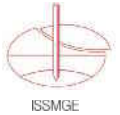




Comité Français
de Mécanique
des Sols



International Society
for Soil Mechanics and
Geotechnical Engineering



Proceedings of the 18th International
Conference on Soil Mechanics and
Geotechnical Engineering

CHALLENGES AND INNOVATIONS IN GEOTECHNICS

*Actes du 18^e Congrès International
de Mécanique des sols et de
Géotechnique*

DÉFIS ET INNOVATIONS EN GÉOTECHNIQUE

Paris 2013

Edited by / Sous la direction de

Pierre Delage, Jacques Desrues, Roger Frank, Alain Puech, François Schlosser

VOLUME 1



Presses des Ponts

Technical Committee 207

Soil-Structure Interaction and Retaining Walls

Comité technique 207

Interaction sol-structure et murs de soutènements

General Report of TC 207 Foundations and Retaining Structures

Rapport général du TC 207 Fondations et ouvrages de soutènement

Bilfinger W.
Vecttor Projetos, Brazil

ABSTRACT: Forty nine papers were included in the theme Soil Structure Interaction. These papers were divided into those related to foundations and retaining structures. The number of research papers and case histories are almost equal, showing equilibrium between academicians and practitioners. Different types of foundations are presented, as well as different types of retaining structures.

RÉSUMÉ : Quarante neuf articles ont été inclus dans le thème « Interaction Sol-Structure ». Ces documents ont été divisés entre ceux qui sont liés aux fondations et ceux liés aux ouvrages de soutènement. Le nombre d'articles de recherche et d'études de cas sont presque égaux, montrant l'équilibre entre les universitaires et les praticiens. Sont présentés différents types de fondations, ainsi que différents types d'ouvrages de soutènement.

KEYWORDS: soil-structure interaction, foundation, retaining structure, excavation.

1 INTRODUCTION

Foundations and retaining structures are traditional and widely used geotechnical structures in which soil-structure interaction plays a major role. For this reason, this technical session was organized by TC 207 – Soil Structure Interaction.

A total of 49 papers were included in this session, 12 focused on foundations and 37 about retaining structures. Contributions came from 28 countries, divided regionally as presented in Figure 1. Almost $\frac{3}{4}$ of all technical papers come from Europe.

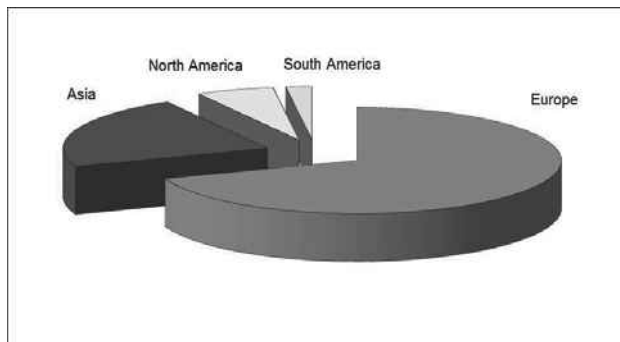


Figure 1. Origin of published papers: Europe – 39, Asia – 11, North America – 3 and 1 – South America.

23 papers present case histories and 26 research results, which show a desired equilibrium between academia and practice.

This report includes:

- A brief summary of the papers related to foundations;
- Some selected topics related to foundations;
- A brief summary of the papers related to retaining structures;
- Some selected topics related to retaining structures;
- Conclusions.

2 BRIEF REVIEW OF PAPERS RELATED TO FOUNDATIONS

12 papers focusing on foundations were selected for this session, 5 of them describing case histories and 7 presenting

research results. Variable topics were presented and discussed, including shallow and deep foundations, as well as soil structure interaction, specially the interaction between foundations and deep excavations.

M. Bidasaria presents a case history about the cofferdam for the Indira Sagar Project in India. This cofferdam was built as a gravity dam, using precast hollow concrete blocks on the upstream and downstream faces. Between the two faces, rubble was filled and later grouted by a cement-sand mixture, forming a so called stonecrete. The paper presents interesting constructive details about the construction of the cofferdam.

E. M. Comodromos et al. present numerical simulations to evaluate the influence of diaphragm wall construction on adjacent buildings. The 3D simulations are specific about the excavation phase, where soil is substituted by bentonite slurry, and the concrete tremied into the pannel. Obtained results showed maximum settlements in the order of 5 mm, for a 6 story building founded on direct footings located closely to the wall.

F. Cuira and B. Simon present an analytical model to evaluate soil reinforced by vertical inclusions, considering the interaction between the reinforced and un-reinforced soil along their boundary. An analytical method is compared to 3D FE simulations and good results are obtained. Further research using centrifuges is recommended in the conclusions.

W. Guo and J. Chu present results of model tests of suction caissons, focusing on shallow water for near shore use. The obtained results were in good agreement with an analytical results.

G. Hannink and O. Oung present a case history with prediction and monitoring results of the induced movements of a 9 story high apartment building, due to excavation of a 20 m deep closely located (7m distance) excavation, retained by strutted diaphragm walls. Measured horizontal and vertical movements of the apartment building were in the order of 10 mm.

Horn-Da Lin et al. present numerical simulation results, where the influence of a deep excavation on nearby located buildings is evaluated. The excavation depth is around 20 m. As benchmark, results of a documented published case history are used, and good agreement was obtained. Horizontal wall

deflections were in the order of 110 mm and maximum settlements at the surface, around 80 mm.

R. Katzenbach and S. Leppla describe results of ground heave and settlement due to excavations, building construction and de-construction. The measured behavior is time dependent and occurs during years and the magnitude of the displacements is in the order of several cm. The soil responsible for this time dependent behavior is the overconsolidated Frankfurt clay. An empirical formulation that approximately describes the time dependent behavior is also proposed.

M. Korff and R. Mair present building settlement results due to deep excavations in Amsterdam. The difference between ground surface and building response as a function of foundation is highlighted and a methodology to evaluate buildings response is presented. Surface settlements in the order of 70 to 110 mm are presented, while the piled building settles only in the order of 20 to 40 mm.

T. Mizutani and Y. Kikuchi describe shaking table model tests to test seismic behavior of caisson type quay walls. The aim of the tests was to verify the possibility to increase water depth in front of the quay after soil treatment – “solidification” in the caisson foundation. It was found, that six different factors affect the caissons improved by the “solidification”. Further research will be performed to allow the development of a design methodology.

T. Pucker and J. Grabe present the structural optimization method applied to geotechnical engineering design. This use is new and, according to the authors, promising results were obtained, showing potential economy and/or improvement in performance.

V. Sesov et al. present a methodology developed for the evaluation of seismic response of historical monuments in Macedonia. 3 Case histories are presented, where this methodology was used.

A. Siemińska-Lewandowska et al. describe different uses of diaphragm walls: retaining structures and foundations. Vertical load test results are presented, with up to 7,5 mm settlement for 150% of the working load. Interesting retaining structures using T shaped diaphragm walls are also presented.

3 SELECTED TOPICS RELATED TO FOUNDATIONS

The papers presented related to foundations cover a wide range of issues and foundation types:

Direct foundations:

- Gravity “concrete” dam;
- shallow footings (influence by diaphragm wall construction; influence by nearby deep excavations);
- caissons – quay wall;
- suction caissons;

Soil treatment for vertical loads by rigid inclusions;

Deep foundations:

- Driven timber piles (influenced by nearby excavation);
- Precast concrete piles (influenced by nearby excavation);
- Barrettes and Diaphragm walls (as foundations and retaining structures);

Seismic design and retrofitting of different foundations;

Long term settlement and heave in highly overconsolidated clay;

Structural optimization technique – use of new technique to optimize foundations.

Two topics were selected, among this wide range presented, and are discussed in more detail.

Specifically seismic issues will not be discussed in detail in this session, as a specific session at this same conference deals with the theme.

3.1 Influence of Excavations on Foundations

The evaluations of E. M. Comodromos et al. showed that the construction of diaphragm walls alone lead to settlement of closely located direct foundations in the order of 5 mm. The approach presented considered complex 3D nonlinear modeling, where the excavated soil is replaced by bentonite slurry.

Additionally to this theoretical aspect, it could be added that, in the field, several times, especially in sandy soil below the groundwater level or soft clays, the operation and movements of the excavation equipment (clam shell, etc) can generate temporary negative suction pressures, leading to “cave-ins” and additional settlements, that can be in the order of several cm.

M. Korff and R. Mair and G. Hannink and O. Oung, present monitoring results, as well as simulations of settlements induced by deep excavations.

The results presented show significant difference between measured settlements: Korff and Mair show settlements, in Amsterdam, at the ground surface of more than 100 mm and, at 10 m from a 31 m deep excavation, building settlements of almost 40 mm. G. Hannink and O. Oung, on the other hand, present settlement measurements, in Rotterdam, of less than 10 mm for a building located 7 m from a 20 m deep excavation. Both excavations are supported by braced diaphragm walls. Possible explanations for these differences are probably:

- Different soil profiles;
- Different excavation depths;
- Different diaphragm and bracing stiffnesses;

Appart from these rather obvious aspects, certainly:

- Different pile length: in the case of the excavation in Amsterdam, the piles are located well above the excavation bottom, but in the case of Rotterdam, pile toes are located almost at the same elevations;
- Location of the buildings in relation to the excavation. No specific information is available from Amsterdam, but in Rotterdam, the building is located close to the excavation, as can be seen in figure 2.

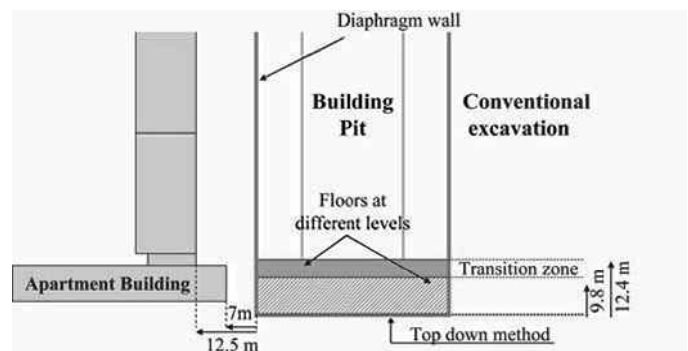


Figure 2. Position of building with relation to excavation (G. Hannink and O. Oung)

This last topic can be confirmed by the analysis of the results presented by Horn-Da Lin et al: the evaluations presented show, qualitatively, that close to the excavation borders, settlements are significantly lower than in the central part, as can be seen in figure 3. The arrows show an approximate position of the apartment building. It is clear that the settlements are significantly lower than in the central part.

Depending of the geometrical conditions, it becomes clear that 3D analyses may be necessary to adequately evaluate soil-structure interaction.

With relation to settlements induced by excavation, in the author’s opinion, the methodologies presented and discussed in Korff and Mair present tools to adequately predict building response to deep excavations, in the case of deep foundations.

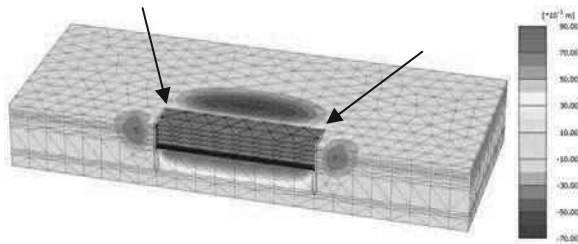


Figure 3. Settlements due to excavation (*Horn-Da Lin et al.*).

3.2 Loading and Unloading due to high rise buildings and excavations

The paper presented by *R. Katzenbach and S. Leppla* presents results of ground heave and settlement measurements due to excavations, building construction and de-construction. This behavior, which could be expected not only in Frankfurt, but also in other geological environments, was adequately documented during a significant time period for some buildings.

The first important issue, often neglected due to lack of reliable information, is the fact that unloading generates significant upward movement, in the order of some or even several cm.

The second issue is the time dependent behavior: a significant part of total displacements are measured at the end of construction, but between 30 and 50% of the observed behavior, occur during months or years after completion of the construction works.

Katzenbach and Leppla propose an empirical equation to represent this time dependent behavior. Just as an exercise, Figure 4 presents monitoring results and the equation proposed by *Katzenbach and Leppla*, and, additionally, settlements estimated using conventional consolidation theory. A consolidation coefficient at the recompression stage of $c_v = 9 \times 10^{-2}$ cm/s was backanalyzed from the measured settlements. This value can be considered representative of overconsolidated clays.

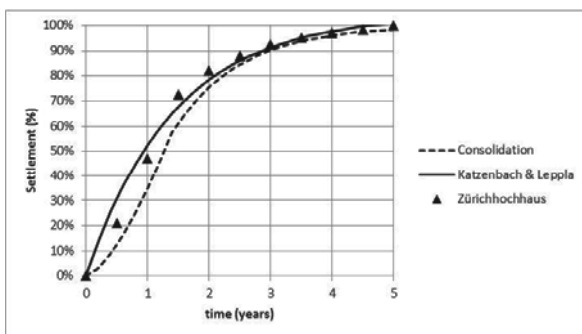


Figure 4. Settlement in % using conventional consolidation theory, the equation proposed by *Katzenbach & Leppla* and monitoring results.

From the discussion above, it becomes clear that, especially in urban environments, even for material considered relatively stiff, time dependent behavior cannot be neglected, depending of local geology.

4 BRIEF REVIEW OF PAPERS RELATED TO RETAINING STRUCTURES

37 papers focusing on retaining structures were selected for this session, 18 of them associated to case histories and 19 with research results. A broad range of topics related to retaining structures was presented.

M. Abramento et al. present a case history from Brazil, of a mixed retaining structure, reinforced earth at the top and anchored wall at the bottom, in a geotechnical environment of expansive soils. The case history includes laboratory tests of the expansive soils and anchor pull out tests, demonstrating that

injection pressures have significant impact on anchor resistance. Monitoring results of the retaining structure are also presented, showing significant horizontal displacement of the reinforced earth face, and negligible horizontal displacements of the anchored stretch.

D. Alexiew and H. Hangen discuss a case history from Bulgaria, where reinforced earth structures were used as retaining structures. Relatively steep, 1H:10V, and high, over 20 m, structures are presented; constructive details are included. Design considerations, including seismic actions, are also discussed.

S. Bagheri present the case history of the deep excavation, in marl and weather marl, associated to the construction of the "Tour Odeon" in Monaco. The excavation is more than 70 m deep and the excavation is supported by anchors.

Ö. Bilgin and E. Mansour discuss theoretical analysis of sheet piles in expansive soils. For a typical sheet pile wall, 10 m high and with an anchor level at 2,5 m, significant increases in anchor reactions and bending moments occur, as swelling pressure increases. Higher wall penetrations also become necessary. Swelling pressures were associated to the Plasticity Index and moisture content variations.

C. M. Chow and Y.C. Tan. present data related the performance of soil nails in weathered granite and fill. Several soil nail pull out tests were performed in excavations up to 20 m depth. Lateral friction measurement results varied between 50 and 140 KPa. A conservative correlation for lateral friction of 5 x SPT (in KPa) blowcount is also proposed.

I.P. Damians et al. discuss the influence of vertical facing stiffness on reinforced soil wall design. Numerical results showed that the loads at the base of the vertical facing and in the reinforcement are affected by the backfill and foundation material, and that the face stiffness also affects reinforcement tensile forces.

T. Durgunoglu et al. present a case history from Turkey, an over 20 m deep excavation close to the Bosphorus. Top down construction method was used, including excavation of rock sockets into rock with a uniaxial compressive strength varying between less than 10 MPa, up to almost 100 MPa.

R.J. Finno et al. discuss ground movements due to top-down construction in Chicago. For this type of construction, according to these authors, normalized horizontal movements of 0,15% to 0,2% are expected. Approximately 40% of these movements can be attributed to time dependent behavior of the concrete slabs. Significant movements can be associated to activities other than the excavation, like potholing.

R. Frischknecht et al. present an environmental impact evaluation, comparing a conventional concrete structure with a geosynthetic reinforced earth structure. The conclusion of the evaluation is that geosynthetic retaining structure shows a 63% to 87% lower environmental impact.

P.P. Ganne and X. Raucroix discuss the design of cantilever walls with a relief floor. For unsaturated, sandy, silty and alluvial clayey soils, an analytical design methodology is proposed, including pre-design recommendations.

A. Gomes Correia et al. present a case history of a 13 m high CSM anchored retaining wall built in Portugal. The CSM wall was built in fill, sands and weathered sandstone, reinforced by steel beams with a horizontal spacing of 1,1m. Maximum measured horizontal displacements were of 16 mm.

A. Guilloux et al. discuss the design, modeling and monitoring of the Tour Odeon, also presented by *Bagheri*. A 3D numerical model is presented as main design tool. The use of the observational model with a maximum horizontal displacement of 17 mm is described.

E. Guler et al. present the case history of a 23 m deep excavation in Istanbul. 2D and 3D numerical modeling was used to evaluate interaction between 2 tunnels, a circular shaft and a deep braced excavation. 2D and 3D models were compared and the 2D analysis showed results on the safe side. Monitoring results obtained during construction yielded reduced

horizontal displacements, in the order of 8 mm, compatible with the 3D FE analysis.

I. Gutjahr et al. discuss comparisons between subgrade reaction calculations, FE analysis using 2 different softwares and monitoring results of an anchored retaining structure of the Vieux Blanc-Mesnil Basin, in France.

V.A.Ilyichev and Y.A. Gotman present a method to optimize diaphragm wall displacements in deep excavations, by means of using soil cement mix in the active and passive parts of the soil massif. The dimensions and stiffness of the soil cement mix can be estimated using the proposed computational method. FE calculations were used to calibrate the proposed calculation method and good agreement was obtained.

Y. S. Jang et al. discuss two case histories from Korea of deep excavations supported by diaphragm walls. Excavations depths of 1 case is 20 m and of the other, 31 m. The retaining walls are concrete diaphragm walls, steel profiles and timber, and steel profiles and shotcrete. Horizontally, the walls are supported by anchors, in one case, and by steel struts, in the other case. Horizontal movements of 30 to almost 100 mm were measured. Forces in anchors and struts were also measured and compared to numerical simulations.

S. Jessee and K. Rollins present model tests to evaluate the passive pressure on skewed bridge abutments. The performed tests showed that a significant reduction was measured, as the skew angle increases. These results were compatible with numerical simulations and a simple correction factor is proposed.

M. Long et al. present a number of case histories of excavations in glacial tills of Ireland. 12 cases are presented, where horizontal displacements were measured. The displacements were, in most of the cases, less than 0,1% H. The conclusion of the authors are that design has been conservative and more realistic design methods and construction methods can lead to more economic design.

D. Loukidis and R. Salgado discuss the results of numerical simulations of earth pressure on walls supporting granular soils. The simulations, using Ottawa and Toyoura sands, with varying relative densities, showed that a minimum active pressure is obtained at 0,5% H displacement. But with higher displacements, in the order of 10% H, critical state inside the soil mass is mobilized. An equation is proposed to estimate the variation of the earth pressure coefficient as a function of the wall crest displacement.

R. Lüftenegger et al. present case histories of non conventional retaining structures. The structures were conceived based on the necessity to avoid the installation under neighboring buildings. 3D FE analyses were used to understand behavior. Good adherence between prediction and monitoring was not obtained, and for this reason the use of the observational method is recommended.

T. Maeda et al. discuss the use of inclined braceless retaining structures in sandy soil. Instead of using a vertical face, inclining it slightly, 10°, allowed the excavation of an almost 10 m deep excavation without any bracing or anchor. An analytical design method was developed and verified by centrifuge tests. Monitoring results from the site showed that the design method lead to results on the safe side.

S. Nakajima et al. present a methodology to inspect exiting retaining structures. The methodology includes percussion tests and vibration tests, where the natural frequency of the structures is measured to evaluate its condition.

C.Y. Ou et al. discuss the mechanism of settlement influence zone due to deep excavation in soft clay. The USC model is used for parametric analyses a method for predicting the settlements is proposed.

J. Philipsen discusses the case history of a braced excavation, built under difficult conditions, in Copenhagen. The excavation was built in quaternary clays and sands, overlaying limestone.

A. Pinto et al. present a case history of an anchored excavation in Lisbon. The excavation was 13 m deep and supported by vertical steel profiles associated to a CSM wall and anchors. The geotechnical profile includes superficial fill, medium sands and sandstones, and GWT 5 m below the surface. The excavation was monitored through inclinometers, with maximum horizontal displacements close to the surface of around 40 mm.

Another paper by *A. Pinto et al.* present the case history of excavations for the Leixões Terminal in Portugal. 2 different solutions are presented: CSM panels with steel profiles and CSM panels with micropiles. The excavation is around 6,5 m deep and the geotechnical profile includes hydraulic fill placed on weathered schist. CSM UCS minimum measured values were of 4 MPa.

H. Popa et al. discuss a case history from Bucharest. 16 m had to be excavated to accommodate a 4 to 6 m deep basement mat and 2 basements. The subsoil profile included interbedded layers of medium to compact sands and medium to stiff clays, with groundwater level 2 to 3 m above the excavation bottom. An anchored diaphragm wall was designed, built and monitored, with maximum horizontal displacements of less than 10 mm.

C. di Prisco and F. Pisanò, present a new anchor type. FE analyses are used to evaluate the pull out behavior of the anchor. Based on the FE analyses, an analytical method is also developed and presented.

N. Sanvitale et al. discuss the role of the facing on the behaviour of soil-nailed slopes under surcharge loading, using small physical models in sand. Flexional and axial stiffness influence the performance of the soil nailing system.

T. Tanaka et al. present results of physical and numerical models, where 3D seepage effects influence stability. Uniform sand are used for the evaluations and results show that the 3D conditions differs from those of typical 2D conditions. Correction factors from an axisymmetric simulation to no axisymmetric conditions are also presented.

P. Turček et al. discuss case histories of deep excavations in Bratislava. Local subsoil includes superficial quaternary sediments, mainly gravel and sand, overlaying neogene marine sediments, mainly stiff clays. Groundwater is normally at shallow depth and its control is one of the main challenges for successful construction.

M J Turner and N A Smith present a case history of the stabilization of a gravity quay wall in the UK. The 17 m high wall, originally built at the end of the 19th century, suffered stability problems since the mid 1980s, with horizontal displacements of around 400 mm. Evaluations showed that the difference between the high tidal variations, more than 6 m, and the groundwater level behind the wall, were leading to increasing horizontal displacements. Stabilization measures included groundwater lowering and installation of anchors.

L. Vollmert et al. discuss results of large scale in situ tests, as well as long term monitoring results of a reinforced earth structure. For the monitored cases, with full height panel walls as facing, the actual lateral stress measured is significantly lower than FE calculations or classic earth pressure theory, showing that current design methods are on the safe side and, possibly, a correction factor can be introduced to EBGeo design methodology.

G. Vukotić et al. present results of anchor bond measurements in different soils and anchor length. The influence of the fixed anchor lengths is evaluated, showing that longer anchors are less efficient than shorter anchors. A proposition or design methodology is presented, including possible use of single bore multiple anchors – “SBMA”.

L. Warren et al. discuss the use of drystone retaining walls, including model tests performed in the UK. Different types of walls, based on their construction methods, horizontal, vertical and random, are discussed. The type of wall is presented as a

sustainable type of structure, due to lack of mortar, use of local materials and providing habitat for animals and plants.

C. A. Wiggan *et al.* present a numerical evaluation of potential pore pressure reduction on retaining walls due to the flow between piles. Not considering a wall of secant of contiguous piles impermeable, lead pore pressure reductions that act on the wall. Results of parametric evaluations are presented, where the distance between the piles are varied, showing significant pore pressure reductions. This approach, however, leads to increased settlements at the surface.

C. Yoo and D.W. Jang discuss results of laboratory tests performed on reduced models, to evaluate the influence of rainfall on the performance of reinforced earth structures. Test results showed that wetting and drying cycles may have cause additional wall displacements, especially for structures with low safety factor.

5 SELECTED TOPICS RELATED TO RETAINING STRUCTURES

The technical papers related to retaining structures cover a wide range of topics, including:

- Reinforced soil – 5 papers;
- Diaphragm walls – 4 papers;
- Secant pile walls – 1 paper;
- Sheet pile walls – 3 papers;
- Soldier type walls – 3 papers;
- Mixed in place soil structures – 5 papers;
- Soil nailing and anchors – 3 papers;
- Gravity and cantilver walls – 3 papers;
- Others.

From this wide range, some topics were selected and are discussed in more detail:

- Horizontal displacements;
- Earth pressures;
- Soil nailing and anchor lateral friction;
- Soil-cement mixtures.

Unfortunately, not all papers present sufficient technical data, to allow analyses and comparisons.

5.1 Horizontal displacements

The selected papers present, in some cases, monitoring results, specifically, horizontal displacements, which are summarized in Figure 5 and 6.

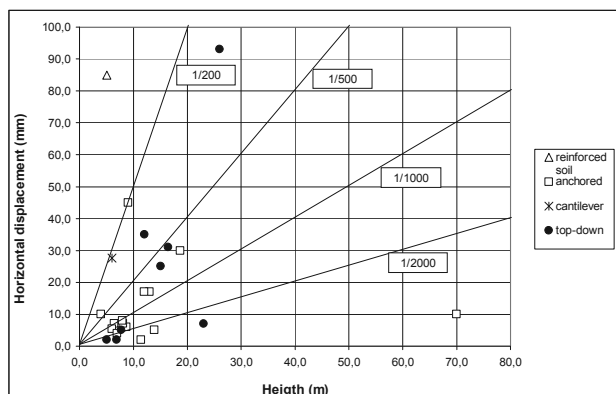


Figure 5. Horizontal displacements x excavation depths.

Very variable results can be seen; horizontal displacements / heights (H/D) from less than 1/2000 to more than 1/200 were presented.

No clear tendency can be identified in figure 5. Visually, one possible conclusion is that deeper excavations, apparently, present lower D/H values, meaning that this type of construction is, due to its complexity, designed and built with higher safety margins and possibly, more rigid. Figure 6 below presents the same data, showing normalized horizontal displacements and

excluding 1 extreme value: the 70 m high excavation (in rock) presented by S. Bagheri and A. Guilloux *et al.*

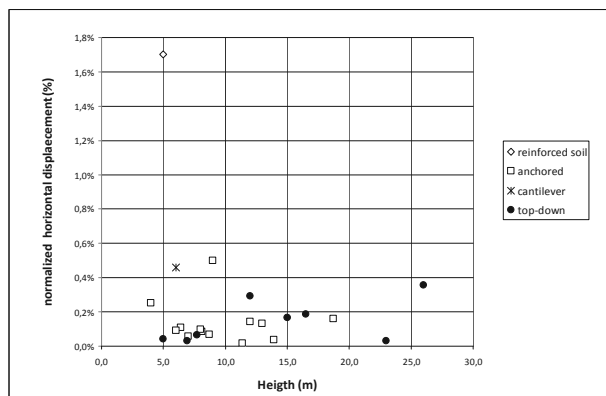


Figure 6. Normalized horizontal displacements with respect to excavation heights (depths)

In comparison to other retaining structures, relatively high horizontal displacements (85 mm => 1,7%) were measured for a reinforced earth structure (M. Abramento *et al.*). However, this magnitude of displacement, according to common practice, can be considered normal for reinforced soil structures (Sayão *et al.*, 2004).

Figure 7 shows the same results, plotted together with the data presented by Long (2001).

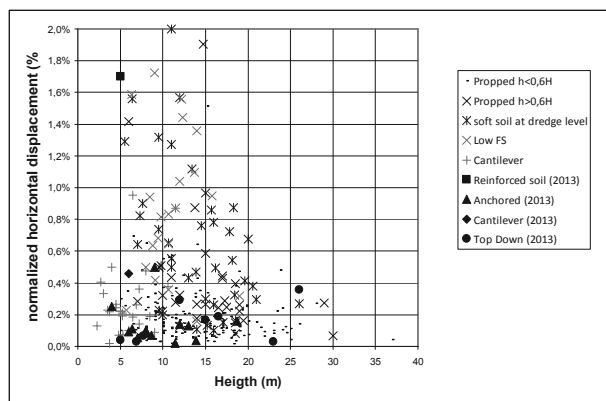


Figure 7. Normalized horizontal displacements x excavation heights, including data presented by Long (2001).

It can be seen that the published horizontal displacements are compatible with several other measurements as compiled and published in 2001.

Other published databases are also compatible with the presented data:

- Leung and Ng (2007): 0,13 %H to 0,23 % H, depending on soil stiffness;
- Wang *et al.* (2010): 0,27%H to 1,5%H, depending of retaining structure type and soil stiffness.

Common conclusion of Long (2001), Leung and Ng (2007) and Wang *et al.* (2010) are that horizontal displacements are affected mainly by safety margins, system stiffness, soil type and construction method.

Finally, the conclusions presented by R.J. Finno *et al.* are interesting: for the cases where small displacements are measured, a significant part of these displacements may be caused by time dependant behavior of concrete floor slabs.

5.2 Earth Pressures

Four papers deal specifically with earth pressures: Ö. Bilgin and E. Mansour, S. Jessee and K. Rollins, D. Loukidis and R. Salgado, T. Maeda *et al.*

Ö. Bilgin and E. Mansour discuss theoretical analysis of sheet piles in expansive soils. The presented analyses are based on a correlation between the plasticity index (PI) and swelling potential. The analyses presented assume that swelling pressure will act in the zone where moisture varies, relatively close to the surface. Figure 8 presents results of the authors analyses, correlating anchor loads of sheet pile wall to the PI

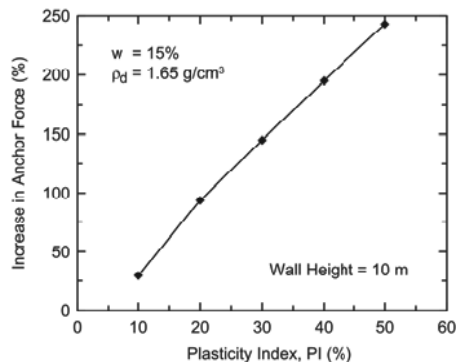


Figure 8. Effect of expansive soils on anchor force, according to Ö. Bilgin and E. Mansour

S. Jessee and K. Rollins present model tests to evaluate passive earth pressure on a “skewed” surface. Figure 9 presents a proposed reduction factor for the passive force, as a function of the skew angle.

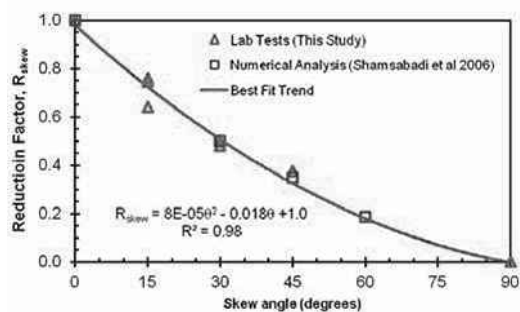


Figure 9. Test results presented by S. Jessee and K. Rollins.

The performed tests showed that a significant reduction was obtained as the skew angle increases. These results were compatible with numerical simulations and a simple correction factor is proposed. Peak passive pressure was developed at 2,5% to 3,5% of abutment height. Significant reductions in passive pressure were measured beyond peak (4% to 6%), with a residual stress around 40%.

Results are interesting, but direct use of results for design shall be evaluated with care.

D. Loukidis and R. Salgado present the results of sophisticated numerical simulations of variation of earth pressure on walls supporting granular soils. Figure 10 present one of the presented outputs and some interesting qualitative conclusions can be drawn:

For horizontal displacements of around 0,5%, minimum lateral earth pressure develops. Considering K_0 around 0,5, K_a results around 0,125. As horizontal displacement increases, K_a results in the order of 0,2. The authors state that the minimum earth pressure coefficient should not be used, at least for ultimate limit state design. However, when analyzing figure 7, where a significant number of case histories showed horizontal displacements of less than 0,4 %, possibly some optimization in terms of design earth pressures can be possible.

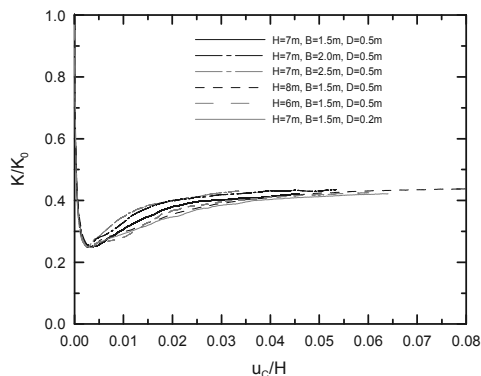


Figure 10. Results presented by D. Loukidis and R. Salgado: Variation of normalized lateral earth pressure coefficient with wall crest displacement from analyses with medium dense Toyoura sand ($D_R=60\%$)

T. Maeda et al. discuss the use of inclined braceless retaining structures in sandy soil. The presented evaluations showed that significant reduction in earth pressures acting on a cantilever wall can be obtained by inclining the wall facing. Figure 11 present horizontal displacements measured on model tests. It can be seen that, even for a reduced inclination of 10°, horizontal displacements reduced around 30%.

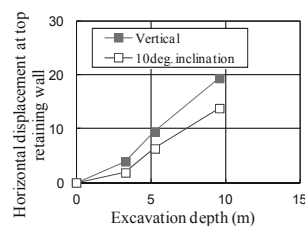


Figure 11. Relationship between excavation depth and horizontal displacement of retaining walls, considering horizontal and inclined structures, presented by T. Maeda et al.

Figure 12 presents earth pressures for the inclined and the vertical structure. It can be seen that, especially for deeper excavations, a significant reduction in earth pressures occurs.

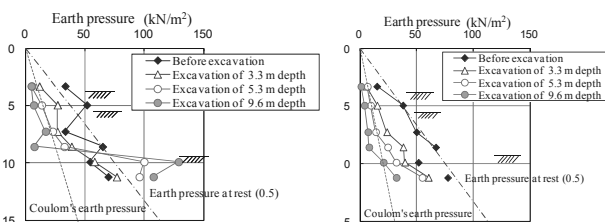


Figure 12. Earth pressures for vertical and inclined structure, presented by T. Maeda et al.

In the author’s opinion, the simple approach of inclining slightly a cantilever structure can bring significant saving, should be further investigated and can be used in practice.

5.3 Soil nailing and anchor lateral resistance

C. M. Chow and Y.C. Tan. present data related to the performance of soil nails in weathered granite and fill. Several soil nail pull out tests were performed in excavations of up to 20 m depth. Figure 13 presents typical pull out results, showing that maximum load is obtained between 4 and 6 mm of displacement. After a peak value, only slight increases can be seen.

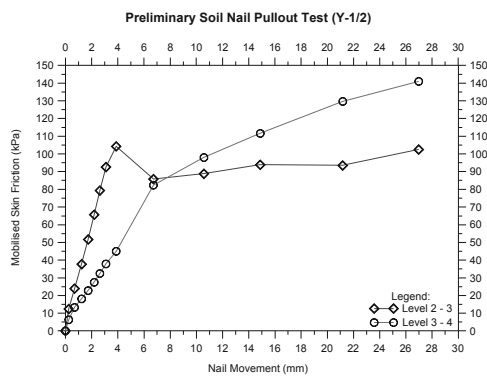


Figure 13. Pull out test results, presented by *C. M. Chow and Y.C. Tan*.

Lateral friction measurement results varied between 50 and 140 KPa. A conservative correlation for lateral friction of 5 x SPT (in KPa) blowcount is also proposed.

These results are comparable with data presented in Ortigão and Sayão (2004): for sands, approximate ratio between SPT blowcount and lateral friction is around 5, and for clays, around 3,4.

M. Abramento et al. presented results of pull out tests of anchors for different grouting conditions and resulting lateral friction between 80 KPa and 140 KPa. The soil where the anchors were built has an approximate SPT blowcount between 20 and 30.

Finally, just for comparison, Décourt (1982) presented a correlation between SPT blowcount and lateral friction for piles:

$$\text{Lateral friction} = 10 \times (\text{SPT} / 3 + 1).$$

Figure 14 presents graphically the lateral frictions and corresponding SPT blowcount values.

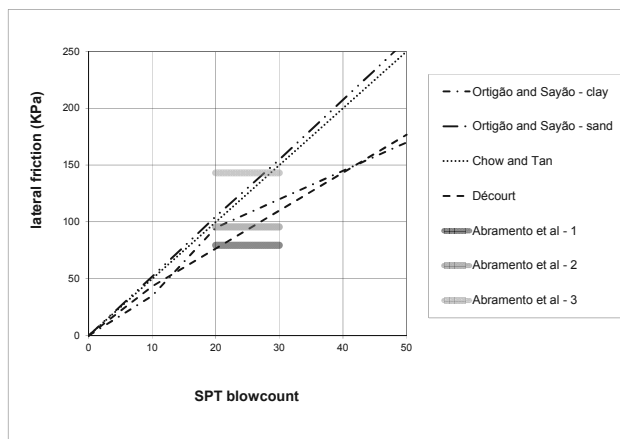


Figure 14. Lateral friction results, presented by *C. M. Chow and Y.C. Tan*, including values published by Ortigão and Sayão (2004) and Décourt (1982).

A. Gomes Correia et al. present results of anchor tests in medium dense sands, resulting in a lateral friction of 275 KPa. Similar results and even higher lateral frictions are presented by *G. Vukotic et al.* for tests in different soils. Unfortunately, there is no specific information available about the SPT blowcount, but probably results will be well above the graphs presented in Figure 14. Possibly, this difference occurs due the use of pressure grouting.

Even considering the limitations of the SPT blowcount as geotechnical design parameter, the correlations between the SPT and lateral friction proposed by *C. M. Chow and Y.C. Tan* seem compatible with previously published results for soil nails. Grout injection influence, in the author's opinion, shall be further investigated. Special anchor devices, like the one presented by *C. di Prisco and F. Pisanò* work completely different from cylindrical nails / anchors and further research is necessary to allow reliable comparisons.

5.4 Soil mixing compressive strength

A. Gomes Correia et al. present a case history where CSM material, with a cement consumption of 600 kg/m^3 , was tested and a minimum uniaxial compressive strength of 4 MPa was obtained. Minimum E_{50} values were 1 GPa. Unfortunately, few results with information about this important design parameter were presented. As complementary information, Figure 15 presents data published by Bilfinger et al, with results from uniaxial compressive strength tests results in soil treated with jet grouting technology.

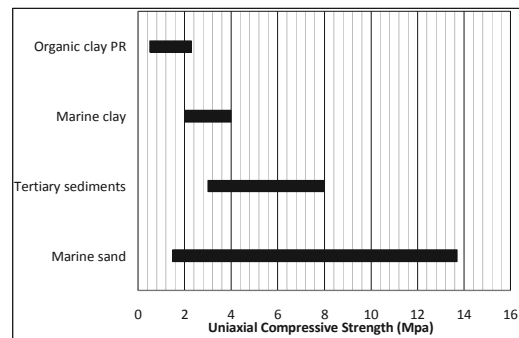


Figure 15. Uniaxial compressive strength, Bilfinger et al. (2012).

It can be seen that soil type has major influence on uniaxial compressive strength, specially the organic matter content.

6 CONCLUSIONS

The technical papers included in this session cover a wide range of topics. In items 3 and 5 some of these topics were discussed in more detail.

Some conclusions may be drawn with relation to three areas:

Design: No detailed design procedures were presented, but some interesting conclusions can be drawn from the published papers:

- Numerical modeling is a common tool to model soil and structure interaction;
- Limit equilibrium analysis and beam-spring models continue to be used in design practice;
- The observational method, meaning, the use of monitoring to control and, possibly, adjust the design, is a widespread design “philosophy”.

Construction: Different construction techniques and structures are discussed and presented:

- Foundations: direct footings, caissons and suction caissons, barretes and diaphragm walls, soil treatment by rigid inclusions;
- Retaining structures: diaphragm walls, secant pile walls, sheet pile walls, soldier type walls, mixed in place structures, anchored and nailed structures, reinforced soil, cantilever and gravity walls.

Most of these construction techniques and structures are already well known and the focus and innovation presented in the papers are performance, size, depth and proximity to other structures. Two exceptions are: soil treatment techniques, used in different conditions and suction caissons.

Research: Different research themes were presented, but one of the important investigated issues is earth pressures for different conditions. Another topic researched are mathematical models associated to techniques to optimize design procedures, and not to represent soil constitutive models.

REFERENCES

- Bilfinger, W., da Silva, M.A.A.P., Rocha, H.C., Celestino, T.B. (2012) Tunnels in São Paulo, in Soils of the Metropolitan Regions of São Paulo and Curitiba, ABMS (in Portuguese)

- Décourt, L. (1982): "Prediction of the Bearing Capacity of Piles based exclusively on N values of the SPT", 2nd European Symposium on Penetration Testing, Amsterdam, pp. 29-34.
- Long, M. (2001) "Database for retaining wall and ground movements due to deep excavations", *J Geotech Geoenviron Eng, ASCE* 127 (3), 203–224.
- Leung, E.H.Y., Ng, C.W.W. (2007). "Wall and ground movements associated with deep excavations supported by cast in situ wall in mixed ground conditions". *J Geotech Geoenviron Eng, ASCE*, 133 (2), 129–143.
- Ortigão, J.A.R., Sayão, A.S.F.J. Handbook of Slope Stabilization. Springer, New York, 2004.
- Sayão, A.S.F.J., Azambuja, E. Ehrlich, M., Gomes, R.C. (2004) "Reinforced Walls and Slopes" in Brazilian Geosynthetic Manual, ed. Vertematti, J.C. Edgar Blücher, São Paulo (in Portuguese)
- Wang, J., Xu, Z., and Wang, W. (2010). "Wall and Ground Movements due to Deep Excavations in Shanghai Soft Soils." *J. Geotech. Geoenviron. Eng.*, 136(7), 985–994.
- APPENDIX - List of papers submitted for this session:
- FOUNDATIONS:
- Bidasaria, M. Foundation and Geotechnical Problems, Geology, Design and Construction of Cofferd Dam on Narmada River for Indira Sagar Project in Central India.
- Comodromos E. M., Papadopoulou, M.C., Konstantinidis, G.K. Effects on adjacent buildings from diaphragm wall installation.
- Cuira, F., Simon, B. Prise en compte des effets de bord dans un massif renforcé par inclusions rigides.
- Guo, W., Chu, J. Suction Caisson Installation in Shallow Water: Model Tests and Prediction.
- Hannink, G., Oung, O. Displacement of an apartment building next to a deep excavation in Rotterdam.
- Lin, H.D., Dang, H.P., Hsieh, Y.M. Assessment of Ground and Building Responses Due to Nearby Excavations Using 3D Simulation.
- Katzenbach, R., Leppla, S. Deformation behaviour of clay due to unloading and the consequences on construction problems in inner cities.
- Korff, M., Mair, R.J. Response of piled buildings to deep excavations in soft soils.
- Mizutani, T., Kikuchi, Y. Shaking table tests on caisson-type quay wall with stabilized mound.
- Pucker, T., Grabe, J. Structural Optimization in Geotechnical Engineering.
- Sesov, V., Cvetanovska, J., Edip, K. Geotechnical aspects in sustainable protection of cultural and historical monuments.
- Sieminska-Lewandowska, A., Mitew-Czajewska, M., Tomczak, U. Various use of Diaphragm walls for construction of multilevel road junction - design and monitoring of displacements.
- RETAINING STRUCTURES
- Abramento, M., Fujii, J., Cogliati, B., Assakura, V. Design, Construction and Monitoring of a Mixed Soil-Reinforced and Anchored Retaining Wall in Expansive Soil.
- Alexiew, D., Hangen, H. Design and construction of high bermless geogrid walls in a problematic mountainous seismic region in Bulgaria.
- Baghery, S. La Fouille de la Tour Odéon à Monaco : Les quatre éléments remarquables de sa conception.
- Bilgin, Ö., Mansour, E. Anchored sheet pile wall design in expansive soils.
- Chow, C.M., Tan, Y.C. Performance of Soil Nails in Weathered Granite and Fill.
- Damians, I.P., Lloret, A., Josa, A., Bathurst, R.J. Influence of facing vertical stiffness on reinforced soil wall design.
- Durgunoglu, T., Kulac, F., Ikiz, S., Akcakal, O. Top Down Construction Alongside Of Bosphorus – A Case Study.
- Finno, R.J., Arboleda, L. Kern, K., Kim, T., Sarabia, F. Computed and observed ground movements during top-down construction in Chicago.
- Frischknecht, R., Büsser-Knöpfel, S., Itten, R., Stucki, M. Comparative Life Cycle Assessment of Geosynthetics versus Concrete Retaining Wall.
- Ganne, P.P., Raucroix, X. Design of inverted T-shaped Cantilever Wall with a Relief Floor.
- Gomes Correia, A., Tinoco, J., Pinto, A., Tomásio, R. An Anchored Retaining Wall in CSM.
- Guilloux, A., Porquet, M., De Lavernée, P., Lyonnet, P., Roman, P. Conception, modélisation et auscultation d'une très grande excavation à Monaco.
- Guler, E., Osmanoglu, U., Koç, M. A Case Study of 3D FE Analysis of a Deep Excavation Adjacent to a Tunnel Construction.
- Gutjahr, I. Doucerain, M., Schmitt, P. Heumez, S., Maurel, C. Instrumentation de la paroi moulée du bassin de Blanc-Mesnil : retro-analyse et calage des modèles de calcul.
- Ilyichev, V.A., Gotman, Y.A. Calculation method of optimization the soil-cement mass dimensions to reduce the enclosure displacements in deep excavations.
- Jang, Y.S., Choi, H.C., Shin, S.M., Kim, D.Y. Case Studies of Complicate Urban Excavation from Design to Construction.
- Jessee, S., Rollins, K. Passive Pressure on Skewed Bridge Abutments.
- Long, M., O'Leary, F., Ryan, M., Looby, M. Deep excavation in Irish glacial deposits.
- Loukidis, D., Salgado, R. Active earth thrust on walls supporting granular soils: effect of wall movement.
- Lüftenegger, R., Schweiger, H.F., Marte, F. Innovative solutions for supporting excavations in slopes.
- Maeda, T., Shimada, Y., Takahashi, S., Sakahira, Y. Design and Construction of Inclined Braceless Excavation Support Applicable to Deep Excavation.
- Nakajima, S., Shinoda, M., Abe K. Inspection of structural health of existing railway retaining walls.
- Ou, C.Y., Teng, F.C., Hsieh, P.G., Chien, S.C. Mechanism of Settlement Influence due to Deep Excavation in Soft Clay.
- Philipsen, J. Establishing a high risk construction pit in a hurry.
- Pinto, A., Tomásio, R., Godinho, P. Innovative Solution of King Post Walls combined with CSM Panels.
- Pinto, A. Pita, X., Neves, M. Unusual Geotechnical Solutions at the Leixões Cruise Terminal.
- Popa, H., Manea, S., Batali, L., Olteanu, A. Aspects on designing and monitoring a deep excavation for a highly important structure.
- di Prisco, C., Pisanò, F. FEM – aided design of a novel device for soil anchoring.
- Sanvitale, N., Simonini, P., Bisson, A., Cola, S. Role of the facing on the behaviour of soil-nailed slopes under surcharge loading.
- Tanaka, T., Kusumi, S., Inoue, K. Effects of plane shapes of a cofferdam on 3D seepage failure stability and axisymmetric approximation.
- Turček, P., Frankovská, J., Súfovská, M. Stability and dewatering problems of deep excavations in Bratislava.
- Turner, M.J., Smith, N.A. Managed remediation of a large Victorian gravity quay wall using the observational method.
- Vollmert, L., Niehues, C. Concrete panel walls – Current development on interaction of earthworks, geosynthetic reinforcement and facing.
- Vukotić, G., González, J., Soriano, A. The influence of bond stress distribution on ground anchor fixed length design. Field trial results and proposal for design methodology.
- Warren, L., McCombie, P., Donohue, S. The sustainability and assessment of drystone retaining walls.
- Wiggan, C., A., Richards, D.J., Powrie, W. Numerical modelling of groundwater flow around contiguous pile retaining walls.
- Yoo, C., Jang, D.W. Geosynthetic Reinforced Soil Wall Performance under Heavy Rainfall.

Design, Construction and Monitoring of a Mixed Soil-Reinforced and Anchored Retaining Wall in Expansive Soil

Conception, construction et surveillance d'un mur mixte de sol renforcé et ancré dans un sol gonflant

Abramento M.

CEG Engenharia and Escola Politécnica da USP

Fujii J.; Cogliati B., Assakura V.

Yamamichi and CEG Engenharia

ABSTRACT: Due to traffic volume increase a large stretch of a major highway linking São Paulo and Campinas City, Brazil, has recently been widened. In order to achieve the construction of additional lanes, a construction of a mixed-type retaining wall became necessary. This mixed-retaining structure consisted of a 5m high anchored wall at the bottom and a 5m high steel-reinforced retaining wall at the top, totalling a 10m high retaining wall. The bottom wall was built in a cut slope in a stiff, highly expansive, clayey soil. The steel-reinforced retaining wall was built over the lower anchored wall with both faces aligned. Anchor loads at the bottom wall were applied in stages in order to account for the increasing loads during the construction of the top wall. In order to correctly design the bottom anchored wall several undisturbed soil samples were obtained from the stiff clay. Laboratory tests included complete characterization, shear strength and expansion pressure determination. The retaining system was monitored during all construction stages. This paper presents details on the laboratory tests results, design of the retaining walls, construction steps and monitoring.

RÉSUMÉ : En raison du volume de trafic une portion d'une route importante reliant São Paulo et Campinas, au Brésil, a récemment été élargie. Afin de réaliser la construction de voies supplémentaires, une construction d'un mur de type mixte devenait nécessaire. Cette structure mixte consistait en un mur ancré de 5m de haut en partie basse et un mur en sol renforcé en partie haute, pour une hauteur totale de 10m de soutènement. La paroi en partie basse a été construite dans une pente en déblai dans un sol argileux raide et très expansif. Le mur en sol renforcé a été construit sur la paroi inférieure ancrée avec les deux parements alignés. Les charges d'ancrage de la paroi en partie basse ont été appliquées par paliers afin de tenir compte des charges croissantes au cours de la construction de la paroi supérieure. Afin de concevoir correctement le mur ancré plusieurs échantillons de sol intacts ont été prélevés sur l'argile raide. Les tests de laboratoire incluent la caractérisation complète, la résistance au cisaillement et à la détermination des pressions de gonflement. Le système de soutènement a été suivi pendant toutes les étapes de la construction. Cet article présente des détails des résultats des tests de laboratoire, la conception des murs de soutènement, la construction et le suivi des mesures.

KEYWORDS: Reinforced wall, anchored wall, expansive soil, monitoring

1 INTRODUCTION

Due to traffic volume increase a section of approximately 3km of a major highway linking São Paulo and Campinas city, Brazil, had to be widened. In order to achieve the construction of additional lanes, and due to geometric constraints, a mixed-type retaining wall became necessary. This mixed-retaining structure is shown in Figure 1 and consists in a 5m high anchored wall at the bottom and a 5m high steel-reinforced retaining wall at the top, totalling a 10m high retaining wall.

This paper presents details on the laboratory tests results, design of the retaining walls, construction steps and monitoring, as well as a comparison of measured and predicted displacements and loads at the top and bottom retaining walls.

2 SITE INVESTIGATION AND LABORATORY TESTS

SPT borings show that the local soil consists of a superficial colluvial soil characterized as a soft porous silty clay 2 to 3m thick and with blowcounts varying from 2 to 3, followed by a medium, stiff and hard clay with blowcounts larger than 15 and reaching up to 40. A picture of this last layer is shown in Figure

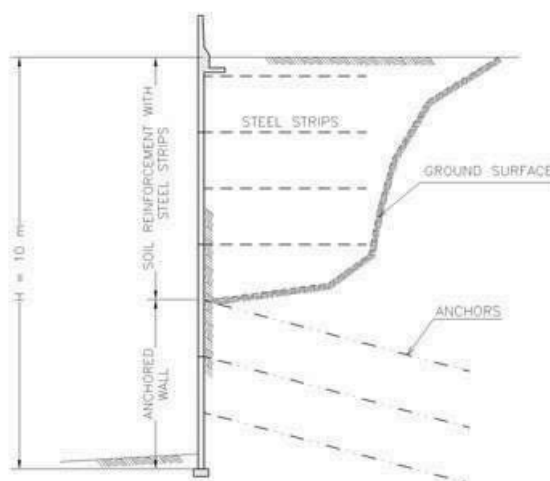


Figure 1. Typical cross-section of mixed reinforced fill-anchored wall.

2. Figures 3 and 4 show typical SPT borings results for two of the wall sections. This stiff clay layer receives the load from the

reinforced fill and had to be cut and anchored in order to widen the roadway.

Therefore, this layer was fully investigated with:

- Several SPT borings.
- Laboratory tests: direct shear and expansion tests on undisturbed samples and characterization.
- Pullout tests on anchors.

Moreover, compaction and direct shear tests were carried out on fill materials.



Figure 2. Stiff to hard silty clay layer to be cut and retained with anchored wall and surcharged with reinforced soil fill.

3 TEST RESULTS – STIFF TO HARD CLAY

Table 1 presents results from direct shear tests. It is worth noting the large drop in shear strength for large displacements (residual conditions). Peak strength typically occurs for very small displacements, in the range of 1mm.

Table 1. Direct shear test results.

Sample	Specimen	σ (kPa)	τ_{max} (kPa)	τ_{res} (kPa)
Natural	CP-1	51	232	32
	CP-2	154	305	22
	CP-3	306	419	92
Saturated	CP-1	51	228	77
	CP-2	151	264	72
	CP-3	304	304	34

Table 2 presents results from expansion tests carried out on the horizontal and vertical directions. The expansion pressure is very high in the vertical direction, whereas the expansion pressure in the horizontal direction is around 6% of the vertical pressure, showing the marked influence of clay structure on its behavior (Figure 2).

Table 2. Expansion pressure for vertical and horizontal directions.

Direction	Expansion Pressure (kPa)
Vertical	440
Horizontal	30

Table 3 presents results from pullout tests on anchors 10cm in diameter and 6m long as a function of injection pressure. Anchors 202, 207 and 212 had, respectively, one, three and two functioning pressure valves. Therefore, adhesion values varied significantly from 25 to 45kN/m, demonstrating marked influence of injection pressure on adhesion.

Table 3. Pullout tests on anchors.

Segment	Adhesion (kN/m)	Injection Pressure (kgf/cm ²)
202	25	$\phi/\phi/20$ (1 valve)
207	45	50/20/30 (3 valves)
212	30	$\phi/30/20$ (2 valves)

4 DESIGN PARAMETERS

The following design conditions and strength parameters were considered for design:

- End-of-Construction (EOC): peak shear strength parameters and natural water content, with and without expansion pressure.
- Long-Term and Peak Condition (LTP): saturated peak shear strength parameters, with and without expansion pressure.
- Long-Term and Residual Condition (LTR): saturated residual shear strength parameters, with expansion pressure.

A possible decrease in adhesion due to soil saturation was also considered in adhesion. Increase in anchor loads due to expansion pressure was taken into account for anchor design.

With basis on the laboratory and field tests, and following the procedures outlined in ABNT NBR 11.682 – Slope Stability, the parameters presented in Table 5 were used in wall design.

Table 5 – Design parameters.

Parameter	Condition/			
	EOC	LTP	LTR	MSE*
Soil unit weight (kN/m ³)	20	20	20	20
Cohesion intercept (kPa)	60	40	0	30
Friction angle (°)	30	18	18	25
Anchor adhesion (kPa)	Average	100	90	125
	Maximum	140	125	
Same with expansion (kPa)	Average	70	65	-
	Maximum	100	90	
Puncture anchor head (kN)		430		

*MSE :Soil Parameters for Mechanically Stabilized Earth Wall

5 DESIGN AND CONSTRUCTION OF ANCHORED WALL

A limit equilibrium program was used to design the anchored wall, considering the reinforced wall on the top and a traffic surcharge of 25kPa. Potential failure surfaces were always very close to the anchored wall face. As a result, the free section of the anchors were short, in the order of 3.0m. This is the minimum length accepted by ABNT NBR 5629 – Anchored Walls. Anchor length was varied in order to achieve minimum Safety Factor of 1.8 for EOC, 1.5 for LTP, and 1.2 for LTR conditions, resulting the following anchor distribution:

- Cable anchors, 5x12,7mm 190RB, yield stress= 1708MPa
- Working load = 430kN
- Testing load = 760kN
- Minimum spacing = 1,6m
- Maximum spacing = 2,0m
- Inclination with horizontal = 20 degrees
- Free length = 3,0m
- Anchored length = varying from 6.0 to 9.0m
- Anchor diameter = 100mm

Water table close to the base of the anchored wall was found in several SPT bores. Therefore, horizontal drains 15m long were installed every 2.4m along the wall base. The stiff clay layer was carefully excavated to install the anchors and build the reinforced concrete face 30cm thick. For each anchor level the anchors were loaded to 50% of the working load. Construction of the reinforced fill started after the completion of the anchored wall. When the reinforced fill height reached around 70% of the final fill height the anchors were re-loaded with 100% of the final working load.

6 WALL MONITORING

In order to monitor wall behavior a monitoring system was installed along the wall. It consisted of:

- 3 inclinometers 15m deep installed
- 3 load cells installed at selected anchor heads
- 20 displacement pins

Inclinometers were installed in boreholes along the front face of the anchored wall, and extended upwards during placement of the reinforced fill.

Several readings were obtained during construction of the lower anchored section and continued during construction of the upper reinforced fill section.

7 MONITORING RESULTS

Figures 3 and 4 show inclinometers results for 2 of the instrumented sections: Section I-200 and Section I-205. The results show that:

- The displacements increase continuously with construction of the lower anchored wall and the upper reinforced soil wall.
- Displacements of the lower anchored wall were generally small, in the range of 5 to 10mm.
- Small face displacements were expected for the stiff clay layer. However, for these displacements level it is possible that residual conditions may be attained by the clay layer during wall construction.
- For the upper reinforced fill, however, face displacements were relatively high. Measured displacements varied from around 10mm at the bottom up to 70 to 80mm for the upper part of the fill.

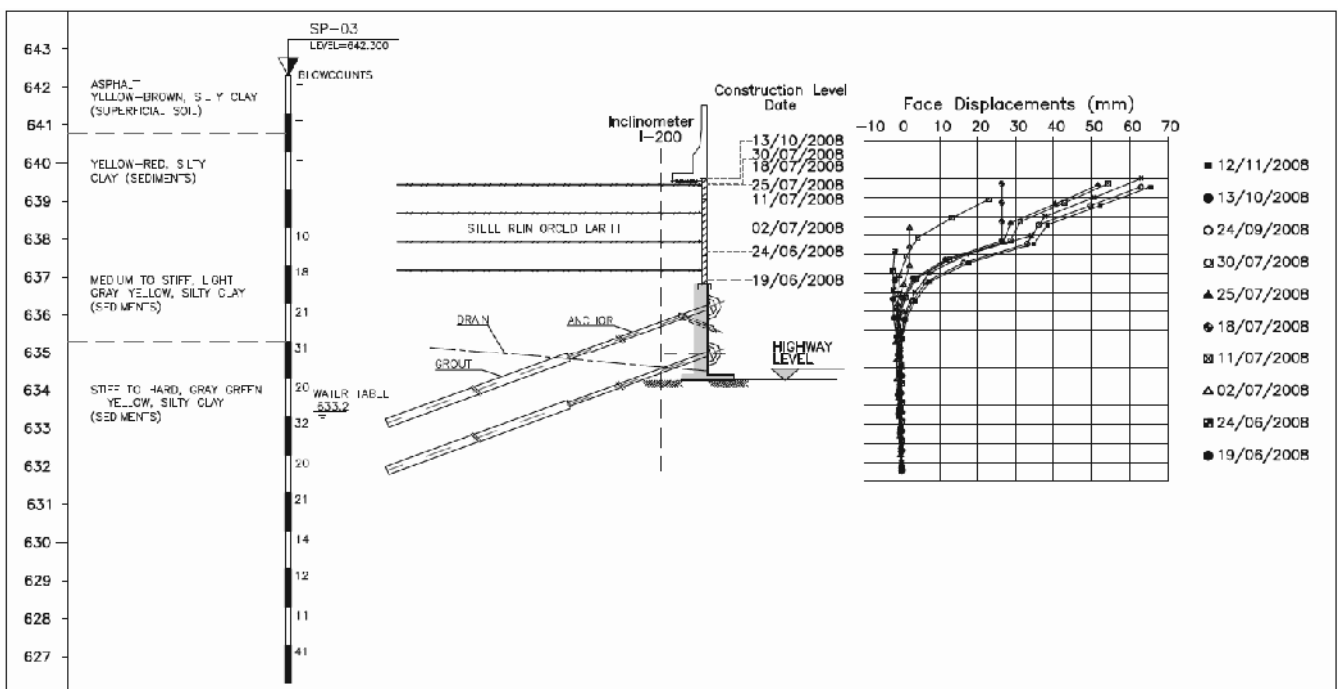


Figure 3. Inclinometer results in Section I-200.

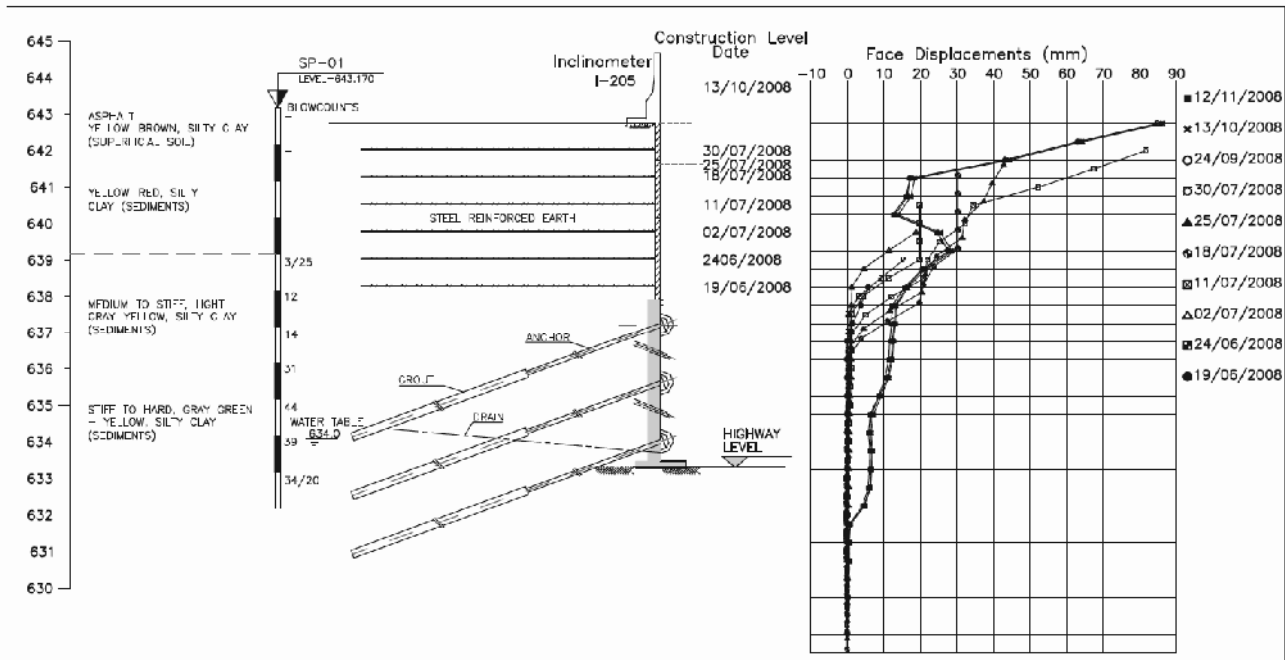


Figure 4. Inclinometer results in Section I-205.

8 CONSTRUCTION CONDITIONS

Figures 5 and 6 show construction conditions, especially the upper part of the reinforced soil fill with the reinforcing steel strips and the face of the anchored wall face at the bottom.



Figure 5. General view of the top part of the reinforced soil fill.



Figure 6. General view of the highest section of wall.

9 CONCLUSIONS

The following conclusions can be summarized:

- The stiff clay layer has relatively high strength parameters for peak conditions.
- Residual conditions are achieved for relatively low displacements, around 1mm.
- Due to structural conditions the stiff clay has relatively high vertical expansion pressures, around 440kPa, whereas horizontal pressures are relatively low, around 30kPa.
- Displacements of the lower anchored wall were generally small, in the range of 5 to 10mm.
- These small face displacements were expected for the stiff clay layer. However, for these displacements level it is possible that residual conditions may be attained by the clay layer during wall construction.
- For the upper reinforced fill, however, face displacements were relatively high. Measured displacements varied from around 10mm at the bottom up to 70 to 80mm for the upper part of the fill.

10 ACKNOWLEDGEMENTS

The authors are grateful to Ms. Karina Tomoko Hentona for helping in preparing the figures.

11 REFERENCES

- ABNT NBR 61822 – 2007. Slope Stability.
 ABNT NBR 5629 – 2006. Anchored Walls.

Design and construction of high bermless geogrid walls in a problematic mountainous seismic region in Bulgaria

Conception et construction de murs renforcés par des géogrilles de grande hauteur et sans risberme dans une région montagneuse sismique problématique en Bulgarie

Alexiew D., Hangen H.
HUESKER Synthetic GmbH, Gescher, Germany

Geogrids made of geosynthetics can replace conventional building materials like concrete. In this article, goal and scope, basic data and the results of a comparative life cycle assessment of concrete reinforced retaining walls (CRRW) and geosynthetics reinforced retaining walls (GRRW) are described. One running meter of a three meters high retaining wall forms the basis for comparison. The two walls have the same technical performance and an equal life time of 100 years. The GRRW has a lower demand of steel and concrete compared to the CRRW. The product system includes the supply of the raw materials, the manufacture of the geotextiles and the concrete, the construction of the wall, its use and its end of life. The life cycle assessment reveals that the GRRW causes lower environmental impacts. The cumulative greenhouse gas emissions of 300 m CRRW are 400 t and 70 t in case of GRRW. The use of an environmentally friendlier lorry in a sensitivity analysis and monte carlo simulation confirm the lower environmental impacts caused by the construction of a GRRW compared to a CRRW. More than 70 % of the environmental impacts of the geogrids production are caused by the raw material provision (plastic granulate) and the electricity demand in manufacturing.

RÉSUMÉ : Les Géogrilles peuvent remplacer les matériaux conventionnels comme le béton. Cet article contient une description de l'objectif et du champ d'étude, l'inventaire et les résultats d'une analyse comparative du cycle de vie d'un épaulement géotextile et d'un soutènement conventionnel. La comparaison est faite sur un mètre courant d'un épaulement de trois mètres de hauteur. Les deux alternatives ont les mêmes propriétés techniques et la même durée de vie de 100 ans. Les systèmes contiennent la provision des matériaux, la fabrication des géotextiles et du béton, la construction, l'utilisation et l'évacuation de l'épaulement. L'analyse de cycle de vie démontre qu'un mètre courant d'un épaulement géotextile cause moins d'impacts environnementaux qu'un mètre courant d'un épaulement de béton. 300 mètres d'un épaulement de béton entraînent 400 t CO₂-eq, celui de géotextile 70 t CO₂-eq des émissions des gaz à effet de serre. L'utilisation de camions avec des émissions réduites ne change pas les résultats. Une simulation « monte carlo » confirme la stabilité des résultats. La provision des matériaux et l'électricité utilisé dans la fabrication de la couche de filtre géotextile sont des facteurs primordiaux (plus de 70 %) en ce qui concerne les impacts environnementaux du géogrille utilisé dans l'épaulement géotextile.

KEYWORDS: geogrid-reinforced walls, facing, seismicity, slope instability, steep slopes
MOTS-CLÉS: épaulement, géotextile, géogrillé, béton, analyse de cycle de vie, ACV

1. INTRODUCTION

In the Rhodope Mountains in the south of Bulgaria the route of the important Road III-868 from Devin to Mihalkovo being part of the National Road Network had to be completely changed due to the erection of a new dam on the River Vacha. The old road along the river had to be moved from the river valley to the hills by up to some hundred meters. The new route has a length of 11 km (Figure 1). Figure 2 provides an overview of the mountainous terrain, of the position of the old road in the valley and of the new road uphill. The mountainous terrain is characterized by sophisticated topography (very steep irregular slopes, Figure 2), varying geological and hydro logical conditions, instability tendencies in some places and non-availability of easy access for construction. Additionally, the region has a significant seismic activity.

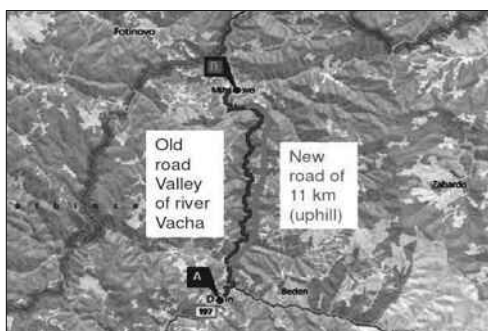


Figure 1. Old route of Road III-868 in the valley and new one uphill through the mountains.



Figure 2. Overview of the mountainous terrain and exemplary positions of the old and new road.

The solution had to meet a wide range of criteria and goals: low costs, quick and easy construction, soil-mass balance (say minimum export / import of soil, say maximum re-use of excavated local soils), minimal environmental impact, as light as possible additional construction materials to ensure easy transportation and low energy consumption ("carbon finger print"), minimum use of heavy equipment, narrow base for retaining walls for an easy into-slope-adaptation, seismic resistance, and last but not least a tight time schedule of less than three years for the 11 km of new road incl. of a tunnel.

The final optimized solution meeting the criteria mentioned above in a balanced way included twenty walls from geogrid-reinforced soil (GRS) with a total length of 2 km, heights of up to 20+ m and a face inclination of 10v:1h (say nearly vertical) without any berms, what is quite unique (see below).

The GRS-walls were chosen (besides other advantages, e.g. more than 30% costs savings versus “common” concrete solutions) due to their excellent adaptation to the environment and their high ductility resulting in high robustness against seismic impact and slope movements. Flexible geogrids were used as reinforcement.

A special type of thin stone-filled wall facing was adapted to fit the landscape, to use local rocky material and to speed up construction. The facing is very flexible and thus of higher resistance against earthquakes and possible slope movements.

2. GENERAL CONCEPTS AND PHILOSOPHY

The project was developed by the General Consultant “Energoprojekt - Hydropower” (Sweco Group) Bulgaria and by the Road Designer “Burda Engineering” Bulgaria with consultancy from the company of the authors. Some specific points have to be mentioned:

A. Because of the very steep natural slopes (sometimes steeper than 1v:1h) the optimal positioning and foundation of all walls asked for almost vertical front inclinations of 10v:1h to achieve a better adaptation to the slope geometry. The base width of the cross-sections had to be minimized thus minimizing excavation (Figure 3c) and expansion down the slope as well (Figure 3a).

B. To optimize the soil mass balance but also based on common practice and conservatism three types of cross-sections were foreseen: without berms (typically up to 6-8 m), with one berm (typically up to 14 m) and with two berms (up to 22 m) (Figure 3).

C. The final stability analyses and design of the GRS-walls were to be completed after beginning of construction (due to site logistics few of the structures could be started at the same time, in reality a progressive construction was carried out along sections of the route). The specifications put to tender were founded on the basic concept and on the typical cross-sections in Figure 3 a, b, c (these were

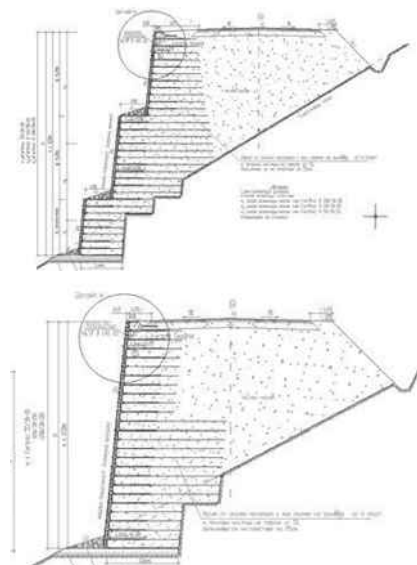


Figure 3. Basic concepts for typical cross-sections: front (facing) inclination always 10v:1h, but different number of berms; from top to bottom: a, b, c.

indicative only, being based on preliminary stability analyses); it was assumed that these will be not the final solutions. The reason for this philosophy was the uncertainty in the real geotechnical and topographical conditions along the 11 km of road, because due to the extremely difficult access the survey and site investigation had been relatively modest.

D. The facing was an important issue. After checking different options the so called “Muralex® Stone” facing system was chosen. Its

concept is based on the idea of a “hanging facade” added and connected in a later construction stage to the “real” bearing geogrid structure (Figure 4).

The system leads to important advantages:

- the geogrids are hidden and protected against UV, impact, fire and vandalism;
- possible wall deformations during construction occur before facing installation - the facing starts its design life deformation-free;
- ductile behavior of the facing under seismic impact and generally under wall deformations of any type in the post-construction stage, because it is quite flexible, say there is no rigid connection to the “real” GRS (Figure 4);
- no special facing foundation is needed;
- a wide range of rocky material available from the excavations on site can be used etc.

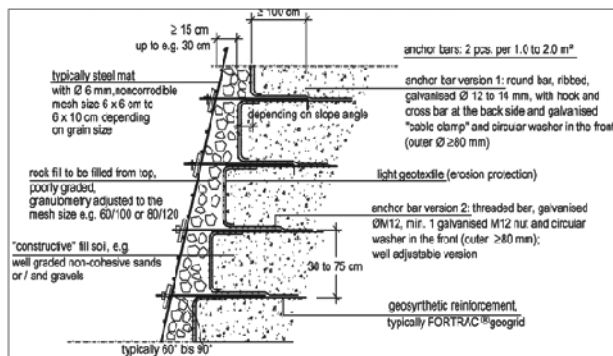


Figure 4. A typical version of the facing system Muralex®.

3. GEOLOGICAL AND HYDROLOGICAL CONDITIONS

The geology along the new route varies significantly (Figure 5). The GRS-walls and their foundations can contact at the back resp. be embedded in (Figure 3) any local soil from silty or sandy clays with stone inclusions (slope talus) to more or less monolithic rock. This enormous inhomogeneity resulted in a low level of predictability not only regarding the local slope soils, but also regarding the parameters of the fill soil; the latter consists (although after pre-selection) from excavated local materials from different cuts along the new route.

The geotechnical survey before beginning of construction was not very detailed. It was decided together with the General Investor “National Electricity Company”, Bulgaria, the General Contractor “Alpine Bau”, Austria, the Consultants (see above) and the Bulgarian Subcontractors for the road construction to assume in all final stability analyses relatively conservative average local soils and fill parameters. Many of the walls cross small valleys; in such cases standard culverts were planned being integrated into the GRS-walls. No water veins were known before beginning of execution. Nevertheless for all walls drainage blankets were implemented at the wall base.

4. SOME STABILITY ANALYSIS ISSUES

For all stability analyses the well known method of circles according to Bishop was used together with additional analyses of polygonal failure planes using the so called Sliding Blocks Method. All analyses were performed in the Engineering Department of the company of the authors. The concept of global factor of safety (FOS) acc. to the German Codes (e.g. DIN 4084) was applied throughout the project from the same beginning (preliminary designs in 2004) until the last adaptations and changes under running execution in 2009, although in the meantime the Codes had changed to partial factors of safety.

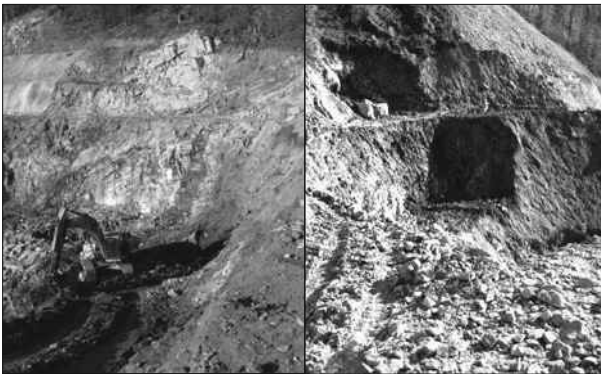


Figure 5. Examples of the enormous inhomogeneity of the local soils and rocks.

“Internal”, “external” and “compound” stability modes were separately checked to keep conformity with the preliminary designs in 2004, although this differentiation is questionable; for more details see Alexiew (2004 & 2005).

Note that in the meantime in the new issue of the German recommendations EBGeo (2010) the distinction internal-external-compound was eliminated, as well as e.g. the formal distinction between “slopes” and “walls”.

Geogrids from the “FORTRAC® T”-family were chosen as reinforcement due to their high specific short- and long-term strength, low short- and long-term strain, low creep, high coefficient of bond to a wide range of soils and flexibility resulting into an easy installation. The range of geogrids for this project was from FORTRAC® T 55 to FORTRAC® T 200.

The required factors of safety (FOS) were chosen according to the Bulgarian Standards with $FOS > 1.3$ for normal (static) conditions. In Figure 6 a typical Bishop circle analysis is shown (for the internal stability only, say the failure surface crosses exclusively the reinforced zone).

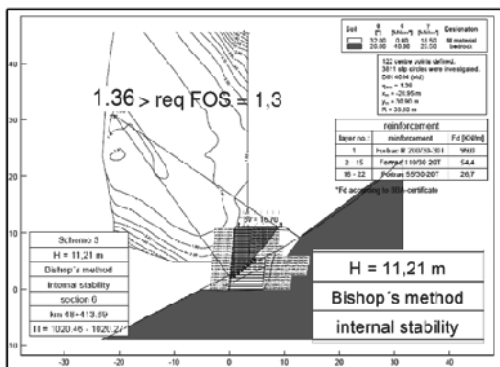


Figure 6. Typical example of stability analysis according to Bishop (only “internal” shown).

A specific issue was the seismic analysis; the region is of significant seismic activity with a magnitude of VII acc. to Richter.

The Bulgarian concepts for seismic design from 1980 being still valid with small modifications during the period of analysis were adopted throughout the project (CDBSSR 1987, CDRW 1986, SGDSR 1987).

Figure 7 shows an overview of the seismic activity in Bulgaria together with the position of the Devin-Mihalkovo project and the zone with VII acc. to Richter with a coefficient of horizontal acceleration $k_h = 0.15$. A vertical acceleration is not being taken into account.

For the acting seismic forces F_{seismic} the Equation 1 can be used (CDBSSR 1987, CDRW 1986, SGDSR 1987):



Figure 7. Seismic activities in Bulgaria, the project position is marked.

$$F_{\text{seismic}} = 1.30 \cdot R_{\text{response}} \cdot k_h \cdot (\text{permanent loads} + 0.50 \cdot \text{traffic loads}) \quad (1)$$

where R_{response} = coefficient of response of the structure to seismic impact; k_h = coefficient of horizontal acceleration; 1.30 and 0.50 = partial safety factors on the side of action for seismic design cases.

R_{response} has higher values e.g. up to 0.40 for rigid (brittle, e.g. masonry, concrete) structures and lower values e.g. 0.25 for ductile structures like earth dams and embankments. It seems logic and conclusive that earth systems reinforced by flexible geogrids should be at least so ductile and able to dissipate seismic energy remaining intact as non-reinforced earth dams.

This concept and the corresponding calculation results seem to be coherent with the experience, conclusions and recommendations in e.g. Tatsuoka et al (1998) and other publications confirming the very advantageous behavior of GRS-walls under seismic impact.

Note that for seismic analyses the Bulgarian codes (CDBSSR 1987, CDRW 1986, SGDSR 1987) ask for a $FOS > 1.1$, for more details and previous “seismic” projects see e.g. Jossifowa & Alexiew (2002).

One specific issue more in the Bulgarian codes is the reduction of the angle of internal friction acc. to Equations 2 & 3 depending on the intensity of earthquake:

$$\Phi_{\text{characteristic, seismic}} = \Phi_{\text{characteristic, static}} - \Delta\Phi \quad (2)$$

where

$$\Delta\Phi = \Delta\Phi (\text{magnitude acc. to Richter}) \quad (3)$$

For the project under discussion with a magnitude of VII acc. to Richter $\Delta\Phi = 3.5^\circ$.

Because the software used (GGU Stability by Civil Serve) does not include a calculation conform to Equation 1 and considers only directly k_h , the latter had to be modified “by hand” before the input.

5. EXECUTION, PROBLEMS, SOLUTIONS, EXPERIENCE

Execution started in summer 2007. First problems arose soon: the topography deviated sometimes significantly from the expected one, the real terrain was sometimes higher or lower than it should be, the real slope inclination often steeper. Step by step many of the cross-sections had to be re-designed. At the end of the day all GRS-walls, even the highest with over 20 m height, became “bermless”, what is quite unique.

The “bermless” solution offers significant advantages: the base width of the cross-sections becomes minimal (Figure 3). This helped to avoid deep cuts into the hillside and/or an expansion of the trapezoid beyond the steep slope line (to the left in Figure 3). Additionally, in some cases the geology deviated significantly from the assumptions; this resulted in re-design as well.

Often surprising water veins in the natural slopes had to be drained promptly. For this purpose thick wicks from rolled non-woven geotextiles were installed ending on the front side of wall as a quick ad hoc solution.

In Figure 8 typical construction stages and details are depicted. Figure 9 shows one of the completed walls just before handing the route over for operation.



Figure 8. Left: construction stages (formwork, geogrids, anchor bars, facing), right: top view of the stone-filled facing used.



Figure 9. Top view of a completed GRS-wall.

6. FINAL REMARKS

The new Road III-868 from Devin to Mihalkovo in the Rhodope Mountains in southern Bulgaria was a challenge in terms of optimal concept, design, execution, re-design during execution, time schedule and costs. It crosses a terrain with sophisticated topography and geology in a seismic region. Its length amounts to 11 km comprising one tunnel and twenty geogrid-reinforced almost vertical soil walls of totally 2 km length and up to 20+ m height.

A specific type of facing was adopted to fulfil a wide range of requirements.

Almost all GRS-walls had to be re-designed and adopted under running route execution, resulting throughout in non-common high bermless solutions.

Nevertheless, it was possible to meet all project goals regarding time schedule and costs (among others; see the description of criteria, goals and optimized solution in Chapter 1). The success is based on the one hand on the advantages and flexibility of geosynthetic solutions in geotechnical engineering in terms of easy and quick construction process and adaptation and on the other hand on the excellent co-operation of all participants: Investor, Owner, Consultants, Contractors and Geosynthetic Company.

The road is since summer 2010 under traffic, the GRS-walls demonstrate until now an excellent behavior both in terms of stability and low deformability.

This transportation project is may be the most distinctive in the Balkan region during the last years.

7. ACKNOWLEDGEMENTS

The authors would like to express their gratitude to all colleagues with the Investor, Consultants and Contractors for the excellent and competent collaboration during all project stages and even (and particularly) in some difficult phases.

8. REFERENCES

- Alexiew, D. (2004): Geosynthetic Reinforced Slopes: Basics of Design and some Projects. *Proc. of the Indian Conference Geosynthetics – New Horizons*, New Delhi, India: 73 – 85.
- Alexiew, D. (2005). Zur Berechnung und Ausführung geokunststoffbewehrter "Böschungen" und "Wände": aktuelle Kommentare und Projektbeispiele. *Proc. 5. Österreichische Geotechniktagung*, ÖIAV, Wien, Austria: 87 – 105.
- CDBSSR Code for the design of buildings and structures in seismic regions (1987). *KTSU & BAN*, Sofia, Bulgaria. (in Bulgarian)
- CDRW Code for the design of retaining walls (1986). *MBI Ministry for building industry*, Bulletin BSA, Vol. XXX/10, Sofia, Bulgaria. (in Bulgarian).
- DIN 1054. Baugrund - Sicherheitsnachweise im Erd- und Grundbau (Ground - Verification of the safety of earthworks and foundations), *Deutsches Institut für Normung*, Berlin, Deutschland.
- DIN 4084. Baugrund - Geländebruchberechnungen (Soil - Calculation of embankment failure and overall stability of retaining structures), *Deutsches Institut für Normung*, Berlin, Deutschland.
- EBGEO 2010 Recommendations for Design and Analysis of Earth Structures using Geosynthetic Reinforcement, *DGGT / Ernst & Sohn*, Essen/Berlin, Deutschland.
- Jossifowa, S. and Alexiew, D. (2002). Geogitterbewehrte Stützbauwerke an Autobahnen und Nationalstrassen in Bulgarien, *Proc. 12. Donau-Europäische Konferenz „Geotechnisches Ingenieurwesen“*, DGGT, Passau, Deutschland: 389-396.
- SGDSR Specialties in the geotechnical design in seismic regions (1987). *MBI Ministry for building industry*, Bulletin BSA, Vol. XXXII/11, Sofia, Bulgaria. (in Bulgarian).
- Tatsuoka, F., Koseki, J., Tateyama, M., Munaf, Y. and Horii, N. (1998): Seismic stability against high seismic loads of geosynthetic-reinforced soil retaining structures. Keynote Lecture. *Proc. 6th International Conference on Geosynthetics*, Atlanta, USA, 1: 103 - 142.

La fouille de la tour Odéon à Monaco : les quatre éléments remarquables de sa conception

The Deep Excavation of the Odéon Tower in Monaco: The four outstanding elements in its design

Baghery S.

Tractebel Engineering (France)/Coyne et Bellier, Gennevilliers (92), France

RÉSUMÉ : La construction de la tour Odéon à Monaco nécessite la réalisation d'une fouille profonde au sein d'un versant très pentu, dans des terrains de caractéristiques médiocres. Le soutènement en a été rendu possible par quatre options remarquables prises par le concepteur, à savoir (1) une construction « top-down » à l'aide d'appuis pré-fondés, (2) la constitution d'une voûte élastique dans le sol côté montagne, ceci par modulation de l'effort de pré-charge par tirants d'ancrage, (3) le fretage du sol au pied des parois à l'aide de clous verticaux en fibre de verre et (4) la prise en compte des effets du déchargement du sol sur les appuis pré-fondés.

ABSTRACT: The construction of the 180-meters-tall Odéon skyscraper building in Monaco calls for a 72-meters-deep excavation to be dug in a steep hillside. The design of the retaining system for this excavation was made possible by Tractebel Engineering (France)/Coyne et Bellier making four unique design choices, namely (1) a "top-down" construction method, (2) the mobilization of an elastic arch in the foundation soil on the upstream side of the works, (3) reinforcing by fibre glass nails the soil below the deepest elements of the foundation, and (4) taking into account the effects, on the supports, of the sequence of construction.

KEYWORDS: Retaining walls, top-and-down construction, vault effect, soil reinforcement, heaving

MOTS-CLÉS: Soutènement, Construction en taupe, Top-Down, Effet de voûte, renforcement de sol, gonflement de sol.

1 INTRODUCTION

Avec une hauteur totale de 180 mètres, la tour Odéon, actuellement construite à Monaco sous la maîtrise d'ouvrage de la SCI-Odéon, restera pour un certain temps la plus haute tour de la Principauté. Alexandre Giraldi en est l'architecte. Elle est construite par l'entreprise Vinci, avec la contribution de Soletanche-Bachy pour les travaux de la fouille.

La réalisation de cet ouvrage nécessite l'excavation d'une fouille atteignant 72 mètres dans la partie la plus profonde (Figure 1). Alors que de nombreuses constructions sensibles situées au voisinage doivent être maintenues intactes, les travaux d'excavation exigent la conception de solutions originales, à la hauteur de ce projet audacieux.

tour, en tant qu'éléments de contreventement et raidisseurs parasismiques. Tractebel Engineering (France)/Coyne et Bellier a assuré la conception de ces deux parties du projet.

Lorsque les profondeurs d'une excavation dépassent les valeurs critiques eu égard aux caractéristiques du sol, le concepteur est confronté à un déficit intrinsèque de butée dans le sol. Il doit alors adopter des mesures innovantes. C'est grâce à de telles mesures que la réalisation d'une fouille avec une profondeur rarement atteinte dans des terrains de telles caractéristiques a été possible. Des études et investigations très poussées ont été nécessaires en amont des phases de contractualisation. Elles ont notamment comporté des modélisations tridimensionnelles des travaux, du massif et des constructions environnantes.

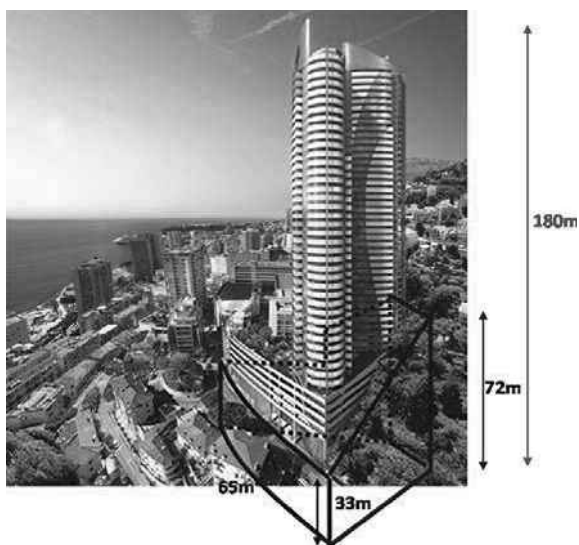


Figure 1: Le site, la tour et sa fouille

La conception du soutènement a été étroitement associée à la méthode et au phasage de construction de la tour, à la géométrie de la fouille et à la topographie du site. Les ouvrages de soutènement remplissent eux-mêmes un rôle structurel pour la

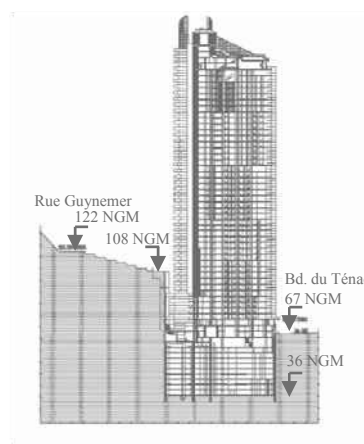


Figure 2: Versant en terrasse, le dénivelé, nivellement

2 LE SITE

Il s'agit d'un site très exigu, sur un versant en terrasses. Le dénivelé du terrain naturel entre l'amont et l'aval de la tour est de l'ordre de 40 mètres (Figure 2).

Les profils géotechniques indiquent une couche supérieure de remblai et d'éboulis sur une épaisseur qui atteint 25 mètres en amont, tandis qu'en aval, cette épaisseur varie fortement du fait des constructions récentes. Sous cette couche superficielle, on rencontre une couche marno-calcaire avec des poches plus

ou moins altérées vers les profondeurs 35-50 NGM. La couche marno-calcaire repose sur un substratum calcaire profond. Le toit du calcaire dessine une surface chaotique et variable. Il se situe en général sous la cote 30 NGM (Figure 3).

Le pendage général de la couche marno-calcaire (non représenté ci-dessous) est dirigé de l'amont vers l'aval. Il est donc favorable, lors de l'ouverture de la fouille, à la stabilité au glissement du massif soutenu côté montagne.

Une grande partie des niveaux piézométriques varie entre 10 et 20 mètres sous le niveau du terrain naturel, avec des fluctuations importantes qui atteignent fréquemment 4 à 5 mètres. Il s'agit d'une nappe superficielle qui coule à la surface de la couche marno-calcaire. A cause de sa faible perméabilité, cette dernière sépare la nappe superficielle d'une nappe plus profonde qui baigne dans le calcaire avec un niveau piézométrique situé environ 40 mètres plus bas que celui de la nappe superficielle.

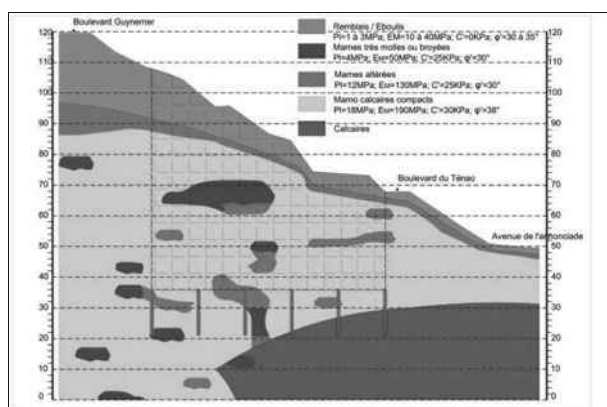


Figure 3: Coupe géologique, caractéristiques géotechniques

La bordure de la fouille est occupée par des bâtiments publics ou privés à des distances plus ou moins proches de la fouille. Compte tenu de la profondeur des excavations, un certain nombre d'entre eux se situe dans les zones d'influence des déplacements engendrés par les travaux d'excavation. Ce voisinage impose des contraintes d'exécution, notamment en termes du respect de déplacements admissibles.

3 OUVRAGES DE SOUTÈNEMENT: LES QUATRE ÉLÉMENTS REMARQUABLES

Les dix niveaux d'infrastructure comportent des planchers « butonnants » confinés entre les parois de la fouille. Ces planchers n'ont pas de joints et peuvent donc transmettre entre parois opposées les efforts de poussée ou de butée. La superstructure se développe au-dessus du boulevard du Ténao sur environ cinquante niveaux supplémentaires.

Si la stabilisation des parois de soutènement sous le boulevard du Ténao peut être assurée au moyen d'un système de planchers butonnants, ce n'est pas le cas pour les parois situées au-dessus de ce boulevard, à cause de l'absence de terrain offrant butée en vis-à-vis. C'est pourquoi les parois poussant au vide ont été stabilisées à l'aide de tirants d'ancrage.

Par ailleurs, l'exiguïté et les contraintes d'accès au site ont donné lieu à une solution de soutènement étagé des parois. En effet, la configuration des lieux avant les premiers travaux n'était pas défavorable à l'utilisation d'engins lourds. Ainsi, la réalisation des premiers écrans de soutènement à l'aide d'engins de taille réduite permet la réalisation de plateformes pouvant recevoir des engins plus encombrants. C'est pourquoi les premiers écrans de soutènement sont de type « mini-berlinoise », passant ensuite à des écrans de type berlinoise, avant de voir apparaître des écrans en paroi-moulée.

3.1 Une construction "Top-Down"

Deux objectifs principaux nous ont conduit à adopter cette méthode de construction : a) Avantages offerts par des planchers butonnants (Figure 4) comme solution plus sûre d'équilibre des poussées en profondeur et dispositifs plus rigide pour limiter les déplacements des parois, et, b) Gain de temps dans la réalisation de la tour. En ce qui concerne ce dernier point, il a été considéré que dans le délai nécessaire à l'extraction des quelques 65 000 m³ de terre des niveaux de sous-sol et à la réalisation en « taupe » des 10 niveaux de plancher correspondants, on pourrait construire simultanément les 50 niveaux de superstructure. Pour atteindre cet objectif, il a fallu réaliser des appuis profondés de la tour avant le démarrage de sa construction. Il s'agit des barrettes de fondation d'épaisseur 1m, forées aux environs de la cote 70 NGM, après les travaux d'excavation et de soutènement de la partie tirantée des parois. Il est à noter que la contrainte de compression moyenne développée dans ces barrettes par la tour en phase d'exploitation s'approchera de la valeur de 10 MPa. Ce niveau de sollicitation aurait pu rendre la solution non-faisable sans l'évolution des textes réglementaires, évolution apparue avec la mise en vigueur de la norme NF94-282 en février 2010, au moment de l'élaboration de la conception.

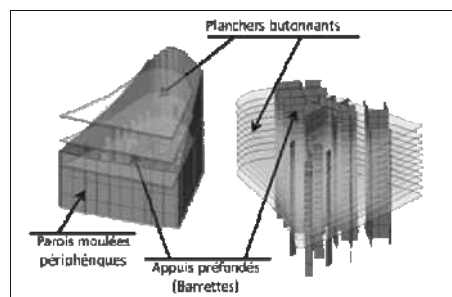


Figure 4 : Parois périphériques, barrettes et planchers butonnants

Au fur et à mesure de la construction des structures, les barrettes profondées reçoivent des charges gravitaires alors que les planchers de sous-sol, portés par les barrettes assurent le rôle simultané de diaphragmes dans la transmission des efforts horizontaux.

3.2 Une voûte en sol

La topographie et la géométrie de l'excavation ont été mises au service de la conception du soutènement de la paroi la plus profonde de la fouille, dans la zone où les poussées sont les plus importantes du fait de la profondeur et de la pente du versant. Mais la portée de la paroi dans cette même zone est plus courte, ce qui nous a encouragé à en profiter pour inscrire dans le terrain le funiculaire des poussées, évitant notamment de solliciter la paroi profonde et limitant ainsi les déplacements. On aurait pu penser, a priori, que ce funiculaire existait en soi par le fait de la géométrie ("effet de voûte"). Mais cette affirmation ne tient pas compte du trop grand déviateur des contraintes (tangentielle et radiale), qui amène le sol de la "voûte" à se déformer à l'état plastique. Pour profiter de l'effet bénéfique de la voûte il a fallu ramener le sol qui la constitue à l'état élastique.

Si la limite élastique dans le sol à l'arrière de la paroi n'est pas dépassée à l'état initial, ce n'est pas forcément le cas avec l'excavation des sols devant la paroi, qui augmente progressivement la contrainte tangentielle dans le sol arrière. Dans le cas où la contrainte radiale reste trop faible, le déviateur s'agrandit et "pousse" le sol dans la plasticité qui engendre à son tour des déplacements importants (Figure 5).

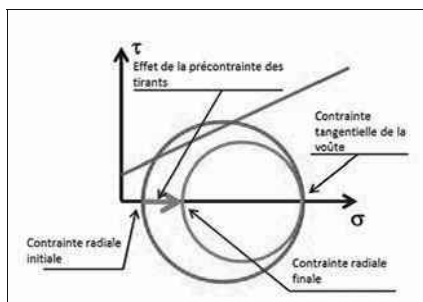


Figure 5 : État de contraintes de la voûte en sol

La solution réside donc dans l'augmentation de la précontrainte radiale à l'aide des tirants d'ancrage qui sont disposés dans la même direction en amont de la fouille.

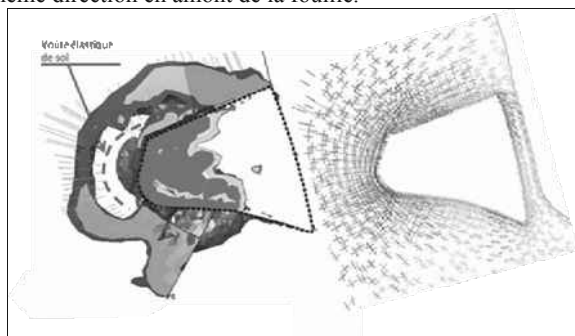


Figure 6: Voûte élastique dans le sol amont (gauche), cheminement des contraintes de la voûte vers les côtés latéraux de la fouille (droite)

La figure 6 (à gauche) montre une voûte en sol créée à l'arrière de la paroi amont, voûte qui redirige les poussées vers les côtés latéraux de la fouille (à droite), soulageant ainsi la paroi la plus profonde exposée à soutenir les charges les plus importantes.



Figure 7: Etat d'avancement du chantier à ≈40% des excavations

En revanche, on peut y remarquer les zones plastiques formées dans la zone des bulbes d'ancrage et à l'arrière des parois plus ou moins rectilignes. Elle illustre également le cheminement des contraintes dans le sol et l'efficacité de la voûte élastique inscrite dans le sol. La figure 7 montre l'état d'avancement du chantier (à environ 40%) de soutènement et des excavations.

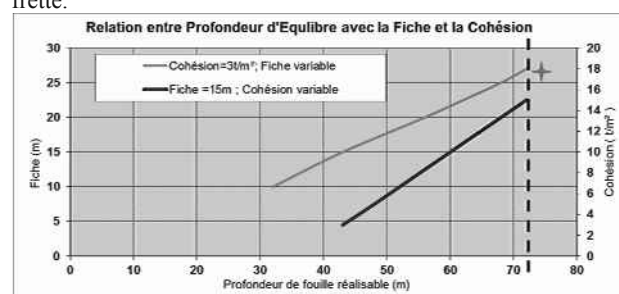
3.3 Fretage du sol

Lorsqu'une fouille dépasse 40 ou 50 mètres de profondeur dans des sols de cohésion faible à moyenne, deux solutions se présentent. La première consiste à mobiliser une masse très importante de sol en butée, ce qui nécessite une fiche de paroi très rigide et surtout très profonde. La seconde fait appel à une amélioration de la cohésion apparente du sol (Figure 8). Nous avons opté pour cette deuxième solution en frettant le sol au

pied des parois de grande profondeur à l'aide de clous verticaux en fibre de verre.

Notons que les barrettes de fondation réalisées par anticipation (appuis préfondés) contribuent, pour leur part, au frettage du sol. Néanmoins, il faudra tenir compte des sollicitations qu'elles encaissent par ailleurs. On vérifiera donc que l'accumulation des contraintes suivant les différents modes de fonctionnement (fondation, frette, inclusion soumise aux effets dus à l'expansion du sol –voir §3.4-) ne dépasse pas la résistance admissible de ces éléments.

L'évaluation de la cohésion apparente apportée par des frettes se fait en comparant la résistance (au glissement par exemple) du sol non-fretté, mais augmenté en cohésion, avec sa configuration frettée muni de la cohésion d'origine. Une analyse itérative des deux schémas aboutira à la valeur de la cohésion apparente qu'il faudra attribuer au sol d'origine pour être équivalent, en termes du critère de résistance choisie, avec le sol fretté.



✦ Dans ce terrain, l'équilibre des poussées exige, soit 28 mètres de fiche rigide avec la cohésion de base (3 t/m²), soit une cohésion améliorée de 18 t/m² avec 15 mètres de fiche.

Figure 8: Profondeur d'équilibre poussées-butées en fonction de la profondeur de la fiche ou de la valeur de la cohésion

3.4 Effets du déchargement du sol sur les préfondés

Comme il a été rappelé plus haut (§3.1), des barrettes de fondation ont été conçues pour être réalisées à un stade où il reste encore à excaver 35 mètres de terrain. Comme fondations, elles supportent les charges de la tour au fur et à mesure de sa construction. De ce fait, elles sont soumises à des contraintes de cisaillement puisqu'elles s'enfoncent dans le sol encaissant. Dans ce schéma, la contrainte de cisaillement développée le long du fût d'une barrette est dans la même direction que le mouvement du sol par rapport au fût, du bas vers le haut. Autrement dit, l'action du sol sur le fût est une contrainte tangentielle (frottement) dans le sens ascendant. Nous lui attribuons le signe « + ». Ces contraintes de cisaillement varient d'une valeur minimale à la base du fût vers une valeur maximale à sa tête (figure 9-a). Si la limite de plasticité devait être atteinte, elle le serait d'abord dans la partie supérieure où la courbe des valeurs serait plafonnée à la valeur plastique.

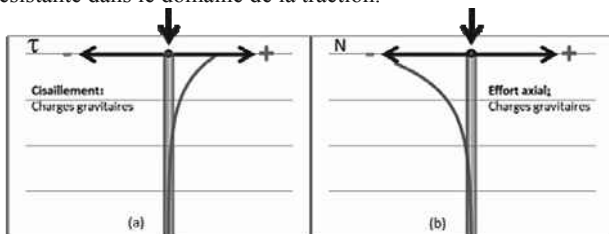
Par ailleurs, sous l'action des charges gravitaires, la valeur de l'effort de compression dans le fût diminue en profondeur, puisqu'une partie de cet effort est absorbée par le sol avec la mobilisation du cisaillement autour du fût (figure 9-b).

Avec l'excavation en présence des appuis préfondés, le sol encaissant autour de ces appuis (barrettes) se décharge et subit de ce fait une extension (gonflement), à l'opposé du phénomène de tassement, développant ainsi autour du fût des barrettes une deuxième catégorie de contraintes de cisaillement. Dans ce type de schéma (gonflement ou tassement du sol encaissant), et dans l'hypothèse d'un sol homogène doté d'un comportement linéaire, le bilan du cisaillement développé autour du fût est nul si l'effet sur le terme de pointe est négligé. La courbe de cisaillement à l'interface sol-fût, sous l'effet du gonflement du sol, possède un point d'inflexion (figure 10-a). Les contraintes de cisaillement changent de signe de part et d'autre de ce point. Dans le cas de gonflement du sol, les contraintes de cisaillement

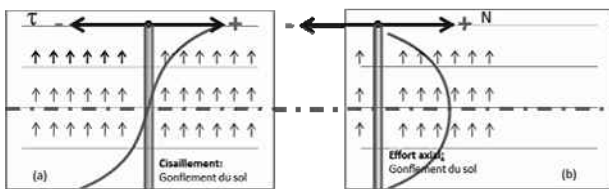
sur la partie située au-dessus du point d'inflexion sont du même signe que les cisaillements provoqués par les charges gravitaires. Dans cette partie, les cisaillements dus à ces deux phénomènes se cumulent (figure 11-a). Nous sommes donc, en cas de gonflement du sol encaissant, face à des contraintes majorées de cisaillement dans la partie supérieure du fût. Sur la partie située sous le point d'inflexion, le signe de la contrainte de cisaillement à l'interface sol-fût provoquée par le gonflement du sol est à l'opposé du signe des cisaillements dus aux charges gravitaires. Sur cette partie, les deux catégories de cisaillements se retranchent et les contraintes de cisaillement résultantes sont minorées.

L'effort axial dû au seul phénomène de gonflement du sol est une traction (figure 10-b) et sa courbe de variation le long du fût est une courbe pseudo-parabolique. Sa valeur maximale se situe au droit du point d'inflexion de la courbe de cisaillement provoqué par le gonflement. En l'absence d'effet sur le terme de pointe, c'est une force interne et elle se retranche de l'effort de compression engendré par les charges gravitaires (figure 11-b). C'est précisément cette valeur résultante qu'il convient de contrôler à chaque phase en mettant en parallèle la vitesse de la construction des structures (« Top » - compression des barrettes) avec la vitesse des excavations (« Down » - traction des barrettes). Le risque est bien l'apparition d'une traction excessive à une phase donnée des travaux, traction qui serait incompatible avec la résistance admissible de la section des barrettes. Ce risque est d'autant plus grand que l'effort de compression axial dû aux charges gravitaires n'est pas grand, le module du sol au déchargement est faible, la raideur axiale des appuis profonds est forte et la raideur au cisaillement du sol est élevée.

On peut conclure, ici, que le gonflement du sol réduit l'effort de compression dû aux charges gravitaires dans le fût. Sous certaines conditions il peut même l'annuler et pousser la section résistante dans le domaine de la traction.

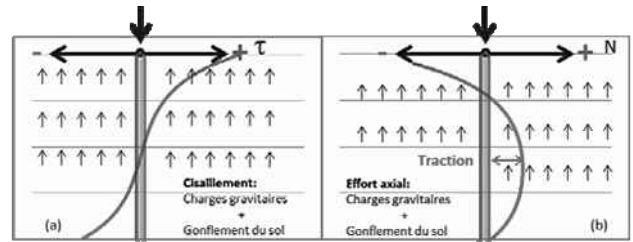


Figures 9(a,b): Cisaillement et effort axial dans les appuis profonds dus aux charges gravitaires (sans terme de pointe)

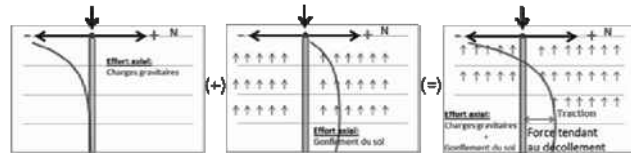


Figures 10(a,b): Cisaillement et effort axial dans appuis profonds dus au gonflement du sol encaissant (sans terme de pointe)

Il est à noter qu'en présence d'un terme de pointe à la base des appuis profonds, les contraintes de cisaillement et les efforts axiaux dus aux charges gravitaires ne se cumulent pas toujours linéairement. En effet, lorsqu'il devient prépondérant, le phénomène de gonflement peut totalement annuler le terme de pointe (effort de compression) dû aux charges gravitaires et créer ainsi une tendance au décollement de la pointe (figure 12). Dans ce cas, une analyse non-linéaire à chacune des phases de chargement où ce phénomène apparaît devient nécessaire.



Figures 11(a,b): Cisaillement et effort axial dans appuis profonds dus aux charges gravitaires + gonflement du sol encaissant (sans terme de pointe)



Figures 12: Cisaillement et effort axial dans appuis profonds dus aux charges gravitaires + gonflement du sol encaissant (avec terme de pointe) – Risque de décollement en pointe

Ce type d'analyse a été conduit sur l'ensemble des profonds (barrettes) de la tour Odéon. L'appréciation de l'amplitude du gonflement du sol dû aux excavations (déchargement) est un préalable à ce type d'analyse. Cela a été possible grâce aux études tridimensionnelles tenant compte du comportement non-linéaire du sol, englobant une large partie du massif et simulant les différentes phases de la construction. Toutes ces études complexes ont été conduites au stade de la conception, avant la contractualisation du marché d'entreprise.

4 CONCLUSIONS

La construction de la tour Odéon nécessite la réalisation d'une fouille de 72 mètres de profondeur au sein d'un versant très pentu, dans des terrains de caractéristiques médiocres et sur un site urbain majeur. Les travaux et leurs séquences de réalisation devaient être conçus de telle sorte que les mouvements de nombreuses constructions sensibles situées en bordure immédiate de la fouille restent dans des limites restreintes. Quatre éléments remarquables et innovants de la conception ont été développés dans cet article :

- a) : une construction « top-down » à l'aide d'appuis pré-fondés,
- b) : la constitution d'une voûte élastique dans le sol côté montage,
- c) : le fretage du sol en pied des parois les plus hautes,
- d) : la prise en compte des effets du déchargement du sol sur les appuis pré-fondés.

Le premier élément (a) permet de réduire d'un an le délai global de la construction, qui est de quatre ans. Le deuxième élément (b) transforme le sol en une structure en voûte pour réorienter les poussées qu'il génère. Les deux derniers éléments (c et d) rendent possible le choix technique indiqué en (a).

5 REFERENCES

- Baghery S., Bouvard A., Miszlai I. (2012). Conception et dimensionnement des ouvrages de soutènement de la fouille de la Tour Odéon à Monaco. *Journées Nationales de Géotechnique et de Géologie de l'Ingénieur JNGG2012*–Bordeaux 4-6 juillet 2012.
- Gastbled O.J., Baghery S. (2010). 3D modeling of a deep excavation in a sloping site for the assessment of induced ground movements. *7th European Conference on Numerical Methods in Geotechnical Engineering (NUMGE)*, Trondheim, Norvège.

3D Finite Element Analyses for a Laterally Loaded Pile Wall in Marine Environment— Case History

Analyses 3D par éléments finis pour un mur de quai chargés latéralement dans un port – Etude de cas

Bahr M.A., Tarek M.F., El-Ghamrawy M.K., Abouzaid K.S.
Al-Azhar University, Egypt

Shaarawi E.M.
Fayum University, Egypt.

ABSTRACT: This paper presents a 3D finite element study on a model to simulate an horizontal load test on a retaining pile wall. The piles wall was constructed at the site of Port Ghalib marina on the Red-Sea coast of Egypt which is considered as an active seismic area. The subsoil layers consist of 2 m to 3 m gravelly sand followed by a deep clayey silt layer. The ground water was observed at a depth of about 1.10 m below ground surface. The purpose of the test is to evaluate the pile displacement characteristics under exposed loads. Numerically a 10 m – length pile was modelled to simulate the actual case. Effect of surcharge, earth pressure and earthquake loads were taken into consideration. The numerical analysis was performed and the results have been found to be in good agreement with the measured field test results. In addition the finite element method make an ability to predict the deflection along the pile length.

RÉSUMÉ : Cet article présente un modèle 3D éléments de dimension par élément finie pour' simuler un chargement horizontal d'un mur de quai du port de plaisance de Port Ghalib sur les côtes égyptienne de la mer Rouge qui est une zone sismique. La stratigraphie est constitué d'une couche de 2 à 3 m de sable graveleux, en surface, suivie d'une couche de limon argileux, en profondeur. La nappe phréatique est située à 1,1 m de la surface. L'objectif de l'analyse est de caractériser le déplacement latéral du mur en fonction du chargement. Le modèle numérique a été construit pour simuler le cas réel. Les effets de la surcharge, pression des terres et effets des seismes, ont été pris en compte dans le modèle. L'analyse numérique et les résultats sont en accord avec les résultats des expérimentaux de terrain. En outre, la méthode des éléments finis donne une prédiction de la déviation le long du mur.

KEYWORDS: 3-D FEE model, analysis, earthquake load, lateral loading, pile wall, Red sea.

MOTS-CLÉS : modèle FEE 3-D, analyse, la charge tremblement de terre, chargement latéral, palplanches, Mer Rouge.

1. SUBSOIL PROFILE CONDITIONS AND PILE GEOMETRY

Soil investigation showed that the soil profile at the site is as follows:

Top layer (yellowish brown, gravel and sand) from ground surface with depth ranging from 2 to 3 m, followed by a layer of grey clayey silt, some fine sand, traces of broken shells, extended to the end of executed boreholes (at depth of about 20 m).

The Standard penetration test (SPT) shows the N values as follows:

- From depth of 2 m to 7 m level N has values between 2 and 13
- From depth of 7 m to 11 m level N = 3
- From depth 11m to the end of boring N has values between 7 and 11

Ground water was observed e at 1.10 m below ground surface. The pile wall consists of contiguous bored piles of 1.0m diameter and 10m length.

2. FINITE ELEMENT MODELLING

The finite element mesh considered in three dimensional nonlinear finite element analysis as discussed in Abouzaid et. Al. (2010) is shown in Figure (1-a). Based on symmetry, only one pile of the model is meshed. 20 nodes brick element Solid 95 were used to simulate both soil, and pile with cap. It should be noted that these quadratic elements exhibit high accuracy even for high aspect ratios and can model accurately bending of solid piles. During mesh design stage, a study was performed to

decide on appropriate (balanced) mesh size. The study showed that a much larger mesh, with more elements (of lower aspect ratios) would account for a fairly small change in results, so the current mesh is sufficient for analysis.

The concrete pile section, with a diameter of 1.0 m and pile cap beam have been meshed by Twenty node brick elements as shown in figure (1a-1b) with the elastic property of concrete. The soil domain has been simulated by strip of 1 m width with symmetry conditions on both sides.. The depth of soil considered below the pile tip 10 times the pile diameter. The domain of soil considered has been found very much suitable for the analysis of the laterally loaded pile as when loaded till failure the soil elements at and near boundary do not experience any deflection. Also the soil elements at and near to the bottom boundary do not experience any deflection. The soil has been modeled as elastoplastic medium following Drucker-Prager (1952) .

Soil domain has vertically been divided to 20 layers, each of thickness 1/20 of the pile embedded length to allow the soil variation with depth. The elastic modulus is taken proportional to strength parameter (c).

The boundary conditions considered are shown in Figure (6-8a), the translations UX have been constrained in outer YZ plans, and only UZ and UY have been permitted whereas UY have been constrained in outer XZ plans, and only UZ, and UX have been permitted, also the translation UZ have been constrained over the area the soil block bottom and the translations UX, and UY have been permitted, this have been done to overcome the singularity of matrices and to help to get convergence. All nodes

of the symmetry plane have been constrained in direction perpendicular to the plane of symmetry.

The interface between the pile and soil have been represented by a couple of 8 node contact element named CONTACT 170 and 8 node target elements named TARGET 174, that was described in the chapter 3. The purpose of this couple is to mimic the installation effects on piles (drilled or driven). It also serves a purpose of a simplified interface which allows for tension cut-off (gaping) and controlled, coupled horizontal and vertical stiffness. The contact between pile and soil was supposed to be rough and were simulated by Drucker–Prager model with a friction angle of value corresponding to each layer.

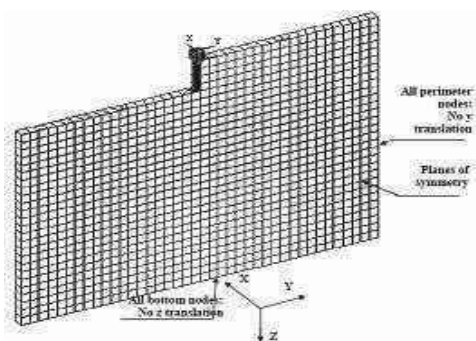


Figure (1-a): 3D Finite Element Model for Contiguous Piles Wall.

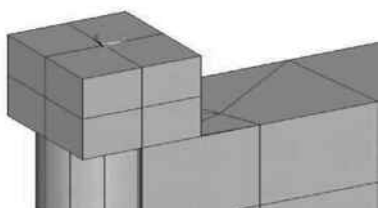


Figure (1-b): Pile Cap Mesh.

3. LOADING CONDITIONS

Loading for this case is presented in Table (1). The pile cap has been proposed to laterally load P at the pile head in the negative direction of y axis, in addition to surcharge load, with excavation at various stages. Ten load cases were performed to simulate the lateral load test loads and study the pile behaviour under different load cases and compare with measured results

Table (1) Applied Load in Each loading Case for Contiguous Piles Wall.

Load case No.	Applied load (P) (kN)
1	Before Applying surcharge load of 20 kN/m
2	Applying surcharge load of 20 kN/m
3	After excavation to -2.5 m from ground level
4	After excavation to -5 m from ground level
5	24 hrs after excavation to -5 m from ground level
6	Applying 21 ton horizontal load
7	After releasing 21 ton horizontal load

8	Just after Applying 300 kN horizontal load
9	24 hrs after Applying 300 kN horizontal load
10	After releasing 300 kN horizontal load

4. RESULTS AND DISCUSSION

4.1 Pile-Soil Deformation

Figures (2-a, b, c, d, and e) show the contour of pile and soil movement in direction Y axis, the deflection along the pile for the load cases no 2, 3, 4, 6, and 8.

In figure (2-a), after applying a vertical surcharge It is interesting to note that the plastic zone propagates deeply with a high densification in top layers till reaches the minimum values at the end of the model and extended below, this means that the settlement under the surcharge induced a lateral movement to the pile towards the settled side (right side), but the pile was rigid enough to retain the other side without movement especially the movements was very low so it does not extend far from the pile. Moreover, the instrumented side (right side) features much larger plastic zone while the plastic zone for the extension side (left side) is confined to the interface layer.

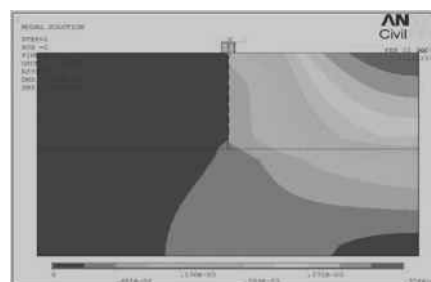


Figure (2-a) Contour of Deflections along the Pile under Surcharge Load .

In figure (2-b), after excavation to -2.5 m from ground level, It is noted that the excavation process resulted in a lateral movement of pile towards the excavation, and a small wedge of soil in front of the pile (left side) exhibits a small movement mobilizing a passive resistance in the front of the pile, but the right side is still affected by the surcharge load settlement which moves the soil very slightly in opposite direction

In figure (2-c), after excavation to -5.0 m from ground level, It is noted that the increase of excavation process resulted in increasing the lateral movement of pile towards the excavation, increasing the wedge of soil in front of the pile (left side) exhibits a bigger movement mobilizing a passive resistance in the front of the pile than the previous case, but the right side is still affected by the surcharge load settlement which moves the soil very slightly in opposite direction but less than the previous case.

In figure (2-d), Applying 21 ton horizontal load, It is noted that applying lateral load in increasing the lateral movement of pile towards the excavation, resulted increasing the wedge of soil in front of the pile (left side) exhibits a bigger movement mobilizing a passive resistance in the front of the pile the movement propagates deeper than the previous case and, but the right side is still affected by the surcharge load settlement which moves the soil very slightly in opposite direction but less than the previous case .

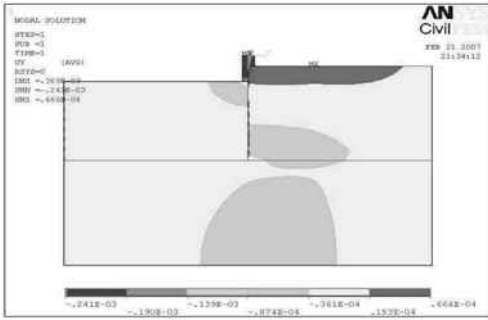


Figure (2-b) Contour of Deflections along the Pile After Excavation to -2.5 m .

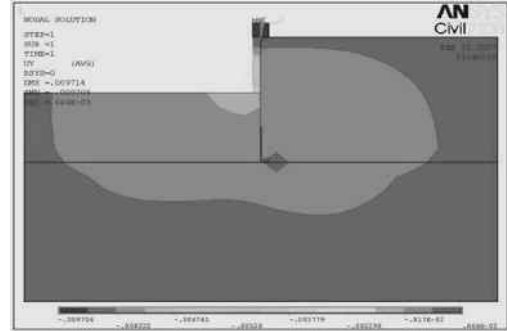


Figure (2-e) Contour of Deflections along Pile for 300 kN Horizontal Load .

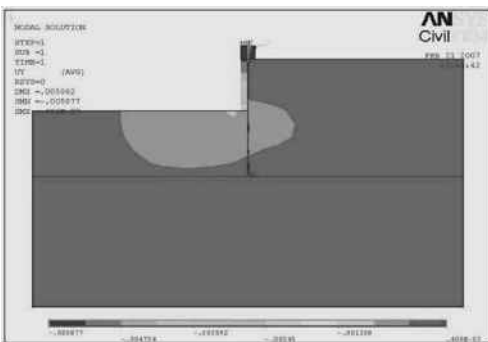


Figure (2-c) Contour of Deflections along the Pile After Excavation to -5 m .

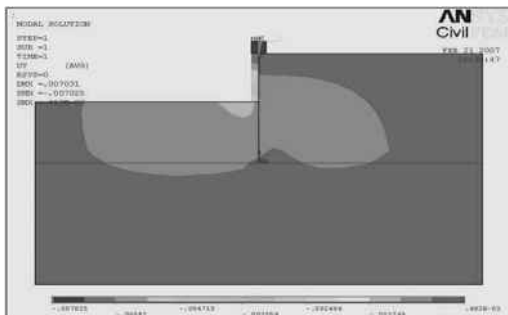


Figure (2-d) Contour of Deflections along the Pile after applying 210 kN Horizontal Load .

In figure (2-e), Applying 30 ton horizontal load, It is noted that increasing the applied lateral load resulted in increasing the lateral movement of pile towards the excavation, increasing the wedge of soil in front of the pile (left side) exhibits a bigger movement mobilizing a passive resistance in the front of the pile the movement propagates deeper than the previous case, the surcharge load settlement effect began to finish and a small passive resistance induced at the pile tip.

figure (3 -a) shows the deformed shape of pile and soil along the pile at failure, and figure (3 -b) shows the vector plot of the deflection of pile and soil along the pile at failure,

It is noted that reaching the ultimate lateral load resulted in increasing the lateral movement of pile towards the excavation, increasing the passive resistance wedge of soil in front of the pile (left side), all these resulted in reaching the pile its yielding and pile rotation increased, consequently, followed by a progressive slope failure on the right side which is clear in figures (3 -b).



Figure (3 -a): Deformed and Undeformed Shapes near Ground Surface .

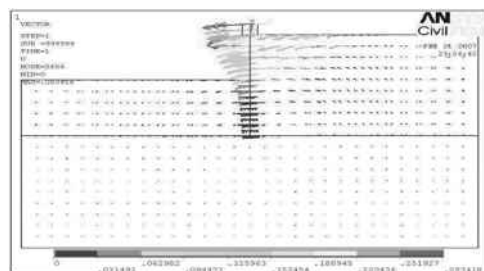


Figure (3 -b) Vector Plot of the Pile and Soil Displacements at Failure.

Considering the lateral displacement UY as the main output, numerical differentiation process were performed to get the slope , bending moment, shear force, and the soil reaction according to equations 1, 2, 3 , and 4 by changing the variable UX by UY .

Where: UY, MX and PY are deflection, bending moment and soil reaction (pressure) respectively. Direct generation of soil

pressure was also performed to check results and it was found that soil pressure were within 97% accuracy.

$$MX = \frac{d(ROTX)}{dz} \tag{2}$$

$$QX = \frac{d(ROTX)}{dz} \tag{3}$$

$$PX = \frac{d(ROTX)}{dz} \tag{4}$$

4.2 Pile Head Displacement.

Figure (4) shows a comparison for the measured pile head displacement and that estimated from the present study. It is noted that a very well agreement between the two curves is existing where the R- squared value is 94%. The pile was just instrumented on the top, thus diagram column represent one case of loading.

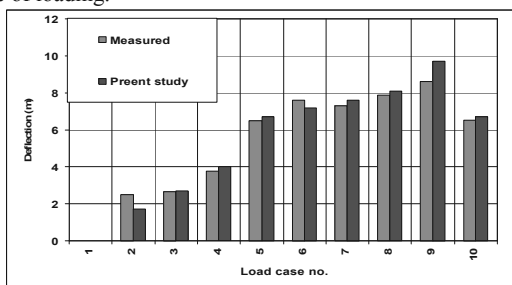
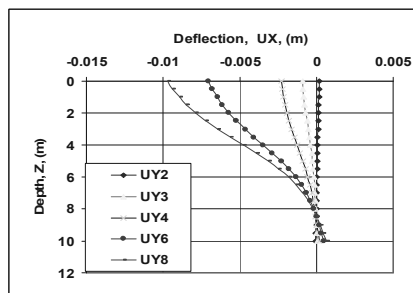


Figure (4) Predicted, and Measured Pile Head Deflection .

4.3 Pile Straining Characteristics

Figures (5- a) to (5- c), show the lateral deflection (UYn), bending moment (MYn), and soil reaction (pressure) (PYn) respectively along Pile Shaft due to the decided loading conditions illustrated in table (1). It is interesting to note that the change in location of maximum bending moment, peak zones of soil reactions, and points of hinges induced in different case of loading, where the point of maximum moment changed from -3 m to -5 m in case of excavation to -2.5m and -4 m , respectively. The beak of soil resistance is observed at -3.0 m in case of excavation to -2.5m and at -5.2 m in case of excavation to -5m. Also, the point of reversing soil reaction was observed at -7.75m.



Figure(5-a): Lateral Deflection along Pile Shaft .

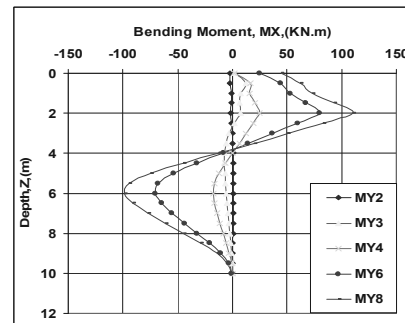


Figure (5-b): Bending Moment along Pile Shaft

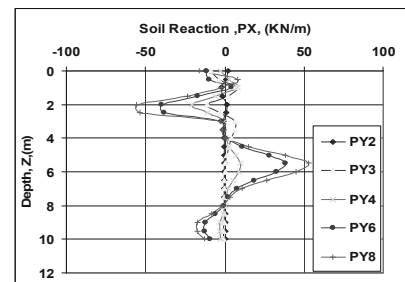


Figure (5-c): Soil Reaction along Pile Shaft.

5. CONCLUSIONS

The main findings can be summarized as follows:

- 3D finite element model gives the possibility of reaching high levels of loading until failure which is not available in full scale load tests.
- 3D finite elements can compensate for performing full scale lateral load tests with a good degree of trust to get reliable behavior of pile under loads saving time, effort , and cost.
- It is noted that good agreement between the measured and estimated from results of the finite element model. It is very important to obtain soil properties from high quality field or laboratory tests, as these will have direct effect on the analysis results.
- Pile and soil geometries must also be determined to a high degree of accuracy as these will also affect analysis outcome. Remembering the adage in computer modelling.

6. REFERENCES

Abouzaid, K.S., Shaarawi, E., El-Ghamrawy, M., Tarek, M.F., and Bahr, M.A., (2010), " Three Dimensional Finite Element Model for a Laterally Loaded Pile in Stiff Clay" Proc. 11th Int Conf., Cairo, Egypt Vol.3, pp. c34.

Alizadeh, M. and Lalvani, L. (2000), Lateral Load-Deflection Response of Single Piles in Sand, Electronic Journal of Geotechnical Engineering. Vol. 5.

Clark, J. I, Mckeown, S., Lester, W. B., and Eibner, L. J. (1985). "The lateral load capacity of large diameter concrete piles." 38th Canadian Geotechnical Conference, Theory and Practice in Foundation Engineering, Bolton, England.

Drucker, D.C. and Prager, W (1952), Soil Mechanics and Plastic Analysis of Limit Design, Quart. Applied Mathematics, Vol. 10, No.2, pp.157-165.

Jeremic, B., and Yang, Z (2002). Numerical analysis of pile behaviour under lateral loads in layered elastic-plastic soils. International Journal for Numerical and Analytical Methods in Geomechanics; 26:1385-1406

Maharaj, D. K. (2003), Load-Deflection Response of Laterally Loaded Single Pile by Nonlinear Finite Element Analysis, Electronic Journal of Geotechnical Engineering. Vol. 8, Bundle C, Paper 0342.

Design and construction of a coffer dam on Narmada River for Indira Sagar project in central India: a case study of innovative foundation

Conception innovante et construction d'un batardeau provisoire pour le barrage sur la rivière Narmada dans le cadre du projet Sagara en Inde centrale

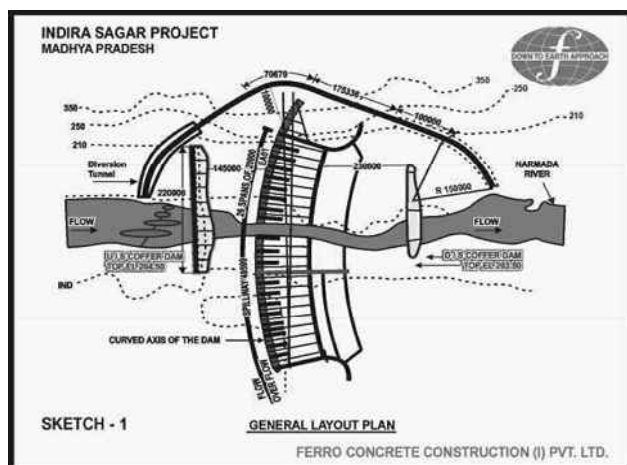
Bidasaria M.
Ferro Concrete Const. (India)

ABSTRACT: Indira Sagar Project in M.P., a multipurpose project, a 92 m high dam on Narmada river was required to be constructed but during off monsoon period flow of 300 cumecs of river Narmada was to be diverted so that dam can be constructed. For this, it was necessary to construct a 24 m high coffer dam to divert the off monsoon flow through a diversion tunnel from left abutment. This coffer dam was to be founded on a complex geological strata. To construct this 24 m high coffer dam, a new concept of innovative design used for first time in any country to construct a coffer dam, using 5 tons pre-cast blocks as shuttering on both faces of a coffer dam and filling the enclosure with boulders and stonecrete them under water. The work of 24 m high coffer dam has been done underground and under water for 12 m height using stonecrete and balance 12 m by conventional stone masonry.

RÉSUMÉ : Pour la construction du projet de barrage principal de 92m de hauteur sur la rivière Narmada des ouvrages provisoires de détournement de la rivière étaient nécessaires dans un contexte géologique difficile. L'article présente la conception innovante de batardeaux utilisant des blocs creux préfabriqués en béton avec bétonnage sous eau après mise en place d'enrochements.

1 INTRODUCTION

Indira Sagar Project is situated near Punasa about 60 Km. from Khandwa Town in Madhya Pradesh. To construct this dam, it was essential to divert Narmada river during off monsoon period from the original flow route, so that dam can be constructed without any hindrances. For this, conceptually it was necessary to have two important Component i.e. one u/s and d/s coffer dam to stop and divert Narmada river flowing from the original flow route, where proposed main dam was to be constructed and another a diversion tunnel through which Narmada post monsoon flow of 300 cumecs can be diverted during working period. That is how the construction of u/s and d/s coffer dam was necessitated. A sketch showing the various component like, u/s and d/s coffer dam diversion tunnel, proposed main dam etc. is shown in sketch – 1.



2. FOUNDATION AND GEOTECHNICAL PROBLEMS AND GEOLOGY

The Geological survey of India had carried out elaborate geological studies at the Indira Sagar Project dam site. It has been indicated that the dam site is located in the upper vindhyan inter bedded sequence of tough quartz arenites (quartzite), sand stones with minor silt stones. The bed in

general has an ENE-WSW strike and dip by 15-25 towards NNW with exceptional steep dips of 40-45 due to local warping. Bedding shears of 10-25 cm thickness confined to the silt stone beds are common features. The dam area in the river bed is occupied by a number of ENE-WSW trending vertical fault/shear zone, indicating horst/graben structure showing relative vertical displacement of blocks. It is WSW continuation of the Sone-Narmada fault. Mapping of the area has identified about five shear zones ranging steep dipping to vertical. These zones are braided with clayey gouge shear seams of 0.10-0.75 m thickness enveloping competent fractured lenses of quartzites and sand stone of 0.50 m to 2.5 m width sketch-2 shows geological L-section along main dam axis.

The fault zone includes the shearing (Sz-5), by virtue of its disposition and continuity, extends beyond the coffer dam located about 80 m upstream of the exposed section and opens in to the water pool, created by the upstream coffer dam in spite of being directly connected to this water pool, created by the upstream coffer dam. In spite of being directly connected to this water pool with a head difference of about 18-20 m the exposed section is completely dry and points to the near impervious nature of the fault zone material. Permeability test carried out in the new test holes in the fault zone confirm this observation (< 1 lugeon).

Except in the highly crushed zone/intrusion dyke, the fault zone material looks well compacted and was expected to have a high in situ density in the range of 2.2-2.3. The shear strength parameters were high and grain porosity may not exceed 20 %. The material did not show any significant deterioration notwithstanding the fact that there has been water to a depth of 1-2 m standing on it for a considerable time.

Even though the strata for foundation of coffer dam looked positive, for further dam design and stability of coffer dam foundation, detailed geotechnical investigation were necessary to eliminate geological surprises. Due to lukewarm report about highly Crushed zone/Intrusion dyke the foundations of coffer dam needed additional treatment to make it water tight. Further site investigation were carried out as given in the table below.

It may be observed that during pre-construction stages, to determine the detailed design parameters, following method of site investigations were performed :-

1	Geological mapping.	Over 0.75 Sq.Km on 1:1000 scale.
2	Core drilling	Double tube barrel – over 3000 m Triple tube barrel – over 500 m
3	Trenches	Three parallel trenches of +30 m. Six cross trenches of + 15 m
4	Shafts	Six shafts of 9.5 to 18m depth, 3.5 m dia.
5	Drifts	Four drifts of +16 – 23 m.
6	Bore hole camera studies	In 2 drill holes to study cavitations in silt stone/bedding shear zones.

This Data indicated that the sheared /crusted rock mass shall get consolidated if consolidation grouting is carried out and after completion of coffer dam, curtain grouting is also recommended, 1 m from the u/s face of coffer dam. Both these treatments were absolutely necessary in view of typical geotechnical problem faced. These treatments were carried out.

3. COFFER DAM - UPSTREAM AND DOWNSTREAM

The u/s coffer dam was necessitated to stop and divert the post monsoon river flow, to facilitate construction of main dam. This post monsoon flow ranging from 300 cumecs to 100 cumecs was required to be diverted from a diversion tunnel which was under construction through the left abutment.

As the construction of diversion tunnel was getting delayed considerably, provision of six sluices in the body of u/s coffer dam was envisaged to pass the post monsoon flow.

3.1 Concept.

The work consists of design and construction of upstream and downstream coffer dam of Indira Sagar Project. This was the new concept of design used for first time in any country to construct a coffer dam using 5 tons pre-cast blocks as shuttering on both faces u/s and d/s side of a dam, and filling the enclosure with boulders and stonecrete them under water. All work of coffer dam has been done underground and under water upto RL 193.5 m.

The maximum height of u/s coffer dam was 24 meter, 12 m under water and 12 m above water. The lowest foundation level in river bed was ± 180.60 m. For under water portion 5 ton hollow pre-cast c.c. blocks were casted and placed on the u/s and d/s face of dam, as a shuttering in a cell of 15 m length with the help of divers. Before placing the blocks, river bed was leveled by using blasting under water and with special technique, PC blocks were placed. Boulders were filled in the enclosure of a 15 m long cell and grout pipe with safety reinforcement were placed. The cell of 15 m was thoroughly caulked from outside, so that river flow does not have any effect in the cell. A colloidal grout, made out of sand, cement water and super plasticiser was pumped through the grout pipe at bottom and level of grout slowly built up from down upward. Thus colloidal grout (colcrete) replacing the water in the voids of the boulder and converting the boulder mass into concrete. This under water work was carried out upto 193.50 m level. About six pre-fabricated construction sluices of 2 m x 3 m were placed to take care of post monsoon discharges upto 300 cumecs as the diversion tunnel was under construction and was not ready.

Stone masonry was constructed above water level over the underwater works from RL 193.5 m and raised upto RL 204.50 m.

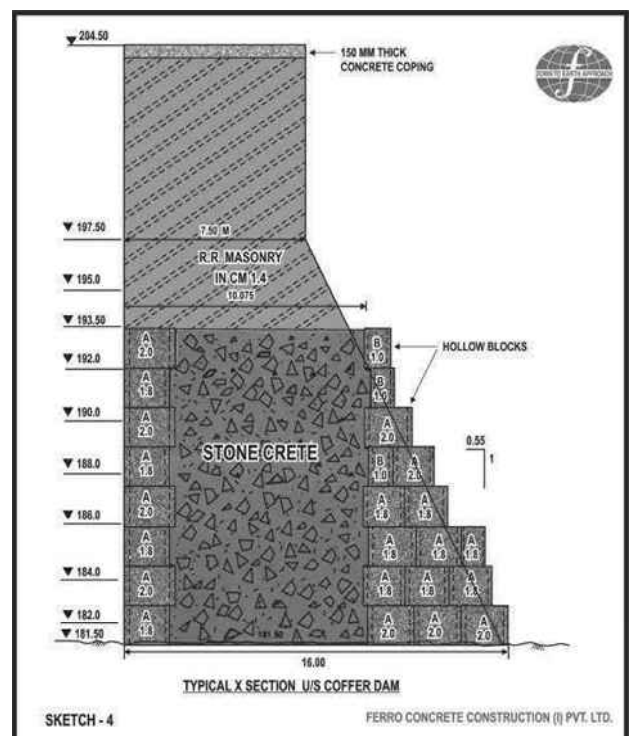
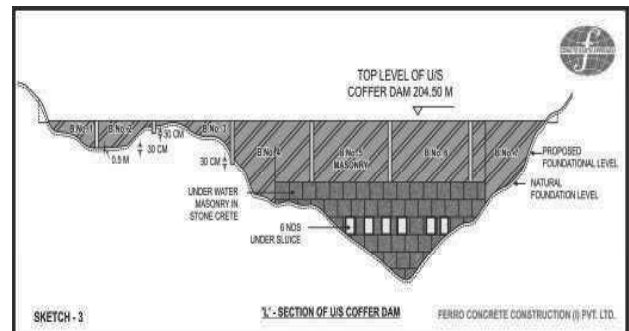
3.2 Design.

Height of u/s coffer dam was 24 m with the lowest foundation level kept at 180.6 and top of coffer dam as RL 204.5m. It has been designed on the principle of gravity dam, duly checked, for stability in various condition like Reservoir empty and Reservoir full etc. with following parameters :-

3.2.1 Coffier dam:

- Above water level, Random rubble masonry with a compressive strength of 10.5 N/mm² (cement mortar 1:4 approximate) with selected stone placed in u/s and d/s face.
- Under water stonecrete masonry in 1:2 and 1:3 concrete with P.C.C. Blocks on u/s & d/s faces.
- PCC blocks in M-15 grade Concrete.
- Coping : Concrete of M20 grade (c.c. 1:1.5:3) with 20 mm graded metal.

It may be observed that for underwater work, PCC blocks were kept on u/s and d/s section of the coffer dam and they were considered as a homogenous part of the full section. Dam cross section and L-section can be seen vide sketch – 3 and 4.



4 CONSTRUCTION SEQUENCE OF COFFER DAM U/S.

Following is the Construction sequence.

4.1 Casting yard for Pre-cast hollow blocks.

A casting yard having all facilities to cast hollow blocks under controlled conditions was made on left bank. The pre-cast/hollow blocks of size of 1.5 m x 1.5 m x 1.5 were casted in this yard. Suitable storage for form work and construction materials like stone grit, sand, water curing tank etc. were arranged on this platform to keep adequate stocks at site. The yard was equipped with form vibrators etc. and the traveling gantry with 10 T capacity. One electric hoist was fitted at this platform. The blocks were handled and loaded in flat bottom trucks by said gantry to carry it upto working platform on left flank from where, finally they were taken for construction using crawler mounted cranes at site.

4.2 Precast Hollow Blocks :-

It was proposed to use hollow-precast blocks in the u/s and d/s of the dam profile under water. This enclosure were termed as stonecrete cell. At a time, 15 m length of coffer dam was undertaken in hand. Selected rubbles were filled within this enclosure along with colgrout pipes to carry out under water work. These colgrout pipe of 80 mm ϕ were kept in a grid of 3 m and individual pipes were surrounded with a circular coil made of 6 mm, Tor to protect them during boulder filling. These blocks in addition to forming the enclosure have helped to stop flow of water within the enclosure as well as in voids of the rubbles.

The shape of the blocks on upstream and down streams faces of the coffer dam were nearly confirming to the designed profile.

To provide necessary interlocking amongst the blocks, male and female grooves were provided in each block. The blocks of special dimensions for maintaining uniform level of courses were casted as per requirement. The necessary shear keys and lifting hooks were provided in each block. The blocks were casted in the rigid steel forms so as to ensure uniform dimensions and minimum tolerances. The blocks were cast in advance and stacked in the casting yard.

4.3 Preparation of Foundation.-

The left and right flanks which were much above water level of river were excavated to reach sound rock level to accommodate the length of coffer dam. Right flank in particular, was braided with clayey gougey shear seam of varying thickness from 2m to 6m. On the left flank excavation bedding shears of 16 to 25 cm thickness confined to the silt stones were commonly seen. Few photographs of the excavation and shear seam are exhibited below.

Foundation preparation in the river portion comprised of removal of silt, debris, loose rock and leveling of bed rock by underwater blasting wherever necessary. This was done using expert divers.

In order that the precast blocks from the pattern masonry walls required to be raised in uniform courses, the precise soundings were taken and loose materials were removed from its underneath. The area was leveled using special sizes of the blocks, or executing under water concreting for leveling course. It was observed that foundation rock was undulated at places. Hence levels were taken at a grid of 2 m and drawn on graph sheet. The gap between the leveled foundation and underneath of the blocks were caulked to achieve reasonable water tight joint.

4.4 Launching of Blocks.

After the river bed is cleared of loose materials and leveled to receive the first course of the blocks as described under preparation of foundation para (III) above, the pre-cast hollow blocks were lifted from the working platform and carried by crane and lowered in position in the cell. Before lowering the PCC blocks, a steel frame made of 100 mm M.S. angle, is first lowered in place on 40 mm bed of stone chips and this frame is leveled horizontally on this bed. Expert divers had positioned the blocks at proper places either on the u/s or d/s of the enclosure as required, but within these steel frames which were leveled horizontally on the bed of 40 mm stone chips.



Each operation of block launching consisted of placement of blocks in the bottom course, to be followed by blocks in upper course. Till they were placed upto the level of 193.50 M. The launching of blocks is shown in photograph above.

Normally the blocks will be placed in required courses on up-stream and downstream sides of the u/s and d/s coffer dams. As the blocks are required to be in course it will be imperative to break the joints between the courses. Proper care was taken to break these joints in subsequent courses. As a matter of abundant precaution, the space in between the rows of blocks, will be filled with selected rubble near the blocks and around the pipes placed for colgrouting, so that the same does not get disturbed while filling up of rubble/stones in the cell

4.5 Packing of Rubbles.

After the blocks are carefully launched and erected on either side in courses and the space in between intersped with colcrete pipes, as stated above, rubble will be placed to fill-up the entire space between the rows of blocks in a 15 m cell. This rubble filling shall be done layer by layer in a systematic way using the large buckets with drop bottoms, handled by cranes.

4.6 Stonecreting Operations.

The stonecrete process consists of making a grout of cement, sand and water in which cement has been so completely hydrated by high speed mechanical mixing, that the grout attains a colloidal form. This grout is stable and particularly fluent. It contains no chemical admixtures which might ultimately be harmful. When colloidal grout is poured in rubble aggregate the voids in the rubble filling are completely filled by penetration and the whole mass sets as a dense, solid concrete which is termed as "STONECRETE".

4.7 Preparation of Colloidal Grout.

The Colloidal grout was prepared in double drum colcrete mixer consisting of sand, cement and water in desired proportions to obtain colloidal grout. In colloidal mixer, the

wetting of solid ingredients results from the shearing action which takes place in the specially designed impellers and matching casings of the colloidal mixers. The colloidal grout of specific gravity upto 1.8 to 2 is obtained using these high velocity mixers. Colloidal grout has enough fluidity to flow like grout and does not get separated when it comes in contact with water. It displaces water from the voids of stone/rubbles due to high specific gravity.

The double drum stonecrete mixer produces colloidal grout at the rate of 5 to 10 M³/hr. of 1:2 mix or 6 to 12 M³/hr. of 1:3 mix. When colloidal grout is stored without agitation in tanks after mixing, a little settlement is to be expected because sand invariably contains some oversize particles. When it is pumped direct by the mixer to the work in normal practice, the oversize particles do not have time to settle out.

4.8 Placement of Colloidal Grout.

Colloidal grout does not mix with water unless agitated with it.

The colloidal grout so prepared is pumped, through 80 mm Φ pipes placed in the rubbles using special roto or colmono pumps. The grout will be pumped at the bottom of pre-packed stones under pressure and will be allowed to rise uniformly in the cell displacing all the water from the voids due to its gravity. Once the grout travels upto the top of the course, the colgrouting is stopped when it emerges out of boulders at a level of 193.50 m of working platform level. After which the crawler mounted cranes will be advanced to tackle the next cell of the coffer dam till entire length 220 m length of u/s coffer dam is completed from one end. Construction sluices were left in the u/s coffer dam for diverting the water in final stages of closure of the coffer dam.

4.9 Construction Sluices.

Pre fabricated M.S. sluice barrel were lowered in the central portion of u/s coffer dam keeping invert level at RL 186. In all, six sluices of 2 m x 3 m were installed. Rigid steel boxes were provided in the blocks for forming the approach tunnel for sluices. The construction sluices were installed under water with the help of the expert divers and is shown in photograph below.



4.10 Masonry Works above water level.

Construction of masonry in the flank blocks and above water level on stonecrete platform, upto top of coffer dam was done using conventional method of construction. The coffer dam above RL 193.5 was constructed in masonry upto RL 204.5 M and is shown in photograph. This was taken up immediately after the construction upto RL 193.5 under water using stonecrete. A coping 150 mm thick was laid at RL 204.5 m on the masonry using M-20 grade concrete.

5. DRILLING AND GROUTING.

5.1 Consolidation Grouting.

Looking to the geology, it was recommended to adopt a grid of drill holes at 3 m c/c on both side, besides about 82 Nos. of special grout holes were identified keeping in mind the location of various fault zones.

Depth of consolidation grout holes was 6 m in foundation rock.

6. CURTAIN GROUTING.

It was recommended to provide a single row of grout curtain, 1 m from the u/s face of the coffer dam, spacing of holes were kept as 3 m c/c. Depth of grout curtain holes in foundation rock was kept as 15 m.

This grout curtain was provided in stages of 5 m of drilling and grouting in descending order method.

It was observed that in consolidation grouting, intake of cement was 45 kg/meter and in curtain grouting it was 26 kg./meter.

7. D/S. COFFER DAM:

The construction of d/s coffer dam was done using the same methodology as explain under para 3 sub para I to IX. The top of d/s coffer dam was kept as 203.50 m i.e. 1 m below the u/s coffer dam. The main purpose of this coffer dam was, not to allow the river water which was diverted through the diversion tunnel (back water) in the d/s of the river.

Closure of Sluices 6 Nos. in coffer dam:

It was essential to ensure following works completed before closure of sluices were taken in hand :-

8 CONCLUSION

Coffer Dam u/s and d/s, for the Indira Sagar Project had been successfully constructed and performed well, as a result the work of 92 m high I.S.P. main dam could be expeditiously carried out on mighty Narmada River.

The unique and innovative design, using 5 Tons Pre-cast hollow blocks with underwater stonecrete technique for the first time in the country, has successfully been used in Indira Sagar Project.

9 REFERENCES

- Ahmed M.J. - Assessment of Geological and Technical inputs for optimization of Designs of Indira Sagar Project, M.P. India.
- Billore M.S., Geed V.K., - Photographs.
- M. Krishnamoorthy, G.C. Vyas, Rajeev Sachedeva – Civil design aspects of Indira Sagar Project.
- Tripathi D.C. Amitabh Sharan, - Shearzone treatment : A case study of Indira Sagar Project on Narmada River, M.P. India.

Anchored sheet pile wall design in expansive soils

Conception d'un mur de palplanches ancré dans les sols expansifs

Bilgin Ö., Mansour E.
University of Dayton, Dayton, Ohio, U.S.A.

ABSTRACT: Expansive soils cause damage to civil engineering structures in various parts of the world, because they swell when absorb water and shrink when dry out. Due to swelling pressures, retaining walls can be subjected to additional lateral pressures causing increased wall deformations and bending moments. Anchor forces can also increase, if the walls are anchored. When expansive soils are present behind retaining walls, swell pressures should also be considered during design in addition to the traditional lateral earth pressures. This study proposes a method to predict potential swell pressures acting on retaining walls for use in design of these walls. A parametric study using the limit equilibrium approach was performed to investigate the effect of swell pressures on the design of anchored sheet pile walls in expansive soils. The results of the study show that the presence of expansive soils can significantly affect earth retaining structures and swell pressures should be considered in the design of retaining walls when the expansive soils are present at the site.

RÉSUMÉ : Les sols expansifs causent des dommages à des structures de génie civil dans diverses parties du monde, ils gonflent quand ils absorbent de l'eau et se contractent quand ils se dessèchent. En raison des pressions de gonflement, les murs de soutènement peuvent être soumis à des pressions latérales supplémentaires augmentant les déformations et les moments fléchissant. Les forces d'ancrage peuvent également augmenter, si les murs sont ancrés. Lorsque les sols expansifs sont présents derrière les murs de soutènement, les pressions de gonflement devraient également être envisagées, en plus des pressions latérales des terres traditionnelles. Dans cette étude, une méthode a été proposée pour prédire d'éventuelles pressions de gonflement agissant sur les murs de soutènement, à utiliser dans la conception de murs de soutènement. Une étude paramétrique en utilisant l'approche d'équilibre limite a été réalisée pour étudier l'effet des pressions de gonflement sur la conception de rideaux de palplanches ancrées dans les sols expansifs. Les résultats de l'étude montrent que la présence de sols expansifs, peut influencer considérablement la conception de structures de soutènement et doit être pris en compte dans la conception des murs lorsque les sols expansifs sont présents sur le site.

KEYWORDS: Retaining wall, anchored sheet pile wall, expansive soil, swell pressure, wall design.

1 INTRODUCTION AND OVERVIEW

The sidewalls of structures and retaining walls may experience additional lateral pressures when they are located within expansive soils. When the expansive soils absorb water the moisture content increases and the soil tends to expand. If the free swelling or expansion of the clay is restricted, then swell pressures develop and this cause an increase in the lateral pressures acting on the structures. The design of retaining walls usually specifies cohesionless soils as a backfill material behind the wall mainly to avoid hydrostatic pressures by providing easy drainage. These cohesionless materials also help to prevent swell pressures that may develop if cohesive soils are used.

Due to economical reasons, local soils which may be expansive are sometimes used as a backfill material (Thomas et al. 2009). However, use of these soils as backfill may result in wall failures (Marsh and Walsh 1996) not only because of the hydrostatic pressures but also due to the additional lateral earth pressures caused by the swelling of expansive soils.

The selection of soils behind the wall is not even optional for in-situ retaining walls, such as cantilever and anchored sheet pile walls, slurry walls, secant and tangent pile walls. These walls are installed in existing soils and front of the wall is usually excavated. When these walls are installed at locations where expansive soils are present, the walls would experience not only the traditional lateral earth pressures but also the swell pressures when soil's moisture content increases.

The objective of this study is to investigate the behavior of anchored sheet pile walls when they are installed in expansive soils and exposed to additional stresses due to the swelling of

these soils.

1.1 Expansive soils

The best way to deal with the shrinkage and swelling of expansive soils is to maintain constant soil moisture. If the soil moisture content does not change, there can be no shrinkage or swelling. However, it is usually not possible to maintain constant soil moisture. Moisture content fluctuates due to several factors, such as precipitation and evaporation. The seasonal variation of soil moisture is much higher at shallower depths and it decreases as the depth below the ground surface increases (Figure 1).

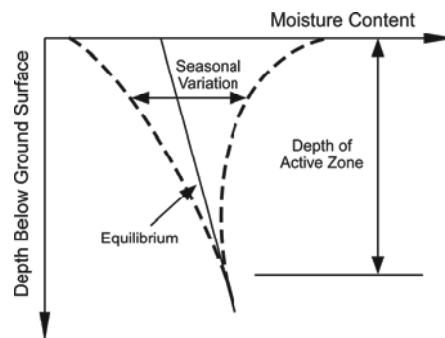


Figure 1. Moisture content fluctuations with depth.

Table 1. Classification of swell potential (after USACE 1983).

Classification of swell potential	Plasticity index, PI (%)
Low	< 25
Marginal	25 – 35
High	> 35

The depth where the seasonal soil moisture variations occur below the ground surface is called the active zone as shown in Figure 1. The depth of active zone is influenced by soil permeability, precipitation and evaporation amounts, seasonal temperature fluctuations, and presence of tree roots. Active zone depths in several U.S. cities were reported by O'Neill and Poormoayed (1980) as: 1.5 to 3.0 m in Houston, Texas; 2.1 to 4.2 m in Dallas, Texas; 3.0 to 4.6 m in Denver, Colorado; and 3.0 to 9.0 m in San Antonio, Texas.

The degree of swell potential of expansive soils can be classified by the soil's liquid limit, LL , or plasticity index, PI . As the liquid limit or plasticity index increases, the swell potential of the soil increases. The classification used by the U.S. Army Corps of Engineers (USACE) (1983) based on the plasticity index is given in Table 1.

1.2 Conventional sheet pile wall design

The design of sheet pile walls is based on active and passive earth pressures which are concerned with the failure condition using the Mohr-Coulomb failure criterion. For a typical wall section, the lateral earth pressures and the resulting forces acting on the wall are shown in Figure 2, where P'_A and P'_P are resultant effective active and passive earth forces, respectively; d_A and d_P are moment arms with respect to the anchor elevation; and FS is factor of safety. The factor of safety is applied to the passive loads during wall design (NAVFAC 1986; USACE 1994). The safety factors are used to take into account the uncertainties in soil conditions, method of stability analysis, loading conditions, as well as to restraint soil movements at an acceptable level (Potts and Fourie 1984).

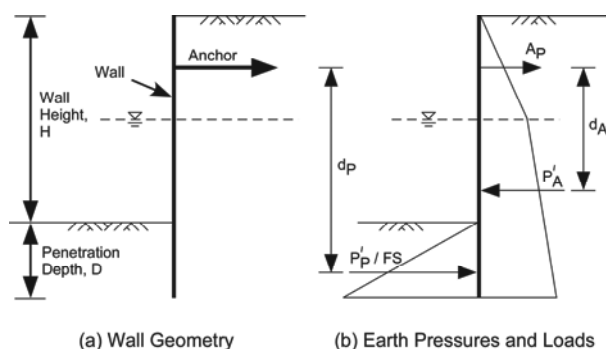


Figure 2. Typical sheet pile wall section and forces acting on the wall.

Wall penetration depth required below the bottom of the excavation is determined by considering the moment equilibrium about the anchor elevation. Because the water level is assumed to be at the same elevation behind and in front of the wall during this study, hydrostatic forces cancel each other. Once the wall penetration depth is determined, the anchor force, A_p , is calculated from horizontal force equilibrium. Based on the active and passive pressure distributions and the calculated anchor force, maximum wall bending moment is determined. The design moment is calculated by applying the moment reduction factor (Rowe 1952) to the calculated maximum bending moment. The steel sheet pile section is then selected based on the design moment, and the wall design is completed by selection and design of an anchorage system. This conventional design approach does not take into account any

swell pressures that may affect walls when they are installed at locations where expansive soils are present.

2 METHOD OF APPROACH

The effect of swelling pressures on anchored sheet pile wall behavior has been investigated through a range of expansive soil activity. The swell pressures were calculated for a range of plasticity index values covering soils from low to high swell potential based on a study performed by Erzin and Erol (2007). Using these swell pressure potentials and moisture change profile in the ground within the active zone, the swell pressure distribution was developed. The swell pressure distribution developed was then applied on the anchored sheet pile wall as potential swell pressure, additional to the lateral earth pressures presented in Figure 2.

A parametric study for a range of plasticity index values, i.e. expansive soil activity and swell potentials, have been performed using the free earth support design method to investigate the effect of swell pressures on anchored sheet pile walls. Design of the wall was first performed for non-expansive soils, i.e. using only the traditional lateral earth pressure distributions, as a baseline case. Then the swell pressures, based on the varying plasticity index values, have been applied and the wall was re-analyzed.

3 SWELL PRESSURES

There are many factors that govern expansive behavior of soils. The primary factors are availability of moisture, amount and type of clay particles, and initial condition of soil in terms of dry density and moisture content (Day 1994). Several earlier studies (e.g., Snethen 1980, Erzin and Erol 2007) indicate that soil suction is the most relevant soil parameter for the characterization of swell behavior of expansive soils.

Multiple regression analyses carried out by Erzin and Erol (2007) revealed that the soil suction relates to the plasticity index and water content as

$$\log s = 2.02 + 0.00603 PI - 0.0769 w \quad (1)$$

where s =soil suction (in bar), PI =plasticity index (in percent), and w =water content (in percent). The study performed by Erzin and Erol (2007) also showed that the swell pressure, for pressures between 0 and 100 kPa, can be given as

$$\sigma_s = -3.72 + 0.0111 PI + 2.077 \rho_{dry} + 0.244 \log s \quad (2)$$

where σ_s =swell pressure (kg/cm^2), PI =plasticity index (in percent), ρ_{dry} =dry density (g/cm^3), and s =soil suction (in bar).

For this study, the plasticity index was used as the only variable to determine swell pressures. The plasticity index values considered ranged from 10% to 50%, which covers low to highly expansive soils as presented in Table 1. A constant value of 15% for the moisture content and a constant value of $1.65 \text{ g}/\text{cm}^3$ for the dry density were used. These selected values represent average values of the ranges considered by Erzin and Erol (2007) in their study. The swell pressures calculated using Eq. 2 for the range of plasticity index values studied, with the moisture content of 15% and dry density of $1.65 \text{ g}/\text{cm}^3$, are shown in Figure 3.

3.1 Distribution of lateral swell pressures behind the wall

As shown in Figure 1, seasonal variation of soil moisture content is the highest at the ground surface and it diminishes as the depth from the ground surface increases. The change in the moisture content with increasing depth is not linear. However, the variation is assumed to be linear in this study. This

assumption is conservative, since the predicted swell pressures will be larger than the actual ones. The simplified linear model is shown in Figure 4.

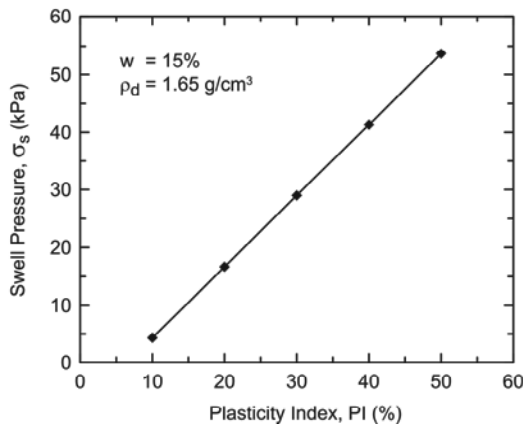


Figure 3. Swell pressure versus plasticity index.

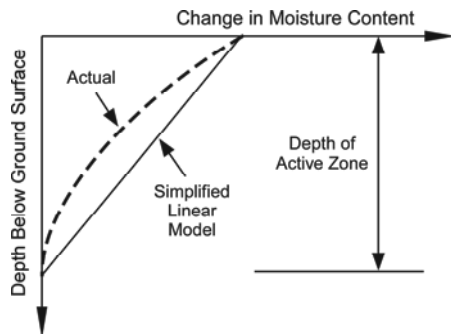


Figure 4. Change in moisture content with depth.

Because the change in moisture content causes the swelling of expansive soils, swell pressure will be maximum at the ground surface and will decrease as the depth increases. These maximum pressures, i.e. potential swell pressures, can be determined using Eq. 2. However, swell pressures close to the ground surface will not reach their potential due to shallow depths where soil confinement pressures are relatively lower. Soils closer to the ground surface will be able to expand, and full swell pressures determined by Eq. 2 will not be able to develop. When swelling occurs, passive lateral earth pressure conditions develop near the ground surface. Therefore, the passive earth pressures can be used as an upper limit for swell pressures near the ground surface. A schematic of the additional lateral pressure developed behind the wall due to the swelling of expansive soil is shown in Figure 5, where the potential swell pressure, σ_s , is determined by Eq. 2. When the swell pressures exceed the passive earth pressures near the ground surface (i.e., within the critical depth, z_c , shown in Figure 5), the additional lateral pressures due to the swelling of soil are capped by the passive earth pressures.

4 ANALYSIS AND RESULTS

The analyses were performed for a fixed wall height of 10 m with anchor level located at 2.5 m below the top of the wall. The anchor level was selected based on a study performed by Bilgin and Erten (2009) which showed that the best anchor location to have minimum wall deformations was $0.25 \times H$ below from the top of wall, where H is the wall height. The active zone depth used in the study was 5.0 m, selected based on the values given by O'Neill and Poormoayed (1980) as mentioned previously. The groundwater table is also assumed to be 5.0 m

below the top of wall and at the same elevation on both sides of the wall. A schematic of the pressure diagrams used to perform parametric study are shown in Figure 6.

The analysis results are shown in Figure 7 through Figure 9, as a percent increase in the wall penetration depth, maximum wall bending moment, and anchor force versus soil plasticity index. The percent increase is given with respect to the baseline case in which the anchored sheet pile wall was installed in non-expansive soil. The results show that as the plasticity index increases the wall penetration depth, maximum wall bending moment, and anchor force can increase significantly.

4.1 Wall penetration depth

The effect of expansive soils and potential swell pressure, calculated based on the soil plasticity index, on anchored sheet pile wall penetration depth is presented in Figure 7. As shown in Figure 7, an increase in the plasticity index, i.e. increase in the activity of expansive soils, can result in significant increase in wall penetration depth. Compared with the wall installed in non-expansive soil, the wall penetration depth can increase more than 85% and 125% for low and marginally expansive soils, respectively. Within the plasticity index range considered during this study, the wall penetration depth can increase as much as 190% which is for the plasticity index of 50%.

4.2 Wall bending moment

The effect of expansive soils and potential swell pressures on wall maximum bending moment is shown in Figure 8. The results show that wall bending moment increases as the plasticity index of soil increases. While the presence of marginally expansive soils with fully reached swell potential can result in approximately 105% increase in wall bending moment, an increase of up to 170% can occur for soils with plastic index values of 50%, i.e. highly expansive soils.

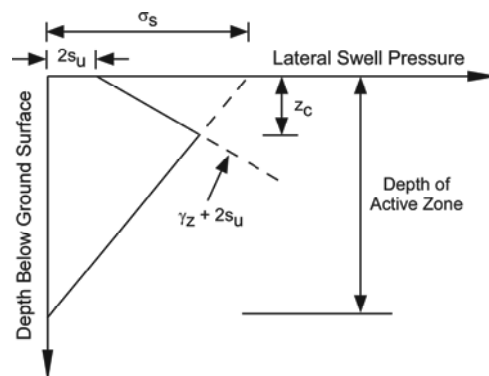


Figure 5. Lateral pressure distribution due to swelling of expansive soil.

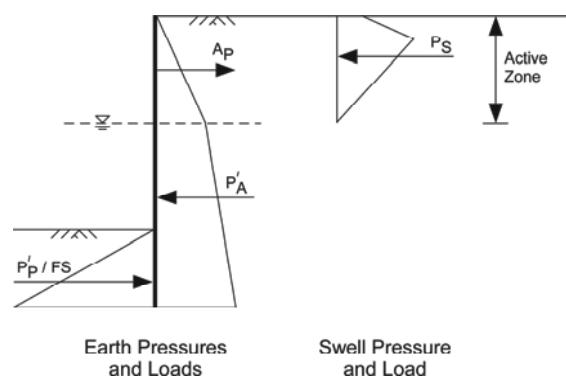


Figure 6. Soil and swell pressures acting on the wall.

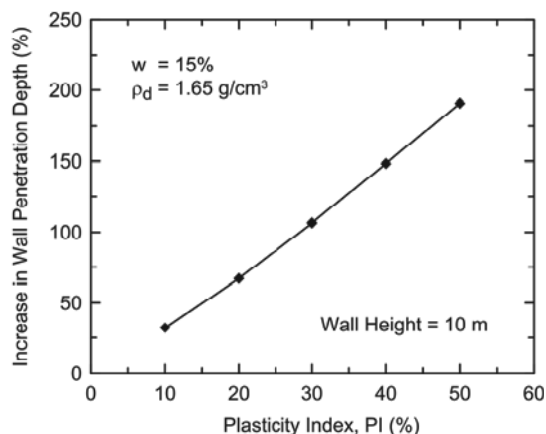


Figure 7. Effect of expansive soils on wall penetration depth.

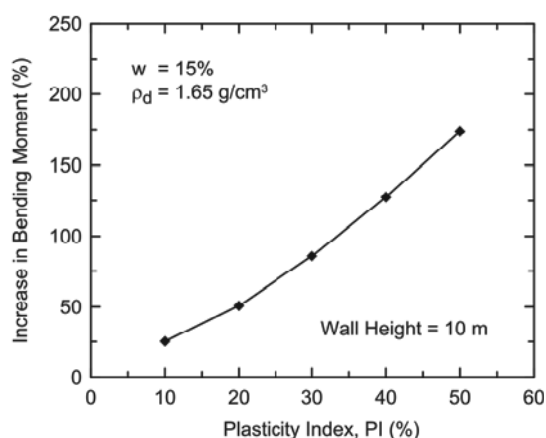


Figure 8. Effect of expansive soils on wall bending moment.

4.3 Anchor force

The effect of expansive soils and potential swell pressure on anchor force is presented in Figure 9. The results show that the anchor force increases as the plasticity index of soil increases, similar to the wall penetration depth and bending moments. However, the presence of expansive soils has the most significant effect on the anchor forces. This is because of the fact that the anchor is located closer to the top of sheet pile wall and the swell pressures are higher closer to the ground surface due to more fluctuations in soil moisture content in this zone. Within the range of parameters considered, an increase in the anchor force can be as much as 240% (when plasticity index is 50%) compared to the condition where the wall is installed in non-expansive soil.

5 SUMMARY AND CONCLUSIONS

The design of retaining walls usually specifies cohesionless soils as a backfill material behind the wall, however, in-situ retaining walls, such as anchored sheet pile walls, are installed in existing soils. Expansive soils exist in many locations around the world, and the design of anchored sheet pile walls needs to consider the effect of soil swell pressures when these walls are installed in these soils.

In this paper the effect of expansive soils and swell pressures on anchored sheet pile walls, in terms of wall penetration depth, wall bending moment, and anchor force were investigated. The swell pressures were determined using the soil plasticity index, based on earlier studies. For the cases studied and range of soil properties considered, the analysis results show that the effect of expansive soils on anchored sheet pile walls can be significant,

even if the soils at the site are low to marginally expansive. For soils with the plasticity index of 50%, indicative of highly expansive soils, and for wall geometry and soil conditions considered during this study, the analysis results show that the wall penetration depth increased 190%, wall bending moments increased 170%, and anchor force increased 240%, compared with the wall design when soils at the site are non-expansive. The maximum increase was observed in the anchor force, because higher swell pressures develop closer to the ground surface due to the seasonal changes in moisture content. It should be noted that the swell pressures determined using the plasticity index values represent the maximum potential swell pressures, i.e. upper limit, and these pressures may not develop during each seasonal changes.

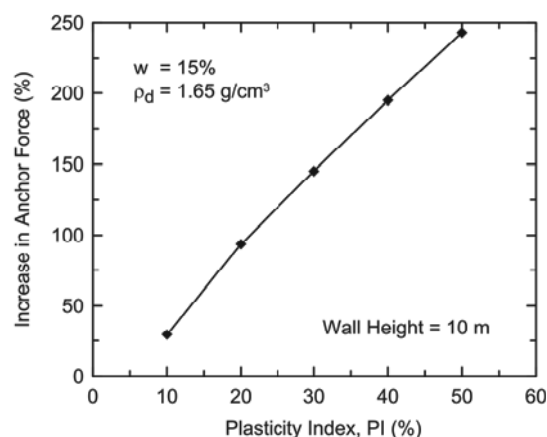


Figure 9. Effect of expansive soils on anchor force.

6 REFERENCES

- Bilgin Ö. and Erten M.B. 2009. Analysis of anchored sheet pile wall deformations. *Contemporary topics in ground modification, problem soils, and geo-support (GSP 187)*. Proceedings, International Foundation Congress & Equipment Expo 2009, Orlando, Florida, 137-144.
- Day R.W. 1994. Performance of slab-on-grade foundations on expansive soils. *Journal of Performance of Constructed Facilities* 8 (2), 129-138.
- Erzin Y. and Erol O. 2007. Swell pressure prediction by suction methods. *Engineering Geology* 92 (3-4), 133-145.
- Marsh E.T. and Walsh R.K. 1996. Common causes of retaining-wall distress: case study. *Journal of Performance of Constructed Facilities* 10 (1), 35-38.
- Naval Facilities Engineering Command (NAVFAC) 1986. *Foundations and earth structures, NAVFAC DM 7.02*, Alexandria, VA.
- O'Neill M.W. and Poormoayed, N. 1980. Methodology for foundations on expansive clays. *Journal of the Geotechnical Engineering Division* 106 (GT12), 1345-1367.
- Potts D.M. and Fourie A.B. 1984. The behavior of a propped retaining wall: Results of a numerical experiment. *Geotechnique* 34 (3), 383-404.
- Rowe P.W. 1952. Anchored sheet-pile walls. *Proc.- Inst. Civ. Eng.* 1 (1), 27-70.
- Sneath D.R. 1980. Characterization of expansive soils using soil suction data. *Proceedings of the 4th International Conference on Expansive Soils*, Denver, Colorado, 54-75.
- Thomas M.G., Puppala A.J., and Hoyos L.R. 2009. Influence of swell pressure from expansive fill on retaining wall stability. *Contemporary topics in ground modification, problem soils, and geo-support (GSP 187)*. Proceedings, International Foundation Congress & Equipment Expo 2009, Orlando, Florida, 590-597.
- U.S. Army Corps of Engineers (USACE) 1983. *Foundations in expansive soils, TM 5-818-7*, Washington, DC.
- U.S. Army Corps of Engineers (USACE) 1994. *Design of sheet pile walls, EM 1110-2-2504*, Washington, DC.

Performance of Soil Nails in Weathered Granite and Fill

Performance de renforcement par clouage du granite altéré et du remblai

Chow C.-M., Chee-Meng, Tan Y.-C.

G&P Geotechnics Sdn Bhd, Kuala Lumpur, Malaysia (www.gnpgeo.com.my)

ABSTRACT: Soil nail is increasingly common in Malaysia for infrastructure works where high cut slope is often formed to accommodate road alignment, facilities, etc. In recent years, soil nailing has also proven to be a viable, cost-effective and environmental friendly alternative solution for deep excavation of basement to replace conventional solutions using vertical retaining wall such as contiguous bored pile, secant pile or diaphragm wall. Applications of soil nail for basement construction of up to 30m deep have been successfully designed and constructed where performance of the soil nailing works have been verified based on monitoring results. Design assumptions for the skin friction between the soil and grouted body of soil nail were also verified using instrumented preliminary and working pull-out tests on the soil nails. This paper discusses results of the pull-out tests on the soil nails and based on analysis of the test results, recommendations on the skin friction applicable for soil nail design are presented.

RÉSUMÉ : Les clous de sols sont de plus en plus communs en Malaisie pour les travaux d'infrastructure où une forte pente de talus est souvent créée pour le tracé de la route, pour accueillir les installations, etc. Ces dernières années, le clouage de sol s'est également avéré être une solution alternative viable, rentable et écologique pour remplacer les solutions classiques utilisant un mur de soutènement vertical tels que les pieux forés contigus, les pieux sécants ou les parois moulées pour les excavations profondes des travaux de fondations. Les applications du clouage de sol dans la construction d'excavations de plus de 30m de profondeur ont été correctement conçues et mises en œuvre et leurs performances ont également été vérifiées sur la base de mesures répétées. Les hypothèses de calcul des efforts d'adhérence entre le sol et les clous de sols avec injection ont également été vérifiées par des tests d'arrachement. Cet article présente les résultats des tests d'arrachement sur des clous de sol et sur la base de l'analyse de ces résultats, propose des recommandations sur la capacité en de scellement à prendre en compte lors de la conception des clous de sol.

KEYWORDS: Soil nail, skin friction, pull-out tests, deep excavation.

1 INTRODUCTION

Soil nails are increasingly common in Malaysia for infrastructure works where high cut slope is often formed to accommodate road alignment, facilities, etc. Soil nail is advantageous compared to other retaining wall system as the soil nails are installed directly onto the final slope/wall profile and as such, minimises earthworks compared to conventional retaining wall. Furthermore, soil nails installation also does not require heavy machineries compared to system such as contiguous bored pile (CBP), diaphragm wall/secant pile. Malaysia's experiences in soil nail design and construction have been discussed by Chow & Tan 2006 and Chow & Tan 2011.

In recent years, the use of soil nails as alternative solution to vertical retaining wall for basement excavation is also gaining popularity and has been successfully designed and constructed for basement excavation of up to 30m deep. This paper discusses the design and construction of a soil nailed slope for basement excavation of a commercial development in Mont' Kiara, Kuala Lumpur, Malaysia with excavation depth of up to 20m.

2 GENERAL GEOLOGY AND SUBSURFACE INFORMATION

The site is underlain by the Kuala Lumpur Granite formation. The granite rocks are generally whitish grey and dark grey in colour except certain parts with iron stained markings that gives orange and dark red colours to the rocks. The texture and composition of the granitic rock generally ranges from coarse to very coarse-grained.

A total of twenty nine boreholes were carried out at the site to facilitate retrieval of undisturbed soil samples for laboratory testing (e.g. Atterberg limits tests, Isotropically Consolidated Undrained Triaxial – CIU tests, etc.) and also in-situ tests such as Standard Penetration Tests (SPT). The interpreted borehole profiles relevant to the soil nail slope showing the SPT-N values, major/minor components of soil and Rock Quality Designation (RQD) for rock are shown in Figure 1. Some of the materials near to the surface, especially for materials with low SPT 'N' values (< 5) are filled materials.

Generally, the subsoil consists mainly silty SAND and sandy SILT with Liquid Limit (LL) ranging from 25% to 71% and Plastic Limit (PL) ranging from 15% to 42% and can be classified as low to high plasticity silty/clayey materials.

A total of eleven Isotropically Consolidated Undrained Triaxial (CIU) tests and four Direct Shear Box tests were carried out to determine the shear strength of the soil. The shear strength parameters of the subsoil adopted for design are $c'=3.5\text{kPa}$, $\phi'=30^\circ$.

3 DESIGN OF SOIL NAIL SLOPE FOR BASEMENT EXCAVATION

The soil nail slope with retained height of up to 20m is designed to ensure minimum long-term factor of safety of 1.4 as the soil nail slope will be permanent.

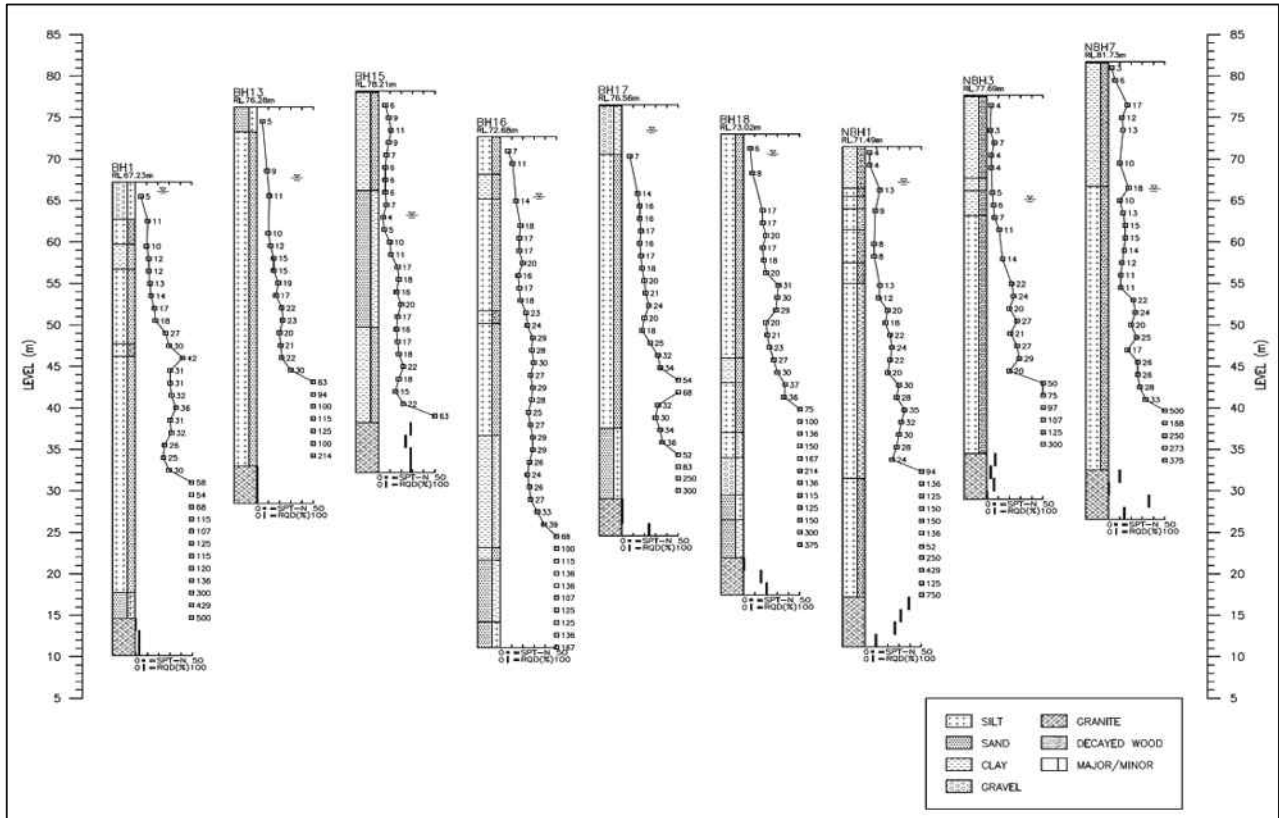


Figure 1. Borehole profiles relevant to soil nail slope.

Critical to the design of the soil nail slope is the assumptions on the skin friction between the ground and the grouted body of soil nail and as such, a series of instrumented pull-out tests on preliminary soil nails (non-working soil nails) were carried out at site to verify the design assumptions. The soil nails adopted at site generally consists of 4m to 18m length soil nails with 16mm to 32mm diameter galvanized high yield reinforcement (yield strength = 460N/mm²) slotted inside a 150mm diameter hole formed by open hole construction (without temporary casing) and filled with Grade 30 non-shrink grout.

3.1 Soil nail pull-out tests

A total of six numbers of instrumented pull-out tests on preliminary soil nails (non-working soil nails) were completed at the time this paper is prepared and the details of the pull-out tests are summarized in Table 1. All the soil nails are 6m length with 5m grouted length and 1m ungrouted length (free length) at the top. Typical set-up for the pull-out tests is shown in Figure 2 while details of the instrumented preliminary soil nails are shown in Figure 3.



Figure 2. Typical set-up for pull-out tests.

tests on preliminary soil nails (non-working soil nails).

Nail No.	Bar Diameter (mm)	Maximum test load achieved (kN)	Nearest borehole
Y-7 (RL 75.19)	25	175.0	BH-15
W/X-16 (RL 71.40)	25	140.0	BH-13
Y-10* (RL 73.24)	25	131.2	BH-15, NBH-3
Y-13* (RL 74.50)	25	148.8	NBH-3
Y-7* (RL 73.24)	25	78.8	BH-15
Y-1/2 (RL 74.00)	32	286.0	NBH-7

Note:

1. Different maximum test load is achieved primarily due to various site issues such as improper test set-up where the dial gauge has reached its maximum travel distance, malfunctioning of the load cell, etc. and not due to inadequate bond strength of the soil.
2. * - Results ignored due to improper preparation of free length at the soil nail head which interferes with instrumentation results.

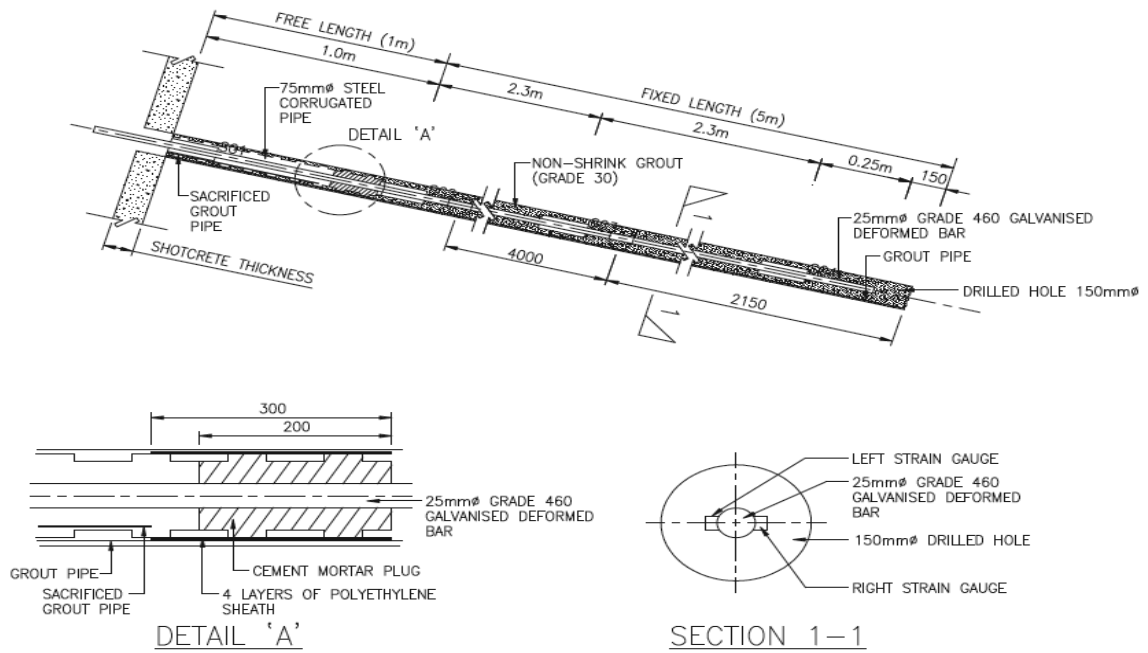


Figure 3. Typical details of instrumented preliminary soil nail.

4 RESULTS OF INSTRUMENTED PULL-OUT TESTS

The test procedures and testing sequence of the soil nails are in accordance with FHWA 1998 and the loading schedule is summarised in Table 2. The pull-out test results showing the mobilised skin friction vs nail movement are shown in Figures 4 to 6.

Table 2. Pull-out tests loading schedule (FHWA 1998).

Load	Hold Time (minutes)
0.25 DTL	10
0.50 DTL	10
0.75 DTL	10
1.00 DTL	10
1.25 DTL	10
1.50 DTL (Creep Test)	60
1.75 DTL	10
2.00 DTL	60
Repeat cycle if test load increased to 3.00 DTL	

Note:

1. DTL – Design test load
2. Test load limited to maximum 80% yield strength of nail reinforcement

The longer holding time of 60 minutes at 1.50 DTL and 2.00 DTL is to monitor creep movement. The acceptance criteria is total creep movement of less than 2mm per log cycle of time between the 6 and 60 minute readings and the creep rate is linear or decreasing throughout the creep test load hold period.

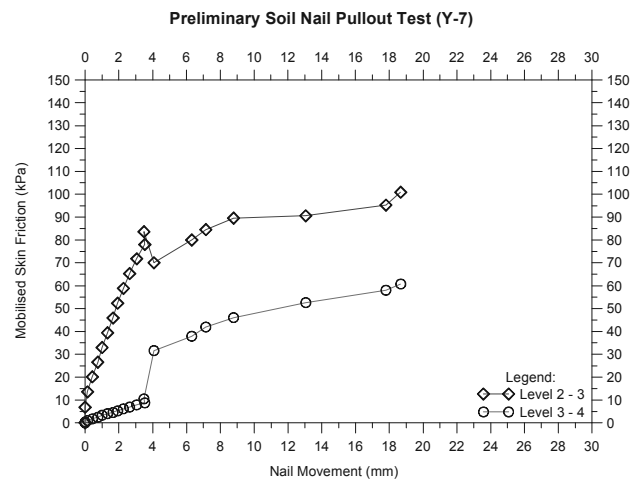


Figure 4. Pull-out test results for nail Y-7.

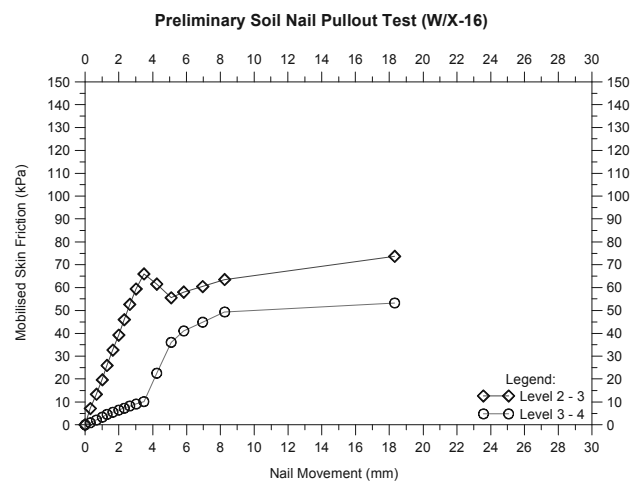


Figure 5. Pull-out test results for nail W/X-16.

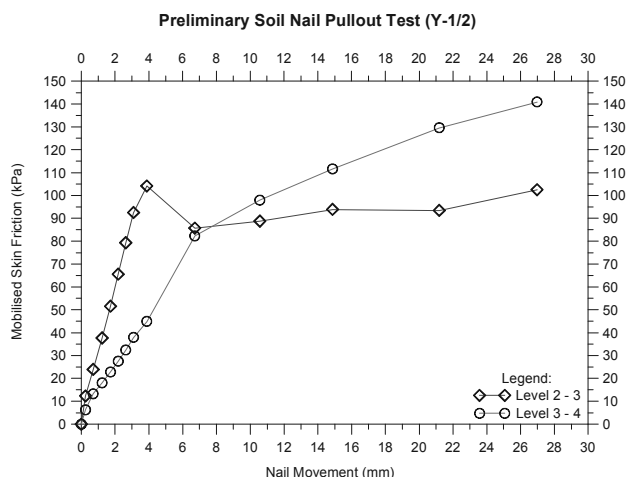


Figure 6. Pull-out test results for nail Y-1/2.

From the pull-out tests, the following observations could be made:

- The ultimate skin friction is mobilised at relatively small nail movement of approximately 4 to 6mm which is about 3-4% of the diameter of the drilled hole.
- Only nail Y-1/2 demonstrates the expected behaviour where initially, more load is transferred to the upper part of the nail until the upper part reaches the ultimate skin friction and thereafter, more load is transferred to the lower part of the nail.
- Other nails (Y-7 and W/X-16) also demonstrated behaviour where initially, more load is transferred to the upper part of the nail. However, the mobilised skin friction for the upper part of the nail has rather unexpectedly continued to increase after the initial drop. This is unexpected and is possibly due to interference from the shotcreted slope surface where the pull-out tests were conducted. It is possible that the shotcreted slope surface restricts the expansion of the soil particles during testing and contributed to the increase in mobilised skin friction for the upper part of the nail.
- The SPT-N values at the level of the tested soil nails typically range from 5 to 13 (average about 10) and the mobilised skin friction recorded range from 50 to 140kPa. This indicate a conservative correlation of skin friction can be 5x SPT-N for soil nail design in weathered granite or fill.
- Results of the pull-out tests also indicate the equation proposed by HA 68/94 (see Eq. 1) underpredicts the mobilised skin friction considerably.

$$Q = \sigma'_n \tan \phi' + c' \text{ (kN/m}^2\text{)} \quad (1)$$

where

σ'_n = average radial effective stress
 ϕ' , c' = soil shear strength parameters

5 CONCLUSIONS

A series of instrumented pull-out tests were carried out for a proposed basement with excavation up to 20m deep supported using soil nailed slope. The pull-out test results indicate a conservative preliminary correlation for skin friction between the ground and the grouted soil nail of 5x SPT-N can be adopted for soil nail design in weathered granite or fill.

Further pull-out tests at deeper layers of the subsoil are currently being carried out at site and the results will be presented in the future. Some improvement to the current test procedures will also be carried out such as hacking a larger area of the shotcreted surface surrounding the test nail in order to ensure the results are not affected by the shotcreted slope surface.

6 ACKNOWLEDGEMENTS

The Authors acknowledge the contributions of Mr. Lim Fang Liang and Mr. Tong Han Seng for their hard work and dedication as part of the geotechnical design team of the project.

7 REFERENCES

- Chow Chee-Meng and Tan Yean-Chin. 2006. Soil nail design: A Malaysian Perspective. *International Conference on Slopes*, 379-400.
- Chow Chee-Meng and Tan Yean-Chin. 2011. Deep excavation for basement via soil nailing method. *APEC Seminar on the State-of-the-practice of Deep Excavation Works from Malaysia, Taiwan and Hong Kong*, 75-94.
- FHWA. 1998. *Manual for design & construction monitoring of soil nail walls*. USA.
- HA 68/94. 1994. *Design Methods for the Reinforcement of Highway Slopes by Reinforced Soil and Soil Nailing Techniques*. UK.

Effects on adjacent buildings from diaphragm wall installation

Effets sur des bâtiments adjacents liés à l'installation de parois moulées

Comodromos E.M., Papadopoulou M.C.
Dept. of Civil Engineering, University of Thessaly, Greece

Konstantinidis G.K.
Manager, Attiko Metro S.A., Greece

ABSTRACT: A new approach for simulating the excavation and construction of subsequent panels is proposed to investigate the effects from the installation of diaphragm walls on the surrounding soil and adjacent buildings. The method has been combined with a 3-D nonlinear analysis and a constitutive law providing bulk and shear modulus variation, depending on the stress path (loading, unloading, reloading). The effects on an adjacent building have been investigated by applying a full soil-structure interaction analysis including the whole building. Contrary to lateral movements, which mostly take place at the panel under construction, it was found that the effect of settlements covers a larger area leading to a progressive settlement increase. The effect highly depends on the distance from the panel under construction. Settlement profiles and settlements at specific points as increasing with subsequent panels installation are given providing the ability of specific monitoring guidelines for the upcoming construction of the diaphragm wall in front of the building.

RÉSUMÉ : Une nouvelle approche pour simuler l'excavation et la construction des panneaux subséquents est proposée pour étudier les effets liés à l'installation de parois moulées adjacents sur les bâtiments et le sol adjacents. La méthode a été associée à une analyse 3-D non linéaire et une loi de comportement qui permet la variation des modules de déformations en fonction des chemins des contraintes. Les effets sur un bâtiment adjacent ont été étudiés en appliquant une analyse d'interaction sol-structures pleine, qui inclut l'ensemble du bâtiment voisin. Contrairement aux mouvements latéraux, qui principalement prennent lieu à partir du panneau en cours de construction, il a été constaté que l'effet des tassements couvre une plus grande région, conduisant à une augmentation progressive de tassements. Les effets dépendent fortement de la distance au panneau en cours de construction. Les profils des tassements et tassements aux points spécifiques augmentant progressivement avec l'installation des panneaux sont donnés en face de l'immeuble où la paroi moulée est en cours de construction.

KEYWORDS: diaphragm walls, soil-structure interaction, multi-stage analysis, buildings settlements.

1 INTRODUCTION

It is widely accepted that the process of installing diaphragm walls can result in potentially significant soil displacements and cause substantial reductions in horizontal stress. Depending on the soil profile, the diaphragm wall configuration (length and construction sequence) and the close existence of adjacent buildings with poor foundations may render the effects of diaphragm wall installation considerable. Field monitoring confirms that ground movements resulting from diaphragm wall installation could be a significant component of the overall displacement (Burland and Hancock 1977, Tedd et al. 1984, Symons and Carder 1993), while centrifuge tests verified the development of the effect as well (Powrie and Kantartzi 1996). Recent field evidences recorded during the on going construction of subway stations in Thessaloniki demonstrated that the component of ground movements resulting from the diaphragm wall installation may be higher than 50% of the overall displacements. It is therefore evident that the simplistic assumption of a 'wished-in-place' wall (installation without any change in stress and cinematic field) commonly applied for design purposes is rather questionable.

The aim of the present paper is to investigate the effect of a diaphragm wall installation to adjacent buildings with relatively poor foundations. The sequential installation of each individual diaphragm wall panel installation was simulated by a substitution of the parameters of excavated elements with those corresponding to the bentonite slurry and later on by the

concrete tremied into the panel. Valuable qualitative and quantitative conclusions regarding the variation of the effects to the adjacent building have been drawn.

1 INSTALLATION PROCEDURE MODELLING

With the aim of minimising disturbance and increase stability during the excavation process, rotary drilling machines for slot excavation have been used in Thessaloniki's underground stations with poor soil conditions. Figure 1, on the left side, shows a rotary drilling machine equipped with cutting wheels and a reverse circulation system. On the right side of Figure 1 the numerical simulation of the excavation process is illustrated. The soil from the surface level down to the upper limit of the rotary wheels (line A), is replaced by a material simulating the bentonite slurry. Appropriate, very small values are attributed to the bulk and the shear modulus of the material. Within that zone the stresses are initialised to the values hydrostatically defined from the weight of bentonite slurry. This simulation process ensures that stresses within this zone remain always equal to the hydrostatic conditions no matter the deformation level. However, in the area occupied by the rotary cutters (area between line A and line B) the development of static hydrostatic pressure is not evident. For this reason, in that zone the stresses are not initialised hydrostatically and only internal gravitational stresses are considered. Within this zone the material (cuttings with bentonite slurry) has higher unit weight and is stiffer than bentonite slurry. The zone undertakes the pressure from the

surrounding elements depending on the internal gravitational stresses, the stiffness and the shear resistance of the surrounding soil elements, and the arching developed around the trench. This complicated mechanism provokes a redistribution of stresses and the surrounding soil elements undergo some deformation. As a result horizontal displacements at the wall/soil interface are governed by the ability of the soil to move in response to the reduction in lateral stresses during the wall installation. The above mechanism leads to a temporary reduction of the horizontal stresses in the surrounding excavation faces, which however increase to the hydrostatic bentonite slurry pressure in the next stage of excavation. When the excavation of a panel is accomplished concrete is cast in place using tremie pipes. The same numerical process is applied to simulate the panel completion, i.e. appropriate values are attributed to the bulk and the shear modulus of the material simulating wet concrete, while, stresses are initialised to the values hydrostatically defined from the weight of wet concrete. When equilibrium is attained, regular concrete values are attributed to bulk and the shear modulus to the panel. The above simulation process is repeated over the entire depth of the panel.

The aforementioned simulation process reflects the construction of a single panel and is applied to all panels in a diaphragm wall. However, the response of each particular panel is greatly influenced by the construction sequence. Obviously when constructing a subsequent panel, with already completed adjacent panels, the effect of arching is strengthened due the high resistance of these elements. As a result a stress increase is observed not only at the adjacent soil, but also on neighbouring panels that have already been casted. Thus over the period of wall construction there will be a progressive transferring of load back and forth laterally, either from a primary panel to the adjacent soil or, as the wall progresses, from new panels to panels previously casted. It can be realised that when accurate prediction of displacements and stresses redistribution are demanded, a profound 3-D nonlinear multi-stage numerical analysis is required.

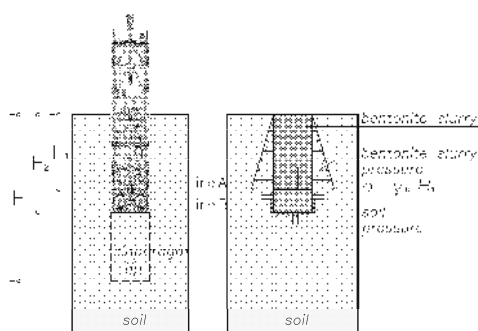


Figure 1. Schematic illustration of the proposed approach for simulating a single panel excavation

2 NUMERICAL SIMULATION

2.1 Project description

The station of Analipsis, 210 m long and 16.4 m wide, is considered as one of the most critical of the underground of Thessaloniki. With the exception of the surficial layer the soil conditions are relatively good. However, the fact that the diaphragm wall is located very close to adjacent buildings with poor foundations, in many cases, renders the construction of the diaphragm wall extremely demanding. According to the guidelines of the German code DIN 4126, the critical zone around the trench excavation extends up to a distance of 70% of the pile length. For this reason a relatively small typical panel length $L = 2.8$ m was applied and a rotary cutting machine was selected to perform the ongoing excavation of the panels. The

thickness of the panels is $t = 1.20$ m, its depth is $H = 44.0$ m and the basement of the station is 28.0 m below the ground surface.

2.2 Soil model and material properties

The ground conditions at the site together with the soil properties of each soil layer, derived from the carried out geotechnical investigation and the evaluation of in-situ and laboratory tests are presented in Table 1. The groundwater level was encountered at 5.0 m below the ground level. Pressuremeter tests were carried out at the area to assess the in situ horizontal stresses and, according to the evaluation of the results, a constant value of $K_0 = 0.54$ has been adopted.

Bearing in mind the crucial effect and the necessity for settlements predictions to the adjacent buildings, a constitutive law with double yielding (FLAC 3D) has been applied in the present study. The model includes a volumetric yield cap surface in addition to Mohr-Coulomb shear and tensile failure envelopes. The cap surface is independent of the shear strength and it consists of a vertical line on a plot of shear stress vs mean stress with a trace on the mean stress axis defined as cap pressure p_c . Any violation of the cap surface produces volumetric plastic strain following a piecewise-linear law prescribed in a user-supplied table. The tangential bulk and shear moduli evolve as plastic volumetric strain takes place according to a special law defined in terms of a constant factor, R , which is the ratio of elastic bulk modulus, K_e , to plastic bulk modulus, K_p . The relevant values adopted are given in Table 1.

The concrete diaphragm wall behaviour was considered as an isotropic linear elastic. Linear elastic behaviour was attributed to the bentonite slurry with infinitesimal deformation values. The shear strength of bentonite slurry with unit weight of 11 kN/m³ is of the order 50 Pa (DIN4126). A reasonable value for the slurry shear modulus is three hundred times the shear strength, $G_{sl} = 15$ kPa, while the Poisson's ratio was taken equal to 0.49. The application of these values to the analysis produced stresses within the bentonite computational domain equal to hydrostatic gravitational state, ensuring that appropriate hydrostatic pressures were developed at the trench faces. A higher value of unit weight (12.5 kN/m³) has been attributed to cutting products mixed with bentonite slurry and similarly the shear modulus has been taken equal to 25 kPa. Taking into account that the construction schedule, the time period between adjacent panels installation, particularly the primary panels, is quite enough for any excess pore dissipation an effective stress analysis was applied.

Table 1. Geotechnical properties of soil layers.

Layer	Fill	A1a	A1b	A1c	B
Depth (m)	0 - 3	3 - 10	10 - 35	35 - 40	40 - 60
Effective cohesion, c' (kPa)	3	3	5	40	50
Effective angle of friction, ϕ' (deg)	30	25	25	25	25
Poisson's ration, ν	0.3	0.3	0.3	0.3	0.3
Plastic bulk modulus, K_p (kPa)	4,000	5,000	8,500	10,000	10,000
Ratio of elastic to plastic bulk modulus, R	5	6.5	10.5	12	12
Cap pressure, p_c (kPa)	100	100	NC*	NC*	NC*

Remark: NC means that cap pressure is equal to the in-situ mean stress

2.3 Simulation procedure

The effective numerical simulation of typical construction procedure for a cast in situ diaphragm wall must reflect the stages and the mechanisms developed during the excavation and throughout the completion of the wall. The first step was to establish the in-situ state of stresses. The construction of a single panel was simulated in 22 stages during which the excavation was advanced in 2.0 m. Within each stage the soil in

the excavation zone was replaced by cutting-bentonite, while the area above the zone being excavated was replaced by bentonite. The end of the excavation was followed by wet concrete placing and the value of $E_{wc} = 1,000$ MPa was attributed to Young's modulus and $\nu_{wc} = 0.49$ to Poisson's ratio. The last stage of analysis corresponded to concrete hardening. The same process was applied to all panels under consideration. The most critical location in the area of the station corresponds to poor building foundation conditions very close to the diaphragm wall. The analysis is therefore focused on that. Prior to the currently presented full soil-structure interaction analysis including a 6-storey building, numerical analyses of a single panel construction and of a wall and an adjacent foundation verified the proposed simulation process as well as the constitutive law and the values for the parameters. Figure 2 shows the foundation plan of the adjacent building together with the location of the diaphragm wall and a curtain of micropiles used to minimize the effect of panels' installation. Further to the bay number of each panel the figure shows the panel type (primary, P, or secondary, S) and the order of installation in the circles on the right side of each panel. The foundation consists of individual footings connected with $0.20 \text{ m} \times 0.50 \text{ m}$ reinforced concrete beams. The foundation level is at 3.0 m from the ground surface. The F.D. mesh included 89,000 3-D elements, 4,272 shell elements and 225 beam elements. The dead weight of the building has been explicitly introduced by the gravity of each element while a uniform load of 5 kPa has been applied to each slab to simulate all other permanent and variable loads. After the establishment of the initial stresses, the installation of the micropiles was introduced followed by the installation of the 9 panels according to the previously described approach. The sequence of installation is presented in Figure 3.

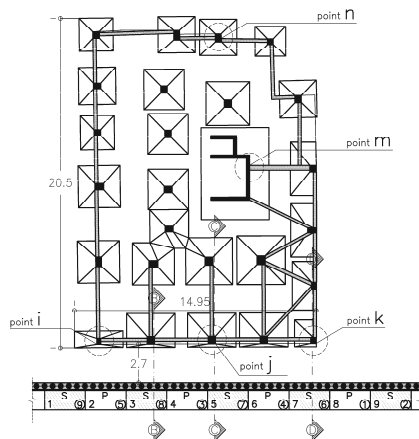


Figure 2. Individual footings of a 6-story building together with the diaphragm wall and the micropiles

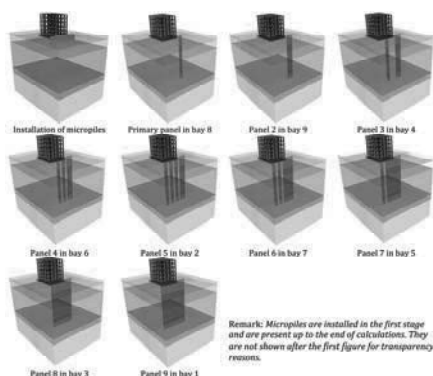


Figure 3. Sequence of panel installation

3 NUMERICAL RESULTS

The contour values for soil settlements, the building floors' settlements and the axial forces of the building columns developed after the completion of the first element (element no 8) are illustrated in Figure 4. For visibility reasons the figure is given in a section at the building face and a cross section at the middle of the building. It can be seen that the maximum soil settlement is located around the excavated panel and is of the order of 2.4 mm. The maximum settlement of the building is located at its corner nearby the excavated panel and the contours show a uniform reduction with distance from that point.

The sequential construction of the next panels provokes the maximum effect in front of each panel, as it has been expected, but at the same time contributes to a progressive increase of settlements in a widespread zone. When the primary panels are installed, an increase of settlements to the value of 4.2 mm is occurred. The soil settlements progressively decrease with the distance from the diaphragm wall and are almost zero at the backside of the building. The completion of the wall with the rest 4 secondary panels does not encounter significant increase to the maximum value of the soil settlements. The final value of maximum settlement is 5.3 mm and the same value is developed at the external side of the building close to the diaphragm wall. From the comparison of the axial forces variation throughout the construction of the panel arises that the panels' installation does not practically affect them.

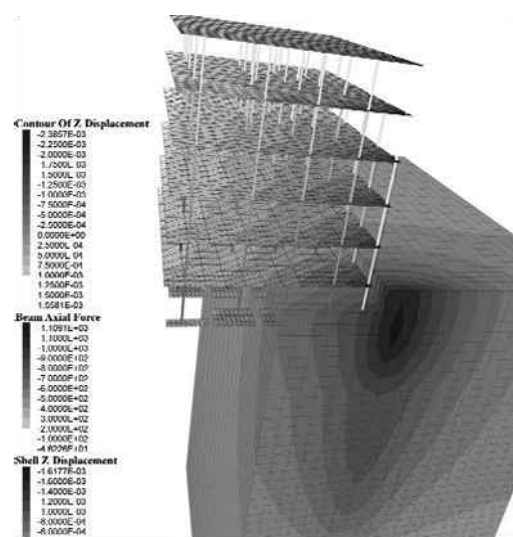


Figure 4. Soil and building settlement contours together with column axial forces after the completion of the first panel (bay no 8)

Figure 5a illustrates the variation of the horizontal displacements with depth below the external boundary of a footing at the front side of the building (cross section 'C-C'). The values are not exceeding the order of 1.0 mm and this is mainly due to the existence of the micropiles. The construction of the panels with bay no 8 and 9 (first and second in construction sequence) are relatively too far from that point and they do not provoke any horizontal displacement at the point under consideration. The panel with bay no 5 is just in front of the point and this explains the important movement of the displacement field during the construction of this panel. Similar are the results in the case of the point below the footing at the edge of the external footing at section 'D-D', Figure 5b.

The most important effect to the adjacent building is the anticipated settlements, the angular distortion that will develop to the foundation and if that last could be capable of provoking any notable bending moment to the foundation elements. Figure 6 illustrates the progressive increase of the settlements across the section 'C-C'. On the same figure the location of the diaphragm wall and the foundation of the building are shown.

The construction of every panel contributes to a progressive increase of settlements, with the maximum influence experienced when the primary panel close to the cross section is installed. This explains the maximum difference observed when panel no 4 is installed. The maximum settlement is developed at the end of the construction of all panels, its value is of the order of 5.5 mm and occurs at the front side of the building.

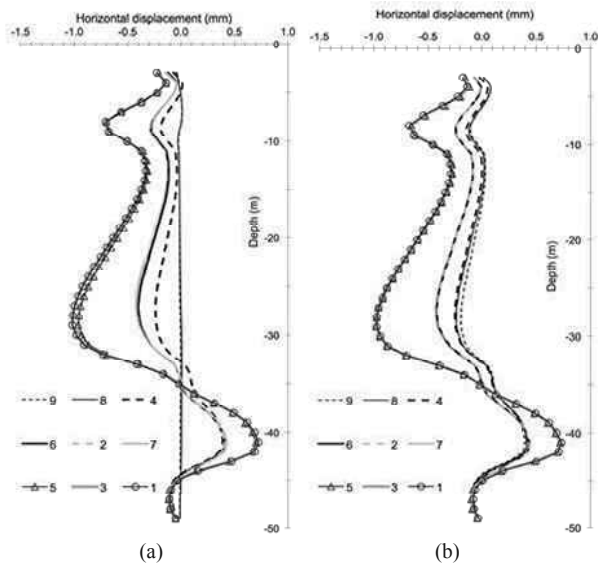


Figure 5. Profile of horizontal displacements below the external footing at (a) the mid-face, point j, and (b) the end-face of the building, point k

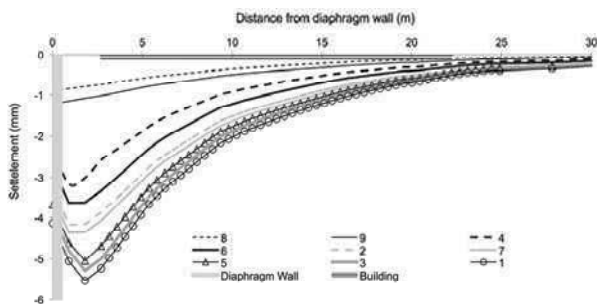


Figure 6. Development of settlement profile with panel sequence construction at cross section 'C-C'

It is worth noticing that the settlement values estimated from the 3-D analysis are leading to an angular distortion of 1:5,000. This value is considerably lower than the limits provided by CIRIA and the CFEM.

An effective design of complex retaining structures, with closely adjacent buildings, includes instrumentation and monitoring to ensure the safety of the construction and control the effect on the adjacent buildings. These data will be available when the diaphragm wall at this area will commence and histograms giving the contribution to cumulative settlements of each particular panel can be drawn. It is therefore extremely helpful to give these histograms resulting from the 3-D analysis and follow up the values as the wall is constructed. Figure 7 illustrates the numerically established cumulative settlements after the completion of each panel, at the characteristic points, i, j, k, m and n. The location of each panel corresponds to relative position from left to right, while the installation sequence is given on the top of the histograms.

It can be seen that the final settlements at the front face of the building (points i, j and k) are of the same magnitude and that the values provided for the points far from the diaphragm wall (points m and n) are drastically lower and with no practical effect on the building. It is clearly evident that Figure 7 can be efficiently used to compare settlements during the up coming

construction and provide alarm signal in case of significantly higher settlements values.

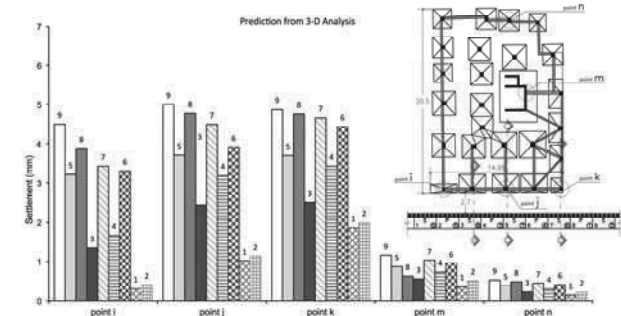


Figure 7. Predicted development of cumulative settlements at points i, j, k, m and n at the end of each panel construction

4 CONCLUSION

In this paper the effects from the installation of diaphragm walls have been investigated using a new approach for simulating the excavation and construction of subsequent panels. The method has been combined with a 3-D nonlinear analysis and a constitutive law providing bulk and shear modulus variation, depending on the stress path (loading, unloading, reloading). It has been observed that the most significant effect in front of a given panel occurs during the installation of that panel and that the effect on stress reduction and lateral movements in front of the subsequent panels is rather limited. The method has been used to estimate the effects on an adjacent 6-storey building by applying a full soil-structure interaction including the whole building. Progressively increased with subsequent panels installation settlement profiles are given along the building foundation. Moreover, settlements at specific points where leveling captures have been installed are given in cumulative form. The predictions indicate that the angular distortion of the building remains under the required limits of serviceability and at the same time provide the guidelines for the monitoring of the upcoming construction of the diaphragm wall in front of the building.

5 REFERENCES

Burland J.B. and Hancock R.J.R. 1977. Underground car park at the House of Commons, London: geo- technical aspects. *Struct Engr* 55 (2), 87-100.
 Tedd P., Chard B.M., Charles J.A. and Symons I.F. 1984. Behaviour of a propped embedded retaining wall in stiff clay at Bell Common Tunnel. *Géotechnique* 34 (4), 513-32.
 Symons I.F. and Carder D.R. 1993. Stress changes in stiff clay caused by the installation of embedded retaining walls. *Retaining structures*. Thomas Telford, London.
 Powrie W. and Kantartzi C. 1996. Ground response during diaphragm wall installation in clay: centrifuge model tests. *Géotechnique* 46 (4), 725-39.
 DIN 4126. 1986. *Cast-in-situ concrete diaphragm walls*. Berlin.
 Itasca. 2009. *FLAC3D, Fast Lagrangian analysis of continua*, version 4.0: User's and theory manuals. Itasca Consulting Group, Inc. Minneapolis.
 CIRIA. 1983. *Settlement of structures on clay soils. Report 113*, London.
 Canadian Geotechnical Society. 1992. *Canadian foundation engineering manual*. British Publishers Ktd, Vancouver.

Prise en compte des effets de bord dans un massif renforcé par inclusions rigides

Modeling edge effects at the periphery of a rigid inclusion reinforced soil volume

Cuira F., Simon B.
TERRASOL, Paris, France

RÉSUMÉ : En périphérie d'un massif de sol renforcé par inclusions rigides il se développe une interaction entre la zone renforcée et la zone non renforcée. Ces effets de bord rendent inapplicables les modèles limités à l'étude d'une cellule élémentaire au sein d'un réseau infini d'inclusions qui adoptent l'hypothèse d'un cisaillement nul sur la frontière de la maille étudiée. Le modèle exposé de type biphasique exprime les équations d'équilibre dans deux domaines apposés, « inclusion » et « sol », en introduisant à la fois le cisaillement interne qui se développe entre l'inclusion et le sol tributaire et le cisaillement externe qui se développe sur tout ou partie de la frontière de la maille, lorsque celle-ci est située en périphérie de la zone renforcée par inclusions. Les cisaillements sont pris en compte en exploitant la notion de loi de transfert t-z appliquée au déplacement relatif entre les domaines considérés. La résolution s'appuie sur une discrétisation 1D des deux domaines et une formulation éléments finis. Différents exemples de semelles sur inclusions sont présentés dont les résultats s'avèrent en bon accord avec ceux de modèles numériques 3D, beaucoup plus complexes à mettre en œuvre. L'évaluation de la méthode se poursuit en exploitant les résultats de modèles physiques en centrifugeuse.

ABSTRACT: At the periphery of a soil volume reinforced by rigid inclusions, interaction between the reinforced soil and the unreinforced soil cannot be neglected. Such edge effects prevent use of the commonly used unit cell model which assumes no shear at the model outer boundary. The proposed model, a simplified form of a two-phase model, expresses equilibrium within two side by side domains « inclusion » and « soil » by introducing shear between inclusion and the tributary soil volume within the cell on the one hand and shear along all or part of the outer “soil” domain boundary, on the other hand, when cell under study is at periphery of the reinforced volume. Shear is taken into account through use of t-z transfer curves based on the domain relative displacements. A 1D discrete model of both domains is used together with a finite element formulation. This is applied to different cases of footings over soil reinforced by rigid inclusions. Results agree well with those obtained by other 3D numerical models, which remain a far more difficult task. Further evaluation is planned using the results of centrifuge test models.

MOTS-CLÉS: renforcement du sol, inclusions rigides, semelle sur inclusions, modèle analytique, effets de bord.

KEYWORDS: soil reinforcement, rigid inclusions, shallow foundations, analytical modelling, edge effects.

1 INTRODUCTION

Le renforcement par inclusions rigides a vu son intérêt largement reconnu pour les ouvrages étendus de type remblais ou dallages (locaux industriels). Le dimensionnement s'appuie généralement sur des modèles de calcul réduits à l'étude d'une cellule élémentaire représentant le comportement d'une maille courante centrée sur une inclusion et incluant le volume de sol et la fondation d'ouvrage afférents (Cuira et Simon, 2009, Simon, 2012). Le caractère répété du motif permet de considérer que le cisaillement est nul au bord du modèle, ce qui en simplifie considérablement la construction. Ces modèles apportent tous les éléments nécessaires au dimensionnement des ouvrages en partie courante ; leur validité a été largement éprouvée dans le cadre du projet national ASIRI (2012) par la confrontation des résultats obtenus avec ceux d'expérimentations en vraie grandeur, de modèles physiques ainsi que de modélisations numériques avancées. Ils sont en revanche insuffisants pour traiter des zones périphériques où les cellules placées au bord sont en interaction avec des cellules intérieures mais aussi avec le massif extérieur non renforcé : l'hypothèse de symétrie permettant de considérer un cisaillement nul aux bords du modèle n'est plus applicable. La validité de ces modèles se heurte également au cas des ouvrages d'emprise limitée tels des semelles sous poteaux ou voiles porteurs, pour lesquels la prise en compte des phénomènes de bord devient là encore une nécessité absolue.

La modélisation de ces configurations particulières (bord d'ouvrage étendu ou ouvrage d'emprise limitée) nécessite en toute rigueur des modèles en trois dimensions dont les limites doivent être étendues largement au-delà du volume de sol renforcé, à la différence des modèles de cellule élémentaire. Une telle modélisation est incontestablement mal adaptée à des études courantes, appelées de surcroît et en dépit du caractère

non exceptionnel des fondations concernées, à examiner un grand nombre de cas de charges. Les Recommandations ASIRI (2012) ont ainsi détaillé plusieurs méthodes simplifiées pour traiter ces configurations dans le cas d'un chargement vertical avec des outils classiques du calcul des fondations. Toutes ces méthodes nécessitent cependant une procédure par étapes.

Cette communication présente la généralisation d'une de ces méthodes qui permet de s'affranchir d'un calcul par étapes, en traitant simultanément les interactions internes se développant au sein du massif renforcé et externes se développant aux bords de celui-ci avec le sol environnant non renforcé. L'équilibre mécanique du volume renforcé est ainsi exprimé en combinant des lois d'interface sol/inclusions (internes) et sol/sol (externes), toutes basées sur les déplacements relatifs afférents.

2 ASPECTS THEORIQUES

2.1 Principe

On considère le cas d'une cellule élémentaire représentant une maille quelconque (courante ou périphérique) centrée sur une inclusion. La cellule est soumise à un chargement vertical et est décomposée en deux domaines complémentaires : le domaine « inclusion » constitué par l'inclusion elle-même et les volumes de sol qui la prolongent jusqu'aux limites inférieure et supérieure du modèle, et le domaine « sol » constitué par le volume de sol complémentaire au domaine « inclusion ». L'interaction entre les deux volumes est supposée entièrement décrite par le cisaillement vertical τ_{int} qui se développe sur leur frontière verticale définie par le périmètre de l'inclusion noté P_{int} . En périphérie de la cellule, l'interaction éventuelle avec le sol environnant non renforcé est supposée entièrement décrite

par un cisaillement vertical extérieur τ_{ext} comme le schématise la figure ci-dessous.

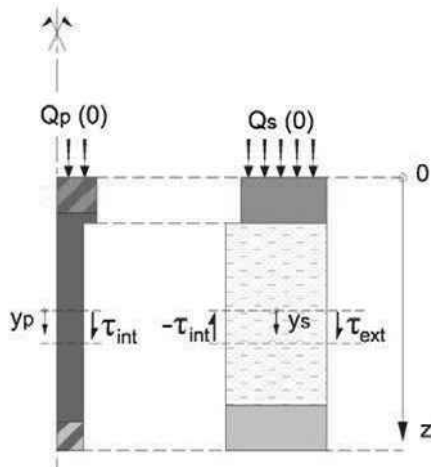


Figure 1. Modèle généralisé de la cellule élémentaire – vue en coupe.

Le cisaillement extérieur τ_{ext} est supposé se développer sur une fraction $\beta \times P_{ext}$ ($0 \leq \beta \leq 1$) du périmètre extérieur total P_{ext} de la cellule comme le schématise la figure ci-dessous.

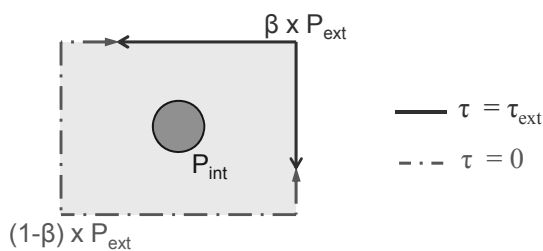


Figure 2. Modèle généralisé de la cellule élémentaire – vue en plan.

Les deux domaines sont assimilés à deux cylindres concentriques de sections équivalentes. On désigne par $S_p(z)$ la section du domaine « inclusion » à la profondeur z . La section du domaine « sol » s'en déduit à l'aide de la relation : $S_s(z) = S_{maille} - S_p(z)$ où S_{maille} désigne l'aire totale de la maille.

2.2 Mise en équation

On désigne par $y_p(z)$ et $y_s(z)$ les tassements respectifs des domaines « inclusion » et « sol ». La combinaison des équations d'équilibre et de comportement des cylindres équivalents aux deux domaines conduit au système d'équations (1), où $E_p(z)$ et $E_s(z)$ représentent respectivement les modules de déformation verticale des domaines « inclusion » et « sol ». Pour le domaine « sol », le tassement $y_s(z)$ est supposé uniforme à toute profondeur z et $E_s(z)$ est assimilé au module équivalent pour l'amplitude de chargement calculée.

$$\text{Domaine inclusion} \quad E_p S_p \frac{d^2 y_p}{dz^2} = \tau_{int} P_{int} \quad (1)$$

$$\text{Domaine sol} \quad E_s S_s \frac{d^2 y_s}{dz^2} = -\tau_{int} P_{int} + \beta \tau_{ext} P_{ext}$$

L'interaction entre les deux domaines est décrite au niveau de chaque couche par une fonction de transfert exprimant la dépendance du cisaillement τ_{int} avec le déplacement relatif entre les deux domaines :

$$\tau_{int} = f(y_p - y_s) \quad (2)$$

L'interaction éventuelle entre la cellule et le sol environnant non renforcé est décrite par une fonction de transfert reliant le

cisaillement extérieur τ_{ext} au déplacement absolu du domaine sol :

$$\tau_{ext} = f(y_s) \quad (3)$$

La combinaison des équations (1), (2) et (3) conduit à un système global à 4 équations et 4 inconnues : y_p , y_s , τ_{int} et τ_{ext} .

2.3 Résolution

Le système précédent est complété par les conditions aux limites suivantes :

- charge totale appliquée en tête du modèle $Q_p(0)+Q_s(0)$;
- fraction de charge transmise en tête du domaine inclusion $E_{QP} = Q_p(0)/[Q_p(0)+Q_s(0)]$;
- loi de mobilisation de l'effort de pointe avec le déplacement relatif.

En présence d'un élément de fondation rigide en surface (radier ou semelle), la valeur de E_{QP} est établie en recherchant l'égalité des tassements en surface $y_p(0)$ et $y_s(0)$, ce qui est justifié par le fait que les déformations de l'élément structural de surface sont négligeables devant celles du sol.

La résolution numérique du système est menée à l'aide d'une formulation en éléments finis. Chacun des deux domaines est discrétisé selon un maillage unidimensionnel avec des éléments à deux nœuds et un degré de liberté par nœud. Dans le cadre de cette discrétisation, le système d'équations précédent s'écrit sous la forme d'un système matriciel équivalent, ce qui simplifie la résolution. La non-linéarité des courbes de transfert implique une procédure itérative visant à assurer la compatibilité en tout point entre cisaillement et déplacement.

2.4 Mise en œuvre pratique

2.4.1 Choix du paramètre β

L'introduction du paramètre β dans le modèle de la cellule élémentaire permet d'aller au-delà de la configuration particulière d'une maille courante où les conditions de symétries justifient l'hypothèse d'un cisaillement nul en périphérie du modèle ($\beta = 0$). Le choix d'un $\beta \neq 0$ implique la prise en compte d'un cisaillement extérieur entre la cellule et le sol environnant non renforcé, sur une partie du périmètre extérieur de la cellule. Dans le cas d'une maille carrée (figure ci-dessous), cela peut être par exemple représentatif d'une cellule située au bord du massif renforcé ($\beta = 0,25$), le cas d'une cellule située à l'angle ($\beta = 0,5$), le cas d'une semelle sur deux inclusions ($\beta = 0,75$) ou une inclusion unique ($\beta = 1$).

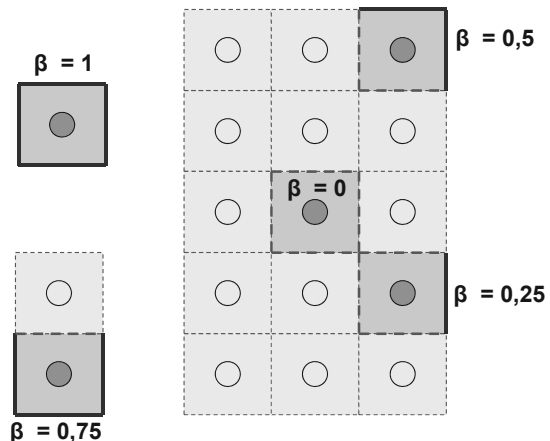


Figure 3. Choix du paramètre β pour le cas d'une maille carrée.

2.4.2 Fonctions de transfert

Ces fonctions de transfert sont utilisées pour caractériser la mobilisation des cisaillements interne (τ_{int}) et externe (τ_{ext}) ainsi que les réactions en pointe. On utilise pour cela les lois bilinéaires du type proposé par Frank et Zhao (1982) caractérisées par deux paramètres : un paramètre de pente (K_i ou K_p) et une valeur de contrainte limite (q_s ou q_p).

Pour le cisaillement interne et la mobilisation des réactions en pointe, ces lois sont construites directement à partir des paramètres pressiométriques.

Pour le cisaillement extérieur τ_{ext} , la valeur de contrainte limite q_s peut être reliée à la contrainte verticale dans le sol non renforcé σ_{v0} par une relation du type $q_s = k \tan \delta \cdot \sigma_{v0}$. Les valeurs choisies pour q_s et le paramètre de pente peuvent être ajustés de manière à retrouver par le modèle du type exposé, appliqué au cas d'une inclusion de section nulle, un tassement identique à celui de la semelle superficielle rigide sur sol non renforcé calculé par la méthode pressiométrique (Frank, 1999).

3 APPLICATION SIMPLE : CAS D'UNE SEMELLE SUR UNE SEULE INCLUSION

3.1 Paramètres d'entrée

L'exemple étudié est celui d'une semelle carrée de 1,33 m de côté, renforcée par une seule inclusion de diamètre 40 cm placée dans l'axe. Deux situations sont étudiées : le cas d'une semelle en contact direct avec l'inclusion (mode « fondation mixte »), et le cas d'une couche de forme intercalaire de 50 cm d'épaisseur (mode « inclusion rigide »). La figure ci-dessous présente la coupe du calcul et les données géotechniques utiles.

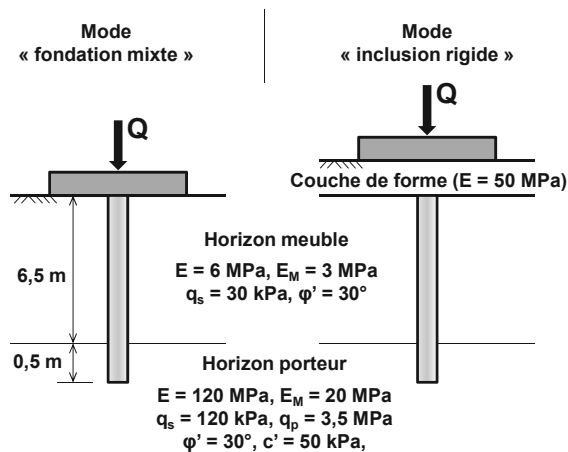


Figure 4. Cas d'une semelle sur une seule inclusion - Coupe de calcul.

Dans le cas d'une maille unique, le paramètre β est pris égal à 1,00 : le cisaillement extérieur avec le massif de sol non renforcé se développe sur tout le périmètre. Les fonctions de transfert sont constituées selon la démarche décrite en §2.4.2 : en particulier, pour le cisaillement extérieur, le calage du paramètre de pente K_i conduit à une valeur équivalente de $K_i = 2,7$ MPa/m. Pour le mode « inclusion rigide », le domaine inclusion est prolongé dans le matelas : la loi d'interface entre les domaines inclusion et sol sur la hauteur du matelas est construite en considérant un module pressiométrique $E_M = 10$ MPa et un frottement unitaire limite égal à $k \tan \delta \cdot \sigma_s$ avec $k \tan \delta = 1$ -et σ_s la contrainte verticale moyenne dans le domaine sol, sur la hauteur du matelas.

Les résultats du calcul sont comparés à ceux d'un traitement en éléments finis sous PLAXIS (modèle axisymétrique équivalent). Dans ce modèle, tous les sols ont un comportement élasto-plastique parfait avec un critère de rupture de Mohr Coulomb : les paramètres d'entrée sont ceux de la Figure 4. Le

choix des paramètres, et notamment ceux décrivant le comportement en pointe (module de déformation et paramètres de cisaillement), a été validé au préalable par calage des courbes de chargement axial d'une inclusion isolée chargée directement en tête (sans semelle), calculées respectivement par un modèle PLAXIS ou un modèle analytique à l'aide des lois de Frank et Zhao.

3.2 Sans matelas de répartition : mode « fondation mixte »

La première situation étudiée est celle d'un contact direct entre la semelle et l'inclusion (fondation mixte). Une partie de la charge totale Q appliquée sur la semelle est reprise par le sol, mais le frottement mobilisé sur la hauteur de l'inclusion demeure positif : la charge maximale dans l'inclusion est obtenue en tête. La figure ci-dessous présente les résultats obtenus selon un diagramme Effort – Tassement. Deux courbes sont représentées : celle du tassement de la semelle en fonction de la charge appliquée (Courbe 1), et celle du tassement de la semelle (= tassement en tête de l'inclusion) en fonction de l'effort maximal dans l'inclusion (Courbe 2). Les résultats se révèlent en bon accord avec ceux de PLAXIS.

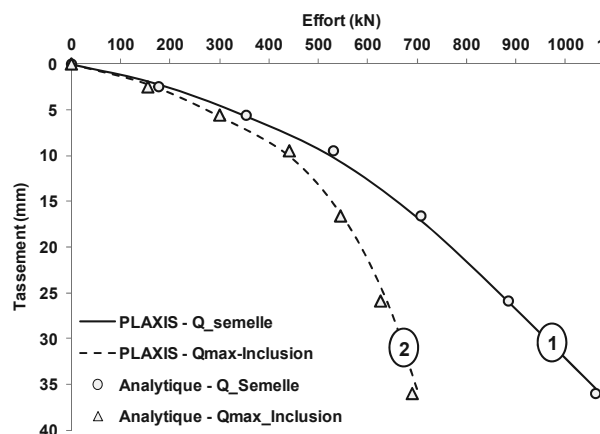


Figure 5. Effort sur la semelle et effort maximal dans l'inclusion en fonction du tassement en tête - cas d'une fondation mixte.

3.3 Avec matelas de répartition : mode « inclusion rigide »

Dans cette situation, une couche de forme sépare la semelle de l'inclusion. La principale différence avec le cas précédent est l'apparition d'un frottement négatif : l'effort maximal dans l'inclusion n'est pas obtenu en tête mais au niveau du plan neutre identifié ici vers 1,0 m de profondeur. La même concordance peut être observée avec PLAXIS.

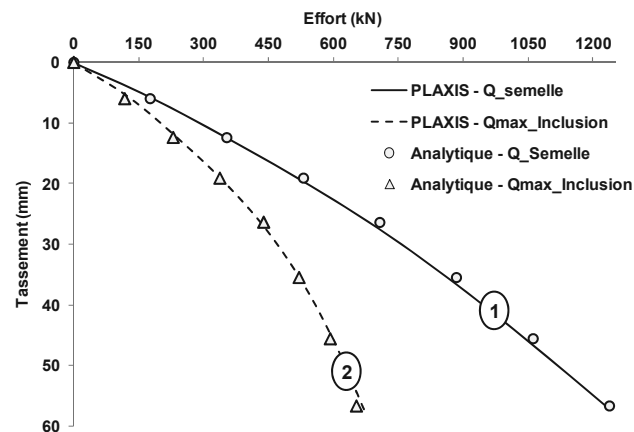


Figure 6. Effort sur la semelle et effort maximal dans l'inclusion en fonction du tassement en tête du modèle - cas d'une inclusion rigide.

4 CAS D'UNE SEMELLE SUR QUATRE INCLUSIONS RIGIDES

La situation choisie correspond à une étude numérique conduite dans le cadre du projet ASIRI. Une semelle carrée de côté 2,8 m repose par l'intermédiaire d'un matelas de répartition d'épaisseur 0,5 m sur un sol compressible renforcé par 4 inclusions de diamètre 0,34 m. Le sol compressible repose sur un substratum rigide et est légèrement surconsolidé (surconsolidation de 10 kPa).

Cette configuration a fait l'objet d'une étude paramétrique détaillée à l'aide du logiciel Flac 3D, couvrant un large éventail de cas de charge appliqués à la semelle (Dias et Simon, 2012). La comparaison concerne le cas d'un chargement de la semelle par un effort vertical centré $Q = 1568$ kN.

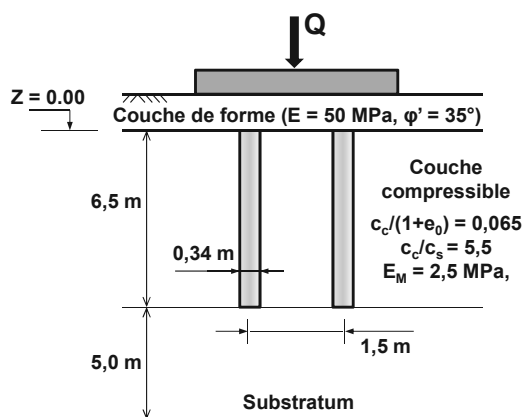


Figure 7. Cas d'une semelle sur quatre inclusions - Coupe de calcul.

La méthode exposée a été appliquée à un modèle représentant un quart de la semelle en adoptant pour le paramètre β la valeur 0,5. Les lois d'interaction sont construites selon la formulation de Frank et Zhao en adoptant les valeurs K_t et K_p calculées avec $E_M = 2,5$ MPa et en ajustant les valeurs limites relatives au cisaillement τ_{int} pour respecter la relation $q_s(z) = K \tan \delta \cdot \sigma_s(z)$ où $\sigma_s(z)$ désigne la contrainte verticale dans le domaine sol à la cote z et celles concernant le cisaillement τ_{ext} pour respecter la relation $q_s(z) = K \tan \delta \cdot \sigma_{v0}'(z)$ où $\sigma_{v0}'(z)$ désigne la contrainte verticale initiale dans le massif non renforcé à la cote z . Le facteur $K \tan \delta$ a été pris égal à 0,3 pour le cisaillement intérieur comme celui extérieur.

La Figure 8 présente les tassements calculés dans les domaines « inclusion » et « sol » en fonction de la profondeur.

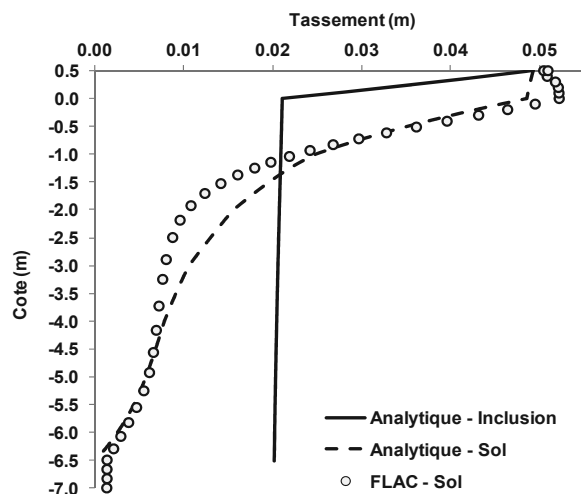


Figure 8. Profils de tassement des domaines « inclusion » et « sol » et comparaison à celui calculé dans l'axe du modèle Flac3D.

Le plan neutre s'établit 1,5 m sous la base du matelas. Le tassement dans le domaine « sol » se révèle proche de celui obtenu dans l'axe de la semelle par le modèle Flac3D.

La Figure 9 présente la distribution des efforts $Q_s(z)$ et $Q_p(z)$ avec la profondeur sous le sommet de la semelle ; l'effort $Q_p(z)$ dans l'inclusion est maximal au niveau du plan neutre. La valeur atteinte se révèle d'un ordre de grandeur comparable à celle du modèle Flac3D, même si celui-ci révèle le plan neutre à une profondeur supérieure.

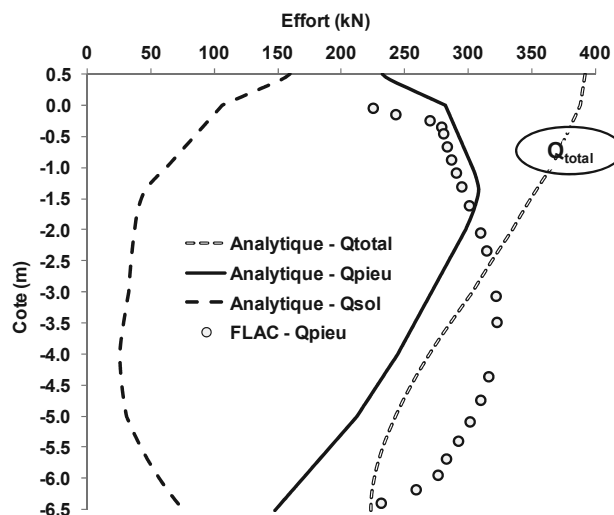


Figure 9. Effort axial dans les domaines « inclusion » et « sol » et comparaison à celui calculé dans une inclusion du modèle Flac3D.

La figure ci-dessus présente également l'évolution de l'effort total [$Q_s(z) + Q_p(z)$] avec la profondeur : celui-ci varie de 392 kN en tête du modèle (seul un quart de la semelle a été modélisé) à 224 kN à la base. La dissipation observée ($392 - 224 = 168$ kN) est liée au cisaillement extérieur représentant les interactions avec le sol environnant non renforcé.

5 CONCLUSION

La méthode analytique exposée permet de prendre en compte les effets de bord qui sont à considérer autour d'un massif de sol renforcé par inclusions rigides. La comparaison des résultats ainsi obtenus à ceux issus de modèles 3D éléments finis ou différences finies, beaucoup plus complexes à mettre en œuvre s'avère tout à fait encourageante. L'évaluation de la méthode se poursuit sur des résultats de modèles physiques en centrifugeuse.

6 REFERENCES BIBLIOGRAPHIQUES

- ASIRI 2012, *Recommendations for the design, construction and control of rigid inclusion ground improvements*, IREX – Presses des Ponts, Paris.
- Cuir F. & Simon B. 2009, Deux outils simples pour traiter des interactions complexes d'un massif renforcé par inclusions rigides, 17th ICSMGE, Alexandria, 1163-1166.
- Dias D. & Simon B. 2012, Spread foundations on rigid inclusions subjected to complex loading: comparison of 3D numerical and simplified analytical modelling, TC211, IS-GI Brussels.
- Frank R. & Zhao S.R. 1982, Estimation par les paramètres pressiométriques de l'enfoncement sous charge axiale des pieux forés dans les sols fins. *Bull. Liaison P. et Ch.*, 119, 17-24.
- Frank R. 1999, *Calcul des fondations superficielles et profondes*, Techniques de l'Ingénieur – Presses des Ponts, Paris.
- Simon B., 2012, General report S5, Rigid inclusions and stone columns, TC211, IS-GI Brussels.

Influence of facing vertical stiffness on reinforced soil wall design

Influence de la rigidité verticale du parement dans la conception des murs en sols renforcés

Damians I.P., Lloret A., Josa A.
Universitat Politècnica de Catalunya (UPC) – BarcelonaTech

Bathurst R.J.
Royal Military College of Canada

ABSTRACT: Current design practices for reinforced soil walls typically ignore the influence of facing type and foundation compressibility on the magnitude and distribution of reinforcement loads in steel reinforced soil walls under operational conditions. In this paper, the effect of the facing vertical stiffness (due to elastomeric bearing pads placed in the horizontal joints between panels) on load capacity of steel reinforced soil walls is examined in a systematic manner using a numerical modelling approach. Numerical modelling was carried out using the commercial finite element program PLAXIS. The numerical model was verified against measurements recorded for an instrumented 6 m-high wall reinforced with steel strips. The influence of the facing stiffness and backfill-foundation stiffness combinations on the vertical load through the facing and on the magnitude and distribution of the reinforcement loads was examined. For walls subjected to operational (working stress) conditions at end of construction, the numerical results confirm that the vertical stiffness of the facing and soil-stiffness combinations can have a great effect on the vertical facing loads and on the magnitude and distribution of the load mobilized in the soil reinforcement layers.

RÉSUMÉ: Les pratiques actuelles de conception des murs en sol renforcé ignorent généralement l'influence du type du parement et de la rigidité de la fondation sur l'ampleur et la répartition des charges de renforcement. Dans cet article, on utilise une approche par modélisation numérique pour examiner systématiquement l'effet de la rigidité du parement vertical (due à la présence de cales en élastomère placées dans les joints horizontaux entre panneaux) sur la capacité de charge des murs renforcés sol/acier. La modélisation numérique a été réalisée à l'aide du code commercial Éléments Finis PLAXIS. Le modèle numérique a été validé sur des mesures enregistrées lors de l'expérimentation d'un mur d'une hauteur de 6 m et renforcé par des bandes d'acier. Le modèle permet de tester l'influence de différentes combinaisons entre la rigidité du parement et celle du remblai-fondation sur les valeurs des charges verticales dans le parement et les efforts dans les éléments de renforcement. Pour les murs travaillant en conditions opérationnelles (sous efforts de service) à la fin de leur construction, les résultats numériques confirment que ces combinaisons ont un grand effet sur les charges verticales et la distribution des efforts mobilisés dans les couches de renforcement.

KEYWORDS: reinforced soil retaining walls, steel strips, facing panels, finite element modelling.

1 INTRODUCTION AND GENERAL APPROACH

The mechanical behaviour of reinforced soil walls is complicated due to the mechanical complexity of the component materials (including soil type/arrangement), their interactions, wall geometry, and the influence of method of construction. Most reinforced soil walls are designed assuming that the wall foundation is rigid and/or does not influence the magnitude and distribution of reinforcement loads under operational conditions. This assumption may not apply to walls constructed over compressible foundations. This paper describes the results of a series of numerical simulations that were carried out on a 6-m high wall with precast concrete panels with metallically reinforced soil and constructed with backfill (reinforced soil and retained fill) and foundation soils having different stiffness, and different number of horizontal joints (i.e. different height of the panel units) along the facing elevation.

The program PLAXIS (PLAXIS 2008) was used to carry out the numerical simulations. The reference case for model calibration is the instrumented 6 m-high precast panel facing wall reinforced with steel strips reported by Chida and Nakagaki (1979). All the results in the present study correspond to operational (working stress) conditions at the end of the construction.

2 NUMERICAL MODEL

2.1 General

The PLAXIS global geometry, structural components, and the numerical mesh to simulate the performance of the reference instrumented case are illustrated in Figure 1.

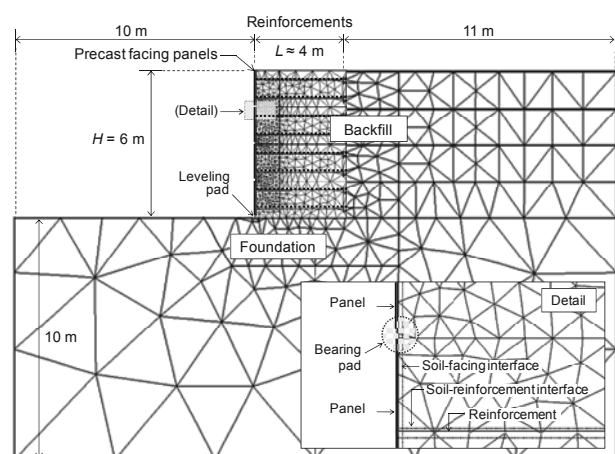


Figure 1. PLAXIS numerical model

2.2 Materials properties

2.3.1 Soil

Material properties for the soil zones (backfill and foundation) are summarized in Table 1. Two different stiffness of the backfill were considered to represent different scenarios due to the effects of compaction. The more compressible soil case (with assumed $E_{backfill} = 10$ MPa) does not imply that poorly compacted soils should be used in the construction of these types of structures, but was used to ensure detectable differences between simulation outcomes. Moreover, the first meter of reinforced soil in contact with the facing is commonly constructed with less compaction energy and hence was assumed to have one half the stiffness of the fully compacted soil. Two other cases were assumed for the foundation soil; nevertheless, the actual foundation stiffness for the reference wall case was not reported by Chida and Nakagaki. The stiffness combinations in Table 1 result in four boundary cases to be examined.

Plane-strain boundary conditions were considered for the selection of the internal friction angle of the soils. The soil material properties also define the strength and stiffness of the interfaces between the soil and the structural elements (panels and reinforcement) using a reduction factor (R_i), which is the ratio of interface shear strength to shear strength of the surrounding soil. The values chosen for this factor in each case (soil-facing and soil-reinforcement) are based on reported data and actual mechanical behavior of these interactions.

Table 1. Model properties of the soil materials

Parameters	Foundation	Backfill	
		> 1.0 m from face	< 1.0 m from face
Unit weight (kN/m ³)	20	18	18
Cohesion (kPa)	1	1	1
Friction angle (°)	36	44	44
Dilatancy angle (°)	6	14	14
Elastic modulus (MPa)	10 – 1000	10 & 100	5 & 50
Poisson's ratio	0.3	0.3	0.3
Interface reduction factor	1	1	0.3 & 0.6

2.3.2 Reinforcement

Reinforcement elements were modelled using the “geogrid” PLAXIS elements as continuous sheets that have only axial stiffness and can transmit load to the surrounding soil through interface shear (R_i parameter). The equivalent linear-elastic axial stiffness of the geogrid element for each layer of reinforcement elements is computed as follows:

$$(EA)_{geogrid} = E_{reinforcement} A_{reinforcement} \frac{n_{reinforcements}}{L_{panel}} \quad (1)$$

Where: $E_{reinforcement}$ is the stiffness modulus of the reinforcement layers (200 GPa for steel); A_{strip} is the cross-sectional area of one strip (100 × 2.3 mm); n_{strips} is the number of strips along one panel (two strip-units), and L_{panel} is the panel width assumed as 1.5 m. The resulting axial stiffness of the geogrid element is about 60 MPa/m. Other analyses considering different axial stiffness modulus equivalent to other steel reinforced types (e.g. bar mats with axial stiffness about 40 MPa/m) do not generate significant variations from the results presented in this study.

2.3.3 Facing-beam elements

The facing was defined by PLAXIS “beam” elements, and is comprised of the panels and the elastomeric bearing pads. The bearing pads are installed in the horizontal joints between contiguous vertical panels and are used in practice to prevent concrete-to-concrete panel contact.

Material properties for the concrete facing panels and horizontal joints are summarized in Table 2. The material type, dimensions and number of bearing pads can vary between projects (Neely and Tan 2010). The same Equation 1 can be used to obtain the parametrical values of the bearing pad elements (Damians et al 2013). In the present analyses, two EPDM (ethylene propylene diene monomer (M-class) rubber) bearing pads were assumed in each horizontal joint between per panel width.

Table 2. Model properties of the beam elements

Parameters	Panels	Bearing pads (EPDM)
Axial stiffness (MN/m)	6.0	0.1
Bending stiffness (kN/m ² /m)	11	0.3
Weight (kN/m/m)	4.5	0.2
Poisson's ratio	0.15	0.49

3 RESULTS

3.1 Numerical and reported physical data comparison

Numerical predicted vertical loads at the base of the facing panels and the reinforcement loads were compared to values reported by Chida and Nakagaki (1979) during calibration of the numerical model.

3.1.1 Vertical loads under facing

Damians et al. (2013) have shown from a review of instrumented case studies that the vertical load at the base of a precast facing wall with steel reinforced soil elements is greater than the self-weight of the panels. The vertical load under facing is a combination of facing self-weight, soil-panel shear and reinforcement down-drag loads, which generate reported load factors from 1.8 to 4.7 times the self-weight of the panels in steel reinforced soil walls (a value of 2.1 is computed for the reference wall reported by Chida and Nakagaki). It should be noted that the studied cases are restricted to steel reinforced soil walls. However, there are similar data for an instrumented full-scale 6-m high geosynthetic-reinforced soil wall with incremental concrete panels constructed in the laboratory (Tariji et al. 1996); the computed vertical load factor is 2.2 for this structure.

Figures 2a and 2b summarize results that take into account the effect of the backfill and foundation stiffness scenarios and the backfill-facing interface shear strength (R_i value of 0.3 and 0.6).

The data show that the larger R_i -value assumed results in a range of total vertical facing loads that vary from the reported value of 53.3 kN/m for the reference case. Assuming a value of $R_i = 0.3$ generates four stiffness scenarios that include the measured case study value more accurately (modifying the $E_{backfill}$ from 100 to 10 MPa when $E_{foundation}$ is 1000 MPa, or modifying $E_{foundation}$ from 1000 to 10 MPa when $E_{backfill}$ is constant at 100 MPa).

Typically, the recommended interface shear strength factor values are about 0.6 times the shear strength of the surrounding soil. However, analysis of a wall reported by Runser et al. (2001) showed that a value of $R_i = 0.3$ was gave more accurate

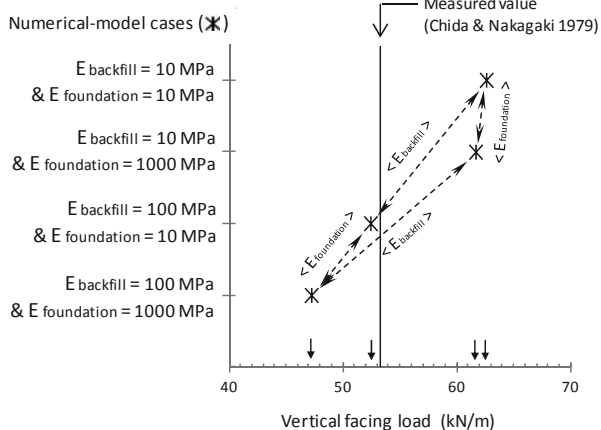
predictions (Damians et al. 2013). This value was adopted in the current study.

3.1.2 Reinforcement loads

In Figure 3 are shown the results of the reinforcement tensile loads obtained from numerical modelling and comparison with measured data for selected strips at different elevations. The reinforcement length considered in this study is 0.6 – 0.7 times the total wall height. Steel strips with lengths from 4.0 to 5.0 m were used in the reference case study, so all locations along any reinforcement layer are normalized with the respect to the layer length.

The presented results show good agreement between the numerical model results and measured data. The backfill-foundation stiffness combination results give different tensile-load distributions in the reinforcement layers. The effect of the less-compacted soil near the facing can be clearly detected with the discontinuity at a normalized distance from 0 to 0.25.

a) $R_i = 0.3$



b) $R_i = 0.6$

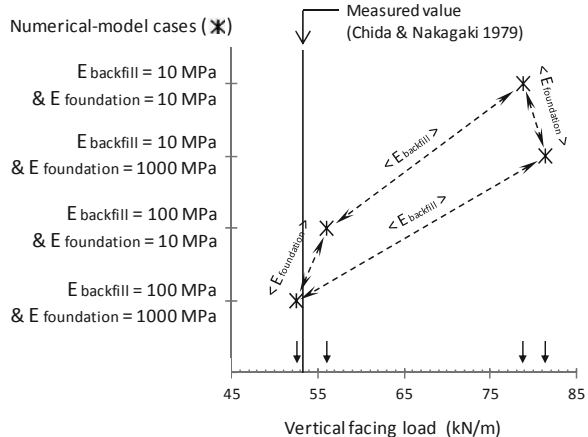


Figure 2. Total vertical loads under the facing assuming soil-facing interface reduction factor $R_i = 0.3$ (a), and $R_i = 0.6$ (b)

3.2 Influence of vertical facing stiffness

As noted earlier, the vertical facing stiffness was modified by changing the number of horizontal joints along the facing height of the wall. The reported case (base-case) had three horizontal joints (four panels of 1.5 m-height). Three other cases were considered to investigate the effect of the vertical facing stiffness (see Figure 4).

Figure 5 shows the numerical model reinforcement tensile-loads with respect to the number of horizontal joints. The values correspond to the maximum load ($T_{maximum}$) of all the reinforcement strips, its related strip, and the normalized

distance of T_{max} to the facing in the strip. Reported values obtained from Chida and Nakagaki (1979) are also shown.

First, it can be noted that there is little difference in the predicted T_{max} value with respect to the backfill and foundation stiffness combinations (less than 4 kN/m in the case with more divergence, i.e. $E_{backfill} = 100 \text{ MPa}$ and $E_{foundation} = 10 \text{ MPa}$ combination). All the T_{max} values (numerical and measured) are located at the bottom zone of the wall (all at the layer located at 1.13 m, except the numerical case with $E_{backfill} = 100 \text{ MPa}$ and $E_{foundation} = 10 \text{ MPa}$). With respect to their location in the reinforcement (normalized distance from the facing), all the T_{max} values are located between 0.3 and 0.5.

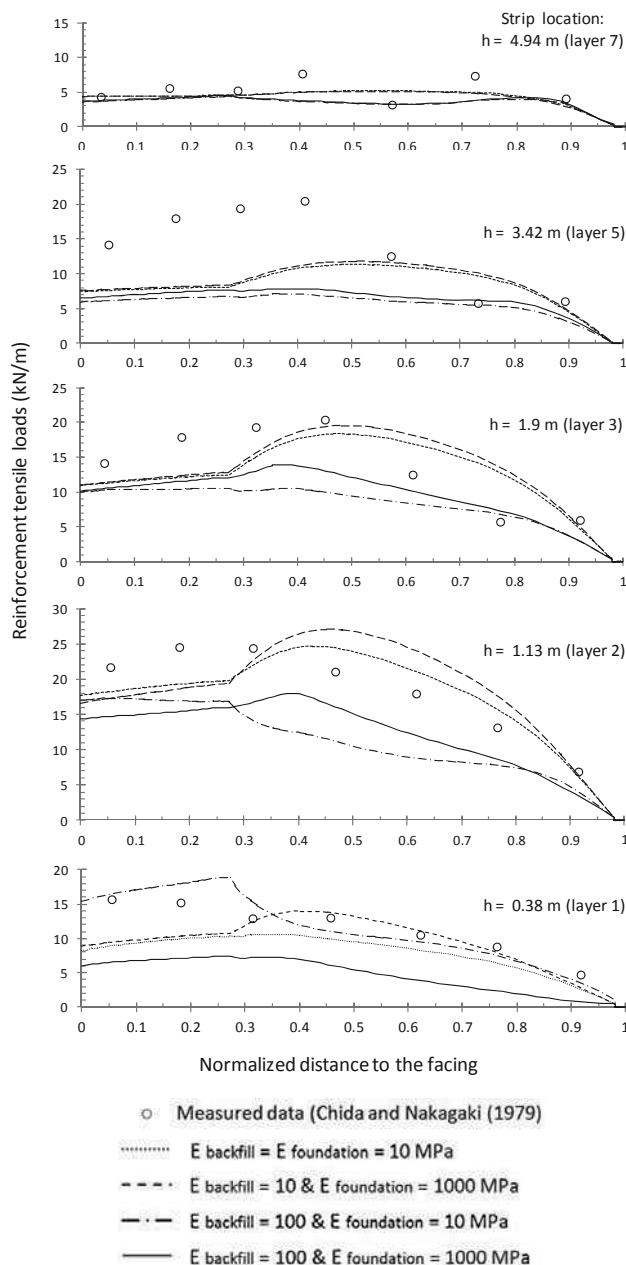


Figure 3. Tensile-load distribution of the wall reinforcements at the end of construction. (Normalized distance = distance to the facing of a stress i-point / total length of the reinforcement)

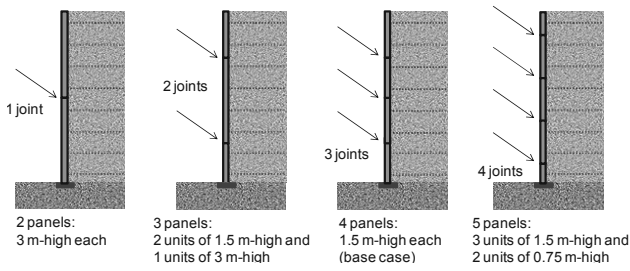


Figure 4. Schema about the horizontal joint options considered

Figure 6 shows the effect of the foundation stiffness and the vertical facing stiffness on the total vertical loads at base of the facing. Three additional foundation stiffness cases are considered here in order to obtain more data points. It can be observed that higher values of the foundation stiffness (elastic modulus) generate lower values of the total vertical load under the facing. If the total vertical load under the facing with respect to the number horizontal joints is analyzed (Figure 6), a significant influence of the vertical facing stiffness on the results can be noted. This influence is less relevant if the lowest modulus of the backfill soil is assumed (i.e. $E_{backfill} = 10$ MPa, which generates a range of about 3 kN/m between boundary cases). If the backfill soil is assumed with higher stiffness value ($E_{backfill} = 100$ MPa), the variation of the vertical load is more significant with a range of 15 kN/m for the single joint case, and 20 kN/m for the four joint case.

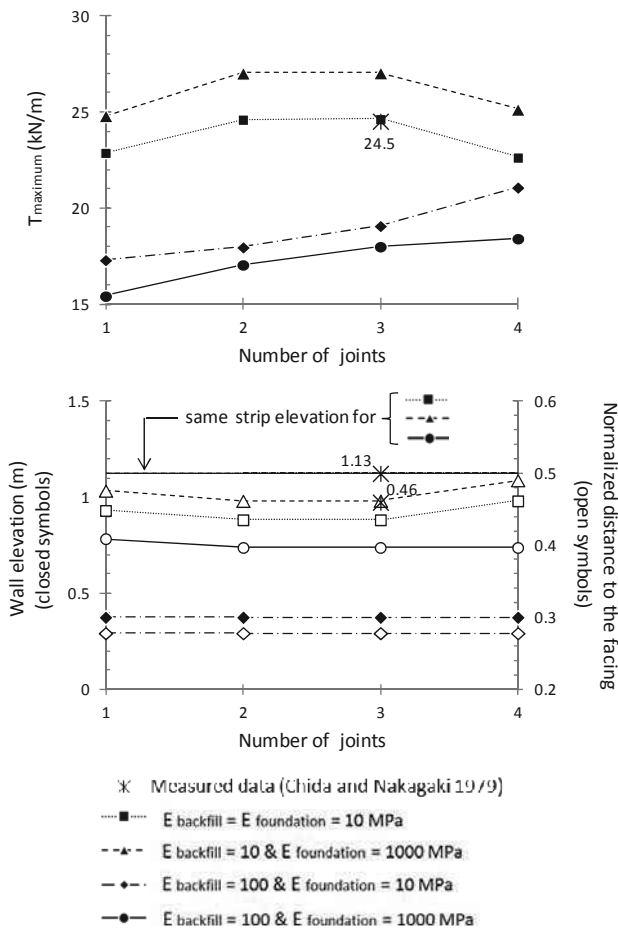


Figure 5. Maximum reinforcement loads (T_{max}) with respect to the number of horizontal joints and backfill-foundation stiffness combination (upper figure), and the T_{max} location in the backfill (reinforcement layer and distance to the facing; bottom figure)

4 CONCLUSIONS

The mechanical behaviour of reinforced soil walls is complicated due to the mechanical complexity of the component materials, their interactions, wall geometry and soil type/arrangement, in addition to the unquantifiable effects of construction method and quality. Nevertheless, current design methods are typically based on classical notions of soil and reinforcement ultimate strength. Furthermore, internal stability design using conventional analytical solutions assumes that the compressibility of the foundation soil does not influence reinforcement loads.

The numerical simulation results in the current study demonstrate, first, that vertical loads at the base of the facing are affected directly by the backfill and foundation stiffness scenario and the soil-facing interface shear strength; second, there is a significant variation of reinforcement tensile load results depending on the combination of the backfill and foundation stiffness values; and third, the vertical stiffness of the facing (represented by the number of horizontal joints along the facing, that can be also be understood as different thicknesses of the bearing pad elements) produce significantly different effects on the vertical facing load and the reinforcement tensile loads. These three outcomes cannot be predicted for walls under operational (working stress) conditions using current strength-based design methods for the calculation of reinforcement loads.

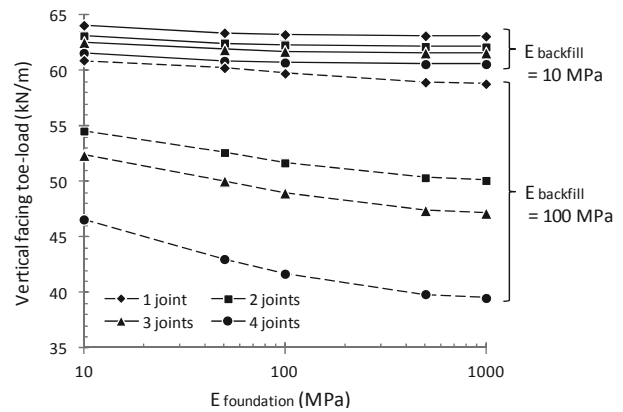


Figure 6. Vertical facing toe-load comparison with facing, foundation and backfill stiffness

5 REFERENCES

Chida, S. and Nakagaki, M. 1979. Test and experiment on a full-scale model of reinforced earth wall. *Proceedings of the International Conference on Soil Reinforcement*, Paris, France, Vol. 2, pp. 533-538.

Damians, I.P., Bathurst, R.J., Josa, A., Lloret, A. and Albuquerque, P.J.R. 2013. Vertical facing loads in steel reinforced soil walls. *ASCE Journal of Geotechnical & Geoenvironmental Engineering* (in press).

Neely, W.J. and Tan, S.L. 2010. Effects of second order design factors on the behaviour of MSE walls. Earth Retention Conference 3. Earth Retaining Structures Committee of the Geo-Institute of ASCE. Geotechnical Special Publications (GSP) n. 208. *Proceedings of the 2010 Earth Retention Conference*, Bellevue, Washington, August 1-4, 2010, pp. 522-530.

PLAXIS. 2008. Reference Manual, 2D - Version 9.0. PLAXIS B.V., Delft University of Technology, The Netherlands.

Runser, D.J., Fox, P.J. and Bourdeau, P.L. 2001. Field performance of a 17 m-high reinforced soil retaining wall. *Geosynthetics International*, 8(5): 367-391.

Tajiri, N., Sasaki, H., Nishimura, J., Ochiai, Y. and Dobashi, K. 1996. Full-scale failure experiments of geotextile-reinforced soil walls with different facings. *IS-Kyushu 96, 3rd International Symposium on Earth Reinforcement*, Fukuoka, Japan, pp. 525-530.

Earth Pressure from Strip Footings on an Anchored Sheet Pile Wall

Poussée des terres provenant de semelles filantes sur un mur de palplanches ancré

Denver H., Kellezi L.

GEO-Danish Geotechnical Institute, Lyngby, Denmark

ABSTRACT : A strip footing is frequently situated near a sheet pile wall. Assessment of the extra pressure on the wall generated by a footing causes theoretical problems for the designer. The distribution of this pressure depends in fact on many parameters. Besides the location and magnitude of the load a characterization of the soil and the wall is necessary for a rational design. Furthermore, the movement of the wall has a significant impact on the pressure. In this paper an anchored wall is investigated where the movement in failure is a rotation about the anchor point. The problem is solved by means of different analytical methods compared with solutions by finite element modeling applied to a number of representative examples. These comprise different strengths for the cohesion-less soil and different load scenarios. After a discussion of the results a simple calculation procedure is proposed.

RÉSUMÉ : Une semelle filante est souvent située à proximité d'un mur de palplanches. L'évaluation de la pression supplémentaire sur la paroi générée par la semelle provoque des problèmes théoriques pour le concepteur. La répartition de cette pression dépend en fait de nombreux paramètres. Outre l'emplacement et l'ampleur de la charge, une caractérisation du sol et du mur est nécessaire pour une conception rationnelle. De plus, tout déplacement de la paroi a un impact significatif sur la pression. Dans cet article, une paroi ancrée est étudiée lorsque le déplacement amenant à une défaillance consiste en une inclinaison autour du point d'ancrage. Le problème est résolu par le biais de différentes méthodes d'analyse que l'on compare aux solutions de modélisation d'éléments finis, appliquées à de nombreux exemples représentatifs. Celles-ci comprennent différentes forces pour un sol sans cohésion ainsi que différentes configurations de charge. Une simple procédure de calcul est proposée après la discussion des résultats.

KEYWORDS: Sheet pile wall, continuous footing, earth pressure, finite element method, sand, stress distribution.

1 INTRODUCTION

Sheet pile wall design methods in Europe generally rely on simplified earth pressure theories where the failure mechanism of the soil is in fact not compatible with the wall deflections. The Danish design method of sheet pile walls is based on Brinch Hansen's earth pressure theory, which assumes plastic behaviour for the wall and the soil. The computer program SPOOKS, which is a product from GEO-Danish Geotechnical Institute, is successfully used for sheet pile wall design in Denmark and abroad. The program calculates the required driving depth, the maximum bending moment and the anchor force for a user defined failure mode of the wall and the adjacent soil. The wall may be either anchored or free and either hinged or fixed in an anchor point. In the limit state a yield hinge in the wall with an ultimate positive moment may develop below the anchor level.

When excavating close to an existing building the effect of the partial distributed loads, from for example strip foundations (two dimensional (2D) conditions), or plate foundations (three dimensional (3D) conditions), are usually implemented in the sheet pile wall plastic design by means of the elasticity theory and the principle of superposition, where the extra earth pressure simply is added to the plastic solution. It is however not correct in the plastic design to separately calculate the active earth pressures from partial distributed loads without taking into account the active pressure from the unit weight of the soil.

The objective of the present paper is to supplement an earlier investigation for a free wall, Denver & Kellezi (2011), with establishment of an empirical relationship to estimate the extra earth pressure on an anchored sheet pile wall from a strip load behind the wall. This relationship is compared with solutions from finite elements (FE) results. The additional pressure is found as the difference between the combined pressure from self weight of the soil and the strip footing and the pressure

from only the self weight. In an attempt to assess the additional pressure on the wall, different approaches are investigated:

- Analytical calculations by the theory of plasticity on a suitable rupture figure.
- Empirical solutions inspired by Coulomb's theory.
- Numerical modelling by the FE method.

2 GENERAL

The earth pressure calculation on a wall is here illustrated by the Danish method denoted as Earth Pressure Calculation. This method has been proposed by J. B. Hansen (1953) and is extensively used in Denmark. The pressure on the wall (e) is calculated as a sum of three terms as given in equation (1).

$$e = \gamma' d K_\gamma + q K_p + (c K_c) \quad (1)$$

These terms and the other parameters used in the calculation are: γ' the effective unit weight of the soil; K the earth pressure coefficient (different for the three terms); c the cohesion of the soil; p the surface load behind the wall, and d the depth along the wall from the soil surface. The last term is enclosed in parenthesis as this paper deals only with frictional soil.

In the Danish method the wall is considered composed of several rigid parts interconnected by yield hinges. Each part is assumed to rotate about a point and the earth pressure coefficients are functions of the position of this point and the direction of rotation (besides the friction angle of the soil, φ). Examples of anchored walls with yield hinges are shown in Figure 1, and examples of rupture figures used for calculation of K are shown in Figure 3. The result of each calculation is the total force on the wall and the point of application. The normal component of this force (E) is distributed along the wall. A part of E is applied near the top as a Prandtl rupture zone.

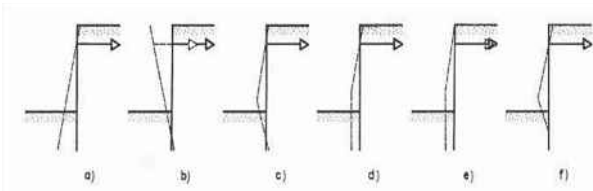


Figure 1, Anchored wall in failure composed of one or more rigid segments connected by yield hinges in failure. This paper deals with failure mode a) marked with rectangular.

A pressure jump near the top is then applied to ensure that the effect of the distribution (in terms of total force and moment) corresponds with the rupture figure. The method has been described in detail by Mortensen & Steinfeldt (2001) and results of calculated examples are compared with FE calculations.

3 COMPUTER PROGRAM ‘SPOOKS’

Although J. B. Hansen has developed a complete set of diagrams to find the values of K , the earth pressure calculation for a specific design situation is rather time consuming. To this end GEO-Danish Geotechnical Institute has made a commercially available computer program named ‘SPOOKS’.

Here, apart from the geometry of the excavation, the soil conditions and water tables, only a selection of the total wall movements (as shown in Figure 1) is necessary as input. The results are a distribution of both earth and water pressures, curve of bending moments along the wall, tip level, and anchor force. All together ready for the final design of the sheet pile wall profile and anchor. However, this program has no facility to include a partial surface load.

4 THEORY OF PLASTICITY

A method to assess the extra soil pressure caused by a partial load has been introduced by J.S. Steinfeldt and B. Hansen (1984). The Danish method to calculate the earth pressure coefficient from a relevant rupture line has been adopted. A circular rupture line is used as an appropriate choice for a rotation about a point at the anchor level. The stresses from the rupture line are determined by the Kötter’s differential equation. The total force is found by integration of this equation presented by Brinch Hansen (1953) and shown as the resulting force (F_o) and moment (M_o) about the centre of the circle as shown in Figure 2 where the significance of the variables is indicated.

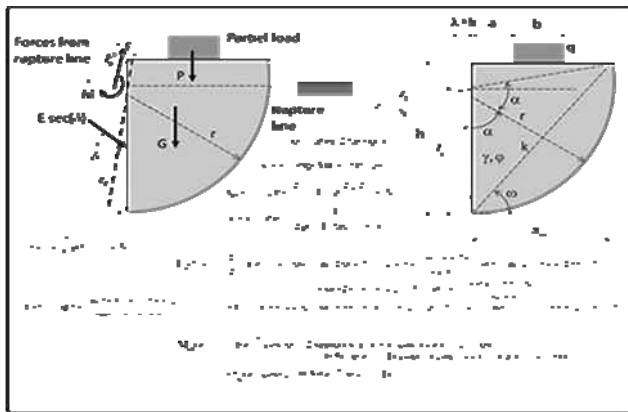


Figure 2, Analytical method where circular rupture figure is applied. Negative values of ϕ and δ shall be applied as the rupture is active.

It should be mentioned that $t_c = \sqrt{q^2 + \tau^2}$ where t_c refers to the starting point of the integration where the rupture circle meets the soil surface and σ and τ are coordinates to the yield point in the Mohr’s circle. The function $q(\lambda)$ refers to the value of q in the point where the circle meets the surface. (q beneath the load

and 0 otherwise). The three unknowns (λ , E , and z_p) are finally found by the three equilibrium equations.

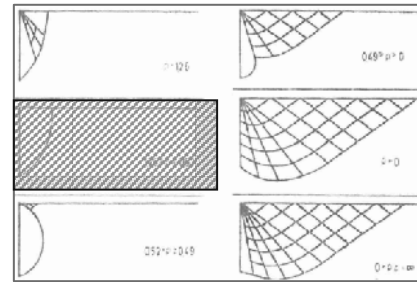


Figure 3, Rupture figures with different rotation points (ρ : relative height from the bottom of the wall). The figures are drawn for $\phi = 30^\circ$, $c = 0$ and rough wall rotating clockwise. The pure line rupture is investigated analytically in this paper (shaded in the figure).

This method (Figure 3 shaded) is in detail introduced and discussed by the authors and the results of a large number of load scenarios are presented in their paper.

5 EMPIRICAL METHOD

It is usual practice to apply a soil pressure derived from the distribution for the uniformly loaded surface. A minor part of this distribution is then used situated to a depth interval defined by inclined lines through the soil.

In Figure 4 a method of this kind often used in Denmark is shown. However, a tail below the lower line has been in this method proposed by K. Mortensen (1973) who has pointed out the complexity of the problem assuming a smooth wall that rotates anti-clockwise about a point below the tip of the wall. Consequently, the upper part with the even distribution is given by an active Rankine rupture figure. The tail is probably inspired by calculations by Coulomb’s method where the lower part is more dependent of other parameters than a and b .

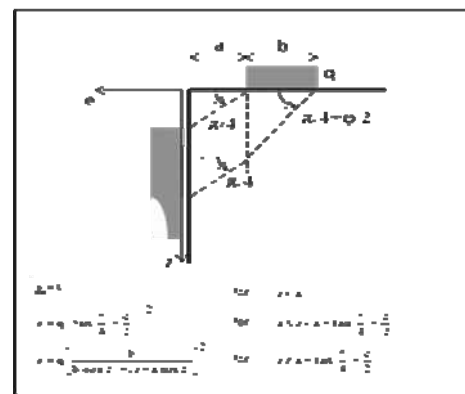


Figure 4, Empirical method based partly on the Coulomb’s earth pressure theory.

As this method is often used also for other movements, en lieu of other procedures it is adopted here as an example of an empirical solution.

6 ELASTIC SOLUTION

An elastic solution developed by Boussinesq (1885) is often used because of its simplicity as shown in Figure 5. Besides the theory of elasticity a smooth vertical wall without any movement is assumed. This method is often questioned as the resulting distribution is too large and situated much too high on the wall with respect to results from model tests and calculations based on the Coulomb’s method.

This is also the authors experience when the movement of the wall is anti clockwise about a low point in the wall. However, if the movement is a clockwise rotation about the anchor (as in this paper) the assumptions for an elastic solution are more justified.

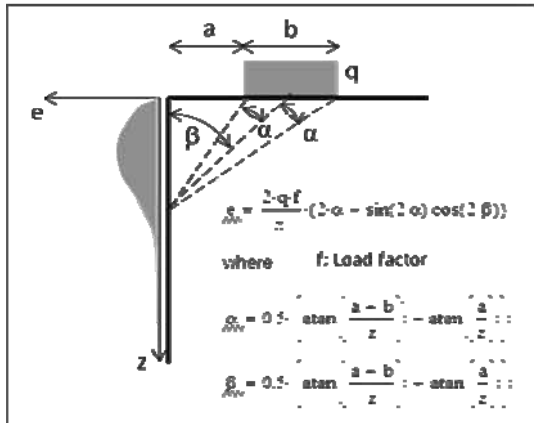


Figure 5, Elastic solution by Boussinesq (1885)

7 FINITE ELEMENT METHOD

In order to validate the method a number of load scenarios have been calculated by the FE program Plaxis 2011.

A 2D mesh pattern has been generated using triangular finite elements (15-noded). Sand is modeled in drained conditions using the Mohr-Coulomb constitutive model. The sheet pile wall is assumed weightless and with a large stiffness to prevent any interaction of stresses caused by deformation of the wall. The initial geostatic conditions are calculated first. Mesh sensitivity analyses have been carried out and an optimal mesh pattern with respect to element size and obtained accuracy has been chosen for the final analyses.

Plaxis plastic analyses (small deformation theory) and Updated Mesh (large deformation theory) have been applied to estimate the effect of the wall movement on the results. The calculations are carried out in different ways considering the impact the staged construction (excavating after, before or at the same time with the load application) has on the results.

Some different load scenarios are modeled and calculated to illustrate the problem. The loads / pressures applied over the foundations are chosen in such a way that the foundation bearing capacity is satisfied. The load scenarios are shown in Table 1.

Table 1, Load scenarios calculated

No	φ (deg)	a (m)	b (m)	q (kPa)	No	φ (deg)	a (m)	b (m)	q (kPa)
1	30	1	2.5	125	6	40	1	2.5	713
2	30	1	1	50	7	40	1	1	285
3	30	2.5	1	50	8	40	2.5	1	285
4	30	5	1	50	9	40	5	1	285
5	30	0	∞	50	10	40	0	∞	285
h = 12 m $\gamma = 14 \text{ kN/m}^3$ c = 0 kPa rough wall									
Height to rotation point: $h_p = 9.6 \text{ m}$									

A unit weight has been applied to the soil to provide a realistic stress distribution near the top of the wall. Interface elements are applied along the wall. However, the soil strength at the interface has not been reduced as a rough wall is considered. The influence of the load on the wall has thus been derived as the difference between results of calculations of the wall with load and unit weight and with unit weight alone.

A rigid anchor is applied at a depth corresponding to 0.8*h referring to the bottom of excavation or the height of the wall h.

The anchor point ensures a rotation around this point during failure (Figure 6).

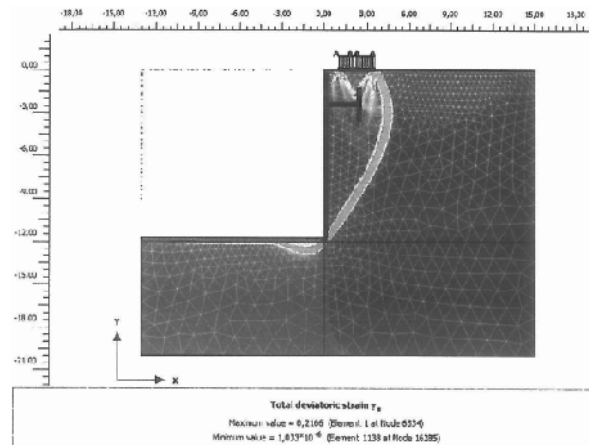


Figure 6 FE model example, ($\varphi=30^\circ$ a=1.0 m b=2.5 m or a/b=0.4 p=125 kPa).

A complete presentation of the results is not included due to lack of space. The normal pressure (e) on wall from the soil, and the soil plus load, and the additional pressure from the load derived as their difference (Delta e) are derived from the interface zone as given in Figure 7 and 8 for both soil types considered. The FE results are used as benchmarks for the accuracy of the other methods and shown relative to those in the discussion.

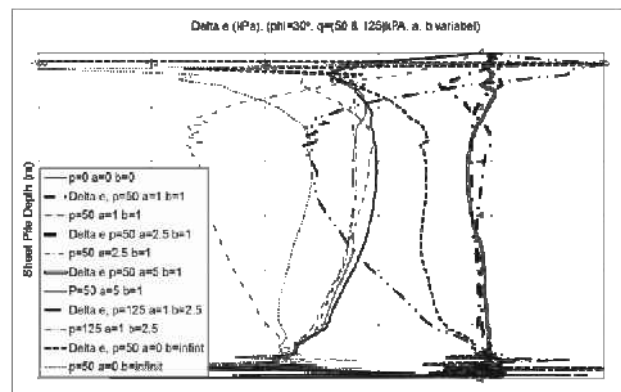


Figure 7 FE models results ($\varphi=30^\circ$)

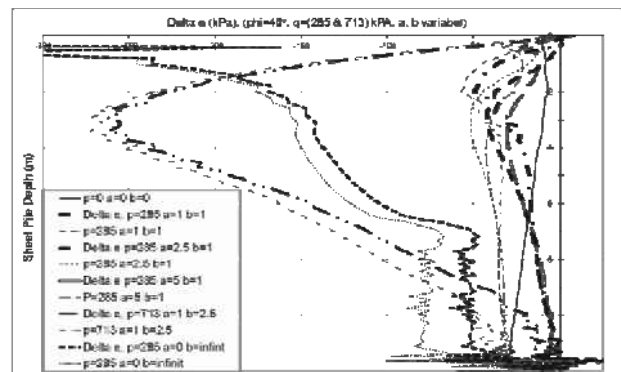


Figure 8 FE models results ($\varphi=40^\circ$)

8 DISCUSSION OF CALCULATIONS

It was expected that a study of the theory of plasticity would yield a deeper insight into the problem and provide useful results. However, our calculations have produced rather scattered results. The calculations presented by Steinfeldt & Hansen do by no means suggest simple relations to the input

parameters. Their recommendation is also to make a computer code using the detailed described procedure and solve the problem in question explicitly. The resulting force from the integration along a rupture line consists together with simple zone ruptures the backbone of the Danish earth pressure theory, and should by no means be questioned here.

It should be mentioned that the procedure involves two calculations: (i) a calculation with both P and G (Figure 2), and (ii) a calculation with G alone. The influence of P is found by a subtraction of the two vectors. As G is great compared to P the latter is poorly determined and also problems with the validity of supposition as assumed here will distort the result.

Another problem is connected with the integration of the Kötter's equation. The only contribution to a change of the ambient stress condition is caused by the unit weight. However, the rupture line will pass through domains in the soil much differently affected by the partial loaded surface.

In every case the method will not provide the distribution of the pressure which is imperative especially to determine the moment in the wall in the anchor level.

9 PROPOSED PROCEDURE

When a procedure to assess the influence of a partial loaded surface it should be taken into consideration that the proposed distribution should converge to the distribution usually applied for a fully loaded surface.

The procedure proposed is:

- Calculate the elastic distribution ($e_e(z)$) using the equations in Figure 5.
- Calculate the distribution usually used for a fully loaded soil surface. Use only the part of this distribution corresponding to the uniform part of the distribution ($e_p(z)$) shown in Figure 4.
- The final distribution is: $e(z) = W * e_p + (1-W) * e_e(z)$, where W is a weight function $W = 1.5 * (F - 0.167) - 2 * (F - 0.5)^3$ and $F = 0.8 * b/h$.

10 VERIFICATION

The benchmark for the verification is chosen as the results of the FE calculations. As before mentioned it is difficult to characterize the distributions by simple means. We have here focused on the usage of the distribution: (i) to calculate the anchor force (A), and (ii) to calculate the moment in the wall in the anchor level (M).

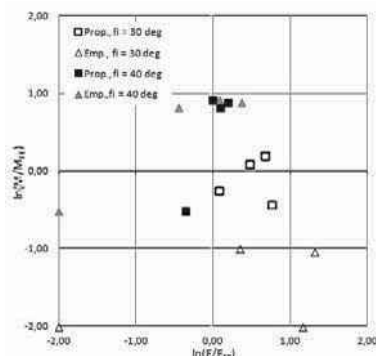


Figure 9, Accuracy of the methods (Empirical, Proposed vs. FE).

The anchor force is estimated as the part of the distribution above the depth z equal to double the height of the wall above the anchor. This procedure excludes the results found by the theory of plasticity to be represented. The quantities $\ln(A/A_{FE})$ and $\ln(M/M_{FE})$ are made where the denominators are the results from the FE calculations. These quantities are plotted against each other in Figure 9 for load cases (1-4) and (6-9).

When a quantity is greater than zero, the predicted value is on the safe side. When a quantity is 1 the corresponding ratio is 2.7. If A , or M is zero the quantity is minus infinity but plotted on the frame of the diagram.

A study of Figure 9 shows that the proposed procedure is superior to the empirical procedure and the fit is surprisingly accurate taking into account the complexity of the problem.

In order to offer a qualitative impression of the results a single distribution from the FE calculations is shown in Figure 10. This distribution is supplemented with distributions from two other methods (Empirical and Proposed).

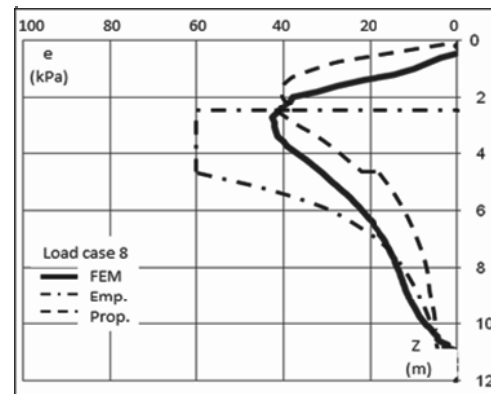


Figure 10, Normal pressure distribution (e) from FE calculations compared with other methods (Empirical, Proposed) for a single load, (Load Case 8).

11 CONCLUSION

A procedure to calculate the pressure distribution has been proposed and has proved an excellent fit with results from FE calculations. The procedure is based on the theory of elasticity where the assumption of an immobile wall is justified by the high rotation point. The result converges to the usually applied when the entire surface is loaded.

12 ACKNOWLEDGEMENT

The authors acknowledge GEO-Danish Geotechnical Institute for the financial support of the project.

13 REFERENCES

Boussinesq, J. 1885, *Application des potentiels a l'etude de l'equilibre et du mouvement des solides elastiques*. Gauthier-Villars, Paris.
 Brinch Hansen J. 1953, *Earth Pressure Calculation*, Danish Technical Press, Copenhagen.
 Coulomb CA. 1776, *Essai sur une application des r\oles des maximis et minimis a quelques problemes de statique*. *Memoires Acad. Royale des Sciences*, Vol. 7. Paris.
 Denver H., Kellezi L. 2011, Earth pressure from a nearby building on sheet pile walls. *Proc. 17th European Conf. Soil Mechanics and Geotechnical Engineering*. Athens.
 Mortensen N., Steenfelt J.S. 2001, Danish plastic design of sheet pile walls revisited in the light of FEM, *Proc. 15th Int. Conf. Soil Mechanics and Geotechnical Engineering*. Istanbul.
 Plaxis, 2011, *FE Code for Soil and Rock Analyses*, User's Manual, A.A. Balkema, Rotterdam.
 Steenfelt J.S., Hansen B. 1984, Sheet pile design earth pressure for strip load, *J. Geotechn. Engrg. ASCE* Vol. 110, No. 7.

Top-Down Construction Alongside Of Bosphorus – A Case Study

Construction en « Top-Down » le long du Bosphore – Une étude de cas

Durgunoglu T., Kulac F., Ikiz S., Akcakal O.
Zetas Zemin Teknolojisi A.S., Istanbul, Turkey

ABSTRACT: Hatice Sultan and Fehime Sultan Residences are two historical Ottoman waterfront mansions placed on the European shore of Bosphorus in Istanbul. Within the restoration campaign of these mansions, it is planned to add four basement levels under the complete plot with the exception of preserved two corners where Hatice Sultan Residence and an old and large tree exist. The depth of the excavation needed for the basements is about 24 m below ground surface of which 21.20 m will be below groundwater level. The excavation should take place just 75 m far from the southwest pylon of the Bosphorus Suspension Bridge. Soil profile consists of uncontrolled fill, marine alluvium layer and bedrock which is sloped towards the seaside with a varying inclination. Steel propping system was set forth by the geotechnical design group of the Client, though this method was eliminated later during the bidding stage, because it was found impractical due to their obstacle in basement construction. The method of top-down construction of the basement levels with permanent diaphragm wall and bored piles socketed into bedrock was agreed to be realized by the Client based on the alternative proposal given by the foundation subcontractor during the bidding stage. THY -Do&Co JV Ortakoy Hotel Project is an interesting case-study where a challenging supporting system is being implemented near the Bosphorus in very poor soil conditions, under high seismicity.

RÉSUMÉ : Les Résidences de Hatice Sultan et de Fehime Sultan sont deux yalis Ottomanes historiques situées sur la côte Européenne du Bosphore, à Istanbul. Le projet de rénovation de ces yalis prévoit d'ajouter quatre étages en sous-sol sous l'ensemble du terrain, à l'exception de deux zones préservées où sont situés la Résidence de Hatice Sultan et un arbre centenaire. Une excavation de 24m sous le niveau du terrain naturel est requise pour la réalisation des sous-sols dont environ 21,20 m sous le niveau de la nappe phréatique. L'excavation aura lieu à tout juste 75 m du pylône sud-ouest du Pont sur le Bosphore. Le profil du sol est constitué de remblais non contrôlés, de couches d'alluvions marins reposant sur un substratum rocheux s'enfonçant avec une inclinaison variable en allant vers le Bosphore. Cependant, le design initial du client basé sur la mise en œuvre d'un système de soutènement en acier a été plus tard écarté car ne permettant pas la réalisation ultérieure des niveaux de sous-sol. La méthode de construction en « top-down » utilisant une paroi moulée et des pieux forés ancrés dans le substratum rocheux a finalement été sélectionnée par le Client, sur la base de la proposition alternative remise par le sous-traitant lors de l'appel d'offres. Le Projet de THY - Do&Co JV Ortakoy Hôtel est une étude de cas intéressante pour lequel un soutènement a dû être mis en œuvre à proximité du Bosphore, avec des conditions de sol très difficiles et en prenant en compte de forts risques sismiques.

KEYWORDS: Top-Down Construction

1 INTRODUCTION

Fehime Sultan and Hatice Sultan Residences are one of the historical Ottoman waterfront mansions constructed alongside the Bosphorus. These residences were constructed in the second half of the 19th the Century by Sultan Abdulhamid II as a wedding present for two daughters of Sultan Murat V. Later on, Fehime Sultan Residence was given as a gift to Gazi Osman Pasha for his success in Plevne Defense against Russian Army. During the Turkish Republic period this mansion served as a primary school and unfortunately was seriously damaged in a recent fire in 2002. On the other hand Hatice Sultan Residence served as an orphanage and then as private swimmers club in the later periods. The plot has been recently purchased by Turkish Airlines - Do&Co JV on BOT basis and is planned to be restored and developed to serve as a boutique hotel. Ruins of the Fehime Sultan Residence have been transferred to the restoration workshop. This beautiful and historical mansion is planned to be re-constructed using its original fragments. Within this restoration campaign, it is also planned to add four basement levels under the complete plot with the exception of two corners where Hatice Sultan Residence and an old and large tree exist. This deep excavation is agreed to be implemented with the Top-Down construction method because of the poor soil conditions, high ground water table and important

neighboring infrastructures. On the date of the paper submission, the diaphragm wall construction was just finalized. Therefore, only findings and implications of design and methodology together with diaphragm wall construction are presented within this paper.

2 PROJECT DESCRIPTION

Fehime Sultan and Hatice Sultan residences are located in district of Ortakoy alongside of Bosphorus and approximately 75 m away the southwest pylon of the Bosphorus Suspension Bridge in Istanbul (Figures 1a and 1b). Within the restoration campaign of these residences four basement floors are planned to be constructed in the entire plot. The periphery of the basement floors encloses the plot limit, except two corners on where Hatice Sultan residence and a historical tree exist (Figure 2). Basement excavation will be realized under Fehime Sultan residence location at the left in Figure 2 because ruins of this residence as a result of fire have been removed to restoration workshop area before the commencement of the works. The perimeter of the excavation plot is about 372 m and the area of the plot is approx. 6064 m². Site elevations are varying between +1.00 m to +3.00 m. Excavation elevation is 21.20 m below the

sea level and maximum excavation depth is approximately 24 m.



Figure 1a and 1b. General View of the Site Figure and Location of the Site in Istanbul



Figure 2. Periphery of the Excavation (photo after the fire of 2002 and before the start of the restoration campaign)

During the bidding stage, top-down construction proposed by the foundation subcontractor was considered as a suitable method under the existing conditions. Typical cross section of the basement structures through the perpendicular direction to the seashore is given in Figure 3. It is planned to use the diaphragm walls as permanent periphery walls of the basement floors, construct the bored piles as permanent columns of the underground structure and integrate the foundation and slabs with the permanent wall and columns during the top-down construction method. This choice resulted in the necessity to develop special details for ground water isolation and continuity of the structural elements.

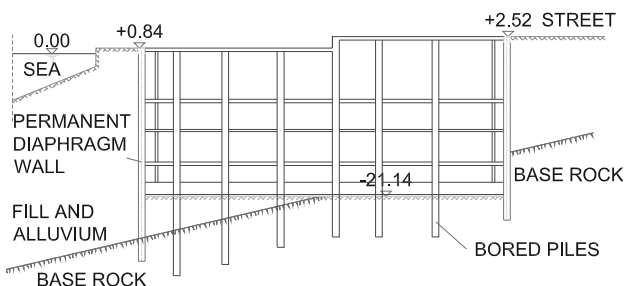


Figure 3. Section of the Basement Structure in Perpendicular to the Seashore

3 GEOTECHNICAL MODELLING

Within the soil investigations ten boreholes were implemented with a maximum length of 50 m. Two of the boreholes adjacent to the seaside were implemented with 45° inclination and length of these boreholes was 100 m. Also within the geophysical measurements, MASW and microtremor studies are implemented in the site to obtain the geodynamic modeling of subsoils.

Soil profile consists in sequence from top to down as of uncontrolled fill, marine alluvium and bedrock. Dyke, sandstone and shale are the commonly encountered rock types at the site. According to the results of vertical boreholes at the site bedrock is located between 13.50 m and 27.20 m under the sea level. Therefore length of the diaphragm wall and bored piles are chosen variable from one location to another in accordance to

encountered bedrock elevations. Typical soil profile is given in Figure 4.

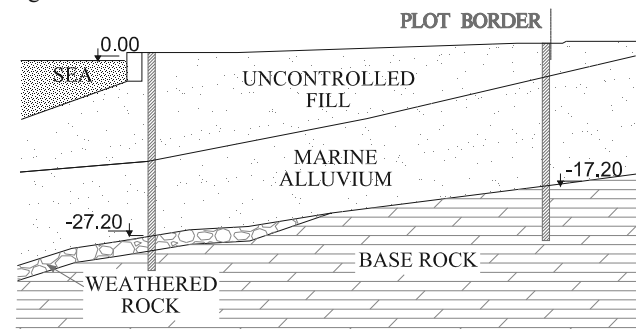


Figure 4. Typical Soil Profile

Simplified average drained shear parameters of the alluvial soil layers based on the field and laboratory testings are given in Table 1. Ground water table is located within 1.0m to 3.0m below the ground surface.

Table 1. Soil Properties

Layer	γ (kN/m ³)	ϕ' (°)	c' (kN/m ²)
Uncontrolled Fill and Marine Alluvium	18	28	1
Weathered Rock	22	33	20
Bedrock	24	33	50

4 PRELIMINARY DESIGN

The preliminary retaining system has been proposed by a geotechnical design group employed by the Client prior to the tender, which consisting a peripheral diaphragm wall and tubular steel struts. Diaphragm wall thickness was considered as 800 mm and planned to be used only temporarily during the excavation. To support the diaphragm wall, four rows of steel struts are proposed to be implemented. The spacing between the struts was 5.0 m in vertical and 8.20 m in horizontal directions. Typical cross section of the tender design is given in Figure 5.

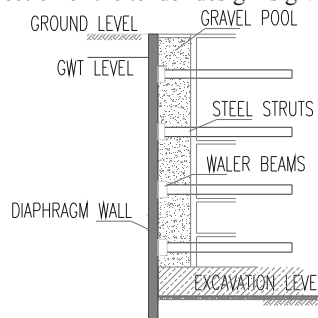


Figure 5. Tender Design Typical Cross Section

Complete underground structure were planned to be constructed 21.20 m below the water table. As a result, the uplift of the underground structure is one of the critical issues for the design.

5 PROPOSED ALTERNATIVE DESIGN

During the bidding stage the applicability towards the construction of underground structure and the cost of the tender design was examined. One of the drawbacks realized was that the space between the steel tubular struts was very limited to implement the excavation works in a safe and efficient manner. As a result, alternative top-down construction method was proposed to eliminate the implications of steel struts. Further, in order to eliminate the gravel filled between the walls; namely

gravel pool, proposed in the preliminary design, uplift loads are proposed to be taken by tension piles under the foundation.

As described in the previous sections, the site is located in a densely populated urban zone and there are important neighboring infrastructures around the plot. In order to minimize the lateral displacements to be realized during excavation implication of the proposed top down procedure was very effective and superior compare to strutted excavation.

In the proposed top down method permanent diaphragm walls and piles are to be constructed prior to excavation works. Later ground level r. c. floor will be constructed except the part behind the Hatice Sultan residence (Figure 6).

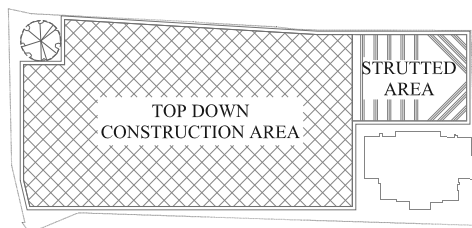


Figure 6. Top Down Construction Area

Soil under the ground level floor will be excavated phase by phase until the bottom elevation of foundation. In parallel to excavation works 1st basement r. c. floor will be constructed. The part of limited excavation plot behind the Hatice Sultan Residence will be supported with steel struts to provide space for ramps which will be used for the transportation of the excavated material. Top down construction steps will continue similarly as 2nd basement floor 3rd basement floor and foundation respectively (Figure 7).

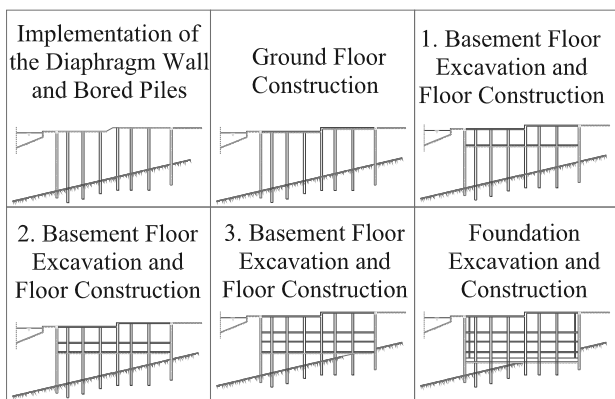


Figure 7. Top Down Construction Steps

Groundwater seepage into the excavation site is evaluated by seepage analysis and optimum socket length in to the bedrock is determined as 5.0 m. Also settlements due to the lowering groundwater table are estimated and found to be less than 18 mm which is considered as tolerable for the existing structures.

Bored piles are designed to be used as compression and tension members depending on the loading conditions. Therefore, piles which will act as permanent columns of the underground structure are extended into the bedrock having minimum socket length of 6.0 m based on the result of pile tension test conducted at the site in order to satisfy the most critical tension loading condition under the uplift forces. Tension capacity of the piles are estimated and taken into account against uplift forces.

In the top down construction, floor and foundation reinforcements will be integrated into the permanent diaphragm wall and piles with the aid of additional link reinforcements

which are already placed in these elements. Details of these link reinforcements are given in the next section.

After the top down construction steps the limited area behind the Hatice Sultan Residence will be constructed with conventional method from bottom to top in parallel to dissembling the steel struts. Special water-proofing works will also be implemented under the foundation and on the constructive inner wall during the down to top construction steps.

6 CONSTRUCTION STAGE OF DIAPHRAGM WALLS

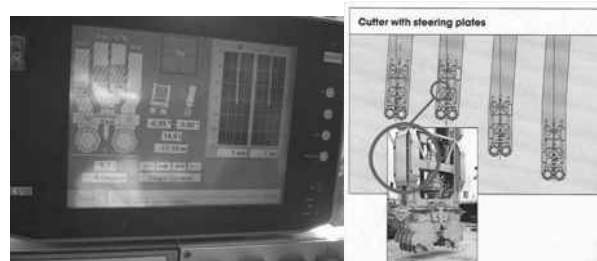
At the time of paper submission, diaphragm wall construction was just completed and preparations have been realized to initiate the piling works. Therefore only diaphragm wall construction stage would be covered within the paper.

To implement the diaphragm wall in required socket lengths in the bedrock formation, hydrofraise machine was mobilized for this project having 81 kNm max. torque per gear box, and 25 rpm max. revolution, with a max cutting depth capacity of 70m (Figure 8).



Figure 8. Diaphragm Wall Machine, Hydrofraise-Cutter

Another reason of implementing the hydrofraise-cutter machine was to provide a better verticality control during the construction of the permanent diaphragm walls. The verticality was monitored parallel to diaphragm wall excavation and direction of the cutter controlled with the help of the flaps on the edges (Figures 9a and 9b).



Figures 9a and 9b. Verticality Control System

During the soil investigations encountered maximum UCS values of the bedrock are given at the Table 2 below.

UCS Value	Intrusive Dyke		Sandstone		Shale Sandstone	
	Min.	Max.	Min.	Max.	Min.	Max.
	0.7	65	3.6	160	1.0	67

The distribution of the UCS values with the depth is given in Figure 10.

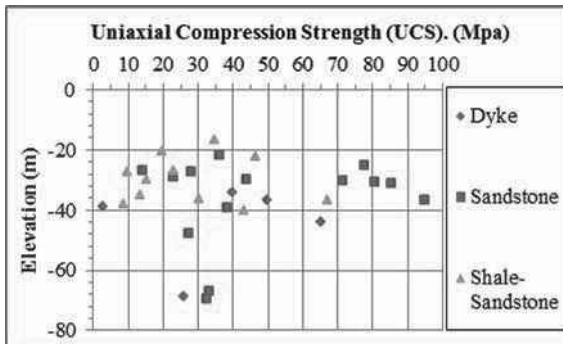


Figure 10. Unconfined Compression Strength (UCS) Values with Depth

The socket length of the diaphragm wall is variable due to the variability of the lithology of bedrock. It is estimated that the minimum 5.0 m socket length in the rock formation will be required. With the utilized hydrofraise cutter diaphragm wall machine, it was possible to construct approximately 2.65 m/day on plan (equals to 60 m² diaphragm wall per day) in average.

To integrate the slabs and foundation with the diaphragm walls additional link reinforcements are placed in the reinforcement cage (Figure 11). It is planned to chip the concrete on these elevations to bend the additional reinforcement into the slab and foundation elements.

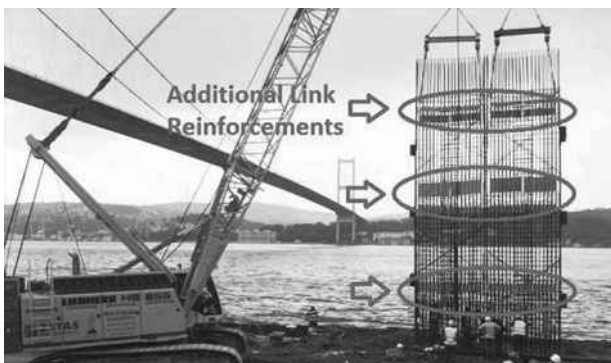


Figure 11. Additional Link Reinforcements on the Slab Elevations

Prior to diaphragm wall construction on the seaside, it was planned to implement sheet piles at the shore to remove the large quay stones at the back side and to prevent the negative fluctuation effect of the sea during the diaphragm wall construction. Sheet piles also contribute to the overall stability of the quay under the weight of heavy diaphragm wall machine. Sheet piling application is presented in the Figures 12a and 12b.



Figures 12a and 12b Sheet Piling

7 CONCLUSIONS

Within the restoration campaign of two beautiful historical mansions from Ottomans alongside the Bosphorus namely Hatice Sultan and Fehime Sultan, four basement floors was planned to be constructed with a maximum excavation depth of 24 m. Tender design for the retaining system of this excavation was temporary diaphragm walls supported with steel tubular struts. Due to the lack of enough spacing between the struts, applicability of the excavation works to achieve the desired speed was found to be questionable. Therefore an alternative system of top down construction method was proposed during the bidding stage. Prior to the excavation, it is proposed to construct the diaphragm wall and bored piles which will be also part of permanent structure of the basement so a remarkable saving and speed together with additional safety could be provided to the project. Another benefit of this system was also allowing extension of bored piles which are also columns of the basement into the bedrock to have desired tension resistance against uplift. This design gave a chance to eliminate the gravel pool proposed in preliminary design and provided additional space in basement floors. Integration of diaphragm wall, slabs and foundation is realized with additional link reinforcements and these reinforcements are placed in their for seen locations during the cage preparation. Sheet piles implemented also successfully prior to the seaside diaphragm wall construction in order to eliminate the negative effect of sea. In spite of the high UCS values it was possible to construct the diaphragm walls socketing 5.0 m deep into the bedrock with high capacity hydrofraise – cutter diaphragm wall machine at a reasonable rate. It is concluded that with the implication of top down construction method, part of this challenging project is completed successfully in economical, safe and timely manner.

8 ACKNOWLEDGMENT

We would like to extend our great appreciation to Mr. Hamdi Topcu, Chairman of Executive committee of Turkish Airlines and Mr. Atilla Dogudan, Chairman of Do-Co Corporation. The coordination and cooperation of Guryapi Construction Company are also gratefully acknowledged.

Experiences with SBMA ground anchors in spanish soils

Etude expérimentale avec les tirants d'ancrage SBMA dans le sol espagnol

Fernandez Vincent J.M.

Universidad de Buenos Aires, Universidad Catolica Argentina, Geotecnika SRL

ABSTRACT: The load transfer mechanism of steel, subjected to axial tension, adhered to a soil or rock through a cement grout is not through a uniform stress distribution. This results from the general incompatibility between the modulus of elasticity of steel, grout and soil, causing the phenomenon known as progressive debonding, as it causes the increase of the load of the anchor. The investigation of this phenomenon, the development of this knowledge and its application to industry has resulted in the SBMA System. This system applies much more efficiently the bond stresses available in the field through the use of various units within a single anchor borehole. We present brief guidelines for their design, and case histories within different geotechnical units in Spain.

RÉSUMÉ : Le mécanisme de transfert de charge d'un tirant en acier, soumis à une traction axiale, scellé dans le sol ou le rocher par un coulis de ciment ne se fait pas avec une répartition uniforme des contraintes. Ceci résulte de l'incompatibilité générale entre le module d'élasticité de l'acier, le coulis et le sol, provoquant un phénomène de décollement progressif et d'augmentation de la charge de l'ancrage. L'étude de ce phénomène, le développement d'un savoir et son application à l'industrie sont synthétisés dans le système SBMA. L'utilisation de plusieurs éléments dans un seul forage permet d'augmenter l'efficacité de l'ancrage. La communication présente des directives de conception, et des cas historiques dans différentes unités géotechniques en Espagne.

KEYWORDS: design – ground anchor – multiple anchor - load transfer – efficiency factor – fixed length

MOTS CLES: Conception, tirants, ancrage multiples, charge de transfert, facteur d'efficacité, longueur de scellement

1 INTRODUCTION.

Anchor design codes allow engineers to assume load is distributed uniformly through the length of an anchor, but experts acknowledge that the ultimate load is not proportional to the anchor's fixed length.

Anthony D. Barley's (1995, 1997, 2003) research and development for over a decade confirmed and extended existing independently works coming to the same conclusion of the non-uniformity of the distribution of adhesion in the fixed length anchor, but finally introducing the efficiency factor for calculating the length of the fixed length of an anchor considering this phenomenon. This research was then applied to the development of a new technology for ground and rock posttensioned anchors called Single Bore Multiple Anchor (SBMA).

In 2004 this technology was introduced in Spain, in which the author was responsible. This was done with the technical support of A. Barley.

2. DESCRIPTION

The system involves the installation of multiple units in a single anchor borehole. Each unit has its own single tendon, his own free length, length of bulb and is loaded using its own tensioning unit. The tensioning of all anchor units is performed simultaneously by a hydraulic jacks synchronized equipment that ensure that the load applied to the various units is always the same. The sum of the loads of the various units loads totaled the anchor total of the SBMA. With the design conception, there is no theoretical limitation on the overall bond length used (the sum of the fixed lengths of the various units), while for the conventional anchors little increase is expected load over fixed lengths of 8 to 10 meters.

Another advantage of the system is the opportunity to take account of the varying strata within the ground, as each anchor

within a bore can be designed for different ground conditions. Experts agree that the SBMA system is most effective in weak soils either to enhance capacity or to reduce the total number of anchors. However, they are not economically viable where the structural loading requires only low load anchors at wide spacings.

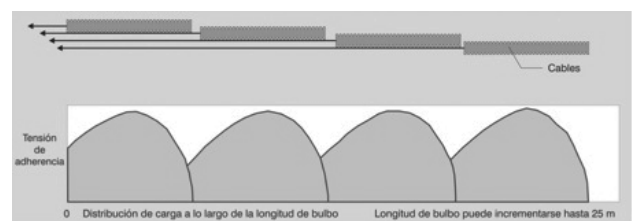


Figure 1. Adhesion stress distribution in several efficient units

3. DESIGN

3.1 Efficiency factor

The relationship between the stiffness of the fixed anchor (controlled by the steel tendon) and the stiffness of the ground governs the rate of progressive debonding as an anchor is loaded and hence affects fixed length efficiency.

The nonlinearity of the mobilization of the value of the grout/ground bond stress (τ_{ult} vs. τ_{res}) along the fixed length could be accounted by the efficiency factor for ground anchors.

$$f_{eff} = 1.6 \cdot L^{-0.57} \quad (1)$$

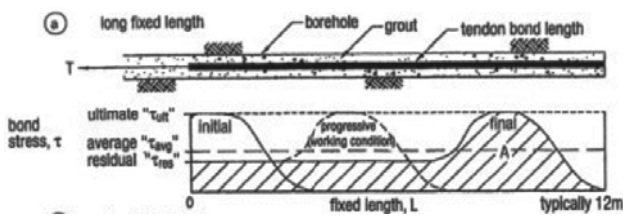


Figure 2. Bond stress distribution in the fixed length for different stages of a load test until failure. The area A is the failure load of the fixed length of the anchor. (Barley and Ostermayer, 2003).

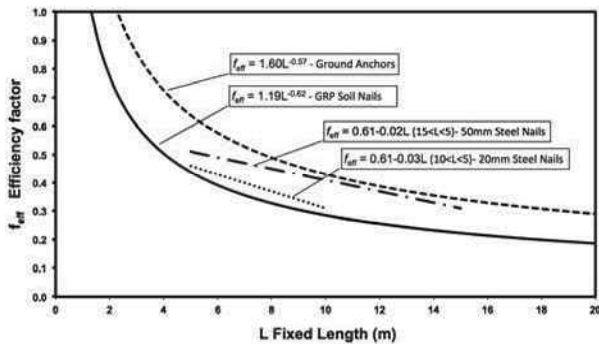


Figure 3. Efficiency factor for Ground Anchors, Steel and GRP Soil Nails (Barley, 1997)

The ultimate geotechnical capacity of the anchor (T_{ult}) is:

$$T_{ult} = (\pi \cdot d \cdot \tau_{ult}) \cdot f_{eff} \cdot L \quad (2)$$

This formula does not apply to granular soils where the capacity to borehole diameter (d) it is not linear and has to be established by meter of fixed length.

All load transfer mechanisms from tendon to grout induce bursting forces in the grout of one degree or another. Generally, the greater the mechanical locking effect (end plate or major deformations) the greater the bursting forces. It follows that the shorter the tendon bond length the greater the mechanical locking to allow the potential transfer of full tendon load capacity. However, this can only be effected where the ground or strong rock will provide adequate confinement of the grout column to prevent bursting failure. So to reduce the inefficiency in load transfer (entire fixed length in shear and tension) it is appropriate to utilize tendon bond lengths long enough to eliminate the risk of bursting failure yet as short as possible to gain maximum efficiency from grout/ground bond (Figure 4).

The high values of bond stress at the grout/ground interface results from the dilatancy effects of the soil in the shear zone, and interlocking at the rough interface, all as a consequence of an increase in radial normal stress.

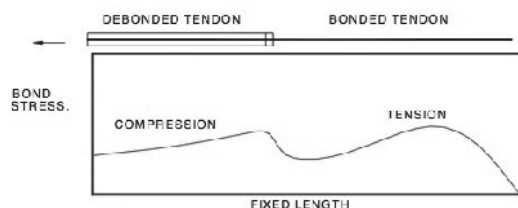


Figure 4. Probable bond stress distribution in compression and combined shear and tension.

3.2 Preliminary tests

Where preliminary trial anchors are tested to failure, each unit anchor yields its own value of ultimate bond capacity and hence more intensive data than conventional test anchors. The in situ testing of many of these multiple anchors with variable unit lengths has therefore recently extended the knowledge and

understanding of the tendon/grout/ground bond mechanism. The SBMA system has been utilized in permanent anchors and temporary anchors (including those with removable tendons).

Test anchors of length 2.5 to 5 metres may easily be taken to failure to establish the ultimate bond stress of that length and then the fixed length of production anchors accurately, designed to provide the required factor of safety. In the trials it is important to control the grouted length tested.



Figure 5. Trial research test with multiple synchronized hydraulic jacks in Parking La Vega, Murcia, 2005.

4. CASE HISTORIES

4.1 La China Stormwater management pond (Madrid)

In carrying out the excavation depth of 15.0 meters, were implemented temporary SBMA anchors of 2000 kN design load, using four units in the soil strata called "Peñuela" (gypsum with interbedded clays). The system was used always in combination with an injection unit located in each bulb known in spanish specification as IR that involves a postgrouting procedure and each units had 3x0,6" steel strand.

Research trials conducted according to the standard UNE 1537, allowed to change the original traditional ground anchors design, for less multiple anchors with increased load and efficiency.

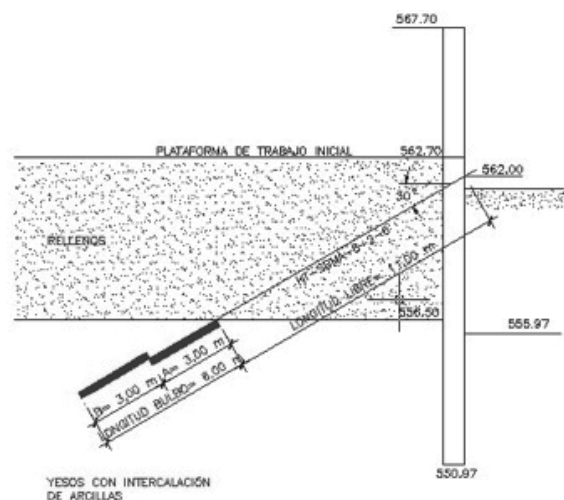


Figure 6. Section of diaphragm wall with trial anchor test TA2.

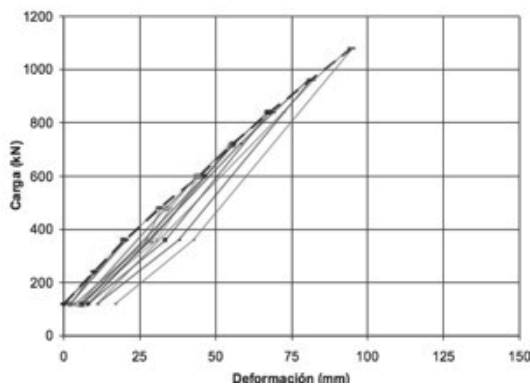


Figure 7. Load-deformation curve of trial test unit TA2-A.

4.2 Parking La Vega (Murcia)

For the excavation of a parking 16.0 meters deep, with 9.0 meters of water thrust, one row of temporary SBMA anchors of 1900 kN were executed using four units in a dense gravel. This bearing layer was underlying clays and silts with medium consistency supported by a diaphragm wall thickness of 0.80 m. This solution as an alternative to a 0.60 m thick wall and two levels of traditional anchors.

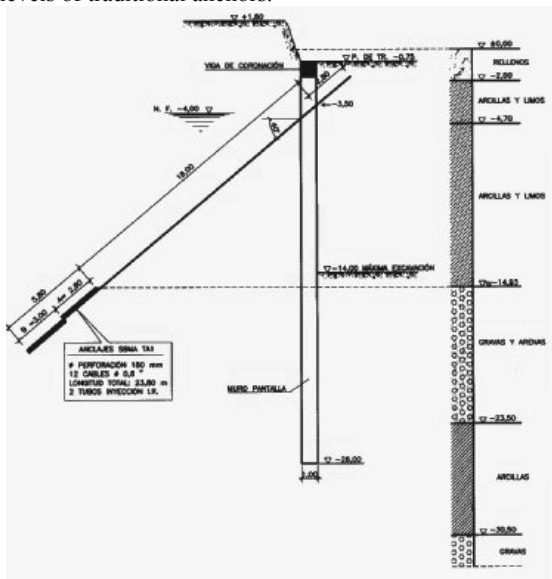


Figure 8. Section of diaphragm wall with trial anchor test TA1.

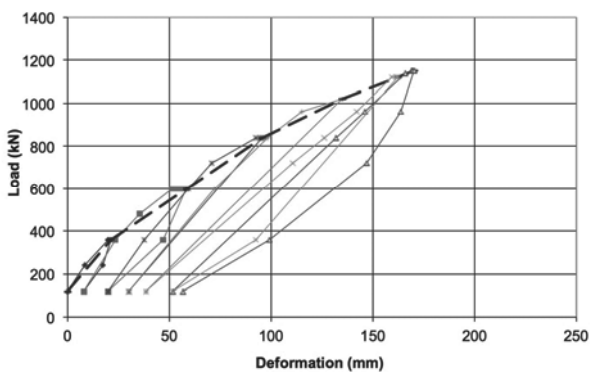


Figure 9. Load-deformation curve of trial test unit TA1-B.

4.3 Palacio de los Congresos (Cartagena)

The Cartagena Convention Centre, located next to the port, run an excavation depth of 13.0 meters, with 10.0 meters of water

pressure. The containment wall was formed by a diaphragm wall 1.00 m thick and 2000 kN temporary anchors, bulb units in both compact red clays, and gravelly dense sands according to the geotechnical profile of each sector, and combinations of both soils in the same anchor. The inclination of the anchors was 30 to 40 degrees to the vertical, in order to avoid obstacles and achieve the desired geotechnical units.



Figure 10. Investigation test in trial SBMA anchor in the port zone.

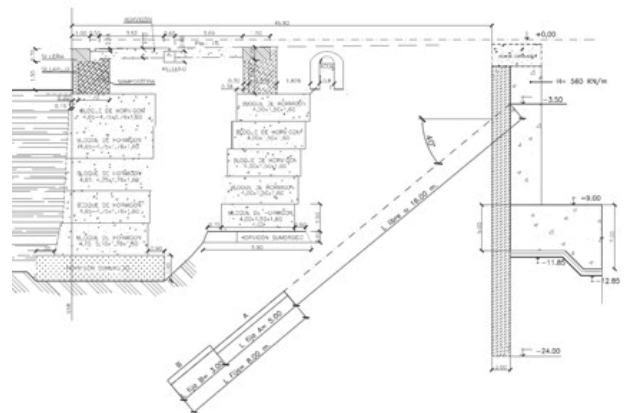


Figure 11. Section of port zone. Diaphragm wall with trial anchor.

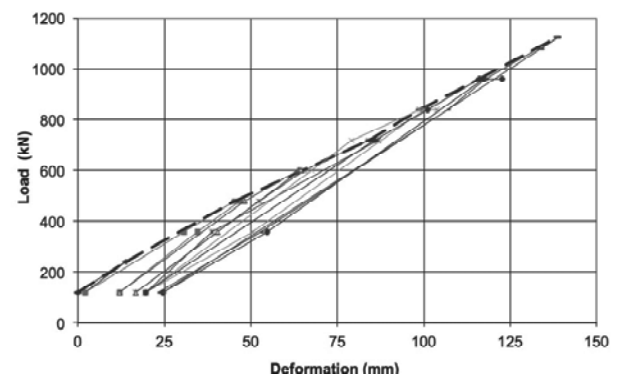


Figure 12. Load-deformation curve of trial test unit 55-B.

4.4 El Corte Ingles (Albacete)

In the execution of the excavation depth of 14.0 meters, were implemented temporary anchors SBMA of 1200-1800 kN

design load, using three and four units in clays and silts of medium consistency, supporting a diaphragm wall of 0,80 m thickness with a water head of 10 meters. They were employed four rows of anchors, the first line with traditional anchors and the other three with SBMA.

In the preliminary research trials, within the present cohesive soils ($N_{SPT} < 8$), the distribution of the adhesion along the fixed lengths tested was close to linear. The same is known of loose granular soils.



Figure 13. General view of the jobsite at design excavation level.



Figure 14. Execution of acceptance tests in El Corte Ingles

Within the reference work, we tested the use of multiple removable anchors as a modern solution to urban problems of public land use. This anchor also employs several units, each consisting of a single tendon lubricated and encapsulated in its entire length, which is bent in a special chair 180 degrees. The chair has a steel bar and the whole performs as a compression anchor, which transfers the load to the cement grout and ground. Thereof the anchorage capacity determines the number of units. The cable of each unit is then removed by pulling one of its ends. The complete withdrawal of steel anchors once their useful life is due, freeing of "pollution" of the ground for future use (subway/metro, underground pipes, buildings with deep foundations or basements, etc.)

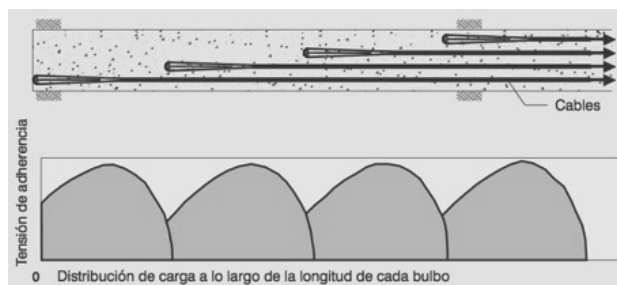


Figure 15. Removable SBMA units, schematic arrangement.



Figure 16. Removing an anchor unit with a force of 50-150 kN.

5. CONCLUSIONS

SBMA ground anchors are currently the most advanced technology for greater efficiency in the use of high adhesion capacity of the ground by the technologies currently employed in the execution of post-tensioned anchors. This system increases the limit loads traditional anchors used in soils, and innovation in paradigms hitherto employed in reference to the design and implementation of the fixed length of an anchor.

The efficiency factor should be complemented with more test data from different soil units with different consistency or relative density; so further detailed test trials research for the better understanding of each geotechnical unit is to be done. Meanwhile, there is experience accumulated in the countries where this technique has been being used the last 20 years.

6. ACKNOWLEDGEMENTS

The author thanks Kellerterra S.L. for the information herein presented, acquired during his service as its Technical Director. Also I am grateful of having met Tony Barley, and having shared professionally and personally these presented works.

7. REFERENCES

- Barley, A.D. 1995. Theory and practice of the Single Bore Multiple Anchor System. Anker in Theorie and Praxis. *Proc. Int. Symposium Salzburg Okt.* Balkema Rotterdam, 293-301
- Barley A.D. and C.R. Windsor. (2000). Recent advances in ground anchor and ground reinforcement technology with reference to the development of the art. *GeoEng 2000 International Conference*, November 19-21, Melbourne, Australia.
- Barley, A.D., Ostermayer, H. 2003. Ground Anchors. *Geotechnical Engineering Handbook*, Ernst & Sohn, 169-215.
- Fernández Vincent, J.M., 2005. Anclajes de Bulbo Múltiple. 5^a Sesión, *Jornadas Técnicas SEMSIG-AETESS - Madrid*.
- Fernández Vincent, J.M., 2010. Teoría y práctica del anclaje de bulbo múltiple. *XX Congreso argentino de Mecánica de Suelos e Ingeniería Geotécnica*, Mendoza, Argentina. 457- 464.
- Fernández Vincent, J.M., 2011. Casos de aplicación del anclaje de bulbo múltiple. *14th Pan-American Conference on Soil Mechanics and Geotechnical Engineering*. Toronto, Canada.
- Ostermayer, H. (1974). Construction carrying behaviour and creep characteristics of Ground Anchors. *ICE Conference on Diaphragm Walls and Anchorages*, London, pp. 141-151.
- UNE 1537 – Execution of special geotechnical works - Ground anchors.

Computed and observed ground movements during top-down construction in Chicago

Mouvements de terrains calculés et observés en construction descendante à Chicago

Finno R.J., Arboleda L., Kern K.

Department of Civil and Environmental Engineering, Northwestern University, Evanston, IL, USA

Kim T.

Korea Railroad Research Institute, Uiwang, Korea

Sarabia F.

AECOM, Vernon Hills, IL, USA

ABSTRACT: Two detailed case studies of deep excavations in Chicago made with top down techniques are presented. The importance of considering all aspects of the construction process when estimating ground movements is emphasized. Detailed construction records were maintained at both sites. Inclinometers located within the walls, close to the walls and 7 m from the wall provided lateral movements throughout construction. Ground surface settlements were obtained by optical survey of several hundred observation points at each project. In addition, one of the projects included 88 strain gages installed in the floor slabs to measure time dependent responses of the concrete slabs used as lateral support for more than four years. The movements are presented in relation to construction activities and causes of incremental movements are identified. The lateral movements that arose from cycles of excavation and bracing accounted for approximately one-quarter and one-half the total movements at the two sites. Of these, field performance data and results of numerical simulations showed that approximately 40% of the movements arose from the time-dependent responses of the concrete floor slabs.

RÉSUMÉ : Deux études de cas détaillées d'excavation profondes réalisées à Chicago en construction descendante sont présentées. L'accent est mis sur l'importance de prendre en considération tous les aspects du procédé de construction. Des registres de construction détaillés ont été maintenus sur les deux projets. Des inclinomètres situés dans les murs, à proximité des murs et à 7m du mur ont mesuré les déplacements horizontaux tout au long de la construction. Les affaissements de surface ont été observés à l'aide d'un relevé topographique optique comprenant plusieurs centaines de points pour chaque projet. De plus, l'un des projets comprenait 88 jauges de déformations installées dans les dalles de plancher pour mesurer les réponses dans le temps des dalles de béton utilisées comme supports latéraux pendant plus de quatre ans. Les mouvements sont mis en relation avec les activités de construction et les causes des mouvements progressifs sont identifiées. Les mouvements latéraux causés par les cycles d'excavation et de contreventement ont représenté environ la moitié et le quart des mouvements totaux sur les deux projets. Pour ceux-ci, les résultats des tests sur le terrain et des simulations numériques ont montré qu'environ un tiers des mouvements était causé par les réponses dans le temps des dalles de planchers en béton.

KEYWORDS: Excavation, top-down support, ground movements, clays, time-dependent concrete response

1 INTRODUCTION

Use of top down construction has increased as more developers have seen the benefit of taking the excavation portion of a project off the critical path. Top down methods use permanent walls and flooring systems as temporary support and thus the support systems are very stiff. Yet, there are conflicting data concerning whether resulting movements are smaller than those associated with bottom-up methods. For example, Long (2001) observed no discernible difference in the performance of internally supported, anchored, or top-down systems based on examination of 296 excavation case studies. Kung (2009) reported results of 26 excavations made through Taipei silty clay which showed the maximum lateral wall deflection induced by the top-down methods were 1.3 times larger than that induced by bottom up methods. These observations are surprising given that the floor slabs are in theory much stiffer than either cross-lot braces or ground anchors, and that it is not possible to overexcavate the soil – i.e., make a deeper cut than planned so that the support system is essentially more flexible than planned in design - during construction since one must cast each floor on the ground.

This paper summarizes two case studies of deep excavations in Chicago made with top down techniques. Detailed construction records were maintained at both the Block 37 and One Museum Park West (OMPW) projects. Performance during construction is illustrated with results of inclinometers

located close to the walls and optical surveys of points on the ground adjacent to the excavations. In addition, one of the projects included 88 strain gages installed in the floor slabs to measure for four years the time-dependent responses of the concrete slabs used as lateral support. The movements are presented in relation to construction activities at both sites and causes of incremental movements are identified. It is shown that the movements that occurred during cycles of excavation and bracing are small, and about 40% of these movements are attributable to the time-dependent responses of the concrete slabs. The importance of considering all aspects of the construction process when evaluating movements is emphasized.

2 SUBSURFACE CONDITIONS

The subsurface conditions at the two sites are summarized in Figure 1 which shows the natural water contents and undrained shear strengths found from results of site investigations at each location. The surficial layer is an urban fill material consisting of sandy soils and construction debris. Underlying the fill material is a sequence of glacially deposited clays. The first two layers are soft to medium stiff clays which are very similar mineralogically, but exhibit different geotechnical characteristics due to the type of glacial deposition. The Blodgett stratum underlies the urban fill and was deposited in a

supra-glacial environment, which include glaciolucustrine clays and melt-out and flow tills (Chung and Finno, 1992). Because of this complicated depositional environment, the Blodgett generally has variable geotechnical characteristics, including water content, strength and stiffness. A desiccated crust is often present on top of the Blodgett stratum. At these sites, the crust is relatively thin, and in some cases is not present at all. Underlying the Blodgett stratum is a medium stiff clay, called the Deerfield stratum. This stratum exhibits much more uniform geotechnical characteristics than the Blodgett because the Deerfield was deposited as a basal melt-out till or a waterlain paratill. The stiff Park Ridge clay underlies the Deerfield layer. It is generally a little more overconsolidated than the upper clays, with an OCR of about 1.5. A deposit locally known as “hardpan” is found beneath the Park Ridge stratum. The soils in the hardpan are very stiff to hard and consist of silty clays to clayey silts and contain occasional lenses of sandy soils. These soils are basal tills and overconsolidated.

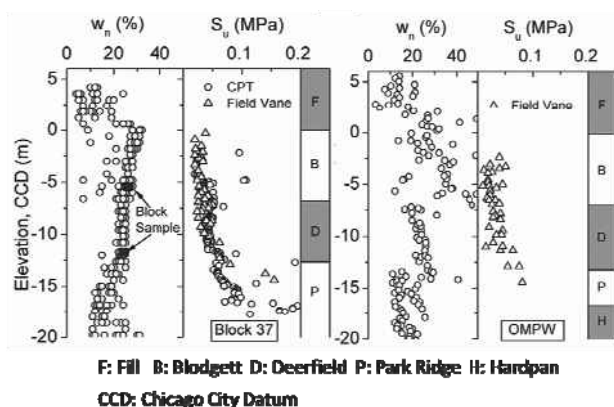


Figure 1. Subsurface conditions

3 BLOCK 37 PROJECT

Lateral support for the Block 37 excavation consisted of a 0.9 m thick reinforced concrete slurry wall and four levels of reinforced concrete floor slabs. After installation of the slurry wall, existing foundations from previous buildings were removed. These potholing activities were extensive near the north end of the excavation, and excavations reached as deep as 6 m. After the abandoned foundations and walls were removed, the excavations were backfilled.

Thereafter the excavation progressed in stages to the levels of the four basement floors (B1, B2, B3 and B4). Because the “ground” slab was placed after slab B1, the slurry wall was cantilevered with an unsupported length of about 7 m before any lateral support was placed. Thus this excavation deviated from an ideal top-down construction system because the lateral support was not installed prior to any significant excavation. The contractor made the decision to delay placement of the ground surface slab on the basis of construction expediency. A complete description of the activities at the site and performance of the excavation is found in Kern (2011).

3.1 Ground movements during construction

The development of ground movements during construction is summarized in Figure 2. The optical survey points and inclinometer were located adjacent to the north wall of the excavation. The settlements are typical of the maximum values measured along this side of the excavation. The horizontal movements were taken from an inclinometer located 1 m behind the slurry wall near its center and were taken from elevation – 9 m CCD. Lateral movements versus depth will be discussed in the next section. Also shown on the figure is a record of the

construction activities so the causes of the movements are apparent.

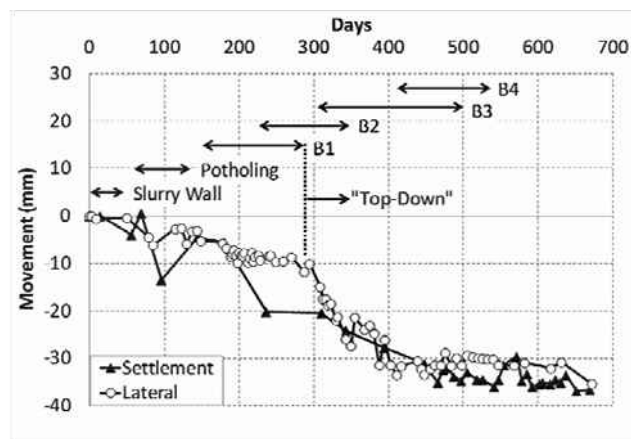


Figure 2. Settlements and lateral movements at Block 37

The maximum settlement and lateral movement observed at this section was 36 mm. As is apparent from the figure, significant ground movements developed during both the potholing activities and the first portion of the excavation when the large cantilever stage existed as the contractor excavated to the B1 slab level. These activities caused about 60% of the settlements that developed throughout the entire construction process. This large percentage was caused by the contractor’s decision to start the top-down process after the first level basement was constructed. The removal of the old foundations and slabs also contributed to the relatively large movements observed along this wall.

3.2 Lateral movements adjacent to wall

Typical distributions of lateral ground movements with depth are shown in Figure 3 for inclinometers located 1 m and 7 m from the wall. These inclinometers were installed prior to any construction at the site and thus indicate the complete lateral response. The large influence of the potholing and initial cantilever stage of the excavation is seen clearly in the results.

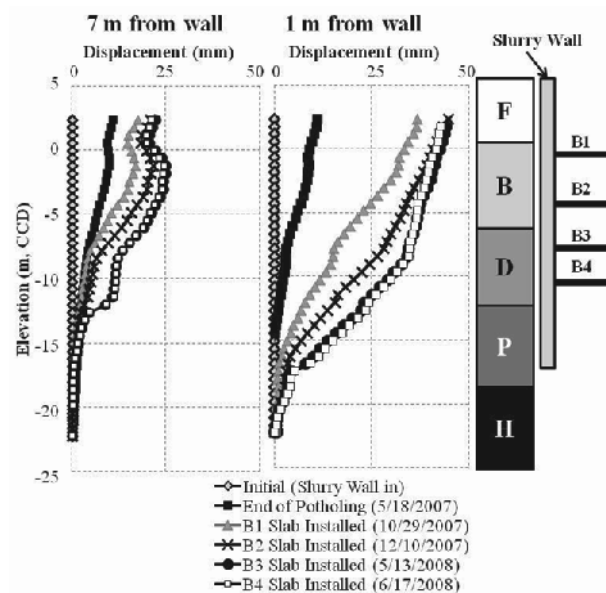


Figure 3. Lateral ground movements at Block 37

4 ONE MUSEUM PARK WEST PROJECT.

The One Museum Park West project involved constructing a 53-story reinforced concrete tower with a central core and four or five basement levels that extended approximately 15.3 m

below grade. The central core was excavated using a circular cofferdam, consisting of a sheet-pile wall and horizontal ring beams for internal bracing. The construction of the tower core was performed in a conventional “bottom-up” manner. The basement was constructed with steel beam reinforced concrete secant pile walls using top-down construction procedures. After leveling the site, the perimeter wall was installed and caisson foundations constructed. After the central core cofferdam was built, the excavation of the remainder of the site is being made with “top-down” construction methods. The perimeter secant pile wall is utilized as a permanent load bearing wall. Lateral bracing is provided by 4 or 5 levels of permanent floor slabs, depending on the location within the structure. After the ground level slab was cast integrally with the slurry wall, excavation proceed top-down by excavating to the bottom of the second level floor slab, casting that slab integrally to the slurry wall, and repeating the process until the final excavation depth was reached. Detailed descriptions of the construction and performance of this project are found in Sarabia (2012) and Arboleda (2013).

The development of ground movements during construction is summarized in Figure 4. Again, both settlements and lateral movements are represented in the figure. In this case, only the settlements provide a complete record of the ground response during construction. The inclinometers were located within 1 m of the secant pile wall at all locations, and were damaged as the wall was installed. Replacement inclinometers were initialized prior to the start of top-down excavation, so these data do not reflect deformations that developed as the wall and caissons were installed, or as the central core cofferdam was constructed. The data for the lateral movements were taken from the location of the maximum lateral movement recorded by the inclinometer, in this case, from elevation -8 m CCD. The settlements are typical of the maximum values measured along the west side of the excavation. Also shown on the figure is a record of the construction activities so the causes of the movements are apparent.

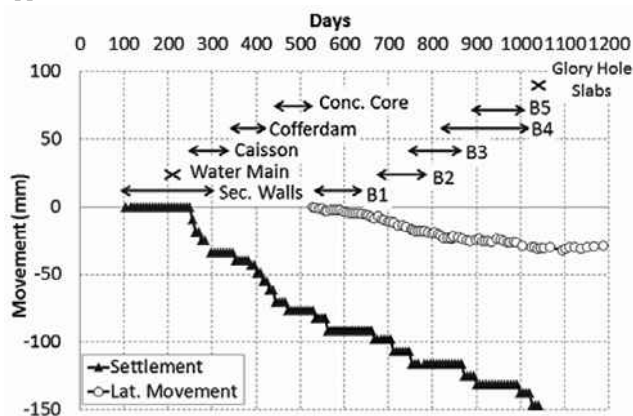


Figure 4. Settlements and lateral movements at OMPW

The maximum settlement observed at this section was 150 mm and the maximum lateral movement was 30 mm. As is apparent from the figure, significant ground movements developed throughout construction. The portions of the settlements that occurred during different phases of construction are summarized in Table 1. The activities before the top down portion of the project started resulted in 75% of the total settlements observed during construction.

Table 1. Settlements during construction activities

Construction activity	Settlement (mm)
Secant pile wall installation	11
Caisson installation	12
Water main relocation	5
Central cofferdam construction	12
Top-down construction	13

5 WALL MOVEMENTS DURING EXCAVATION

The lateral deformations that were recorded at OMPW only reflect those that occurred during top-down construction. Data from an inclinometer located in the middle of the west wall are shown on Figure 5. Also shown on the figure are the lateral movements that developed at Block 37 during the top-down phase of that construction, i.e., those after slab B1 was cast.

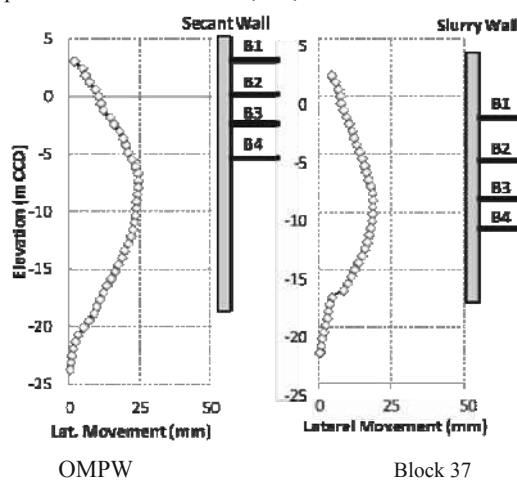


Figure 5. Lateral movements during top-down excavation only

The trends in these data reflect expected responses for an excavation made using top-down methods with very stiff walls and supports. Very little lateral movement is observed at the uppermost slab which was cast at the ground surface. The normalized maximum horizontal movements (movement/depth of excavation) were 0.14% and 0.2% at the Block 37 and OMPW sections, respectively. These values are more in line with what one would expect from a very stiff excavation with no overexcavation. However, it is clear that movements developed at both sites as a result of other construction activities or procedures that were not employed with the goal of minimizing ground movements. When using precedent for a first order estimate of expected ground movements for a top-down procedure, these data provide useful estimates. One should not indiscriminately use performance data without considering all activities that occurred during construction.

6 TIME-DEPENDENT RESPONSES OF FLOOR SLABS

The concrete floor slabs that serve as lateral bracing for these two projects were cast integrally with the support walls. As such, the floor slabs contracted as the concrete cured and crept under load. This time-dependent component of movement contributed to the wall deformations and analyses were conducted to evaluate the magnitude of this effect. Eighty-eight vibrating wire strain gages were cast into the OMPW slabs at four levels and at five sections so as to directly measure the strains in the slab that developed over time. Detailed descriptions of the instrumentation and results of analyses are given in Arboleda (2013).

To illustrate the influence of the time-dependent properties of concrete on the lateral movements of the secant walls, 3D

finite element simulations of the top-down construction process were conducted using SAP2000. The nonlinear time-dependent concrete effects of shrinkage, creep and variation of the modulus of elasticity with time were considered in the analysis. The analysis was performed in a step-by-step basis for the entire construction sequence using nonlinear stage construction without geometric nonlinearity.

Figure 6 shows the model after the first basement level was placed. The reinforced concrete columns and caissons were modeled as frame elements whereas the basement slabs, secant walls, foundation mat, corewalls, and interior shear walls were modeled as thin shell elements. The cross section of the secant walls consisted of concrete elements with embedded wide flange sections (W24, W33) and was modeled using an equivalent thickness based on the transformed section. Structural loads were applied, but lateral earth loads were not.

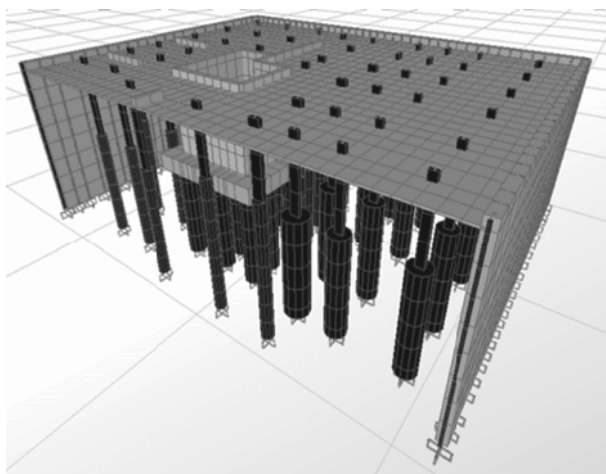


Figure 6. Model for time-dependent slab response at OMPW

The concrete was assumed isotropic with compressive strength taken from the as-built structural drawings and verified with the concrete reports provided by the contractor. The time-dependent behavior of concrete was included only for the basement slabs. The concrete properties were calculated based on standard concrete practice methods defined in ACI (2011) for a Poisson ratio of 0.2. The nonlinear variation of shrinkage with time was based on average values of the standard concrete practice codes: ACI 209, CEB-FIP 1990, AASHTO LRFD 2010, AS3600-2009, and NEN 6720.

The results of the analyses are given in Figure 7, where both the computed time-dependent movements of the walls at the end of each slab placement stage are compared to the total lateral movements of an inclinometer 1 m behind the wall. The lateral movements shown correspond to those that developed after the excavation to the first slab level was made, so that one can directly see the contributions of the time-dependent movements to the lateral deformations. About 40% of the lateral movements can be attributed to the time dependent effects of the concrete slabs.

7 CONCLUSION

Based on the results of the data and analyses summarized herein, the following conclusions can be drawn regarding these two excavations:

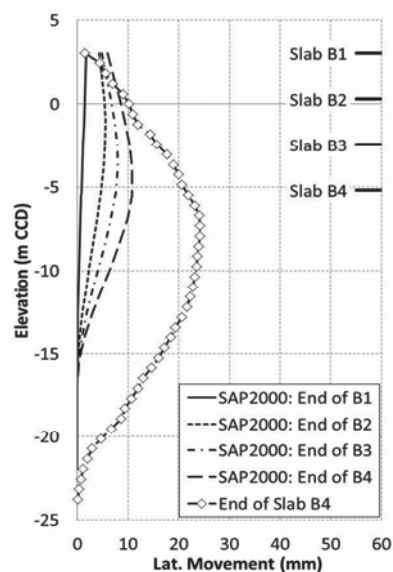


Figure 7. Computed time-dependent and observed lateral movements after slab B4 placed at OMPW

1. Top-down excavations in clays can be expected to result in normalized horizontal movements of approximately 0.15 to .2% when the uppermost slab is placed close to the ground surface so as to minimize the cantilever movements associated with the excavation process.
2. Of these “top-down” movements, approximately 40 % could be attributed to the time-dependent response of the concrete floor slabs.
3. Other construction activities or expedient excavation procedures led to movements that constituted 60 to 75% of the total movements that developed during construction. Use of precedence in estimating ground movements must be tempered by a realization of other site activities that can lead to ground movements.

6 ACKNOWLEDGEMENTS

Financial support for this work was provided by National Science Foundation grant CMMI-0928184 and the Infrastructure Technology Institute of Northwestern University.

7 REFERENCES

- American Concrete Institute (2011), "Building Code Requirements for Structural Concrete (ACI 318-11) and Commentary," Farmington Hills, MI.
- Arboleda, L. (2013). "Influence of time-dependent effects on movements associated with top-down excavations," PhD dissertation, Northwestern University, Evanston, IL
- Chung, C.-K. and Finno, R.J., "Influence of depositional processes on the geotechnical parameters of Chicago glacial clays," *Engineering Geology*, 32, 1992, 225-242.
- Kern, K. (2011). "Analysis of top-down construction at the Block 37 project in Chicago II," MS thesis, Northwestern University, Evanston, IL
- Kung, G. T.-C. (2009). "Comparison of excavation-induced wall deflection using top-down and bottom-up construction methods in Taipei silty clay," *Computers and Geotechnics*, Volume 36, Issue 3, April, 373-385.
- Long, M. (2001) "Database for retaining wall and ground movements due to deep excavations," *J Geotech Geoenviron Eng, ASCE*, 127 (3), 203-224.
- Sarabia, F. (2012). "Hypoplastic constitutive law adapted to simulate excavations in Chicago glacial clays," PhD thesis, Northwestern University, Evanston, IL

Comparative Life Cycle Assessment of Geosynthetics versus Concrete Retaining Wall

Analyse de cycle de vie comparative d'un épaulement géotextile et conventionnel

Frischknecht R., Büsser-Knöpfel S., Itten R.
treeze Ltd., Kanzleistrasse 4, 8610 Uster, Switzerland

Stucki M.
Zurich University of Applied Sciences, Institute of Natural Resource Sciences, Campus Grüental, 8820 Wädenswil Switzerland

Wallbaum H.
Chalmers University of Technology, Civil and Environmental Engineering, 412 96 Göteborg, Sweden

ABSTRACT: Geogrids made of geosynthetics can replace conventional building materials like concrete. In this article, goal and scope, basic data and the results of a comparative life cycle assessment of concrete reinforced retaining walls (CRRW) and geosynthetics reinforced retaining walls (GRRW) are described. One running meter of a three meters high retaining wall forms the basis for comparison. The two walls have the same technical performance and an equal life time of 100 years. The GRRW has a lower demand of steel and concrete compared to the CRRW. The product system includes the supply of the raw materials, the manufacture of the geotextiles and the concrete, the construction of the wall, its use and its end of life. The life cycle assessment reveals that the GRRW causes lower environmental impacts. The cumulative greenhouse gas emissions of 300 m CRRW are 400 t and 70 t in case of GRRW. The use of an environmentally friendlier lorry in a sensitivity analysis and monte carlo simulation confirm the lower environmental impacts caused by the construction of a GRRW compared to a CRRW. More than 70 % of the environmental impacts of the geogrids production are caused by the raw material provision (plastic granulate) and the electricity demand in manufacturing.

RÉSUMÉ : Géogrids peuvent remplacer les matériaux conventionnels comme le béton. Cet article contient une description de la définition de l'objectif et du champ d'étude, de l'analyse de l'inventaire et des résultats d'un analyse de cycle de vie comparative d'un épaulement géotextile et conventionnel. La comparaison est faite sur un mètre courant d'un épaulement de trois mètre d'hauteur. Les deux alternatives ont les mêmes propriétés techniques et la même durée de vie de 100 ans. Les systèmes contiennent la provision des matériaux, la fabrication des géotextiles et du béton, la construction, l'utilisation et l'évacuation de l'épaulement. L'analyse de cycle de vie démontre qu'un mètre courant d'un épaulement géotextile cause moins d'impacts environnementaux qu'un mètre courant d'un épaulement de béton. 300 mètres d'un épaulement de béton entraîne 400 t CO₂-eq, celui de géotextile 70 t CO₂-eq des émissions des gaz à effet de serre. L'utilisation des camions avec les émissions réduites ne change pas les résultats. Une simulation « monte carlo » confirme la stabilité des résultats. La provision des matériaux et l'électricité utilisé dans la fabrication de la couche de filtre géotextile sont des facteurs primordiaux (plus que 70 %) en ce qui concerne les impacts environnementaux du géogrid utilisé dans l'épaulement géotextile.

KEYWORDS: retaining wall, slope retention, geosynthetics, concrete, geogrid, life cycle assessment, LCA

MOTS CLÉS : épaulement, géotextile, géogrid, béton, analyse de cycle de vie, ACV

1 INTRODUCTION

Geosynthetic materials are used in many different applications in civil and underground engineering, such as in road construction, in foundation stabilisation, in landfill construction and in slope retention. In most cases they are used instead of minerals based materials such as concrete, gravel or lime.

Environmental aspects get more and more relevant in the construction sector. That is why the environmental performance of technical solutions in the civil and underground engineering sector gets more and more attention.

The European Association for Geosynthetic Manufacturers (E.A.G.M.) commissioned ETH Zürich and Rolf Frischknecht (formerly working at ESU-services Ltd.) to quantify the environmental performance of commonly applied construction materials (such as concrete, cement, lime or gravel) versus geosynthetics (Stucki et al. 2011).

In this article, the results of a comparative Life Cycle Assessment (LCA) of slope retention are described. The slope retention is either provided by a concrete reinforced retaining

wall (CRRW) or a geosynthetics reinforced retaining wall (GRRW).

The environmental performance is assessed with eight impact category indicators. These are Cumulative Energy Demand (CED, Frischknecht et al. 2007), Climate Change (Global Warming Potential, GWP100, Solomon et al. 2007), Photochemical Ozone Formation (Guinée et al. 2001a; b), Particulate Formation (Goedkoop et al. 2009), Acidification (Guinée et al. 2001a; b), Eutrophication (effects of nitrate and phosphate accumulation on aquatic systems, Guinée et al. 2001a; b), Land competition (Guinée et al. 2001a; b), and Water use (indicator developed by the authors). The calculations are performed with the software SimaPro (PRÉ Consultants 2012).

2 GEOSYNTHETIC VERSUS CONCRETE RETAINING WALL

It may be necessary in some cases, especially in the construction of traffic infrastructure, to build-up very steep walls. For such walls, supporting structures are necessary. The retaining walls need to meet defined tensile and shear

strengths. Retaining walls can be reinforced with concrete or geogrid made of geosynthetics.

The functional unit is defined as the construction and disposal of 1 m slope retention with a 3 meters high wall, referring to a standard cross-section. Thus, the functional unit is independent of the length of the wall.

Polyethylene and PET granules are used as basic material of the geogrid. The geogrid has to achieve a long-term strength of 14 kN/m. A scheme of both types of retaining walls are shown in Fig. 1.

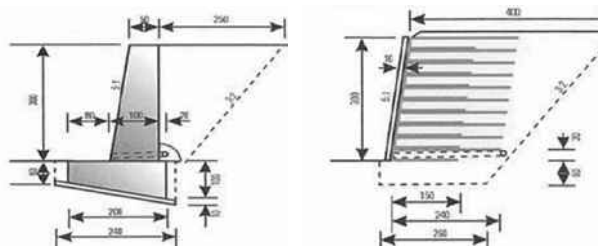


Figure 1. Scheme of the concrete reinforced retaining wall (CRRW, left) and the geosynthetics reinforced retaining wall (GRRW, right)

Some important key figures of the construction of a reinforced retaining wall are summarized in Tab. 1. The information refers to one meter of slope retention infrastructure and a time period of 100 years. Diesel is used in building machines for the excavation of the foundation and the compaction of the ground. The NMVOC emissions shown are released from the bitumen used to seal the concrete wall. The use of recycled gravel is not considered, since usually no onsite recycled gravel with specific properties is available when building reinforced retaining wall for the first time.

Tab. 1 shows specific values of the retaining walls for both alternatives. The material on site is used as fill material, wall embankments and cover material in case of a GRRW. A drainage layer made of gravel with a thickness of at least 30 cm behind the concrete lining is necessary. To be consistent with the CRRW, a gravel layer thickness of 80 cm is assumed in both cases. Round gravel is used for drainage purposes.

Table 1. Selected key figures describing the two constructions of one meter reinforced retaining wall

	Unit	CRRW	GRRW
Concrete	m ³ /m	1.60	-
Lean mix concrete	m ³ /m	0.24	-
Structural concrete	m ³ /m	2.10	0.31
Reinforcing steel	kg/m	153	-
Gravel	t/m	4.3	4.3
Bitumen	kg/m	2.84	-
Three layered laminated board	m ³ /m	0.01	-
Geosynthetic	m ² /m	-	39.2
Polystyrene foam slab	kg/m	0.25	-
Polyethylene	kg/m	1.74	2.02
Diesel in building machine	MJ/m	11.6	53.9
Transport, lorry	tkm/m	701	265
Transport, freight, rail	tkm/m	33.2	6.9
Land use	m ² /m	1.0	0.6
NMVOC	g/m	20	-

The difference between the CRRW and GRRW lies in the amount of concrete, steel and bitumen used, the energy con-

sumption that is related to the slope retention used (material transportation, excavation etc.), and the use of geosynthetics.

In a sensitivity analysis, it is analysed how the results of the slope retention change, when a low emission Euro5 lorry (>32 t) is used for the transportation of the materials to the construction site instead of an average European lorry (>16 t).

3 MANUFACTURING OF THE GEOGRID

Data about geosynthetic material production are gathered at the numerous companies participating in the project using pre-designed questionnaires. The company specific life cycle inventories are used to establish average life cycle inventories of geosynthetic material.

The data collected include qualitative information of system relevant products and processes from the producer, information from suppliers of the producer (where possible) as well as data from technical reference documents (e.g. related studies, product declarations, etc.). Average LCI are established on the basis of equally weighted averages of the environmental performance of the products manufactured by the participating companies.

The primary source of background inventory data used in this study is the ecoinvent data v2.2 (ecoinvent Centre 2010), which contain inventory data of many basic materials and services. In total, data from 5 questionnaires concerning the production of geosynthetic geogrids used in slope retention applications are included. The quality of the data received is considered to be accurate. The level of detail is balanced in a few cases before modelling an average geosynthetic layer.

Tab. 2 shows important key figures of the production of an average geosynthetic geogrid

Table 2. Selected key figures referring to the production of 1 kg geosynthetic layer used in slope retention

	Unit	Value
Raw materials	kg/kg	1.02
Water	kg/kg	0.86
Lubricating oil	kg/kg	7.30*10 ⁻⁵
Electricity	kWh/kg	0.73
Thermal energy	MJ/kg	1.24
Fuel for forklifts	MJ/kg	0.13
Building hall	m ² /kg	6.32*10 ⁻⁶

4 LIFE CYCLE IMPACT ASSESSMENT

In this section the environmental impacts of 1 m slope retention with a height of 3 m over the full life cycle are evaluated. The life cycle includes the provision of raw materials as well as the construction and disposal phases.

In Fig. 2 the environmental impacts over the full life cycle of the slope retention are shown. The environmental impacts of the case with the highest environmental impacts are scaled to 100%. The total impacts are divided into the sections wall, raw materials (concrete, gravel, geosynthetic layers, reinforcing steel, bitumen, wooden board), building machine (construction requirements), transports (of raw materials to construction site) and disposal of the wall (includes transports from the construction site to the disposal site and impacts of the disposal of the different materials).

The GRRW (4B) causes lower environmental impacts compared to the CRRW (4A) in all impact categories considered. The non-renewable cumulative energy demand of the construction and disposal of 1 meter CRRW (4A) with a height of 3 meters is 12'700 MJ-eq and 3'100 MJ-eq in case

of GRRW (4B). The cumulative greenhouse gas emissions amount to 1.3 t CO₂-eq in case of the CRRW (4A) and 0.2 t CO₂-eq in case of the GRRW (4B). Correspondingly, the cumulative greenhouse gas emissions of 300 m CRRW (4A) are 400 t and 70 t in case of GRRW (4B).

The most relevant aspects concerning the environmental impacts of the life cycle of the CRRW (4A) are concrete, reinforcing steel, transportation and disposal. This order of relevance changes depending on the impact category indicators. The high share of concrete in the global warming indicator can be explained by the production process of clinker. During its calcination process geogenic CO₂ emissions arise. Reinforcing steel consists of 63 % primary steel and 37 % recycled steel. Most environmental impacts of the reinforcing steel arise from the fuel consumption and the emissions during the sinter and pig iron production in the supply chain of the primary steel. Disposal includes the disposal as well as transports from the construction site to the disposal site in case the material is not recycled. Impacts of disposal are dominated by the high amount of concrete which is landfilled. While direct emissions of landfilling concrete are negligible, the construction of the landfill and the transport of concrete to the landfill site are important. The land competition indicator is strongly influenced by the direct land use of the slope retention as well as by the wooden board used in the formworks. Gravel is responsible for a considerable share of the total amount of water used because substantial amounts of water are needed in gravel production.

Concrete, the geosynthetic and transportation mostly cause the highest burdens of the life cycle of the GRRW (4B). The share of the geogrid to the overall impacts is relatively high because on one hand several layers, and thus a considerable amount of geogrid, are required. On the other hand most materials used in the construction of the slope retention are available on-site and thus do not cause substantial environmental impacts (compare Tab. 1). The disposal gains importance in the categories eutrophication and global warming. The global warming impacts of disposal are caused by burning geogrids in waste incineration plants, which leads to fossil CO₂ emissions. Gravel dominates the water use indicator and the direct land use of the slope retention wall during its use is dominating land competition.

The main driving forces for the difference between CRRW (4A) and GRRW (4B) are the higher amount of concrete used in CRRW (4A) as well as the use of reinforcing steel, which additionally leads to higher transport expenditures. With regard to CED renewable and land competition the wooden board additionally increases the difference in total impacts because wood is a renewable resource with a high direct land occupation. Direct land competition is lower for the GRRW (4B) because the sprayed concrete lining is thinner than the CRRW (4A) and the embankment and backfilling area is not considered as occupied land.

The share of the geosynthetic material on the overall environmental impacts is between 3 % and 44 % (water use and CED non-renewable, respectively).

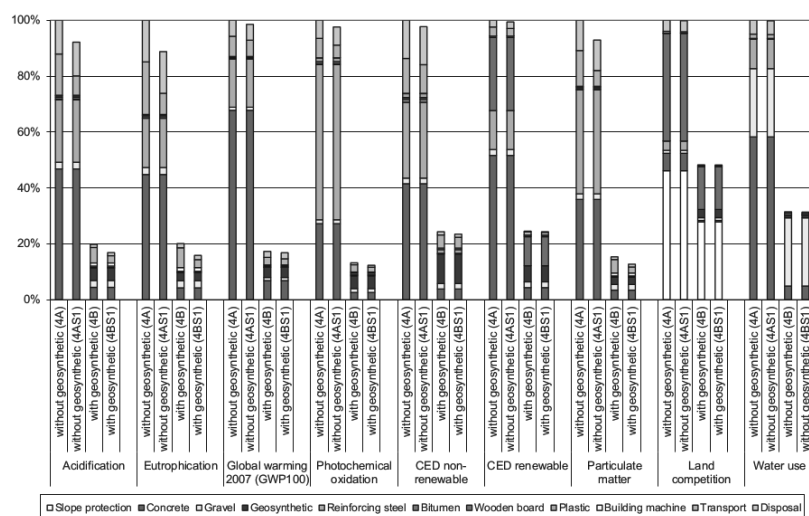


Figure 2. Sensitivity analysis: Environmental impacts of the life cycle of 1 m conventional (4A) and geosynthetic retaining wall (4B). 4AS1 and 4BS1 refer to the sensitivity analysis with a Euro5 lorry transportation. For each indicator, the case with highest environmental impacts is scaled to 100%.

4.1 Sensitivity analysis

In a sensitivity analysis, it is analysed how the results of the slope retention change, when a Euro5 lorry (>32 t) is used for the transportation of the materials to the construction site instead of an average European lorry (>16 t).

Fig. 2 reveals that if a Euro5 lorry with lower exhaust emissions is used for the transportation, the environmental impacts of the GRRW (4BS1) are reduced between 0.1 % and 22.8 % (land competition and eutrophication respectively), whereas the environmental impacts of the CRRW (4AS1) are decreased between 0.2 % and 13.2 % (land competition and eutrophication respectively). The use of a Euro5 lorry leads among others to lower NO_x emissions, which influences eutrophication. Land competition is obviously not influenced much by using another type of lorry.

4.2 Contribution Analysis Geosynthetic Production

In this section the environmental impacts of 1 kg geogrid are evaluated. The life cycle includes the provision and use of raw materials, working materials, energy carriers, infrastructure and disposal processes. The category geosynthetic in Fig. 3 comprises the direct burdens of the geosynthetic production. This includes land occupied to produce the geosynthetic as well as process emissions (e.g. NMVOC, particulate and COD emissions) from the production process but not emissions from electricity and fuel combustion which are displayed separately. The environmental impacts of the geogrid are shown in Fig. 3. The cumulative greenhouse gas emissions amount to 3.4 kg CO₂-eq per kg.

Environmental impacts are mostly dominated by the raw material provision and electricity consumption. Raw material

includes different types of plastics. Country-specific electricity mixes are modelled for each company and thus impacts of electricity consumption depend not only on the amount of electricity needed but also on its mix. The higher share of electricity in CED renewable can be explained by the use of hydroelectric power plants in the electricity mixes of several factories. And the relatively high share in eutrophication is mainly due to electricity from lignite. The share of heating energy and fuel consumption for forklifts is between 0.01 % (land competition) and 2.8 % (global warming) and is thus not considered to be of primary

importance. With regard to land competition the geosynthetic production plays an important role. The impacts are dominated by the direct land use, i.e. land which is occupied by the manufacturer plant in which the geosynthetic is produced. Indirect land uses, i.e. land occupation stemming from upstream processes, are significantly lower because no land occupation is reported in the inventories of plastic feedstock and no land intensive products such as wood are used in considerable amounts. Water consumption is included in the working materials. As a consequence, this category bears about 5 % of the total amount of water used.

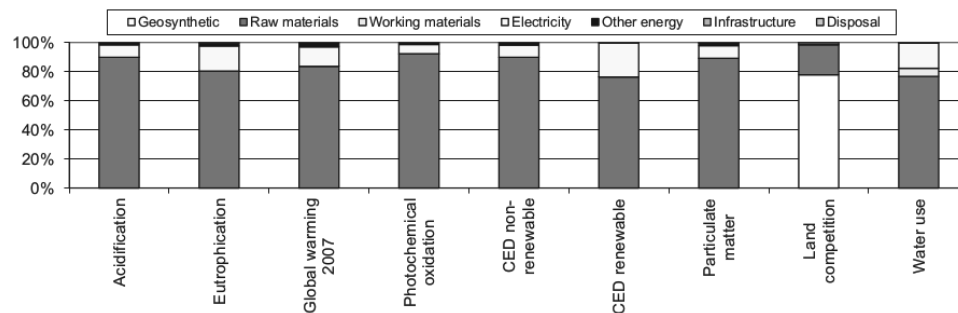


Figure 3. Environmental impacts of the life cycle of 1 kg geogrid. Geosynthetic includes direct burdens of the geosynthetic production. Raw materials include plastic, extrusion if necessary and additives, working materials include water (tap and deionised) and lubricating oil, other energy includes thermal energy and fuels, infrastructure covers the production plant and disposal comprises wastewater treatment and disposal of different types of waste.

5 DISCUSSION AND CONCLUSION

The use of geosynthetics leads to lower environmental impacts of slope retention in all indicators investigated. The specific climate change impact of the construction of the slope retention (1 m slope retention with a 3 meters high wall) using geosynthetics is about 1 ton CO₂-eq per meter lower compared to a conventional alternative. This difference is equal to about 84 % of the overall climate change impact of the construction and disposal efforts of an entire conventional slope retention system during its 100 years lifetime.

If a Euro5 lorry with lower exhaust emissions than an average fleet lorry is used for the transportation of materials, the environmental impacts of both cases are somewhat reduced regarding some indicators. However, this does not affect the overall conclusions of the comparison.

Slope retentions are individual solutions in a particular situation. The height of slope retention walls and the horizontal loads on it may differ, which may lead to differences in thickness and reinforcement. Thus, generalising assumptions were necessary to model a typical slope retention. Data about on-site material used, gravel extraction, concrete and the use of building machines are based on generic data and knowledge of individual civil engineering experts.

Based on the uncertainty assessment it can be safely stated that the geosynthetics reinforced slope retention shows lower environmental impacts than the concrete wall. Despite the necessary simplifications and assumptions, the results of the comparison are considered to be significant and reliable.

A geosynthetic reinforced wall used for slope retention constitutes a different system compared to a concrete reinforced wall. Nevertheless, both systems provide the same function by enabling the build-up of steep walls. Compared to the conventional slope retention, the geosynthetic reinforced wall substitutes the use of concrete and reinforcing steel, which results between 63 % and 87 % lower environmental impacts.

6 REFERENCES

ecoinvent Centre (2010) ecoinvent data v2.2, ecoinvent reports No. 1-25. Swiss Centre for Life Cycle Inventories, Dübendorf, Switzerland, retrieved from: www.ecoinvent.org.

- Frischknecht R., Jungbluth N., Althaus H.-J., Bauer C., Doka G., Dones R., Hellweg S., Hischier R., Humbert S., Margni M. and Nemecek T. (2007) Implementation of Life Cycle Impact Assessment Methods. ecoinvent report No. 3, v2.0. Swiss Centre for Life Cycle Inventories, Dübendorf, CH, retrieved from: www.ecoinvent.org.
- Goedkoop M., Heijungs R., Huijbregts M. A. J., De Schryver A., Struijs J. and van Zelm R. (2009) ReCiPe 2008 - A life cycle impact assessment method which comprises harmonised category indicators at the midpoint and the endpoint level. First edition. Report I: Characterisation, NL, retrieved from: lcia-recipe.net/.
- Guinée J. B., (final editor), Gorrée M., Heijungs R., Huppes G., Kleijn R., de Koning A., van Oers L., Wegener Sleswijk A., Suh S., Udo de Haes H. A., de Bruijn H., van Duin R., Huijbregts M. A. J., Lindeijer E., Roorda A. A. H. and Weidema B. P. (2001a) Life cycle assessment; An operational guide to the ISO standards; Part 3: Scientific Background. Ministry of Housing, Spatial Planning and Environment (VROM) and Centre of Environmental Science (CML), Den Haag and Leiden, The Netherlands, retrieved from: www.leidenuniv.nl/cml/ssp/projects/lca2/lca2.html.
- Guinée J. B., (final editor), Gorrée M., Heijungs R., Huppes G., Kleijn R., de Koning A., van Oers L., Wegener Sleswijk A., Suh S., Udo de Haes H. A., de Bruijn H., van Duin R., Huijbregts M. A. J., Lindeijer E., Roorda A. A. H. and Weidema B. P. (2001b) Life cycle assessment; An operational guide to the ISO standards; Parts 1 and 2. Ministry of Housing, Spatial Planning and Environment (VROM) and Centre of Environmental Science (CML), Den Haag and Leiden, The Netherlands, retrieved from: www.leidenuniv.nl/cml/ssp/projects/lca2/lca2.html.
- PRÉ Consultants (2012) SimaPro 7.3.3, Amersfoort, NL, retrieved from: www.esu-services.ch/simapro/.
- Solomon S., Qin D., Manning M., Alley R. B., Berntsen T., Bindoff N. L., Chen Z., Chidthaisong A., Gregory J. M., Hegerl G. C., Heimann M., Hewitson B., Hoskins B. J., Joos F., Jouzel J., Kattsov V., Lohmann U., Matsuno T., Molina M., Nicholls N., Overpeck J., Raga G., Ramaswamy V., Ren J., Rusticucci M., Somerville R., Stocker T. F., Whetton P., Wood R. A. and Wratt D. (2007) Technical Summary. In: Climate Change 2007: The Physical Science Basis. Contribution of Working Group I to the Fourth Assessment Report of the Intergovernmental Panel on Climate Change (IPCC), Cambridge University Press, Cambridge, United Kingdom and New York, NY, USA.
- Stucki M., Büsser S., Itten R., Frischknecht R. and Wallbaum H. (2011) Comparative Life Cycle Assessment of Geosynthetics versus Conventional Construction Material. ESU-services Ltd. commissioned by European Association for Geosynthetic Manufacturers (EAGM), Uster and Zürich, CH.

Design of inverted T-shaped Cantilever Wall with a Relief Floor

Conception d'un mur équerre avec dalle de délestage

Ganne P.P., Raucroix X.

Engineering department, BESIX, Gemeenschappenlaan 100, 1200 Brussels, Belgium

ABSTRACT: Cantilever walls are widely used as ground retaining structures. The analytical approach of L-shaped and inverted T-shaped cantilever walls results in reliable designs. This paper proposes and discusses an analytical approach for the geotechnical design of inverted T-shaped cantilever walls with relief floor. This approach combines the analytical approaches of inverted T-shaped walls and of relief floors. The resulting analytical approach is verified by numerical simulations of inverted T-shaped cantilever walls with relief floor for 5m till 10m high retaining structures in unsaturated sandy soils, silty soils and alluvial clayey soils. Finally, rules of thumbs for typical dimensions of the inverted T-shaped cantilever wall with relief floor are given, based on experience, analytical calculations and numerical simulations.

RÉSUMÉ : Les murs équerres sont communément répandus comme structure de soutènement. D'un point de vue de la conception géotechnique, les méthodes analytiques sont éprouvées. Cet article propose et discute une approche analytique pour la conception géotechnique des murs équerres avec dalle de délestage. Cette approche combine l'approche de dimensionnement analytique des murs équerres avec l'effet d'ombre des dalles de délestage. L'approche analytique proposée est justifiée à l'aide de simulations numériques modélisant des murs équerres avec dalle de délestage reprenant des différences de niveau allant de 5m à 10m et ce, dans des sols non-saturés de nature sableuse, silteuse et alluvio-argileuse. En conclusion, des dimensions typiques de murs équerres avec dalle de délestage sont données, basées sur l'expérience, des calculs analytiques et des simulations numériques.

KEYWORDS: inverted T-shaped cantilever wall, relief floor, soil retaining structure, finite element code

1 INTRODUCTION

In recent decades, the number of installations of permanent ground retaining structures is drastically increasing. One of the oldest ground retaining structures are the gravity walls. They have a very easy way of realization and are particularly suitable for retained heights of less than 3m. While they can be designed for greater heights, other types of retaining walls such as L-shaped cantilever walls are usually more economical as the height increases.

L-shaped cantilever walls uses the soil upon the heel to stabilize the horizontal soil pressures. One of the disadvantages of the L-shaped cantilever walls is the high ratio between the horizontal loads due to soil pressures and the vertical soil weight, causing a disadvantageous eccentricity of the forces at the base slab. Therefore, the length of the base slab can amount up to 70% (sandy soils) and up to 120% (alluvial clay) of the retaining height. In most projects, the realization of L-shape structure is not possible due to the lack of required space to excavate up to the rear edge of the base slab level with a reasonable slope.

It is usually more economical to design the L-shaped cantilever wall with a toe at its front side: the inverted T-shaped cantilever wall. This increases the moment arm and reduces the disadvantageous eccentricity of the forces in the base slab. The distance between the front of the stem and the back of the heel of the cantilever wall amounts to 50% (sandy soils) or to 60% (alluvial clay) of the retaining height.

In some cases, it is more economical to further reduce the required space between the front wall face and the temporary slope at the back of the structure. In these cases, a relief floor

could be added : the inverted T-shaped cantilever wall with relief floor. In this way, (1) the disadvantageous horizontal soil forces are reduced and (2) the disadvantageous eccentricity of the forces at the base slab could be reduced, generally down to a negligible low value. The distance between the front of the stem and the back of the heel of the cantilever wall amounts only 20% (sandy soils) or to 40% (alluvial clay) of the retaining height.

The construction of the inverted T-shaped cantilever wall with a relief floor itself is in most of the cases of lower economical interest than the inverted T-shaped cantilever wall. Nevertheless, reducing the space between the front of the stem and the heel, increases the available space for the excavation, necessary to reach the level of the base slab. The possible economic benefit may be found in the less expensive temporary excavation method.

The geometry of an inverted T-shaped cantilever wall with a relief floor depends on the conditions of the specific project. Therefore, each realization must be based on thorough geotechnical evaluation of its design, a hydrogeological evaluation, a detailed structural design, an analyses of the construction methodology and a general risk evaluation.

This paper proposes a simplified analytical approach for the geotechnical design of the inverted T-shaped cantilever wall with a relief floor. This simplified analytical approach is checked by numerical simulations for unsaturated sandy soils, silty soils and alluvial clays. Finally, typical dimensions which can be used for predesign estimations are given, based on experience, analytical and numerical calculations.

1 ANALYTICAL APPROACH OF A L-SHAPED WALL WITH A RELIEF FLOOR

The envisaged geotechnical structure is an inverted T-shaped cantilever wall with a relief floor. Figure 1 shows a typical section of this construction with a retaining soil height of 8.6m. The foundation level is 0.8m below ground surface, in order to place it under the frost line. In order to study the behavior of this structure, a brief review of the behavior of L-shaped cantilever walls and the influence of a relief floor is given, before the global analytical approach is proposed.

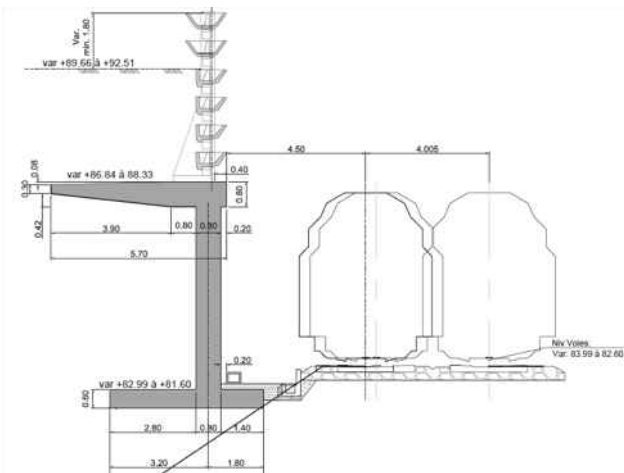


Figure 1. View of the inverted T-shaped cantilever wall with a relief floor of 3.9 m.

1.1 Geotechnical principle of L-shaped cantilever wall

The geotechnical behavior of a L-shaped or an inverted T-shaped cantilever wall is quite complex (Figure 2). When the L-shaped wall fails geotechnically, the failure surfaces E-F, A-D and A-C occur. All these failure surfaces have an inclination of $\pi/4 - \varphi/2$ from the vertical A-B (further called 'virtual back'). All the soil in the block A-C-D can be described as active Rankine soil. The block A-C-F-E deforms and slides downwards simultaneously. The soil pressure distribution in the block A-C-D is symmetrical about the vertical A-B, on which horizontal soil pressures are present. This theory is confirmed by numerical modeling (e.g. Arnold, 2010).

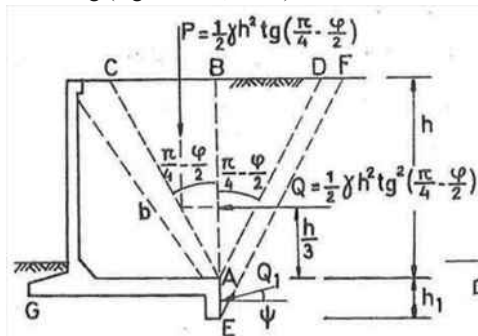


Figure 2. Soil rupture surface (wing shape : C-A and E-F) of a L-shaped cantilever wall (after Vandepitte, 1979).

It is shown that this complex geotechnical behavior of the L-shaped or an inverted T-shaped cantilever wall is equivalent to the following simplified structure (Rouili et al. 2005; Vandepitte 1979). The wall together with the backfill up to a vertical plane above its heel (A-B i.e. 'virtual back') is treated as a monolithic block. Gravity forces, surface loads and horizontal active soil pressures acting at the virtual back may be assumed. This block is checked against sliding, overturning and

bearing capacity failures in the ultimate limit state (GEO 2000; Frank et al. 2004).

This approach is mathematically equivalent to the consideration of the wall together with the backfill up to the plane A-C (Figure 3).

It has to be stressed that though the two above approaches are equivalent for the design of the L-shaped or an inverted T-shaped cantilever wall, the wing-shaped soil rupture surface is the only physical failure mode.

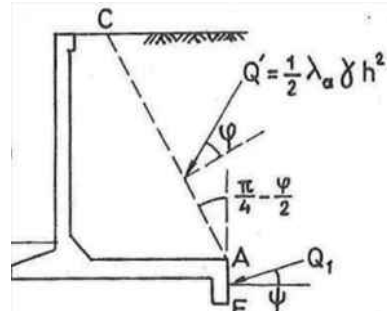


Figure 3. Alternative design rupture surface C-A-E of a L-shaped cantilever wall (after Vandepitte, 1979).

1.2 Geotechnical principle of a relief floor

Geotechnical constructions sometimes uses a relief floor. If the relief floor is rigidly build-in in the geotechnical construction, it implies three stabilizing effects (Figure 4):

1. the backfill in the area A'-A-B engenders a stabilizing moment against overturning,
2. a reduction of the total horizontal soil pressure, increasing the safety to sliding,
3. a reduced eccentricity of the global force at the base, increasing the bearing capacity.

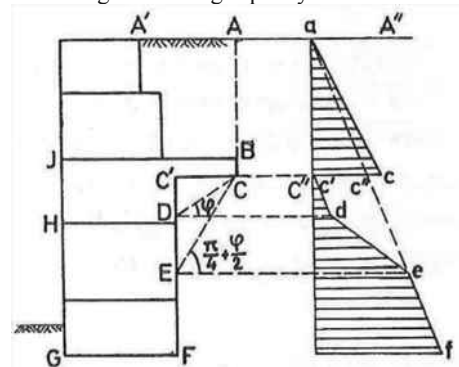


Figure 4. Four zones of soil pressure distribution A-C, C'-D, D-E and E-F. (after Vandepitte, 1979).

Four zones of horizontal soil pressure can be distinguished: Zone 1 : A-C is not influenced by the relief floor.

Zone 2 : C'-D is totally influenced by the relief floor. The horizontal soil pressure is 0 in C'.

Zone 3 : D-E is partly influenced by the relief floor. The horizontal soil pressures increases linearly from d to e.

Zone 4 : E-F is not influenced by the relief floor. The horizontal soil pressure correspond to the active soil pressure, taking into account the surface level A'A and the present surface load.

1.3 Simplified analytical approach of an inverted T-shaped cantilever wall with a relief floor.

The proposed simplified analytical approach combines the theory of the L-shaped cantilever wall and the theory of the relief floor. Two virtual backs are defined : upper virtual back A-B and lower virtual back C'-F (Figure 5).

The wall together with the backfill up to the virtual backs (A-B and C'-F) is treated as a monolithic block. Surcharges and horizontal active soil pressures acting on the virtual backs and gravity forces may be taken into account. On the lower virtual back (under the relief floor level), horizontal soil pressures as described in §1.2 are assumed. This monolithic block is checked against sliding, overturning and bearing capacity failures in the ultimate limit state.

It has to be stressed that the above approach is a simplification of the physical behavior. The physical soil rupture surface does not follow the two virtual backs, but corresponds more with wing-shapes.

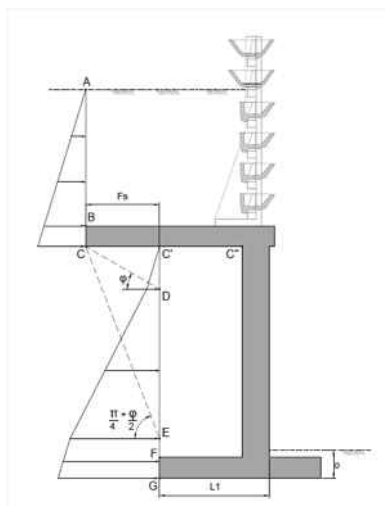


Figure 5. Virtual backs as in the analytical approach of an inverted T-shaped cantilever wall with a relief floor.

2 NUMERICAL SIMULATION OF INVERTED T-SHAPED CANTILEVER WALL WITH RELIEF FLOOR

For the numerical validation of the inverted T-shaped cantilever wall with a relief floor, two-dimensional finite element code PLAXIS is used. The Hardening soil model in plane strain is used to model the soil (Brinkgreve et al. 2002).

2.1 Simulation of excavation stages

Accomplishment of physical modeling, including simulation for gravity stresses is followed with the calculation program. Simulation of the entire inverted T-shaped cantilever wall with relief floor is carried out in a sequence of construction stages. In each construction stage a sufficient number of calculation steps are used to obtain an equilibrium-state:

- Stage 1 : initial situation (gravity loading, soil with temporary cohesion)
- Stage 2 : excavation till bottom level of the cantilever wall (soil with temporary cohesion)

Table 1. Soil parameters of sandy soil, silty soil and clayey soil, as used in the numerical simulations (the stiffness is expressed at a reference pressure of 100 kPa).

	Sandy soil	Silty soil	Clayey soil
γ_{unsat}	17kN/m ³	18kN/m ³	17kN/m ³
$E^{\text{ref}}_{\text{oed}}$	22,30.10 ³ kN/m ²	6.10 ³ kN/m ²	4.10 ³ kN/m ²
E^{ref}_{50}	22,30.10 ³ kN/m ²	9.10 ³ kN/m ²	8.10 ³ kN/m ²
$E^{\text{ref}}_{\text{ur}}$	66,90.10 ³ kN/m ²	36.10 ³ kN/m ²	40.10 ³ kN/m ²
m	0,50	0,75	1,00
c^{temp}	4kPa	4kPa	4kPa
c^{perm}	0,1kPa	2kPa	4kPa
ϕ^{temp}	30°	25°	22°

- Stage 3 : construction and back fill of the cantilever wall till level of relief floor (soil with temporary cohesion)
- Stage 4 : Construction and back fill of the relief floor till final level (final situation, permanent soil parameters, SLS)
- Stage 5 : Determination of factor of safety using c-phi reduction (ULS).

The model simulates 100m (length) by 50m (depth) using 4825 elements (15-noded). The elements around the inverted T-shaped cantilever with relief floor are highly refined. The geotechnical behavior is simulated in unsaturated sandy soils, silty soils and alluvial clayey soils (Table 1).

2.2 Numerical simulation of an inverted T-shaped cantilever wall in sandy soil

A typical section of inverted T-shaped cantilever wall is simulated (Figure 1), retaining the soil over 8,6 m of height. The used geometry implies a L1 = 3,6m and a Fs = 1,9m (Figure 5). The buried depth of the base slab D is in this case 0,6m. The used type of in situ soil and the backfill soil are in this example the above described 'Sandy soil'.

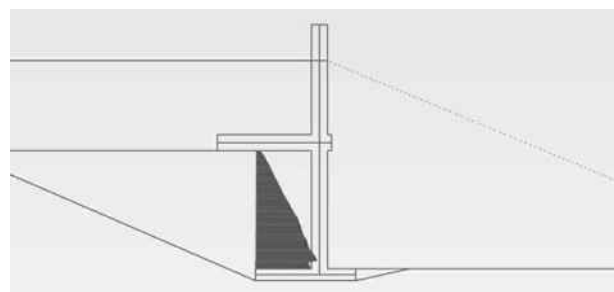


Figure 6. Horizontal effective soil pressures at the lower virtual back up to 61,3kPa at stage 4 (c-phi reduction of 1,20).

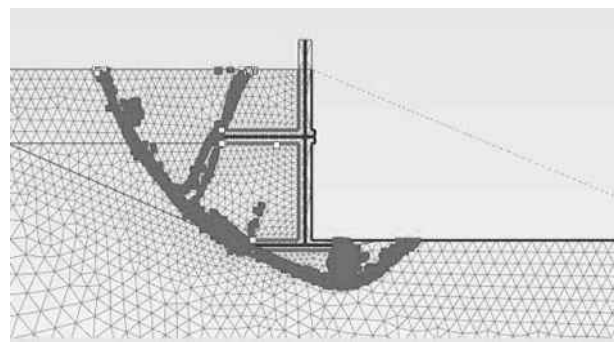


Figure 7. Positions of elements with a Mohr-Coulomb plastic behavior in stage 4 (c-phi reduction of 1,20).

The global geotechnical safety, calculated by the c-phi reduction is 1,20. Figure 7 shows the positions of the elements which are in the plastic zone of the Mohr-Coulomb law. The failure surface underneath the foundation level suggests a failure mode of bearing capacity. As the inverted T-shaped cantilever wall deforms, failure surfaces, inclined at $\pi/4 - \phi'/2$ from the vertical, at the upper and lower virtual backs occur. This corresponds with the described failure 'wings' in § 1.1.

The effective horizontal stresses at the upper virtual back increases from 0kPa up to 29kPa. At the lower virtual back, the effective horizontal stresses increases from 2kPa up to 70kPa. Figure 6 shows that the influence of the relief floor isn't total : the relief floor deforms 3cm downwards, causing a small horizontal effective stress (2kPa) at the top of the lower virtual back. The mean effective vertical stress at the base slab amounts to 228kPa.

2.3 Comparison of the numerical simulation with the proposed analytical approach

The inverted T-shaped cantilever wall with a relief floor in § 3.2 is compared with the analytical calculation as described in § 2.3. The geometry and the soil parameters are similar inputs in both approaches.

Remember that the analytical calculations consider active soil pressures. Therefore, the analytical approach assumes a displacement of the structure. In the numerical simulations, this displacement of the structure occurs only in stage 5 ‘c-phi-reduction’. When forces in the analytical calculations are compared to those in the c-phi reduction stage of the numerical simulations, it is important to notify that the actual cohesion c' and angle of internal friction of the soil ϕ' are reduced.

In the analytical approach, the factor of safety is 3,39 for the overturning failure mode, 1,98 for the sliding and 2,14 for the bearing failure mode. Figure 7 suggests that the failure mode of the numerical model is the bearing capacity (c-phi reduction safety factor = 1,20).

Table 2 shows that the difference of the horizontal forces at the virtual backs in the analytical approach and in the numerical simulations is below 8%. The difference of the vertical force at the foundation amounts to 15%.

Table 2. Comparison of the horizontal and vertical forces at the virtual backs and the foundation in the analytical approach and the numerical simulations.

	Anal. approach	Num. simulation
Horizontal force at upper virtual back	57kN/m ²	62kN/m ²
Horizontal force at lower virtual back	230kN/m ²	211kN/m ²
Vertical force at foundation	951kN/m ²	1117kN/m ²

3 PREDESIGN OF L-SHAPED CANTILEVER WITH RELIEF FLOOR

Based on experience, numerical modeling and hand calculations, typical dimensions of reliable inverted T-shaped cantilever walls with a relief floor could be estimated. For sandy soil and a buried depth of 0,8m and 1,3m; the L1 is about 20% to 40% of the retained soil height H; the Fs (as defined in Figure 5) is about 1,5 to 2,5 m (Figure 8).

The level of the relief floor is of less importance for the geotechnical design, as long as the full stress relief is applied on the virtual back of the inverted T-shaped wall. Furthermore, it is good practice to design the level of the relief floor at about the half of the retained soil height.

The type of soil in situ is an important geotechnical parameter, specially for the bearing capacity and sliding failure mode. For inverted T-shaped walls with relief floor, retaining a soil height of 5 m, a buried depth $D = 1,3$ m; the length L1 varies from 1m (sandy soil) to 2m (clayey soil) (Figure 9).

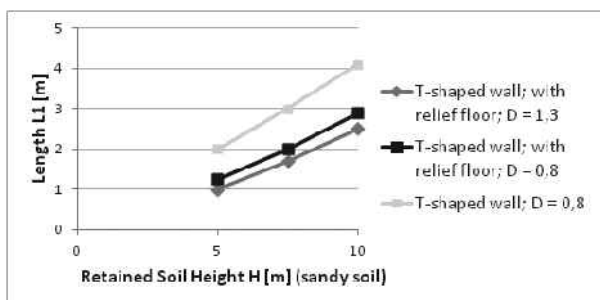


Figure 8. Typical distance between the front of the stem and the back of the heel (L1 [m]) of inverted T-shaped cantilever walls with and without relief floor in sandy soils.

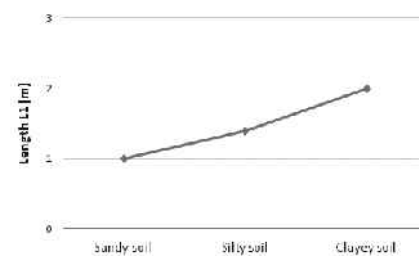


Figure 9. Typical distance between the front of the stem and the back of the heel (L1 [m]) of inverted T-shaped cantilever walls with a relief floor in sandy, silty and clayey soils (retained soil height of 5,0m; buried depth of base slab $D = 1,3$).

4 CONCLUSIONS

The geometry of an inverted T-shaped cantilever wall with a relief floor depends on the height of the retaining soil, the surcharges, the depth of the foundation base slab, the geotechnical parameters of the soil in situ and of the backfill, the possible length of the toe and so forth.

In the case of unsaturated sandy soils, silty soils and alluvial clayey soils, an analytical approach is proposed and confirmed by numerical simulations. The analytical approach is based on an upper and a lower vertical virtual back. The wall together with the backfill up to the virtual backs are treated as a monolithic block. At the lower virtual back, the horizontal soil pressures are reduced, due to the presence of the relief floor. This monolithic block is checked against sliding, overturning and bearing capacity failures in the ultimate limit state.

For predesign estimations, a typical inverted T-shaped cantilever wall with a relief floor may be considered:

- the distance between the front of the stem and the back of the heel is about 20% to 40% of the retained soil height,
- the length of the toe is similar to the length of the heel,
- the base slab is buried deeper than the frost line,
- the difference between the length of the relief floor and the length of the heel is about 1,5m to 2,5m,
- the level of the relief floor is about the half of the retained soil height.

Though some general rules of thumbs for the dimensions of an inverted T-shaped cantilever wall with relief floor are given, each realization must be based on thorough geotechnical evaluation of its design, a hydrogeological evaluation, a detailed structural design, an analyses of the construction methodology and a general risk evaluation.

5 REFERENCES

- Arnold M. 2010. Physical modeling of L-shaped retaining walls. *Physical Modeling in Geotechnics*, Proceedings of the 7th International Conference on Physical Modelling in Geotechnics (ICPMG 2010) 425-430 Zurich.
- Brinkgreve R., Al-Khoury R., Bakker K., Bonnier P., Brand P., Broere W., Burd H., Sotys G., Vermeer P. and Haag D. 2002. *Plaxis - finite element code for soil and rock analyses. User's manual Ver. 8.0*. A.A. Balkema, Rotterdam.
- Frank R., Bauduin C., Driscoll R., Kavvas M., Krebs Ovesen N., Orr T. and Schuppener B. 2004. *Designers' Guide to EN 1997-1 Eurocode 7 : Geotechnical design - General rules*. Thomas Telford, London.
- GEO - geotechnical engineering office. 2000. *Guide to retaining wall design*. Hong Kong.
- Rouili A., Djerbib Y. and Touahmia M. 2005. Numerical modeling of an L-shaped very stiff concrete retaining wall. *Sciences & Technique* 24 (B) 69-74.
- Vandepitte D., 1979. *Berekening van constructies*. Scientia, Genth. (in Dutch).

An Anchored Retaining Wall in CSM

Un soutènement ancré en CSM

Gomes Correia A., Tinoco J.
C-TAC - University of Minho, Guimarães, Portugal

Pinto A., Tomásio R.
JetSJ Geotecnia, Lisboa, Portugal

ABSTRACT: Cutter soil mixing (CSM) is being recently used in Portugal in several applications. This paper describes a solution in cutter soil mixing reinforced with vertical steel profiles IPE270 for a retaining wall with 66 m long and 13 m high constructed in geological formations of landfill materials, Miocene sandy soils and sandstones, with a phreatic level around 8 m depth. This construction is done nearby commercial buildings. The solution is justified against more classical solutions for anchored retaining walls considering the following aspects: feasibility of CSM in the geological and environment conditions, predict behaviour during and post construction, simplicity of construction process, time of construction, economy and quality assurance. Numerical modelling using a commercial program is carried out, based in geotechnical parameters established at the project level, showing a good agreement of the observed data, in terms of horizontal displacements of the wall and also of the safety levels against bending, shear and compression.

RÉSUMÉ : La technique « cutter soil mixing » (CSM) a été récemment utilisée au Portugal dans plusieurs applications. Cet article décrit une solution CSM renforcé avec des profilés verticaux IPE270 pour un mur de soutènement avec 66 m de long et 13 m de haut construit dans des formations géologiques de matériaux de remblai, des formations du Miocène de sols sablonneux et des grès, avec un niveau de nappe phréatique autour de 8 m de profondeur. Cette construction se fait à proximité de bâtiments commerciaux. La solution est justifiée par rapport aux solutions plus classiques des murs de soutènement ancrés tenant compte des aspects suivants: faisabilité du CSM dans une vaste gamme des conditions géologiques et de l'environnement, prévoir le comportement durant et après construction, simplicité du processus de construction, le temps de construction, l'économie et l'assurance-qualité. Une modélisation numérique au moyen d'un programme commercial est effectuée avec l'utilisation des paramètres géotechniques établis au niveau du projet, montrant une bonne concordance des données observées, en termes de déplacements horizontaux de la paroi, autant que des niveaux de sécurité contre la flexion, le cisaillement et la compression.

KEYWORDS: soil treatment, deep soil mixing, cutter soil mixing, retaining wall.

1 INTRODUCTION

Deep Mixing is an in situ soil treatment method that makes use of a technology in which the soil is mechanically mixed with other materials, mainly binders. The composite material will have improved benefits in terms of resistance, compressibility and permeability (Larsson 2003, Bruce 2000). One of the variants of Deep Mixing is the Cutter Soil Mixing (CSM) technique, which produces panel elements with an accurate geometry, vertically and direction. Additionally, low disturbance is induced on the soil and nearby structures, making their use appropriate in urban areas. Furthermore, this technique has shown a great technical versatility and efficiency, as well as economical advantages, including the optimization of the construction schedule (Ameratunga et al., 2009, Capelo et al. 2012, Marzano et al., 2009, Pinto et al. 2011).

This paper describes an innovative solution involving CSM panels combined with a reinforced concrete wall, for a permanent ground anchored retained structure, with about 66 m long and 13 m high constructed in geological formations of heterogeneous landfill materials, Miocene sandy soils and medium weathered sandstones, with a phreatic level around 8 m depth. This construction is done nearby industrial buildings. Consequently their main purpose was to act as a support system maintaining the stability of the excavation against lateral earth pressures, while controlling the deformation and settlement of the surrounding structures (Porbaha, 2000).

The retaining wall uses soil-cement panels with a minimum depth above the excavation level of 4 m and cross-section of 2.4 x 0.5 m², including 0.20 m of overlapping, were built using the

CSM technology. The panels were reinforced with vertical IPE270 (S275JR) hot rolled steel profiles (Euronorm 19-57), spaced in average 1,1m, in order to resist both to the earth and water pressures, as well as to ensure a better control of deformations. The steel profiles were placed inside the panels, before the cement started the curing process. The wall was braced by four (case study) or three levels of permanent ground anchors, applied at the capping beam as well as at the distribution beams, integrated on the reinforced concrete lining wall (Figure 1). As already stated, the soil-cement panels were lined with a reinforced concrete 0.20m thickness wall, connected to the vertical IPE270 profiles with steel cantilevers, allowing the mobilization of the global resistance of both the steel profiles and the lining reinforced concrete wall, acting a Berlin wall combined with CSM panels. The design criteria, verifying Ultimate Limit State and the Serviceability Limit State, as well as the limitation of the water inflow, were established by the support of 2D FEM analysis using commercial PLAXIS[®] software. In this paper a comparison between the control and monitoring parameters with design parameters is done in order to support the discussion about the reliability of both the solution and the construction method.

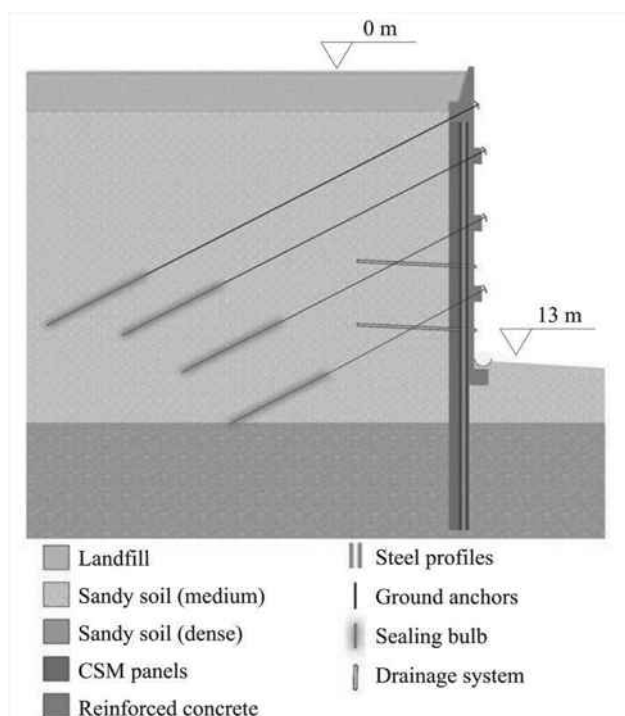


Figure 1. Representative schema of the solution proposed for the retained wall.

2 SITE AND SUBSURFACE CONDITIONS

The local geological conditions were heterogeneous. The excavation works intersected, from the surface, heterogeneous landfills and Miocene medium dense to dense sands and medium weathered sandstones. The ground water table was located about 5m above the final excavation level. Taking into account this scenario, an initial solution of Berlin walls was considered. A more detailed information about the site and subsurface conditions can be consulted in Pinto et al (2013).

3 CSM WALL MODELLING AND DESIGN CRITERIA

The modelling work was carried out using the commercial PLAXIS[®] software. The *Hardening-Soil* model was adopted for the different soil layers based in the available geotechnical laboratory and field data and taking into account all the excavation phases. Table 1 summarizes the main soil parameters.

Table 1. Main soil properties for modeling.

Constitutive model: Hardening-Soil	Landfill	Sandy soil (medium)	Sandy soil (dense)
γ_t (kN/m ³)	16	17	19
E_{50}^{ref} (kN/m ²)	10,000	20,000	35,000
E_{oed}^{ref} (kN/m ²)	10,000	20,000	35,000
E_{ur}^{ref} (kN/m ²)	30,000	60,000	105,000
Parameter m	0.5	0.5	0.6
c'	0	0	0
ϕ' (°)	22	33	35

For the soil-cement material produced by the CSM technology, using a cement consumption ratio of about 600kg/m³, the Mohr-Coulomb constitutive model was adopted and the parameters summarized in Table 2 were used.

Table 2. Main CSM panels parameters used in the modeling.

Constitutive model: Mohr-Coulomb	CSM panels
γ_t (kN/m ³)	22
E_{ref} (kN/m ²)	1000000
ν	0.3
c' (kN/m ²)	600
ϕ' (°)	35

With the purpose to approximate the behavior of the structure to the real behavior, the three configurations shown in Figure 2 were considered: a) two half vertical IPE270 spaced in 1.1 m, b) two half vertical IPE270 spaced in 1.1 m plus lining wall and c) two half vertical IPE270 spaced in 1.1 m plus lining wall and CSM panels.

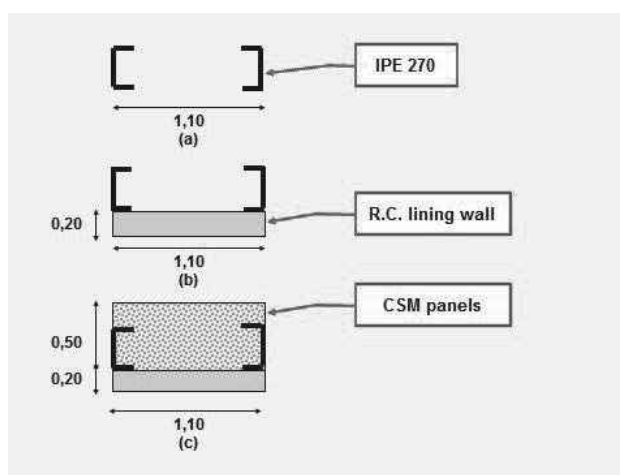


Figure 2. Configurations adopted in the modeling: a) two half vertical IPE270 spaced in 1.1 m, b) two half vertical IPE270 spaced in 1.1 m plus lining wall and c) two half vertical IPE270 spaced in 1.1 m plus lining wall and CSM panels.

For the structural analysis, load combinations for the Ultimate Limit State and for the Serviceability Limit State were defined according to Pereira (2011). The obtained results of 2D FEM analysis (mesh consisted of plane strain, 15-node elements) in terms of efforts and displacements are illustrated in Figure 3 and Figure 4 respectively.

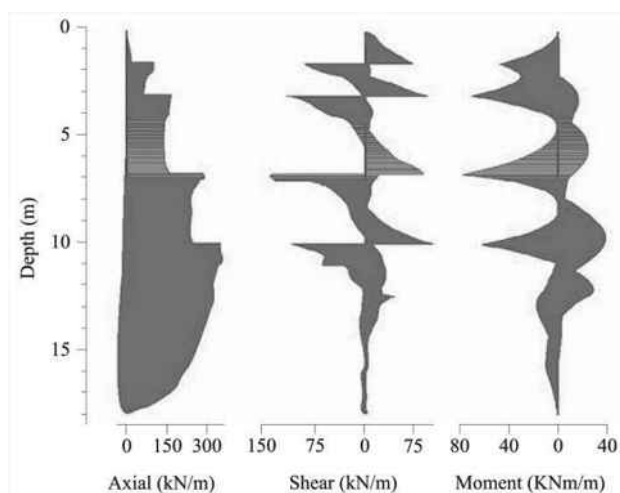


Figure 3. Efforts diagrams.

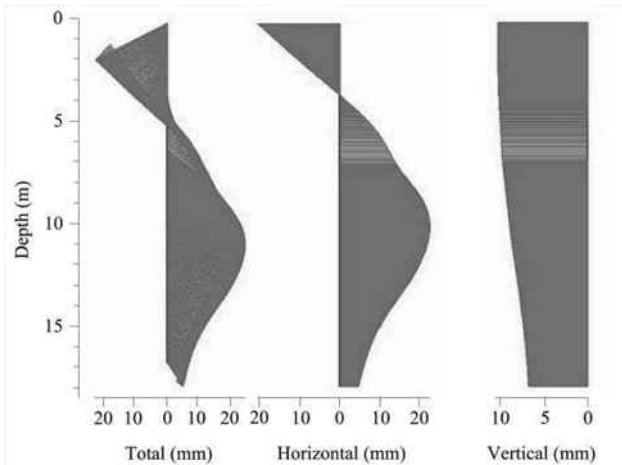


Figure 4. Displacement diagrams.

For the verification of the ultimate limit states was assumed a simplified approach. Thus, it was considered that the strength capacity is the individual combination of the strength resistance of the CSM panels, the IPE270 profiles and the reinforced concrete lining wall.

Summarising the main results obtained are the following:

- M_{Rd} (resistant bending moment) = 167 kNm/m > 1.5 M_{Ed} (maximum acting bending moment) = 119 kNm/m;
- V_{Rd} (resistant shear force) = 251 kN/m > 1.5 V_{Ed} (maximum acting shear force) = 207 kN/m;
- σ_{Rd} (resistant compression stress of CSM) = 2 MPa (with FS=2) > 1.5 σ_{Ed} (maximum acting normal stress) = 1.1 MPa;
- S_H (maximum horizontal displacement) = 22.7 mm at about 10m depth.

Based in these results the following design criteria were established: take into account the resistance and stiffness of both the steel profiles and the reinforced concrete lining wall. The contribution of the CSM panels was considered in order to protect and confine the steel profiles (exploration phase) and to perform as preliminary ground improvement, allowing the execution of the excavation works without any restriction, in each level.

4 QUALITY CONTROL / QUALITY ASSURANCE

4.1 Control of production parameters

One of the major issues of the CSM technology is the high quality control and quality assurance (QC/QA), allowing on real time the monitoring and correction of important parameters, such as: depth, inclination, speed of mixing tools, pressure (ground and binder slurry) on cutter wheels, rate and total volume of pumped slurry (Figure 5).



Figure 5. CSM on line execution control.

4.2 Control of mechanical soil-cement properties

The execution control is complemented by a tight quality control and quality assurance, allowing the confirmation of both the main resistance, homogeneity and deformability of the soil-cement (soil-binder) parameters. For this purpose, samples from fresh material (before on suitability tested panels and during construction) and cores from the executed panels (after a certain curing age ranging from 7 to 28 days) were collected in order to access the material homogeneity, as well as to perform laboratorial tests with different ages, mainly unconfined compression strength (UCS) and Modulus (E_{s50} – secant modulus at 50% of maximum stress of UCS). The results obtained confirm an UCS minimal of 4MPa and a E_{s50} not lesser than 1GPa, satisfying the design criteria (Figure 6).

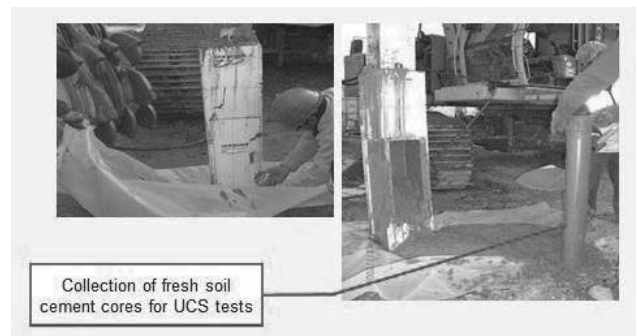


Figure 6. Collection of soil - cement fresh cores.

Taking into account the results of the UCS load tests, mainly on the suitability test panels, the following parameters were adopted for the execution of the CSM panels are presented on Figure 7.

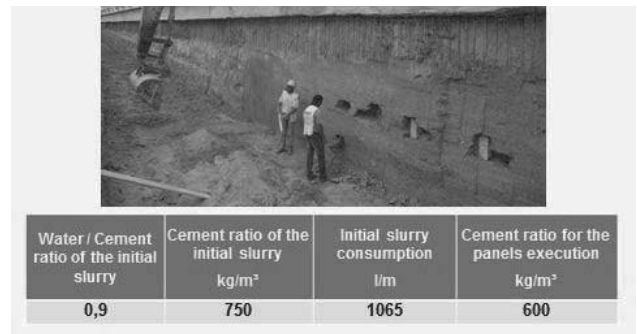


Figure 7. Adopted values for the CSM panels execution parameters.

Regarding the QC/QA of the solution, it should also be pointed out the execution of suitability and reception tests for all the permanent ground anchors, allowing the optimization of the anchors grout body length (Figures 8 and 9).

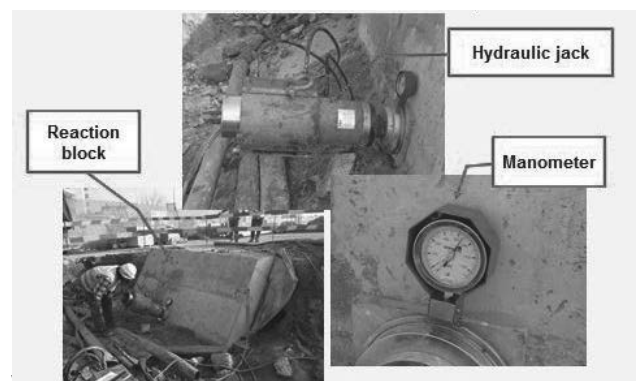


Figure 8. Permanent ground anchor suitability test.

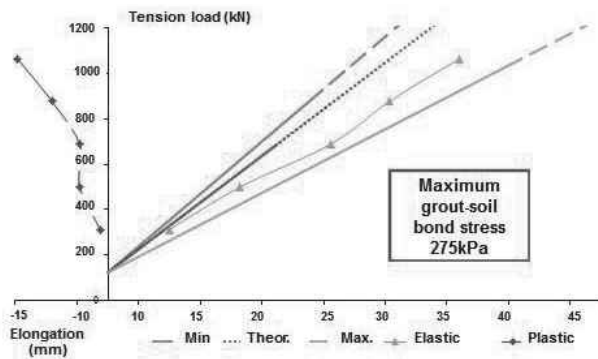


Figure 9. Main results of the ground anchor suitability test.

5 CSM WALL PERFORMANCE

The implemented monitoring and observation plan, is shown on Figure 10, including 2 inclinometers and 7 topographic targets.

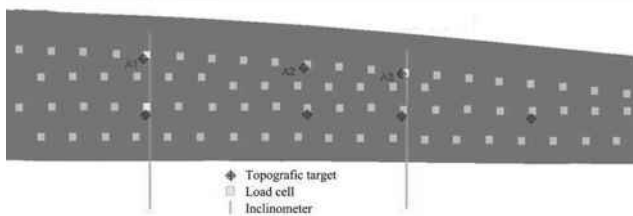


Figure 10. Monitoring and observation plan.

Figure 11 shows that the maximum displacement was observed at 10 m depth, corresponding to 15 mm (inclinometer I8).

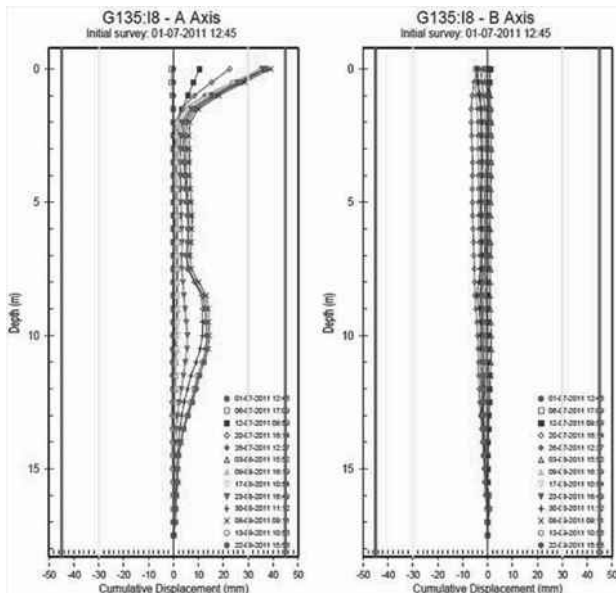


Figure 11. Displacement recorded at the inclinometer I8.

In Figure 12 it is observed that the maximum vertical displacement is 4 mm and that the maximum horizontal displacement is 17 mm.

These results show that the FEM analysis, with the presented input data, has given a good analytical prediction of the observed horizontal displacement, mainly confirming the depth where the maximum horizontal displacement occurred.

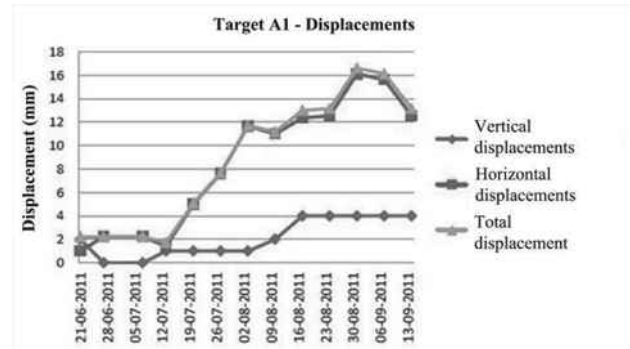


Figure 12. Displacement recorded at the topographic target A1.

6 MAIN CONCLUSIONS

The case study presented in this paper shows the good performance, mainly low deformations, of an anchored retaining structure, combining CSM panels with a reinforced concrete lining wall, leading to the optimization of both the construction overall schedule and budget in a complex geotechnical and site conditions. It was also shown that the use of commercial FEM software with appropriated input data gives a reasonable prediction of the main displacements, which are critical for the verification of both the ultimate and serviceability limit states, for all the excavation phases.

7 ACKNOWLEDGEMENTS

The authors wish to thank to “Fundação para a Ciência e a Tecnologia” (FCT) for the financial support under the strategic project PEst-OE/ ECI/UI4047/2011. In addition, the authors would like to thank the contribution of Ângelo Pereira.

8 REFERENCES

Ameratunga J.; Brown D.; Ramachadran R.; Denny R. (2009). “Ground improvement for a large above ground storage tank using cutter soil mixing columns.” *Proc. 17th International Conference on Soil Mechanics and Geotechnical Engineering*, Alexandria, Egypt, pp. 2280-2283.

Bruce D.A. 2000. An introduction to the deep soil mixing methods as used in geotechnical applications. *Federal Highway Administration*, Georgetown.

Capelo A., Gomes Correia A., Ramos L.R., Pinto A. And Tomásio R. 2012. Modeling and monitoring of an excavation support using CSM. *4th International Conference on Grouting and Deep Mixing*, New Orleans, Louisiana, USA, ASCE, GSP (in printing).

Larsson S. 2003. Mixing processes for ground improvement by deep mixing. *Department of Civil and Environmental Engineering, Royal Institute of Technology in Stockholm*.

Marzano I.P., Osman A.A-M., Grisolia M., Al-Tabbaa A. 2009. Mechanical performance of different stabilised soils for application in stratified ground. *17th International Conference on Soil Mechanics and Geotechnical Engineering*, Alexandria, Egypt, pp. 2276-2279.

Pereira A. 2011. *Application of Cutter Soil Mixing Technology in containment of a retaining wall anchored linear*. MSc dissertation, Guimarães (in Portuguese).

Pinto A., Tomásio R., Pita X., Pereira A. and Peixoto A. 2011. Cutter Soil Mixing Solutions in Portugal on Hard Soils and Weak Rocks. *Proc. 15th European Conference on Soil Mechanics and Geotechnical Engineering*, September 2011, Athens, Greece, Part 2 – 3.3 – Ground Reinforcement, pp. 1037-1042.

Pinto A., Tomásio R., Godinho P., 2013. Innovative Solution of King Post Walls combined with CSM. *Proc. 18th European Conference on Soil Mechanics and Geotechnical Engineering*, Paris, France.

Porbaha, A. (2000). State of the Art in Deep Mixing Technology. Part IV: Design Considerations. *Ground Improvement*, 4(3), 111-125.

Conception, modélisation et auscultation d'une très grande excavation à Monaco

Design, modelization and monitoring for a very large excavation in Monaco

Guilloux A., Porquet M.
Terrasol, Paris France

De Lavernée P., Lyonnet P.
Soletanche-Bachy, Rueil Malmaison, France

Roman P.
Vinci Construction, Monaco

RÉSUMÉ : la construction d'une grande tour à Monaco, de 160 m de hauteur avec 10 niveaux de sous-sols et sur un terrain en forte pente, conduit à réaliser une excavation de 70 m de profondeur, dans un environnement très urbanisé. La communication présente les principes de conception de cet ouvrage exceptionnel, et notamment les modélisations numériques 3D mises en œuvre pour prédire les déformations de l'ouvrage et des avoisinants. On décrit ensuite le comportement de l'ouvrage pendant l'excavation, suivi selon les principes de la méthode observationnelle, ainsi que quelques adaptations rendues nécessaires au cours des travaux dans certaines parties d'ouvrage dont le comportement s'écartait des prévisions.

ABSTRACT: the construction of a high rise building in Monaco, of 160 m high with 10 basements levels and over a steep slope, required a 70 m deep excavation in an urbanized environment. The paper describes the main features of the design for this outstanding geotechnical structure, together with the 3D FE models developed for prediction of deformations of the retaining structures and the existing surrounding buildings. The actual behavior during the excavation, analyzed according to the principle of the observational method, will be described, as well as some changes in the work progress required in some areas due to a behavior somewhat different from the predictions.

MOTS-CLES : grande excavation, modélisation, auscultation, méthode observationnelle –

KEYWORDS: deep excavation, modelization, monitoring, observational method.

1 PRESENTATION

Le projet Odéon à Monaco consiste en la construction d'une tour de 160 m de hauteur sur un versant en forte pente et dans un contexte déjà fortement urbanisé. L'emprise du projet, la topographie, et la construction de 10 niveaux de sous-sol en infrastructures de la tour conduisent à réaliser un ouvrage de soutènement de très grande hauteur, environ 70 m, dont 35 m en parois berlinoises ancrées par tirants actifs et près de 40 m en paroi moulées butonnées par les planchers de sous-sols.

La géologie du site est constituée d'éboulis surmontant des marnes noires de qualité médiocre et des calcaires profonds. La tour elle-même repose sur des barrettes préfondées, permettant la construction selon la méthode « up and down », ancrées en moyenne à 50 m de profondeur sous le niveau du rez de chaussée.

Outre les dimensions tout à fait exceptionnelles de l'excavation, l'enjeu géotechnique majeur consistait à garantir des déplacements des ouvrages avoisinants existants inférieurs à 5 mm, et la méthode observationnelle était imposée pour garantir le succès de l'opération.

La communication présente :

- La conception globale du projet et le dimensionnement des divers éléments de soutènement et fondation ;
- Les modélisations numériques géotechniques 3D qui ont été élaborés à différents stades du projet, intégrant l'ensemble des fondations (parois moulées périmétriques et barrettes, planchers des sous sols) et des soutènements, y compris tirants et pieux des berlinoises, et reproduisant les phases de construction. Ces modèles ont globalement permis de valider les méthodes et phasages de construction ;
- Les performances réellement observées, notamment en termes de déplacements sur les avoisinants, qui ont dans l'ensemble confirmé les ordres de grandeur attendus.

Elle décrit également quelques adaptations du projet qui ont été mises en œuvre dans le cadre de la méthode observationnelle, et qui ont permis de gérer les situations où les déplacements observés sur des bâtiments avoisinants ont dépassés les seuils.

2 DESCRIPTION DU PROJET

2.1 L'ouvrage et son phasage de réalisation

La tour s'inscrit dans un talus naturel de pente moyenne 25°, qui doit être en conséquence rogné sur un dénivelé de plus de 40 m, entre la cote 110.0 NGM en amont et le niveau de la rue en aval à 67.0 NGM. Elle se compose de 2 parties en forme de pétales ayant respectivement 44 et 48 étages au-dessus d'un parking de 10 niveaux en sous-sol. L'ensemble est fondé sur une paroi moulée périphérique en forme d'auge vue en plan, et sur un réseau de barrettes intérieures. La paroi moulée est prolongée verticalement en superstructure par un voile pour épouser le versant sculpté en amphithéâtre, constituant un socle rigide dont le rôle est capital vis-à-vis de la reprise des efforts liés à la dissymétrie du site.

L'ouverture de la fouille se fait à l'abri de 3 soutènements étagés successifs (Figure 1) :

- Une microberloise de 15 m, avec micropieux ϕ 219 ayant une fiche de 8 m et espacés d'environ 1 m ;
- Une berlinoise de 20 m, avec pieux ϕ 1000 espacés de 2 m et ancrés d'en moyenne 12 m ;
- Et enfin la paroi moulée de 30 à 40 m de haut renforcée dans certaines zones par des contreforts.

Ces dispositions visent, au fur et à mesure du terrassement, à la constitution de plates-formes de travail de plus en plus larges pour l'utilisation d'un matériel de plus forte capacité permettant la mise en œuvre de soutènements de plus forte inertie.

Ente les cotes 110.0 NGM et 64.0 NGM, les berlinoises et la partie supérieure de la paroi moulée sont ancrées par 18 lignes de tirants de longueur maximum 42 m.

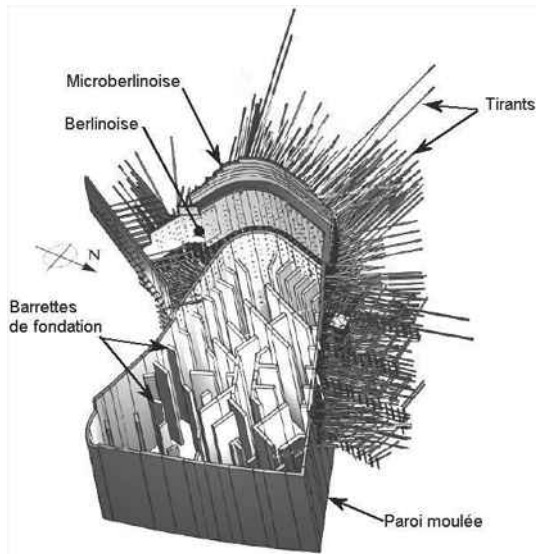


Figure 1 : Vue 3D des soutènements et fondations

A la cote 64.0/67.0 NGM, la dalle de couverture du parking est coulée, après quoi la construction de la tour en up & down peut débuter : il s'agit de construire simultanément la superstructure et l'infrastructure, à raison de trois étages de superstructure pour un niveau d'infrastructure en taupe, la paroi moulée et ses contreforts prenant appui sur les dalles de sous-sols coulées à l'avancement et portées par les barrettes de fondations profondées.

2.2 Le contexte géotechnique

Géologiquement la structure tectonique régionale est complexe : l'ensemble du versant est constitué d'un système d'écaillés, et au droit du site on rencontre des marnes Cénomaniennes. Ces dernières, qui ont déjà été à l'origine de difficultés lors de la réalisation de grandes excavations à Monaco, constituent l'essentiel des terrains à excaver, avec localement un substratum calcaire, qui remonte à la faveur d'une faille. Notons que la faille du Larvotto se situe légèrement en aval du site.

Le site a fait l'objet d'une importante reconnaissance, avec environ 35 sondages, carottés, destructifs et pressiométriques, sur des profondeurs atteignant couramment 90 m, et jusqu'à 120 m. La Figure 2 montre une coupe transversale, mettant en évidence la couche de colluvions épaisse de 25 m en amont du site, puis les marnes du Cénomaniens, plus ou moins déstructurées, et localement les calcaires profonds.

On notera tout particulièrement la présence de niveaux décomprimés dans les marnes, mis en évidence par leur description sur carottes et par des modules pressiométriques très faibles (< 50 MPa), alors qu'ils sont de l'ordre de 200 à 300 MPa dans les marnes saines. Cette conséquence probable de la tectonique du site a été l'un des enjeux importants du projet de soutènement.

L'hydrogéologie montre une nappe de surface dans les éboulis, suivant la pente à 15-20 m sous le TN et une nappe captive en charge dans les calcaires profonds. Mais les capteurs de pression interstitielle dans les marnes montrent également des valeurs de pression correspondant à la nappe de surface, et ce au moins localement et temporairement : la conception du projet a du également tenir compte de ces fortes charges piézométriques.

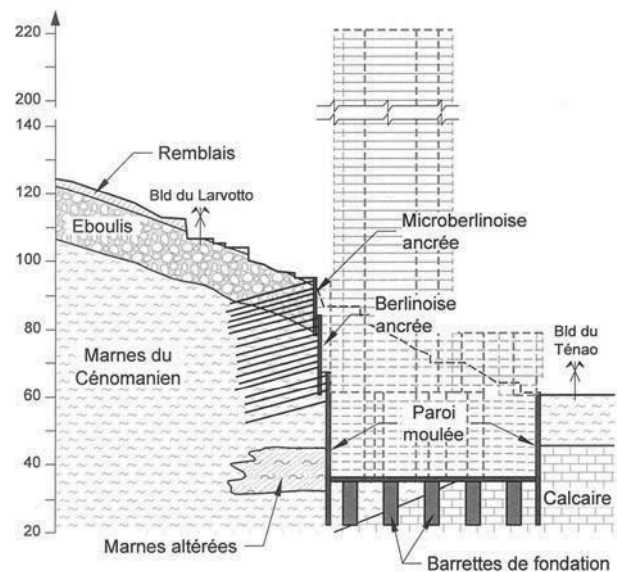


Figure 2 : Profil géologique et projet

2.3 La conception des soutènements et fondations

La hauteur importante de la tour, et les actions qui en résultent sur les fondations sous l'effet du vent et du séisme, ont nécessité une étroite liaison entre les études de la structure et des soutènements. En effet, la paroi moulée périphérique fonctionne à la fois comme soutènement des terres et comme fondation de la tour. Les effets de renversement sur la tour, notamment sous séisme, mettent en traction la paroi moulée amont. Par ailleurs, en phase de service, la tour doit être calculée sous l'hypothèse d'une détente des tirants des berlinoises, les massifs de terre s'appuyant directement sur le socle de la superstructure.

Pour ces diverses raisons, les soutènements ont fait l'objet de plusieurs vérifications. En phase d'excavation, ils ont été dimensionnés par la méthode classique des calculs au coefficient de réaction, complétée par des calculs de stabilité générale faisant intervenir la longueur des tirants. L'ensemble a été conduit selon des profils transversaux bidimensionnels, malgré le caractère fortement tridimensionnel du projet, conduisant à une approche a priori sécuritaire.

En phase de service, pour vérifier le comportement de la paroi moulée associée à la tour, un modèle 3D structurel des infrastructures a été élaboré, sur lequel ont été appliquées les poussées issues des calculs de soutènement au coefficient de réaction, et les actions propres à la tour (vent, séisme, charges verticales). Afin de prendre en compte l'effet des phases de terrassement sur les sollicitations finales dans la paroi moulée, il a été également introduit un cas de charge élémentaire représentant le décalage de moment et d'effort tranchant dans la paroi entre un calcul phasé et un calcul non phasé négligeant les terrassements. Le modèle de l'infrastructure ainsi étudiée fournit les cartographies d'armatures à prendre en compte dans le dessin des cages de paroi moulée et conduit à un dimensionnement rigoureux et optimum.

La méthodologie de construction de la tour en up & down permet d'assurer la stabilité générale et de maîtriser au mieux les modifications de contraintes dans le massif. En effet :

- En phase de terrassement, le poids de la tour compense partiellement le poids des terres excavées qui sont stabilisatrices vis-à-vis des cercles de grand glissement ;
- Les tassements se produisent au fur et à mesure de la construction et sont compensés par le soulèvement du fond de fouille.

Enfin, malgré le caractère de roche tendre des terrains, un clouage vertical en fibres de verre a été nécessaire devant la paroi moulée amont, afin d'améliorer la butée mobilisable lors des dernières passes de terrassement où la paroi est soumise à

une poussée approchant les 1000 kPa dans les zones de marnes altérées.

3 LES MODÉLISATIONS NUMÉRIQUES

3.1 Modélisation 3D globale sous CESAR 3D

Après un premier modèle géotechnique tridimensionnel réalisé par Coyne et Bellier dans le cadre des études de conception, nous avons conduit, dès le démarrage des études d'exécution, une nouvelle modélisation géotechnique 3D de l'ensemble du projet, intégrant les interfaces géologiques, les avoisinants existants et les nouvelles infrastructures, réalisée avec CESAR 3D v5. Le modèle (Figure 5) comporte 57 phases de calcul reproduisant toutes les étapes des travaux depuis l'excavation des premières plateformes jusqu'à l'application des charges de superstructures sur les barrettes de fondations.

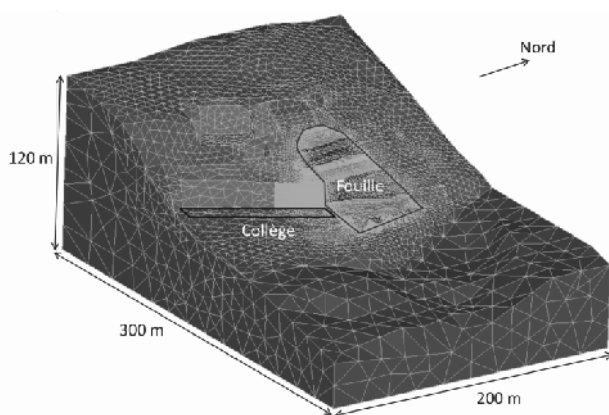


Figure 3 : Vue du modèle 3D général

Les résultats mettent en évidence l'effet de voûte lié à la forme de l'excavation et conduisent à des déplacements des avoisinants de l'ordre de 5 mm en déplacement horizontal, et presque toujours inférieurs à 5 mm en soulèvement. Les déplacements calculés les plus importants sont situés près du collège Charles III.

3.2 Modélisation 3D locale sous Plaxis 3D

Suite à un changement de méthode pour réaliser les soutènements au niveau du collège, un autre calcul centré sur ce bâtiment a été réalisé avec Plaxis 3D. Ce modèle « simplifié » (Figure 4) ne comprend que les structures existantes du collège, la variante de soutènement, et une moitié de l'excavation principale. La stabilité de l'ensemble est assurée par les conditions aux limites, et l'effet de voûte est reproduit par une surcharge à l'arrière du modèle.

Les déplacements calculés restent comparables à ceux obtenus précédemment et montrent que la nouvelle solution de soutènement garantit bien la stabilité de l'ensemble.

3.3 Apport des modélisations

Ces modélisations 3D ont permis la prise en compte des effets 3D tels que l'effet de voûte et la validation de systèmes de soutènement complexes, notamment vis-à-vis des déplacements des structures et des avoisinants. Le comportement fortement 3D de l'ouvrage est bien mis en évidence, avec notamment des déplacements des soutènements de l'ordre de 10 mm au maximum, très inférieurs aux 30 mm évalués par les calculs 2D au modules de réaction.

En outre, une approche de la stabilité générale a pu être conduite sur la base du modèle global, en affectant les paramètres de résistance au cisaillement des terrains de coefficients réducteurs partiels, et en vérifiant l'équilibre numérique du modèle avec ses caractéristiques réduites.

4 L'APPLICATION DE LA MÉTHODE OBSERVATIONNELLE

4.1 Auscultation mise en œuvre

L'auscultation de l'ouvrage et de ses avoisinants est organisée selon 10 profils verticaux (3 à l'amont côté ouest, 3 côté collège au sud, 2 côté Nord et 2 à l'aval côté Est) tel qu'illustré sur Figure 4. Sur chacun de ces profils, les différents instruments de mesures permettent de recouper les informations.



Figure 4 : Vue en plan du projet et des profils d'auscultation

La mise en place du dispositif d'auscultation de l'ouvrage et de ses avoisinants s'est faite de manière progressive :

- En premier lieu, dès le début des travaux, les avoisinants (villas et immeubles aux alentours, collège Charles III, paroi moulée amont du collège) ont été équipés de cibles topographiques ; des inclinomètres profonds ont été réalisés dans le terrain (jusqu'à 80 m de profondeur) à l'amont et autour de l'emprise de la future fouille, et une dizaine de piézomètres a également été réalisée tout autour de la fouille ;
- Puis les ouvrages ont été équipés au fur et à mesure de la réalisation : mise en place d'inclinomètres noyés dans les micropieux, pieux et paroi moulée, de cibles topographiques, d'extensomètres de forages, de cellules dynamométriques en tête de tirants, ainsi que de jauges de contraintes dans les barrettes et certaines dalles. L'auscultation des avoisinants a également été renforcée tout au long du chantier avec l'ajout de cibles complémentaires et de fissuromètres dans les zones ayant subi des déplacements au cours de travaux.

Pour les profils les plus hauts côté amont, 3 séries d'inclinomètres sont placées en recouvrement relatif sur la microberlinoise, la berlinoise et la paroi-moulée, de façon à reconstituer un profil inclinométrique complet intéressant les divers soutènements. Ils sont également équipés d'environ 7 cellules de charges sur les têtes de tirants, réparties sur les 18 lits.

Les cibles topographiques sont elles aussi disposées le long des profils à raison d'une cible toutes les 2 passes de terrassement soit environ une cible tous les 5 mètres, avec une cible en tête de chaque ouvrage.

Les extensomètres de forage sont pour certains ancrés à une profondeur de 60 m à l'arrière du soutènement, au-delà des tirants les plus longs, avec une ancre tous les 10 m.

Inévitablement un certain nombre d'instruments situés dans le terrain à l'amont du projet a été détruit au moment de la réalisation des tirants de la berlinoise, et a dû être remplacé. C'est notamment le cas des piézomètres, qui ont été remplacés le plus souvent par des capteurs de pression interstitielle.

4.2 Choix des seuils

La limite admissible de déplacements des immeubles mitoyens a été fixée contractuellement à 5 mm, avec un seuil d’alerte à 3 mm.

Vis-à-vis des soutènements eux-mêmes, le contrat spécifiait uniquement des critères de déplacements pour le dimensionnement selon la méthode de calcul au coefficient de réaction (calcul 2D) :

- 30 mm pour les parois non joutées par des immeubles ;
- 15 mm pour les points situés à plus de 10 m des fondations des immeubles ;
- 3 à 10 mm pour les points entre 5 et 10 m de ces fondations ;
- 3 mm pour les points situés à moins de 5 m des fondations.

Il faut souligner que les déplacements calculés par les méthodes aux éléments finis (3D) sont largement inférieurs à ceux obtenus par les méthodes 2D.

5 LE COMPORTEMENT EN COURS DE TRAVAUX

5.1 En zone courante

On notera tout d’abord que la précision du théodolite automatique est tout à fait remarquable : avec une mesure toutes les trois heures, la précision obtenue est de l’ordre de +/- 0,5 mm, comme cela apparait sur les courbes de suivi topographique. De même la précision des extensomètres de forage est tout aussi remarquable : +/- 0,1 mm. Seule la précision des inclinomètres est plus aléatoire : il apparait que celle-ci dépend fortement de la qualité du scellement, en relation avec la qualité des terrains trouvés et bien sûr de la hauteur de l’inclinomètre. Un post-traitement de type correction de pied, ou autre, améliore nettement la fiabilité des résultats.

En vue de l’analyse des mesures, le Bureau d’Etudes avait transmis, pour les profils types, les courbes de déplacements calculés phase par phase, pour comparaison avec les mesures inclinométriques.

Les mesures montrent, notamment en zone amont, des déplacements inclinométriques de la paroi moulée de quelques millimètres, nettement plus faibles que ceux calculés avec la méthode au coefficient de réaction en 2D, qui atteignaient 10 à 15 mm dans cette zone (Figure 5).

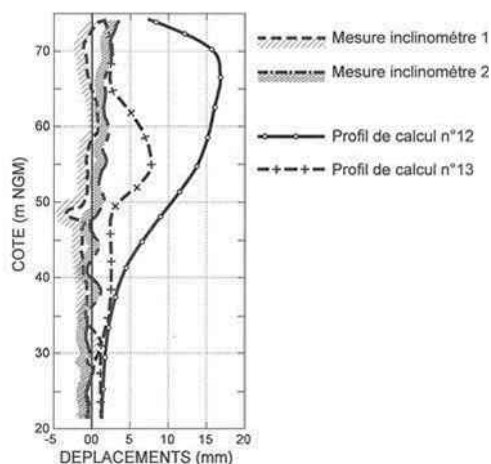


Figure 5 : déplacements calculés et mesurés des parois

Ceci était prévisible, comme le montraient les résultats des calculs numériques 3D, du fait de la géométrie de la fouille beaucoup plus haute que large, qui favorise la formation de voûtes de décharge horizontales, réduisant ainsi la poussée effective sur le soutènement.

D’une façon générale, on peut souligner que les déplacements maximaux δ des parois de soutènement restent de l’ordre de 10 mm au maximum, ce qui est remarquable pour un soutènement de hauteur totale $H = 70$ m : $\delta/H \approx 0.15/1000^\circ$.

5.2 Exemple d’écarts par rapport au modèle et adaptations du projet

D’une façon générale, il n’a été constaté que peu d’écarts significatifs entre le comportement observé et les prévisions de déplacements fournies par les calculs.

Les premiers écarts l’ont été dès le début du chantier, lors de la foration des premiers tirants dans les éboulis qui ont conduit à des déplacements centimétriques, dépassant les seuils, sur certains avoisinants. Ces premiers mouvements, attribués à l’effet de la foration et du scellement des tirants dans les éboulis, nous ont conduits à adapter la méthode de forage : abandon des forages à l’air en faveur de méthodes au tricône sous coulis, et forage « Sonic ».

Ainsi, pour la villa Bataglia, située au nord-ouest du projet et qui avait subi des déplacements allant jusqu’à 14 mm, nous avons été conduits à réaliser un soutènement spécifique en aval de la villa : longrines en béton armé de 1 m de haut sur deux niveaux, ancrées par 8 tirants de 15 m de long scellés dans les éboulis, et 3 tirants de 21 m dans les marnes. Ce soutènement a permis d’éviter l’évolution des mouvements jusqu’à la fin des travaux de perforation et d’injection de coulis dans cette zone. A ce jour, soit environ un an et demi après ces travaux, plus aucun déplacement complémentaire n’a été observé.

Un autre écart de comportement structurel a pu être constaté, cette fois-ci sur l’ouvrage en construction : dans la zone située au droit du collège, la paroi moulée se trouvait localement en console maintenue par trois lits de tirants, après un terrassement de 7 m pour le coulage de la dalle RDC. Les déplacements mesurés en tête de la paroi moulée ont atteint 13 mm, supérieurs aux déplacements calculés. Le bureau d’études a alors lancé une rétro-analyse, qui a montré que ces mouvements pouvaient être attribués à une « surcharge » résultant de l’accumulation d’eau derrière la paroi, en relation avec les venues d’eau rencontrées lors de la foration de certains tirants.

Nous avons donc réalisé des drains complémentaires et trois tirants d’ancrages supplémentaires. Lors de la foration des drains complémentaires, il a été constaté un fort débit pendant les premiers jours et une atténuation par la suite. Ce dispositif a permis de stopper les déplacements, en attendant le butonnage par la réalisation des planchers correspondants.

6 CONCLUSION

Cet ouvrage, exceptionnel par sa hauteur (70 m de soutènement) et par son environnement imposant des contraintes très strictes de déplacements, a pu être mené à bien grâce à une conception d’origine adaptée, notamment par sa géométrie en voûte et par la méthode de construction en « Top & Down », et par des études alliant des approches traditionnelles négligeant tout effet tridimensionnel, et des modélisations numériques 3D permettant d’évaluer les effets bénéfiques de cette géométrie en reproduisant tous les éléments de soutènement et d’infrastructure et le phasage détaillé de l’opération.

Mais tout autant que la conception, c’est le suivi rigoureux du chantier, conduit selon les principes de la méthode observationnelle, qui a permis d’atteindre les performances attendues (déplacement horizontal en tête de l’ordre de $0.15/1000^\circ$ de la hauteur), et de traiter à temps les rares, mais inévitables, anomalies de comportement local.

7 REMERCIEMENTS

Les auteurs remercient : le Maître d’Ouvrage : Groupe Marzocco, la Maîtrise d’œuvre générale : Cabinet d’Architecte GIRALDI, le Bureau d’Etudes Structure : Coyne et Bellier, le Bureau de contrôle : SOCOTEC, et le Bureau d’Etudes Géotechnique : E&G.

A Case Study of 3D FE Analysis of a Deep Excavation Adjacent to a Tunnel Construction

Une étude de cas d'une simulation tridimensionnelle d'analyse par éléments finis d'une excavation profonde adjacente à une construction d'un tunnel

Guler E.

Bosphorus University, Istanbul, Turkey

Osmanoglu U., Koç M.

ELC Group Inc. (Royal HaskoningDHV Turkey), Istanbul, Turkey

ABSTRACT: This paper describes the 3D geotechnical FE analysis and design of a deep excavation bracing system. The location is situated in a very dense business area in Istanbul. The maximum height of the excavation is ~23 m to accommodate 7 basement floors. The layout has a non-uniform shape, surrounded with existing high rise structures with multi-basement floors, and an underpass connection to E-5 Motorway. In addition to these, the most outstanding characteristic of this design is the pedestrian tunnel and the shaft that is very close to the excavation pit. Both of these underground structures were being constructed throughout the same construction period as the deep excavation. At the non-anchoring zones adjacent to the tunnel and shaft, steel struts have been used. As a compound engineering service, soil investigation – design – site supervision – geotechnical instrumentation works was carried out. Therefore a comprehensive data for comparison between design results and in-situ performance could be gathered. This paper focuses on the details of the sophisticated 3D FE analysis and the comparison with the in-situ performance of the shoring system.

RÉSUMÉ : Ce document décrit l'analyse géotechnique 3D par éléments finis et la conception d'un système de contreventement utilisé dans l'excavation profonde. L'emplacement est situé dans un quartier très dense à Istanbul. La hauteur maximale de l'excavation est de 23 m pour 7 sous-sols. Le site a une forme non uniforme, entouré de structures existantes de grande hauteur avec multi-sous-sols, une connexion souterraine de l'autoroute E-5. En plus de cela, la caractéristique la plus remarquable de cette conception est le tunnel pour piétons et l'arbre qui est très proche de l'excavation. Ces deux structures souterraines ont été construites pendant la même période que la construction de l'excavation profonde. Au niveau des zones de non-ancrage adjacentes au tunnel et à l'arbre, des entretoises en acier sont utilisées. En tant que service d'ingénierie l'étude du sol, - la conception - la supervision de chantier - les travaux en instrumentation géotechnique ont été réalisées. Par conséquent un ensemble de données complètes pour la comparaison entre les résultats de la conception et de la performance in-situ aurait pu être recueillie. Ce document se concentre sur les détails d'une simulation 3D sophistiquée d'Analyse par éléments finis et la comparaison des performances in-situ du système d'étaie.

KEYWORDS: 3D FE Analysis, Deep Excavation, Case Study, Excavation-Tunnel-Shaft interaction.

1 INTRODUCTION

The deep excavation retaining system project is located at the European side of Istanbul. The plan view of the site is presented in Figure 1. The depth of the excavation is 23 m. The ongoing construction of a pedestrian tunnel and entrance shaft adjacent to this excavation makes the design of the retaining system complicated. Interaction with this deep excavation work was not considered in the design of the tunnel and shaft. Hence, the shoring design for the deep excavation had to consider the very close tunnel and shaft which were still being constructed and standing with their temporary support systems during the excavation works. Since the interaction between the deep excavation and the simultaneously constructed shaft and tunnel cannot be modeled with only a 2D analysis (plain-strain model), a 3D Geotechnical FE analysis (especially for the shaft location) had to be conducted.

The pedestrian tunnel has a span of 7 m at a distance of 7 m to the piles of the shoring system. The shaft has a diameter of 6 m at 2.5 m distance to the piles of the shoring system. The tunnel and shaft's temporary support system was composing of ~20 cm shotcrete facing and rock bolts. In the tunnel 4 m long rock bolts were used only at the top heading. In the shaft 2 m long radial rock bolts were used. The temporary excavation system of the building is designed with micro piles, pre-stressed anchors and steel struts at non-anchoring zones due to tunnel and shaft. The elevation corresponds roughly to the foundation level of the excavation pit.

The software used in this project were TNO DIANA for 3D modeling and Plaxis V.11 for 2D modeling (for the analysis at the tunnel side).

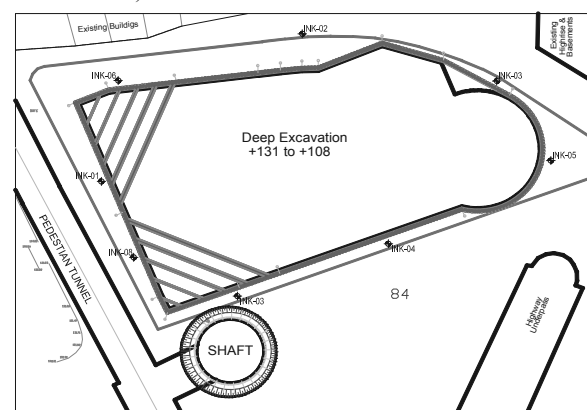


Figure 1. Site layout with surrounding structures

2 DESIGN PHASE

The design works were carried out based on the geological & geotechnical data obtained from the site investigations. Surcharge loads were considered wherever necessary.

2.1 Geological & Geotechnical Conditions

The geology of the site mainly consists of Carboniferous aged Trace Formation’s intercalation of sandstone – siltstone layers. The bedrock is overlain by weathered particles of the Trace Formation in clay matrix with thicknesses varying between 3 ~ 4 m. Finally the site is covered with artificial fill with a thickness of ~2 m. The bedrock is divided in to two fictitious layers at a depth of 14 m according to the increasing rock mass quality. Except leakage water from the discontinuities and fractures, no groundwater table was encountered at the site. The proposed stratigraphy and the engineering parameters used in modeling are presented in Table 1.

Table 1. Proposed stratigraphy and engineering parameters

Layer	Fill	Residual Zone	Bedrock-1	Bedrock-2
Thickness (m)	2	5	7	-
c (kPa)	0	1	5	10
ϕ (°)	25	30	35	38
γ (kN/m ³)	18	20	22.5	23
E (kN/m ²)	5,000	25,000	100,000	150,000
ν	0.35	0.30	0.28	0.25

2.2 Design Philosophy

Since the construction of the pedestrian tunnel and shaft were ongoing at the time, the initiation of the phased construction model had to be started with simulation of these structures. The design work was aiming to find out the effects of the deep excavation on the tunnel and shaft structures. In order to detect the magnitude (after initial phase) and variations of the section forces together with the deformations of the tunnel and shafts’ temporary support system throughout the deep excavation, dewatering and basement construction stages, the shotcrete facing was modeled with shell elements.

The deep excavation support system was designed contiguous (without a gap) to the basement walls that will be constructed after the completion of the deep excavation. This is mainly due to the clients’ demand for minimum space loss. This philosophy turned in to an advantage for the adjacent tunnel and shaft, since every constructed basement floor constituted a rigid support to the shoring system, hence the effects of dewatering stages could be minimized on tunnel and shaft.

Both the 2D and 3D finite elements models were constituted in compliance with in-situ construction steps (tunnel & shaft construction, staged deep excavation procedure, staged basement construction and dewatering of the steel struts).

The steel struts, piles of shoring system, shotcrete facing and the rockbolts were modeled as linear elastic materials. The properties of these linear elastic materials are given in Table 2. All struts used were tubular steel with a thickness of 10.3 mm.

Table 2. Elastic and rigidity variables

Material	E (kN/m ²)	D Spacing (m)	d Diameter	ν
Micropiles	2.5E7	0.60	30 cm	0.20
Shotcrete	2.0E7	cont.	20 cm	0.20
Steel struts	2.1E8	3	16” ~ 32”	0.28
Rockbolts	1E7	1.5	51 mm	0.28

2.3 2D FE Analysis

General approach to model a deep excavation in geotechnical engineering is to execute Limit Equilibrium stability analysis to get the satisfactory factor of safety and a FEA to check the

compliance of deformation criteria. Since 2D FEA is a fast and effective design tool, the same methodology was used for the subjected project.

The 2D FE model at the adjacent tunnel location is given in Figure 2.

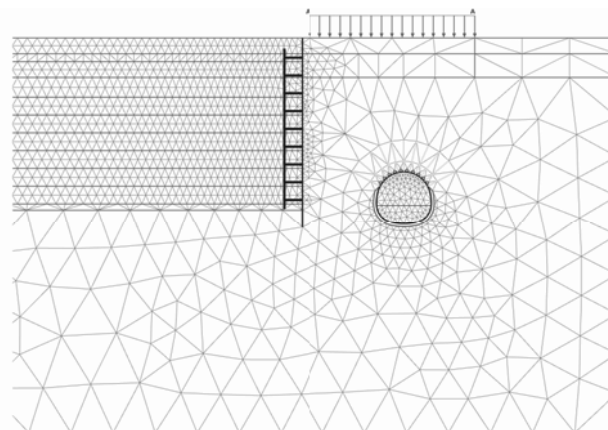


Figure 2. 2D FE model from tunnel section

Deformation analyses were carried out with commercial software package of PLAXIS. Mohr Coulomb material model was used for the design based on the expertise of deep excavation designs and their feedback from in-situ performance, in similar geological circumstances which is very widespread in Istanbul.

2.4 3D FE Analysis

A 3D FE Analysis had to be conducted in order to simulate the interaction between the deep excavation works and tunnel&shaft. The main goal of the 3D modeling study was to establish an appropriate excavation system and sequence, hence only the related part of the system was focused in the analysis. By this means, the processing time in such a complex model could be reduced to a reasonable level. As it is in 2D FEA, also Mohr-Coulomb material model was used in the 3D FEA. All engineering parameters were kept same.

The 3D FE model is given in Figure 3.

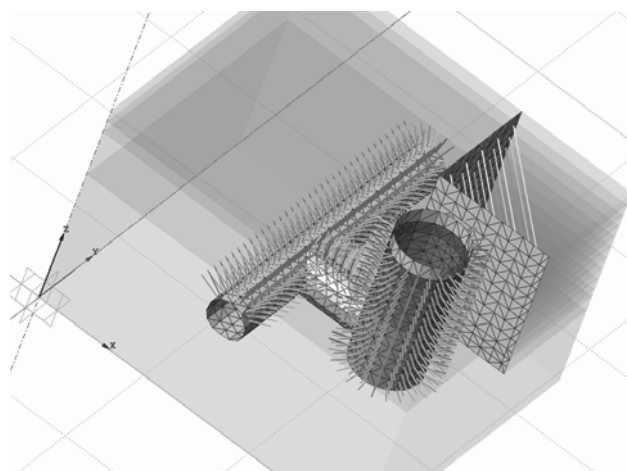


Figure 3. 3D FE model from with nearby tunnel and shaft

3 RESULTS FROM THE ANALYSES

The main purpose of this modeling study was to find out the interaction between the tunnel&shaft structures with (and during) the deep excavation works. Therefore, the specific values (bending moments, shear forces, normal forces, and

displacements) are presented in this paper (both from 2D FEA and 3D FEA) in Table 3. The given results for the tunnel and shaft structures are values prior to excavation and final values after completion of deep excavation work.

Table 3. Results of FEA

Result	2D FEA	3D FEA
Deformation of shoring (mm)	7.8	4.2
Deformation of Tunnel (mm)	9 / 3	2.0
Deformation of Shaft (mm)	NA	3.2
Bnd.Moment on Shoring (kNm/m)	97.3	31
Bnd.Moment on Tunnel (kNm/m)	9 / 16.4	8.4 / 8.7
Bnd.Moment on Shaft (kNm/m)	NA	13.9 / 16.1
Shear Force on Shoring (kN/m)	132.4	83
Shear Force on Tunnel (kN/m)	20.2 / 22.5	26.8 / 25.3
Shear Force on Shaft (kN/m)	NA	20.0 / 19.6
Normal Force on Shoring (kN/m)	416.8	366
Normal Force on Tunnel (kN/m)	470.7 / 633.4	545 / 532
Normal Force on Shaft (kN/m)	NA	800 / 666

The result for total deformation from the 3D FEA is presented in Figure 4. The result for total deformation from the 2D FEA is presented in Figure 5.

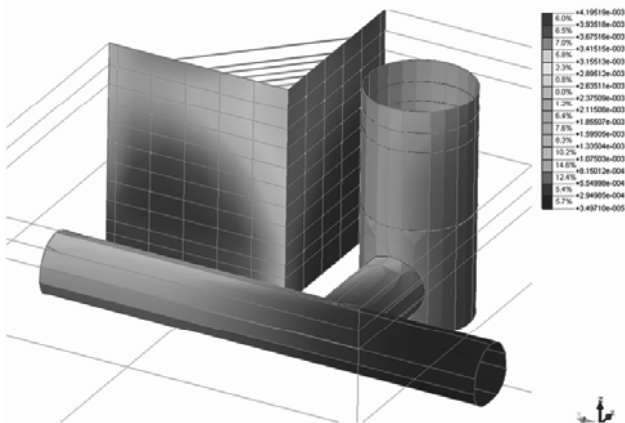


Figure 4. Total displacement from 3D FEA (max. 4.2 mm)

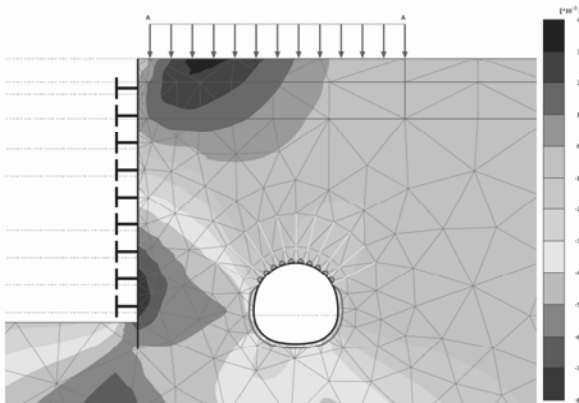


Figure 5. Total displacement from 2D FEA (max. 7.8 mm)

The result for bending moments (on all shell elements) is presented in Figure 6.

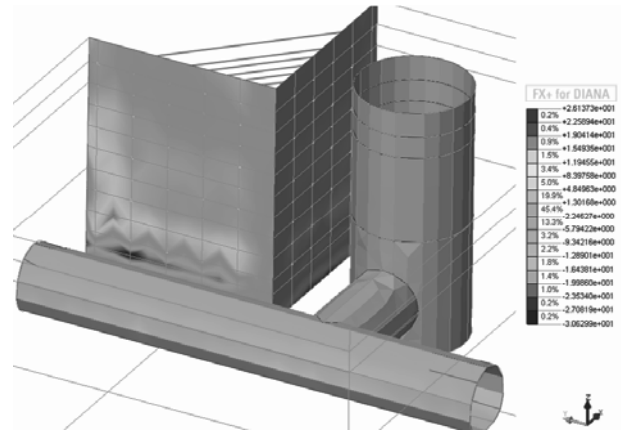


Figure 6. Bending moments from 3D FEA (max. 31 kNm/m shoring, max. 8.7 kNm/m tunnel, max. 16.1 kNm/m shaft).

In addition to deformations and section forces, the axial forces on the steel struts are also calculated and compared with both 2D and 3D FEA. The values are presented (as the envelope values for all construction and demounting stages) in Table 4.

Table 4. Results of Axial Forces in struts

Result	2D FEA	3D FEA
Axial Forces (kN)	263 kN/m	627-765 kN*

*The assumed length of struts in 2D is 20 m hence the results of 17-23 m struts in 3D model are given. The spacing of the struts in 2D model is 4.0 m, so that the value of 263 kN/m (perpendicular to the surface) shall be multiplied by 3 in order to get the axial perpendicular force of an individual strut.

The results for steel strut axial forces from 3D FEA are presented in Figure 7.

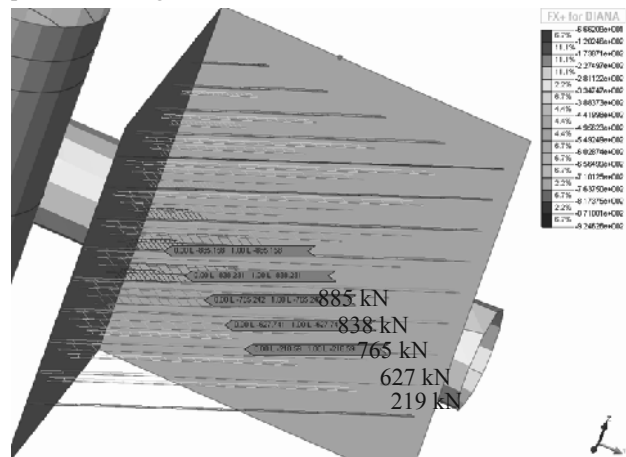


Figure 7. Total strut forces from 3D FEA (max. 885 kN)

4 CONSTRUCTION AND MONITORING PHASE

During construction period, a geotechnical instrumentation program, consisting of inclinometers, optic survey points (for deformation monitoring) and strain-gauges (for axial force and dependently stresses on steel struts), has been carried out. This monitoring program gave reliable data and so it was possible to verify the design results with in-situ performance that has been gathered.

The maximum deformation on the inclinometer at shaft location (INK-07) was measured as ~7 mm. The maximum deformation values received from optical surveys are also ~7 mm at shaft location and ~8 mm at the tunnel location. Inclinometer and optic survey results are presented in Figure 8.

Suction Caisson Installation in Shallow Water: Model Tests and Prediction

Installation de caissons à succion en eau peu profonde: essais et prédiction

Guo W.

School of Civil & Environmental Engineering, Nanyang Technological University, Singapore

Chu J.

Department Civil, Construction & Environmental Engineering, Iowa State University, USA

ABSTRACT: Suction caissons have been used as foundations to support mainly offshore structures such as offshore oil rigs in deep water where a large suction pressure can be generated. Studies have been made recently to use this method for near shore foundations in shallow water where the suction that can be applied is much smaller. In this paper, a study on the installation of suction caissons in clay in shallow water using large scale model tests is presented. The model test setup and test results are discussed. The effects of soil plug and side friction are evaluated. An analytical method proposed by Houlsby and Byrne is adopted to predict the penetration versus time relationship. The analytical solutions agree well with the model test results.

RÉSUMÉ: Les caissons à succion ont été utilisés principalement pour les fondations de structures offshore en eau profonde permettant de générer de fortes pressions de succion. Cet article présente une étude sur une installation de caisson dans de l'argile à faible profondeur en utilisant un modèle à grande échelle. Les résistances d'arrachement et frottements latéraux sont évalués. La méthode analytique proposée par Houlsby et Byrne est adoptée pour prédire la relation pénétration-temps et donne de bons résultats

KEYWORDS: Caisson; Clay; Model Test.

1 INTRODUCTION

A research project to use super-size cylindrical structures to form underwater space and at the same time create land on top is being carried out in Singapore. As the seabed soil is mainly soft clay, suction caissons were considered on possible form of foundations to support part of the reclaimed land for buildings or other types of structures to be built on top of it, the foundation types for the offshore structures have to be developed using innovative solutions. The most difficult design condition is when the seabed soil is soft. It would be too costly to treat the soft soil offshore. One innovative solution is to use suction caissons.

Normally suction caissons are large, hollow, cylindrical steel or concrete structures in form of upturned bucket shape, and are penetrated into the seafloor bottom sediments by self-weight and suction pressure. The principle of the suction caisson technique is to apply suction inside a sealed cylindrical caisson to create a downward net force to sink the caisson into the seabed soil. After the suction is removed, the foundation is constructed without treating the soft soil. The suction caisson have been successfully employed in recent years in many projects including mooring anchors (Andersen and Jostad, 1999; Andresen et al., 2011; Randolph et al., 2011; Wang et al., 1975), beak water or sea walls (Chu et al., 2012), offshore platforms (Zhang et al., 2007; Zhang and Ding, 2011) and foundation for wind turbine in deep waters (Byrne et al., 2002; Gavin et al., 2011; Houlsby et al., 2005c).

For caissons used in deep water, the hydrostatic water pressure as provided by the water depth can contribute to suction pressure to compress the caisson into seabed. However, in relatively shallow water, there may not be sufficient suction to allow the caisson to penetrate to the required depth. Another factor affecting the penetration of a suction caisson is the soil plug formed inside the caisson. When a caisson is penetrated into clay, soil will go inside the open ended hollow caisson and form soil plug. The soil plug resists the penetration of the caisson. For this purpose and for the development of suitable design methods, model tests and numerical studies were carried out.

Analytical methods for analyzing the installation process of suction caisson have also been proposed (Andersen et al., 2005;

Chen et al., 2009; Houlsby and Byrne, 2005a, 2005b; House and Randolph, 2001; House et al., 1999; Tran and Randolph, 2008). In the method by Houlsby and Byrne (2005a, 2005b), a constant penetration velocity was assumed. The driving forces and soil resistance were also assumed to be balanced during the whole installation process. This method was adopted to calculate the amount of penetration of suction caisson subjected to a constant driving force. The solution of this method was compared with those from the model tests and good agreement was achieved. Some of the key design parameters were also evaluated based on the model test results.

2 MODEL TESTS

2.1 Soil Preparation

The soil used for the model tests was consolidated from kaolin slurry. Factory made kaolin powder was used because of its high coefficient of consolidation, low compressibility and commercial availability. The kaolin used was supplied by Kaolin Malaysia Sdn. Bhd. It has a specific gravity of 2.61, a liquid limit of 61% and a plastic limit of 38%.

The kaolin powder was mixed with tap water into a slurry form with water content of 81.3%. After mixing, the desired slurry was transferred to the consolidation tank as shown in Figure 1. Then the top cap and piston were mounted onto the cylindrical tank. A compressed air pressure of 60kPa was applied on top of the piston to consolidate the kaolin slurry for about 10 days. The friction between the piston and the tank wall was 17.35 kN measured by a calibration test before the test. Therefore, the effective consolidation pressure was 37.9 kPa only.

The consolidated water was allowed to drain freely through a drainage valve at the bottom of base plate. In order to consolidate the kaolin slurry faster, a filter layer were designed on the bottom of the tank including two layers of geotextile, fine sand and gravel. The movement of piston was monitored by a laser sensor (Keyence®IL-600). After the consolidation was completed, the air pressure was reduced to zero and the top cap was removed to allow soil samples to be taken for undrained shear strength and water content tests. The water content of the tested soil was 42.7%. The average undrained shear strength

(S_u) was 13 kPa as measured by lab shear vane method along the tank depth.

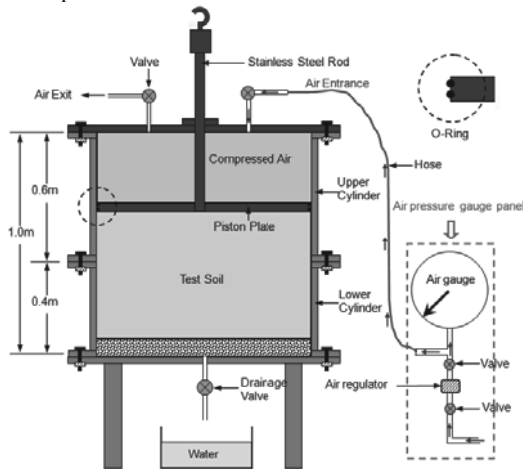


Figure 1 Consolidation procedure of kaolin

2.2 Caisson Installation

The caisson was made by an inner steel skirt and covered by a layer of concrete with its total height of 400mm, diameter of 205mm and wall thickness of 22.5mm. The Caisson was assembled with a designed piston which made it possible to monitor the process of soil plug during installation tests. The piston consisted of a ‘Teflon’ plate and a steel rod. The plate was 25 mm thick and 150 mm in diameter with steel rod mounted in the middle. A crew with a height of 20 mm was used to strengthen the connection of the rod and the plate. Thus the clear internal skirt length of the caisson reduced from 400mm to 335 mm. The total weight of caisson and piston was 27.2kg.

The vacuum loading system was composed by a vacuum pump (EVISA E25), a vacuum gauge, two bowl vacuum filters, a vacuum tank, and a hose, as illustrate in Figure 2. Note that during suction installation tests, one more absolute pressure transducer was mounted in the caisson cavity to test the vacuum pressure.

The miniature pore water pressure transducers (PPTs) were used in this model test to measure the pore water pressure changes. Such a miniature size was necessary to minimize the influence of the measuring device to the overall soil behavior during model test. Before a model test, all PPTs were calibrated by using water pressure generated in a triaxial cell. The preinstalled positions of the PPTs on the top cap are shown in Figure 2.

The displacement of the piston in the consolidation tank or that of the suction caisson during the model test was measured by laser sensor (KEYENCE IL series) which had an effective measurement range from 20cm to 1.0m. The displacement of piston rod in caisson was also measure by another laser sensor by mounting an aluminum plate on to the rod. The third laser sensor was mounted on the frame to measure the displacement of suction caisson. Two other laser sensors were used to measure the soil movement on caisson sides as shown in Figure 2. This contact-free displacement measuring method offered both reliability and convenience.

2.3 Model Test Results

The model test results of caisson penetrated into the soil bed assisted by vacuum pressure was discussed in this section. Since the self-weight was not able to provide enough penetration force for caisson insertion, the caisson was manually penetrated into soil in a short distance to ensure that the applied suction would not leakage. The applied vacuum pressures in Model Test No. 1 and No. 2 during the suction installation are shown in Figure 3. It can be seen that the vacuum pressure increased very slowly

till to the largest magnitude of -80kPa. The displacements of the caisson and soil plug are shown in Figure 4 and Figure 5, respectively. It can be seen that the soil plug was moving upward throughout the installation procedure. At the beginning, the soil plugs increased nearly linearly with the time. At the time of 81s for test No. 1 and 96s for test No. 2, there was a sudden jump in the displacement. This happened because the soil plug was broken suddenly. During this period, the caisson had no penetration.

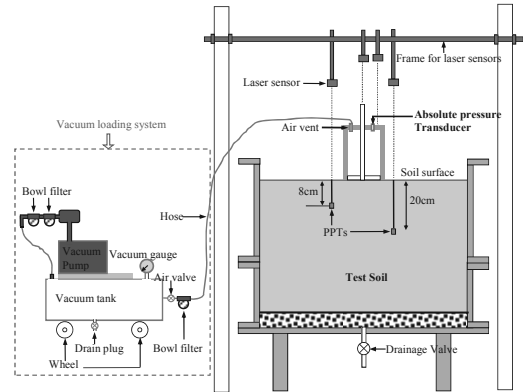


Figure 2 Installation of suction caisson

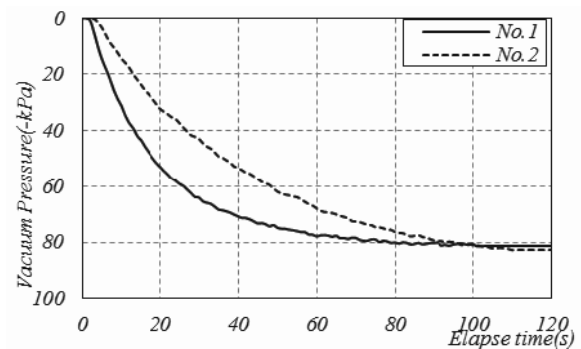


Figure 3 Vacuum pressure vs. time curve

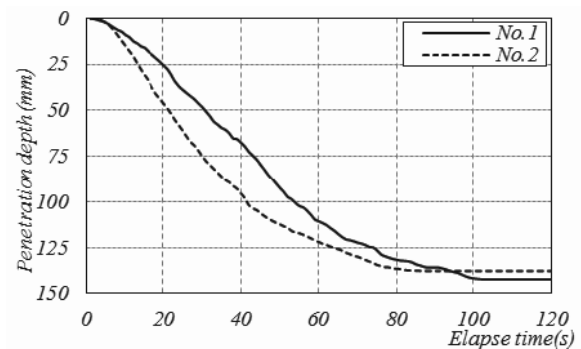


Figure 4 Penetration depth vs. time curve

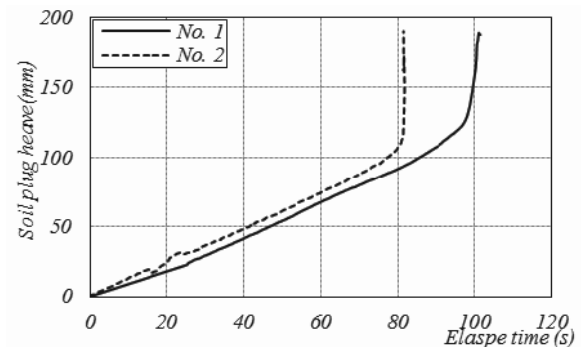


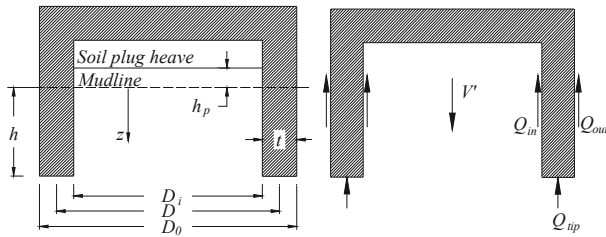
Figure 5 Penetration depth vs. soil plug heave curve

3 ANALYTICAL SOLUTIONS

An analytical method to simulate the penetration procedure for suction caisson in clay has been proposed by Houlsby and Byne (2005b). The friction between internal caisson wall and internal clay and that between external wall and external clay were considered separately by using different friction coefficient (different α value). The self-weight penetration and suction assistant penetration have been made a clear distinction. As the self-weight penetration is very small in our 1-g model tests, only the suction assistant penetration process is discussed in this paper.

A simplified cross-section of the suction caisson is shown in Figure 6. The vertical coordinates, measured at a depth below the mud line, is set up with z . The inside, outside and average diameters of the caisson are represented by D_i , D_o , D respectively. Therefore, $D_i = D_o - 2t$ and $D = (D_i + D_o)/2$ where t is the thickness of the caisson wall. The total height of the caisson is L and height embedment into the seabed is h . The soil plug higher than the mud line inside of the caisson is denoted as h_p . The unit weight of water is γ_w and that of soil is γ .

As illustrated in Figure 6(b), the total effective weight of suction caisson is presented as V' . The side frictions between soil with outside and inside of the caisson are written as Q_{in} and Q_{out} , respectively. The end bearing capacity on the tip of suction caisson is defined as Q_{tip} .



(a) Parameters definition (b) Free body diagram
Figure 6 Cross section of suction caisson (Modified after Houlsby and Byne, 2005b)

When the caisson penetrates into the soil, a bearing capacity failure will occur around the wall tip. It is assumed that the soil plug is mainly due to these displaced soil flow into the caisson. We make the simplifying assumptions that: (a) there is a volume of clay, V_s , flows into the caisson because of the replacement of caisson walls, V_c , and $V_s = mV_c$; (b) the flowed clay does not change the original unit weight of clay within the caisson; and (c) the flowed clay forms the soil plug with its height shown in Eq. (1). These assumptions were especially valid for the suction caisson installed in clay which have already been verified by model test results (Whittle et al., 1998), prototype behavior (Colliat et al., 1996), and finite element analyses (Andersen and Jostad, 2002; Andersen and Jostad, 2004). The values of m will be calculated using the model test results.

$$h_p = m(D_o^2 / D_i^2 - 1)h \quad (1)$$

For the case of suction caisson installation in clay, the calculation neglects the effect of the applied suction pressure and the side frictions along the caisson walls. Then this procedure can be treated as undrained conditions. Therefore, the side frictions are calculated by applying a factor α to the value of the undrained strength (α -method), i.e. $Q_{in} = h\alpha_i s_{ui}(\pi D_i)$ and $Q_{out} = h\alpha_o s_{uo}(\pi D_o)$ where s_{uo} is average undrained strength between mud line and depth h . If the undrained strength of clay increased along depth linearly, i.e. $s_u = s_{u1} + \rho z$, the average undrained strength of soil, s_{uo} , can be calculated as $s_{uo} = s_{u1} + \rho h/2$ where ρ is the coefficient of undrained strength increasing. Similar calculation method can also be applied to the internal

undrained strength, s_{ui} . The bearing capacity on the tip is calculated according to the standard bearing capacity calculation, i.e. $\sigma'_{tip} = \gamma' h N_q + s_{u2} N_c$ and $s_{u2} = s_{u0} + \rho h$, where N_c is the capacity factor for a deep strip footing in clay (a typical value of 9 may be adopted) and $N_q = 1$ for undrained analysis. During the suction assisted penetrations, the driving force is the weight of suction caisson and applied suction pressure. The resistance to the caisson is calculated as the sum of the side frictions ($Q_{in} + Q_{out}$) and the end bearing capacity on the tip (Q_{tip}). The force equilibrium along the vertical direction yields the following equation:

$$V' + s\left(\frac{\pi D_o^2}{4}\right) = h\alpha_o s_{uo}(\pi D_o) + (h + h_p)\alpha_i s_{ui}(\pi D_i) + (\gamma' h + s_{u2} N_c)(\pi D t) \quad (2)$$

The internal and external side frictions calculated by $(h + h_p)\alpha_i s_{ui}$ and $h\alpha_o s_{uo}$ may be assumed to have the same magnitude. This is reasonable as the internally remold clay will have a lower undrained shear strength and a lower coefficient of side friction (Andersen and Jostad, 2004). Then Eq. (2) can be further simplified as follows:

$$V' + s\left(\frac{\pi D_o^2}{4}\right) = 2h\alpha_o s_{uo} \pi D + (\gamma' h + s_{u2} N_c)(\pi D t) \quad (3)$$

The penetration depth h can be derived from Eq. (3) and shown as follows:

$$h = \frac{V' + s\left(\frac{\pi D_o^2}{4}\right) - s_{u2} N_c (\pi D t)}{2\alpha_o s_{uo} \pi D + \gamma' (\pi D t)} \quad (4)$$

4 COMPARISON BETWEEN THE TWO METHODS

It should be point out that the analytical method for caisson penetration is only applicable when the caisson is penetrating into clay with a constant velocity. Then the driving forces and resistance forces can be treated as balanced during each calculation step. The results shown in Figure 4, the penetration depth versus time curve is almost in a linear relationship. The comparisons between these two sets of results were made by assuming the caisson was penetrated into the clay in a constant speed or the forces in each calculation step were balanced.

In the following calculation, the tested vacuum pressures were taken as inputs. This procedure maybe not the way for engineering designing but could be used to verify the accuracy of this theoretical method. The comparison could also give a way to evaluate the key design parameters for caisson designing. The average undrained shear strength of soil bed used for calculation was $13kPa$ as discussed in section 2.1. The values of N_c and N_q for undrained analysis were adopted as 9.0 and 1.0, respectively. The average unit weight of soil bed is $12.3kN/m^3$ which can easily be derived from $w\%$ (42.7%) and G_s (2.61). The total weight of concrete caisson is $0.272kN$ ($27.2 \times 10kN$).

The model test results and the analytical results for the displacement of suction caisson are compared in Figure 7. It can be seen that when $\alpha = 0.72$, the two sets of results agree well with each other. The analytical results show that the penetration of suction caisson needs a minimum driving suction pressure. However, the model tests show a much smaller value. Furthermore, the penetration procedure for model No. 2 was delayed (start time of $t = 25s$) comparing to model No. 1 (starting time of $t = 13s$) because the applying speed of vacuum pressure for model No. 2 is lower than that for model No. 1.

The comparison between the theoretical and the model test results regarding the heave of soil plug is shown in Figure 8. The analytical model indicates that a minimum vacuum pressure is required for the soil plug to start to heave as there is no plug

movement at the beginning. This is related to the assumption that the heave of soil plug is caused by the penetration of caisson walls. A fitting of the experimental curves using a value of $m=1.4$ was also made. $m=1.4$ implies that the volume of the soil going into the caisson cavity was 140% of the volume of the soil replaced. This is possible as the additional 40% could come from the expansion of the remolded soil or flow of soil beneath the caisson. As discussed before, the soil plug was broken at the end of the experiments. This aspect could not be modeled by the analytical method.

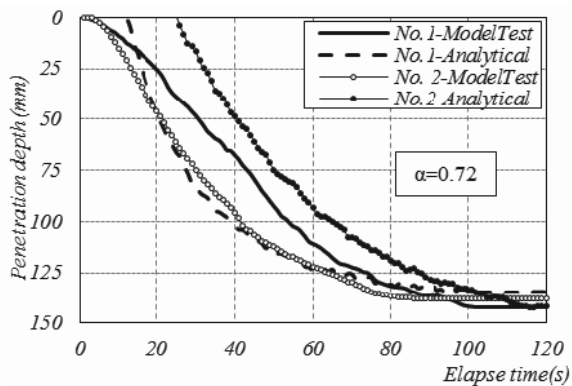


Figure 7 Predicted and measured penetration depth vs. time curves

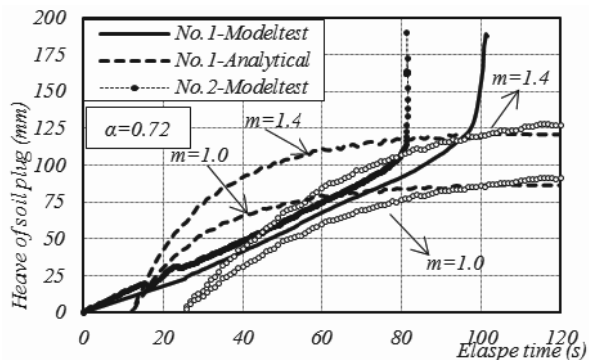


Figure 8 Predicted and measured heave vs. time curves

5 CONCLUSIONS

Suction caissons have been used mainly as foundations to support offshore structures in deep water. Their applications in shallow water are more challenging as the amount of suction that can be applied to install the caissons is much less. Several model tests on the use of suction caisson in clay in shallow water were carried out. The height of soil plug, displacement of the suction caisson and applied vacuum pressure were measured during the model tests. An analytical method proposed by Housby and Byrne (2005b) were adopted to simulate the model test results. The analytical results agree well with the model test results with the selection of appropriate parameters.

6 ACKNOWLEDGEMENT

The authors would like to thank Dr. LIU Kejin, WU Shifan and LI Mangyuan for their contribution to the research program and Prof YAN Shuwang for useful discussions with him.

7 REFERENCES

Andersen, K.H., Jeanjean, P., Luger, D., Jostad, H.P., 2005. Centrifuge tests on installation of suction anchors in soft clay. *Ocean Engineering* 32, 845-863.

- Andersen, K.H., Jostad, H.P., 1999. Foundation Design of Skirted Foundations and Anchors in Clay, *Offshore Technology Conference*, Houston, Texas.
- Andersen, K.H., Jostad, H.P., 2002. Shear Strength Along Outside Wall of Suction Anchors in Clay after Installation, *Proceedings of The Twelfth (2002) International Offshore and Polar Engineering Conference*. Kitakyushu, Japan.
- Andersen, K.H., Jostad, H.P., 2004. Shear Strength Along Inside of Suction Anchor Skirt Wall in Clay, *Offshore Technology Conference*, Houston, Texas.
- Andresen, L., Jostad, H.P., Andersen, K.H., 2011. Finite Element Analyses Applied in Design of Foundations and Anchors for Offshore Structures. *International Journal of Geomechanics* 11, 417-430.
- Byrne, B.W., Housby, G.T., Martin, C.M., Fish, P., 2002. Suction caisson foundation for offshore wind turbines. *Wind Engineering* 26, 145-155.
- Chen, W., Zhou, H., Randolph, M.F., 2009. Effect of Installation Method on External Shaft Friction of Caissons in Soft Clay. *Journal of Geotechnical and Geoenvironmental Engineering* 135, 605-615.
- Chu, J., Yan, S.W., Li, W., 2012. Innovative methods for dike construction – An overview. *Geotextiles and Geomembranes* 30, 35-42.
- Colliat, J.-L., Boisard, P., Gramet, J.-C., Sparrevik, P., 1996. Design and installation of suction anchor piles at a soft clay site in the Gulf of Guinea. *Paper OTC 8150, Offshore Technology Conference*, Houston, Texas.
- Gavin, K., Igoe, D., Doherty, P., 2011. Piles for offshore wind turbines: A state of the art review. *Ice Geotechnical Engineering Journal* 164 245-256.
- Housby, G.T., Byrne, B.W., 2000. Suction Caisson Foundations for Offshore Wind Turbines and Anemometer Masts. *Wind Engineering* 24, 249-255.
- Housby, G.T., Byrne, B.W., 2005a. Design procedures for installation of suction caissons in sand. *Proceedings of the ICE - Geotechnical Engineering* 158, 135 -144.
- Housby, G.T., Byrne, B.W., 2005b. Design procedures for installation of suction caissons in clay and other materials. *Proceedings of the ICE - Geotechnical Engineering* 158, 75 -82.
- Housby, G.T., Kelly, R.B., Huxtable, J., Byrne, B.W., 2005c. Field trials of suction caissons in clay for offshore wind turbine foundations. *Géotechnique* 55, 287-296.
- House, A.R., Randolph, M.F., 2001. Installation and Pull-Out Capacity of Stiffened Suction Caissons in Cohesive Sediments, *Proceedings of the Eleventh (2001) International Offshore and Polar Engineering Conference*, Stavanger, Norway, pp. 17-22.
- House, A.R., Randolph, M.F., Borbas, M.E., 1999. Limiting Aspect Ratio for Suction Caisson Installation in Clay, *Proceedings of the Ninth (1999) International Offshore and Polar Engineering Conference*. Brest, France.
- Randolph, M.F., Gaudin, C., Gourvenec, S.M., White, D.J., Boylan, N., Cassidy, M.J., 2011. Recent advances in offshore geotechnics for deep water oil and gas developments. *Ocean Engineering* 38, 818-834.
- Tran, M.N., Randolph, M.F., 2008. Variation of suction pressure during caisson installation in sand. *Géotechnique* 58, 1-11.
- Wang, M.C., Nacci, V.A., Demars, K.R., 1975. Behavior of underwater suction anchor in soil. *Ocean Engineering* 3, 47-62.
- Whittle, A.J., Germaine, J.T., Cauble, D.F., 1998. Behavior of Miniature Suction Caissons in Clay, *Proc., Offshore Site Inv. Found. Behavior '98*. London, UK, pp. 279-300.
- Zhang, J.H., Zhang, L.M., Lu, X.B., 2007. Centrifuge modeling of suction bucket foundations for platforms under ice-sheet-induced cyclic lateral loadings. *Ocean Engineering* 34, 1069-1079.
- Zhang, P., Ding, H., 2011. Bearing capacity of the bucket spudcan foundation for offshore jack-up drilling platforms. *Petroleum Exploration and Development* 38, 237-242.

Instrumentation de la paroi moulée du bassin de Blanc-Mesnil : retro-analyse et calage des modèles de calcul

Instrumentation of the diaphragm wall of the Blanc-Mesnil Basin : retro-analysis and calibration of calculation models

Gutjahr I., Doucerain M., Schmitt P.
SOLETANCHE-BACHY, Paris, France

Heumez S., Maurel C.
CETE-IF, Le Bourget, France

RÉSUMÉ : Le chantier du bassin du Vieux Blanc-Mesnil a fait l'objet d'une instrumentation afin de confronter le comportement réel de l'ouvrage aux calculs aux coefficients de réaction menés lors des études d'exécution, puis en complément aux calculs aux éléments finis. Une particularité de ce projet réside dans le fait que le soutènement est surmonté d'un talus de grande hauteur, le suivi du comportement du soutènement permet donc également de comparer les différentes modélisations d'un talus à la réalité. Suite aux différences constatées entre les courbes de déformée réelle et calculée lors des études d'exécution, il a été procédé à un affinage du modèle géotechnique consistant à ne tenir compte que des sondages les plus proches des sections instrumentées. Il a ainsi été possible de valider les résultats obtenus par les différentes méthodes (coefficient de réaction et éléments finis), moyennant la prise en compte d'une modélisation réaliste du talus et l'utilisation de paramètres de sols équivalents et représentatifs.

ABSTRACT: The diaphragm wall of the Blanc-Mesnil Basin was subject to instrumentation in order to compare the structure's actual behaviour to calculations based on the coefficient of subgrade reaction, as used in the execution studies, as well as to calculations based on the finite element model. A peculiarity of this project lies in the fact that the retaining wall is surmounted by a high slope, thus the monitoring also permits to compare different slope calculation models to reality. Following the differences observed between the measured and calculated displacement curves, the geotechnical model was refined considering the boreholes closest to the surveyed sections. Thus it has been possible to validate the results obtained by different calculation models (finite element and coefficient of subgrade reaction).

Mots-Clés : suivi inclinométrique, modélisation d'un talus, calcul aux coefficients de réaction, calcul aux éléments finis

Keywords: inclinometer survey, slope calculation model, coefficient of subgrade reaction calculation, finite elements calculation

1 INTRODUCTION

Le soutènement périphérique du bassin de retenue du Vieux Blanc-Mesnil est constitué d'une paroi moulée d'épaisseur 0.80m ancrée par un niveau de tirants précontraints à caractère permanent.

Deux sections distinctes ont fait l'objet d'une instrumentation et d'un suivi complets dans le cadre de l'action de recherche FONDAMS pilotée par l'IFSTTAR afin de permettre une analyse du comportement réel de l'ouvrage puis ensuite le comparer non seulement aux calculs aux coefficients de réaction utilisés pour le dimensionnement, mais encore aux calculs aux éléments finis réalisés *a posteriori*.

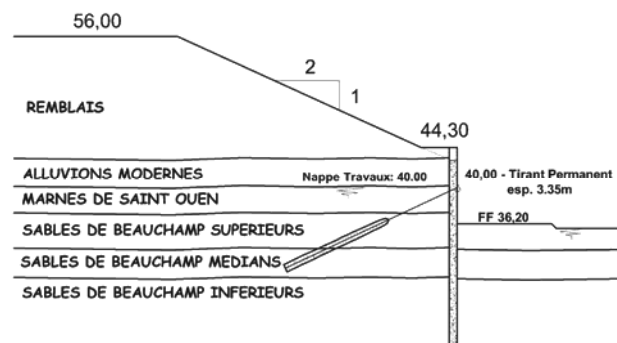


Figure 1. Profil de mesure « Coupe 1 B ».

Un intérêt particulier du projet est la présence d'un talus surmontant la paroi moulée sur une forte hauteur, variable de 7

à 12 m au droit des deux profils de mesure. La comparaison entre le comportement réel de l'ouvrage et les calculs permettra ainsi de confronter les différentes modélisations d'un talus utilisées dans la pratique courante à la réalité des mesures.

On a utilisé le logiciel PARIS (logiciel de calcul interne Solétanche-Bachy) pour les calculs aux coefficients de réaction et le logiciel PLAXIS 2D pour les calculs aux éléments finis.

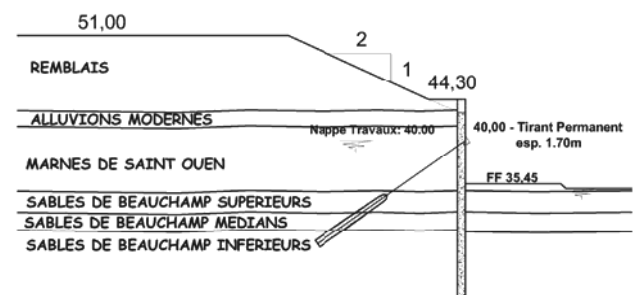


Figure 2. Profil de mesure « Coupe 2 B ».

2 PRÉSENTATION DES MESURES

L'instrumentation de la paroi a consisté en la mise en place de deux inclinomètres scellés dans des tubes de réservation liés aux cages d'armatures de deux panneaux distincts. Plusieurs relevés inclinométriques ont donc été possibles au cours de la réalisation du bassin (un point zéro avant le début des excavations, une mesure lors de la phase en console avant la

mise en tension des tirants, et une mesure en phase fond de fouille). La précision des mesures inclinométriques est de l'ordre de 0,1 mm/m.

Afin de suivre l'évolution des efforts dans les tirants, des cales dynamométriques ont également été installées.

3 MODÉLISATION D'UN TALUS POUR LES CALCULS AUX COEFFICIENTS DE REACTION

Avant de procéder aux calculs de recalage, nous avons d'abord tenté d'établir quelle modélisation du talus est la mieux adaptée à la géométrie et au phasage du projet.

Pour cela nous avons mené une étude comparative portant sur la géométrie de la Coupe 1 B.

3.1 Modélisations étudiées

Nous avons comparé la modélisation du talus fini par différentes méthodes :

- approches en plasticité avec hypothèse sur le schéma de rupture : méthodes de Graux (Graux, 1967) ou Houy par bandes horizontales
- approches en élasticité : méthode de Boussinesq par bandes horizontales ou verticales
- approche en plasticité avec recherche du schéma de rupture critique : module de calcul « talus-risberme » de PARIS par recherche automatique de lignes de rupture critiques (voir figure 3) (Schmitt et al, 2002)

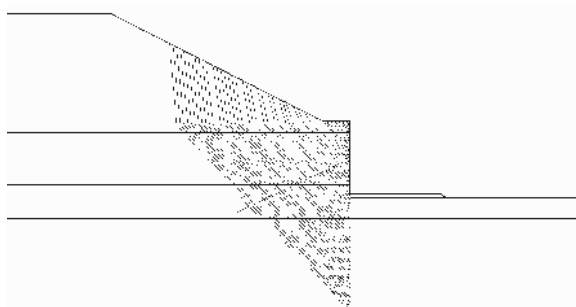


Figure 3. Lignes de rupture – modèle « Talus-Risberme ».

Nous avons complété ces approches par le calcul des talus infinis par les coefficients de Caquot-Kérisel (1990), constituant dans le cadre de notre projet une méthode de référence car :

- l'angle du talus (27°) est inférieur à l'angle de frottement interne des remblais (30°).
- le talus peut être considéré infini par rapport à la hauteur excavée.

Afin de prendre en compte le retrait du talus par rapport à la paroi, nous avons réalisé 2 calculs de talus infini avec 2 cotes de pied de talus correspondant pour l'un à l'impact du prolongement du talus réel avec la paroi (42.90 NGF) et pour l'autre au sommet de la paroi (44.30 NGF) duquel on fait partir un talus fictif parallèle au talus réel, constituant ainsi les 2 bornes de référence pour la comparaison des différentes modélisations.

3.2 Analyse des résultats et conclusion

Les calculs ont été menés avec le logiciel PARIS. Nous avons analysé l'influence des différentes modélisations sur les poussées actives et réelles ainsi que sur les déformées du soutènement par rapport aux bornes de référence données par les calculs des talus infinis.

Les conclusions sont les mêmes pour l'ensemble des paramètres comparés.

On constate notamment que les approches en élasticité donnent des poussées et déformées largement supérieures aux

autres modèles et aux bornes de référence, comme il fallait s'y attendre.

Les approches en plasticité avec hypothèse sur le schéma de rupture donnent des poussées et déformées supérieures aux bornes de référence et au modèle « talus risberme ».

Enfin la modélisation « talus risberme » donne les résultats les plus proches des bornes de référence. De plus, on constate que cette modélisation donne des courbes de poussée lissées, ne présentant pas les sauts observés dans les calculs « talus infini », ce qui devrait se rapprocher le plus des poussées réelles dans le terrain.

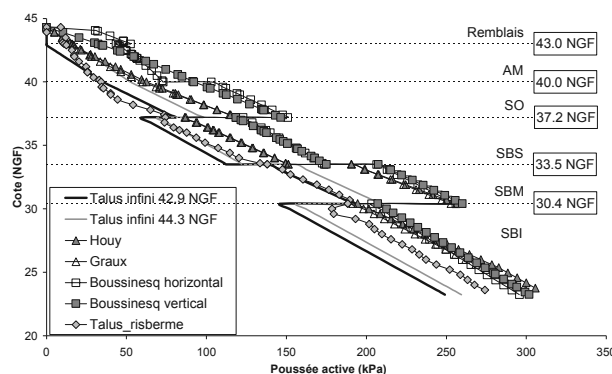


Figure 4. Comparaison des poussées actives selon modèle.

Notons que la modélisation « talus risberme » permet de modéliser l'aménagement d'une plateforme de circulation à l'arrière du soutènement, subtilité ne pouvant pas être prise en compte par les modèles « talus infini » ce qui explique que la poussée calculée par PARIS soit localement inférieure à la borne minimale : ceci traduit simplement le fait que la ligne d'influence du talus intercepte l'écran à une cote inférieure à 42.90, comme on le voit sur la figure 3.

Nous avons donc retenu la modélisation « talus risberme » pour les calculs aux coefficients de réaction.

4 COMPARAISON DES COURBES INCLINOMÉTRIQUES AVEC COURBES DE CALCUL CORRESPONDANT AUX CALCULS D'EXÉCUTION

Après avoir adapté les stratigraphies en fonction des sondages situés à proximité des inclinomètres, nous avons estimé les courbes de déformées théoriques à l'aide de calculs aux coefficients de réaction, en considérant les caractéristiques géotechniques des terrains tels que considérés lors des études d'exécution.

Tableau 1. Caractéristiques des terrains « Etudes d'exécution »

Terrain	EM / pl (MPa)	γ / γ' (kN/m ³)	ϕ (°)	c (kPa)	k (MN/m ³)
Remblais	8.3 / 1.1	20 / 10	30	0	8.1
Alluvions Modernes	6.2 / 0.7	20 / 10	30	0	8.1
Marnes de St. Ouen	8.3 / 1.1	20 / 10	30	0	11.2
Beauchamp Supérieurs	23 / 2.3	22 / 12	35	0	36.5
Beauchamp médians	16 / 2.2	22 / 12	30	5	22.5
Beauchamp Inférieurs	37 / 3.8	22 / 12	35	10	67.5

EM / pl : module pressiométrique / pression limite

γ / γ' : poids volumique / poids volumique déjaugé

ϕ : angle de frottement interne

c : cohésion

k : coefficient de réaction estimé selon la formule de Schmitt(1998)

4.1 Coupe 1 B

On constate que les courbes obtenues pour la phase console divergent tandis qu'elles sont proches pour la phase fond de fouille. Nous en déduisons que pour la phase console les caractéristiques et modèles de calcul initialement retenus sont globalement réalistes, mais les propriétés mécaniques des terrains supérieurs semblent sous-évaluées.

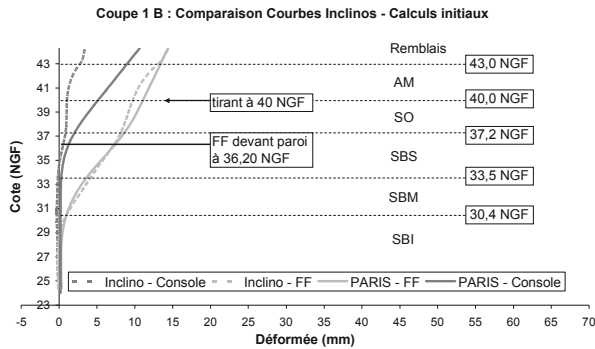


Figure 5. Coupe 1 B : Comparaison des Courbes de Déformées.

4.2 Coupe 2 B

Nous observons que les déplacements calculés sont supérieurs aux déplacements mesurés. Bien que l'influence du talus soit moindre en raison de sa plus faible hauteur, l'écart entre les déplacements calculés et mesurés est systématiquement plus important que dans la coupe 1B, ce qui tend à montrer que les caractéristiques réelles des terrains sont globalement meilleures.

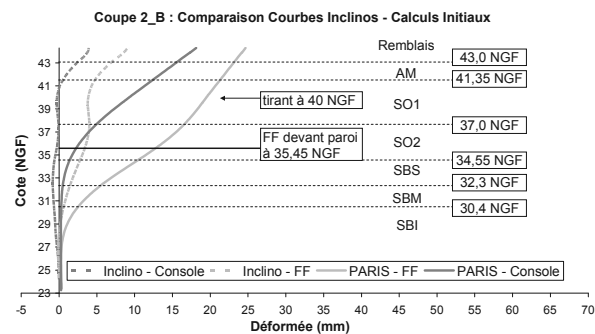


Figure 6. Coupe 2 B : Comparaison des Courbes de Déformées.

L'amplitude des déformations mesurée est parfois très faible, ce qui rend illusoire toute interprétation précise de l'allure des déformées. Par ailleurs des paramètres ne pouvant pas être pris en compte dans les calculs peuvent avoir une influence : la qualité du scellement des tubes inclinométriques, la poutre de couronnement (poids important et discontinuité du bétonnage), la température....

Afin de permettre une bonne interprétation des courbes de déformées obtenues par les mesures inclinométriques, il est toujours utile de disposer de plusieurs relevés concomitants (cibles topographiques, cales des tirants, niveaux piézométriques).

5 CALCULS DE RECALAGE

Suite aux divergences entre les courbes de déformées réelles et théoriques, nous avons recalé le modèle géotechnique en ne tenant compte que des sondages proches des sections étudiées.

En l'absence de mesures du niveau de la nappe phréatique nous avons gardé le niveau de calcul.

5.1 Calculs aux coefficients de réaction

Nous avons introduit deux couches de St.Ouen suite à l'analyse du sondage PR107 situé au droit du profil 2B et qui montre des caractéristiques pressiométriques nettement meilleures dans la partie basse de cette couche. Etant donné que l'épaisseur de la couche de St.Ouen est plus importante au droit du profil 2B (7m) qu'au droit du profil 1B (3m), nous avons considéré cette deuxième partie du St.Ouen uniquement pour les calculs de recalage du profil 2B.

Nous avons également introduit une cohésion à court-terme dans les Alluvions Modernes ainsi que dans les deux couches du St.Ouen, justifiée par la faible durée entre la mesure 0 des inclinomètres et la mesure de la phase console (1 mois).

De plus nous avons revu les valeurs des coefficients de réaction des terrains suite à l'analyse du sondage PR107 montrant des valeurs pressiométriques plus élevées que celles considérées lors des études d'exécution.

Tableau 2. Caractéristiques des terrains obtenus après recalage.

Terrain	E_M / pl (MPa)	γ / γ' (kN/m ³)	ϕ (°)	$c - ct$ (kPa)	$c - lt$ (kPa)	k (MN/m ³)
Remblais	8.3 / 1.1	20 / 10	30	0	0	8.1
Alluvions Modernes	6.2 / 0.7	20 / 10	30	5	0	8.1
Marnes de St. Ouen 1	6.4 / 0.9	20 / 10	30	15	0	20
Marnes de St. Ouen 2	30 / 3.0	20 / 10	30	40	15	75
Beauchamp Supérieurs	40 / 3.2	22 / 12	35	0	0	65
Beauchamp médians	29 / 2.6	22 / 12	30	5	5	35
Beauchamp Inférieurs	55 / 3.5	22 / 12	35	10	10	80

Modifications par rapport aux paramètres initiaux en gras.

Nous obtenons les courbes suivantes :

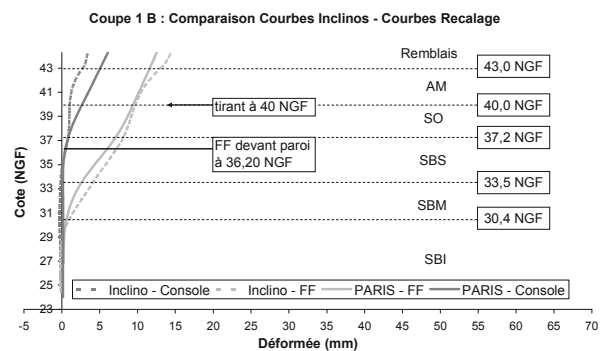


Figure 7. Coupe 1 B : Comparaison des Courbes de Déformées après recalage.

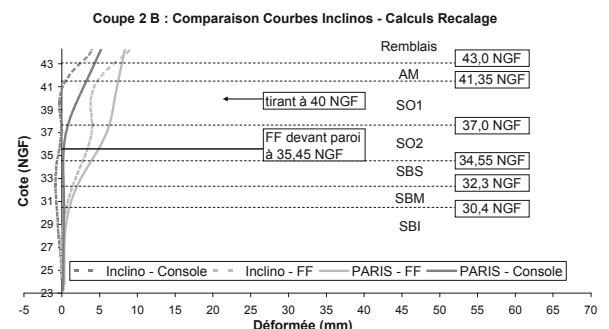


Figure 8. Coupe 2 B : Comparaison des déformées après recalage.

Concernant les efforts dans les tirants, nous observons que les efforts trouvés par le calcul de recalage sont environ 10%

plus importants que les efforts mesurés après le terrassement au fond de fouille.

5.2 Calculs aux éléments finis

Parallèlement aux calculs aux coefficients de réaction, des calculs par la méthode des éléments finis ont été menés à l'aide du logiciel Plaxis2D. Afin de permettre la comparaison entre les deux méthodes de calcul, nous avons repris les mêmes caractéristiques des sols (issues du recalage).

La loi de comportement considérée est élasto-plastique avec critère de plasticité de Mohr-Coulomb. Les modules d'Young ont été fixés grâce à la relation $E_Y=4E_M/\alpha$ (avec E_M module pressiométrique, et α coefficient rhéologique des sols).

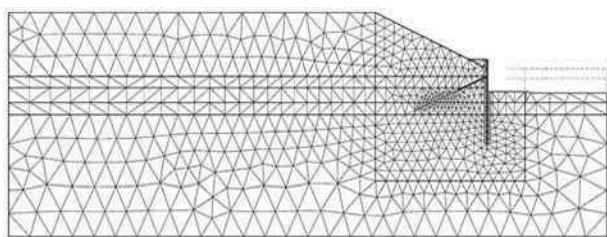


Figure 9. Vue du maillage de la coupe 1B.

La présence de la pente oblige à éloigner assez fortement la limite gauche du modèle pour minimiser l'influence des conditions limites (tout en ne l'éloignant pas trop car cela a une incidence sur la propagation des déformations). La limite droite a été choisie sur l'axe de symétrie du bassin.

Afin de prendre en compte l'inclinaison des contraintes dans la pente, la première phase de calcul a été une phase fictive d'application de la gravité.

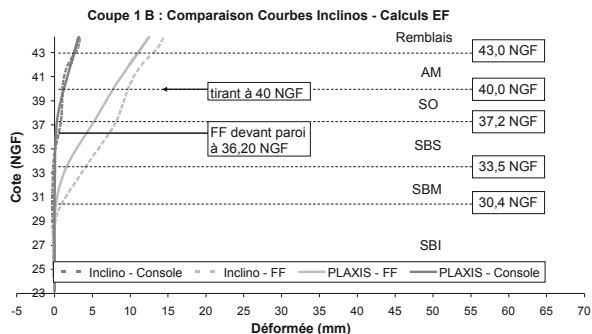


Figure 10. Coupe 1 B : Comparaison des Courbes de Déformées mesurées et calculées par EF.

On constate qu'il existe une bonne concordance entre les déformées mesurées et calculées. Certains phénomènes ne sont cependant pas retrouvés par le calcul, comme la déformation vers 41 m NGF de la coupe 2B (cette déformation est présente dès la phase console, et pourrait être due à la réalisation de la poutre de couronnement).

On notera également qu'il existe un déplacement d'ensemble de la paroi (translation horizontale vers la fouille de 3,2 mm pour 1B et de 1,5 mm pour 2B), non représenté sur les courbes de déformées. Ce déplacement d'ensemble est peu réaliste et est certainement lié à la modélisation numérique, mais en l'absence de suivi topométrique, et avec des mesures inclinométriques ne descendant pas sous la base de la paroi, il n'est pas possible de certifier que ce mouvement d'ensemble n'existe pas.

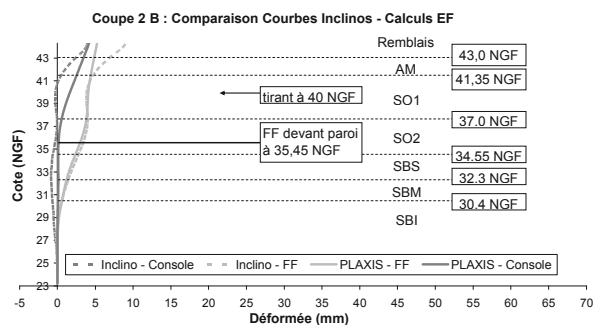


Figure 11. Coupe 2 B : Comparaison des déformées mesurées et calculées par EF.

Quant aux efforts calculés dans les tirants, on constate qu'ils sont sous-estimés de 15% pour la coupe 1B, et surestimés de 20% pour la coupe 2B.

6 CONCLUSIONS

On observe que les résultats des calculs de recalage obtenus avec PARIS et PLAXIS avec les mêmes caractéristiques de terrain, sont très similaires, tant en valeur qu'en allure de déformée et relativement proches des mesures inclinométriques.

L'ensemble des calculs menés, et notamment la similarité des résultats obtenus par PARIS et PLAXIS 2D, montre la validité du modèle « talus risberme » avec recherche automatique des lignes de rupture critiques dans le cadre de cette étude, ainsi que la bonne concordance du calcul aux éléments finis en modèle Mohr-Coulomb ($E_Y=4E_M/\alpha$) avec le calcul aux coefficients de réaction estimés selon Schmitt, ce qui confirme les résultats obtenus sur des chantiers antérieurs (Schmitt 2009)

7 REMERCIEMENTS

Remerciements à l'IFSTTAR qui a permis la mise en place de l'instrumentation et une partie de cette étude dans le cadre de l'opération de recherche FONDAMS.

8 RÉFÉRENCES

Mestat P., Prat M. 1999. *Ouvrages en interaction*. Hermès.
 Marten S., Delattre L., Magnan J-P. 2005. *Etude expérimentale et méthodologique sur le comportement des écrans de soutènement*. LCPC.
 Schmitt P., 1998. *De l'élasticité linéaire au coefficient de réaction*. Revue Française de Géotechnique n°85.
 Caquot A., Kérisel J. 1990. *Tables de Poussée et Butée 3^{ème} édition*. Presse de l'Ecole Nationale des Ponts et Chaussées.
 Graux D, 1967. *Fondations et Excavations Profondes – Tome 1 : Géotechnique Appliquée*. Editions Eyrolles.
 Schmitt P., Dodel E. 2002. *Méthodes Numériques en Géotechnique*. 5^{ème} conférence européenne. NUMGE 2002.
 Schmitt P., 2009. *De l'importance du suivi pour maîtriser le dimensionnement des ouvrages géotechniques*. Revue Française de Géotechnique n°126-127.

Displacement of an apartment building next to a deep excavation in Rotterdam

Déplacements d'un bâtiment d'habitation adjacent à un chantier profond d'excavation à Rotterdam

Hannink G., Oung O.

Engineering Consultancy Division, City of Rotterdam, The Netherlands

ABSTRACT: A new underground car park is being realized near the Rotterdam Central Railway Station. The car park will contain five stories and will be about 150 m long and 35 m wide. The depth of the underground car park is about 20 m. Tall office buildings are present at both sides. A 30 m high apartment building is situated perpendicular to the car park, and the distance of this building to the car park is only 7 m. This building is founded on prefabricated concrete piles with a base level that equals the excavation depth of the car park. The underground car park is being realized inside a dry building pit surrounded by 40 m deep diaphragm walls. Predictions, based on calculations with analytical as well as 2D and 3D finite element models, showed that the expected settlements of the apartment building were acceptable. The measured displacements remained well within the limits that were predicted.

RÉSUMÉ : Près de la gare ferroviaire centrale de Rotterdam, un parking souterrain est encore en construction. Ce parking sera pourvu de cinq niveaux et aura les dimensions de 150 m de long en 35 m de large. La profondeur de ce parking sera de 20 m. Le long des côtés du parking en construction se trouve de hauts bâtiments. En particulier, un bâtiment d'environ 30 m de haut est situé à peine à une distance de 7 m de ce parking et se tient perpendiculairement à celui-ci. Ce bâtiment est fondé sur des pieux en béton préfabriqués dont la base est au même niveau que celui de l'excavation réalisée pour la construction du parking. Cette excavation est délimitée par des parois moulées dont la base se trouve à 40 m de profondeur. Les prédictions, basées sur des calculs pour lesquelles des modèles d'éléments finis bi- et tridimensionnels ont été montés, ont montré que les tassements de ce bâtiment prédits étaient acceptables. Les déplacements mesurés durant la réalisation de l'excavation sont restés dans les limites des calculs de prédiction.

KEYWORDS: deep excavation, settlement of structures, finite element models, prediction, monitoring.

1 INTRODUCTION

In the centre of Rotterdam, extensive reconstruction works are executed as part of the overall project Rotterdam Centraal. The reconstruction comprises of the building of a large Public Transport Terminal to facilitate passenger transfer between (inter)national trains including the high-speed train, and local public transport like trams, buses and underground trains. The project also includes a new underground metro station, a new underground parking facility for bicycles, a new traffic tunnel below a newly created square, and a new underground car park.

The car park will contain five stories and will be about 150 m long and 35 m wide. The depth of the underground car park is about 20 m. Tall office buildings are present at both sides. A 30 m high apartment building is situated perpendicular to the car park and the distance of this building to the car park is only 7 m (see Figure 1).

The apartment building is founded on prefabricated concrete piles with a base level that equals the excavation depth of the car park. The underground car park is being realized inside a dry building pit surrounded by 40 m deep diaphragm walls.

Calculations of the expected settlement of the apartment building were made in the design stage of the project, and a fall-back option was thought out in case the settlement would exceed the criteria.

The apartment building was continuously monitored during the construction of the parking facility. This paper describes the expected impact of the construction of the underground car park on the apartment building, and the results of the monitoring. The car park is presently in the final stage of construction.

Engineering of the car park Kruisplein, and supervision of the execution of the project is performed by the Engineering Consultancy Division of the City of Rotterdam.



Figure 1. The construction of the underground car park Kruisplein (February 2012). The apartment building is situated in front, at the left (perpendicular to the car park). Photograph Nick de Jonge – Skeyes fotografie.

1.1 Subsoil

The ground level in the area is situated at about sea level (this corresponds to the Dutch reference level NAP). The subsurface conditions at the building site are presented in Table 1. The hydraulic head in the fill is about 1.5 m below sea level, and in the Pleistocene sand layers about 2 m below sea level.

Table 1. Soil conditions

Elevation (m NAP)		Origin – Type of soil
from	to	
-0.3	-4.5	Fill - sand
-4.5	-5.5	Holocene - soft clay
-5.5	-8.0	Holocene - peat
-8.0	-17.0	Holocene - soft clay
-17.0	-35.0	Pleistocene - sand
-35.0	-37.0	Pleistocene - stiff clay
-37.0	-40.0	Pleistocene - sand

1.2 Challenge

The horizontal as well as the vertical equilibrium of the foundation of the apartment building may be influenced by the building activities (see Figure 2). The foundation piles of the apartment building:

- will be horizontally loaded by the soil that displaces into the direction of the diaphragm wall, because of its deflection;
- will displace vertically, because the soil that displaces into the direction of the diaphragm walls also displaces slightly into the vertical direction;
- will displace vertically, because the deflection of the diaphragm wall causes some relaxation of the sand layer, and therefore results in a decrease of the bearing capacity.

The effects of these phenomena had to be assessed, and taken into account during the design stage of the construction of the underground car park.

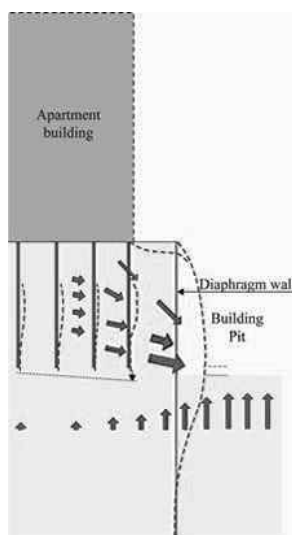


Figure 2. The consequences of the deflection of the diaphragm wall to the apartment building.

2 APARTMENT BUILDING

The length of the apartment building is 50 m, the width is 10 m. Prefabricated concrete piles 380 mm square and 450 mm square support the building. The foundation piles are connected by beams in north-south direction. The pile rows in the vicinity of the building pit support via columns bearing walls (see Figure 3). These walls distribute the load to the piles. The apartment

building can therefore be considered as stiff in the north-south direction. In the east-west direction pile rows are not able to redistribute the loads. In that direction the apartment building is considered as flexible.



Figure 3. The apartment building.

Before analyzing the expected settlement behavior of the apartment building, the building regulations of the period in which the apartment building was constructed had to be translated, and compared with the current building regulations. Therefore calculations of the vertical bearing capacity of the foundation piles were made, based on the Dutch standard NEN 6743-1. The original building documents of the apartment building mentioned the design loads on the piles. These had to be converted first into representative and design values. This resulted in a ratio of 1.9 between the average bearing capacity of the pile foundation and the representative value of the load. This fits reasonably well with the overall safety factor of 2.0 that was used for this type of piles in the period the apartment building was constructed. Because of this small difference in safety level NEN 6743-1 was used to analyze the settlement behavior of the apartment building.

3 ANALYSIS

3.1 Settlement due to the relaxation of the subsoil

The analysis was directed to the first five rows of piles of the apartment building. The first row is situated at about 7 m distance of the diaphragm wall; the fifth at about 23 m. The distance between the pile rows is 3.9 m. Load-settlement diagrams have been derived for a single prefabricated concrete pile based on general curves presented in NEN 6743-1. Both a pile 380 mm square and a pile 450 mm square were considered.

The calculations with the computer code MFoundation 5.3.1.4 were based on data of six CPT's. The maximum bearing capacity for each CPT, the representative value of the average bearing capacity and the design value of the bearing capacity were determined for both pile sizes. The magnitude of the negative skin friction was also calculated.

The subsoil, in particularly the sand layer with the top at 17 m below sea level, will relax as a result of the excavation of the

building pit. Based on CPT-measurements of the cone resistance at a comparable building pit, it was assumed that the relaxation amounts to 20% up to a distance of 12 m of the building pit, and that the relaxation from this distance decreases with 2.5% every 5 m. The decrease of the vertical bearing capacity was assumed to be proportional to the relaxation of the sand layer.

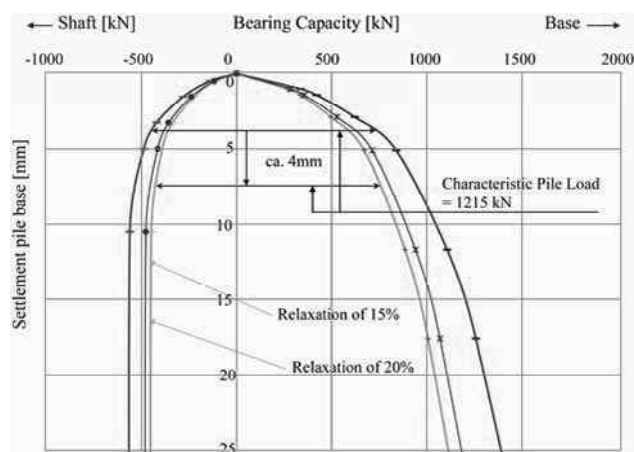


Figure 4. Graphical determination of the pile base settlement.

Load-settlement diagrams have been composed for the serviceability limit state, based on NEN 6743-1 (see Figure 4). For example, a pile base settlement of 4 mm is expected for the original situation. Due to a relaxation of the sand layer of 20% a pile base settlement of 8 mm is calculated, thus an additional settlement of 4 mm as a consequence of the relaxation.

It was concluded that the piles 380 mm square could settle 2 to 4 mm as a result of a relaxation of the sand layer of 12.5 to 20%. For piles 450 mm square these values varied between 3.5 and 5 mm.

3.2 Horizontal soil displacement due to the deflection of the diaphragm wall

The greenfield horizontal soil displacement at the position of the relevant foundation piles of the apartment building has been calculated by using the Hardening Soil (HS) model with the Small Strain Stiffness (HSS), of the computer code Plaxis 2D 8.5. Three cross-sections were considered (see Figure 5):

- at the middle section of the building pit where the excavation took place according to the conventional method;
- next to the apartment building, where the car park was built according to the top down method: after the construction of the diaphragm wall the roof is built, and after that the soil is excavated below the roof and the successive floors are made;
- in the transition zone between the two building methods.

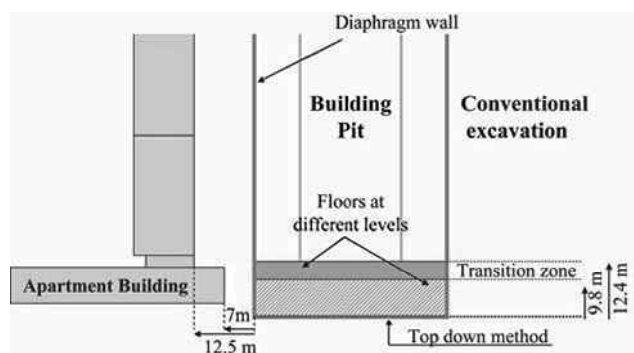


Figure 5. The cross-sections of the building pit that were considered with the Plaxis 2D computer code.

The different stages of the excavation with the corresponding lowering of the groundwater pressures in the building pit, and the installation of the successive layers of struts have been

considered, and the displacements have been calculated. The stiffness of the diaphragm wall was based on cracked concrete.

The calculated deflection of the diaphragm wall was about 70 mm in the middle section of the building pit, at a depth of 18 m. Next to the apartment building, the deflection was about 40 mm, at a depth of 20 m. The expected deflection of the diaphragm wall was about 55 mm in the transition zone.

At the location of the first pile row of the apartment building, the calculated greenfield horizontal soil displacement was 20 mm. At the following pile rows this displacement was according to the calculations 10 to 15 mm.

From additional calculations with the elastoplastic spring model of the computer code MSheet 7.7, it was concluded that the expected moments and shear forces in the foundation piles would remain smaller than the acceptable values.

3.3 Consequences of the soil displacement to the pile foundation

The computer code Plaxis 3D Foundation 2.1 has been used to determine the combined effect of the horizontal and vertical ground displacements. With the computer code MFoundation 5.3.1.4 the vertical displacement was considered, and with the computer code Plaxis 2D 8.5 the greenfield horizontal soil displacement.

The diaphragm wall has been modeled from the southern wall up to the middle of the conventionally built section. The floors that are part of the section that was built according to the top down method form part of the model. Only the five pile rows next to the building pit, and the complete ground floor were part of the model.

The piles were modeled as embedded piles. This made it possible to determine the moments and shear forces as well as the displacement of the foundation piles directly from the calculations. The calculated settlements of the pile base may be exaggerated, because the model does not take into account the densification of the soil as a result of the installation of the piles.

The with the computer code Plaxis 2D calculated deflection of the different parts of the diaphragm wall was used to calibrate the Plaxis 3D model. For the greater part of the building pit the calculated maximum horizontal displacement of the diaphragm wall was about 70 mm, in accordance with the results of the calculations with the Plaxis 2D computer code. Near the southern part of the diaphragm wall the calculated displacement varied between 15 and 40 mm.

According to the calculations, the pile base of both the 380 mm pile, and the 450 mm piles will settle 8 to 12 mm as a consequence of the soil displacement. The calculated horizontal deflection of the foundation piles was 25 mm as a maximum. The calculated moments and shear forces are relatively small.

4 PREDICTION

Based on the calculations the predicted settlement of the apartment building was 2 to 5 mm due to relaxation and 8 to 12 mm due to the soil displacement. This means in total 10 to 15 mm as a consequence of the building activities for the underground car park. Damage was not expected, because of the decrease of settlement with distance from the building pit. The settlement difference of the piles was expected to be small.

Horizontal displacements of the pile foundation, varying between 10 and 25 mm, were also expected. Also no damage was expected in this case, because the displacement would manifest itself underground, with only a limited effect on the foundation piles and the superstructure.

5 MONITORING

5.1 Set-up

Measuring points at 4 m above ground level were installed on the columns that were supported by the first four rows of piles of the apartment building (see Figure 6).

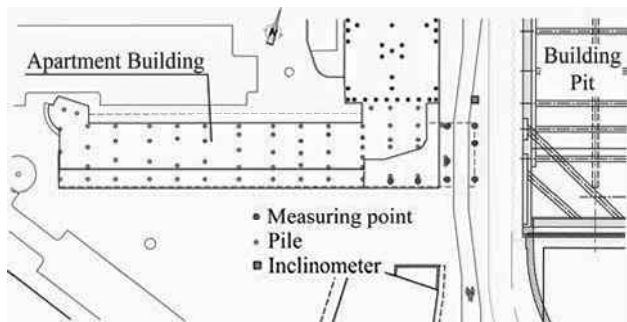


Figure 6. Measuring points on the apartment building.

Vertical and horizontal displacements were continuously monitored by a measuring device on top of a building at a distance of more than 50 m. The results of these measurements were periodically checked by measurements that were discontinuously executed as part of an extensive measuring program around the building pit.

The results of periodically executed inclinometer measurements offered another way to check the actual displacements. The inclinometers were situated next to the apartment building at a distance of 7 m from the diaphragm wall. This corresponds to the distance of the first pile row of the apartment building from the diaphragm wall.

The owner of the apartment building was fortnightly informed about the monitoring results.

5.2 Criteria

A relative rotation of the apartment building of 1:600 was used as the value to intervene, and a relative rotation of 1:750 served as the value to prepare mitigating measures. Because of practical reasons these values have been converted to settlement values of 15 and 12 mm respectively at any specific point.

5.3 Results

The continuous measurements started in January 2010. The measured displacements appear to be according to the prediction (see Figure 7). Meanwhile the apartment building is stable, and only a limited settlement has occurred.

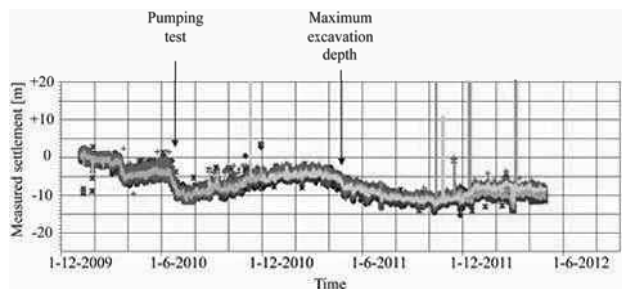


Figure 7. Measured vertical displacements in the period from January 2010 till May 2012.

The in June 2010 measured vertical displacement of the east front of the apartment building was the reason that the fall-back option was prepared. However, the further development of the settlement did not give rise to the actual installment of additional foundation piles below the east front.

The measurement results show that the apartment building rose again some 5 mm after the execution of the water tightness test. During the excavation of the deepest part of the building pit the apartment building settled some 8 mm. The maximum settlement of the east front appeared to be 10 to 15 mm, in accordance with the prediction.

The measured horizontal displacement of the apartment building varied between +10 and -10 mm (see Figure 8).

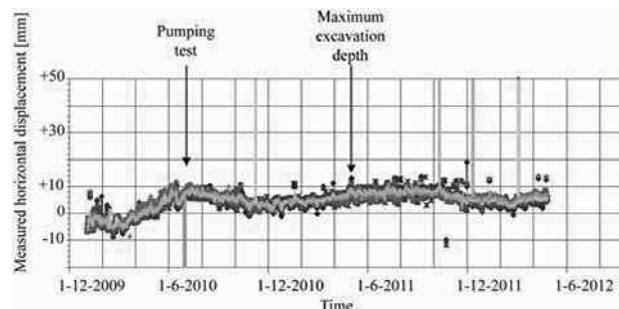


Figure 8. Measured horizontal displacements in the period from January 2010 till May 2012.

Inclinometer measurements started in July 2010, after the execution of the water tightness test. Next to the apartment building the maximum measured deflection of the diaphragm wall was about 35 mm at 15 m depth. At a distance of 7 m from the diaphragm wall the maximum horizontal soil displacement was about 40 mm at a depth between 5 and 10 m. From additional calculations with the elastoplastic spring model, it was concluded that the moments and shear forces in the foundation piles were smaller than the acceptable values.

6 CONCLUSIONS

Diaphragm walls are an appropriate type of retaining wall in an urban environment, but will also deflect as a result of a deep excavation. The consequences for adjacent structures must therefore be studied in the design stage.

A risk analysis helped to find the optimal design for the building pit as to restrict the uncertainties for adjacent structures to a minimum. It also helped to create fall-back options.

The results of the test of the water tightness of the building pit showed in an early stage that the apartment building was vulnerable to deformations of the subsoil. This resulted in a great attention for monitoring results during the whole construction period by all persons concerned.

Accurate predictions about the expected vertical and horizontal displacements appeared to be possible with the help of the available computer codes.

The case of the apartment building next to a deep building pit showed for all that a systematic approach is needed to overcome the presented challenges.

7 REFERENCES

- NEN 6743-1 2006. *Geotechnics – Calculation method for bearing capacity of pile foundation – Compression piles*. Nederlands Normalisatie-instituut, Delft (in Dutch).

Calculation method of optimization the soil-cement mass dimensions to reduce the enclosure displacements in deep excavation

Calcul des dimensions optimales du massif du sol-ciment pour réduire les déplacements de fouilles profondes

Ilyichev V.A.
Russian Academy of Architecture and Construction Sciences, Moscow, Russia

Gotman Y.A.
Company Ltd 'Podzemproekt', Moscow, Russia

ABSTRACT: In the article basic condition to the calculation the soil-cement massif optimum dimensions, which ensure the assigned value of deep excavation wall displacement are presented. Problem statement and it's solution with the application of a Winkler-bed model, standard procedures for analysis of massive retaining walls and theory of optimum design are described. Some results of calculations and benchmark of these results with the use of PLAXIS 2D software package are given.

RÉSUMÉ : Le procédé de calcul est décrit pour la détermination des dimensions d'une masse de sol-ciment en utilisant un modèle de "Winkler-bed", des procédures standard pour l'analyse des murs de soutènement poids, et la théorie de la conception optimale. Les résultats des calculs et leur évaluation à l'aide du logiciel PLAXIS 2D sont présentés.

KEYWORDS: diaphragm wall, optimal design, Winkler-bed model, coefficient of stiffness.

1 INTRODUCTION

Acceleration of work execution for underground space constructing in dense urban conditions with the minimum influence upon surrounding buildings is one of the main problems of underground structures design today. The given paper presents the design method of optimization of the raised problem design decision. The method of excavation "top-down" is used as technological scheme only with upper floor installation and as optimized (variable) parameter, the dimensions of soil-cement mass (SCM) combined with enclosure (diaphragm wall) that provides the excavation without intermediate strutting system and minimization of wall displacement (Fig. 1).

So the main task is to determine the minimum volume of the SCM with the condition that the horizontal displacements of the enclosure during excavation of the pit do not exceed the assigned value $S^v_{max} \leq S^h_{pred}$.

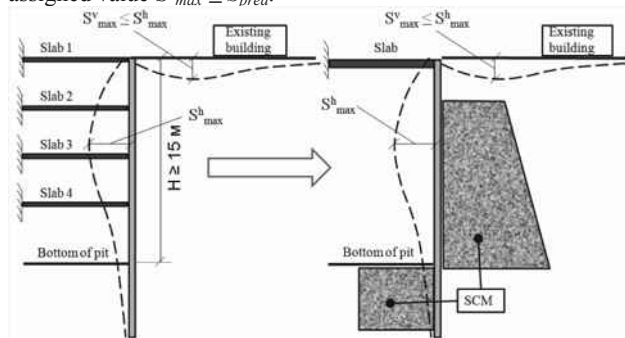


Figure 1. Problem condition

1 PROBLEM STATEMENT

The computational model of the optimized "wall-SCM-soil" system can be represented as a beam on an elastic Winkler bed, where the beam simulates the pit enclosure, and the SCM working in consort with the soil of the elastic bed. The stiffness coefficient of the bed, which varies over the height of the enclosure, is the only parameter of the model used to

determine the dimensions of the SCM. The stiffness coefficient of the elastic bed, and the development of a procedure to determine the SCM dimensions corresponding to the optimal solution will therefore be the subject of optimization problem.

In its initial state of rest, the enclosure is treated as a beam affixed on two sides by prestressed springs that describe the "SCM-soil" system (Fig. 2, a, b), whereupon the prestress corresponds to the lateral pressure of the soil q_{01} in a state of rest (Fig. 2, c, d). As the pit is excavated, the prestressed springs (soil) then disappears on one side together with the pressure, which they have created, and the system is taken out of equilibrium. To attain equilibrium, the enclosure is displaced within the pit (Fig. 2, e). Here, the springs below the bottom of the pit are mutually disturbed on the inside, but are undisturbed on the outside, altering the pressure of the springs against the enclosure (Fig. 2, f). During compression, this pressure is increased, and is

$$q_2 = q_{02} + kz, \quad (1)$$

but is diminished on release

$$q_1 = q_{01} - kz, \quad (2)$$

whereupon the change in pressure will depend on the coefficient of stiffness k of each spring, and the displacement z of the enclosure at the corresponding point.

During excavation, therefore, the SCM as a component part of the soil, which is simulated by the springs (Fig. 2, g) is displaced inside the pit, and the pressure against the enclosure is changed in conformity with (1) and (2), and the pressure against the SCM remains as before q_{02} and q_{01} on the side of the soil, when no Coulomb active or passive pressure is formed.

Considering that the displacement of the soil and beam below the bottom of the pit is less than that within the bounds of the pit over its height, let us simplify the computational diagram. The work of the springs on the outside of the pit below its bottom can be neglected (Fig. 2, h), and replaced by a constant pressure of the soil in a state of rest. If these springs are eliminated from the computational diagram of the beam on the outside of the pit, the pressure of the soil against the enclosure below the bottom of pit will be $q_0 = q_{01} - q_{02}$, and the springs on the inside beneath its bottom will be under no prestress.

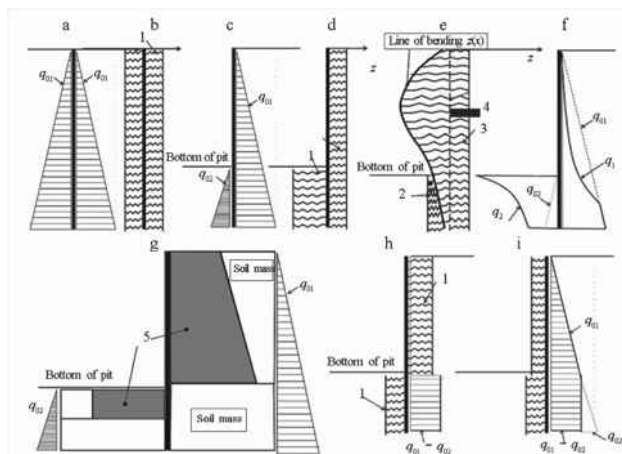


Figure 2. Steps in formulation of computational diagram: 1) elastic prestressed springs; 2) and 3) compression and release of springs; 4) position of enclosure prior to excavation of pit; 5) SCM.

Considering that the displacement of the soil and beam below the bottom of the pit is less than that within the bounds of the pit over its height, let us simplify the computational diagram. The work of the springs on the outside of the pit below its bottom can be neglected (Fig. 2, h), and replaced by a constant pressure of the soil in a state of rest. If these springs are eliminated from the computational diagram of the beam on the outside of the pit, the pressure of the soil against the enclosure below the bottom of pit will be $q_0 = q_{01} - q_{02}$, and the springs on the inside beneath its bottom will be under no prestress.

To convert to the standard diagram of a beam on an elastic bed, let us point out that the amount $k \cdot z$ by which the pressure of the springs is reduced against the enclosure during release in (2) is the reaction of ordinary springs with no prestress, which are positioned on the opposite side when acted upon by force q_{01} . The work of the prestressed springs is then equivalent to the work of stress-free springs under a load equal to the prestress.

Consequently, the problem reduces to one of a beam on an elastic bed (Fig. 2, i), where the beam represents the pit enclosure, the external load is the lateral pressure of the soil in a state of rest $q_0 = q_{01} - q_{02}$, and the coefficients of the elastic bed are the stiffness coefficients k of the "SCM-soil" system, which depend on the dimensions and shape of the SCM, as well on the strength and deformation characteristics of the soil. Considering the above, let us determine the following for further analysis:

1) the active pressure against the "enclosure-SCM-soil" system – the pressure q_0 of the soil at rest;

2) the contact pressure on the enclosure, which can be transmitted through the SCM

$$q = q_0 - kz; \quad (3)$$

3) the reactive pressure of the SCM – that portion of the active pressure against the system, which can be taken up by the SCM as the system transitions to a new equilibrium position after excavation of the pit

$$r = kz. \quad (4)$$

Depending on the displacements of the enclosure, the soil mass may function in an elastic stage, which can be described by the work of elastic springs, or a plastic stage when the contact pressure against the enclosure attains the active or passive pressure of the soil. Since the basic purpose of SCM use is to ensure preservation of surrounding development, the stress-strain state (SSS) of the surrounding soil mass should not go over into a plastic state, and the displacements of the enclosure during excavation should be so small that Coulomb's limiting equilibrium will not be realized. In the analyses, therefore, only the elastic work of the system, where the SCM ensures that the soil, and, accordingly, the "SCM-soil"

system, will function elastically, is ensured. This enables us to perform the calculations in a linear statement, appreciably simplifying solution of the problem of the optimal design of the system under consideration.

In conformity with the physical essence of the problem, the contact pressure against the enclosure above the bottom of the pit cannot be less than zero (cannot act in the opposite direction due to excavation of the pit). For stiffness coefficients above the bottom of the pit should be satisfied the condition

$$q = q_0 - kz \geq 0. \quad (5)$$

Using (5) the "enclosure-SCM-soil" system, therefore, it is possible to use a finite-element formulation of a beam on an elastic bed, where the lateral pressure of the soil in a state of rest is the load.

Let us borrow terminology from (Hogg and Arora 1983) to construct the mathematical optimal-design model. Terms of the theory of matrix calculus can also be used when necessary.

In the computational model selected:

– the *equation of state* is the matrix equation of the finite-element method (FEM)

$$K(k)Z - Q = 0, \quad (6)$$

where $K(k)$ is the global stiffness matrix of the system, the elements of which will depend on k , and Q and Z are the vectors of the nodal loads and displacements, respectively;

– the *state variables* are the displacements Z at the nodes of the finite-element diagram, which describe the behavior of the system in question under load. The transposed form of the vector

$$Z = [Z_1, Z_2, Z_3, \dots, Z_m], \quad (7)$$

where m is the number of degrees of freedom and state variables $m = 2n + 2$, and n is the number of finite elements. After exclusion the angle of rotation from vector Z the vector z of horizontal displacements expressed as follows

$$z = [Z_1, Z_3, \dots, Z_{m-1}] = [z_1, z_2, z_3, \dots, z_{n+1}]; \quad (7a)$$

– the *design variables* are contained in the set of coefficients k , which describes the system itself, but not its behavior.

$$k = [k_1, k_2, k_3, \dots, k_n]. \quad (8)$$

For the computational diagram under consideration, let us write in the terms of the problem statement of an optimal finite-dimensional design in state space.

It is required to determine the set of design variables k , which will minimize the efficiency function, as determined by the total stiffness coefficient with respect to all finite elements of the model

$$\psi_0 = \psi_0(k) = \sum k_i \rightarrow \min, i = 1 \dots n \quad (9)$$

when state equations

$$h(k, z) = K(k)Z - Q = 0 \quad (10)$$

and constraints

$$\psi(k, z) = [\psi_1(Z), \psi_2(k), \psi_3(k), \psi_4(k, Z)]^T \leq 0 \quad (11)$$

exist, where $\psi(k, Z)$ is the set of its type of constraints, $i = 1-4$.

Let us define the types of bounded functions.

1. Bounded-function vector $\psi_1(Z)$ is determined from the conditions of the problem for which limits should be placed on horizontal displacements z (7, a) at all $n + 1$ nodes of the enclosure, which is broken down into n elements. The expressions $\psi_1(Z)$ are derived proceeding from the inequalities

$$z_1 \leq S_{\max}, i = 1 \dots n + 1 \quad (12)$$

2. The vector function $\psi_2(k)$ reflects the limits placed on the design variables k . Expressions for

$\psi_2(k)$ are derived, proceeding from the inequalities

$$k_i \leq k_{\max}, k_i \geq k_{\min}; i = 1 \dots e, \quad (13)$$

where e is the number of the last element situated above the base of the pit, k_{\max} is the value defining the upper limit of the variation of a variable, and $k_{\min} = 0$ is the lower limit of variation in the absence of an SCM.

3. The vector function $\psi_3(k)$ reflects the limits placed on the design variables k below the bottom of the pit. The expressions for $\psi_3(k)$ are derived from the inequalities

$$k_i < k_{max}; k_i > k_{min}; i = e + 1 \dots n, \quad (14)$$

where k_{min} is the lower limit of variation, and $k_{min} = k_{so}$ corresponds to the stiffness coefficient of the soil when functioning elastically.

4. The vector function $\psi_4(k, Z)$ reflects the constraint that ensures fulfillment of (5) – a reduction in pressure on the elements residing above the base of the pit, and cannot exceed the active horizontal load of the soil at rest on the corresponding element. The expressions for $\psi_4(k, Z)$ are derived from the inequalities

$$r_i = k_i \cdot z_i < q; i = 1 \dots e + 1 \quad (15)$$

where r_i is the reduction in pressure, or the reaction of the elastic bed at the itch node, k_i is the coefficient of the elastic bed at the itch node, and z_i is the horizontal displacement z (7, a) at the itch node.

In the problem under consideration, the limits are represented by the following type of set:

$$\psi(k, z) = [\psi_1(Z), \psi_2(k), \psi_3(k), \psi_4(k, z)] \quad (16)$$

Using (9), (10), and (16), the structure and analytical form of the components of the mathematical optimal-design model are entirely defined and ready for the solution.

2 PROBLEM SOLUTION

The search algorithm for optimization based on the method of gradient projection, where that variation in design variables, for which the efficiency function is decreased, and the limits are not violated, is determined in each interval, is compiled for the problem's solution, and is implemented in the software package MATLAB v.7.9.0. The gradients of the efficiency and bounded functions with respect to design variables are required for construction of the algorithm are determined from analysis of the sensitivity of the design in state space (Hogg and Arora 1983).

The search strategies consist in the plotting of a succession of k^p points calculated in accordance with the rule

$$k^{p+1} = k^p + \delta k^p, p = 0, 1, \dots, \quad (17)$$

where p is the number of iterations, k^p is a vector in the form of (8), and δk^p is the vector of variation in the design variables, which decreases the efficiency function as determined for each p using the gradients obtained from sensitivity analysis of the design.

Figure 3 shows a geometric interpretation of the performance of the algorithm for a two-dimensional space. The resultant vector of the variation in the design δk^p is obtained as a result and the iteration process of the search for the conditional extremum acquires the form shown in Fig. 3

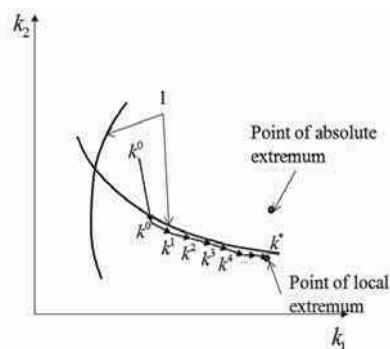


Figure 3. Geometric interpretation of algorithm performance:

1) curve of bounded function;

After running the algorithm, the succession of points converges on the optimal value of the efficiency function, i.e., the optimal distribution of k^* . As a result of running the

algorithm, the sequence of points converges to the optimal value of the efficiency function, i.e., to the optimal distribution of the coefficient k^* of the bed's stiffness.

The dimensions of the SCM corresponding to this stiffness are required for determination of the optimal distribution of the coefficient k . The following are basic initial data for determination of the optimal dimensions of the SCM:

- the minimum height h of the SCM, as determined above and below the bottom of the pit based on the distribution curves of k and the reactive pressure R ;

- the total reactive pressure of the SCM over the height h , which should be taken up by the SCM as a component part of the soil in order that the "SCM-soil" system correspond to the elastic behavior

$$R = \sum r_i, \quad (18)$$

where i is the number of nodes over the height h , and the point of application of the force R resides at the level of the center of gravity r of the plot; and,

- the average displacement z_{avg} of the enclosure over height h , which corresponds to the displacement of the SCM under the action of R

$$z_{avg} = \sum z_i / v, \quad (19)$$

where v and i are the number of nodes, and the numbers of the nodes over height h .

Use of R and z_{avg} enable us to convert to the assumption that as a component part of the soil, the SCM functions as a solid body, and is not calculated for individual elements over the height.

It is therefore required to determine the minimum dimensions of the SCM for which it will experience a horizontal displacement z_{avg} under the horizontal force R .

Let us examine the application of the above-indicated computational principles in an example of the calculation of optimal SCM dimensions for the excavation of a pit in sand with the following initial data: specific weight $\gamma = 20 \text{ kN/m}^3$, overall compression modulus $E = 25,000 \text{ kPa}$, angle of internal friction in shear $\varphi = 30^\circ$, cohesion $c = 1.0 \text{ kPa}$, pit depth of 20 m, enclosure depth of 30 m, a "diaphragm wall" enclosure with a thickness of 800 mm, and an upper thrust bracing consisting of a reinforced concrete span with a thickness of 500 mm.

Solution of the optimal-design problem (Fig. 4) includes curves of enclosure displacements (Fig. 4, a), distributions of the optimal stiffness coefficient over the height of the enclosure (Fig. 4, b), the reactive pressure (Fig. 4, c), and the contact pressure (Fig. 4, d).

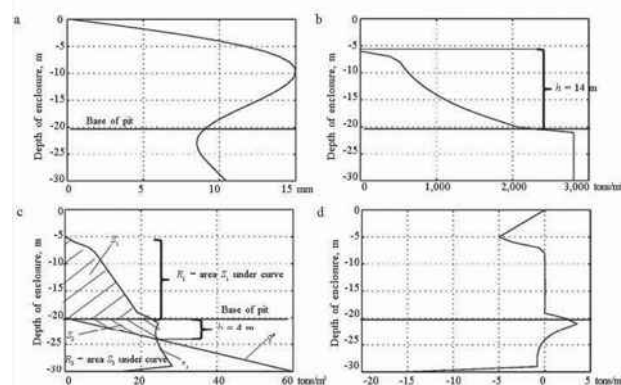


Figure 4. Results of calculation for $S_{max} = 15 \text{ mm}$: a) displacement; b) stiffness coefficient diagram; c) reactive pressure; d) contact pressure

To determine the optimal dimensions, let us examine the SCM above and below the bottom of the pit.

According to the plot (Fig. 4, b), the SCM above the bottom of the pit extends to the point along the height where $k = 0$ and $h = 14 \text{ m}$. For the enclosure above the bottom of the pit where $k = 0$, no soil cement is required. Let us consider the SCM a massive retaining wall 14 m high, the upper and lower bases a and b of which should be determined from calculation of (18) for a

horizontal load R_1 corresponding to area S_1 under the reactive-pressure curve in Fig. 4, c and the displacements z_{avg} (19).

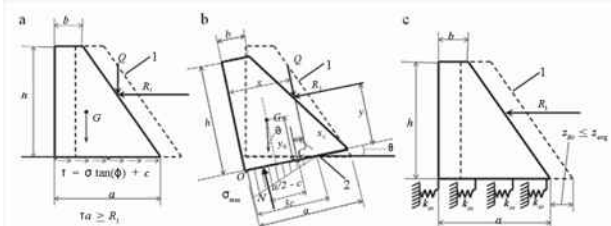


Figure 5. Computational diagrams for SCM above bottom of pit: 1) initial position; 2) turning point.

The optimal dimensions of the SCM on the outside of the pit were found by solving the other optimization problem which minimize cross sectional area of the massive retaining wall (trapezoid)

$$\Psi_0(a, b) = (a+b)h/2 \rightarrow \min \quad (20)$$

for limits ensuring observance of the following conditions:

1) stability against shear (Fig. 5, a)

$$(Q(a, b) + G(a, b))\tan(\varphi) + ca \geq R_1, \quad (21)$$

where Q is the weight of the soil in the SCM benches;

2) stability against overturning about a certain point (Fig. 5, b) with consideration of the deforming bed in accordance with Klein's procedure (Klein 1964)

$$M_{re}(a, b) = N(a/2 - c) \geq M_d(a, b) = R_1y + G(a/2 - x) - Qx_c; \quad (22)$$

3) the displacement z_{sc} of the SCM under the action of R_1 should not exceed the displacement

z_{avg} averaged over the height h (Fig. 5, c).

$$z_{sc} = \frac{R_1}{k_{sp} \cdot a \cdot tg\varphi} \leq z_{cp};$$

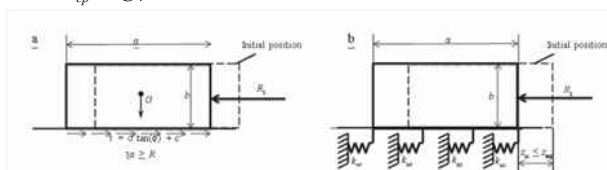


Figure 6. Computational diagram for SCM below bottom of pit

If the first two stability conditions are observed, the displacement of the SCM is determined only by the horizontal deformation of the soil in the bed, which is described by the stiffness coefficient k_{so} of the soil when the rotation of the mass is disregarded.

In order for the system to function in the elastic stage, the dimensions of the SCM below the bottom of the pit are determined with consideration of the fact the soil takes up the reactive pressure, and the SCM the remaining portion. Above the point of intersection, the reactive pressure exceeds the passive pressure of the soil q_p (see Fig. 4, c), but is lower than the passive pressure below the point; the minimal height of the SCM will therefore correspond to the distance from the bottom of the pit to the point of intersection of the r and q_p curves. Here, the design load on the SCM is calculated based on area S_2 (see Fig. 4, c)

The optimal dimensions of the SCM under the bottom of the pit are determined by solving the optimization problem which minimize the value of the efficiency function corresponding to the cross-sectional area of the mass

$$\Psi_0(a, b) = ab \rightarrow \min \quad (25)$$

with limits ensuring observance of the following conditions:

- the stability of the SCM against shear (Fig. 6, a)

$$R_2 \leq F_n = G\tan(\varphi) + ca; \quad (26)$$

- the displacement z_{sc} of the SCM under load R_2 is no greater than the displacement z_{avg} averaged over height h (Fig. 6, b)

$$z_{sc} = \frac{R_2}{k_{so} \cdot a \cdot tg\varphi} \leq z_{avg} \quad (27)$$

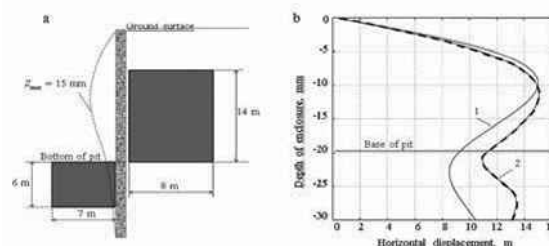


Figure 7. Results of problem solution: a) optimal SCM dimensions when $S_{max} = 15$ mm; b) results of comparison: 1) elastic bed; 2) PLAXIS 2D.

The optimal dimensions are determined for the allowable displacement of the enclosure $S_{max} = 15$ mm as a result of solution of the problems described (Fig. 7, a).

The numerical modeling was performed in the software package PLAXIS 2D with consideration of the SCM dimensions obtained, and plots of the horizontal displacements were compared (Fig. 7, b). The discrepancy between the maximum horizontal displacements was insignificant, although the pattern of the curves differed somewhat. Similar calculations and comparison with PLAXIS were conducted for the same initial data, but with limits placed on the displacements $S_{max} = 30$ and 60 mm. It was established that the SCM dimensions obtained with use of the proposed method yielded a high safety factor with respect to displacements with increasing tolerances. Application of the method in question is therefore restricted to the region of small enclosure displacements; this does not contradict the goals of the stated problem.

3 CONCLUSIONS

A computational method is developed for determination of the optimal dimensions of a soil-cement mass (SCM) that reduces the displacements of an enclosure to required values. The method includes:

- a computerized-search algorithm for optimal engineering of the coefficient of stiffness of an elastic bed; and,
- calculation of optimal SCM dimensions corresponding to the optimal stiffness using standard procedures for analysis of massive retaining walls.

The computational method makes it possible to determine optimal SCM dimensions for the excavation of deep pits in a dense urban setting, when it is necessary to shorten considerably the construction time, and ensure a minimal effect of excavation on surrounding development.

4 REFERENCES

Gotman Yu.A. 2010. Variant design of using the jet-grouting technology for reduction of the settlements of existing buildings during construction of an underground complex in Moscow., *Geotechnical Engineering 20. View of Young European Geotechnical Engineers*, Brno, 134-139.

Hogg E. and Arora Ya. 1983. Applied Optimal Design. *Mechanical Systems and Structures* [Russian translation], Mir, Moscow.

Klein G.K. 1964. *Analysis of Retaining Walls* [in Russian], Vysshaya Shkola, Moscow.

Case Studies of Complicate Urban Excavation from Design to Construction

Études de cas d'excavations complexes en site urbain: de la conception à la construction

Jang Y.S.

Dept. of Civil & Env. Eng., Dongguk Univ., Seoul, Korea

Choi H.C.

Architectural Structure Team. SK E&C

Shin S.M., Kim D.Y.

Saegil Engineering & Consulting. Co. Ltd., Seoul, Korea

ABSTRACT: Various types of retaining walls, e.g. H-Pile with Timber, C.I.P (cast in place pile) and subsurface continuous walls, are domestically used for excavation sites in Korea depending on the site conditions, architectural structure and geotechnical conditions. Ground Anchor, strut and permanent slab are used as support methods. The wall displacements and axial forces of the struts are variable depending on the excavation depth, groundwater level and construction methods, etc. In this study, case studies are performed for the excavation sites, where the modified slab methods, e.g. S.P.S, and S.T.D are used and the ground anchors as temporary supports. The wall displacements and the axial forces predicted at the design stage and monitored in the actual excavation stage are analyzed. The advantage of construction time using the permanent slab method is discussed.

RÉSUMÉ : Différents types de murs de soutènement, par exemple pieu en H avec du bois, CIP (Pieu en béton coulé en place) et des parois continues ancrées dans le sol, sont à usage domestique pour les sites d'excavation en Corée suivant les conditions du site, la structure architecturale et les conditions géotechniques. Ancrage au sol, entretoise et dalle fixe sont utilisés comme méthodes d'étaie. Les déplacements du mur et les forces axiales des entretoises sont variables en fonction de la profondeur de l'excavation, du niveau des eaux souterraines et des méthodes de construction, etc. Dans cet article, des études de cas sont réalisées pour les sites d'excavation, où les méthodes de dalle modifiées (SPS, MST) sont utilisées et aussi les ancrages au sol comme des appuis temporaires. Les déplacements du mur et les forces axiales prévus au stade de la conception sont examinés et analysés dans la phase réelle d'excavation. L'avantage de la durée de construction en utilisant la méthode de dalle permanente est discuté dans cet article.

KEYWORDS: S.P.S, S.T.D, C.I.P, Ground Anchor, Strut, Slab, Displacement, Axial force, Construction time

MOTS-CLÉS : S.P.S, S.T.D, C.I.P, Ancrage au sol, entretoise, dalle, déplacement, force axiale, durée de construction

1 INTRODUCTION

Recent urban building construction has trends of deep excavation and the methods of excavation are diversified. In addition, various types of structures, e.g. the subway tunnels and utility lines and pre-existing buildings are located around the excavation sites. Therefore, when the excavation is done in the metropolitan area, the excavation plans must be made considering the safety, constructability and cost effectiveness synthetically.

In this paper, the retaining wall displacements and the axial forces of the excavation sites which are constructed using the various supports, e.g. C.I.P. with ground anchor, and the permanent slab methods, i.e. S.P.S and S.T.D., are monitored and analyzed using the related case histories.

2 EXCAVATION METHODS

In the case studies, two new excavation methods, i.e. S.P.S and S.T.D, are used and the concepts of each methods are introduced. In the S.P.S(Strut as Permanent system) method, the subsurface steel frame and beams are designed strong enough to endure the temporary and permanent external pressures. They are used as temporary retaining walls while the excavation is going on. They can also be used as the walls of main structures without dismantling of strut after the excavation is finished. Fig. 1 shows the conceptual diagram and the field example.

S.T.D (Strut Top Down) method can use the struts which increase the resistance to horizontal pressures. It can also use various types of basement slabs such as beam & girder as well

as one or two way wide beams (Sho et al. 2004). Fig. 2 shows the conceptual view of S.T.D construction and the field example.

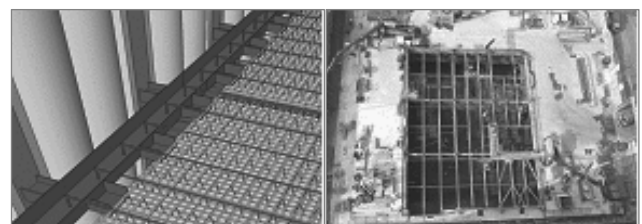


Figure 1. Conceptual diagram and field example of S.P.S

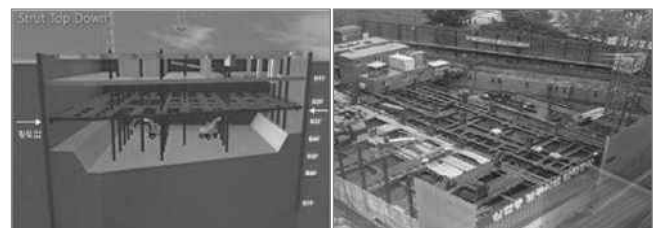


Figure 2. Conceptual diagram and field example of S.T.D

3 SITE CONDITIONS

3.1 Site 1: S.P.S and ground anchor on C.I.P wall

Site 1 is the office facility of 7th floor on the ground and 3rd floor in the basement. The building is located at Chung Ju in the central region of Korea (Saegil E&C, 2011a). The excavation depth is in the range of of GL.-14.0m~GL.-20.0m. High apartments with deep parking lot are in the southern part of the site. A building with basement is located 20m apart from the site in the west. Roads of 35m and 23m are located at the north and the east part of the site.

Two types of retaining walls are used, i.e. rigid C.I.P wall and H-Pile & Timber. Ground anchor is used as the support of both walls. Considering the tall buildings with basements, S.P.S method is used at the southern part (Fig. 3).

The soil profile of the excavated site is composed of buried soil layer, alluvial layer, weathered soil and rock layers from the surface. Most of the excavated parts are composed of soils (Fig.4). Two sections, i.e. S.P.S and ground anchor, are selected as the analysis section in this paper (Fig. 5).

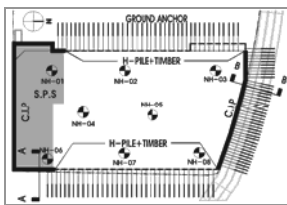


Figure 3. Plan view of site 1

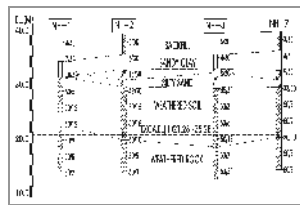
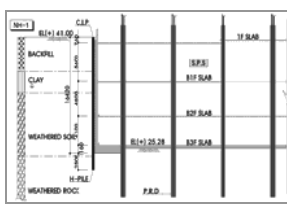
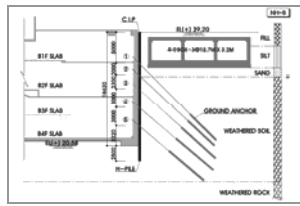


Figure 4. Soil profile of site 1



a) Sec. A-A' (C.I.P & S.P.S)



b) Sec. B-B' (C.I.P & Anchor)

Figure 5. Section view of Site 1

3.2 Site 2: S.T.D and C.I.P

Site 2 is the office facility of 23rd floor on the ground and 7th floor in the basement. The building is located at Sang Am dong, Seoul, Korea (Saegil E&C, 2011b). The excavation depth is in the range of GL.-25.0m~GL.-31.0m. A building of 20th floor on the ground and 5th floor in the basements is located to the north of the site. In the east, the road of 30m wide and the building with 21st floor on the ground and 7th floor in the basements is located. The roads of 30m wide are located to the south and the west directions.

The retaining wall is composed of C.I.P in the soil layer and H-Pile & shotcrete in the rock layer. S.T.D method is used as the support of the excavation site (Fig. 6).

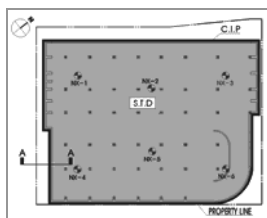


Figure 6. Plan view of site 2

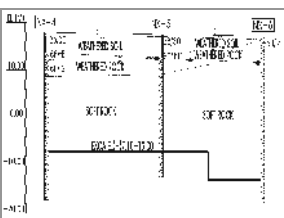


Figure 7. Soil profile of site 2

The soil profile of the excavated site is composed of buried soil layer, weathered soil and rock layers, and soft rock layer from the surface. The geotechnical investigation shows that the

soft rock appears at the shallow depth of GL.-2.4m and GL.-9.2m (Fig. 7).

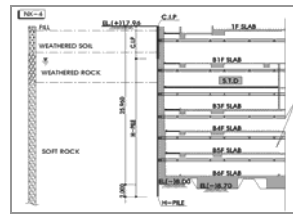


Figure 8. S.T.D Section A-A'

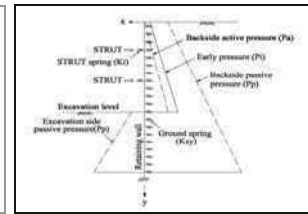


Figure 9. Schematic section for Analysis Program

The sections of retaining walls, i.e. C.I.P in the soil layer and H-Pile & shotcrete in the rock layer are selected for analysis. S.T.D method is used as the supports of the excavated site (Fig. 8).

4 ANALYSIS PROGRAM FOR DESIGN

The program used in the design stage is SUNEX(Step Under ground EXcavation), which is a stress-strain analysis program commonly used for the design of the deep excavation site in Korea (Geogroup Eng., 2010). This program calculates earth pressure on the braced earth retaining system, horizontal displacement, shear force and bending moment of vertical wall and axial force of supports and tieback anchors for step by step excavation.

The program adopts elasto-plastic behavior of soil to calculate earth pressure on the retaining wall. Calculation model includes elastic beam for vertical wall (elastic-plastic beam optional), elastic spring for strut and tieback anchor, elasto-plastic spring for active and passive soil (Fig. 9).

5 COMPARISON OF DESIGN AND MONITORED VALUES

Both the wall displacement and the axial stress of the struts obtained either from the design stage using the SUNEX or from the field monitoring using the field installed instruments. In this section, The two values are compared by separating to the mid and the final stage of the excavation.

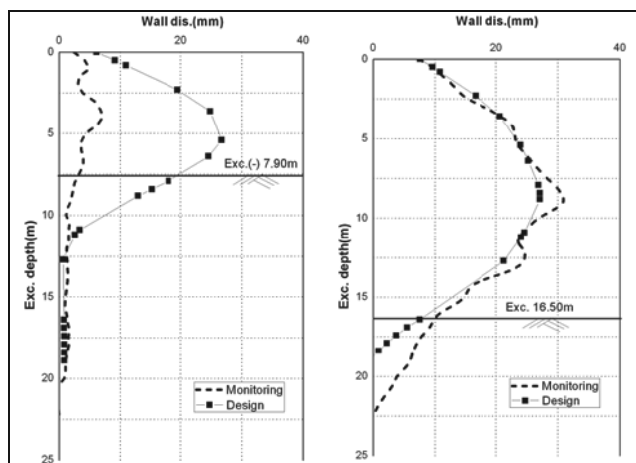
5.1 Wall displacements

5.1.1 Site 1 : S.P.S and ground anchor on C.I.P wall

The displacements of wall in which S.P.S method is applied are shown in Fig. 10 for the mid and final stages of excavation, i.e. GL.-7.9m and GL.-16.5 m.

In the mid stage of excavation, the predicted design displacement was 26.7mm and was greater about 20mm than the monitored displacement of 7.0 mm. This discrepancy seemed to come from the fact that the influence factors, e.g. the loads behind the wall, the excavation height for installation of supports, and weak soil profiles near the ground surface, were selected conservatively compared with the real field conditions.

However, in the final stage the two values were come out quite close. The reasons for this consistency are: (1) The construction conditions was very similar to the one adopted in the design stage, according to the construction process identified at the site; (2) In S.P.S method, it is able to install the steel supports immediately after the excavation. This gives an advantage of reducing the time delayed displacement of the wall, which developed the quite consistent displacements between the design stage and the actual excavation.

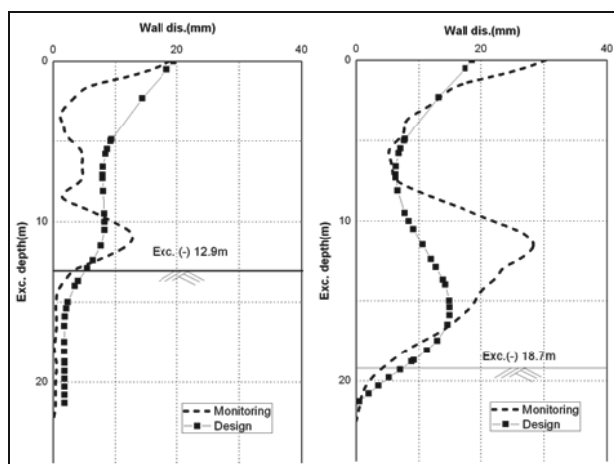


a) Mid stage (GL.-7.9m) b) final stage (GL.-16.5m)
Figure 10. Wall displacements for S.P.S applied section

The displacements of the wall where the ground anchors are applied are shown in Fig. 11. As can be recognized in the figure, the predicted displacement in the mid stage was larger than the monitored value. In the final stage, the two displacements are consistent partly but larger displacements of 10mm are monitored at the upper and central positions of the wall.

This large displacement seems to come from the initial over-excitation length of more than 5m due to the sewage culvert box near the ground surface in Fig. 5b. As the excavation went on the final stage, the spacing of the ground anchors was about 3m and the over-excitation which was greater than the designed strut spacing was made in the field.

Therefore, it is judged that a particular sites like this one which has large sewage culvert box near the ground surface and the over excavation is made near the final stage needs the detailed design and construction considering all the factors related to spacing of the ground anchor and strut, initial displacement of the wall near the ground surface and the geotechnical conditions included.



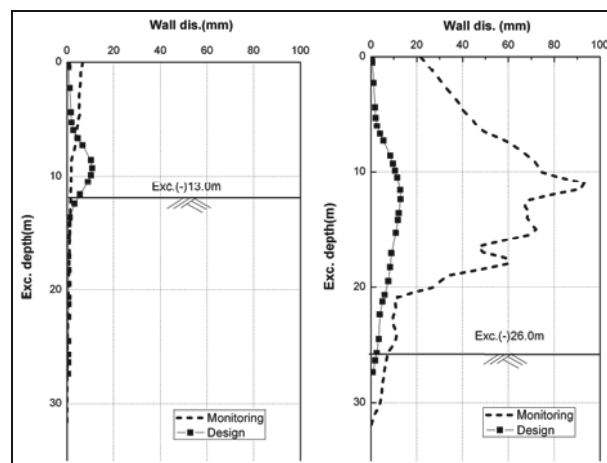
a) Mid stage (GL.-12.9m) b) final stage (GL.-18.7m)
Figure 11. Wall displacements for ground anchor applied section

5.1.2 Site 2: S.T.D and C.I.P

Fig. 12 shows the wall displacements for mid and final stages of excavation in the site 2 where S.T.D method is applied. The excavation depths of mid and final excavation stages were GL.-13.0m and GL.-26.0m, respectively. In the mid stage, the predicted and monitored displacements came out very similar. In the final stage, large discrepancy was recognized for the

predicted and the monitored displacements, i.e. 13mm and 93.1mm, respectively.

Proper construction process and the favorable soil conditions near ground surface seemed to create the consistent wall displacements in the mid stage. Large monitored wall displacements may come from the fact that (1) The design condition would not include the time effect of concrete curing in the slab; (2) over excavation was made since the weathered and soft rocks appeared in the initial stages of excavation. The large discrepancy of the wall displacement about 80mm was the accumulated displacement of the 26m deep excavation.



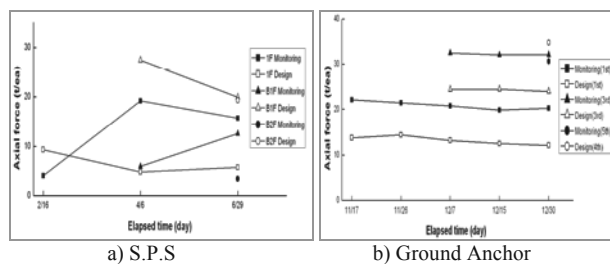
a) Mid stage (GL.-13m) b) final stage (GL.-26m)
Figure 12. Wall displacements in S.T.D method applied

6 AXIAL FORCES OF RESISTANT BODIES

6.1 Site 1 : S.P.S and ground anchor on C.I.P wall

Fig. 13a shows the predicted and monitored axial forces acting the struts of S.P.S. The two axial forces in the initial stage showed large difference, because the construction conditions, e.g. ambient temperature and impacts, etc, create large changes in the strain gages measuring the axial forces. However, this discrepancy was reduced as the predicted and monitored displacements became similar (see Fig. 10b).

It is necessary to identify the wall displacements together when the axial forces in the supports of S.P.S are analyzed.



a) S.P.S b) Ground Anchor
Figure 13 Axial forces for site 1

Fig 13b shows the axial forces of ground anchors in the locations where the ground anchors were applied. In general, the pre-stress considered in the design stage is sufficiently reflected on the ground anchors constructed in the field. However, the monitored axial forces tend to be larger than the predicted values in the design stage in site 1, although the pre-stresses are fully reflected at the excavation.

According to Fig. 11b, the axial forces were large at the locations in which the large wall displacements are detected. At the location of 5th floor in which the design and monitored

displacements are closer to each other, the two axial forces were also close to the values of 35tons.

High correlation is recognized between the wall displacements and the axial forces in the struts. In addition, the changes of axial forces were negligible as the time elapses at the locations where the large wall displacements are detected. This means that the ground anchors are working quite well at such locations (Jang et al., 2012).

6.2 Site 2: S.T.D and C.I.P

Fig. 14 shows the axial forces which act on the slab of S.T.D method by comparing design and monitored values. The monitored axial forces are mostly larger than the predicted values set in the design stage. This result came from the increased wall displacement due to over-excavation and the characteristics of S.T.D. method.

Contrary to the direction of the soil pressures, tensile forces are developed on the 1st anchor from the top. This may come from the large displacement in the central part of the wall, i.e. B2F and B3F, which gave reverse stresses on the upper part of the wall.

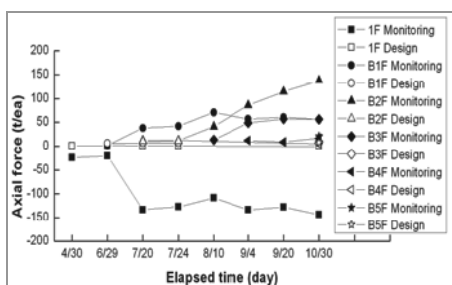


Figure 14. Section A-A' Slab axial forces

7 COMPARISON OF CONSTRUCTION TIME

The current retaining wall design, which uses slab as the support of the wall, applies S.P.S and S.T.D methods. These methods can save the construction time because they can support the retaining walls as well as can use the slabs as the permanent basement structure of the building. The two sites have different excavation area and depth. Hence a direct comparison of the construction period was difficult. In this study, construction period was calculated and relative comparison was made based on the Site 1, which was quantified by area (15,000 m²) and the excavation depth (GL.-19m).

Table 1 shows the comparison of the construction time of the basement for different support methods. In Site 1 where the ground anchors are partly used, the construction time was 9 months. However, in Site 2 where the slab support S.T.D is used, the slabs are installed simultaneously with the excavation and the time taken to finish the basement structure was 7 months.

Table 1. Comparison of construction time for two sites

Construction Method		Site 1: Chung Ju	Site 2 : Sang Am
		S.P.S & Anchor	S.T.D
Excavation Depth		GL.-19m	GL.-26m
Excavation And Sub- structure	Start	2010.10	2012.04
	End	2011.06	2012.11
	Period	9 month	7 month

8 CONCLUSIONS

In this study the displacement on the C.I.P. walls and the axial forces on the slabs are monitored in the two excavation sites. In the sites, two new top down methods, S.P.S & S.T.D, are applied with the traditional support method, i.e. ground anchor. The monitored values are analyzed and compared with those predicted at the design stage. The conclusions obtained are the following:

- 1) The monitored displacements of C.I.P rigid walls with S.P.S support were similar to the predicted values. The displacement of the S.P.S support wall came from the characteristics of the support which does not applies the pre-stresses to the wall. The displacement of the wall is allowed by the slab without restriction.
- 2) Even though the rock layer is appeared in the shallow depth, large displacements and axial forces are monitored compared to the values predicted at the design stage in the site where S.T.D. method is applied. This is because the excavation depth is deep and the over-excavation was made at the final stage of construction to reduce the construction time.
- 3) It is necessary to reflect the characteristics of the excavation method and the soil conditions when the retaining walls are planned for excavation site. At the site of excavation, the monitored value in each stage should be reviewed and compared with the designed values. Feedback analysis is sometimes needed when some field problems are anticipated.
- 4) Quantitative inspection of the construction time of the selected sites identifies the significant reduction of the construction time when the slab support methods are applied compared with the traditional ground anchor supports.

9 ACKNOWLEDGEMENTS

This research was supported by the Basic Science Research Program through the National Research Foundation of Korea (NRF), funded by the Ministry of Education, Science and Technology (No.2012-0002408). This paper is also a part of the result from the "Maintenance of Foundation Design Criteria under the Construction Facilities for Standardization", the "Construction & Transportation R&D Policy and Infrastructure Project".

10 REFERENCES

Geogroup Eng.(2010),"SUNEX Manual, 13th Ver. 6.01. SI Version", P1-3.
 Jang ,Y. S., S.M Shin and J.H. Hoe (2012), "A Study on Design and Construction of Earth Retaining Wall Using Multi-Supporting System", KGS-IGS Geotechnical Workshop, I.I.T., New Delhi, December 12.
 Saegil E&C (2011a), "Hyundai Department Chung Ju Excavation Design and Field Monitoring Report"
 Saegil E&C (2011b), "SANG-AM DMC E2-3BL Excavation Design and Field Monitoring Report"
 Sho, Kwang-Ho (2011) "Study on the Application of Semi-open cut Top-Down Construction for Framework" Journal of the Korean Association for Spatial Structures, Vol.11, No.2, pp.129~138.

Passive Pressure on Skewed Bridge Abutments

Pression passive sur des culées de pont asymétriques

Jessee S.

Terracon Consultants, Oklahoma City, Oklahoma, USA

Rollins K.

Brigham Young University, Provo, Utah, USA

ABSTRACT: The passive force-deflection relationship for abutment walls is important for bridges subjected to thermal expansion and seismic forces. Although a number of tests have been performed to investigate these relationships for non-skewed abutments, no tests have been performed for skewed abutments. To determine the influence of skew angle on the development of passive force, lab tests were performed on a wall with skew angles of 0°, 15°, 30°, and 45°. The wall was 1.26 m wide and 0.61 m high and the backfill consisted of dense compacted sand. As the skew angle increased, the passive force decreased substantially with a reduction of 50% at a skew of 30°. An adjustment factor was developed to account for the reduced capacity as a function of skew angle. The horizontal displacement necessary to develop the peak passive force was typically about 2.5 to 3.5% of the wall height, H, and the residual passive force typically dropped by 40% at a deflection of 4 to 6% of H. For the no-skew case, the shape of the failure plane closely resembled that predicted by the Rankine theory but was much shorter than that predicted by the log-spiral approach. Nevertheless, the log-spiral method accurately predicted the measured force while the Rankine method grossly under predicted the force.

RÉSUMÉ: La relation force- déformation passive des murs en retour est importante pour les ponts soumis à la dilatation thermique et des forces sismiques. Bien qu'un certain nombre de tests aient été réalisés afin d'étudier ces relations pour les murs non-biais, aucun test n'a été effectué pour les murs biais. Pour déterminer l'influence de l'angle du biais sur le développement de la force passive, des tests de laboratoire ont été effectués sur un mur ayant des angles de 0°, 15°, 30° et 45°. Le mur a une largeur de 1.26 m et 0.61 m de hauteur, le remblai se compose de sable compacté. Lorsque l'angle du biais augmente, la force passive diminue considérablement avec une réduction de 50% pour un biais de 30°. Un facteur d'ajustement a été mis au point pour tenir compte de la réduction de capacité en fonction de l'angle du biais. Le déplacement horizontal nécessaire pour développer la force maximale passive est généralement d'environ de 2.5 à 3.5% de la hauteur du mur H, et la force résiduelle passive chute généralement de 40% pour un biais de 4 à 6% de H. Pour les cas non-biais, la forme du plan de rupture est proche de celle prévue par la théorie de Rankine, mais beaucoup plus courte que celle prédite par la méthode de la spirale logarithmique. Néanmoins, la méthode de la spirale logarithmique prédit avec précision la force mesurée alors que la méthode de Rankine sous-évalue largement la force.

KEYWORDS: Passive force, Passive Pressure, Skewed abutments, Earth pressure, Dense sand, Plane Strain, Log-Spiral.

1 INTRODUCTION

The passive force-deflection relationship for abutment walls is important for bridges subjected to thermal expansion and seismic forces. Although a number of tests have been performed to investigate these relationships for non-skewed abutments (Maroney 1995, Duncan and Mokwa 2001, Rollins and Cole 2006, Rollins and Sparks 2002, Lemnitzer et al 2009), no tests have been performed to investigate these relationships for skewed abutments. Performance of skewed bridges during the 2010 M8.8 Chilean earthquake suggests that this may be an issue of concern as several such bridges were observed to have rotated about a vertical axis, becoming unseated in their acute corners (EERI, 2010).

While current design codes (AASHTO 2011) consider that the ultimate passive force will be the same for a skewed abutment as for a non-skewed abutment, numerical analyses performed by Shamsabadi et al. (2006) indicate that the passive force will decrease substantially as the skew angle increases. Reduced passive force on skewed abutments would be particularly important for bridges subject to seismic forces or integral abutments subject to thermal expansion. To better determine the influence of skew angle on the development of passive force, a series of large size laboratory tests were performed on a wall that was 1.26 m (4.1 ft) wide and 0.61 m (2 ft) high. A dense sand was compacted behind the wall to simulate a bridge approach fill. Passive force-deflection curves were measured for skew angles of 0°, 15°, 30°, and 45°. Vertical

columns of red soil were embedded into the backfill sand so that the failure surface could be located at the completion of the testing. This paper describes the test program, the test results, and the implications for design practice based on analysis of the test results.

1 BACKGROUND

The distribution of forces at the interface between a skewed bridge and the adjacent backfill soil is illustrated in Fig. 1 as originally outlined by Burke (1994). The longitudinal force (P_L) can be induced by thermal expansion or seismic forces. For static or simplified pseudo-static analyses, the components of the longitudinal force normal and transverse to the abutment must be resisted by the passive force (P_p) normal to the abutment backwall and the shear resistance (P_R) on the backwall. Summing forces normal to the abutment produces the equation

$$P_p = P_L \cos\theta \quad (1)$$

where θ is the skew angle of the backwall.

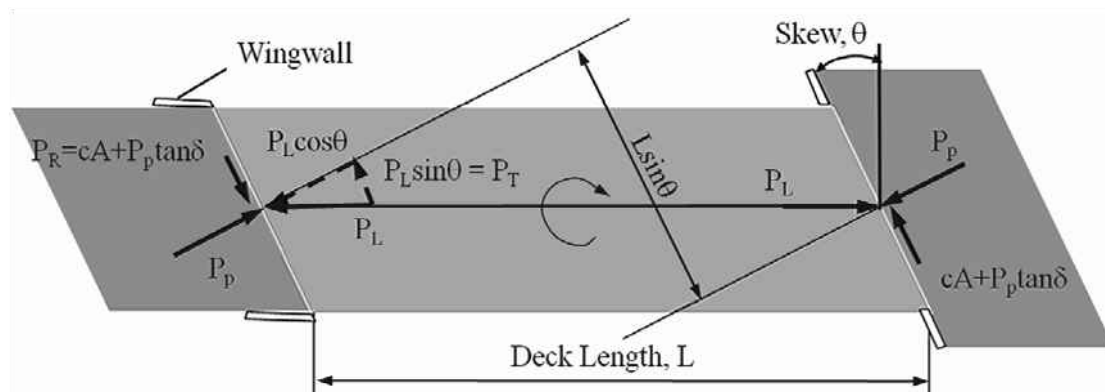


Figure 1. Illustration of forces acting on a skewed bridge at the soil-abutment interface

The transverse applied shear force (P_T) can be computed using the equation

$$P_T = P_L \sin \theta \quad (2)$$

while the transverse shear resistance (P_R) can be given by the equation

$$P_R = cA + P_p \tan \delta \quad (3)$$

Summing forces transverse to the backwall produces the equation

$$(cA + P_p \tan \delta) / F_s \geq P_L \sin \theta \quad (4)$$

where c is the soil cohesion, A is the area of the backwall, δ is the angle of wall friction between the backfill soil and the concrete abutment backwall, and F_s is a factor of safety. If the applied transverse shear resistance exceeds the ultimate shear resistance, the abutment could slide against the soil leading to an unstable condition.

In addition, the offset in passive force on the abutments produce a force couple which must be resisted by the force couple produced by the shear resistances on each abutment. Summing moments about a vertical axis leads to the equation

$$(cA + P_p \tan \delta) L \cos \theta / F_s \geq P_p L \sin \theta \quad (5)$$

Again, if the shear resistance is insufficient, the bridge will tend to rotate, which would likely change the distribution of passive force on the abutments. Based on Eq 5, Burke (1994) suggested that rotation would be expected for skew angles greater than 15° with smooth abutment-soil interfaces and no cohesion as the factor of safety dropped from 1.5 to 1.0. If cohesion is ignored, the potential for rotation is independent of both P_p and the length of the bridge, L .

2 TEST LAYOUT

The test layout is illustrated in Fig. 2. A concrete wall 1.26 m (4.13 ft) wide and 0.61 m (2 ft) high was used to model the backwall of an abutment. Passive force-deflection tests were performed with skew angles (θ) of 0° , 15° , 30° , and 45° . Two tests were performed for each skew angle to evaluate repeatability. A dense sand was compacted behind the wall to simulate the backfill in a typical approach fill. The sand backfill was 0.9 m (3 ft) thick and extended 0.3 m (1 ft) below the base of the wall. The backfill was 3 to 4 m (10 to 13 ft) long to completely contain the failure surface and was slightly wider than the wall 1.28 m (4.21 ft) to allow the backwall to move into the sand backfill without any friction on the concrete sidewall. To support the sand backfill during compaction, two

1.5 m concrete blocks were bolted to the structural floor of the laboratory on either side of the fill near the wall. Beyond the concrete blocks, plywood walls were braced into a vertical position. Two plastic sheets were placed along the sidewalls to create a low friction surface and produce a 2D or approximately plane strain geometry. A base was constructed below the concrete backwall and rollers were placed at the interface between the backwall and the base to provide a normal force but minimize base friction.

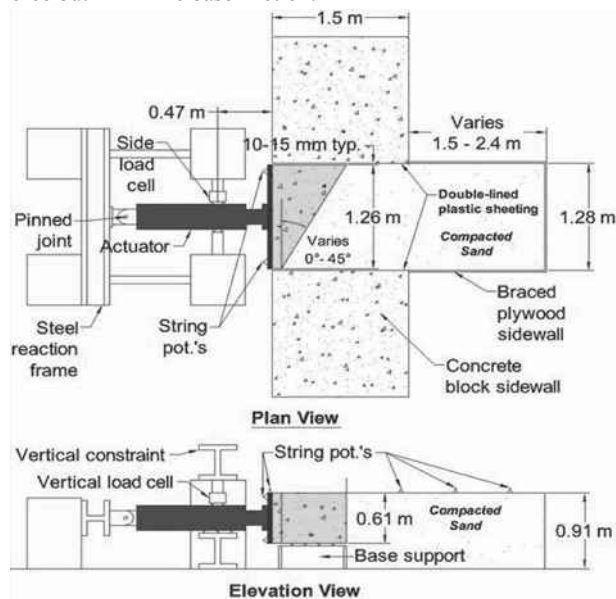


Figure 2. Plan and elevation views of the test layout.

Tests were performed by pushing the backwall longitudinally into the backfill sand using a 490 kN (110 kip) hydraulic actuator which was bolted to the backwall. Load was applied at a rate of 0.25 mm/min (0.1 inch/min); but sand is not very rate sensitive. Vertical and horizontal load cells were mounted between the reaction frame and the actuator so that the loads necessary to hold the wall in place could be measured.

2.1 Instrumentation

Load was measured by pressure transducers in the actuator. To measure the movement of the backwall, four longitudinal string potentiometers were positioned at the corners of the wall and two transverse string pots were positioned at the top and bottom of one side. In addition, a final string pot was used to monitor the vertical movement.

The position of the failure surface was monitored by marking 0.3 m (1 ft) square grids at the backfill surface. The subsurface failure plane position was located by placing vertical

columns of red sand spaced along the longitudinal axis behind the wall.

2.2 Backfill soil properties

The sand backfill is clean poorly-graded sand classifying as SP according to the Unified Soil Classification System and A-1-b according to the AASHTO system. The particle size distribution curve falls within the gradation limits for washed concrete sand (ASTM C33) with C_u of 3.7 and C_c of 0.7. A modified Proctor test was performed on the sand and indicated a maximum dry unit weight of 17.8 kN/m³ (113.5 lbs/ft³). The sand was placed in 150 mm (6 in) lifts and the average relative compaction achieved was typically about 98%.

Load testing was generally performed two days after compaction and moisture content measurements at various depths were made immediately after testing. These measurements indicated good consistency between tests, with the moisture content typically falling within 7 to 9%.

Based on a direct shear test the drained friction angle (ϕ') was found to be 46° with a cohesion of 7 kPa (140 psf). Interface friction tests were also performed between the sand and the concrete and a wall friction angle (ϕ) of 33° was measured.

Because the compacted sand in a partially saturated state could be excavated with a vertical face and remained stable for long periods, the potential for apparent cohesion owing to matric suction was also investigated. Suction measurements indicated that the sand at the moisture content during testing had a matric suction (ψ) (negative pressure relative to atmospheric pressure) of approximately 4 to 5 kPa (80 to 100 psf). Based on recommendations of Likos et al (2010), this magnitude of suction produces an apparent cohesion (c_a) of approximately 4 to 5 kPa (80 to 100 psf).

3 TEST RESULTS

3.1 Passive force-deflection curves

The passive force versus longitudinal deflection curves for the tests at each of the skew angles are plotted in Fig. 3. Although the initial stiffness for each curve is remarkably similar, the peak passive force clearly decreases as the skew angle increases. In addition, there appear to be some differences in the shape of the passive force displacement curves as skew angle increases.

The passive force-deflection curve appears to exhibit a typical hyperbolic curve shape for the no skew case however, it transitions to a different shape as the skew angle increases. As the skew angle increases, the passive force exhibits a longer plateau where the force remains relatively constant or increases gradually with deflection before reaching a peak and abruptly decreasing to a residual value. The peak passive force typically developed at a normalized deflection of 2.5% to 3.5% of the wall height (H), and did not change consistently with skew angle. The tests typically showed a reduction in the passive force to a residual value at a normalized displacement of 0.04H to 0.06H. The post-peak residual strength ranged from 53 to 72% of the peak value with an average of 60%. This decrease in post peak resistance is consistent with results from the direct shear tests.

The peak passive force for each test at a given skew angle has been divided by the peak passive force at zero skew and the results are plotted as a function of skew angle in Fig. 4. Normalized data from numerical analyses of skew abutments reported by Shamsabadi et al (2006) are also shown in Fig. 4 and the results follow the same trend line. The curve has been extrapolated to zero at a skew angle of 90°. The no skew case involves pure passive resistance and zero shear force. A skewed wall is subject to a combination of both passive resistance and side shear force. At the largest possible skew angle, 90°, the

forces acting on the wall transition to pure side shear force with zero passive resistance.

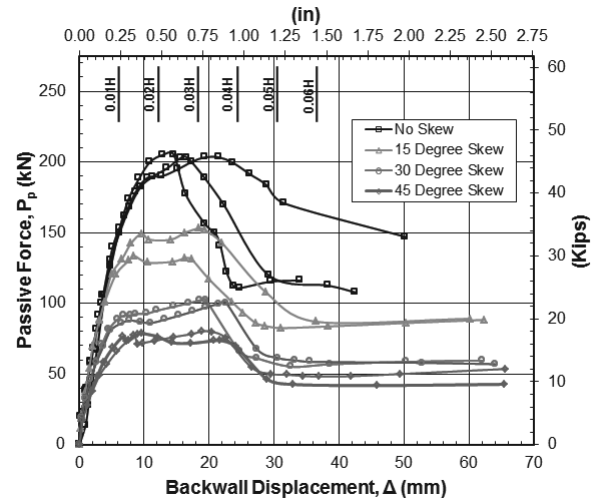


Figure 3. Passive force versus longitudinal backwall displacement for the tests at each skew angle.

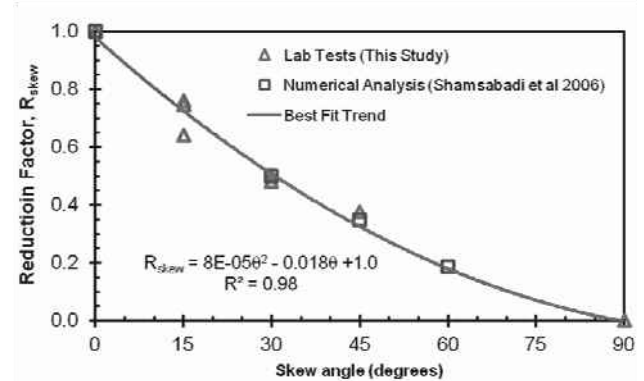


Figure 4. Normalized peak passive force versus skew angle from lab tests and numerical model results.

As indicated previously, vertical and horizontal displacements of the wall during the tests were minimal. Wall displacement was less than 4.4 mm for vertical movement and less than 2.3 mm for transverse movement for the skew angles tested.

3.2 Failure surface geometry

The failure surface for the no skew case was approximately the same length across the width of the sand box; however, when a skew angle was involved, the failure surface also exhibited a skew across the width of the sand box. The failure surface did not manifest itself at the ground surface until after the peak force had been reached.

The failure surface within the sand was clearly identifiable from the offset in the red sand columns. The failure surface geometry is shown as a function of distance behind the middle of the wall for the various skew angles in Fig. 5. In addition, the ground surface heave is also plotted for each test. The average length of the failure surface behind the middle of the wall was 2.1 m (7.0 ft) with a standard deviation of 0.3 m (1.0 ft). The length of the failure surface ranged from 1.8 to 2.6 m (5.9 to 8.6 ft). The failure surface typically extended 75 mm to 300 mm horizontally from the bottom of the wall then exhibited a relatively linear trend line upward to the surface. The angle of inclination of the trend line was between 19° and 21.5° with an average of 20°. Assuming that the angle of inclination (α) of the straight line segment of the log-spiral failure wedge is given by the equation:

$$\alpha = 45 - \phi'/2 \quad (8)$$

as suggested by Terzaghi and Peck (1948), then the interpreted drained friction angle would be between 47° and 52° with an average of 50°. The inferred friction angle value is higher than the measured friction angle from the direct shear test, but is close to the value that would be expected for the plane strain friction angle. The conditions and geometry of the sand box simulated a plane strain condition as well. Based on a number of studies, Kulhawy and Mayne (1990) determined that the plane strain friction angle for dense sand was 11% higher than the triaxial value on average. Thus, the plane strain friction angle for the sand used in the tests would be about 51°, which is approximately the same value as that of the inferred friction angle from the inclination of the failure wedge.

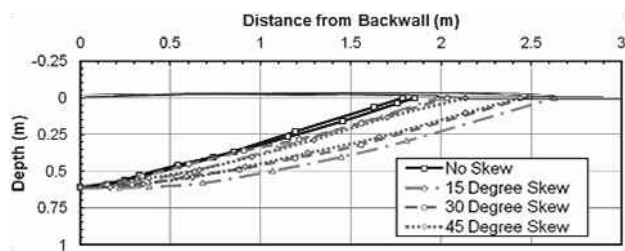


Figure 5. Measured failure surface depth versus distance from the backwall for each test.

4 ANALYSIS OF RESULTS

Test results were analyzed using the Rankine (1857) and log-spiral (Terzaghi, 1948) passive pressure theories. Table 1 shows comparisons of the test results with computed passive force and failure surface orientation for the no-skew case. The measured and theoretical failure surface geometries for the no-skew case relative to the top of the wall are shown in Fig. 6. For the analysis, the soil friction angle was taken as 50°, consistent with the plane strain value, with a cohesion of 4.5 kPa (90 psf), and the wall friction angle was taken as 33° based on interface tests. While the failure plane according to the log-spiral method generally exceeded the length of the failure surface by 45 to 50%, this method was most effective in computing passive force. In contrast, the Rankine method grossly underestimated the measured force, but gave a reasonable approximation of the failure surface geometry. Although the Coulomb theory is widely used, it is limited to cases where δ/ϕ is less than about 0.5. For these tests, δ/ϕ is equal to 0.66. Thus, analyses using the Coulomb method predict an unreasonably high value for the passive force, and the failure surface extent is likewise unreasonably over-predicted (see Table 1).

5 CONCLUSIONS

1. Large scale laboratory tests and numerical analyses indicate that the peak passive force for a skewed abutment significantly decreases as the skew angle increases. Based on available results, this reduction can be accounted for by using a simple reduction factor. This reduction may be dependent on abutment geometry and other unknown factors and should thus be used with caution until further research is performed.
2. For the dense sand typical of approach fills, the peak passive force for all tests typically developed at longitudinal deflections between 0.025H and 0.035H. However, the shape of the passive force-deflection curve up to the peak value transitioned from a typical hyperbolic shape for the no skew case to a bilinear shape for the skewed walls.
3. At wall displacements beyond the peak (0.04 to 0.06H) the passive force decreased substantially and the residual force was typically about 40% below the peak force, which is in agreement with the behavior in the direct shear tests.
4. Based on the measured soil parameters the log spiral method provided the best agreement with the measured passive force,

while the Rankine method grossly underestimated the force. However, the failure surface geometry was closer to that predicted by the Rankine method than the log spiral shape.

Table 1. Summary of measured tests results in comparison with computed values using different passive pressure theories.

	Passive Force		Failure Surface Geometry	
	(kN)	% of measured	Orientation (degrees)	Extent (m)
Avg. Measured	205 (46 kips)	100	20	1.8 (6.0 ft)
Coulomb Theory	1115 (251 kips)	545	3.4	10 (33 ft)
Rankine Theory	51 (12 kips)	25	20	1.8 (5.8 ft)
Log-Spiral Theory	205 (46 kips)	100	-	3.1 (10 ft)

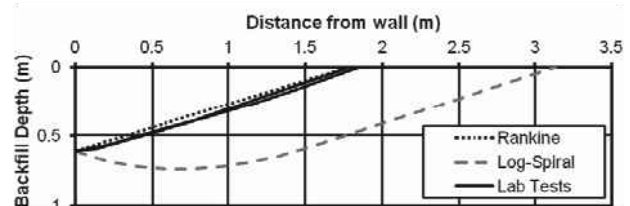


Figure 6. Measured and theoretical failure surface geometries for the no-skew case.

6 REFERENCES

- AASHTO (2011), Guide Specifications for LRFD Seismic Bridge Design, 2nd Edition, 286 p.
- Burke, M.P. Jr. (1994). "Semi-Integral bridges: movements and forces". Transportation Research Record 1460, Transportation Research Board, Washington, D.C., p. 1-7.
- Cole, R.T and Rollins, K.M. (2006). "Passive Earth Pressure Mobilization During Cyclic Loading." *J. Geotech. & Geoenviron. Eng.*, ASCE, 132(9), 1154-1164.
- Duncan, J. M., and Mokwa, R. M. (2001). "Passive earth pressures: theories and tests." *J. Geotech. & Geoenviron. Eng.*, ASCE Vol. 127, No. 3, pp. 248-257.
- EERI (2010). "The M_w 8.8 Chile Earthquake of February 27, 2010". EERI Special Earthquake Report, June, 2010.
- Kulhawy, F. H., and Mayne, P. W. (1990). "Manual on estimating soil properties for foundation design." Research Project 1493-6, EL-6800, Electric Power Research Institute, Palo Alto, California.
- Lemnitzer, A., Ahlberg, E.R., Nigbor, R.L., Shamsabadi, A., Wallace, J.W., and Stewart, J.P. (2009). "Lateral performance of full-scale bridge abutment wall with granular backfill," *J. Geotech. & Geoenviron. Eng.*, ASCE, 135 (4), 506-514.
- Likos, W.J. Wayllace, A., Godt, J., and Ning, L. (2010). "Direct shear apparatus for unsaturated sands at low suction and stress". *Geotech. Testing J.*, ASTM, 33(5)
- Maroney, B.H. (1995) "Large scale abutment tests to determine stiffness and ultimate strength under seismic loading" Ph.D. Dissertation, Civil Engineering Dept., University of California, Davis.
- Rankine, W. J. (1857). On the stability of loose earth. *Philosophical Transactions of the Royal Society of London*, 147.
- Rollins, K.M. and Cole, R.T. (2006). "Cyclic Lateral Load Behavior of a Pile Cap and Backfill." *J. Geotech. & Geoenviron. Eng.*, ASCE, 132(9), 1143-1153.
- Rollins, K.M. and Sparks, A.E. (2002) "Lateral Load Capacity of a Full-Scale Fixed-Head Pile Group." *J. Geotech. & Geoenviron. Eng.*, ASCE, Vol. 128, No. 9, p. 711-723.
- Shamsabadi, A. Kapuskar, M. and Zand, A. (2006). "Three-dimensional nonlinear finite-element soil-Abutment structure interaction model for skewed bridges". 5th National Seismic Conf. on Bridges and Highways, FHWA, p.
- Terzaghi K. and Peck, R. B. (1948). *Soil Mechanics in Engineering Practice*, John Wiley and Sons, New York, p.

Deformation behaviour of clay due to unloading and the consequences on construction projects in inner cities

Étude du comportement en déformations de l'argile suite à un retrait de charge et conséquences lors de projets de constructions en zone urbaine

Katzenbach R., Leppla S.

Technische Universität Darmstadt, Institute and Laboratory of Geotechnics, Germany

ABSTRACT: In the course of construction projects in many cases the soil is unloaded. For example at the construction of excavations or the deconstruction of existing buildings the soil relaxes due to the reduced stress level. Cohesive soil materials like clay react strongly time dependent. At all construction projects in the city of Frankfurt am Main, Germany, which belong to the Geotechnical Category 3 regarding Eurocode EC 7 the deformation of the soil was measured during and after the construction works. It has to be determined that the settlement relevant soil layer, the tertiary Frankfurt Clay, relaxes time-delayed due to the unloading in the dimension of centimetres. The new acknowledgement of the deformation behaviour of the Frankfurt Clay due to unloading the subsoil is presented in detail by typical projects for the development of the city.

RÉSUMÉ : Il arrive régulièrement dans le cadre de projets de construction en zone urbaine que le sol subisse un déchargement. Dans le cas d'excavations par exemple, le sol se détend suite à une baisse des contraintes appliquées. Le comportement des sols cohésifs tels que l'argile dépend fortement du temps. Pour l'ensemble des projets de construction à Francfort en Allemagne, ces projets étant classés en Catégorie Géotechnique 3 selon l'Eurocode 7, les déformations du sol ont été mesurées pendant et après les travaux. Il est à mettre en avant que le sol de la couche pertinente en terme de tassements, l'argile tertiaire de Francfort (Frankfurt Clay), subit un relâchement différé dans le temps suite au retrait de charge de l'ordre du centimètre. Les nouvelles reconnaissances sur le comportement de l'argile de Francfort suite à un déchargement du sol sont présentées ici en détail pour des projets typiques dans le cadre du développement de la ville.

KEYWORDS: Soil-structure-interaction, Frankfurt Clay, time dependent deformation behaviour, observational method.

1 INTRODUCTION

Since the beginning of the large infrastructure and high-rise building constructions in Frankfurt am Main the bearing and deformation behaviour of the Frankfurt Clay has been scientifically researched intensely (Chambosse 1972, Breth and Stroh 1974, Amman et al. 1975, Sommer et al. 1990, König 1994, Katzenbach and Moormann 1999, Breth and Katzenbach 2000, Katzenbach et al. 2001, Moormann 2002, Katzenbach et al. 2002, Dürrwang et al. 2007, Janke et al. 2010, Vogler 2010, Katzenbach et al. 2011). The first research and experiences made with the Frankfurt Clay result from new constructions, i.e. from high-rise buildings and tunnel constructions.

Due to the development of the city a lot of deconstruction activities occur in advance of new construction projects. In the course of these projects new knowledge about the time dependent bearing and deformation behaviour of the Frankfurt Clay is obtained, especially if there is a larger timeframe between the deconstruction (unloading) and the new construction activity (reloading). In such cases the uplifting is not overlapped or compensated by an early reloading. For example a deep excavation base usually heaves up to several centimetres as shown in Figure 1 (Amman et al. 1974).

The time dependent deformation behaviour of the over-consolidated tertiary Frankfurt Clay is presented in detail by 2 large deconstruction projects. The first project is the deconstruction of the building complex of the Zürich Insurance consisting of 2 high-rise buildings (Zürichhochhaus I and II) and the construction of the new high-rise building Opernturm at the same location. The project is located very close to a tunnel of the metro system. The second project is the deconstruction of an up to 14 storeys high-rise building in the historic centre of Frankfurt am Main. The project is located directly over 2 tunnels and an underground station of the metro system.

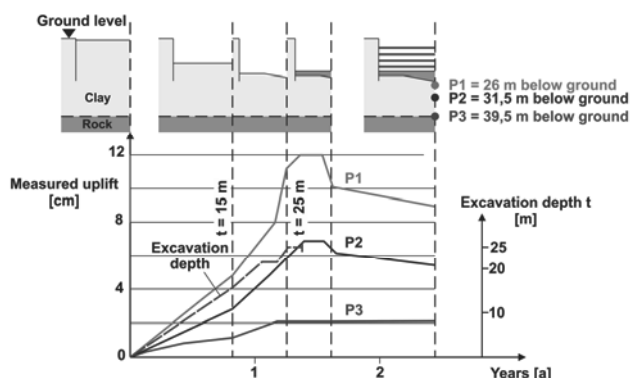


Figure 1. Measured uplift of the surface of the excavation pit at BfG high-rise building (now: European Central Bank ECB).

2 DECONSTRUCTION OF THE ZÜRICH INSURANCE HIGH-RISE BUILDINGS

The Zürich Insurance building complex was built between 1959 and 1963. It consisted of 2 high-rise buildings (Zürichhochhaus I and II) with heights of 70 m and 63 m and annexe to the high-rise buildings with up to 8 storeys. The complex was founded on a raft in a depth of 7 m below the surface. In the years 2001 and 2002 the complex was deconstructed down to the ground

level. The sublevels remained. A cross section through the project area is shown in Figure 2.

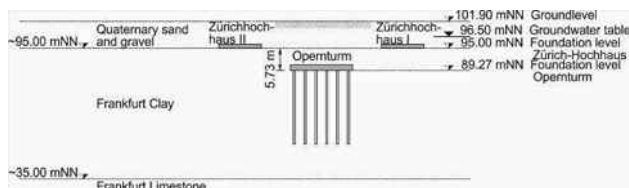


Figure 2. Soil, groundwater and foundation conditions.

5 years after the deconstruction the 177 m high-rise building Opernturm was built. The annexe of the high-rise building is up to 7 storeys high (Fig. 3) and was founded on the existing raft foundation. Under the Opernturm the existing raft was deconstructed and a new sublevel was built.



Figure 3. New high-rise building Opernturm.

The Opernturm is founded on a Combined Pile-Raft-Foundation (CPRF) consisting of a 3 m thick raft and 57 piles with a diameter of 1.5 m and a length of 40 m. For design of the CPRF a whole characteristic load of 1,500 MN was calculated. The bearing behaviour of the CPRF is described by the CPRF-coefficient α_{CPRF} , explained in Equation (1) (Viggiane 1998, Hanisch et al. 2002). The Opernturm has a $\alpha_{CPRF} = 0.9$.

$$\alpha_{CPRF} = \frac{\sum_{j=1}^n R_{pile,k,j}}{R_{tot,k}} \quad (1)$$

The soil and groundwater conditions are typical for the inner city of Frankfurt am Main:

- 0 m to 7 m: quaternary sands and gravel
- 7 m to 67 m: Frankfurt Clay
- below 67 m: Frankfurt Limestone
- groundwater level in a depth of 5.5 m

The measured settlements during the construction of the Zürichhochhaus I and II as well as the uplift during their deconstruction are depicted in Figure 4. The measured settlements increase continuously up to 60 % of the final settlement during the construction time of the superstructure. Due to the consolidation process the deformation rate decreases continuously. About 5 years after the construction the settlement stopped at 9.5 cm at Zürichhochhaus I and 8.5 cm at Zürichhochhaus II. The deconstruction started in the middle of 2001. In March 2002 the deconstruction was completed. Only

the sublevels were kept. After 5 years the measured uplift is in the same magnitude as the settlements before.

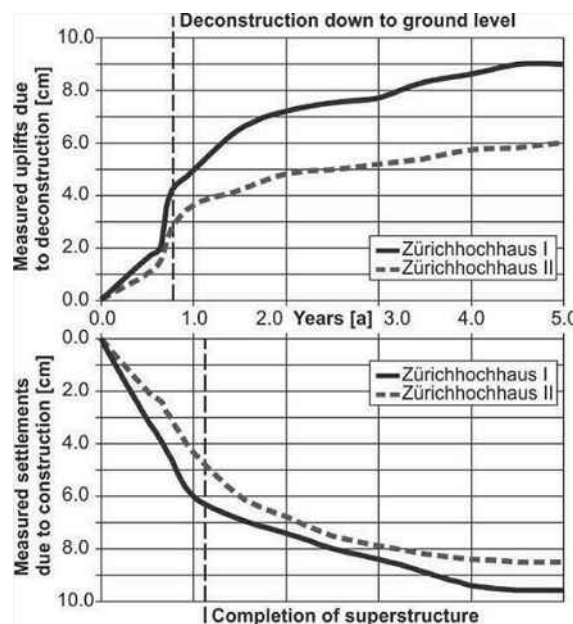


Figure 4. Measured settlements and uplifts of the soil in the area of the high-rise buildings.

The measured time dependent settlement and uplift evolution with reference to the maximum value can be approximately mathematically described by Equation 2. Figure 5 shows the application of Equation 2 to the presented project.

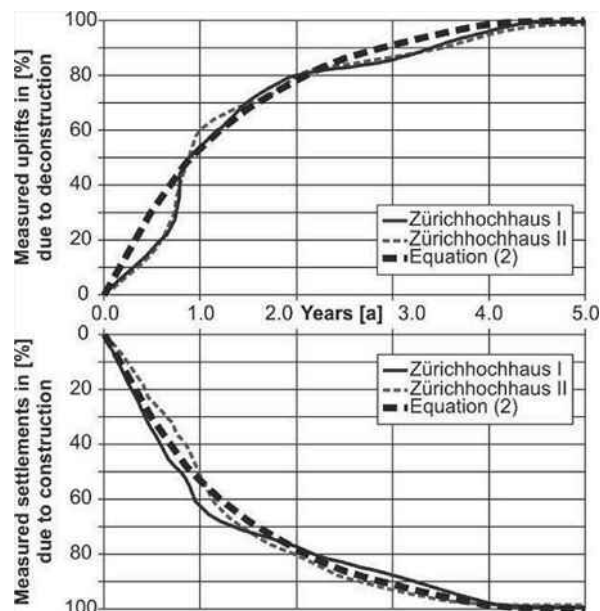


Figure 5. Measured settlement and uplift and correlation to Equation 2.

$$\frac{s(t)}{s_{max}} = k \cdot (1 - e^{-(n \cdot t)}) \quad (2)$$

where : k = Consolidation factor
 here : $k = 0,104 [-]$
 n = Time factor
 here : $n = 0,7 [-]$
 t = Time in years ($t \leq 5$ years)

(3)

$$\frac{s(t)}{s_{\max}} = k \cdot (1 - e^{-(n \cdot t)})$$

where: k = Consolidation factor
 here: $k = 0,104 [-]$
 n = Time factor
 here: $n = 0,7 [-]$
 t = Time in years ($t \leq 5$ years)

To verify Equation 2 the measured time dependent settlement behaviour during the construction of the high-rise building Mainzer Landstraße in Frankfurt am Main is used (Fig. 6). The construction of the 155 m high-rise building began in 1973 and the settlements were measured for 5 years. After this time a settlement of 25.4 cm was measured in the core area of the high-rise building. At the completion of the superstructure after 1.5 years the measured settlement was about 70% of the total settlement. The estimation of the time dependent deformation behaviour can also be described by Equation 2.

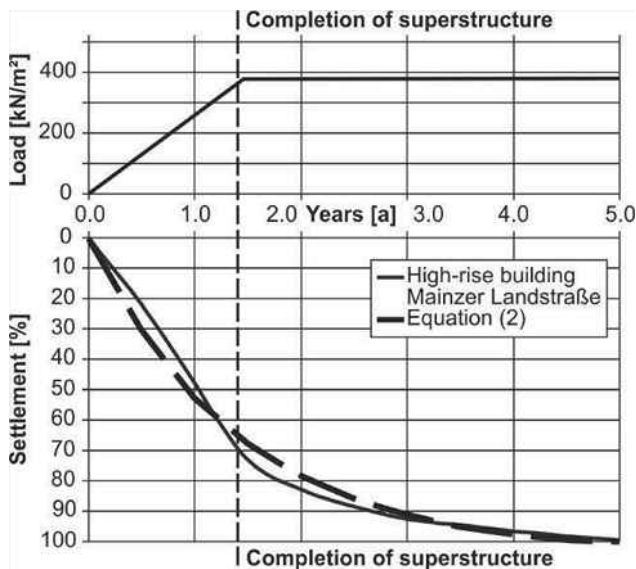


Figure 6. Measured settlement of the high-rise building Mainzer Landstraße.

3 DECONSTRUCTION OF A HIGH-RISE BUILDING FOUNDED ON AN UNDERGROUND STATION

In the context of the urban development the city of Frankfurt am Main plans to redesign the historic centre. Historic façades and buildings will be reconstructed. To create the necessary space on the surface an up to 14 storeys high-rise building was deconstructed. According to the present state of planning the deconstruction was carried out down to the sublevels.

The high-rise building and its underground parking overlay 2 tunnels and an underground station of the urban metro system. The loads of the superstructures are directly transferred onto the tunnels and underground station. Figures 7 and 8 give an overview on the primary situation prior to the deconstruction. The sealing of the structures was made of outside layers of bitumen-based materials. It must be guaranteed that during the deconstruction of the existing high-rise building and the construction of the new buildings the sealing of the underground structures and the sublevels remained intact. For this purpose especially the uplifts due to the deconstruction and the deformations of the underground structures and the sublevels had to be monitored during the execution of the project according to the observational method.

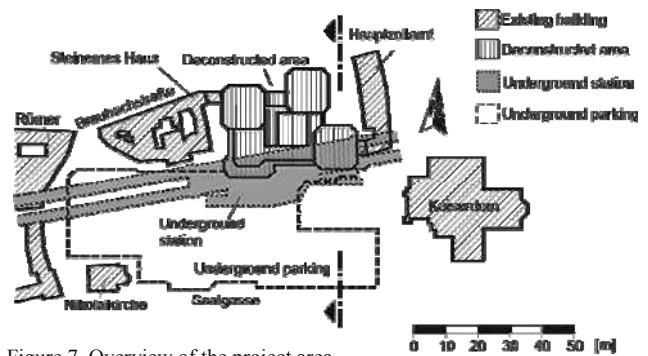


Figure 7. Overview of the project area.

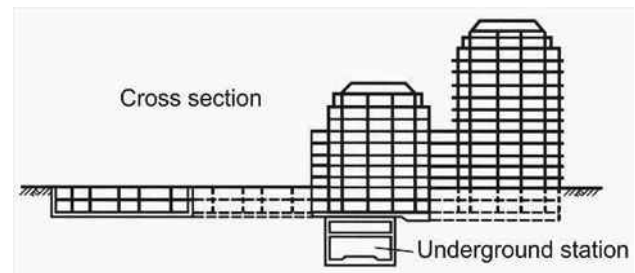


Figure 8. Cross section of Figure 6.

The soil and groundwater conditions are as follows:

- 0 m to 7 m: quaternary sands and gravel
- 7 m to 30 m: Frankfurt Clay
- below 30 m: Frankfurt Limestone
- groundwater level in a depth of 6 m

The groundwater level is influenced by the river Main which is 180 m far away. In the course of the geotechnical survey two aquifers have been encountered. The top aquifer is located in the non-cohesive soil. The lower confined groundwater layer is located in the Frankfurt Clay and in the Frankfurt Limestone.

According to the classification of the project into the Geotechnical Category 3, that is the Category for very difficult projects in EC 7, an extensive geodetic monitoring program with 580 measuring points was installed. 220 measuring points are located around the deconstructed building, 110 are located in the underground parking and in the sublevels of the deconstructed building, 30 are in the underground station and the remaining 220 are located in the tunnels.

The existing buildings were deconstructed down to the 2 sublevels. The uplift that occurred due to the unloaded of the soil is shown on selected points (Figures 9 and 10).

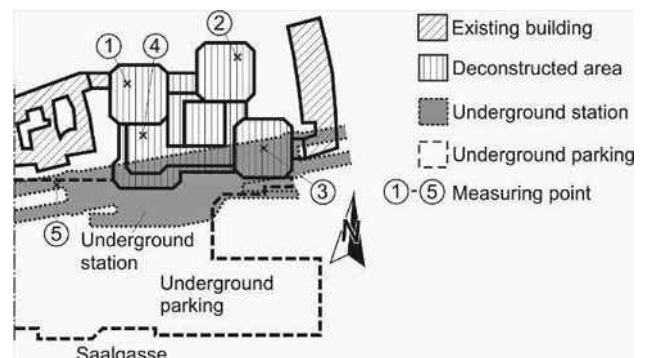


Figure 9. Selected measuring points.

The selected measuring points 1 to 4 are in the sublevel of the former high-rise building. Measuring point 5 is at the transition of the underground station to the tunnel. At the

measuring points 1 to 4 uplift between 1 cm and 5 cm was detected in the deconstruction time (March to December 2010). The measured uplift of measuring point 5 is less than 0.5 cm.

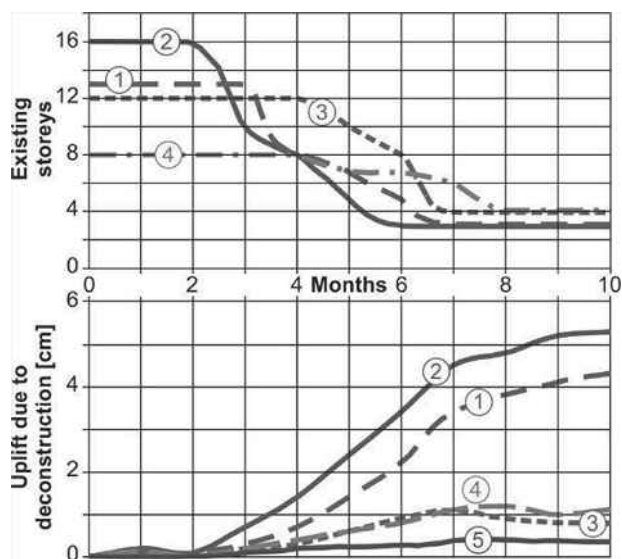


Figure 10. Measured uplift at selected measuring points.

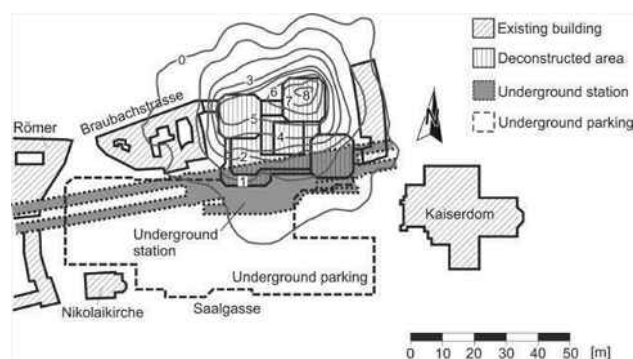


Figure 11. Measured uplift of the whole project area [cm].

After the deconstruction down to the sublevels in December 2010, the modification of the sublevels began. In that phase the loads only were changed insignificantly. The uplift of the whole project area and the neighbourhood in October 2012 is drawn in Figure 11. The uplift due to the reduced stress level of the stress and time related deformation behaviour of the Frankfurt Clay is continuously raising due to the consolidation processes. A maximum uplift of 8.5 cm was measured in the area where the most storeys were deconstructed. The uplifts fade down related to the distance very quickly. So no dangerous deformations of the neighbourhood were measured.

4 CONCLUSIONS

At the construction of excavations or the deconstruction of existing buildings the soil is unloaded and relaxes due to the reduced stress level. Cohesive soil materials like clay react strongly time dependent. For example the tertiary Frankfurt Clay relaxes time-delayed due to the unloading in the dimension of centimetres. Regarding the guarantee of the stability and the serviceability of structures in the neighbourhood the influence of the arising deformation of the soil has to be taken into

account during an early planning stage and has to be considered during analyses and design.

For verification of the analyses and to proof the design all projects with large soil deformations have to be monitored by means of the observational method. Only high-level analyses compared with the observational method are the guarantee for a safe construction phase for the project itself and the influenced structures.

5 REFERENCES

- Amman, P., Breth, H., Stroh, D. 1975. Verformungsverhalten des Baugrundes beim Baugrubenaushub und anschließendem Hochhausbau am Beispiel des Frankfurter Tons. *Mitteilungen des Institutes und der Versuchsanstalt für Geotechnik der Technischen Universität Darmstadt*, Heft 15.
- Breth, H., Stroh, D. 1974. Das Verformungsverhalten des Frankfurter Tons beim Aushub einer tiefen Baugrube und bei anschließender Belastung durch ein Hochhaus. *13. Baugrundtagung der Deutschen Gesellschaft für Geotechnik in Frankfurt am Main*, 51-70
- Breth, H., Katzenbach, R., 2000. Entwicklungen in der Geotechnik, gespiegelt in 75 Bänden des Bauingenieur. *Bauingenieur 75*, Heft 7/8, 365-371.
- Chambosse, G. 1972. Das Verformungsverhalten des Frankfurter Tons beim Tunnelvortrieb. *Mitteilungen des Institutes und der Versuchsanstalt für Geotechnik der Technischen Universität Darmstadt*, Heft 10.
- CEN European Committee of Standardization 2008. Eurocode 7: Geotechnical design – Part 1: General rules.
- Dürwang, R., El-Mossallamy, Y., Reininger-Behrenroth, M. 2007. Neue Erkenntnisse zum Verformungsverhalten des Frankfurter Tons. *Bautechnik 84*, Heft 3, 190-192.
- Hanisch, J., Katzenbach, R., König, G. *Kombinierte Pfahl-Plattengründungen*. Wilhelm Ernst & Sohn, Berlin.
- Katzenbach, R., Moormann, C. 1999. Geotechnical field measurements applied to a 240 m high office tower constructed by top/down methods in Frankfurt Clay. *5th International Symposium on Field Measurements in Geomechanics in Singapore*, 325-330.
- Katzenbach, R., Hoffmann, H., Moormann, C., Vogler, M. 2001. Neue geotechnische Konzepte für den technisch und wirtschaftlich optimierten Hochhausbau. *Bauingenieur 76*, Heft 7/8, 314-325.
- Katzenbach, R., Turek, J., Vogler, M. 2002. Entwicklung einer horizontal belasteten KPP am Beispiel der neuen Messehalle 3 in Frankfurt am Main. *Bauingenieur 77*, Heft 9, 393-398.
- Katzenbach, R., Leppla, S., Seip, M. 2011. Das Verformungsverhalten des Frankfurter Tons infolge Baugrundentlastung. *Bauingenieur 86*, Heft 5, 233-240.
- König, G. 1994. Innovationen im Bauwesen durch Forschung und Entwicklung an den Hochschulen. *Mitteilungen des Institutes und der Versuchsanstalt für Geotechnik der Technischen Universität Darmstadt*, Heft 32, 87-112.
- Janke, O., Zoll, V., Sommer, F., Waberseck, T. 2010. Palais Quartier (Frankfurt HochVier) – Herausfordernde Deckelbauweise im Herzen der City. *Mitteilungen des Institutes und der Versuchsanstalt für Geotechnik der Technischen Universität Darmstadt*, Heft 86, 113-124.
- Moormann, C. 2002. Trag- und Verformungsverhalten tiefer Baugruben in bindigen Böden unter besonderer Berücksichtigung der Baugrund-Tragwerk- und der Baugrund-Grundwasser-Interaktion. *Mitteilungen des Institutes und der Versuchsanstalt für Geotechnik der Technischen Universität Darmstadt*, Heft 59.
- Sommer, H., Katzenbach, R., DeBenedittis, C. 1990. Last-Verformungsverhalten des Messturms in Frankfurt am Main. *28. Baugrundtagung der Deutschen Gesellschaft für Geotechnik in Karlsruhe*, 371-380.
- Viggiane, C. 1998. Pile groups and piled raft behaviour. *3rd International Geotechnical Seminar on Deep Foundations and Bored and Auger Piles*, Ghent, 77-91.
- Vogler, M. 2010. Berücksichtigung innerstädtischer Randbedingungen beim Entwurf tiefer Baugruben und Hochhausgründungen am Beispiel des PalaisQuartier in Frankfurt am Main. *Bauingenieur 85*, Heft 6, 273-281.

Large tailings heaps and the influence on infrastructures due to the resulting soil deformation

Les grands terrils miniers et leur influence sur les infrastructures voisines à travers la déformation des sols

Katzenbach R., Leppla S.

Technische Universität Darmstadt, Institute and Laboratory of Geotechnics, Germany

Seip M.

Ingenieursozietät Professor Dr.-Ing. Katzenbach GmbH, Frankfurt am Main, Germany

Schleinig J.-P.

K+S Aktiengesellschaft, Kassel, Germany

Schnürer F.

K+S KALI GmbH, Kassel, Germany

ABSTRACT: In the context of potassium fertilizer production the residua, mostly consisting of granular rock salt, is stored on large tailings heaps. The salt residue has a strongly visco-plastic material behaviour with a rate-dependant strength. The heaps have a base area up to a square kilometre and heights up to 120 m. Using the Finite-Element-Method (FEM) and a numerical constitutive law for the salt residue, developed at the Technische Universität Darmstadt (TU Darmstadt), the influence of the heaps on infrastructures like buildings, streets, railway tracks and pipelines can be estimated. In the context of the approval procedures of the extension of existing heaps comprehensive numerical investigations regarding stresses and deformations are necessary to guarantee the stability and the serviceability of the heaps and influenced infrastructures. For verification of the numerical investigations according to the observational method monitoring programs have to be installed.

RÉSUMÉ : Dans le contexte actuel de production d'engrais riches en potassium, les résidus, principalement constitués de sel gemme granulaire, sont stockés sous forme de larges terrils. Les résidus salins présentent un important comportement visco-plastique, et une résistance à la rupture fortement dépendante du temps. La surface occupée par ces terrils peut atteindre un kilomètre carré et une hauteur de 120m. L'influence de ces terrils sur les infrastructures du type bâtiments, routes, rails et pipelines peut être estimée en combinant la Méthode des Eléments Finis (MEF) et l'utilisation d'une loi constitutive numérique pour le matériau salin, développée à la Technische Universität Darmstadt (TU Darmstadt). Dans le contexte actuel qui encourage l'extension des terrils existants, il devient nécessaire de mener des études numériques poussées évaluant les contraintes et déformations, afin de garantir la stabilité et le bon fonctionnement des terrils et des infrastructures avoisinantes. Des programmes de contrôle doivent être mis en place afin d'effectuer la vérification des études numériques, obtenues grâce aux méthodes observationnelles.

KEYWORDS: Tailings heap, visco-plastic material behaviour, observational method.

MOTS-CLES : Terrils miniers, comportement visco-plastique, méthode observationnelle

1 INTRODUCTION

During the production of potash and the converting into fertilizer for agriculture and into specialty products for the chemical industry a large amount of residua, mostly consisting of granular rock salt, is deposited on large heaps. The resulting tailings heaps with a ground view up to 1 km² and a height up to 120 m cause normal stresses of 2,200 kN/m² and shear stresses of 550 kN/m² on the contact surface. An impression of the dimensions of such tailings heaps is given in Figure 1.



Figure 1. Rock salt heaps.

For analyses of the load and deformation behaviour of the heaps the Finite-Element-Method (FEM) in combination with elastoplastic constitutive laws for the soil and a viscoplastic constitutive law for the granular rock salt, developed at the Institute and Laboratory of Geotechnics of the TU Darmstadt, are used.

The verification of the developed constitutive law for the granular rock salt was done by back-analyses of laboratory tests and the monitoring data of specific projects. The paper focuses on the challenges of an extension of a tailings heap and the influence on a railway track as only 1 example from engineering practice (Katzenbach et al. 2004, Katzenbach et al. 2006).

2 PROJECT DESCRIPTION

In order to ensure the further production an existing 120 m high tailings heap needs to be extended (Figure 2).

The planned extension of the tailings heap approaches the railway track to the south. The existing heap was stored in blocks with a lower and an upper layer (Figures 3 and 4). The slope ratio is up to 40°. Since 2008 the extension is stored with layers on the slope (Figure 5).

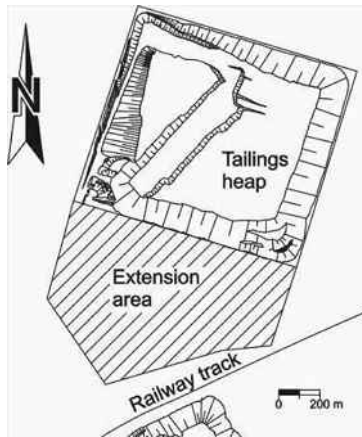


Figure 2. Site plan of the project.



Figure 3. Spreader on a heap.

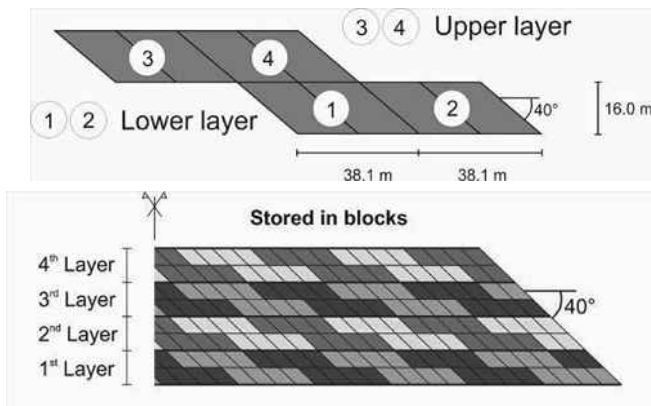


Figure 4. Schematic procedure of the block storing method.

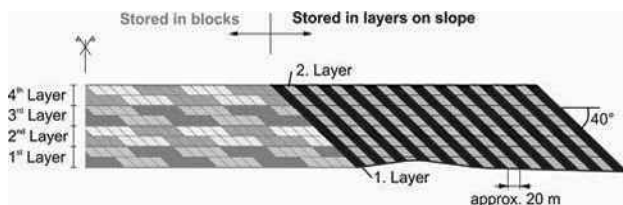


Figure 5. Schematic storing with layers on the slope.

The project area is situated in a glacial plain with a rather flat ground surface. The soil is horizontally stratified. At the surface a 5 m to 10 m thick layer of sand and marl glacial deposits was investigated. Below the sand and marl deposits a 50 m thick layer of quaternary sand with loose density was found, followed by a 130 m to 150 m thick layer of Rupel Clay and dense sand with varying layers of silt. At a depth of approximately 200 m

below the surface the new red sandstone begins. The groundwater level is about 5 m below the surface.

3 MATERIAL BEHAVIOUR OF GRANULAR ROCK SALT

The material behaviour of granular rock salt is characterized by a distinctive time and stress dependence. Initially fresh granular rock salt has a non-cohesive texture. After a short period the loose, granular rock salt converts into a cohesive texture with a high strength (Ankes 1972). The salt material attains a shear strength with a friction angle of $\phi' = 50^\circ$ and a cohesion of $c' = 850 \text{ kN/m}^2$, as well as a stiffness of $E_s = 2,500 \text{ MN/m}^2$. The material behaviour of the granular rock salt is strongly dependent to the deformation rate. High, overcritical deformation rates lead to high strength and stiffness of the rock salt and to brittle fracture. Small, undercritical deformation rates lead to minor strength and stiffness and to a plastic creep without fracture.

Directly after storing the granular stockpiled material has a density of $\rho = 1.4 \text{ to } 1.5 \text{ t/m}^3$. Due to the atmosphere, chemical processes and the pressure because of the increasing covering the granular stockpiled material in the core of the heap transforms nearly into solid body.

Under constant deviatoric stress the stockpiled material presents a constant creep behaviour despite a huge strength. The material behaviour of stockpiled material is strongly dependent on the state of stress and of the deformation rate. Figure 6 shows the results of two strain controlled triaxial tests on specimen of stockpiled material, obtained from core drillings from the top of a heap. For both tests a cell pressure of $\sigma_3 = 0.5 \text{ MN/m}^2$ was specified. Both deformation rates vary by the factor 1,000.

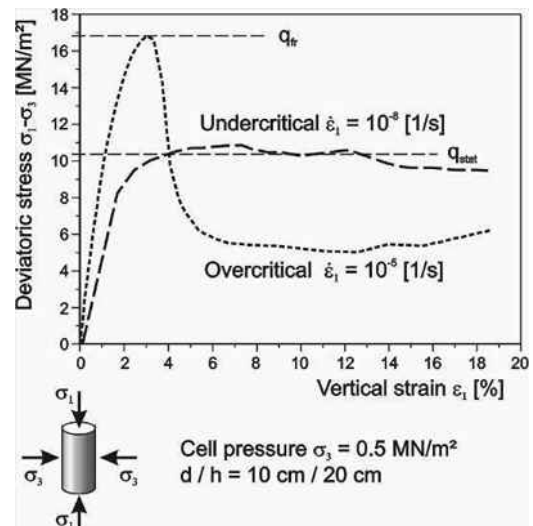


Figure 6. Typical results of strain controlled triaxial tests on stockpiled material samples.

The sample with the higher, overcritical deformation rate of $d\epsilon/dt = 10^{-5} \text{ 1/s}$ presents the usual material behaviour on high deformation rates. After the peak stress q_{fr} follows a deep drop of the deviatoric stress (brittle fracture). The sample with the lower (undercritical) deformation rate of $d\epsilon/dt = 10^{-8} \text{ 1/s}$ does not collapse. The sample creeps under a constant deviatoric stress q_{stat} .

On the left in Figure 7 is shown the specimen after the test with undercritical deformation rate. On the right is shown the specimen after the test with overcritical deformation rate.

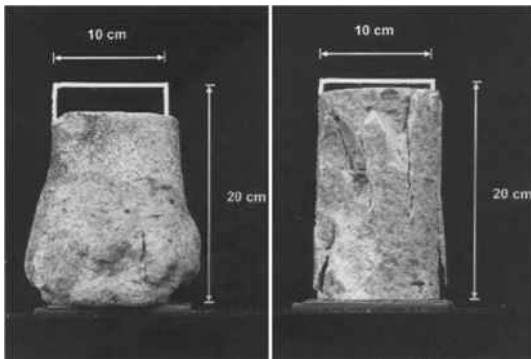


Figure 7. Specimens of triaxial tests with undercritical (left) and overcritical (right) deformation rates.

Due to deviatoric stress levels the stockpiled material creeps with high deformation rates at the beginning. The deformation rate decreases under constant deviatoric stress dependent on the time and approaches asymptotic the stationary creep rate (Figure 8).

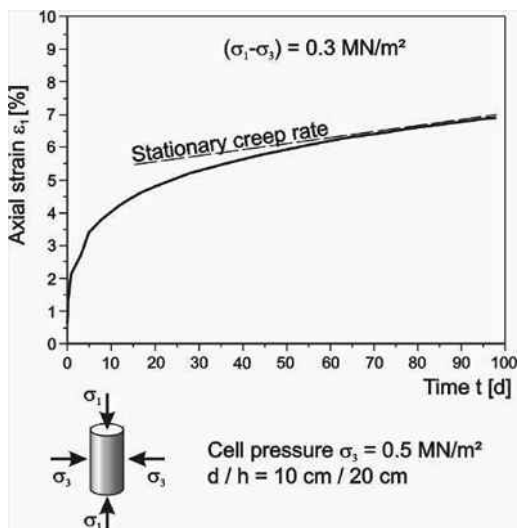


Figure 8. Typical creep curve of granular stockpiled material.

For further information of the material behaviour of granular rock salt see *Fordham 1988, Munsan and Wawersik 1991, Chumbe et al. 1996 and Boley 1999*.

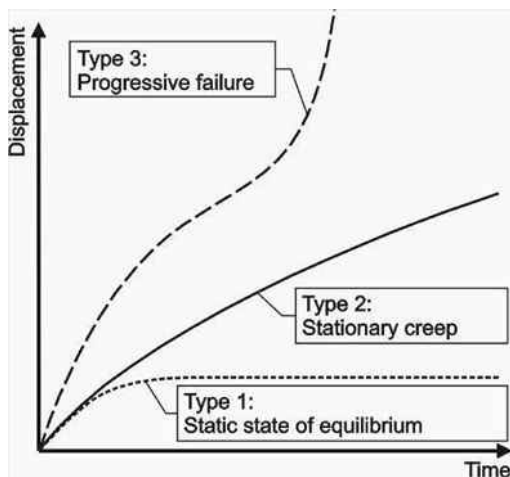


Figure 9. Deformation rate dependent system behaviour.

Although the heaps have a slow creep deformation and the soil has a continuously, slow changing load the heaps do not collapse due to the viscoplastic material behaviour of the granular rock salt as long as the deformation rate is undercritical. The collapse of the slope of a heap only results from a progressive failure (Figure 9) due to an increasing overcritical deformation rate. The system behaviour of a heap consisting of granular rock salt normally is like type 2 in Figure 9, if there is no weakening in the contact area.

On the basis of more than 150 triaxial tests a constitutive law for the material behaviour of granular stockpiled material was developed at the Institute and Laboratory of Geotechnics of TU Darmstadt (Boley 1999, Wachter 2009, Wachter and Katzenbach 2009). This constitutive law was implemented in a Finite-Element-Software for analyses of the ultimate limit state (ULS) and serviceability limit state (SLS) of granular rock salt heaps and infrastructures and buildings in the influenced area around the heaps.

4 ANALYSES OF THE EXTENSION OF THE HEAP

For analyses of the extension of a tailings heap and the influence on the railway track numerical simulations using the FEM were carried out. The model has a length of 1,800 m. The heap is 120 m high. Regarding the analyses of an extreme situation the groundwater level was set to the surface. The soil is modelled with an elastoplastic constitutive law based on a modified Drucker-Prager-Modell, the new red sandstone was modelled with an elastic constitutive law. The FE-Model is shown in Figure 10.

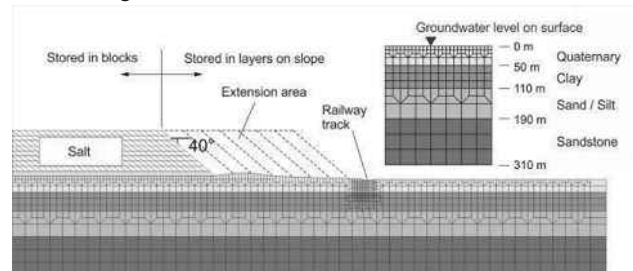


Figure 10. FE-Model of the soil and the heap before and after the extension.

The interaction between the tailings heap and the soil is modelled by a contact surface. The shear strength is defined by the friction law of *Coulomb*. The shear stress is proportional to the vertical stress. The time dependent material behaviour and the changing geometry of the heap are considered by a step-by-step analysis.

Figure 11 shows the analysed cross sections. The horizontal distance s_i of the toe of the slope to the railway track is varying along the track.

The relative deformations and the deformation rates have been calculated. The deformation rates increase when the extension approaches the railway track and decrease to a low rate when the extension area is totally filled up.

Due to the complexity of the project and the interaction between soil, heap and the infrastructure an extensive monitoring program according to the observational method was installed. The main part of the monitoring program consists of geodetic and geotechnical measurements (Figure 12).

For example the measured, absolute, horizontal displacements orthogonal to the toe of the slope of 2 measurement points are presented. The measurement point MR 54 is at the toe of the slope before the extension started. The measurement point MR 51 had a distance of 150 m to the toe of the slope before the extension started.

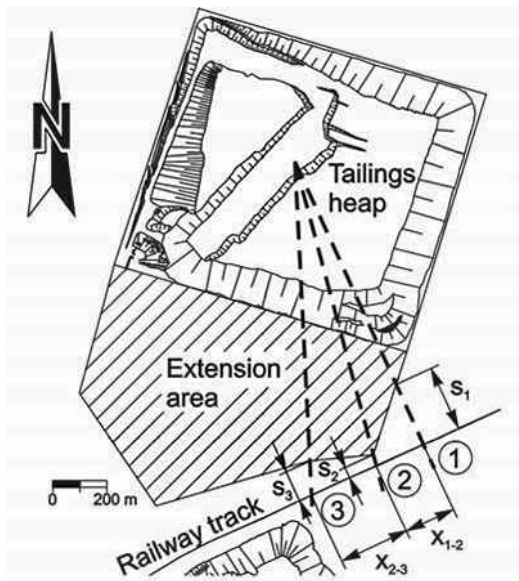


Figure 11. Cross sections for the analyses of the deformation of the railway track.

The measurement point MR 54 had a horizontal displacement of 0.30 m before it was covered with salt. After the covering no further measurement data for this point existed. The measurement point MR 51 had a horizontal displacement of 0.45 m before it was covered with salt.

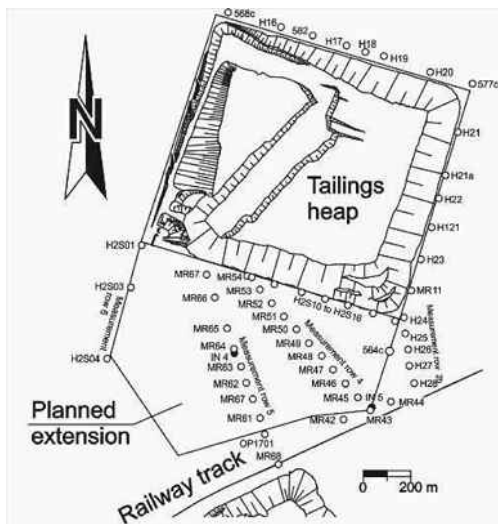


Figure 12. Geodetic and geotechnical monitoring program.

For calibration of the numerical simulations the calculated displacements are compared to the measurement data. In result numerical simulations supply horizontal displacements in a comparable range.

5 CONCLUSIONS

Due to the storing of granular residues of potash production on large tailings heaps enormous loads are transferred into the soil. In this context vertical and horizontal deformation occur even in a distance of hundreds of metres. For analyses of the ultimate limit state and the serviceability limit state of the heaps and infrastructures and buildings in the area of influence realistic simulations are necessary.

Using a complex constitutive law for the viscoplastic stockpiled material, developed at the Institute and the Laboratory of Geotechnics of TU Darmstadt, the numerical simulations of an extension of a heap and the influence on a railway track were investigated. The comparison of the results of the numerical simulations and the monitoring program shows a good accordance.

The developed constitutive law can be judged as a robust, efficient and purposeful material routine which offers an instrument for the simulation and investigation of complicated, time variant systems using numerical simulations.

6 REFERENCES

- Ankes, A. 1972. Untersuchung bodenphysikalischer Eigenschaften von Rückstand. *Dissertation an der Fakultät für Technische Wissenschaften der Bergakademie Freiberg.*
- Boley, C. 1999. Untersuchungen zur Viskoplastizität und Festigkeit von Steinsalz. *Mitteilungen des Institutes und der Versuchsanstalt für Geotechnik der Technischen Universität Darmstadt, Heft 48.*
- Chumbe, D., Lloret, A., Alonso, E. 1996. Creep and permeability tests on compacted granular salt. *4th Conference on the Mechanical Behaviour of Salt*, Montreal, Canada, 331-339.
- Fordham, C.J. 1988. Behaviour of granular halite for use as a backfill in potash mines. *Dissertation at University of Waterloo, Canada.*
- Katzenbach, R., Giere, J., Seip, M. 2004. Stability and serviceability of a railway track and a gas pipeline at the base of steep creeping slopes. *1st European Regional International Association for Engineering Geology Conference*, Liège, Belgium, 11 p.
- Katzenbach, R., Giere, J., Seip, M. 2006. Aspects of safety and serviceability of heaps with viscoplastic materials due to man-made liners or natural slip-surfaces. *Geo Environmental Engineering Conference*, Kyoto, Japan, 237-244.
- Munson, D.E., Wawersik, W.R. 1991. Constitutive modelling of salt behaviour – state of the technology. *7th International Conference on rock mechanics, Workshop on Rock Salt Mechanics*, 1797-1810.
- Wachter, S. 2009. Dreidimensionale, zeitvariante stoffliche Modellierung von granularem Steinsalz. *Mitteilungen des Institutes und der Versuchsanstalt für Geotechnik der Technischen Universität Darmstadt, Heft 82.*
- Wachter, S., Katzenbach, R. 2009. CAPCREEP – Ein benutzerdefiniertes Stoffmodell zur Untersuchung von Rückstandshalden. *Bauingenieur 84, Heft 9*, 368-373.

In-situ tests of permanent prestressed ground anchors with alternative designs of anchor bond length

Essais in situ des tirants d'ancrage précontraints permanents avec des conceptions alternatives de la longueur de scellement

Klemenc I.
Slovenian National Building and Civil Engineering Institute

Logar J.
University of Ljubljana, Faculty of Civil and Geodetic Engineering

ABSTRACT: Some concepts of cost efficient ground anchors with enhanced pull-out resistance from single borehole already exist: single bore multiple anchors (Barley, 1990) and prestressed ground anchors of variable stiffness (Škrabl, 2004). A third alternative with anchor bond length of increased stiffness has been proposed. All three concepts have been combined with the concept of comprehensive corrosion protection. Five anchors of all three design alternatives as well as ten investigation tests on standard permanent prestressed ground anchors were tested in-situ on a large retaining wall in N-E Slovenia. The paper presents the design of each type of anchor bond length, test procedure and test results. The test results of our in-situ research on the specific location show that the highest anchor pull-out resistance was obtained for the anchor bond length of increased stiffness.

RÉSUMÉ: En plus des conceptions existantes d'augmentation de la résistance des tirants d'ancrage dans un même forage avec un bon rapport coûts-efficacité, tels les tirants à torons multiples (technologie SBMA – Barley, 1990) et les tirants précontraints de rigidité variable (Škrabl, 2004), nous proposons une troisième alternative: les tirants d'ancrage à rigidité renforcée. Les trois types étudiés ont été combinés parallèlement avec une conception de protection anti-corrosion. Nous avons testé in situ des ensembles de cinq groupes de chacun des trois types proposés et de dix tirants d'ancrage standard, sur une construction de soutènement importante réalisée dans la partie nord-est de la Slovénie. Dans cet article nous présentons le dimensionnement de la longueur de scellement de tous les types de tirants d'ancrage ainsi que le déroulement et les résultats des essais effectués. Les résultats des essais in situ démontrent que la résistance maximale est obtenue avec la longueur de scellement du tirant à rigidité renforcée.

KEYWORDS: ground anchor, design of bond length, pull-out resistance, in-situ test, comprehensive corrosion protection.

1 INTRODUCTION

In 1934 the first prestressed ground anchors were built during the raising of the Cheurfas Dam (Algeria). Such anchors have been increasingly used since then, in cases, where the execution of other geotechnical measures is significantly more difficult, more expensive or even impossible. The most widespread is the use of the friction tensile type of ground anchors (Limelette, 2008), with which the technological design and implementation of the corrosion protection has reached a level that promises a long-term operation (provided that adequate maintenance is ensured). This especially applies to anchors with a comprehensive corrosion protection, which was two decades ago developed in Switzerland: the steel parts of these anchors are encapsulated by a waterproof polyethylene (PE) cover, which also provides electrical isolation of steel parts against the environment. In parallel with technological improvements, the price of anchors has also grown. Therefore, increasing tendencies to rationalize anchors have appeared.

Three different simple modifications of a permanent prestressed anchor bond length were designed and investigated in order to achieve higher values of pull-out resistances and better efficiencies of anchors. The prototypes of such alternative anchors were installed and tested in a testing field. The obtained results were compared with those of reference anchors.

2 ALTERNATIVE DESIGNS OF BOND LENGTHS

The starting-point in the task of searching for the most effective concept of permanent prestressed ground anchors with the tendon contained within joint PE cover were reference (standard) anchors **RCP/D**. These anchors were used in a retaining wall that served as a test site. The total length of each

individual anchor is $l = 35$ m with the tendon bond length of $l_v = 7$ m, consisting of six low-relaxation strands $\varnothing 15.2$ mm ($f_{p0.1k}/f_{pk} = 1670/1860$ MPa).

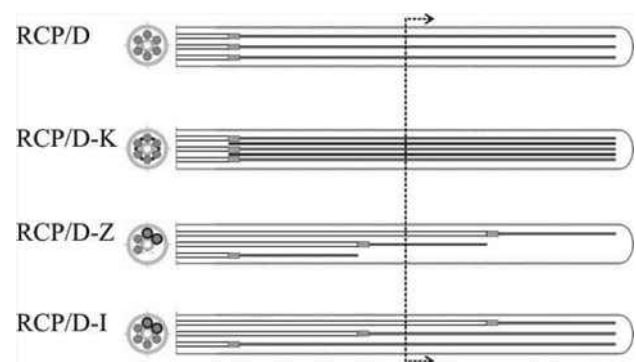


Figure 1. Conceptual designs of bond lengths of permanent prestressed strand anchors with joint PE encapsulation: reference anchor RCP/D, alternative types of anchors RCP/D-K (increased stiffness of bond length), RCP/D-Z (multiple anchor) and RCP/D-I (anchor of variable stiffness).

Three different conceptual designs of anchor bond lengths (Fig. 1) were conceived and implemented with the intention to improve stress distribution along the tendon bond length and to consequently increase the pull-out capacity of anchors:

- anchors with *increased stiffness of bond length*, with which six additional steel wires $\varnothing 5$ mm were placed in empty spaces among bond lengths of strands (type **RCP/D-K** with strand free lengths of 28 m and strand bond lengths of 7 m),
- *multiple anchors with staggered anchor units* based on the idea of Barley's anchors SBMA, only that three anchor units

(two strands each) of 2.2 m bond length were not installed into a borehole as independent elements but were placed into the joint corrugated PE duct (type **RCP/D-Z** with strand free lengths of 28 m, 30.4 m and 32.8 m),

- *anchors with variable stiffness of bond length* after the patent of Škrabl, 2004, with the tendon combined of three anchor units (2 strands each), with strand free lengths of 28.0 m, 30.4 m and 32.8 m, and with strand bond lengths of 7.0 m, 4.6 m and 2.2 m (type **RCP/D-I**).

3 IN-SITU TESTING

The test field has been located at the level of the middle berm of a larger retaining wall, where load-bearing stratum consists of marl and silty marls with thin lenses of siltstone and sandstone. A total of 18 anchors were installed: three reference RCP/D anchors and five anchors of each alternative type (RCP/D-K, RCP/D-Z and RCP/D-I). Boreholes, deflected 15° downwards, were drilled with a chisel (Ø 140 mm) using air-flushing for the removal of drill spoil. The ratio of 6-strand anchor steel cross-sectional area to cross-sectional area of the borehole equaled 5.5% of the theoretical cross-sectional area of the borehole. The appearance of moist in the ground was repeatedly detected in the region of the anchor bond lengths. Cement grout with w/c ratio of 0.42 was used for grouting within the PE encapsulation as well as for the collar of the borehole with an average grout consumption of about 17 dm³/m¹.

At in-situ testing individual strands were tensioned with monostrand jacks, connected to a joint hydraulically synchronized system (Fig. 2). An electrical load cell was used for the precise adjustment of stressing forces. Extensions and creep behavior of strands were measured with digital displacement transducers, attached on the monostrand jacks.



Figure 2. Test setup for simultaneous stressing of all strands of prestressed ground anchors using monostrand jacks.

As a measure for the assessment of load-bearing characteristics of anchor bond lengths creep displacement rate k was used (Ostermayer, 1975):

$$k = \frac{s_2 - s_1}{\log \square t_2/t_1} \quad (1)$$

where s_1 and s_2 are head displacements at times t_1 and t_2 , respectively. For the failure of anchor bond length the critical creep displacement rate $k_{crit} = 2$ mm was used.

All reference anchors and one anchor of each alternative type were tested up to the maximum test load $P_{pv} = 1254$ kN (80 % steel tensile strength R_m) or until failure of anchor bond length was reached (*investigation test* - IT). Other alternative

anchors were tested using the same procedure, except that the test was stopped at the first sign of anchor bond length failure, i.e. as soon as k_{crit} appeared (*comprehensive suitability test* - CST). All test field anchors were tested according to the loading procedure and methodology for IT as described in Swiss standard SIA 267/1, which is very similar to test Method 1 of standard EN 1537: each anchor was loaded in eight incremental cycles from a datum load $P_a = 150$ kN (10 % R_m) to the maximum test load P_{pv} . The increments of strand extensions were measured at the end of specified time intervals, which were used for the evaluation of k values. Individual strand extensions as well as average extensions for all strands of the RCP/D-I anchor SBZ-33 at load level $P_6 = 978$ kN of CST are presented on the left diagram of Fig. 3. The right diagram shows the development of apparent free lengths l_f of individual strands during the same CST, which is based on the measured elastic displacement Δs_{el} at load decreasing from current level P_i to the initial level P_a , knowing the characteristics of the tendon (cross-section area A_p and modulus of elasticity E_p):

$$l_f(P_i) = \frac{\Delta s_{el}}{P_i - P_a} A_p E_p \quad (2)$$

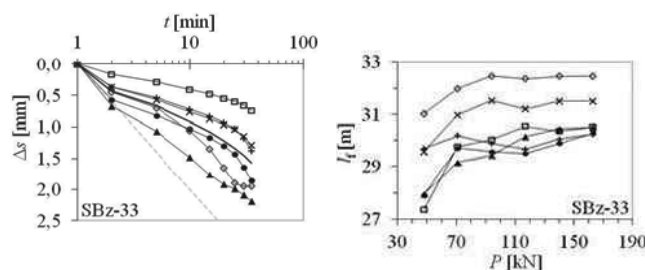


Figure 3. Measured increments of displacements of the anchor SBZ-33 (type RCP/D-I) at load level P_6 of CST (left), apparent free lengths of individual strands l_f during CST (right).

The behaviour characteristics of anchor bond length could be recognized only on the basis of strand extensions, measured on displacement transducers, fixed on the monostrand jacks. The problem is that due to the limited amount of data and the inability of physical insight into the bond lengths deep in the load bearing stratum, we cannot always directly link measured extensions with creep displacement rate k of the bond length (i.e. it is not necessary that each measured strand extension actually originates from the bond length deterioration). Therefore, in the analysis of the in-situ test results it is recommendable to compare the k values of individual strand with the k values of other individual strands of the same tendon, with k values of anchor units (average of two strands, only at types RCP/D-Z and RCP/D-I), with the average k values of all strands, as well as with the permanent displacements Δs_{bl} and apparent free lengths l_f , obtained after each loading stage. In order to prevent sudden failures of bond lengths at CST, an appropriate software tool was prepared to enable simultaneous recording and evaluation of the most important behaviour parameters of an anchor during in-situ test.

4 ANALYSIS OF RESULTS OF THE IN-SITU TESTING

There are several possible failure mechanisms at the anchor bond length, which occur at the IT of prestressed ground anchor with a comprehensive corrosion protection: inside or outside the PE corrugated duct, under some circumstances it may also come to the rupture of PE duct. The types and incidences of individual mechanisms depend on the design of bond length and packing connections at the transition between strand free and bond lengths, possible surface contamination of the bare strand bond length, the design, dimensions and distribution of the constituent components of anchors, local conditions in the ground,

configuration of strands in the bond length, drilling and flushing techniques as well as specifics of grouting. According to the principle of the weakest link in the chain, there starts a mechanism that occurs at the lowest load level, although in the following load steps some additional mechanisms may also occur.

The bond lengths (2.2 m) of the shortest anchor units (RCP/D-Z and RCP/D-I anchors) were determined according to the available anchor bond length 7 m and previous experience (Barley and Windsor, 2000, Bruce et al., 2007). The bare strands of the bond length of RCP/D and RCP/D-K anchors were spirally rotated along the longitudinal axis, while the strands of the short bond length of RCP/D-Z and RCP/D-I anchors were straight. The bare strands of the bond length of RCP/D anchors (and to a certain extent of RCP/D-K anchors) were additionally arranged in a pattern of alternating spatial extension and compression of strands. Although the lengths of strand bond lengths were selected in accordance with the aforementioned recommendations, the analysis of the in-situ test results of RCP/D-Z and RCP/D-I anchors showed predominant mechanism of pull-out of strands bond length from cement grout inside the corrugated PE duct. Such behavior can be associated with the greasing technology of strand free length, in which some strands in bond lengths can be locally stained with vaseline, although most of the stains were later on removed. Contrary to expectations, only in individual cases of RCP/D and RCP/D-K anchors, there appeared the pull-out mechanism of the whole tendon from the cement grout inside corrugated PE duct. Such behaviour can be partly ascribed to the local contamination of bare strands with vaseline stains, and partly to the direct contact of strand bond lengths with the bottom part of the corrugated PE duct (no minimum grout cover was provided).

The behaviour of anchor bond length is reflected in the most important outcome of the IT: pull-out resistance R_a , which is determined as the intersection of experimentally obtained curve of interval creep displacement rate k_{int} to the assumed margin that denotes the failure of an anchor $k_{crit} = 2$ mm. In cases where such intersection does not exist, the failure of anchor bond length is not reached – in these cases the standard SIA 267/1 allows for an extrapolation of R_a as a proof load extrapolated up to 10%. The problem with this assessment remains when the anchor bond length can be assessed as failed, or in other words, in those cases when it is a reasonable to expect that the anchor bond length would be able to sustain a load of $1.10 P_{pv}$. The analysis of in-situ obtained test results for the considered type of anchors showed: if the following criteria are satisfied, this could be a suitable basis for 10 % extrapolation of P_{pv} , provided that the estimate is made by an experienced specialist:

- linear trend approximation of the creep displacement rates at the proof load P_{pv} (considering all strands and the anchor as a whole) should not exhibit any noticeable increase in creep rate,
- maximum creep displacement rate in each time interval after the second minute of observation (for each strand and the anchor as a whole) must not exceed the criterion of failure k_{crit} ,
- the interval creep displacement rate $k_{int}(P_{pv})$, of each strand and the anchor as a whole should not be greater than 1.35.

Results of all performed in-situ tests are presented as values of pull-out resistances R_a [kN] (Table 1) as well as in the diagrams of interval creep displacement rates k_{int} obtained at all stages of IT and CST (Fig. 4).

The general impression in the ratio of pull-out resistances among various types of tested anchors can already be obtained on the basis of visual assessment of the curves in the diagrams: the highest values of anchor bond length resistance (i.e. high loads P reached at low values of k_{int}) were achieved at RCP/D-K anchors with increased stiffness of bond length, which slightly exceeded the bond length resistance of reference RCP/D anchors. An unexpectedly rapid failure of two reference RCP/D anchors was a result of problems at grouting (anchor SBz-23)

and distinctive slip of two strands, probably due to bare strand contamination with vaseline (anchor SBz-59). On the other hand, multiple anchors with staggered bond lengths (RCP/D-Z type) demonstrated the poorest performance of all tested anchors due to early failure of bond lengths at low load stages of IT or CST (deterioration of bond between strands and cement grout resulted in the pull-out of the strands). The behaviour of RCP/D-Z and RCP/D-I anchors was probably influenced by the surface contamination with vaseline as well as configuration of strands in the bond length. Additional impairment of the conditions within the corrugated PE duct was caused by the use of soft and relatively spacious packing connections in the transition between anchor unit bond and free length.

Table 1. Results of in-situ tests: pull-out resistances R_a [kN] of all tested anchors of reference and alternative types.

RCP/D	RCP/D/K	RCP/D/Z	RCP/D/I
Anchor R_a [kN]	Anchor R_a [kN]	Anchor R_a [kN]	Anchor R_a [kN]
TS-01* 800	SBz-89* 1254	SBz-56* 702	SBz-86* 1144
TS-02* 979	SBz-18# 978	SBz-36# 694	SBz-12# 604
TS-03* 981	SBz-39# 1231	SBz-63# 469	SBz-33# 1248
TS-04* 1015	SBz-66# 1220	SBz-81# 837	SBz-60# 789
TS-05* 1095	SBz-84# 978	SBz-15# 400	SBz-78# 840
TS-06* 1195			
TS-07* 1227	* ... Result of IT.		
SBz-23* 651	# ... Result of CST.		
SBz-56* 1211			
SBz-59* 642			

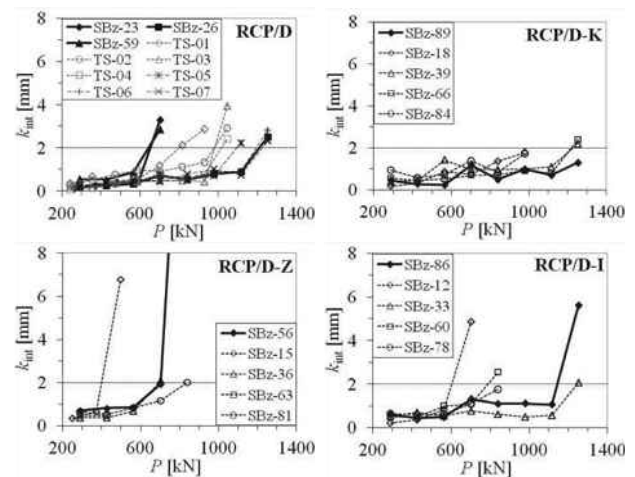


Figure 4. Interval creep displacement rates k_{int} for reference testing anchors as well as for all types of alternative anchors.

To confirm the relationships among pull-out resistances R_a (Table 1) a one-sided Student's T-test with unequal variance was used to check whether the average values of different types of anchors differ significantly from each other.

Results of testing the hypothesis of the equality of the means of two normal populations at the 5 % significance level showed that the mean value of RCP/D-Z anchor pull-out resistance was statistically typically lower than the mean values of pull-out resistance of reference RCP/D and alternative RCP/D-K anchors (Table 2). Somewhat unexpectedly, using statistical methods we could not confirm that the mean value of RCP/D-Z anchor pull-out resistance was statistically typically lower than the mean value of pull-out resistance of RCP/D-I anchors, as it

could be inferred only on the basis of visual comparison of the curves in the graphs in Fig. 4.

Table 2. Results of one-sided Student's T-test with unequal variance of mean pull-out resistances R_a for reference and alternative anchors.

	RCP/D	RCP/D-K	RCP/D-Z	RCP/D-I
Mean	980	1132	620	925
Variance	47770	19965	32622	70263
Standard deviation	218,6	141,3	180,6	265,1
Coef. of variation	0,223	0,125	0,291	0,287
RCP/D	–			
RCP/D-K	13,0 %	–		
RCP/D-Z	0,7 %	0,1 %	–	
RCP/D-I	70,3 %	17,3 %	7,1 %	–

5 CONCLUSIONS

Based on the theoretical background of bond length behaviour of a prestressed ground anchor and the patents of Barley and Škrabl, three types of anchors with alternative concepts of bond lengths inside PE encapsulation (RCP/D-K, RCP/D-Z and RCP/D-I types) were designed, installed and tested at a test field. The behaviour of alternative types of anchors was compared with the behaviour of the reference RCP/D anchors. Different aspects of design (especially limited anchor bond length of 7 m, the diameter of available type of corrugated PE duct), formation, manufacturing details and installation of testing field anchors resulted in different pull-out resistances R_a and they indicate the relations among bond length capacities of different anchor types.

Test results of 25 anchors showed that the maximum values of pull-out resistance R_a were reached at the modified RCP/D-K anchors with increased stiffness of bond length - the mean values of R_a of RCP/D-K anchors exceeded the mean values of R_a of RCP/D anchors by 16 %. Although the free space within the corrugated PE duct of bond length of the RCP/D-K anchors was very restricted, allowing only \varnothing 5 mm additional steel wires to be installed (instead of originally planned \varnothing 12.5 mm steel strands), high values of pull-out resistances of RCP/D-K anchors were obtained. The behaviour of RCP/D-Z and RCP/D-I anchors was probably influenced by the surface contamination with vaseline as well as the configuration of strands in the bond length. Additional impairment of the conditions within the corrugated PE duct was caused by the use of soft and relatively spacious packing connections in the transition between anchor units bond and free length. The RCP/D-Z anchors demonstrated the poorest performance of all tested anchors (the bond length of RCP/D-Z anchors failed at low force levels of IT and CST). In all cases local debonding at the strand/grout interface resulted in the pull-out of strands. With improvement of particular technological details of alternative anchors, higher values of pull-out resistances can be expected. According to the experiences of Barley with multiple anchors, the pull-out resistances of RCP/D-Z anchors should attain (and probably exceed) the pull-out resistances of reference RCP/D anchors, provided that the pull-out of strands from cement grout, placed within the corrugated PE duct, is prevented. At least it is necessary to provide the immaculate condition of bare strands in the bond length within the PE encapsulation. Moreover, it is also possible that instead of RCP/D-K anchors the highest values of pull-out resistance could be achieved at one of the other alternative types (RCP/D-I or RCP/D-Z).

With the intention to increase the efficiency of alternative types of permanent prestressed anchors (RCP/D-K, RCP/D-Z and RCP/D-I) the following improvements are suggested:

- Results of field testing confirm the already known fact (Littlejohn, 1993, Hanna, 1982) that for effective performance of bond length the bare strands should be covered with sufficiently thick layer of cement grout, irrespective of the anchor bond length design.
- The efficiency of anchor bond length could be improved with the increase of corrugated PE duct diameter. In that case the region around bare strands within corrugated PE duct could be reinforced (spiral micro reinforcement, cement grout with admixed fibres, etc.). Simultaneously, extra space would be gained for noding or local deforming of strands.
- The efficiency of RCP/D-Z and RCP/D-I anchors could also be improved by upgrading the technological detail of anchor unit packing connections at the transition between strand bond and free lengths. Performance of RCP/D-z and RCP/D-I anchors could also be improved if the greased and sheathed strands in the free length would possibly be replaced with some other solution that offers higher stiffness in radial direction.
- For specific design of RCP/D-Z and RCP/D-I anchors the combination of strand and anchor unit noding is suggested, whereat the minimal anchor unit strands bond length should be 2.5 m (in case of the increased diameter of corrugated PE duct) and 3.0 m (in case of the unchanged diameter of corrugated PE duct).

6 ACKNOWLEDGEMENTS

The authors are grateful to the Slovenian motorway agency DARS, for their financing of the research project. We are also much obliged to the manufacturer CA.TI. Carnica Tiranti, Srl, Italy for their donation of the anchors, and to the contractor GEOT for successful installation and in-situ testing of anchors.

7 REFERENCES

- Barley A.D. 1990. Ground anchorage containing a multiple of ground anchorages : patent number EP 0 356 215 A2. European Patent Office.
- Barley A.D. and Windsor C.R. 2000. Recent advances in ground anchor and reinforcement technology with reference to the development of the art. International conference on geotechnics and geotechnical engineering, vol. 1. 19th – 24th November 2000, Melbourne, Australia. Basel, Lancaster: 1157-1252.
- Bruce M.E.C., Gómez J., Traylor R.P. 2007. Repeated lift-off testing of single bore multiple anchors for dam retaining wall over a 5-year period. V: Littlejohn, G.S. (ed.). International conference on ground anchorages and anchored structures in service. ICE London, November 2007. London, Thomas Telford: str. 111-119.
- Hanna T.H. 1982. Foundations in tension : ground anchors. Trans Tech Publications. New York, McGraw Hill Book Co.
- Hutchinson D. and Diederichs M. 1996. Cablebolting in underground mines. Richmond, Canada, BiTech Publisher Ltd.
- Klemenc I. 2011. Investigation tests of permanent prestressed strand ground anchors with various designs of tendon bond length : doctoral thesis (in Slovene). Ljubljana.
- Limelette test fields results. 2008. Proceedings of the international symposium ground anchors. 14 May 2008, Brussels, Belgium.
- Littlejohn S. 1993. Overview of rock anchorages. Hudson, J.A. (ed.). Comprehensive rock engineering : excavation, support and monitoring, vol. 4. Oxford, Pergamon Press.
- Ostermayer H. 1975. Construction, carrying behaviour and creep characteristics of ground anchors. Conference on Diaphragm Walls and Anchorages. ICE London, September 1974, 141-151.
- Škrabl S. 2004. Prestressed ground anchors of variable stiffness : patent number 21320 (in Slovene). Ljubljana : SIPO.

Response of piled buildings to deep excavations in soft soils

Déformations des bâtiments liés aux excavations profondes situés dans les sols mous

Korff M.
Delft and Cambridge University

Mair R.J.
Cambridge University

ABSTRACT: This paper explores the building displacements related to deep excavations for a case study from the Netherlands: the construction of the North South Metro Line in Amsterdam. The overall goal of the analysis of the displacement is to study the interaction of deep excavations with piled buildings. The response of buildings is governed by the soil displacements resulting from the excavation. These displacements are described in a second, related paper in this conference. In this paper, the response of the piled buildings is described.

RÉSUMÉ : Les auteurs ont analysé déformations des bâtiments liés aux excavations profondes à Amsterdam pour la Ligne nord/sud. L'objectif général de l'analyse des déformations est d'étudier l'interaction des excavations profondes avec des bâtiments sur pieux. La réponse des bâtiments est régie par les déformations du sol résultant de l'excavation. Ces déformations, du niveau de la surface et de niveaux plus profonds, sont décrites dans un article connexe à cette conférence. Dans le document présent, la réponse des bâtiments sur pieux est décrite.

KEYWORDS: deep excavation, ground displacement, piles.

1 INTRODUCTION

The North-South Line in Amsterdam passes under the historical centre of the city in twin tunnels. Five underground stations are currently under construction. Rokin, Vijzelgracht and Ceintuurbaan Station are three of the deep stations in the historic city centre. They are built using the top down method, see Figure 1. In a related paper for this conference by the same authors, the construction method and ground displacements related to the deep excavations have been described. The settlement measurements for the Amsterdam deep excavations have been compared to several, mostly empirical, relationships to determine the green field surface displacements and displacements at depth. In summary, the surface displacement behind the wall is 0.3 – 1.0% of the excavation depth, if all construction works are included. Surface displacements behind the wall can be much larger than the wall deflections and become negligible at 2-3 times the excavated depth away from the wall. The shape of the displacement fits the proposed profile by (Hsieh and Ou 1998) best. In all three of the Amsterdam cases, the largest effect on the ground surface displacement can be attributed to the preliminary activities, which include amongst others the diaphragm wall construction, jet grout strut installation and construction of the roof, and took in total about 4 years. See Table 1 for details.

Table 1 Construction activities and dates for Ceintuurbaan

Construction activity	End date
Base monitoring start 2001	2003-11-01
Preliminary activities	2007-04-01
Excavation to NAP -6.2m	2007-09-13
Excavation to NAP -15.3 m	2007-12-10
Excavation to NAP -19.4 m	2008-03-01
Excavation to NAP -24 m	2008-08-01
Excavation to NAP -25.6 m	2009-06-24
Floor construction, pumping test	

The actual excavation stage caused only about 25-45% of the surface displacements, with 55-75% attributed to the

preliminary activities. At larger excavation depths the influence zone is significantly smaller than 2 times the excavation depth.

This paper describes the building displacements related to the excavation works in more detail.

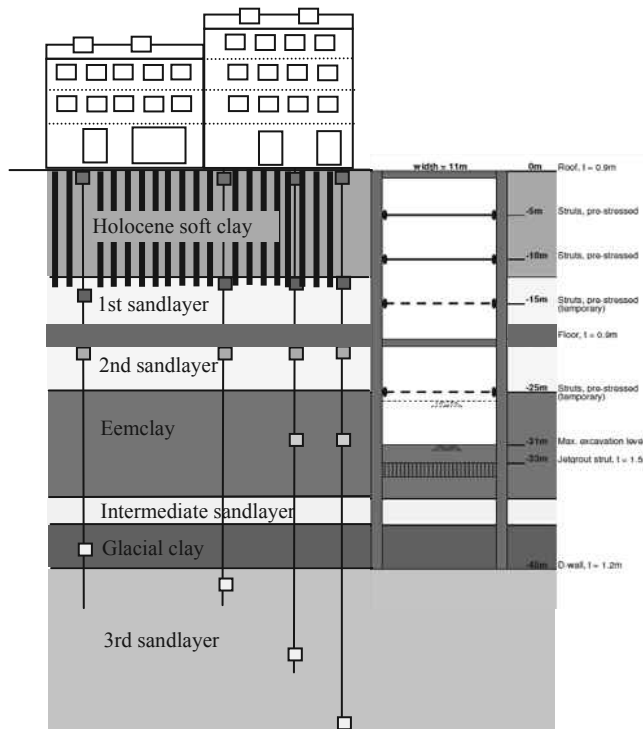


Figure 1 Cross section of Ceintuurbaan Station with soil profile and extensometer locations.

2 SOIL-STRUCTURE INTERACTION

The excavation-induced displacements described in the related paper can be considered as green field displacements. To assess the potential impact of these ground displacements on buildings, these displacements are usually directly projected onto the building, leading to bending and shear strains in the structure. It is however known that the presence of the building and the interface between building and soil also influences the settlement trough and transfer of deformations to the building. (Potts and Addenbrooke 1996, Franzius et al. 2006 and Farrell 2010) have shown this for displacements related to tunnels and (Goh and Mair 2011) for buildings influenced by deep excavations. (Goh and Mair 2011) modified the relative stiffness proposed by Potts and Addenbrooke for tunnelling to the following for deep excavations:

$$\rho_{exc}^* = \frac{EI}{E_s L^3} \quad (1)$$

$$\alpha_{exc}^* = \frac{EA}{E_s B} \quad (2)$$

where EI is the building stiffness, E_s a representative soil stiffness and L the length of the building in either hogging or sagging. EA is the axial stiffness of the building and B is the total length of the building.

Furthermore (Jacobsz et al. 2005) described the soil-structure interaction in more detail for piled buildings related to tunnelling. In Amsterdam the piled buildings were influenced by deep excavations, which requires a combined approach influenced by the presence of pile foundations: the initial stresses in the foundation and the ground, and possible load transfer within the building. If these effects are not considered, the current assessment methods may be too conservative or too optimistic, leading to costly measures either being taken unnecessarily or having to be applied at a late stage in the project.

3 BUILDING AND FOUNDATION CHARACTERISTICS

Most buildings in the historic centre of Amsterdam are built with masonry walls, wooden floors and timber pile foundations, the piles being founded in the First Sand Layer at about 12m below the surface level (see Figure 1). More recent buildings with 1-4 storeys are built with concrete walls and floors and prefabricated concrete or steel piles. Foundations for some recent buildings are in deeper layers such as the second sand layer. The buildings considered in this paper are from the older type, see Figure 2.



Figure 2 Historic buildings at Vijzelgracht (left) and Ceintuurbaan Station (right), dated 1880-1920

The wooden piles are installed in pairs, see Figure 3, with 0.8m between the pairs. Pile diameters for the timber piles vary from

160 - 300 mm (typical 180-200 mm) at the head and usually diminish by 8 mm/m to about 70-200 mm (typical 120-140 mm) at the toe. Based on several pile load tests in the historic centre it is known that the wooden pile foundations have low factors of safety. Up to 15% of the buildings of this age in Amsterdam are not up to current standards, according to (van Tol 1994). A large number of timber piles deteriorate due to decay of the wood, which may lead to a different kind of building response; this effect is not described here.

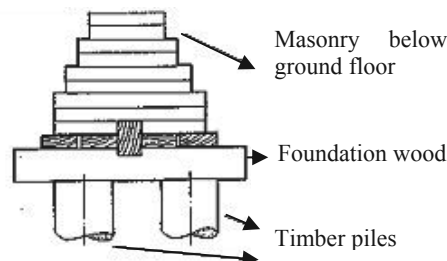


Figure 3 Typical cross section of base of the wall in masonry buildings (Zantkuyl 1993)

Two typical load-displacement curves are shown in Figure 4. The timber piles in failure generally find 60% of their capacity at the toe, 10% as friction in the sand layer and 30% as friction in the Holocene clay the maximum shaft friction develops at a relative displacement of about 25 mm and in the base sand layer at about 15 mm. The maximum base capacity for piles with average diameter at the base of 130 mm is reached at about 10% of the diameter, which is consistent with common design methods. The high horizontal flexibility assures that the piles can move rather easily with the soil in horizontal direction, compared to concrete piles.

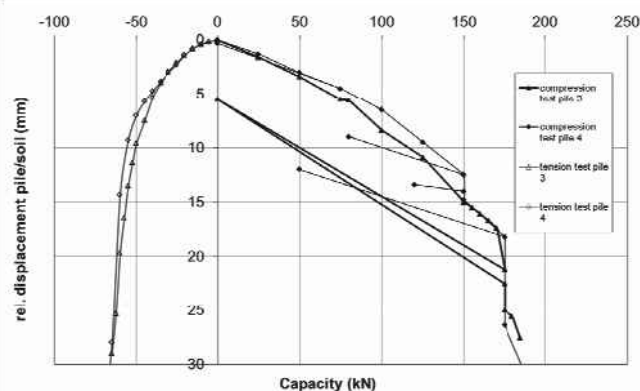


Figure 4 Representative load-settlement curves for timber piles in Amsterdam (Hoekstra 1974)

To determine the response of piled buildings to excavations knowledge of the current state of the piles is essential. Most piles in the historic centre of Amsterdam will already have experienced the maximum negative skin friction possible over time. The presence of soft soil layers combined with earlier city developments which included raising of the ground level causes on-going subsidence due to consolidation and creep. Negative skin friction develops as a result along the shaft of a pile when the soil surrounding the pile settles more than the pile itself. Positive skin friction occurs in opposite circumstances when the pile settles more than the surrounding soil. Both forces are likely to act on the timber piles in Amsterdam, see Figure 5.

4 RESPONSE OF PILED BUILDINGS

For end bearing piles with sufficient factor of safety the neutral level is found close to the location of the bearing layer. For the most historic Amsterdam foundations, the reserve capacity is smaller, and positive skin friction is also found in the soft or settling layers. The maximum force in the pile is found at the neutral level (the level at which the soil and pile settlements are the same and the shear stresses acting on the pile change direction). Usually in Amsterdam, it is considered that the negative skin friction is already fully mobilized before the excavation takes place.

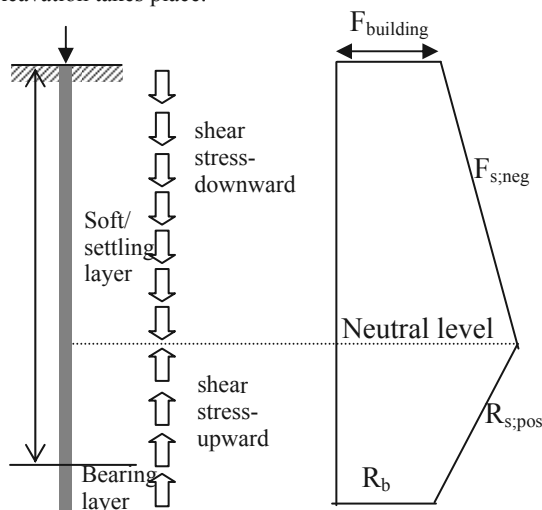


Figure 5 Development of negative and positive skin friction along a pile with low factor of safety

Buildings in the influence zone of the excavation may experience several phenomena:

1. reduction of pile capacity due to lower stress levels (s_1)
2. settlement of soil below the pile base (s_2)
3. development of negative (or positive) skin friction due to relative movements of the soil and the pile shaft (s_3)
4. redistribution of pile load between the piles (s_4)
5. horizontal deformations of the piles.

The settlement of the pile head is determined by the combination of the first four effects described above:

$$s = s_1 + s_2 + s_3 + s_4 \quad (3)$$

Settlement s_1 for end bearing piles is significant if the pile tips are very close to the excavation and stress relief takes place around the pile tip. Settlement s_2 does not involve interaction with the piles, whereas s_3 is a true interaction component. For end bearing piles complying with current standards negative skin friction, if already fully developed, will not cause additional settlements, which means $s_3 = 0$. For all other piles s_3 depends on the amount of negative skin friction mobilized in the initial state. If the shaft friction is already fully mobilized, the neutral level will remain at about the same level and the pile follows the settlement of the soil at this level. If the shaft friction initially is not developed completely, the neutral level will change if soil displacements take place. For piles close to failure, the neutral level is found close to the surface and s_3 is about equal to the surface settlement.

An important issue is to determine the initial neutral level. This could be done theoretically based on CPT data or from historic data of relative building settlements to surface settlements. Based on the average pile capacity, the neutral level for an old pile in Amsterdam is found to be between NAP -7 and NAP -12 m, depending on the load on the pile, see (Korff 2012). Assuming a linear relationship between the ground settlement at surface and pile tip level, the pile-soil interaction

can be determined from the relative position of the neutral level to the surface and the tip level, see Figure 6.

If the negative skin friction is not fully mobilized at the initial state or if the tip resistance reduces, the skin friction will further mobilize, which will raise the neutral level. Settlement s_3 might also include an elastic component of the shortening of the pile if the total stress in the pile increases with increasing negative skin friction. If the pile redistributes its load, s_4 needs to be determined together with s_3 . This could occur if the piles closest to the excavation settle more than the piles further away. The building stiffness will prevent the building from following the different pile movements and the pile load will redistribute accordingly. If this happens, the external load on the pile changes, leading to a new equilibrium. This effect should be determined by a coupled analysis for a pile group, such as with a boundary element method as described by (Xu and Poulos 2000).

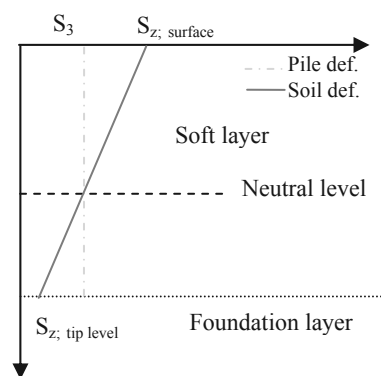


Figure 6 Settlement profile and neutral level, assuming linear relationship

5 BUILDING DISPLACEMENTS

The effects that cause the piles and hence the buildings to settle have been evaluated by analysing substantial amounts of monitoring data available from the Amsterdam cases. The settlement of the building is compared to the greenfield soil deformations at surface and pile tip level. It is not possible to distinguish between the contributions of s_1 , s_3 and s_4 . Settlement s_2 however can be directly evaluated against the results of the extensometer measurements at pile tip level. Figure 7 shows the building displacements (LevelingS) compared to the soil displacements at surface (GroundSurface) and pile tip level (ExtensioNAP-12m) for a series of buildings with old timber piles. The settlement of these buildings is equal to the soil settlement at approximately 0.3 to 0.5 times the pile length if a linear soil settlement profile between the surface settlement and the settlement at the first sand layer is assumed.

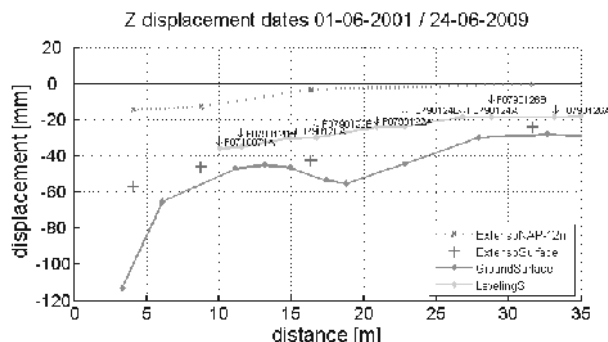


Figure 7 Ground and building displacements for CS13044 (at Ceintuurbaan).

In most cases in practice, no detailed information is present about the foundation and the soil-pile interaction has to be estimated or measured during construction.

For a second series of buildings with more modern foundations (old timber piles combined with renovation steel piles), the depth at which the pile and soil settlement are equal is found at approximately 0.8 – 1.0 times the pile length, see Figure 8.

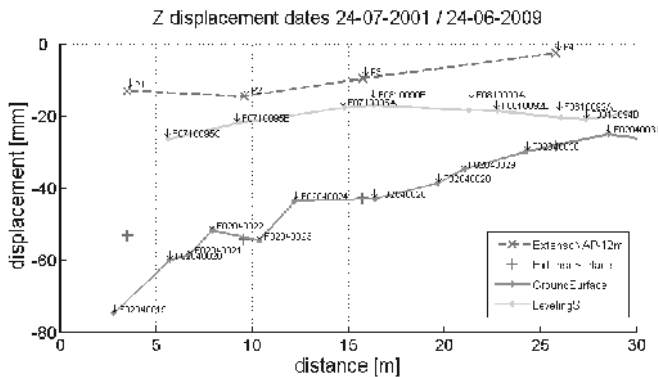


Figure 8 Ground and building displacements for CS13110 (at Ceintuurbaan) in the period 2001-2009

Based on the soil and building displacements as presented in more detail in (Korff 2012), the average interaction between pile and soil is found at 0.3 – 0.8 times the pile length for most original timber pile foundations and 0.8-1.0 times the pile length for most renewed foundations in the first sand layer. Some modern buildings settle very little and the pile settles the same as the pile tip level (1.0).

The settlement of the piles is shown to be between the settlement of the surface and the foundation layer. The deflection of the building is smaller than the deflection of either of the surface or base level soil deflections due to the stiffness of the building. The (Goh and Mair 2011) method to compare building settlement with greenfield settlement was used to determine the modification factors. In this case this was done comparing with greenfield surface settlement and with greenfield settlement of the foundation layer (first sand). For the deflection of buildings next to excavations, deforming in hogging shape, the modification factor is based on (Potts and Addenbrooke 1996):

$$M_{hog}^{DR} = \frac{\Delta/L \text{ hog, building}}{\Delta/L \text{ hog, greenfield}} \quad (4)$$

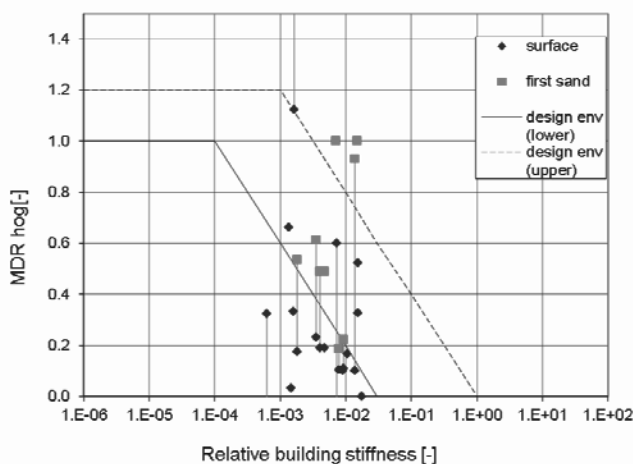


Figure 9 Modification factors from Amsterdam deep excavation for surface level and foundation level, compared with the design envelope presented by (Mair 2011)

The deflection of the buildings is clearly less than the deflected shape of the surface (70% reduction). A reduction of the deflection of 45% is found compared to the foundation level. The variation in these factors can to a certain degree be explained by the relative stiffness of the buildings compared to the soil as shown in Figure 9.

6 CONCLUSIONS

Piled buildings adjacent to deep excavations have to be assessed differently from buildings with shallow foundations. Piled buildings settle an amount between the surface settlement (for friction piles in failure) and tip level settlement (for end bearing piles with sufficient capacity to take full negative skin friction). The precise soil-pile interaction can be estimated based on the pile load, the pile capacity and the shaft friction development based on a method described in (Korff 2012). Based on measurements of Amsterdam timber pile foundations, the pile settlement is equal to the soil settlement at a depth of 0.3 – 0.8 times the pile length for most original timber pile foundations and 0.8-1.0 times the pile length for most renewed foundations in the first sand layer. Most of the modern buildings settle not more than the pile tip level.

The method proposed by (Goh and Mair 2011) provides a realistic, although rather large, range of possible modification factors to estimate the building deflection compared to the deflected shape of the soil surface and foundation level.

ACKNOWLEDGEMENTS

This research was performed in cooperation with the Dutch Centre for Underground Construction (COB). The authors wish to thank the city of Amsterdam for permission to use the data.

REFERENCES

- Franzius J. N. Potts D. M. and Burland J. B. 2006. The response of surface structures to tunnel construction. *Proc. Institution of the Civil Engineers Geotechnical Engineering* 1591, 3–17
- Farrell R.P. 2010. *Tunnelling in sands and the response of buildings*. Ph.D thesis Cambridge University UK.
- Goh K.H. and Mair R.J. 2011. The response of buildings to movements induced by deep excavations. *Geotechnical Aspects of Underground Construction in Soft Ground - Proceedings of the 7th International Symposium on Geotechnical Aspects of Underground Construction in Soft Ground* Rome, 903-910.
- Hoekstra J. and Bokhoven W. 1974. *Systematisch funderingsonderzoek van de Dapperbuurt* "Systematic foundation research in the Dapperbuurt area". Laboratorium voor Grondmechnica Delft reference CO-21606/503 In Dutch.
- Hsieh P. G. and Ou C. Y. 1998.. Shape of ground surface settlement profiles caused by excavation. *Canadian Geotechnical Journal* 35, 1004–1017.
- Jacobsz S. W.; Bowers K.H.; Moss N.A.; Zanardo G. 2005. The effects of tunnelling on piled structures on the CTRL. *Geotechnical Aspects of Underground Construction in Soft Ground* Amsterdam Taylor&Francis Group London.
- Korff M. 2012. *Response of piled buildings to the construction of deep excavations*. Ph.D thesis Cambridge University
- Mair R.J. 2011. Tunnelling and deep excavations - Ground movements and their effects. Keynote Lecture. *Proceedings of the XV European Conference in Soil Mechanics and Geotechnical Engineering ECSMGE-Athens*.
- Potts D. M. and Addenbrooke T. I. 1996. The influence of an existing structure on the ground movements due to tunnelling. *Geotechnical Aspects of Underground Construction in Soft Ground* London.
- van Tol A.F. 1994. *Hoe betrouwbaar is de paalfundering?* Lecture at installation as professor at Delft University of Technology
- Xu K.J. and Poulos H.G. 2000. Theoretical Study of Pile Behaviour Induced by a Soil Cut. *Proceedings GeoEng 2000*, CD volume.
- Zantkuijl H. J. 1993. *Bouwen in Amsterdam - Het woonhuis in de stad Building in Amsterdam*. Amsterdam Architectura & Natura.

Deep excavation in Irish glacial deposits

Excavation profonde des dépôts glaciaires Irlandais

Long M., O'Leary F.

Department of Civil, Structural and Environmental Engineering, University College Dublin (UCD), Ireland

Ryan M., Looby M.

Byrne Looby Partners, Dublin, Ireland

ABSTRACT: A good number of deep excavations have been recently completed in Irish glacial deposits. These have included propped walls up to 12 m deep. Experience elsewhere in the world was used to design and construct these walls. However case history data has shown that the behaviour of these walls is very rigid and much stiffer than comparable systems worldwide. It appears this behaviour is due to the inherent natural strength and stiffness of the soil and the slow dissipation of excavation induced depressed pore pressures or suctions. There appears to be scope for developing more efficient designs and in particular for greater use of cantilever walls and less stiff systems with smaller piles and reducing propping requirements. For temporary works, the use of undrained parameters in serviceability limit state calculations together with implementation of the observational approach on site could be considered for future schemes.

RÉSUMÉ : Un bon nombre d'excavations profondes ont été récemment réalisées dans les dépôts glaciaires Irlandais. Elles ont inclus des murs de soutènement jusqu'à 12 mètre de profondeur. La conception de ces murs a été réalisée grâce aux méthodes utilisées dans les autres pays du monde. Toutefois, les analyses a posteriori ont montré que les caractéristiques de ces murs étaient extrêmement rigides et bien plus rigide que d'autres systèmes comparables dans le monde. Il semble que ces caractéristiques sont dues à la résistance naturelle et à la rigidité du sol ainsi qu'à la lente dissipation des pressions interstitielles déprimées ou aux suctions induites par la réalisation des excavations. Il semble y avoir des possibilités de développer des méthodes de conceptions plus réalistes et moins conservatives permettant en particulier une utilisation accrue des murs cantilevers et des systèmes moins rigides avec de petits pieux de fondation et en réduisant les besoins de butonnage ou d'ancrage. Pour les travaux temporaires, l'utilisation de paramètres non drainés dans les calculs des états limite de service ainsi que la mise en œuvre de l'approche observationnelle sur le chantier, pourraient être envisagées pour de futurs projets.

KEYWORDS: deep excavations; retaining walls; glacial deposits; ground movements

1 INTRODUCTION.

Over the previous 15 years, economic growth in Ireland has led to an increase in the use of underground space, with some development now including four underground levels. Valuable full scale data has been obtained from a good number of these projects. The purpose of this paper is to provide an overview of aspects relating to the design, construction and behaviour of retaining walls in Irish glacial deposits.

This paper will exclude projects located in the two main cities of Dublin and Cork. Case histories from these two locations have already been well documented (Long et al., 2012a; Long et al., 2012b; Long et al., 2012c; Long et al., 2013).

Specifically the paper will:

- Briefly review the background geology and ground conditions,
- Outline the presently used design approach,
- Review in detail the general behavior of walls in Irish glacial deposits by reference to two case histories namely:
 - lightly supported "regular" wall for 6 m excavation in Limerick,
 - 6 m excavation in Middleton, Co. Cork where a cantilever solution was used,
- Present an overall summary of the behavior of retaining walls in Irish glacial deposits compared to similar support systems worldwide,
- Provide some overall conclusions and recommendations for the design and construction of future similar schemes.

2 BACKGROUND GEOLOGY

Broadly speaking the coastline of Ireland is formed of strong older igneous and metamorphic rocks such as sandstones, granites and quartzite. The central basin of Ireland is formed of Carboniferous limestone. However the engineering geology of Ireland is dominated by the mantle of 10,000 to 15,000 year old glacial tills and glacial sands and gravels which cover much of the country. These deposits generally have a high gravel, cobble and boulder content and are usually medium dense to dense or stiff to very stiff in consistency. They form a thin layer (but usually greater than 3 m in thickness) draped over and conforming to the underlying bedrock topography. Later alluvial activity has covered the glacial deposits with soft clays, silts and peats in some low lying areas, in estuaries and along river flood plains (Edwards and Warren, 1985).

3 THE SITES

The location of the study sites is shown on Figure 1 and some details of the projects under consideration are given on Table 1. The sites are located throughout Ireland but mostly in the most populated areas to the east and south-east.

At each of the chosen sites inclinometers had been used to measure the lateral pile retaining wall movements. Details given on Table 1 include the depth of excavation (H), the support details including the spacing of the structural piles and the maximum measured pile deflection (δ_h max).

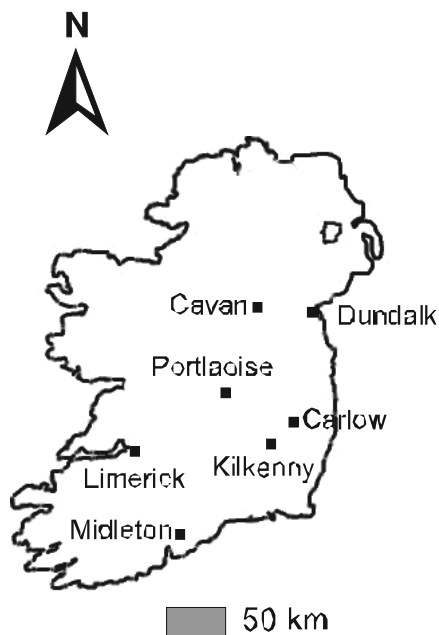


Figure 1. Location of study sites

Table 1. Details of study sites

Site No.	Location	H (m)	Support Configuration	Wall type
1	Savoy Limerick 1	6.4	Single anchor	Secant
2	Savoy Limerick 2	5.8	Single anchor	Secant
3	Main St. Cavan	9.0	Two anchors	Contiguous
4	Dundalk Cellar	8.7	Single anchor	Secant
5	Dundalk Bunker	8.1	Single anchor	Secant
6	Midleton Cantilever	6.0	Cantilever	Secant
7	Midleton Anchored	6.0	Single anchor	Secant
8	Kilkenny	7.7	Single prop	Contiguous
9	Kilkenny	6.9	Single prop	Contiguous
10	Shaws Carlow	5.0	Single prop	
11	Portlaoise SC Phase 1	12.0	Two anchors	Secant
12	Portlaoise SC Phase 2	7.0	Single anchor	Secant

Table 1 continued

Site No	Pile dia. (mm) / spacing (m) / length (m)	δ_h max (mm)	Reference
1	600 / 1 / 8.4	7	BLP files
2	600 / 1 / 7.8	2	BLP files
3	192 / 0.25 / 14	45	BLP files
4	640 / 1.4 / 10	6	BLP files
5	640 / 1.4 / 12	7	BLP files
6	640 / 1.2 / 16.5	27.5	BLP files
7	640 / 1.2 / 14	5.5	BLP files
8	600 / 0.75	5	Arup files
9	600 / 0.75	2	Arup files
10	n/a	2	NVM files
11	640 / 1.0 / 14	17	BLP files
12	640 / 1.0 / 7	4	BLP files

4 DESIGN

Current geotechnical design procedures for retaining walls in Irish glacial deposits often involves the following steps:

- Following the general guidelines of Gaba et al. (2003) or BS8002 (BSI, 1994), for ultimate limit state, determine the required retaining wall toe penetration. Calculations use effective stresses and are often performed by hand, using conventional Rankine active and passive earth pressure theory, or with a relatively simple piece of software,
- Check that this toe penetration is adequate to support any vertical loads and also to prevent significant water seepage,
- Determine wall bending moments, shears, prop / waler forces and lateral wall movements (serviceability limit state) by means of a beam – spring computer program such as OASYS – FREW[®],
- Determine the associated ground movements using empirical based methods, such as those developed by Clough and O'Rourke (1990). Possible adjacent building damage is then assessed by comparing parameters such as differential settlement with empirically based tolerable limits, e.g. those of Burland et al. (1977)

5 OVERVIEW ALL SITES

Data for the 12 available case histories are presented in Table 1. A plot of maximum measured lateral movement (δ_h) versus retained height (H) is shown on Figure 2. Except for the Main St. Cavan, Portlaoise Phase 1 and the Midleton cantilever excavations, δ_h values are less than 7 mm. There does appear to be some weak tendency for an increase in δ_h with H.

Also shown on Figure 2 are lines representing normalised movement (δ_h/H) of 0.08% and 0.4%. The former relationship was obtained by Long et al. (2012a) for projects in Dublin boulder clay – a very stiff glacial lodgement till. The behaviour of the projects presented here is similar if not better than the Dublin sites. The 0.4% line represents a typical design value as recommended by Gaba et al. (2003) in CIRIA Report C580 and clearly this relationship is very conservative for most of the cases presented but is consistent with the data from the Cavan and Midleton cantilever sites.

The data shown on Figure 2 takes no account of the retaining wall type, its stiffness or the prop / anchor configuration. In order to attempt to include these factors, the data are replotted on Figure 3 in the normalised form of δ_h/H against Clough et al. (1989) system stiffness. This is defined on Figure 3 where EI = wall stiffness, γ_w = unit weight of water (so as to make expression unitless) and s = support spacing.

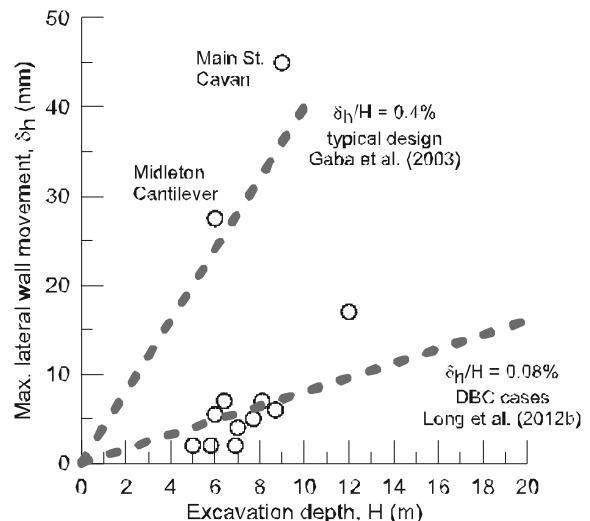


Figure 2. Maximum lateral wall movement versus excavation depth

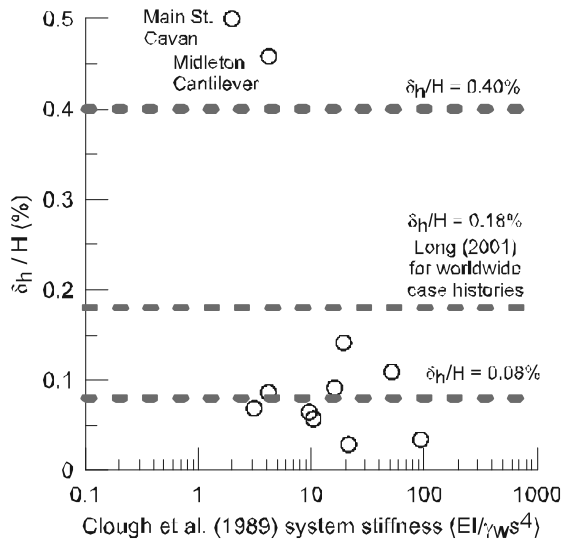


Figure 3. Normalised maximum lateral wall movement versus Clough et al. (1989) system stiffness

The two relationships included in Figure 2 are also shown here. In addition the relationship $\delta_h/H = 0.18$, which was obtained by Long (2001) for an average of 169 case histories worldwide where there was stiff soil at dredge level, is also shown. Lateral movement is clearly a function of system stiffness with the two walls with low system stiffness showing relatively high movements. The Cavan wall had very slender piles and the Midleton wall had no props or anchors. However the remaining data plot well below the worldwide trend suggesting that a more flexible (and hence a more economic) wall may perform adequately in many cases.

Some of the trends shown on Figure 2 and 3 are explored further by examining two detailed case histories as follows

6 CASE HISTORY OF A LIGHTLY SUPPORTED "REGULAR" WALL – SAVOY, LIMERICK

Details of this site are shown on Figure 4. The approach and techniques used at the Savoy Site are typical of those used at many sites in Ireland. The site is underlain by about 2 m of made ground over about 5 m of glacial deposits over limestone bedrock. The glacial deposits have standard penetration test (SPT) N values increasing from about 20 blows / 300 mm near the top of the stratum to an average of 60 blows / 300 mm with depth.

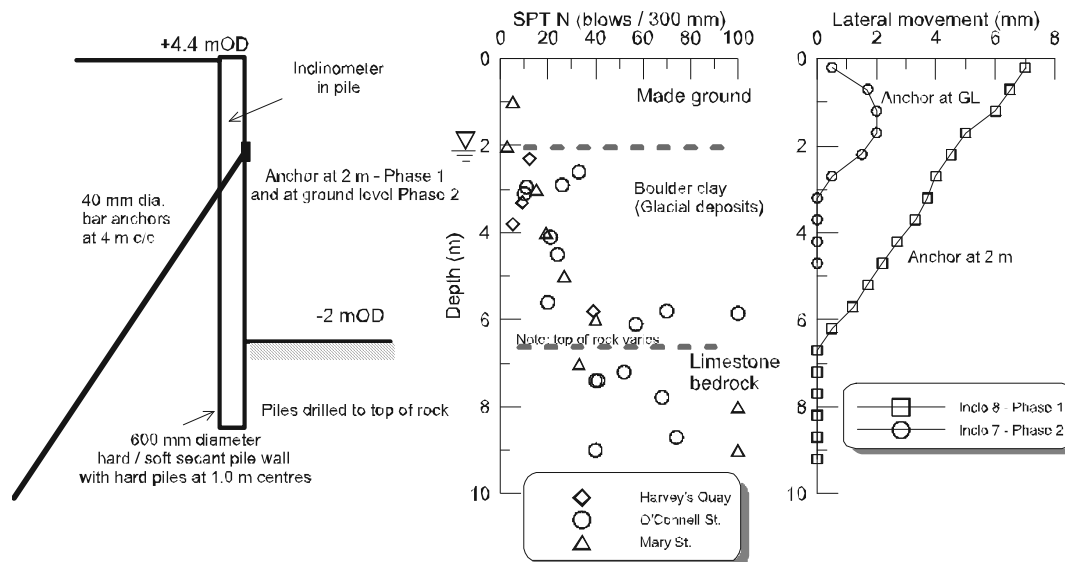


Figure 4. Savoy, Limerick

The retaining wall was required for temporary works purposes only and comprised a 600 mm diameter “hard / soft” secant wall with a single anchor. For the Phase 1 excavation the anchor was located at about 2 m depth. Much of the 7 mm or so movement recorded occurred while the wall was acting in a cantilever mode during the installation of the anchors. This is consistent with the findings of Long (2001) for a good number of world wide projects. Thus for Phase 2 the anchor was relocated to ground level and the measured movements were much smaller.

It would seem that a less stiff system, e.g. smaller diameter / more widely spaced piles or a cantilever wall would have performed perfectly adequately in this case.

7 CASE HISTORY OF CANTILEVER WALL

Details for the Midleton site are shown on Figure 5. This project was carried out in 2012 and thus many of the lessons learned over the previous 10 to 15 years could be used. Again the wall was required for temporary works purposes. It comprised a “hard / firm” secant pile wall with 640 mm diameter structural “male” piles and 900 mm diameter “female”. A single anchor was used at locations where sensitive adjacent buildings were present. However for non sensitive areas of the site and based on the experiences listed above a cantilever solution was used.

Ground conditions are more complex than those at Limerick and comprised a variable sequence of glacial clays, silts, sands and gravels. SPT N values increase from about 10 blows / 300 mm at the surface to an average of 25 blows / 300 mm at 7 m depth and thereafter remain approximately constant.

As would have been expected from previous experience measured movements for anchored section were very small. For the cantilever sections the wall also behaved very well and maximum lateral movements were of the order of 20 mm

Predicted wall deflections, using *FREW*[®] for the anchored wall are also shown on Figure 5. The key input parameters are the effective friction angle (ϕ'), the undrained shear strength (s_u) and the Young's modulus (E_u or E'). These were determined from correlations with SPT N. For the clay layers it was assumed $s_u = 5$ N and $E_u = 750$ N (Gaba et al., 2003; Stroud, 1988). For the granular soils E' was assumed = 2500 N and ϕ' was found from the relationships of Peck et al. (1974).

It can be seen that the predicted values considerably overestimate the measured ones. A similar finding was made for the cantilever wall at Midleton.

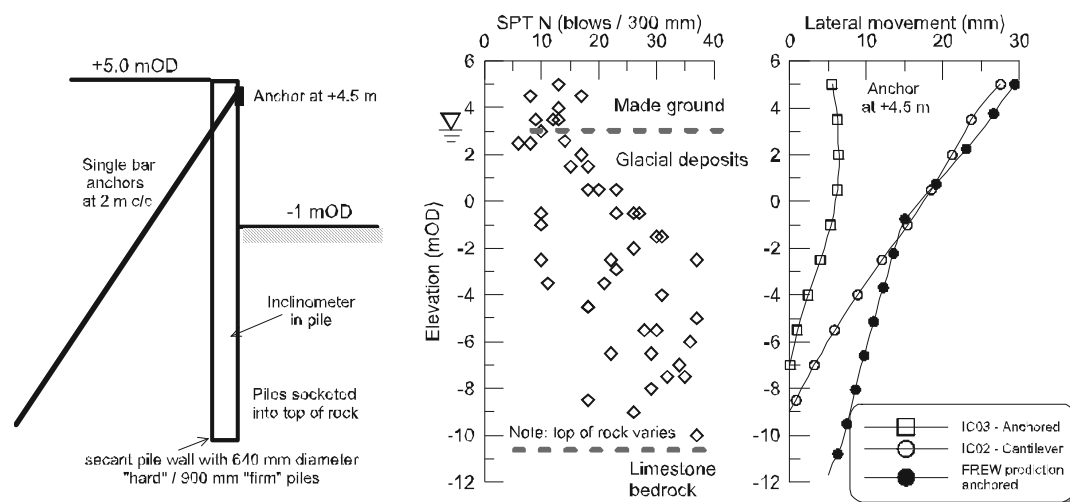


Figure 5. Midleton

8 DISCUSSION

The reasons for the very stiff behaviour of the retaining walls in Irish glacial deposits are complex but are due to a combination of the following factors:

- Excavation induced depressed pore pressures (or even suctions) in the material. These result in increased effective stress and hence stability (Long et al., 2012a).
- The low permeability of the clay fraction of the material (10^{-10} m/s or less) meaning that the dissipation of the depressed pore pressures takes a long time.
- The material has extremely high strength and stiffness.

A possible approach for the design of temporary retaining structures in the clay fraction of the material may be in the use of undrained parameters in conjunction with the observational approach. This approach should only be considered where the predicted deflections using an effective stress approach would be within defect limits to prevent the possibility of damage, economic loss or unsafe situations. The risk associated with the decision should be clearly assessed in terms of understanding of the site geology, type and condition of structures to the rear of the pile wall and the quality of monitoring procedures and contingency measures put in place.

It seems there is scope for the greater use of cantilever walls, less stiff walls (e.g. smaller diameter piles) and also greater retained heights at least for temporary works purposes. It must also be emphasised that an effective stress design approach is always needed for the ultimate limit state analysis in permanent works as the suctions will eventually dissipate.

9 CONCLUSIONS

Case history data confirms that retaining wall behaviour in Irish glacial deposits is extremely stiff.

The reasons for this stiff behaviour lie in the low permeability and high strength and stiffness of the material and the resulting very slow dissipation of depressed excavation induced pore pressures.

It appears that the current approach, for serviceability limit state calculations, which usually involves beam – spring type computer programs is clearly conservative.

For temporary works, the use of undrained parameters in conjunction with the observational approach may be considered for reducing predicted deflections to simplify the construction sequence and reduce costs.

There is scope for greater use of cantilever walls and walls and systems with lower stiffness.

10 ACKNOWLEDGEMENTS

Some of the data used in this paper was kindly provided by Mr. Tony O'Dowd of PJ Edwards & Co., Mr. Pat Fox of Murphy International Ltd., Mr. Patrick Casey of Arup Consulting Engineers and Mr. Eddie Meade of NVM Ltd. and their co-operation is gratefully acknowledged.

11 REFERENCES

- BSI, 1994. *Code of practice for earth retaining structures*
- Burland, J.B., Broms, B.B. and De Mello, V., 1977. Behaviour of foundations and structures, *Proceedings IXth International Conference on Soil Mechanics and Foundation Engineering*, Tokyo, pp. 495 - 546.
- Clough, G.W. and O'Rourke, T.D., 1990. Construction induced movements of in situ walls, *Proceedings ASCE Conf. on Design and Performance of Earth Retaining Structures*, ASCE Pub. No. 25, Cornell, pp. 439 - 470.
- Clough, G.W., Smith, E.M. and Sweeney, B.P., 1989. Movement control of excavation support systems by iterative design, *Proceedings ASCE Foundation Eng: Current Principles and Practices*, ASCE, pp. 869 - 884.
- Edwards, K.J. and Warren, W.P., 1985. The Quaternary studies in Ireland. In: K.J. Edwards and W.P. Warren (Editors), *The Quaternary History of Ireland*. Academic Press, London, pp. 1 - 16.
- Gaba, A.R., Simpson, B., Powrie, W. and Beadman, D.R., 2003. Embedded retaining walls - Guidance for economic design, *CIRIA Report No. C580*.
- Long, M., 2001. A database for retaining wall and ground movements due to deep excavations. *Journal of Geotechnical and Geoenvironmental Engineering*, ASCE, 127(3): 203 - 224.
- Long, M., Brangan, C., Menkiti, C., Looby, M. and Casey, P., 2012a. Retaining walls in Dublin Boulder Clay, Ireland. *Institution of Civil Engineers Journal of Geotechnical Engineering*, 165(GE4, August): 247 - 266.
- Long, M., Daynes, P.J., Donohue, S. and Looby, M., 2012b. Retaining wall behaviour in Dublin's fluvio-glacial gravel, Ireland. *Institution of Civil Engineers Journal of Geotechnical Engineering*, 165(GE5, October): 289 - 307.
- Long, M., Menkiti, C., Skipper, J., Brangan, C. and Looby, M., 2012c. Retaining wall behaviour in Dublin's estuarine deposits, Ireland. *Institution of Civil Engineers Journal of Geotechnical Engineering*, 165(GE6, December): 351 - 365.
- Long, M., Murphy, M., Roberts, T., Clancy, N. and Murphy, P., 2013. Deep excavations in water bearing gravels in Cork. *Quarterly Journal of Engineering Geology (QJEGH)* Paper submitted November 2012.
- Peck, R.B., Hanson, W.E. and Thorburn, T.H., 1974. *Foundation Engineering* 2nd Ed. John Wiley and Sons, New York.
- Stroud, M.A., 1988. The standard penetration test: its application and interpretation, *Proceedings ICE Conference on Penetration Testing in the UK*. Thomas Telford, London, University of Birmingham, pp. 29 - 51.

Active earth thrust on walls supporting granular soils: effect of wall movement

Pression active des terres sur des murs soutenant des sols granulaires: l'effet du mouvement du mur

Loukidis D.
University of Cyprus, Cyprus

Salgado R.
Purdue University, USA

ABSTRACT: The methods currently used in the design practice of retaining walls supporting granular soils (sand, gravel, silt, and their mixtures) assume that the soil friction angle and, consequently, the active earth pressure coefficient K_A are independent of wall movement. However, the mobilized friction angle inside the retained soil in reality first reaches a peak value and then decreases towards the critical state value as shear strain increases with wall movement. This study aims to investigate the development and evolution of the active earth pressure by modeling the soil mechanical behavior in a realistic way in a series of finite element analyses. Based on the numerical results, an equation is proposed for the estimation of K_A as a function of the initial relative density and the wall crest displacement.

RÉSUMÉ : Les méthodes actuellement utilisées dans la pratique de la conception des murs de soutènement supportant des sols granulaires (sable, gravier, limon et leurs mélanges) supposent que l'angle de frottement du sol et, par conséquent, le coefficient de pression active des terres K_A sont indépendantes du mouvement du mur. Toutefois, l'angle de frottement mobilisé à l'intérieur du sol retenu atteint en réalité d'abord une valeur de pic, puis diminue vers la valeur d'état critique à mesure que la déformation en cisaillement augmente avec le mouvement du mur. Cette étude vise à étudier le développement et l'évolution de la pression active des terres par la modélisation du comportement mécanique des sols de manière réaliste dans une série d'analyses par éléments finis. Sur la base des résultats numériques, une équation est proposée pour l'estimation de K_A en fonction de la densité relative initiale et le déplacement en crête du mur.

KEYWORDS: retaining wall, active earth pressure, sands, finite element analysis.

1 INTRODUCTION

The active earth pressure is expressed as the product of the vertical effective stress σ'_v in the retained soil mass or backfill and the active earth pressure coefficient K_A . The earliest and simplest methods for the calculation of the active earth pressure for purely frictional soils are those based on the Coulomb and Rankine theories. For a retained soil with horizontal free surface and a vertical wall backface, Coulomb's solution yields

$$K_A = \frac{\cos^2 \phi}{\cos \delta \left[1 + \sqrt{\frac{\sin(\phi + \delta) \sin \phi}{\cos \delta}} \right]^2} \quad (1)$$

The Coulomb solution can be proven to be equivalent to a rigorous limit analysis upper bound solution. It is also in good agreement with other upper bound solutions (Chen 1975, Soubra and Macuh 2002), as well as the lower bound solution by Lancellotta (2002), with the differences not exceeding 7%.

Furthermore, these methods, which are currently used in design practice, assume that ϕ and, consequently, the active earth pressure coefficient K_A are constant, i.e. their values do not change as the wall moves. However, the value of the mobilized friction angle in reality depends on a number of factors, such as the current mean effective stress, and, most importantly, the shear strain. Granular soils, unless in a very loose state, are strain-softening materials, meaning that the mobilized friction angle first reaches a peak value ϕ_p and then decreases towards the critical state value ϕ_c . Hence, the active state developing inside the mass of the supported soil is a function of the wall movement.

The goal of this study is to investigate the development and evolution of the active earth pressure as the wall moves away from the retained soil using finite element (FE) analysis. The study focuses on retaining wall that are free to translate and rotate, such as gravity walls, cantilever walls and self-supported (cantilevered) sheet pile, secant pile or slurry walls. The mechanical behavior of the soil is captured realistically using a two-surface constitutive model based on critical state soil mechanics.

2 FINITE ELEMENT METHODOLOGY

The FE analyses were performed using the code SNAC (Abbo and Sloan 2000). A typical finite element mesh is shown in Fig. 1. The mesh consists of 8-noded, plane-strain quadrilateral elements and includes the wall, the supported soil and the foundation soil. The free surface of the supported soil is horizontal and without surcharge. The wall has a rectangular cross-section with width B and height H , and is modeled as a linear elastic material with very large Young's modulus so that it can be considered rigid. The retaining wall is also embedded a small distance D into the foundation soil. The analyses start with the supported soil at rest (K_0 state). No interface elements are placed between the soil and the wall. As a consequence, slippage between the wall and retained soil occurs due to the formation inside the soil mass of a shear band parallel to the wall backface. This roughness condition is realistic for walls made out of concrete; however, this may not be the case for sheet pile walls.

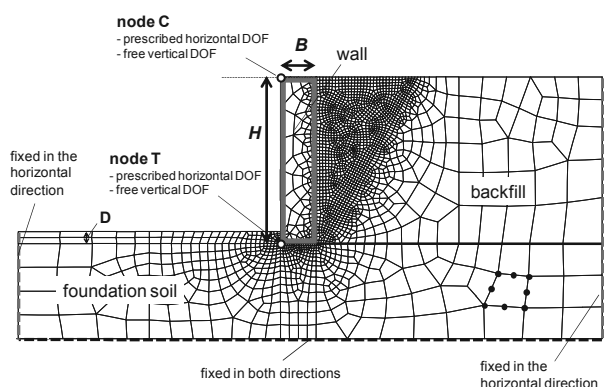


Figure 1. Typical mesh and boundary conditions used in the FE analyses.

The constitutive model used in this study is the two-surface plasticity model based on critical state soil mechanics developed originally by Manzari and Dafalias (1997) and subsequently modified by Dafalias et al. (2004) and Loukidis and Salgado (2009). The model parameters were determined by Loukidis and Salgado (2009) for two sands: air-pluviated/dry-deposited Toyoura sand and Ottawa sand. The model takes into account inherent and stress-induced anisotropy, and predicts accurately the soil response at both small and large strain regimes.

Because the problem under investigation involves material softening, the numerical simulations were inherently unstable. For this reason, the analyses were performed under displacement control. In the beginning of the analysis, the wall is fully supported at two points, namely the crest (node C) and the toe (node T), shown in Fig. 1, where the corresponding horizontal reactions are $R_{C,0}$ and $R_{T,0}$, respectively. Equivalently, the wall is initially prevented to move horizontally or rotate because of the external application of a horizontal force $F_{ext,0} = R_{C,0} + R_{T,0}$ and a moment $M_{ext,0} = R_{C,0}/H$. The analysis proceeds by the application of horizontal displacement increments Δu_C and Δu_T pointing away from the retained soil. As a result, the reactions F_{ext} ($=R_C + R_T$) and $M_{ext} = R_C/H$ begin to decrease. These displacement increments are applied in such way that the ratio $F_{ext}/F_{ext,0}$ is maintained equal to the ratio $M_{ext}/M_{ext,0}$. As a consequence, the prescribed displacements u_C and u_T are not equal to each other, leading to an overall wall motion that includes both translation and rotation. The wall is allowed to move vertically as no restraints are imposed on its nodes in the vertical direction.

3 SIMULATION RESULTS

Finite element analyses were performed for B ranging from 1.5m to 2.5m and H ranging from 6m to 8m. The sand unit weight γ was set equal to 18kN/m^3 , while the coefficient K_0 was set equal to 0.5. For the sake of simplicity, the foundation soil is assumed to be of the same type and density as the retained soil.

3.1 Failure mechanism

Fig. 2 shows contours of the incremental maximum shear strain γ_{max} at the final stages of the simulations. The failure mechanism inside the supported soil consists of a wedge shaped sliding mass delimited by the wall backface and an oblique shear band originating from the heel of the wall. It can be seen also that families of secondary shear bands develop inside the sliding wedge. This is consistent with experimental observations by Leśniewska and Mróz (2001), as well as with FE analysis results by Gudehus and Nubel (2004). As shown in Fig. 2, the inclination angle of the shear bands in the retained

soil mass with respect to the horizontal is larger in the case of dense than loose sand. A shear band running parallel to the wall back face also forms in all analyses, representing sliding between the sliding soil mass (wedge) and the wall.

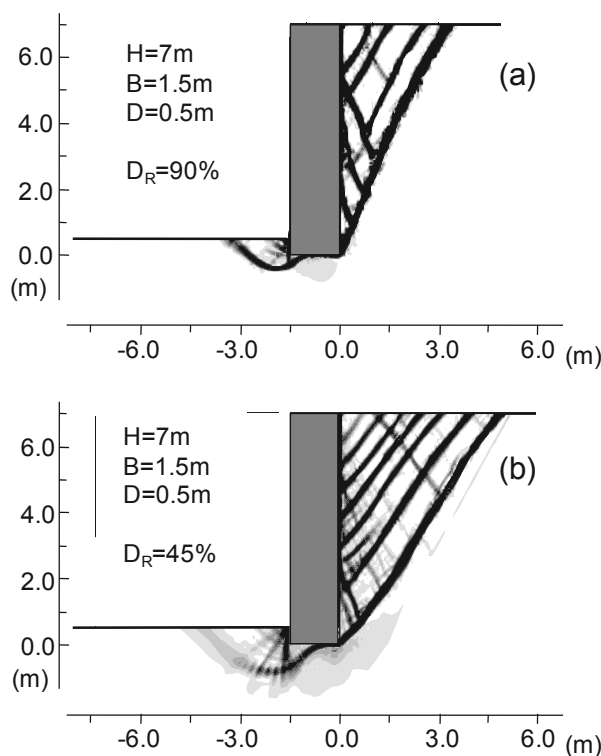


Figure 2. Contours of incremental γ_{max} from analyses with dense and loose Ottawa sand.

Below the wall base, a bearing capacity mechanism forms, the shape of which resembles that of mechanisms presented by Loukidis et al. (2008) for the case of strip footings on purely frictional material and subjected to eccentric and inclined loading.

3.2 Active earth pressure evolution

Fig. 3 illustrates how the normal (horizontal) stress distribution along the back of the wall changes during an analysis. At the beginning, there is the triangular stress distribution corresponding to geostatic stress conditions ($K=K_0$). With increasing wall displacement, the horizontal stress decreases progressively until a minimum active pressure state (MPS) is reached. From that point on, the average horizontal stress increases, but at a much lower rate than the rate at which it decreased earlier. Although before the MPS the stress distribution is smooth, afterwards, local peaks and valleys develop as consequence of bifurcation and the shear banding inside the sliding mass.

The evolution of the lateral earth pressure coefficient K with crest displacement u_C is shown in Fig. 4 for analyses with Toyoura sand with 60% relative density but different values of H , B , and D . It can be seen that K drops sharply towards a minimum value ($K_{A,min}$) corresponding to MPS at u_C approximately equal to $0.003H$ and, subsequently, rises smoothly, approaching a residual value ($K_{A,cr}$) related to the full development of critical state inside the sliding wedge. The results in Fig. 4 suggest that $K_{A,min}$ and $K_{A,cr}$ are practically independent of the wall dimensions and the embedment.

Fig. 5 shows the K/K_0 evolution for Toyoura and Ottawa sands with different values of relative density. The figure also

shows the K_A value resulting from finite element analyses for an elastic-perfectly plastic soil following the Mohr-Coulomb failure criterion (M-C analyses) with friction angle ϕ equal to the critical state friction angle value ϕ_c of each sand for plane strain conditions and dilatancy angle ψ equal to zero (consistent with the constant volume response at critical state).

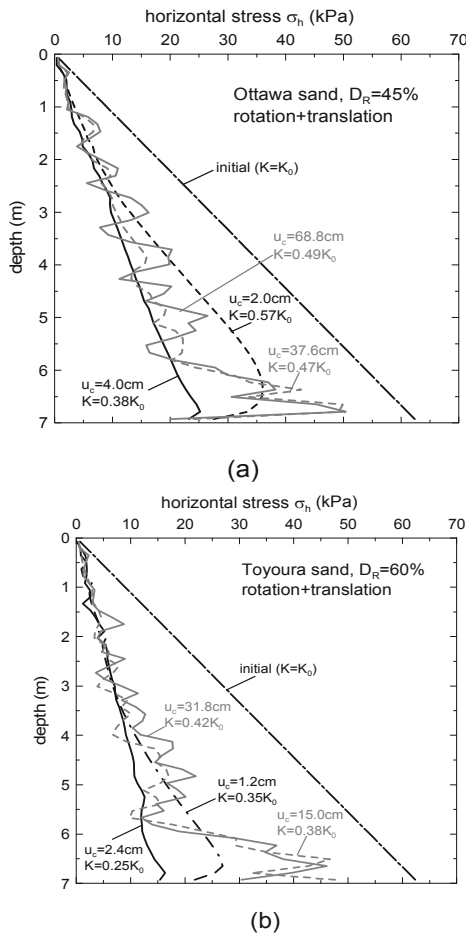


Figure 3. Examples of horizontal stress distribution acting on the wall backface at different stages during the analysis.

As expected, $K_{A,min}$ decreases with increasing relative density and, consequently, peak friction angle. The crest displacement required for reaching the MPS is in the $0.003H$ to $0.006H$ range, regardless the D_R value. On the other hand, attainment of $K_{A,cr}$ requires u_c larger than $0.10H$.

Interestingly, $K_{A,cr}$ seems also to depend on the relative density despite the fact that ϕ_c is independent of D_R . Only the curves for loose sand appear to attain $K_{A,cr}$ values that are in agreement with the K_A from the analyses with a perfectly plastic soil with material parameters consistent with critical state. This is because the inclination of the sliding plane delimiting the wedge depends on the dilatancy that the soil exhibits during the early stages of the wall movement, since the theoretical value of the shear band inclination with respect to the minor stress (i.e. horizontal) axis is equal to $45^\circ + (\phi + \psi)/4$ (Vardoulakis 1980). The sliding wedge forms at MPS, when the soil mass close to the wall is strongly dilative for all except very loose sand. Once the main inclined shear band forms, it tends to stay more or less at that location because of strain localization.

In most of the analyses, the u_c values required to cause bearing capacity failure of the wall foundation is in the $0.01H$ to $0.09H$ range, corresponding to toe displacement of $0.01B$ to $0.065B$. Hence, the foundation is expected to fail before full development of the residual active earth pressure state.

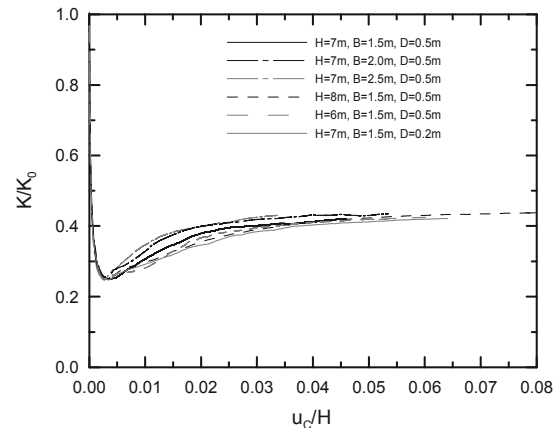


Figure 4. Variation of normalized lateral earth pressure coefficient with wall crest displacement from analyses with medium dense Toyoura sand ($D_R=60\%$).

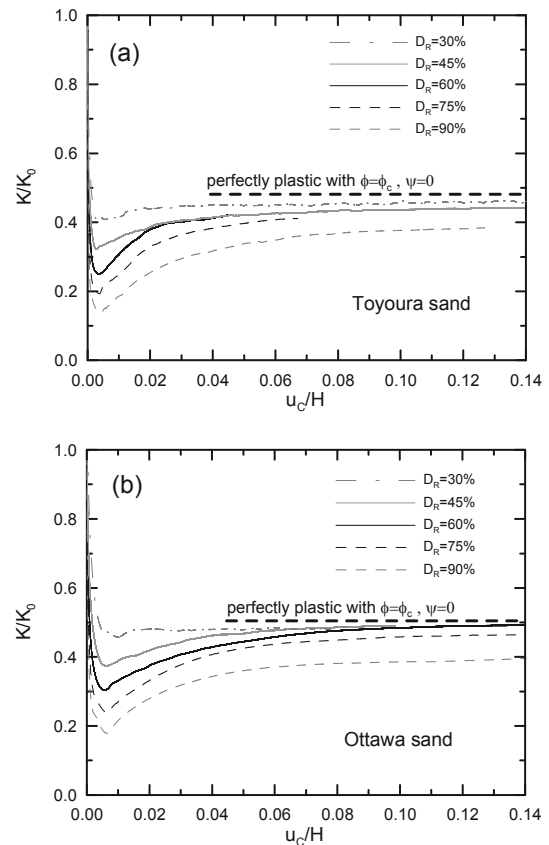


Figure 5. Variation of normalized lateral earth pressure coefficient with wall crest displacement from analyses of a wall with $H=7m$, $B=1.5m$ and $D=0.5m$.

3.3 Mobilized resistance along the wall-soil interface

The mobilized friction coefficient μ ($=\tan\delta$) on the wall backface reaches a peak value at very early stages of the analyses, before the attainment of the MPS. After the peak, δ decreases quickly towards a residual value δ_c that is consistent with development of critical state inside the thin shear band that runs parallel to the wall backface. Despite this, it can be seen that the mobilized friction angle δ_{mob} at MPS ranges from 1.0 to 1.25 times the δ_c (Fig. 6). The δ_c values are 30.8° and 29.6° for Toyoura sand and Ottawa sand, respectively. These are consistent with the theoretical δ_c values calculated as $\arctan(\sin\phi_{c,ps})$, where $\phi_{c,ps}$ is the critical state friction angle for plane strain conditions. For Toyoura and Ottawa sands, this takes the values of 36.6° and 34.6° , respectively, which are

roughly 4° to 5° larger than the values corresponding to triaxial compression conditions $\phi_{c,TX}$ (=31.6° and 30.2°, respectively).

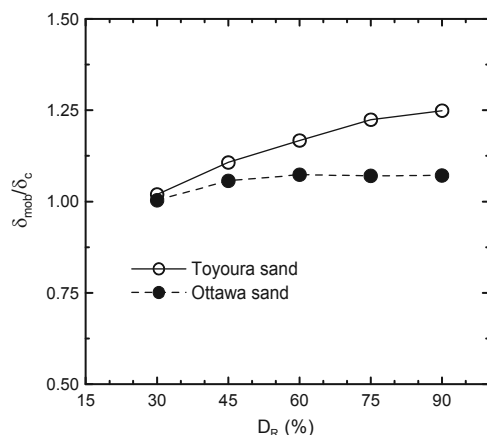


Figure 6. Ratio of the δ mobilized along the wall-soil interface at MPS to the δ corresponding to critical state conditions.

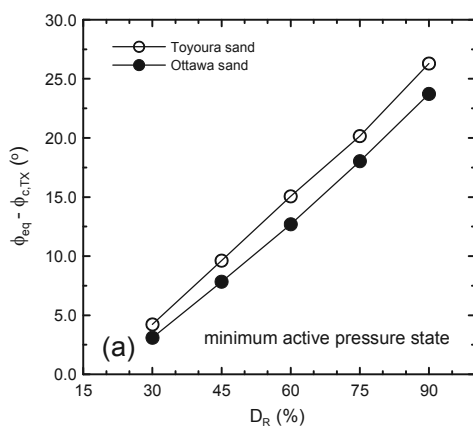


Figure 7. Equivalent value of the friction angle to be used in the calculation of $K_{A,min}$.

3.4 Expression for the estimation of K_A

The variation of the earth pressure coefficient K with crest displacement u_C observed in Figs. 4 and 5 can be described mathematically by the following equation:

$$K = \left[\frac{\frac{(K_0 - K_{A,cr})}{(K_0 - K_{A,min})} u_{Cp} - 2u_C}{\frac{u_{Cp}}{(K_0 - K_{A,min})} + \frac{u_C^2}{(K_{A,cr} - K_{A,min}) u_{Cp}}} \right] + K_{A,cr} \quad (2)$$

where u_{Cp} is the crest displacement needed to reach MPS. Based on the previous discussion, u_{Cp} can be taken equal to $0.005H$.

The characteristic values of the active earth pressure coefficient, $K_{A,min}$ and $K_{A,cr}$, can be calculated using the Coulomb's equation (Eq. 1) with suitable (equivalent) values ϕ_{eq} for the mobilized friction angle inside the sliding wedge. In Fig. 7, we see that there is a linear dependence between ϕ_{eq} for MPS and $\phi_{c,TX}$, which can be expressed by

$$\phi_{eq}^{(MPS)} = \phi_{c,TX} + \left(35 \frac{D_R}{100\%} - 7^\circ \right) \quad (3)$$

We consider $\phi_{c,TX}$ instead the more physically suitable $\phi_{c,PS}$ because it is easier to estimate through empirical relationships, measurements of the angle of repose on a conical soil heap, or a few triaxial compression tests. On the other hand, to calculate $K_{A,cr}$, the friction angle can be estimated using

$$\phi_{eq}^{(cr)} = \phi_{c,TX} + \left(9 \frac{D_R}{100\%} - 2^\circ \right) \quad (4)$$

For the calculation of both $K_{A,min}$ and $K_{A,cr}$ using Eq. (1), the wall-soil interface friction angle δ can be conservatively set equal to δ_c estimated as $\arctan[\sin(\phi_{c,TX} + 4^\circ)]$. Finally, it should be pointed out that, according to the numerical results, the point of application of the active earth thrust at MPS is at a distance roughly $H/3$ from the wall base, while for the residual state is slightly smaller (roughly $0.3H$).

4 CONCLUSIONS

This paper presented the results of a set of finite element analyses of a retaining wall supporting sand. Based on numerical results, the active earth pressure coefficient attains a minimum value $K_{A,min}$ at wall crest displacements of the order of $0.005H$. Hence, from a practical standpoint, this state is of limited relevance to ultimate limit state (ULS) design; it is possibly representative of a serviceability limit state (SLS) design. A residual (maximum) value $K_{A,cr}$ associated to full mobilization of critical state inside the soil mass is practically reached at crest displacements of the order of $0.1H$.

The K_A to be used in ULS calculations can be estimated using the proposed Eq. (2), provided that the designer knows *a priori* the wall crest displacement u_C corresponding to ULS. In case there is a structure founded on the supported soil, the u_C can be set equal to the allowable foundation displacement value compatible with the ULS for the structure, established according to design code provisions. In the opposite case, the u_C could be set equal to 7 times the horizontal base displacement required for wall foundation failure. In the case of granular foundation soils, this base displacement can be conservatively taken as 0.05 times the base width.

5 REFERENCES

- Abbo, A.J. and Sloan, S.W. 2000. *SNAC, User manual, Version 2.0*. Department of Civil, Surveying and Environmental Engineering, University of Newcastle, Callaghan, Australia.
- Dafalias, Y.F., Papadimitriou, A. G. and Li, X. S. 2004. Sand plasticity model accounting for inherent fabric anisotropy. *Journal of Engineering Mechanics*, ASCE, 130(11), 1319-1333.
- Gudehus, G. and Nübel, K. 2004. Evolution of shear bands in sand. *Géotechnique*, 54(3), 187-201.
- Lancellotta, R. 2002. Analytical solution of passive earth pressure. *Géotechnique*, 52(8), 617-619.
- Leśniewska, D. & Mróz, Z. 2001. Study of evolution of shear band systems in sand retained by flexible wall. *International Journal for Numerical and Analytical Methods in Geomechanics*, 25, 909-932.
- Loukidis, D. and Salgado, R. 2009. Modeling sand response using two-surface plasticity. *Computers and Geotechnics*, 36(1-2), 166-186.
- Loukidis, D., Chakraborty, T. and Salgado, R. 2008. Bearing capacity of strip footings on purely frictional soil under eccentric and inclined loads. *Canadian Geotechnical Journal*, 45(6), 768-787.
- Manzari, M.T. and Dafalias, Y.F. 1997. A critical state two-surface plasticity model for sands. *Géotechnique*, 47(2), 255-272.
- Soubra, A-H and Macuh, B. 2002. Active and passive earth pressure coefficients by a kinematical approach. *Proceedings of the Institution of Civil Engineers – Geotechnical Engineering*, 155(2), 119-131.
- Vardoulakis, I. 1980. Shear band inclination and shear modulus of sand in biaxial tests. *International Journal for Numerical and Analytical Methods in Geomechanics*, 4(2), 103-119.

Innovative solutions for supporting excavations in slopes

Solutions innovantes pour le soutien d'excavations situées dans des terrains en pente

Lüftenecker R.
GDP ZT-OG, Austria

Schweiger H.F., Marte R.
Institute for Soil Mechanics and Foundation Engineering, Graz University of Technology, Austria

ABSTRACT: The design of support measures for deep excavations is one of the key tasks in geotechnical engineering. The choice of the most appropriate support system depends on various obvious factors such as ground conditions and excavation depth but sometimes also on less obvious boundary conditions, for example when construction of ground anchors is not possible because permission of placing them in neighbouring property is not given. In these cases other options have to be pursued, resulting sometimes in non-conventional solutions. Examples for such innovative support systems are presented in this paper. In the first case the arching effect of the retaining structure was used to design an excavation pit without any anchors reaching on the neighbouring ground, because there was no permission for construction elements there. The 6 meter spanned arches consist of mixed in place columns (MIP), which rest on supporting walls (also mixed in place columns) oriented in the direction of the slope. In the second example the behaviour of a serrated sheet pile has been investigated. Comprehensive 3D finite element analyses have been performed in order to prove that the suggested retaining structures are feasible solutions.

RÉSUMÉ : La conception des mesures de soutènement pour les excavations profondes est une des tâches fondamentales dans la géotechnique. Le choix du système le plus approprié dépend de plusieurs facteurs évidents comme les conditions de sol ou la profondeur de l'excavation, mais parfois aussi de contraintes moins évidentes comme par exemple le cas où des ancrages ne sont pas possibles parce qu'il n'y a pas d'autorisation pour l'installation dans la propriété voisine. Dans ces cas, d'autres options doivent être envisagées, qui résultent parfois dans des solutions non-conventionnelles. Quelques exemples de telles solutions sont présentés. Dans le premier cas, l'effet de voûte de la structure de soutènement a été utilisé pour la conception d'une excavation qui bordait une propriété pour laquelle il n'y avait pas d'autorisation pour l'installation des éléments d'ancrage. Les voûtes avec une portée de 6 mètres ont été réalisées avec des colonnes « Mixed in Place » (MIP) qui prenaient appui sur des parois orientées dans la direction de la pente. Dans le deuxième exemple, le comportement d'une palplanche dentelée a été examiné. Des analyses par la méthode des éléments finis 3D complètes ont été effectuées afin de prouver que la structure de soutien proposée était une solution réalisable.

KEYWORDS: deep excavation, finite element method, three-dimensional analysis.

1 INTRODUCTION

The design of support measures for deep excavations is one of the key tasks in geotechnical engineering and, depending on soil conditions and adjacent infrastructure, many different options exist. One of the most difficult situations to overcome is when space for support measures is limited and due to legal reasons support elements such as ground anchors cannot be built on neighbouring ground. The obvious solution in these cases, namely putting struts, is often not very convenient for the excavation process and sometimes even not possible, e.g. if the excavation is situated in a slope. These cases require special attention and two case histories where innovative solutions have been found are presented in this paper.

2 NUMERICAL ANALYSIS

In order to demonstrate the feasibility of the proposed design and to assess expected deformations a number of three-dimensional finite element analyses have been carried out. These analyses also served as basis for the design of the structural elements. The finite element code Plaxis 3D Foundation has been used for all analyses presented in this paper (Brinkgreve and Swolfs 2007).

It is well established that for this type of analysis simple linear elastic-perfectly plastic constitutive models are not very well suited and therefore a more advanced model, namely the

Hardening Soil model, has been employed. This model is a so-called double hardening model and allows for plastic compaction (cap hardening) as well as plastic shearing due to deviatoric loading (friction hardening). The main features of this model, as implemented in Plaxis, can be summarized as following.

- Stress dependent stiffness according to a power law.
- Plastic straining due to primary deviatoric loading.
- Plastic straining due to primary compression.
- Elastic unloading / reloading.
- Failure according to the Mohr-Coulomb criterion.

A more detailed description of the Hardening Soil model can be found e.g. in Schanz et al. 1999.

3 CASE HISTORY 1 – MIXED IN PLACE COLUMNS

The first example is concerned with an excavation situated in a slope, just below existing buildings. The owner of one of the buildings was particularly alerted because he experienced significant damage to his building in the past due to nearby construction activities. He did not allow ground anchors to reach his property. Thus the task was to stabilize the excavation without ground anchors and at the same time provide sufficient support to keep deformations, which could lead to damage of the building located above the excavation, to an absolute minimum. This could be achieved by arches of 6 meter span

constructed by mixed in place columns (MIP), which rest on supporting walls (also mixed in place columns) oriented in the direction of the slope. The earth pressure exerted from the slope was transferred to 5 meter deep mixed in place walls underneath the planed building at the base of the slope. Figure 1 shows the slope with the supporting structure and Figure 2 a detail of the MIP columns.

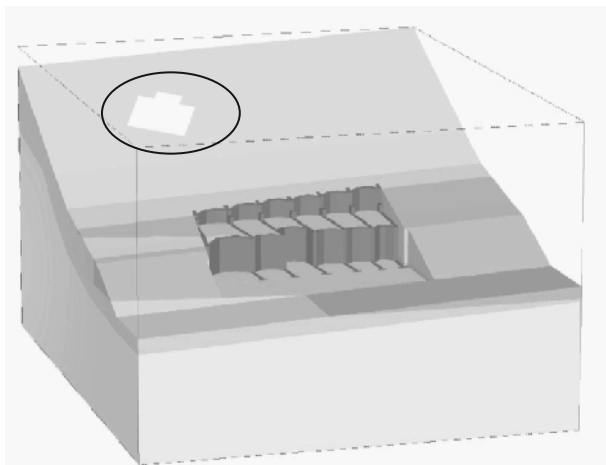


Figure 1. Overview of slope and support structure including critical building.

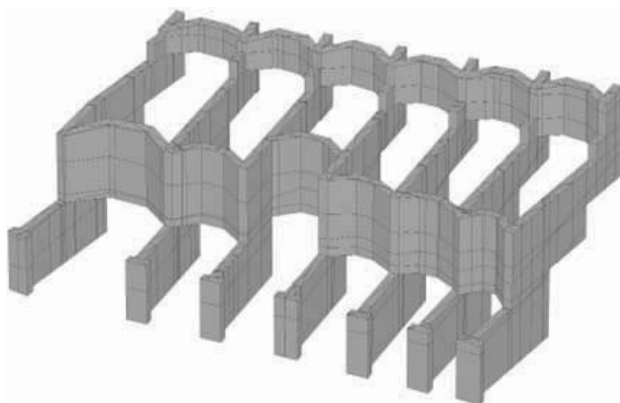


Figure 2. Layout of support structure (MIP columns).

Based on the results from site investigations a representative underground model consisting of three layers was established for the 3D finite element analysis, namely soft sandy silt (0-4 m below surface), stiff laminated sand-silt (4-8 m below surface) and semi-solid sand-silt (below 8 m from surface). The most important parameters for these layers are summarized in Table 1. E_{oed}^{ref} is the stiffness from an oedometer test for the reference vertical effective stress of 100 kPa, E_{50}^{ref} is a secant stiffness at 50% of maximum deviatoric stress in a triaxial compression test at a reference cell pressure $\sigma_3' = 100$ kPa, E_{ur}^{ref} is the unloading/reloading stiffness, again at a reference cell pressure of 100 kPa from a triaxial test, and m is a parameter determining the stress dependency of above stiffness parameters. ϕ' , c' and ψ are the conventional Mohr-Coulomb strength parameters which define ultimate strength in the Hardening Soil model.

The MIP-method improves the mechanical properties of a soil by mechanically mixing and adding binder slurry. The result is a "soil-concrete-mixture" in which the soil is used as aggregate. For the MIP-columns a constitutive model based on the Mohr-Coulomb failure criterion was applied. Based on an unconfined compressive strength of 5 MN/m², whereas this value includes a partial factor of safety on material strength, the material parameters listed in Table 2 have been adopted.

Table 1. Material parameters for Hardening Soil model for soil layers.

Parameter	Layer 1	Layer 2	Layer 3
Friction angle, ϕ' (°)	25	27.5	30
Cohesion, c' (kPa)	0	1	5
Dilatancy angle, ψ (°)	0	0	0
Unit weight, γ (kN/m ³)	20	20.5	21
$E_{oed}^{ref} = E_{50}^{ref}$ (kPa)	10000	25000	45000
E_{ur}^{ref} (kPa)	30000	75000	135000
m (-)	0.5	0.5	0.5

Table 2. Material parameters for MIP-columns.

Parameter	MIP
Friction angle, ϕ' (°)	30
Cohesion, c' (kPa)	250
Unit weight, γ (kN/m ³)	22
Elasticity modulus (kPa)	300000
Tension cut off* σ_t (kPa)	125

* based on reinforcement by steel rods and nails

The results of the calculation show the expected stiff behaviour of the chosen support system. The maximum calculated horizontal deformation of about 15 mm occurs at the front upper corner of the lower excavation step (Figure 3). At the back of the wall (near the border of the neighbouring property) deformations are in the order of millimetres and thus the expected settlements in this area can be considered to be not significant and will not cause any damage to the building (Figure 4). However, the finite element analysis could not model the construction process of the MIP-columns, i.e. the columns were assumed "wished-in-place" before excavation starts and therefore displacements due to the construction process have to be added to these values.

The 3D-model was also used to check the tension zones in the MIP-body. The main tension stresses were located at the connections of the arches and the wall elements. In this area the MIP-wall was reinforced with steel beams (HE-B profiles).

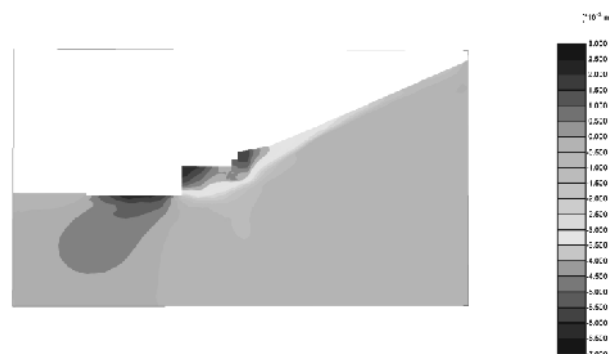


Figure 3. Calculated horizontal displacements, cross section

The measurements during construction on one hand confirmed the results for the numerical analysis but on the other hand showed that significant deformations occurred during construction of the MIP-columns itself (Figure 5). After construction of the columns (panels) deformation measured were less than 15 mm, comparing well with the finite element

predictions. Figure 5 shows the deformations of different points on the top of the MIP-wall. At the neighbouring buildings no movements were recorded. Figure 6 presents a view of excavated MIP-walls.

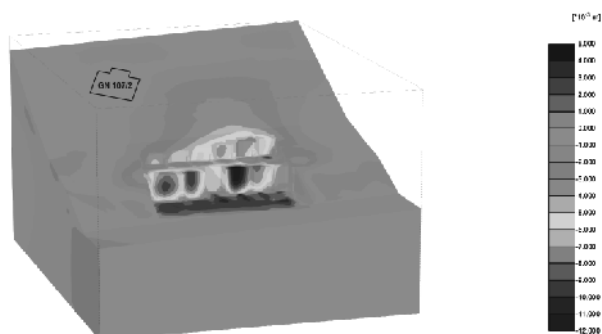


Figure 4. Calculated horizontal displacements with critical building

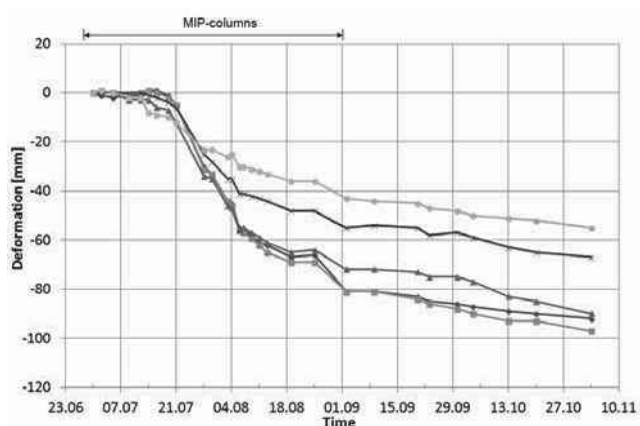


Figure 5. Measured horizontal displacements at several points at the top of the MIP-wall



Figure 6. View of excavated MIP-walls

The large deformations during the production of the columns had two main reasons. In the first part of the production too many MIP columns were produced within a small area. The MIP columns, which take some time to gain strength, weakened the slope during construction, which was already close to critical state. Furthermore, to reduce the length of the MIP columns (in order to save money), deeper working planes than planned were excavated.

This presented case study clearly shows that it is possible to support the earth pressure exerted from a slope by arches constructed by means of soil improvement techniques without

any anchors reaching on neighbouring ground. The numerical analysis was able to prove that the design concept is feasible, however, it is important to observe the deformation during the construction stages because not all aspects of the construction process, in this case of the MIP-columns, can be taken into account in the numerical model.

4 EXAMPLE 2 - SERRATED SHEET PILE WALL

The second example is concerned with the same problem, namely limited space for support measures, but this time it is in an urban environment, namely in the city of Salzburg, Austria. Again the excavation was very close to the adjacent property and it was not allowed to put any construction elements, such as ground anchors, there. In this case the solution chosen was a serrated sheet pile wall. Generally, the subsoil conditions in Salzburg consist of a top layer with backfill and gravel, and soft silty sand and clayey silt layers underneath. The layout of the sheet pile wall follows from Figure 7 (3D finite element model). Every 6 to 8 m there is a 3 m deep indentation in the sheet pile wall. The construction of diagonal compression and tension bars at the top transfers the earth pressure to the right-angled parts of the sheet pile walls. A steel construction, similar to a whaler beam, on top prevents non-homogeneous deformations of the wall. After excavation a drainage layer and a concrete slab is installed to prevent long term movements of the wall and to reduce the influence of the soft layers below excavation level.

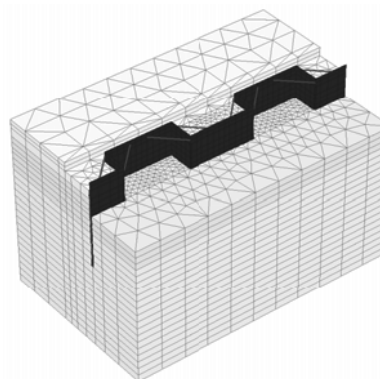


Figure 7. 3D finite element model

The key material parameters for the soil layers considered in the analysis are listed in Table 3. Again the Hardening Soil model has been employed.

Table 3. Material parameters for Hardening Soil model for soil layers.

Parameter	<i>backfill</i>	<i>silty sand</i>	<i>clayey silt</i>
Friction angle, φ' (°)	35	27.5	25
Cohesion, c' (kPa)	0,1	3	5
Dilatancy angle, ψ (°)	0	0	0
Unit weight, (kN/m ³)	19/21	20/21	18/20
$E_{oed}^{ref} = E_{50}^{ref}$ (kPa)	52000	30000	15000
E_{ur}^{ref} (kPa)	208000	120000	60000
m (-)	0	0.5	0.5

The 3D model showed that deformations can be kept to a minimum with maximum values below 10 mm (Figure 8), which was also confirmed by observations during construction. Deformations due to driving and removing of the sheet pile wall are not considered in the analysis. Experience has shown that in this type of soils settlements can reach 20 to 30 mm, and in this particular case observed values were within the lower range.

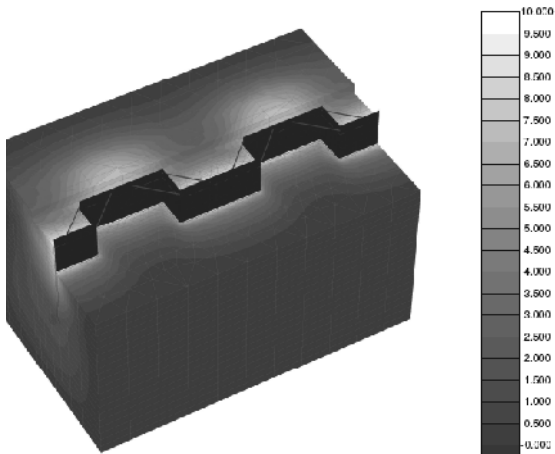


Figure 8. Calculated horizontal displacements

The bending moments of a sheet pile wall with this particular shape and the strengthening construction on top of the wall is not the same as for a cantilever wall, which one would obtain from a 2D analysis and therefore the 3D analysis was essential and helped to estimate the influence of the special support measures. However, 3D finite element analyses are quite time consuming if many different scenarios have to be investigated.

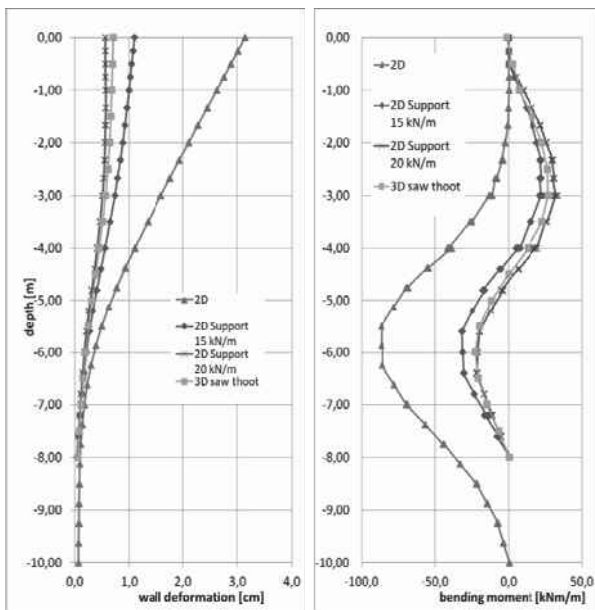


Figure 9. Comparison of 2D and 3D analysis of wall deformation and bending moments

An attempt was therefore made to develop an equivalent 2D analysis for performing parametric studies for a preliminary design. For that reason a 2D model of the sheet pile wall with a supporting force on top of the wall was created. It turned out that for the case of a 8 m deep sheet pile wall and a 4 m deep excavation (groundwater is also at 4 m depth) a supporting force between 15 kN/m und 20 kN/m lead to similar wall deformations und bending moments (Figure 9). This supporting force has to be carried from the additional wall elements spanning across the edges of the two lines of the serrated sheet pile wall (see also Figure 8). The calculations revealed that the earth pressure distribution of the rectangular part of the serrated sheet pile wall is between the active and the at-rest earth pressure (see Figure 10).

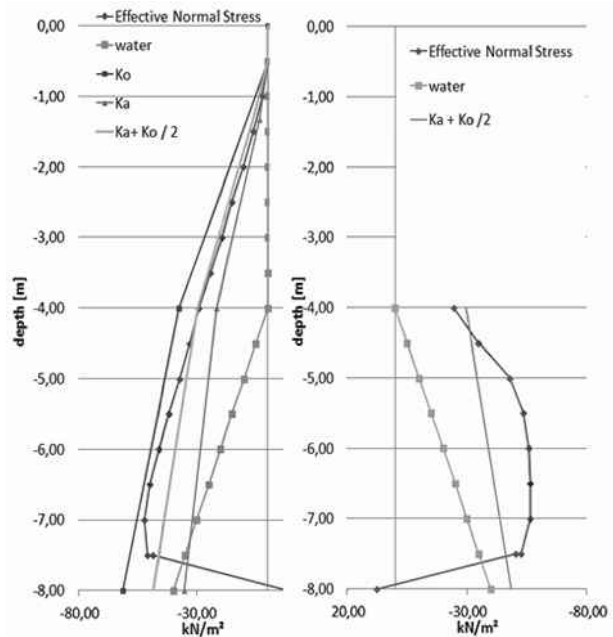


Figure 10. Earth pressure distribution on active and passive side

For the given geometry (distance of 8 m between the rectangular walls) this earth pressure distribution leads to a maximum resistance by wall friction of about 20 kN/m. This shows a good correlation with the presented calculations.

5 CONCLUSIONS

3D finite element modelling allows complex geotechnical structures to be analysed. In the two presented case histories the calculations helped to estimate the arching effect of a curved retaining structure in order to design an excavation pit without any anchors reaching on the neighbouring ground. In the second example the behaviour of a serrated sheet pile has been investigated. In both case the numerical analyses proved the feasibility of the chosen design and improved the understanding how these complex structures behave.

However, even with 3D models it is usually not possible to include all excavation stages in great detail and, more importantly, installation effects are beyond the capabilities of standard numerical tools and this has to be kept in mind when assessing numerical results. Therefore it is essential to monitor the behaviour of the structure during construction and have appropriate counter measures in mind when deformations due to installation effects or unforeseen ground conditions reach critical limits.

6 REFERENCES

- Brinkgreve R.B.J. and Swolfs W.M. 2007. Plaxis 3D Foundation, Users Manual, Plaxis bv, Delft, The Netherlands
- Schanz T., Vermeer P.A. and Bonnier P. 1999. The Hardening-Soil model: Formulation and verification. *Beyond 2000 in Computational Geotechnics*, R.J.B. Brinkgreve (ed.), Balkema, Rotterdam, 281-290.

Design and Construction of Inclined-Braceless Excavation Support Applicable to Deep Excavation

Dimensionnement et Construction du Support d'Excavation Incliné Sans Butons Applicable à une Excavation Profonde

Maeda T., Shimada Y., Takahashi S., Sakahira Y.
Obayashi Corporation

ABSTRACT: The inclined-braceless excavation support (IBES) construction method is characterized by allowing the reduction of retaining wall rigidity and omission of shoring because it reduces the earth pressure acting on the wall, compared with construction using vertical retaining walls. Thus, there are cases where inclined retaining walls are more beneficial in terms of workability and economy than vertical retaining walls, depending on the excavation depth or ground conditions. For the inclined-braceless excavation support construction method applied at open-cut (excavation depth of 9.6m) construction site, this paper presents results of centrifugal model experiments that reflected the actual excavation cross section, the design of the retaining walls in consideration of the inclination of the wall, applied construction method, and measurement results at the site.

RÉSUMÉ: On peut s'attendre à ce qu'une paroi de soutènement inclinée subisse une pression du sol moindre qu'une paroi verticale classique. Le Support d'Excavation Incliné Sans Butons (SEISB) pourrait donc offrir des avantages: un besoin de rigidité réduit et la disparation des étrésillons ou des ancrages. Selon la profondeur d'excavation et les conditions de sol, il peut aussi être plus efficace qu'un système vertical en termes de coût et de durée des travaux. Le présent document rapporte le cas d'un chantier où la méthode SEISB a été utilisée pour une excavation de 9,6m de profondeur: test en centrifugeuse sur un modèle de la coupe d'excavation du chantier, dimensionnement prenant en compte la pression du sol sur un support incliné, méthode de construction adaptée et réalisation des travaux.

KEYWORDS: Inclined-braceless excavation support, steel sheet pile, centrifuge model experiment, earth pressure

1 INTRODUCTION

According to earth pressure theory, the earth pressure acting on temporary earth retaining walls set up during excavation work is reduced when the earth retaining wall is reclined. However, earth retaining walls are generally installed vertically in consideration of workability and construction site limitations, and no earth retaining walls which utilized effect of reduced earth pressure for inclined retaining wall were implemented. Furthermore, deep excavation work requires shoring such as bracing or ground anchors for vertical earth retaining walls with high rigidity (Figure 1).

The inclined-braceless excavation support (IBES) construction method is characterized by allowing the reduction of wall rigidity and omission of shoring because it reduces the earth pressure acting on the wall, compared with construction using vertical retaining walls (Figure 2). Thus, there are cases where inclined retaining walls are more beneficial in terms of workability and economy than vertical retaining walls, depending on the excavation depth or ground conditions.

The authors have previously conducted centrifugal model experiments on inclined-braceless retaining walls using sand ground to examine earth pressure distributions and deformation behavior (Shimada et al. 2010, 2011) and quantitatively confirmed that the earth pressure acting on the retaining walls and deformation arising from excavation can be reduced by inclining the retaining walls.

This paper reports on centrifugal model experiments that reflected the excavation cross section at an actual scale construction site for the inclined-braceless retaining wall construction method to determine its suitability, the design of inclined-braceless retaining walls using reduced earth pressure by inclination of the wall, applied construction method, and measurement results at the site.

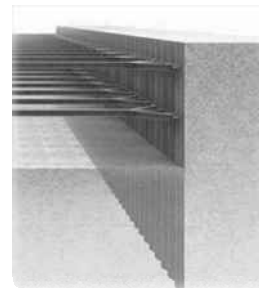


Figure 1 Vertical retaining wall

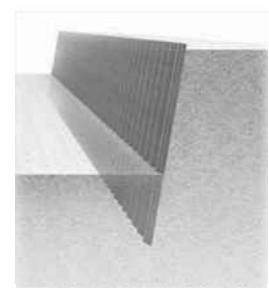


Figure 2. Inclined-braceless retaining wall

2 SUMMARY AND ISSUES OF CONSTRUCTION METHOD FOR INCLINED-BRACELESS RETAINING WALL

Cantilever retaining walls have been widely adopted to retain earth at relatively shallow excavation depths (3–4 m). Inclined-braceless retaining walls are an attempt to switch from the conventional concept of vertical retaining walls in order to reduce earth pressure and make it possible to apply cantilever retaining walls even at deeper excavation depths.

There are no application examples of temporary inclined retaining walls; design issues for the inclined-braceless retaining wall construction method include calculation of the earth pressure while considering the inclination of the retaining wall, and consideration of rollover not only to the excavation side but also to the back side in calculation of embedding of walls. Construction issues include the accuracy of the inclination angle set during retaining wall installation and the construction work cycle time. Centrifuge model experiments conducted to examine these design issues, the applied design

methods, and actual performance at construction sites where the design methods were implemented are described below.

3 CENTRIFUGE MODEL EXPERIMENT OF INCLINED-BRACELESS RETAINING WALL

3.1 Experiment method

A 1/33-scale model ground was prepared to develop excavation cross sections of applicable construction sites (Figure 3) for this experiment. A maximum centrifugal acceleration of 33g was loaded to examine deformation of the retaining wall and distribution of the earth pressure. Figure 4 shows an outline of the model ground. The dimensions of the soil container were 80 cm width × 50 cm height × 20 cm depth. The front side of the container was fabricated from an acrylic plate so that ground displacements could be measured. A Teflon sheet was attached between the soil container, including the acrylic plate, and the model ground to reduce friction. The depth of the model ground was developed with berm to a maximum of 29 cm, and the height of the retaining wall was 36 cm. The model ground is shown in Photo 1. The retaining wall was created assuming that the retaining walls would be made of steel sheet piles. A compact earth pressure gauge (6 mm dia., capacity of 1 MN/m²) was embedded at seven locations on the active side and at four locations on the passive side to measure the earth pressure acting on the wall surface. The retaining wall model was installed and then filled with dry Toyoura standard sand by the airdrop method to prepare the model ground. Excavation steps were simulated during the experiment by repeating the method of loading centrifugal acceleration after the prescribed excavation work was performed at a 1g site. Table 1 shows the experimental cases.

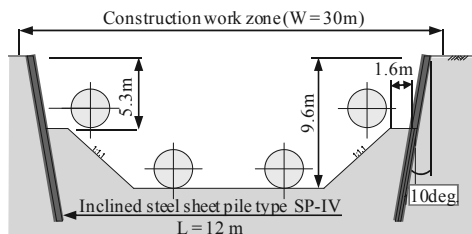


Figure 3. Cross-section of inclined-braceless retaining wall applied at site

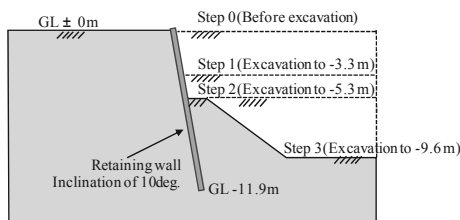


Figure 4. Outline of model ground.

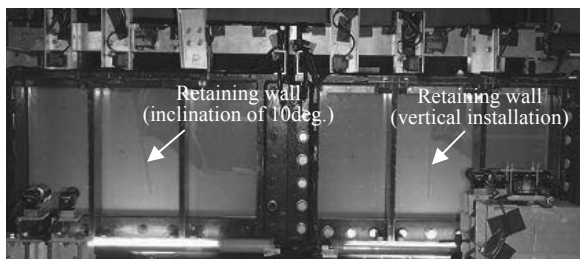


Photo 1. Model ground

Table 1: Experiment Cases

No.	Case 1	Case 2
Retaining wall conditions	Vertical	Inclined (inclination of 10 degree)
Retaining wall model	Made of aluminum, thickness of 7 mm	
Ground	Material: Toyoura standard sand (dry) Density: $\rho_d=1.55 \text{ g/cm}^3$ Preparation method: Airdrop method	
Excavation steps	Step 0: Before excavation Step 1: Excavation depth of 3.3 m Step 2: Excavation depth of 5.3 m Step 3: Excavation depth of 9.6 m	

3.2 Experiment results

Figures 5 and 6 show the deformation behavior of the retaining wall due to excavation work. The displacements shown below were converted to actual-scale displacements by multiplying the experimental measurement results by 33. Figure 5 shows the displacement distribution of the retaining wall for each excavation stage. The horizontal displacement was larger at higher sections of the wall, and deformation occurred in the frontal incline with the lower section of the wall as the axis. Regardless of the excavation depth, the amount of horizontal displacement of the inclined walls was smaller than that of the vertically installed walls. Figure 6 shows the relationship between the excavation depth and horizontal displacement at top of the wall. The deformation increased in correlation to the depth; the displacement of the vertically installed wall was measured at the maximum excavation depth as 20 cm, whereas that of the inclined wall was about 14 cm. Thus, the experimental results confirmed that the amount of deformation was about 30% smaller with inclined walls.

Strain gauges were attached to the front and back surfaces of the wall in the direction of the depth at three locations in order to obtain the bending status of the wall. Figure 7 shows the depth distribution of the bending strain: the maximum value was obtained in the vicinity of the center of the wall regardless of whether the wall was inclined. The maximum bending strain was smaller with inclined walls than with vertically installed walls regardless of the excavation depth. The gap between the two was larger when the excavation depth was 9.6 m than when it was 3.3 m; the effects of inclining the wall were significant and evident.

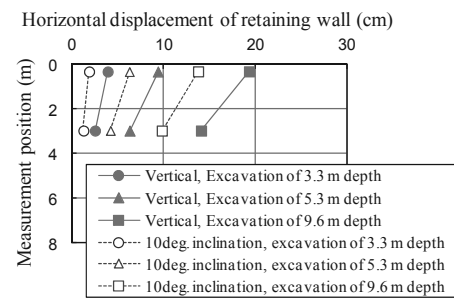


Figure 5. Horizontal displacement distribution of retaining walls

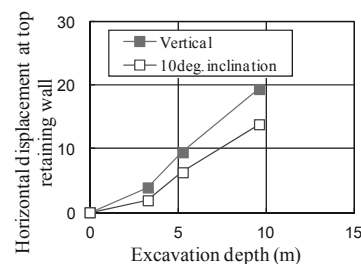


Figure 6. Relationship between excavation depth and horizontal displacement of retaining walls

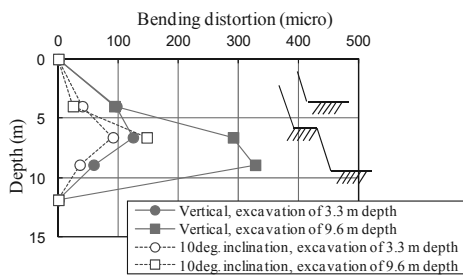


Figure 7. Bending strain distribution of retaining

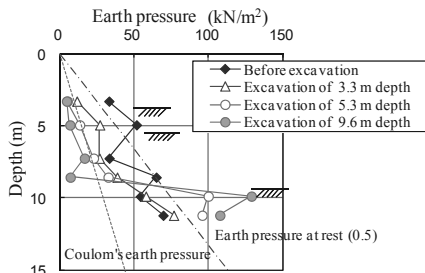


Figure 8. Earth pressure acting on wall surfaces - vertical retaining walls

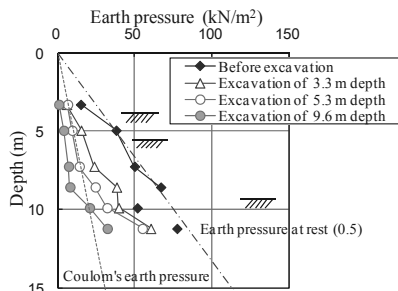


Figure 9. Earth pressure acting on wall surfaces - inclined retaining walls

Figures 8 and 9 show the depth distribution of the active earth pressure that acted on the wall. Although the measurement results for the vertically installed wall showed dispersions prior to excavation, the validity of the earth pressure measurements taken by this equipment were confirmed because they were approximately equal to the earth pressure at rest assuming $K_0 = 0.5$, as noted in the figure. The earth pressure decreased in the excavated sections and increased more than the earth pressure at rest in the embedded sections. The figure shows the Coulomb's earth pressure, where the friction angle of the retaining wall was considered to be $\phi/3$. The active earth pressure measured at the excavated sections was slightly smaller in distribution than the Coulomb's earth pressure. The earth pressure acting on the inclined wall decreased more than the earth pressure at rest regardless of depth. Thus, the acting pressure was smaller than that of the vertically installed wall, which confirmed that inclination of the wall contributed to the stability of the wall in terms of earth pressure as well.

4 DESIGN OF INCLINED-BRACELESS RETAINING WALL

4.1 Calculation method for earth pressure

Ground of the site (Figure 3) was a landfill comprised primarily of loose fine sand (layer thickness: 12 m, N-value: 3–5, and ϕ : 33°). The inclination of the retaining wall could not be considered in the conventional design of the temporary retaining walls, because the Rankine–Resal formula is generally applied to the active earth pressure used. The earth pressure calculation method with Coulomb's formula (Figure 10) used in the design of permanent retaining walls, which considers the inclination of the wall, was therefore applied. Its use was determined safe for design purposes because the earth pressure reduction effect was confirmed in the centrifugal model

experiments with inclined walls. Similarly, the Coulomb's earth pressure was adopted for the passive earth pressure.

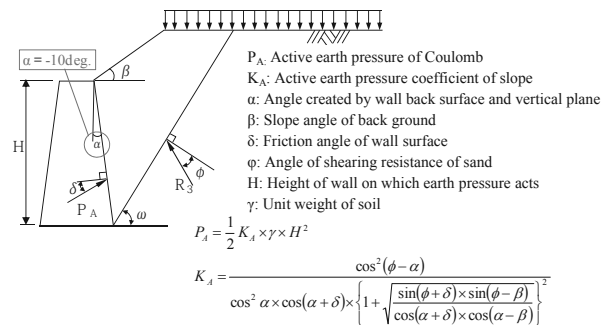


Figure 10. Active earth pressure calculation

4.2 Calculation method for embedding lengths

The embedding length was calculated using not only the “method for determining embedding length to maintain balance based on earth pressure” but also the “overall slippage including the retaining wall.” The circular slipping calculation (Figure 11) was performed to determine the embedding length so that both of the above methods were satisfied. The safety factor for the arc slipping calculation was set to 1.2.

4.3 Calculation of retaining wall displacements and stresses

The displacements and stresses that occurred with the retaining wall were calculated based on elasto-plasticity analysis, which evaluated the earth pressure and wall embedding length given in subsections 4.1 and 4.2 above, by considering the retaining wall as a finite length elastic beam and ground as an elasto-plastic spring (figure 12).

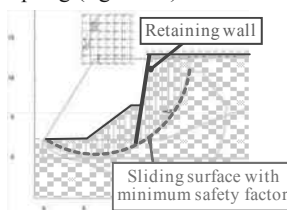


Figure 11. Verification on slipping stability

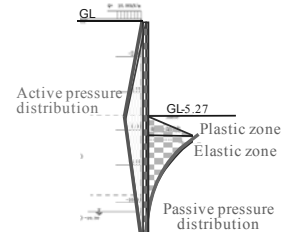


Figure 12. Elasto-plastic analysis

5 CONSTRUCTION WORK IMPLEMENTATION RECORD FOR INCLINED-BRACELESS RETAINING WALLS

5.1 Summary of applied construction sites

The construction sites where the inclined-braceless retaining walls were applied were located within premises used by existing electric power plant and new plant construction. Excavation work had to be performed to install two sets of water intake and water discharge steel pipes (each pipe with a diameter of 2800 mm) in a restricted construction work zone with a width of 30 m (Figures 3 and 13). The period of construction work, which included piping work, needed to be less than six months owing to adjustments that had to be made to accommodate the progress of the main unit construction work being performed at new electric power plant.

In order to satisfy the above conditions, the inclined-braceless excavation retaining wall construction method which reduces earth pressure by inclining the wall, was adopted as it requires no shoring, even when the excavation depth is deep. The retaining wall was fabricated from steel sheet pile type SP-IV, and the inclination of the retaining wall was set to 10 degree owing to restrictions imposed within the construction work zone and the excavation cross section necessary for piping work.

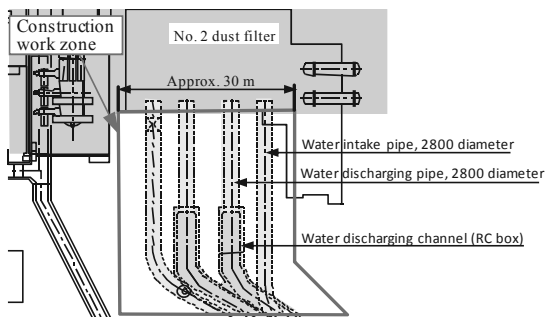


Figure 13. Construction work zone plan

5.2 Inclined-braceless retaining wall construction method

The steel sheet piles driven in at an inclination angle were installed in a manner similar to ordinary vertical installation: a silent piler was used combined with a water jet to reduce the insertion resistance. Because the piler was tilted according to the inclination of the piles being installed, an auxiliary cylinder was installed on the piler main unit to control the angle (Photo 2 and 3). The initial insertion until the piler was set on the piles used a blocking base (110 kN), similar to ordinary vertical installation. The top plate of the blocking base was inclined by 10 degree to accommodate the inclined installation of the piles (Photo 4). The inclination angle was monitored by infrared laser units installed at two locations aside from inclined finishing stake.

5.3 Comparison of onsite measurement results and design values

5.3.1 Earth pressure

The distribution of actual measurements for the earth pressure, which was taken by wall-surface-mounted earth pressure gauges at the time of the final excavation, indicated 20%–50% of the design values on the back side (active side) and 5% of the ultimate value on the excavation side (passive side) (figure 14). The setting method for coefficient of earth pressure (applying the Coulomb’s formula) was considered to be valid because the gradient (equivalent to the earth pressure coefficient) up to GL-3m was roughly equal for the active earth pressure distribution. With regard to the passive earth pressure, the displacement of the retaining wall was small and the ground had a sufficient margin for resistance on the passive side.

5.3.2 Displacements and stresses of steel sheet piles

The maximum displacement during final excavation was 24.1mm, which was about 20% of the design value of 119.2mm (Figure 15). The maximum stress level of the steel sheet piles according to strain gauges was a tensile stress of 8.4N/mm², which is extremely small and about 8% of the design value of 103N/mm². Furthermore, the bending moment distribution obtained by converting the measurement data from the inclinometers was roughly the same as the bending moment distribution obtained from strain gauges.



Photo 2. Overall view of installation work



Photo 3. Auxiliary cylinder



Photo 4. Blocking base

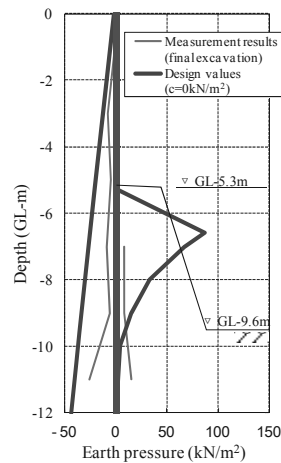


Figure 14. Earth pressure distribution comparison

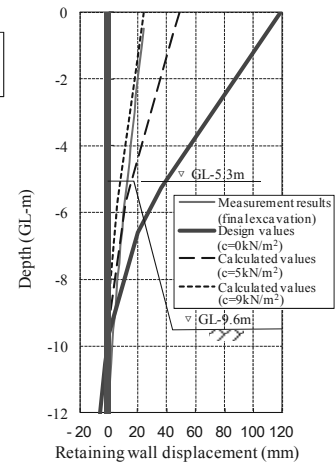


Figure 15. Retaining wall displacement

6 CONCLUSIONS

For the inclined-braceless retaining walls (inclination of 10 degree) with an excavation depth of 9.6 m in sand ground, the effects of earth pressure reduction and stability of retaining wall were verified by a centrifugal model experiment. A design method was developed that considers inclination of the wall by using the Coulomb’s formula in elasto-plastic analysis so that inclined-braceless retaining walls can be adopted at actual construction sites. The actual measurement values taken onsite for the earth pressure acting on the retaining wall and the displacement and stress of the retaining wall both agreed with the design values. Thus, the safety of the retaining wall can be secured using the proposed design method. The inclined retaining wall construction method was used to realize a cantilever retaining wall without shoring despite a deep excavation depth of 9.6 m. Thus, excavation, piping, and building work can be completed in a short term and safely.

We will collect design and construction work track records for the inclined retaining walls under a variety of ground conditions for verification of evaluation methods for analysis models, soil parameters, and earth pressure, and cycle time of construction work, in order to establish more practical design and construction methods.

7 REFERENCES

Shimada Y., Matsumoto S., Takahashi S. and Sugie S. 2010. Centrifugal model experiments pertaining to earth pressure of sand ground acting on cantilever retaining walls. *Proceedings of the 65th Annual Conference of the Japan Society of Civil Engineers*, III-456.
 Shimada Y., Idemitsu M., Takahashi S. and Maeda T. 2011. Centrifugal model experiments pertaining to earth pressure of sand ground acting on steel sheet pile cantilever retaining walls. *46th Japan National Conference on Geotechnical Engineering*, 682.

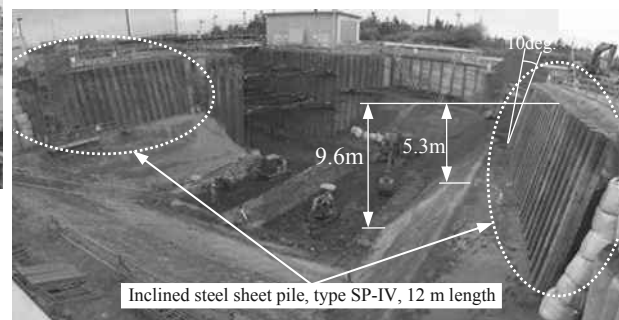


Photo 5. Overall view of excavation completed site

Shaking table tests on caisson-type quay wall with stabilized mound

Essais à table vibrante sur les murs de quai de type caisson avec butte stabilisée

Mizutani T.

Geotechnical Engineering Field, Port and Airport Research Institute

Kikuchi Y.

Professor, Department of Civil Engineering, Tokyo University of Science

ABSTRACT: Caisson-type quay walls were one of the major types of quay walls in Japan. It was desired to increase the front-water depth of them, because vessels coming alongside them become larger and larger. The authors have been studying on a new construction method for the improvement. The method consisted of two steps. Step 1 was to solidify a part of rubble mound beneath a caisson and step 2 was to cut it to increase the front-water depth of the caisson. A series of shaking table tests were conducted to study the seismic behavior of caisson-type quay walls improved by the new method. This paper will introduce the test results and discuss the factors which affected the seismic behavior of the caisson-type quay walls with stabilized mound.

RÉSUMÉ : Les murs de quai de type caisson constituent l'un des types majeurs de murs de quai au Japon. On a désiré augmenter la profondeur frontale face à la mer car les navires venant accoster le long des quais deviennent de plus en plus gros. Les auteurs ont étudié une nouvelle méthode de construction afin d'apporter des améliorations. Cette méthode est constituée de 2 étapes. La 1ère étape consiste à solidifier une partie de la butte de gravats sous le caisson et la 2ème étape à le découper afin d'augmenter la profondeur frontale du caisson. Une série d'essais à table vibrante a été menée afin d'étudier le comportement sismique des murs de quai de type caisson qui ont été améliorés grâce à cette nouvelle méthode. Cette étude présente les résultats des essais et analyse les facteurs qui affectent le comportement sismique des murs de quai de type caisson avec butte stabilisée.

KEYWORDS: caisson-type quay wall, front-water-depth enlargement, shaking table test

1. INTRODUCTION

In recent years, there has been increasing demand to reduce costs for public works in Japan. Correspondingly, great efforts have been directed toward using and upgrading existing infrastructures efficiently. In this context, the authors have been studying methods for enhancement and improvement of existing port facilities.

Because the caisson-type quay wall (see Figure 1) is one of the major types used in Japan (OCDI 2009), it is desirable that this type quay wall have more front-water depth to better accommodate the larger and larger vessels coming alongside. A method often employed for this improvement is to construct a new pier front onto the caisson quay wall as shown in Figure 2. It is impossible, however, to adopt this method for a caisson quay wall when there is not enough frontal space: thus, a new improvement method applicable to such situations is being developed. In the new method, a rubble mound beneath a caisson is solidified then cut to increase the front-water depth of the caisson as shown in Figure 3.

The authors conducted a series of shaking table tests to study the seismic behavior of caisson-type quay walls improved by the new method.

2. TEST METHOD

A model of a caisson quay wall was built in a sand box whose inside dimensions were 85cm in length, 35.4cm in width and 65cm in height. Figure 4 shows a schematic view of the model. The gravel layer at the bottom of the sand box was part of the box (for drainage). It was compacted sufficiently and it was assumed that the deformation of the gravel layer would not affect test results. A non-woven fabric was put on the surface of the gravel layer for sand prevention. The tests focused on the vibrational property and deformation mode of the quay walls

with a stabilized mound; the model ground was dry for simplicity.

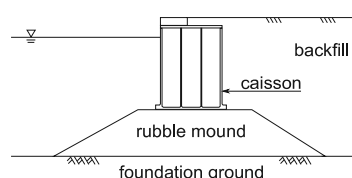


Figure 1. Typical cross-section of the caisson-type quay wall.

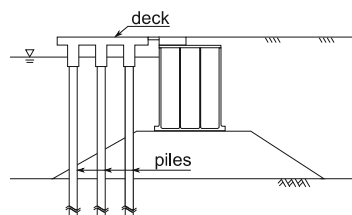


Figure 2. Construction of a new pier to enlarge the front-water depth of the caisson-type quay wall.

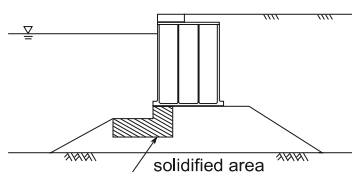


Figure 3. The new method to enlarge the front-water depth of the caisson-type quay wall without change in the face line of the quay wall.

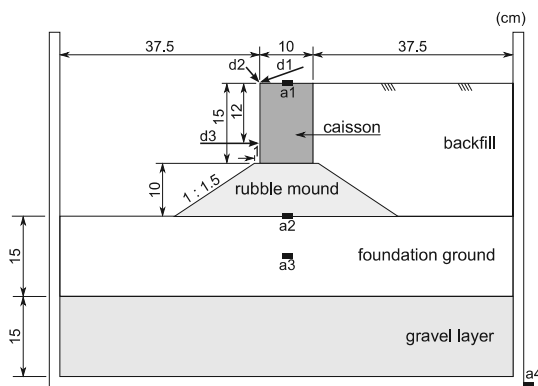


Figure 4. Schematic view of the model ground.

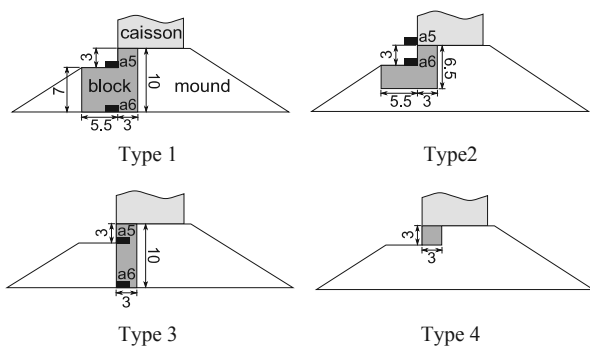


Figure 5. The blocks used in the tests to simulate solidified area in the rubble mound.

First, foundation ground was made by the air pluviation method with Souma sand #6 ($\rho_s = 2.649\text{g/cm}^3$, $\rho_{dmax} = 1.544\text{g/cm}^3$, $\rho_{dmin} = 1.169\text{g/cm}^3$, $D_{60} = 0.161\text{mm}$). Relative density of the foundation ground was about 60%. A rubble mound was built on the foundation ground by gravel #7 (single-sized crushed stone S-5, JIS A 5001) whose particle size was from 2.5 to 5mm. The gravel was placed into a mound by hand, and was not compacted. Density of the rubble mound was about 1.5g/cm^3 . The solidified area in the mound was modeled as a block made of cement paste, and put in the rubble mound. The surface of the rubble mound was covered by gauze to prevent sand particles from dropping into voids within the rubble mound. Then a caisson was located on the mound. The caisson was a wood box in which sand was filled to adjust its weight. Density of the caisson was 0.98g/cm^3 . Finally, backfill was prepared in the same way as the foundation ground.

In the series of tests, blocks having the four shapes, shown in Figure 5, were used. Moreover, the model of the quay wall before improvement, a model without any blocks as shown in Figure 4, was tested.

Accelerometers were placed at points a1-a6 shown in Figures 4 and 5. Acceleration of the shaking table was measured at a4 in Figure 4. Displacement of the caisson was measured at d1-d3. The caisson was divided into three parts in the direction of the face line of the quay wall. The face line is perpendicular to the plane of this page in Figure 4. The measurement was conducted at the center of the caisson to eliminate the effect of friction between the caisson and side walls of the sand box. The blocks, which were the models of solidified area, were divided into three parts in the same manner.

The input wave was a sine wave with a frequency of 10Hz and a wavenumber of 50. Direction of the shaking was perpendicular to the face line of the quay wall. The model was tested by the input wave with 100Gal maximum acceleration, and the residual deformation of the model was recorded by digital camera. Next, the amplitude of the input wave was increased to 200Gal maximum acceleration, and the model was

tested again. In this manner, the model was tested with the input waves whose maximum acceleration was 100, 200, 300, 500, and 800Gal. Several tests were aborted at 500Gal, because deformation of the models was too large to continue the test procedure.

The objective of the tests was to evaluate the variation of vibrational properties and deformation mode caused by the different shapes of the solidified area. The similarity rule for the model was not considered. The tendency of the vibration and deformation of the models was compared relatively, and derivation of the factor which affected the behavior of the quay wall from the comparison was attempted.

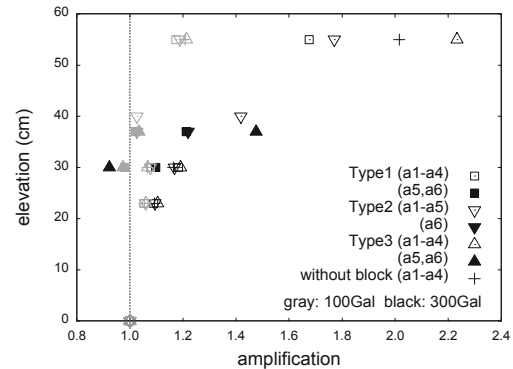


Figure 6. Amplification of acceleration seaward.

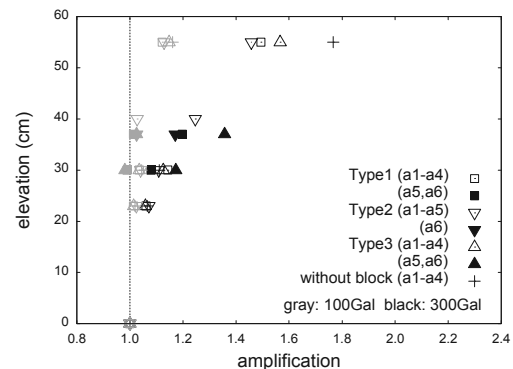


Figure 7. Amplification of acceleration landward.

3. VIBRATIONAL PROPERTY OF QUAY WALL

The vibrational property of the quay wall would be different before and after the improvement. Figures 6 and 7 compare the maximum acceleration amplitude between the models with differently shaped blocks. Figures 6 and 7 also show the amplitude observed in the test of the model without any blocks. Gray marks in the figures show the results observed with the input waves whose maximum acceleration was 100Gal, while black marks show the results with 300Gal. The maximum acceleration amplitudes in figures were calculated as follows: find the maximum acceleration in each cycle of sine waves, calculate the average of the maximum acceleration for the whole of input waves (50 cycles), and divide the average value by the average of the maximum acceleration of a4 (the acceleration of the shaking table, elevation = 0cm). The acceleration time histories were stable for all tests with 100 and 300Gal acceleration, and the maximum acceleration for each cycle remained largely unaltered during the shaking. The calculation was made for each direction; Figure 6 shows the amplitude of acceleration seaward (from the right-hand side to the left in Figure 4) and Figure 7 shows that landward (from left to right in Figure 4). In the case of the tests in which the maximum acceleration of the input wave was larger than 500Gal, large deformation was induced and the accelerometers

tilted; the data were not processed because the accuracy of the measurement of acceleration would be less.

For the test results with 100Gal (gray marks in figures), it could be said that the amplification was small and that there was no large difference among the tests. The amplitude of seaward acceleration was slightly larger than that landward.

In the case of the test with 300Gal (black marks in figures), the amplification tendency differed among the test cases. In the case of quay walls with Type 1 and Type 2 blocks, the acceleration amplitudes at the crown of the caisson were smaller than in the test without blocks both seaward and landward; the stability of the caisson was improved by the blocks. In the case of Type 3 blocks, the amplitude seaward was larger than in the test without blocks at the crown of the caisson, while the amplitude landward was smaller. It was remarkable that the amplitude at the head of the Type 3 block (a5) was much larger in both directions.

Figures 8 and 9 show the phase delay of the acceleration observed in the tests. The phase delay was calculated in the same way as acceleration amplitude. Figure 8 and 9 show that there was no large delay in the case of the tests with 100Gal. Large delay was detected in the landward acceleration observed in the tests with 300Gal acceleration as shown in Figure 9. In the tests with Type 1 and Type 2 blocks, the delay was the same as in the test without any blocks. On the other hand, delay of acceleration landward in the case of the test with Type 3 blocks was much larger than in the case without blocks.

One of the causes of the large acceleration amplitude and delay observed in the test with Type 3 blocks could be the instability of the blocks because the shape was vertically long.

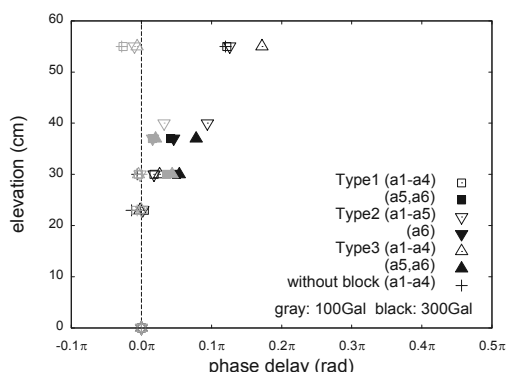


Figure 8. Phase delay of acceleration seaward.

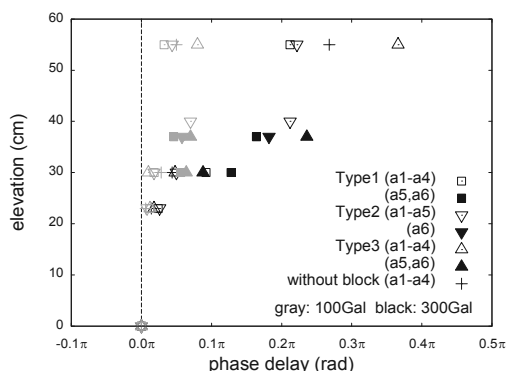


Figure 9. Phase delay of acceleration landward.

4. DISPLACEMENT OF QUAY WALL

The trace of the top-left corner of the caisson in Figure 4 was calculated from displacement measured by d1-d3 for each case. Figure 10 shows the trace observed during the final step of

shaking. The maximum acceleration of the input wave for the final shaking was different among the tests as mentioned before. Tilt angle of the caissons was also calculated from the data of displacement meter; Figure 11 shows the tilt angle observed during the final step.

Figure 12 shows the deformation of the quay wall models observed after the tests. A few millimeters of settlement of the foundation ground were observed in all cases. Sand dropped into clearance gap between the rubble mound and the sand box; the boundary between the mound and the backfill ground was not clear. Figure 12 shows the boundary in outline.

In the case of the model without blocks, the caisson moved seaward with forward inclining as shown in Figures 11 and 12; the large deformation observed with the input wave whose maximum acceleration was 500Gal and the test was aborted (see Figure 12). The caisson in the test with Type 4 blocks showed similar behavior as in the test without blocks. Thus the improved quay wall with Type 4 blocks was comparable in seismic resistance to the quay wall before improvement in spite of the front-water-depth enlargement. Figure 11 shows the tilting of the caisson with Type 4 blocks smaller than the caisson without blocks. The caisson with Type 4 blocks was displaced with small rotation as shown in Figure 12. It could be said that even small blocks like Type 4 had a certain degree of effect on caisson stability.

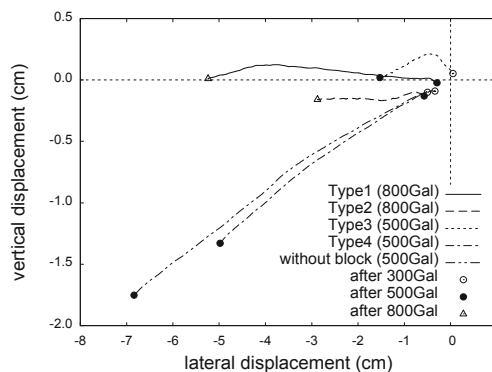


Figure 10. Trace of the top-left corner of the caisson.

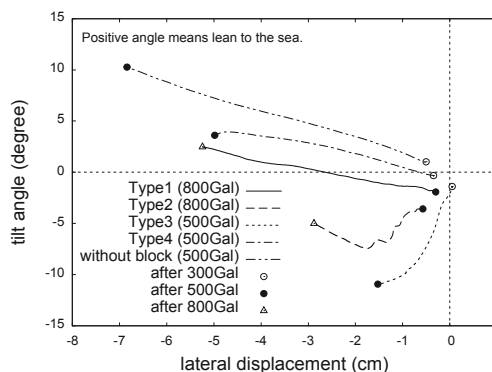


Figure 11. Relationship between tilt angle and lateral displacement of the caisson.

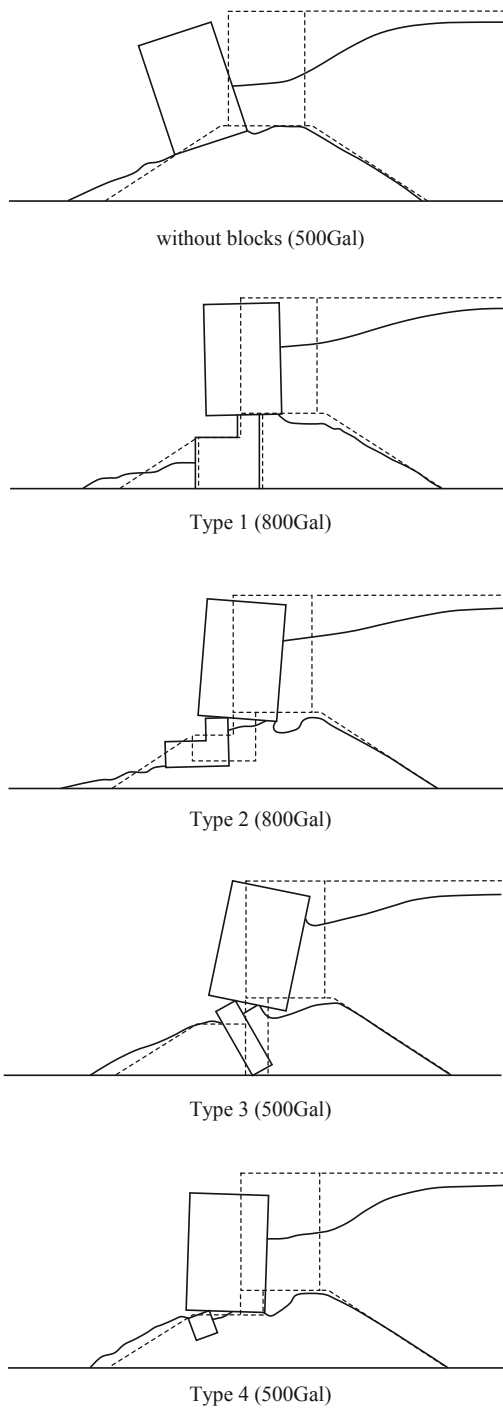


Figure 12. Deformation of the quay wall models after the tests.

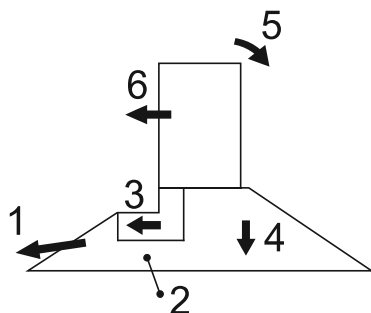


Figure 13. Factors affected the behavior of the improved quay walls.

The caisson with Type 1 blocks had small backward inclining after 500Gal shaking as shown in Figure 11, and was displaced seaward over the block by 800Gal shaking (see Figure 10). After the tests, the tilt angle of the caisson returned to about zero degree. The caisson with Type 2 blocks had backward inclining after 500Gal, the same as the caisson with Type 1 blocks; however, during 800Gal shaking, the blocks moved seaward together with the caisson and the backward inclination of the caisson remained (see Figure 12).

In the case of the model with Type 3 blocks, the blocks leaned seaward, and the caisson had significantly large backward inclining after 500Gal shaking. One of the causes of this result could be the lack of stability of the blocks. The inherent stability of the blocks would be an important factor of the new improvement method.

Based on the final deformation shown in Figure 12 and the results of measurement mentioned above (especially from the observed displacement), it could be said that six factors affected the behavior of the improved quay wall: (1) collapse of foreside slope rubble mound, (2) dimensions of solidified area and ground condition beneath solidified area, (3) displacement of solidified area, (4) settlement of rubble mound and differential settlement between solidified area and rubble mound, (5) leaning of caisson, and (6) displacement of caisson. The numbers correspond to those indicated in Figure 13. These factors correlated strongly with each other, making it difficult to clarify which was the dominant factor on the behavior of quay walls.

5. CONCLUSION

A series of shaking table tests were conducted to study the seismic behavior of caisson-type quay walls improved by the new method. It was derived from the results of the model tests that six factors affected the behavior of the caisson-type quay walls improved by the new method. Further study will be continued to evaluate the effect of each factor, and the design methodology of the new-type quay walls will be discussed based on the results.

6. ACKNOWLEDGEMENTS

This work was supported by the Kanto Regional Development Bureau, Ministry of Land, Infrastructure, Transport and Tourism in Japan, and was a part of cooperative research between the Port and Airport Research Institute and the Japan Dredging and Reclamation Engineering Association. The authors greatly appreciate their contribution.

7. REFERENCES

The Overseas Coastal Area Development Institute of Japan. 2009. *Technical standards and commentaries for port and harbour facilities in Japan*. OCDI, Tokyo.

Inspection of structural health of existing railway retaining walls

Inspection de l'état structurel des murs de soutènement des voies de chemin de fer existantes

Nakajima S., Shinoda M., Abe K.

Railway Technical Research Institute, Japan

ABSTRACT: This study aims to develop an inspection method of a structural health of the existing retaining walls. This paper begins with the brief introduction of the current state of the existing retaining structures. Second, applicability of the percussion test for the evaluation of structural health of existing retaining wall is examined by conducting a large numbers of the percussion test on retaining walls at the site. It was found from the percussion test that structural health of the ashlar wall could be quantitatively evaluated by the percussion test while it was found to be difficult to apply the percussion test for the quantitative evaluation of the leaning type retaining wall. Third, applicability of the small scale vibrator, which was newly developed to improve the disadvantage of the percussion test as the inspection method of the retaining wall, was examined through the prototype scale model test on the existing leaning type retaining wall. It was found from the series of model test that the vibration tests were effective in evaluating the characteristics of dynamic properties of the retaining walls, which were affected by structural health of the retaining walls. This result indicated that the small scale vibration tests could be applicable to evaluate the structural health of the existing retaining structures.

RÉSUMÉ : Cette étude vise au développement d'une méthode d'inspection de l'état structurel des murs de soutènement existants. L'article commence par une brève présentation de l'état actuel des structures de soutènement existantes. Il se poursuit par l'exposition de l'analyse de l'applicabilité des essais aux chocs à l'évaluation de l'état structurel des murs de soutènement existants conduits sur des murs de soutènement sur le terrain. Ces essais aux chocs ont montré qu'ils permettaient une évaluation quantitative des murs de soutènement de type en béton mais qu'ils ne se prêtaient guère à l'évaluation des murs de soutènement de type incliné. Une troisième partie est consacrée à l'applicabilité d'un vibreur à faible échelle nouvellement mis au point qui permet de palier les inconvénients des essais aux chocs comme méthode d'inspection des murs de soutènement. Un appareil prototype a été utilisé pour l'inspection des murs de soutènement de type incliné. La série d'essais modèles conduite a mis en évidence que les essais aux vibrations permettaient de bien évaluer les caractéristiques des propriétés dynamiques des murs de soutènement affectés par leur état structurel. Les auteurs concluent que les essais aux vibrations à petite échelle peuvent être appliqués dans l'évaluation de l'état structurel des murs de soutènement existants.

KEYWORDS: Retaining walls, condition rating, small scale exciter, vibration testing

1 BACKGROUND

In Japan, there are many old existing railway structures and it enhances the importance of the proper maintenance methodology. For the proper management of the railway structures, it is important to detect deformations of the structures in early stage. Once deformations are observed, continuous observations and retrofitting works are also important. As for the Japanese railway structures, it has already developed to evaluate a structural health of bridge piers quantitatively, which makes it possible to maintain structures efficiently. On the other hand, a visual inspection is still conducted to evaluate a structural health of the existing retaining walls because quantitative inspection method for the existing retaining wall has not yet developed. It is required to evaluate a structural health of the existing retaining walls quantitatively because a result of the visual inspection is highly dependent on the subjective judgment of an inspector.

Based on the background above, this study aims to develop an inspection method for the condition rating of the existing retaining walls.

2 CURRENT STATE OF THE RAILWAY RETAINING STRUCTURE

2.1 Maintenance standards in Japan

There are approximately 30 thousand kilometers of the railway lines in Japan, which are operated by many railway organizations (seven Japan Railway companies, over 100 private railway companies and several local governments).

Japanese railway organizations maintain their structures safety conditions by referring to the Japanese maintenance code of Maintenance Standards in Japan (RTRI, 2007). General procedure for structural maintenance in the Management standards and relationships between the soundness and the structure state are shown in Figure 1 and Table 1.

As indicated in Figure 1, "General Inspection" is conducted to all of the railway structures within the intervals of two years mainly by visual inspection. On the other hand, "Individual

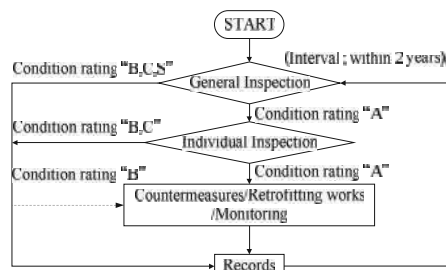


Figure 1. Maintenance procedure according to the Maintenance standards in Japan

Table 1. Relationships between rated condition and structure state

Condition rating	Structure state
A	State that threatens operational safety, safety of passengers, public safety, guarantee of regular train operation, or deterioration that might cause this state
B	Deterioration that might result in a future soundness rank of A
C	Slight deterioration
S	Good condition

Inspection” is performed to the specific structures in which severe deterioration are detected at the time of the General Inspection by means of detailed visual survey or using measuring equipments. As discussed in BACKGROUND, this study aims to develop a methodology which can be used for the condition rating of the retaining walls quantitatively as an alternative method of detailed visual survey.

2.2 Survey on current state of Japanese railway retaining walls

A preliminary survey on current state of Japanese railway retaining structures was conducted. In the preliminary survey, information of typical types of retaining walls in Japan was extracted from the database of the “Structural Management Supporting system (SMS)” (Oyado et al. 2010). In total, the data of 7,989 sites could be extracted. Figure 2 shows the relationships between the type of retaining wall and construction length, which could be obtained using the efficient 1,657 sites data. Construction length of the leaning type retaining wall stands first among all the types of the retaining walls and it accounted for 38.3 % of the efficient data. The percentage of the masonry and ashlar block retaining wall reaches to 37.8 % as well. It was found from the above survey that the leaning type and masonry or ashlar block retaining wall occupies 76.1 % of the total construction length and it indicated the importance of the management of these structures.

2.3 Deformation of retaining walls

Deformation of the railway retaining structures can be divided into two groups; one is the deformation due to destabilization, the other one is the deformation due to deterioration. Typical deformation of the railway retaining structures is schematically illustrated in Figure 3.

Settlement, inclination, swelling, difference in level and difference at construction joint due to external thrusts can be categorized to the deformation due to the destabilization. Exfoliation of concrete, clogging of the drainage facilities is categorized to the deformation due to the deterioration. Cyclic load due to the train passing, increase of earth pressure due to the additional construction of the embankment, increase of dynamic earth pressure due to the earthquake, increase of water

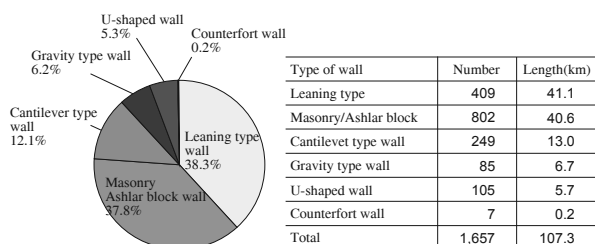


Figure 2. Relationships between construction length and types of retaining wall

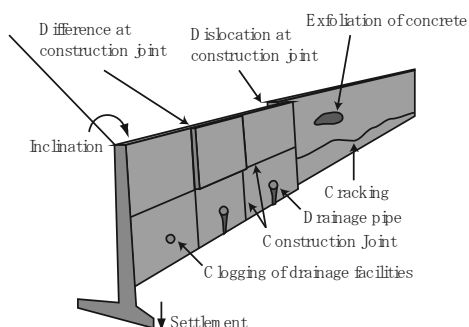


Figure 3. Typical deformation of retaining wall

pressure due to the change of the water level in backfill soil are thought to be the source of the external thrusts, which could cause the deformation due to the destabilization.

On the other hand, deterioration is thought to be caused by the cyclic change of the thermal or humid condition during the long period of its use. Deformation due to the destabilization could be secondary source of the deformation like backfill loosening, bearing capacity failure. Therefore, early detection and retrofitting work against the deformation due to the destabilization are highly important, while it has not yet been developed a methodology to detect such phenomenon by the nondestructive tests. Based on the discussion above, development of a nondestructive evaluation method of the existing retaining wall is attempted in this study.

3 APPLICATION OF PERCUSSION TEST FOR CONDITION RATING OF RETAINING STRUCTURES

3.1 Percussion test

In Japanese railway field works, nondestructive evaluation of the bridge substructure has been carried out by conducting a percussion test (Nishimura et al. 1989). In the percussion test, the natural frequency of the bridge pier is measured with high accuracy and it is used for the evaluation of the structural health of the pier. This method was based on the knowledge that the natural frequency of the bridge substructure decreased with the damage of the structures and increased with the reinforcement.

Natural frequency of the bridge piers is evaluated by carrying out a spectrum analysis using measured free vibration, which is recorded by velocity sensors. Free vibration is induced by hitting the top of the piers using an iron ball. In practice, current performance of bridge pier can be evaluated by comparing the measured natural frequency with the one of immediately after the construction or the criterion of the potential natural frequency. Potential natural frequency is the experimentally-based proposed value by Railway Technical Research Institute so as to be used for the site where the natural frequency immediately after the construction was not recorded.

3.2 Site test results

A series of site test was carried out so as to examine the applicability of percussion test for the condition rating of retaining wall. In the series of site tests, leaning type and ashlar wall are highlighted because construction length of these types of retaining wall was much longer than the other types of walls. As summarized in Table 2, 52 site tests were carried out by selecting the deformed and sound retaining walls so as to investigate into the difference of the vibration characteristics of retaining wall. Percussion test was conducted by hitting the iron ball at the top of the retaining wall and vibration was measured by the velocity sensors attached at the top, middle and bottom of the retaining wall.

Figure 4 shows an example of test result obtained from test No. 3. Predominant frequency of 26.6 Hz could be evaluated based on the changes of phase angle, while the peak amplitude was not clearly observed. This behavior indicates that natural frequency based condition rating, which has been adopted in the condition rating of the bridge substructure, was difficult possibly because the mode of vibration of retaining walls are generally more complicated than the ordinarily bridge substructures. As an alternative index for the condition rating of the retaining wall, the authors proposed the value of spectrum area S_a , which could be evaluated by integrating the Fourier's spectrum of the amplitude as schematically illustrated in Figure 4b), while frequency range of 3 to 40 Hz was selected in this study. Figures 5 and 6 show the relationships between results of condition rating based on visual inspection and the values of

Table 2 Summary of test sites in this study

No.	Company	Type	Height(m)	Deformation	No.	Company	Type	Height(m)	Deformation		
1	A	Leaning	7.2	None	26	F	Leaning	3	None		
2			7.2	None	27			2.64	None		
3			7.2	Cracking	28			3.95	None		
4			7.2	None	29	H	Leaning	5.48	Cracking		
5			7.2	None	30			5.48	Cracking		
6			7.2	None	31			5.48	Cracking		
7			7.2	None	32			5.4	Cracking		
8	B	Leaning	6.3	Cracking	33	I	Ashlars wall	6.4	None		
9			6.3	Cracking	34			2.4	Cracking		
10			6.3	Cracking	35	4.2	None				
11			6.3	None	36	J	Ashlars wall	4.1	None		
12			3.9	Cracking	37			4.1	None		
13			3.35	None	38			4.1	None		
14			3.6	None	39			4	Inclination		
15	C	Leaning	3.6	None	40	K	Ashlars wall	4	Inclination		
16			3.6	None	41			4	Inclination		
17			3.6	None	42			4	Inclination		
18			4.8	None	43			5.7	Cracking		
19	D	Gravity	4.3	None	44	L	Ashlars wall	5.4	None		
20			3.3	None	45			2.6	None		
21			3.7	Cracking	46	M	Ashlars wall	3	None		
22			2.9	Cracking	47			3.4	None		
23			3.2	None	48			3.3	None		
24			E	Leaning	4.15	None	49	N	Ashlars wall	3.3	None
25					4.15	None	50			3.3	None
	4.15	None			51	3.3	None				
					52		3.3	None			

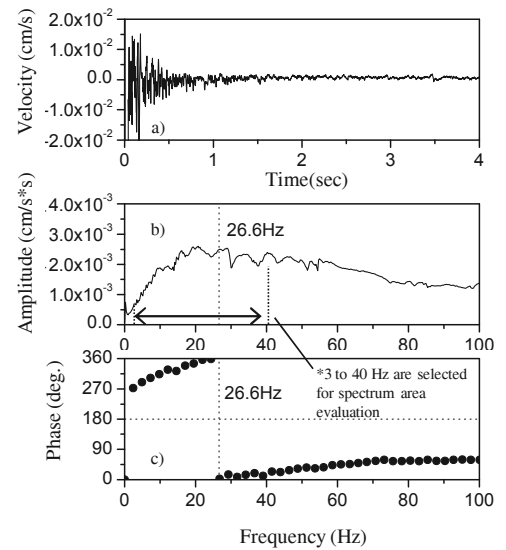


Figure 4. Example of test result obtained from site No.3

spectrum area. In the cases of ashlars wall shown in Figure 5, the values of spectrum area Sa of retaining walls rated as “A(deformed)” were generally larger than the ones of retaining walls rated as “B(no deformation)”, which shows the validity of spectrum area for the condition rating of retaining walls.

In the cases of the leaning type retaining wall shown in Figure 6, a good correlation between the result of visually inspected condition rating and the values of spectrum area could not be found. In the sites No. 6, 20, 21 and 24, the values of spectrum area was much larger than the other sites although they were rated as “B (no deformation)”, which might imply that the progress of the deformation at the part in which is difficult to detect by visual inspection (e.g. subsoil, backfill, etc.). On the other hand, at the sites 27, 26, 25 and 3, the values of spectrum area were not necessarily larger than the other sites although they were categorized as “A(deformed)”.

Percussion test has some problems (Nakajima et al., 2012) ; 1) heavy weight of iron ball (safety, portability) , 2) scattering of impact force depending on inspectors (repeatability) and 3) attenuation of impact force especially in high frequency range(limited range of input frequency). In applying to the condition rating of retaining wall, second and third problems would make it difficult to rate the condition of the retaining wall properly especially in the case of the leaning type retaining wall. Therefore, the authors developed a small scale exciter (Shinoda et al., 2012), which could apply constant sweep sinusoidal excitation under mechanically manipulation, which could solve second and third problems. A prototype scale loading test on leaning type retaining wall model was conducted so as to examine the applicability of the newly developed small scale exciter.

4 PROTOTYPE SCALE LOADING TEST

Cross section of constructed leaning type retaining wall with height of 4.3 m and width of 1.5 m is shown in Figure 7. In Figure 7, the outline of the developed small scale exciter is also summarized. Retaining wall was constructed on the stiff base layer while its backfill consisted of the cobbles, sand backfill with degree of compaction D_c of 90 % and densely compacted gravelly sand. In the loading test, the retaining wall was subjected to the cyclic loading and unloading processes by applying the vertical load at the surface of the backfill using the hydraulic jack while their amplitude were gradually increased as shown in Figure 8. Gravelly sand layer inclined 30 degrees

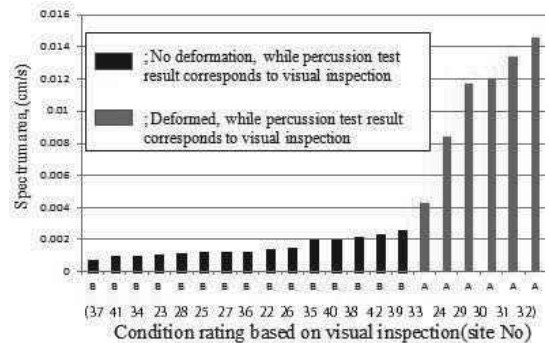


Figure 5. Relationships between condition rating by visual inspection and value of spectrum area (Ashlars wall)

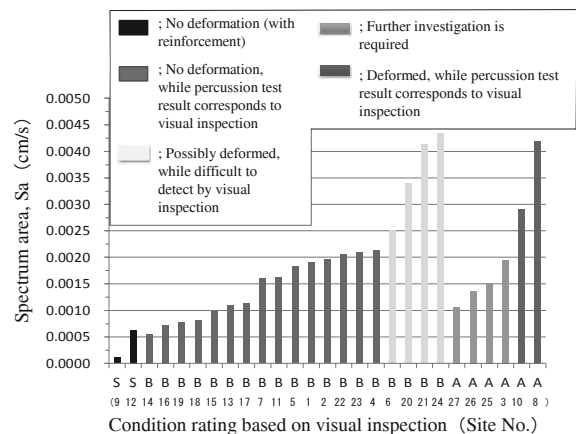


Figure 6. Relationships between condition rating by visual inspection and value of spectrum area (Leaning type retaining wall)

from the horizontal direction so as to apply horizontal load to the retaining wall efficiently.

In the loading test, cyclic loading and unloading processes were applied to the leaning type retaining wall model (Case 1). A soil nailing reinforcement with diameter of 60 mm and length of 4000 mm was installed after horizontal displacement at the wall top exceeded 50 mm. As the second case (Case 2), the model wall reinforced with the top nailing was subjected same loading and unloading processes with Case 1. Lastly, the model wall with top and bottom nailing, which was installed after Case 2, was subjected to the same loading processes while the maximum amplitude of load was applied to the wall in the end

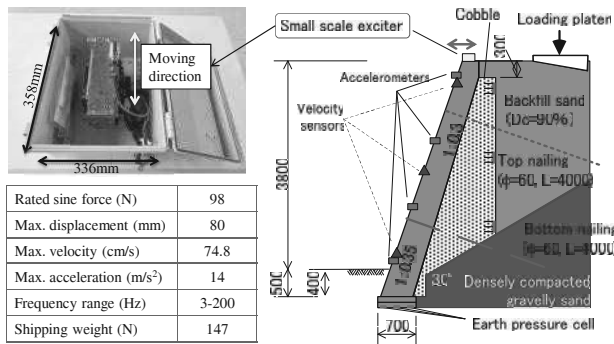


Figure 7. Cross section of model and outline of developed exciter (unit in mm)

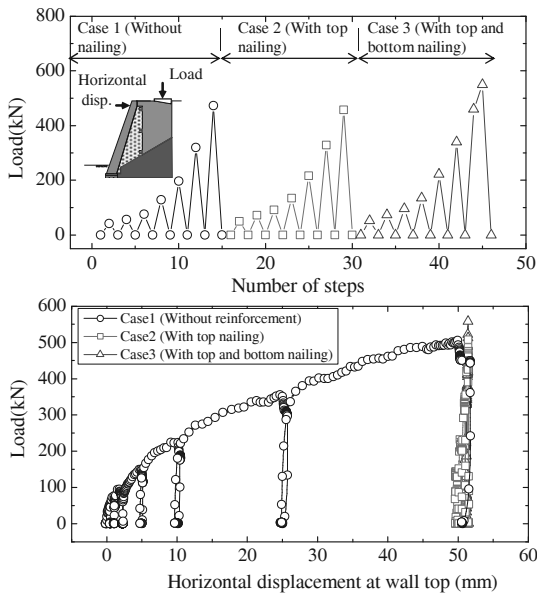


Figure 8. Loading process and load-displacement relationships

of loading process (Case 3). The loading and unloading processes in each case were summarized in Figure 8.

At every loading and unloading process, sets of percussion test with a set of velocity sensors and vibration tests using the developed small scale exciter with a set of accelerometers were conducted so as to investigate into the difference of vibration characteristics obtained from each test. Vibration test was conducted by applying the sinusoidal sweep excitation to the retaining wall model by the small scale exciter fixed at the top of the retaining wall, while the constant amplitude of 1000 gals with frequency range of 3 to 100 Hz and sweeping rate of 3 Hz/sec were adopted as the test condition.

Figure 8 also shows load-displacement relationships obtained from the loadcell installed at the hydraulic jack and displacement transducer at the top of the retaining wall. As clearly shown in Figure 8, the increment of the wall top displacement was drastically reduced by adding the soil nailing although the same amplitude of loading processes were applied to the wall. Displacement increment during a set of loading and unloading processes in Cases 1, 2 and 3 were 50mm, 1.0mm and 0.5 mm respectively.

Figure 9 shows relationships between the number of step and the results from the percussion test and vibration test, while the values of spectrum area of frequency range of 3 to 40 Hz were plotted in the vertical axes. It should be emphasized that the spectrum area evaluated from the percussion test results $Sa[p]$ has the dimension of velocity (cm/sec) because it was evaluated from the integration of the relationships between the Fourier's amplitude of velocity (cm/sec*sec) computed from records of the velocity sensor at the top of the wall and the frequency

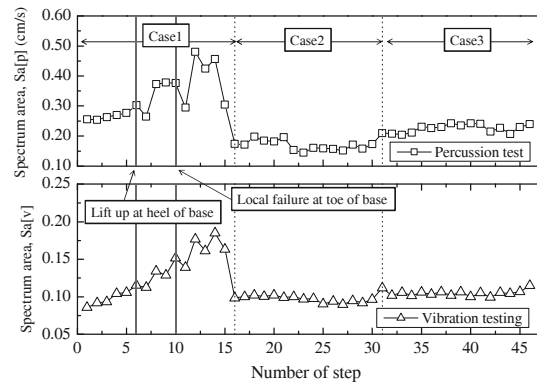


Figure 9. Cross section of model (unit in mm)

(1/sec). On the other hand, the spectrum area calculated from the vibration testing $Sa[v]$ did not have any dimensions because it was evaluated from the transfer function of the top accelerometer against the input acceleration.

It was found from Figure 9 that the values of $Sa[p]$ and $Sa[v]$ increased with the number of step. Moreover, the effect of the nailing could be also detected as the reduction of the values of $Sa[p]$ and $Sa[v]$ in Cases 2 and 3 as compared with Case 1. The difference between $Sa[p]$ and $Sa[v]$ could be found especially in loading and unloading process. The values of $Sa[v]$ increased in the loading process and reduced in the unloading process, which indicated that the spectrum area $Sa[v]$ based condition rating using the vibration testing with the small scale exciter could detect a minor change of the stability of the retaining wall. The value of $Sa[p]$, however, could not detect a minor change during single loading and unloading process, which was possibly because the input force could not be kept constant. It was found from the results of the site tests and prototype scale loading test that the percussion test and the vibration testing could be applicable, while vibration testing could detect a minor change of the stability of the retaining wall.

5 SUMMARY

It was attempted in this study to develop a inspection method of the existing retaining wall. It was found from the preliminary survey on the current state of Japanese railway retaining wall that condition rating of the leaning and the ashlar wall are important because of their huge amount of existing structures. Based on the site test and prototype scale loading test, it was found that the percussion test and vibration test using the spectrum area as an index could be applicable for the condition rating of existing retaining walls.

6 REFERENCES

- Oyado, M., Miyashita, M., Ueda, S. and Sakairi, A., An at-tempt of rationalization for maintenance of railway structure using supporting system, *Proc. of 5th International conference for bridge maintenance, Safety and Management*, pp.3459-3466, 2010.
- Railway Technical Research Institute, *Maintenance Standards for Railway structures*, 2007.
- Nishimura A., Okumura, F. and Tanamura S., Integrity Judgment of Railway Bridges by Percussion Tests for Structure Response, *Quarterly Report of RTRI*, Vol. 29, No.4, pp.184-189., 1988.
- S. Nakajima, M. Shinoda, K. Abe, T. Mai and T. Ehara: Study on inspection method for railway existing retaining walls using vibration testing, *IS-Hokkaido 2012: 2nd international conference on transportation geotechnics*, 2012.
- Shinoda, M., Nakajima, S., Abe, K., Tetsuo M. and Ehara, T.: Development of nondestructive inspection method of railway bridge substructures with small vibration exciter, *Proc of the International workshop on ICT in Geo-Engineering (ICTGE2012)*, 17-18 May 2012.

Mechanism of Settlement Influence Zone due to Deep Excavation in Soft Clay

Mécanisme de la zone d'influence de tassement dû à une excavation profonde dans l'argile molle

Ou C.-Y., Teng F.-C.

National Taiwan University of Science and Technology, Taipei, Taiwan

Hsieh P.-G.

Hwa Hsia Institute of Technology, New Taipei, Taiwan

Chien S.-C.

Aletheia University, New Taipei, Taiwan

ABSTRACT: The objective of this study is to examine the mechanism of settlement induced by deep excavation through finite element analysis. The USC model was selected for this purpose through the calibration of different soil constitutive models. A series of parametric studies were then performed. It was found that in addition to the excavation depth, excavation width, the soft clay thickness and depth to the hard soil are also related to the settlement influence zone. A simple method derived from the basal heave failure mechanism is proposed to predict the settlement influence zone. One case history and one hypothetical excavation with the 80 m thick soft clay were used to verify the proposed method. For comparison, the existing empirical formulae were also used for prediction.

RÉSUMÉ : L'objectif de cette étude est d'examiner le mécanisme de tassement induit par une excavation profonde à travers l'analyse d'éléments finis. Le modèle USC a été choisi à cet effet par le calibrage de différents modèles de sol. Une série d'études paramétriques a ensuite été réalisée. Il a été constaté qu'en plus de la profondeur et de la largeur de l'excavation, l'épaisseur et la profondeur de l'argile molle sur le sol dur sont également liées à la zone d'influence du tassement. Une méthode simple dérivée du mécanisme de rupture par soulèvement basal est proposée pour prédire la zone d'influence du tassement. Une étude de cas et un travail d'excavation hypothétique de l'argile molle sur 80 m d'épaisseur ont été utilisés pour vérifier la méthode proposée. À titre de comparaison, les formules empiriques existantes ont également été utilisées pour la prédiction.

KEYWORDS: Deep Excavation, Soft Clay, Settlement, Constitutive Model, Settlement Mechanism

1 INTRODUCTION

The finite element method and empirical methods are often used to predict the ground settlement induced by deep excavation. The finite element method usually gives better predictions for wall deflection than for ground settlements unless small strain characteristics of soil are taken into account. Ideally, empirical methods should be able to predict ground settlements well because they are mainly derived from field observations of case histories. However, most of them yield poor prediction in ground settlement because settlement mechanism is unclear, case histories adopted is limited, and the excavation depth is the only parameter used in formulas.

The objective of this paper is to investigate the mechanism of ground settlement induced by deep excavation under the plane strain condition through finite element analysis. The study focuses on the settlement under the normal excavation condition, that is, no dewatering induced settlement, no excessively long construction duration causing the occurrence of creep, and no serious construction defects. A suitable soil constitutive model was selected through calibration process. Then a series of parametric studies were performed and the settlement mechanism is proposed.

2 CALIBRATION OF SOIL CONSTITUTIVE MODELS

Since "settlement influence zone" is not rigorously defined, the authors proposed the conception of the primary influence zone (*PIZ*) and the secondary influence zone (*SIZ*) on the basis of the principles of mechanics and regression analysis of excavation case histories (Hsieh and Ou 1998). The settlement curve is steep in the *PIZ* where buildings receive more influence and in the *SIZ* the slope of the curve is gentle and its influence on buildings is insignificant. Finite element analyses are used to capture the characteristics of *PIZ*.

Four soil constitutive models including the Hardening Soil (HS) model, Hardening Soil with Small Strain (HSS) model, $\phi=0$ Mohr-Coulomb (MC) model, and Undrained Soft Clay (USC) model, were adopted. Of these, the HS and HSS model are the effective stress model and the $\phi=0$ MC model and USC model are the total stress model. Both the HSS model and USC model take into account that the soil exhibits high stiffness at small strain.

Though the USC model is a total stress model, it considers the variation of undrained shear strength with principal stress rotation, variation of Young's modulus with the increase of stress level, high stiffness of soil at small strain, and rational way to determine the undrained shear strength (Hsieh and Ou 2011). Similar to Duncan and Chang's model, the tangent Young's modulus (E_t) in the primary loading is derived as

$$E_t = E_{ur}(1 - R_f SL)^2 \quad (1)$$

where R_f is the failure ratio, SL is the stress level, E_{ur} is the unloading/reloading Young's modulus.

The E_{ur} should degrade with the increase of strain or stress level. The degraded Young's modulus is assumed to follow a hyperbolic function as

$$\frac{E_{ur}}{E_i} = 1 - \frac{SL - SL_i}{m + n(SL - SL_i)} \quad (2)$$

where m and n are the degradation parameters relative to the stress level, E_i is the Young's modulus at small strain, SL_i is the stress level corresponding to the threshold value of the small strain or the initial yield strain.

An elastic surface, ES, is defined to represent the small strain characteristics for the state of stress inside the elastic surface. Figure 1 shows the relationships of stress and strain and of

elastic, yield and failure surfaces. Thus, A total of seven parameters are required for the USC model, i.e., s_{uc} (undrained shear strength from K_0 -consolidated undrained compression test), E_i (Young's modulus at small strain) ϵ_s (threshold of small strain) R_f (failure ratio) K_{ss} (ratio of the undrained shear strength from undrained shear strength from K_0 -consolidated undrained compression test to that from undrained shear strength from K_0 -consolidated undrained extension test) as well as m and n (degradation parameters).

The TNEC case history was used for calibration (Ou et al. 1998). Figure 2 shows the comparison of wall deflections and ground movements obtained from field observation and those from finite element analysis using different models. Except for the $\phi=0$ MC model where E_u/s_u was assumed to be 400 according to the local experiences, other soil parameters such as undrained shear strength, E_{50}^{ref} , E_{ur}^{ref} , E_{oed}^{ref} , G_0^{ref} were determined from laboratory tests. $\gamma_{0.7}$ were calibrated to be 5×10^{-5} . Details of the soil parameter evaluation can be found in Lim et al. (2010). Though wall deflections can be predicted well for all models, only the USC model can yield ground settlements close to field observations (Figure 2). Moreover, a hypothetical excavation with an 80 m thick soft clay where its properties were assumed to be the same as the third soil layer of the TNEC case was used for further calibration. The USC model gives a more reasonable prediction in wall deflection and ground settlements than other three soil models (Figure 3). The USC model is thus adopted for parametric studies.

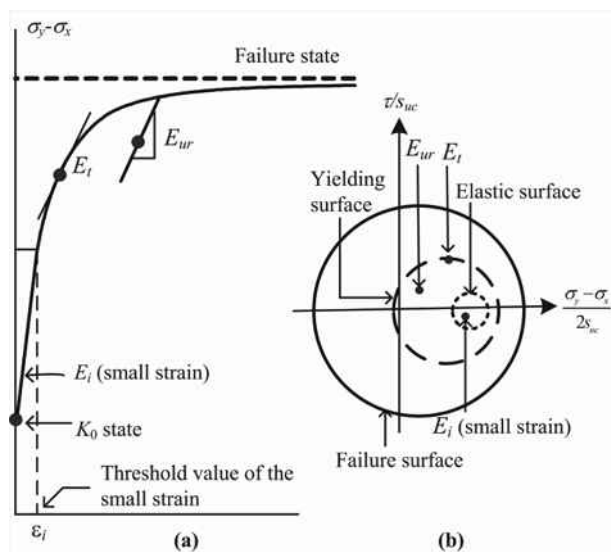


Figure 1. Concept of the USC model (a) Stress-strain behavior (b) Relationship of failure, yield and elastic surfaces.

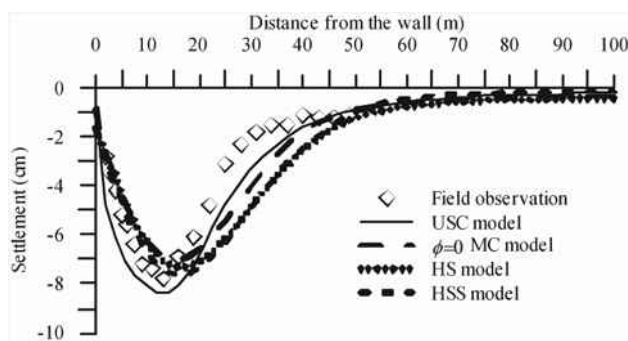


Figure 2. Comparison of settlements from field observation with those from analyses for TNEC

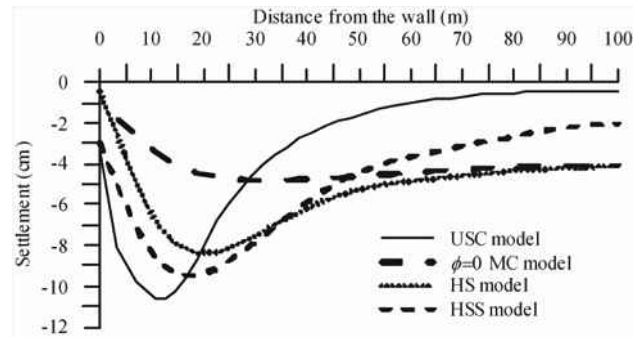


Figure 3. Comparison of settlements from various soil models for a hypothetical excavation with 80 m thick soft clay

3 PARAMETRIC STUDIES AND MECHANISM OF SETTLEMENT

A wide range of assumed excavation cases including excavation depth of 9 to 20 m, excavation width of 20 to 60 m, normalized undrained shear strength (CK_0UC) of 0.28 to 0.34, depth to hard rock of 25 to 50 m was analyzed using the USC model. A typical parametric result, variation of movements with the excavation width, is shown in Figure 4, indicating that the PIZ changes with the excavation width. The excavation depth, excavation depth, thickness of soil clay and depth to hard rock are all affecting the PIZ . Based on the parametric results, we have found the following relationship

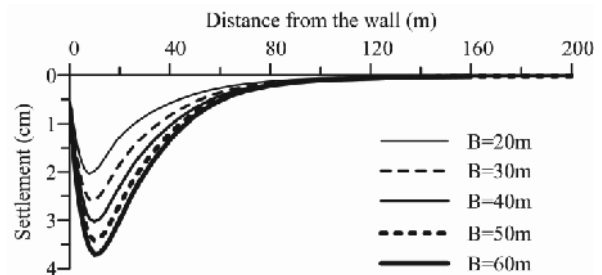


Figure 4. Variation of ground settlement with excavation width (B) for $s_{uc}/\sigma'_v=0.3$.

When the rock-like soil is very deep, i.e., H_g is very large

$$\text{If } \sqrt{B^2 + H_e^2} \leq 2 H_e, PIZ \approx 2H_e$$

$$\text{If } \sqrt{B^2 + H_e^2} > 2 H_e, PIZ \approx \sqrt{B^2 + H_e^2}$$

When the rock-like soil is of the limited depth, i.e., H_g is relatively small

$$\text{If } \sqrt{B^2 + H_e^2} \leq 2 H_e,$$

$$2 H_e \leq H_g, PIZ \approx 2H_e; 2 H_e > H_g, PIZ \approx H_g$$

$$\text{If } \sqrt{B^2 + H_e^2} > 2 H_e,$$

$$\sqrt{B^2 + H_e^2} \leq H_g, PIZ \approx \sqrt{B^2 + H_e^2};$$

$$\sqrt{B^2 + H_e^2} > H_g, PIZ \approx H_g.$$

The above results are summarized below:

$$\text{When } \sqrt{B^2 + H_e^2} > 2 H_e \text{ (wide), } PIZ = \min(\sqrt{B^2 + H_e^2}, H_g) \quad (3)$$

$$\text{When } \sqrt{B^2 + H_e^2} \leq 2 H_e \text{ (narrow), } PIZ = \min(2H_e, H_g) \quad (4)$$

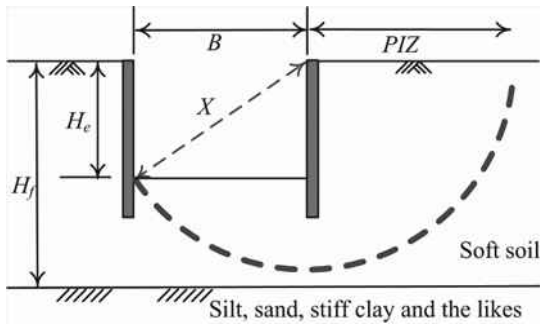


Figure 5. Basal heave failure mode and PIZ.

Comparing Eq. 3 and Figure 5 may show that the PIZ matches the failure zone or potential failure zone. The PIZ also matches the strain contours from the analysis of the TNEC excavation at stage 7 ($H_e=11.8$ m) and that of the plastic-points when the strength is reduced to induce basal heave (Figure 6). This is because the strain in the PIZ should be very large, which in turn induces a relatively large settlement. Therefore, for excavation in soft clay, the PIZ is assumed to be the potential basal heave zone but limited by the non-soft clay, such as silt, sand etc (Figure 5). For simplification, $(B^2+H^2)^{1/2}$ in Eq. 3 is replaced with the excavation width, B . Eq. 3 is thus rewritten as

$$PIZ_1 = \min(H_f, B) \quad (5)$$

where H_f is the thickness of the soft clay.

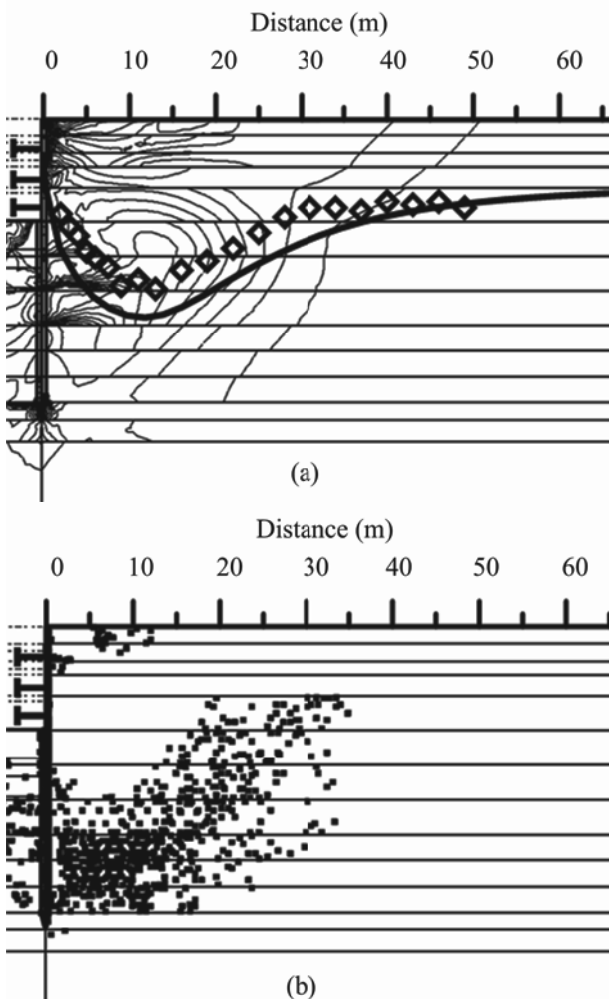


Figure 6. Excavation at Stage 7 for TNEC (a) Strain contours (b) Plastic points when the strength is reduced to cause basal heave.

The relationship in Eq. 4 indicates that the PIZ matches the active zone based on two times the excavation depth. This is because when excavation begins, the wall moves toward the excavation zone and the active zone also occurs behind the wall. Based on the stability analysis, the embedment depth of the wall is usually equal to the excavation depth. The PIZ is coincident with the active failure zone but limited by the rock-like soil. The above equation can be rewritten as

$$PIZ_2 = \min(2H_e, H_g) \quad (6)$$

where H_g is the depth of rock-like soil.

Both PIZ_1 and PIZ_2 are the failure zone or potential failure zones. Therefore, the PIZ is the maximum of the potential failure zones. The method for predicting concave and spandrel types of ground settlement by Hsieh and Ou (1998) is then modified, in which the PIZ derived in this study replaces the $2H_e$, as shown in Figure 7. Details of the derivation can be found in Ou and Hsieh (2011).

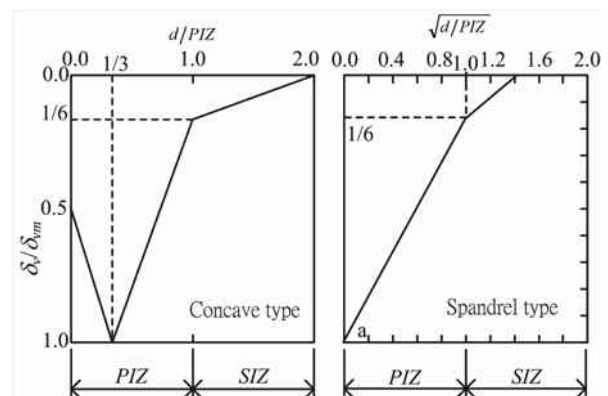


Figure 7. The proposed method for predicting the ground surface settlement.

4 VERIFICATION

The TNEC case history and the ground settlement obtained from finite element analysis of the hypothetical excavation with the 80 thick are used for verification. In the TNEC case history, at stage 5, $2H_e=17.2$ m. If the cobble-gravel soil is regarded as a rock-like soil, $H_g=46$ m. Concerning the active failure zone, $PIZ_2=17.2$ m. With the depth of the bottom of the soft clay (H_f) being 37.5 m, for the potential basal heave failure mode, $PIZ_1=37.5$ m. Thus, the PIZ is 37.5 m. At stage 7, $2H_e=23.6$ m, $H_g=46$ m, $PIZ_2=23.6$ m; $B=40$ m, $H_f=37.5$ m, $PIZ_1=37.5$ m. Thus, the PIZ is 37.5 m. Similarly, the PIZ at the final stage ($2H_e=39.4$ m), is inferred to be 39.4 m. Figure 8 show the comparison between the proposed method (Ou and Hsieh 2011), Hsieh and Ou (1998) and Clough and O'Rourke (1990). The proposed method satisfactorily conforms to the field measurements, while those from other two methods are not.

In the hypothetical excavation with the 80 m thick soft clay, the excavation depths at stages 5, 7 and final are also 8.6, 11.8 and 19.7 m, respectively. The excavation width=40m. The hard soil is located at 80 m. Using the method similar to those in the TNEC case, the estimated PIZ for stages 5, 7 and final are all equal to 40m. Figure 9 shows the comparison of settlement obtained from the USC analysis with those from the three methods. The proposed method is able to give a more reasonable prediction in the settlement of PIZ than the other two methods.

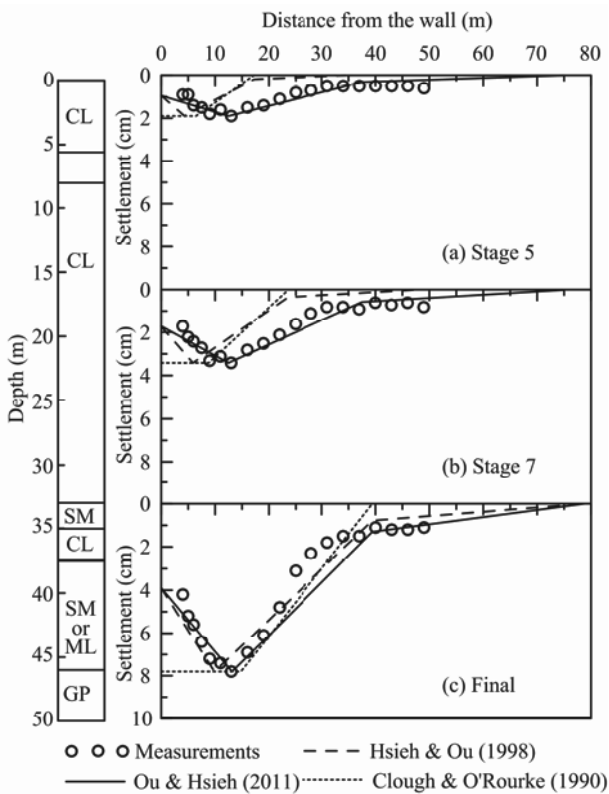


Figure 8. Verification of the proposed method for TNEC excavation.

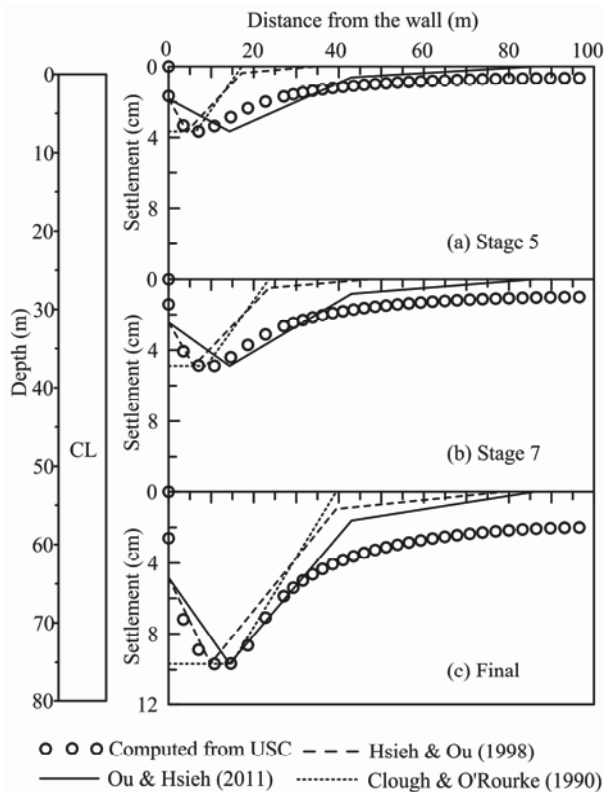


Figure 9. Verification of the proposed method for the hypothetical excavation with the 80 m thick soft clay.

5 CONCLUSION

The objective of this paper is to investigate the mechanism of ground settlement induced by deep excavation under the plane strain condition through finite element analysis. The study

focuses on the settlement under the normal excavation condition, that is, no dewatering induced settlement, no excessively long construction duration causing the occurrence of creep, and no serious construction defects. The USC model was selected to perform parametric studies to find the dominating factors affecting settlement influence zone based on the calibration of a well-documented case history and a hypothetical excavation with 80 m thick soft clay using various soil models. It is found that the primary influence zone is mainly the active failure zone or the potential failure zone due to basal heave. A method is then proposed to estimate the primary influence zone from the relevant parameters such as two times excavation depth, excavation width, depth to rock-like soil layer and depth of the bottom of the soft clay. Case studies reveals that the proposed method improves the prediction of settlement for excavations whose twice the excavation depth are very different than excavation width, depth to rock-like soil layer and depth of the bottom of the soft clay. The methods of Clough and O'Rourke and Hsieh and Ou only yield moderately good prediction results for the settlement at the final stage for most of the cases and largely poor predictions at the intermediate stages, which can be treated as single case histories because the excavation depth is the only parameter used in the formula.

6 REFERENCES

- Clough G.W. and O'Rourke T.D. 1990. Construction-induced movements of in situ walls. Proceedings of the Design and Performance of Earth Retaining Structures, ASCE Special Publication, 439-470.
- Hsieh P.G. and Ou C.Y. 1998. Shape of ground surface settlement profiles caused by excavation. Canadian Geotechnical Journal 35(6), 1004-1017.
- Hsieh, P.G. and Ou, C.Y. 2011, Analysis of nonlinear stress and strain in clay under the undrained condition, Journal of Mechanics, 27 (2), 201-213.
- Lim, A., Ou, C.Y. and Hsieh, P.G. 2010. Evaluation of clay constitutive models for analysis of deep excavation under undrained conditions, Journal of GeoEngineering, 5(1), 9-20.
- Ou, C.Y. and Hsieh, P.G. 2011. A simplified method for predicting ground settlement profiles induced by excavation in soft clay, Computers and Geotechnics 38(12), 987-997.
- Ou, C.Y., Liao, J.T. and Lin, H.D. 1998. Performance of diaphragm wall constructed using top-down method, Journal of Geotechnical and Geoenvironmental Engineering, ASCE, 124(9), 798-808.

Establishing a high risk construction pit in a hurry

L'établissement d'une excavation profonde à risque élevé en court temps

Philipsen J.
Ramboll, Denmark

ABSTRACT: In order to establish a cut & cover road tunnel in Copenhagen, a deep construction pit is established. The future tunnel will run below four railway lines and alongside a fifth, the latter being in poor condition. Since all five railway tracks are vital for the infrastructure in the region, it was not possible to close down all lines during the construction period simultaneously. In fact only two fixed and extremely short closures were allowed for in the construction schedule. This paper presents the thought processes and considerations of the parties involved during the design and planning phase and contains a description of the outcome, that is, the chosen solutions and structural elements.

RÉSUMÉ : Afin de construire un « cut & cover » tunnel routier à Copenhague, une excavation profonde est réalisée. Le futur tunnel est construit sous quatre lignes de chemin de fer et à côté d'une cinquième, cette dernière étant en mauvais état. Étant donné que les cinq voies ferrées sont vitales pour l'infrastructure de la région, il n'était pas possible de fermer toutes les lignes au cours de la période de construction en même temps. En fait, seulement deux fermetures fixes et extrêmement courtes ont été accordées par les autorités. L'article présente les considérations faites par les acteurs concernées lors de la conception et la phase de planification du projet et une description des résultats et les solutions choisies.

KEYWORDS: Construction pit, Temporary retaining structures

1 INTRODUCTION

In Copenhagen a cut & cover tunnel is being established as a part of the new road Nordhavnsvej connecting an existing motorway with the city center of Copenhagen. The construction period is 2011-2015.

The tunnel is a traditional concrete twin tube box tunnel with two road lanes in each tube, build bottom up in a dry construction pit. The length of the tunnel is about 650m.

The alignment of the future tunnel runs below four railway lines at ground level, along a fifth railway line in an old fragile tunnel, below a busy main road and into a narrow path between existing buildings. Figure 1 shows the horizontal alignment and some of the key structures



Figure 1. Horizontal alignment and key structures.

The existing railway lines connect a large part of northern Copenhagen and Zealand to the City centre of Copenhagen, the capital's airport and subsequently to Sweden via the fixed link across the Øresund, which means that they are vital for the infrastructure in the region. Consequently it was not possible to close down all lines during the construction period simultaneously. Only two extremely short main closures were allowed for at each end of the construction schedule.

Figure 2 shows a photo of the 5 railway lines taken from east towards west.



Figure 2. Picture taken prior to project start up showing the 5 railway lines.

The client (the Municipality of Copenhagen) chose Ramboll to be the client's consultants, preparing the detailed design of all permanent works, while the design of the temporary structures was chosen to be split in two parts with different premises and responsibilities.

In the central and most complex part of tunnel alignment - which means at the railway crossing - the client chose a contract form whereby the contractor (Pihl-Zueblin JV) and Rambøll should sit together and optimize the temporary structures at the railway crossing with due consideration, of course, to economy and safety, but most of all with reference to the time schedule.

In the remaining parts of the alignment (the ends) the contractor designed the temporary structures, which e.g. included retaining walls and temporary bridges across the construction pit to facilitate the main road to be open during the complete construction period.

This present paper focuses solely on the temporary retaining structures in the railway crossing which the parties - in close corporation - identified as the optimal.

2 OVERALL GEOMETRY

The vertical alignment of the tunnel is governed by the alignment of the existing rails which are not allowed to be changed. This means that the depth of the construction pit is determined from the height of the future permanent tunnel structure and a required soil cover between the railway tracks and the tunnel roof. The width of the construction pit is about 20m

Figure 3 shows a plan and a longitudinal section at the railway crossing (from St. 5075 to St. 5230).

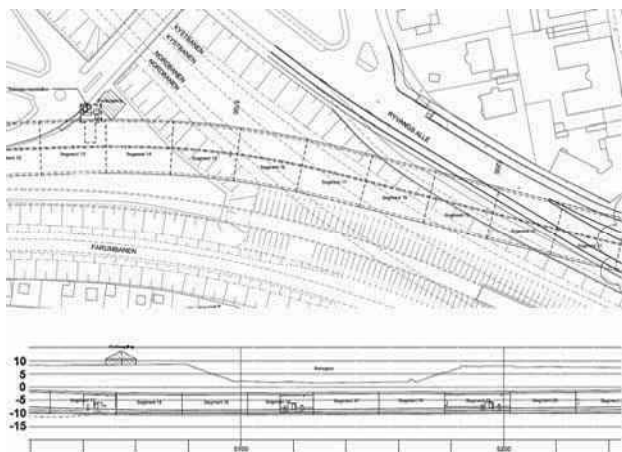


Figure 3. Plan and longitudinal section at the railway crossing.

As shown in Figure 3 the existing railway lines lies in a dell in the terrain. This dell is dug out in the glacial deposits when the railway lines were established.

3 GROUND CONDITIONS

The ground conditions at the railway crossing – and for the Nordhavnsvej project in general - are characteristic for the Copenhagen area.

3.1 Soil

Below a thin layer of fill, the intact soil generally consists of a 10-20m thick quaternary layer of firm clay till with encapsulated layers of melt water sand and gravel. Underneath the quaternary soils limestone is met where the upper 3m is assumed to be glacially disturbed.

As shown in Figure 4 the number of geotechnical investigations in the railway crossing is significant.

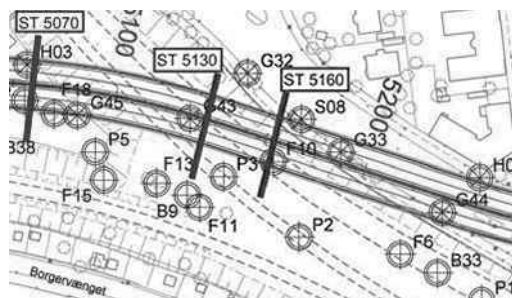


Figure 4. Plan of geotechnical investigations.

The soil parameters are determined from shear vane tests and SPTs carried out in the boreholes, triaxial and oedometer tests

performed in the laboratory on the clay till, VSPs and a priori knowledge of the soil conditions in general.

The sections in St. 5075, St. 5130 and St.5160 shown in Figure 4 indicates the three cross sections being design profiles/representatives for the railway crossing. Figure 5-6 show the assumed geological strata at these three sections

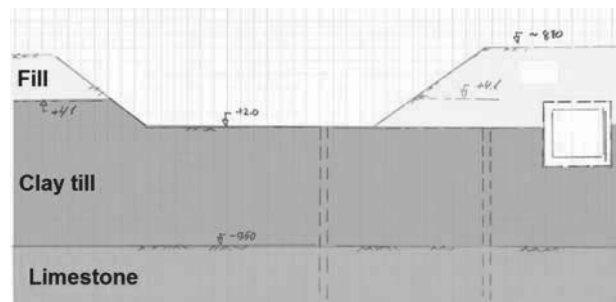


Figure 5. Geological stratum at St. 5075.

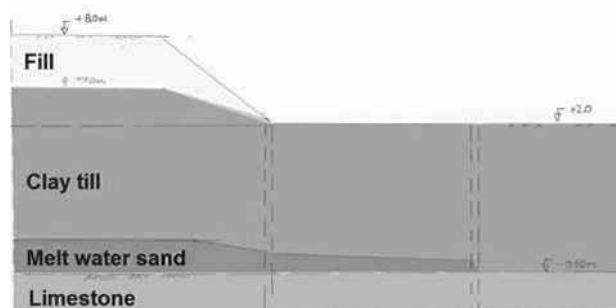


Figure 6. Geological stratum at St. 5130.

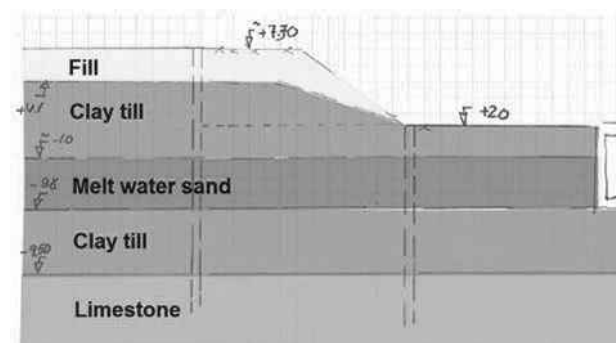


Figure 7. Geological stratum at St. 5160.

3.2 Ground water

At Nordhavnsvej the primary and secondary aquifers are separated. The primary aquifer is the limestone and the secondary aquifer is in the quaternary soils. The water levels are more or less coincident situated a few meters below original glacial ground level except at the railway crossing where the dell in the ground level causes the ground water level down to the terrain.

For the construction of the Nordhavnsvej tunnel it is necessary to lower the ground water level in the limestone temporarily to be able to build the permanent structures. Due to limitations on the allowance of lowering the ground water level in the secondary aquifer, a significant lowering and re-infiltration management system was established.

4 STRUCTURAL SOLUTION

Because of the requirement, that all four crossing railway lines must be in service in the complete construction period except for a few short closures, a number of different solutions to

respect that were considered during the early stages of the project, including pipe arching, top down and the chosen solution, being construction of four temporary steel bridges carrying each a railway line across an open construction pit, facilitating the tunnel to be build bottom up.

Since the railway lines cross the construction pit with rather small angles, the bridge spans are between approx. 40m and 70m. The bridges are prefabricated steel bridges founded on 2-5 bored piles below each bridge placed inside the pit, the retaining walls and concrete foundations with transition slabs at each end.

For safety reasons the bridges are connected in pairs to provide footpaths. Figure 8 shows a cross section in the bridges.

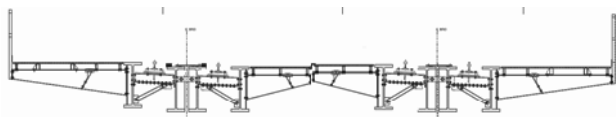


Figure 8. Cross section in temporary bridges.

The type of retaining wall is determined by the constructability in the very hard clay till and the limestone, containing significant amounts of boulders and flint respectively.

In the tender material a solution with steel sheet piles placed in a cement-bentonit slurry trench was prescribed, but during the optimization phase the contractor suggested to use secant pile walls, type hard-firm, since this method is already used outside the railway crossing and consequently well tested before constructing the retaining walls during the railway closure.

The secant piles are established with the Kelly method, cased until 0.5m below excavation level (diameter 1180mm) and below that uncased to the bottom (diameter 1080mm). The walls are staggered so that the firm piles are stopped 1.5m below excavation level. Hard piles are reinforced with 14 or 18pcs. K40 longitudinal reinforcement and K14 spiral shear reinforcement.

To avoid significant crushing works on the secant piles after establishing the tunnel, HEB profiles are casted into the top of the reinforced secant piles or the capping beam and timber lagging is used as infill, forming fixed soldier pile walls, which can easily be cut down and removed respectively. Figure 9 shows one of the encastered soldier pile walls.



Figure 9. Encastered soldier pile wall.

The support system in the railway crossing consist of two levels of walings and steel tube props, supplemented by ground anchors to balance the system where the ground level is significantly different on the two sides of the construction pit.

Where the terrain is at railway level, the upper waling is a concrete capping beam placed on top of the secant piles and attached to the piles by 5 threadbars per reinforced pile as shown in Figure 10. The solution is chosen because it is fast to wash away the upper (poor) concrete in the secant piles, place the prefabricated reinforcement cages for the capping beam and get it all casted together.

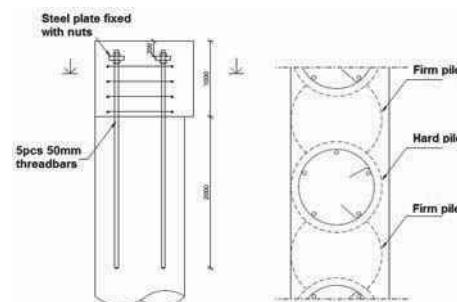


Figure 10. Connection between reinforced secant piles and upper capping beam.

The props in the upper support system are all steel types with 25mm thickness and diameters ranging from 610mm to 820mm and placed unevenly with distances of about 6-8m. The location of the props are of course governed by the capacities of the capping beams and props, but also by the location of the concrete beams spanning from the capping beam to the foundation piles supporting the rail bridges. Figure 11 shows the upper support system and support beams for the bridges and Figure 12 shows a picture of one of the support beams.



Figure 11. Upper support system and support beams.



Figure 12. Picture of support beam.

The props and walings in the lower support system are very temporary. As soon as the bottom slab of the tunnel is established, the props and walings are removed. Consequently a steel solution with double HEB-profiles and steel tube props is chosen, since the establishing and removing of this system is less time consuming than any concrete solution.

5 DESIGN

The design of the retaining walls and the support systems have been carried out using 2D numerical approaches since the effect of asymmetric loading is considerable; different terrain levels, different ground water levels and different loads on each side of the construction pit leading to props pushing excess force from one side to the other. For ULS analyses FEM have been used and cross checked with subgrade reaction models. In SLS small strain stiffness has been considered in FEM analyses.

To ensure that any 3D effects – like the partial loads from trains - were considered realistically in the 2D models, small 3D

FEM models were established and the results were incorporated in the 2D models.

Like for the geological strata, three representative structural cross sections were developed. The sections appear in Figure 13.

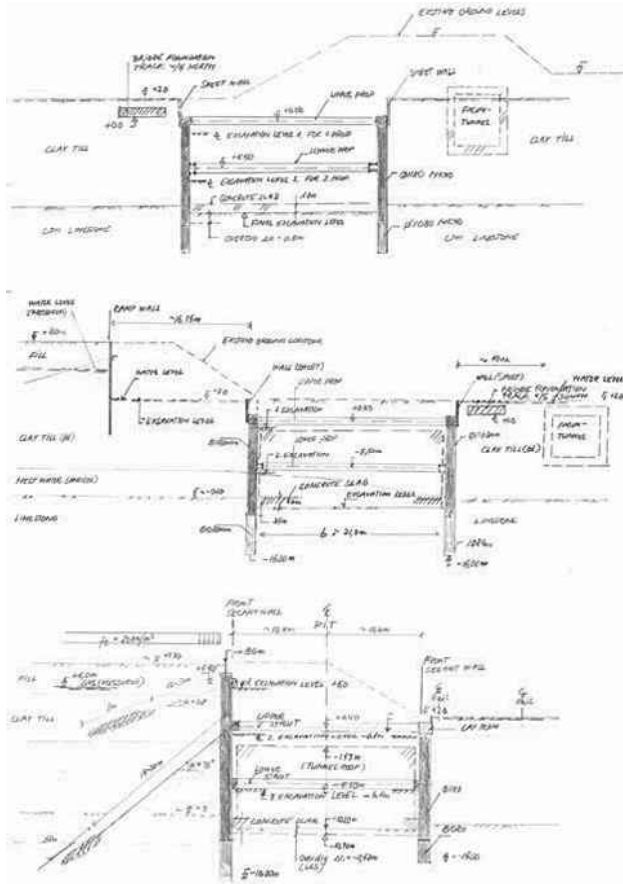


Figure 13. Representative structural cross sections.

The longitudinal reinforcement in the secant piles is checked to behave elastically in SLS, while in ULS and ALS plastic behavior is accepted. The shear reinforcement in the piles are designed using the crack sliding model for a circular cross sections, which is a further development of the plasticity-based crack sliding model originally developed for rectangular beams.

The distribution of sectional forces in props and walings are like the retaining wall design based on numerical methods, in this case spring models taking the stiffness of both the soil and the structural elements into account.

In addition to the load cases considered in the design of the secant pile walls the support systems are designed to withstand temperature loads on the props and the two ALS situations; unintended impacts from a single load and failure of a prop or anchor.

6 MONITORING

Due to strict requirements for deformations of the railway tracks and the aim to avoid structural damage to existing structures, a rather comprehensive monitoring program with accompanying action lists were developed. The monitoring includes; monitoring of rotations and deflections of the secant pile walls via measuring points and inclinometers installed on and in singled out piles, monitoring of forces in certain struts and ground anchors and monitoring of movements of foundations, railway sleepers and terrain in general. Furthermore of course the ground water heads in both the primary and secondary

aquifers are monitored. All monitoring data are stored in a database.

The measured deformations and forces are continuously compared to the expected magnitudes determined in the SLS analyses. In the analyses a number of combinations of different ground water and load conditions are investigated, leading to so called trigger levels for each measuring item in each construction stage. The trigger levels are threshold values of when certain actions must be taken or measures must be done. The trigger levels are presented on a number of drawings, so that they can easily be compared to the monitored conditions on site. Figure 14 shows an example of how the trigger levels are displayed (wall deflections when excavating for establishing of the lower support system at St. 5200).

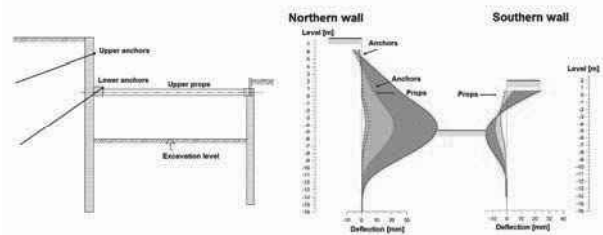


Figure 14. Example of trigger level display.

The monitoring is as a starting point performed with measurements on daily basis, but since most the measurements are performed automatically the frequency can easily be raised if any unexpected development in deformations and/or forces is recorded or lowered if no critical development is recorded.

7 CONCLUSIONS

To be able to construct the future Nordhavnsvej tunnel in Copenhagen, a construction pit with crossing railway lines and a tight construction schedule has been established.

Through corporation between Client, contractor and consultant the mission of not violating short and fixed closures was accomplished. Figure 15 shows a picture of the project stage in December 2012, where installation of the lower support system was ongoing.



Figure 15. Picture of the railway crossing, December 2012.

Innovative Solution of King Post Walls combined with CSM Panels

Solution Innovante de Parois Berlinoise combinée avec des Panneaux de CSM

Pinto A., Tomásio R., Godinho P.
JetSJ Geotecnia Lda

ABSTRACT: The aim of this paper is to present the main design and execution criteria related with the innovative solution of earth retaining walls combining the King Post Walls (Berlin) with the CSM (Cutter Soil Mixing) panel's technology. A case study where the solution was applied is presented, confirming the solution excellent overall performance.

RÉSUMÉ : Dans cet article sont présentés les critères principaux de conception et d'exécution de la solution innovante qui combine des parois de soutènement (Berlinoise) avec de panneaux de CSM (Cutter Soil Mixing). Un cas d'étude avec ce type de solution est présenté, confirmant l'excellente performance globale de la solution.

KEYWORDS: cutter soil mixing, Berlin wall

1 INTRODUCTION

The traditional and widespread King Post Walls (Berlin) technology has some disadvantages, mainly the excavation schedule as well as the confinement reduction of the supported soil during the excavations works, mainly in cohesionless soils (Figure 1). In order to overcome this disadvantage, the Berlin solution can be combined with the CSM technology, which acts as a preliminary treatment of the supported soil.

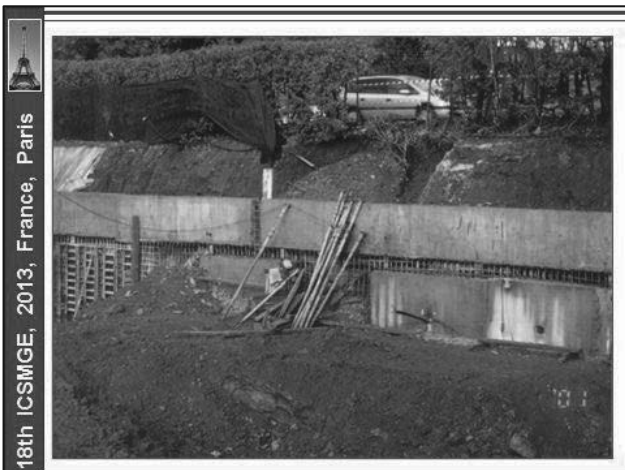


Figure 1. View of the confinement reduction of the supported soil during the excavation works using the Berlin Wall technology.

As an example of this combined solution the case of the enlargement of a railway platform, in order to accommodate the new infrastructures at the connection between two main railway lines in Lisbon, Portugal, is presented (Gomes Correia et al., 2013), following previous works using the CSM technology (Pinto A. et al., 2011). For this purpose it was necessary to perform several excavations with 13m of maximum depth. Due to neighbourhood conditions, three retaining structures (M1, M2 and M3) were built using the combination of Berlin wall with the CSM technology. In this paper the case of the M3 wall is presented, with 13m height and about 66m wide (Figure 2).

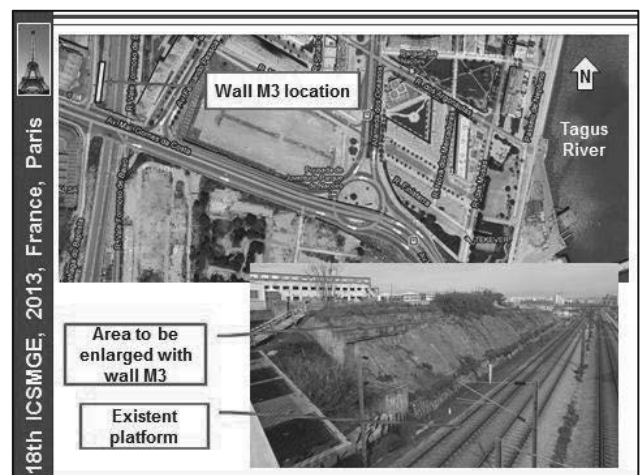


Figure 2. Wall M3 location.

2 MAIN CONDITIONS

2.1 Geological and geotechnical conditions

The local geological conditions were heterogeneous. The excavation works intersected, from the surface, heterogeneous landfills and Miocene medium dense to dense sands and sandstones. The ground water table was located about 5m above the final excavation level (Figures 3 and 6).

2.2 Other conditions

The main neighbourhood conditions included the existent railway lines (under operation and connecting the two Portuguese main cities), several industrial and sensitive buildings, located behind the walls, as well as the important viaduct of the Marechal Gomes da Costa Avenue, over the railway lines, pointing out the importance to control the walls deformation during and after the excavation works (Figure 4).

Geotechnical Conditions						
Geotechnical zone	Ground	SPT n	γ kN/m ³	E kPa	ϕ	c' kPa
ZG1	Fills	-	19	10.000	22	0
ZG2	Medium compacted sands	20	20	20.000	33	0
ZG3	Dense sands and sandstones	60	21	35.000	35	0
CSM panels			22	1.000.000	600	35

Ground water table was observed at a depth of about 10m, some times above the final excavation level

Figure 3. Main geotechnical conditions.

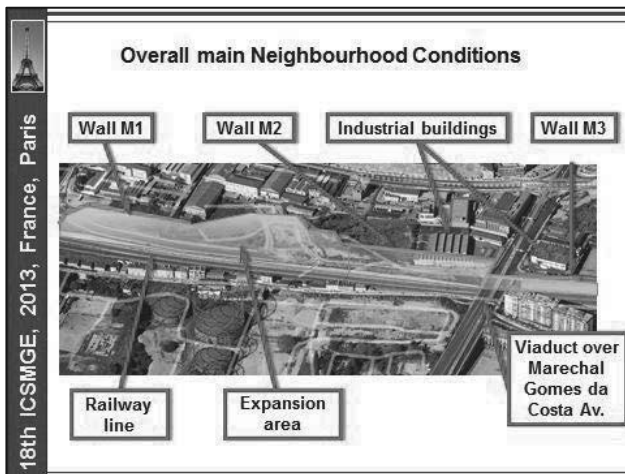


Figure 4. Overall main neighbourhood conditions.

3 ADOPTED SOLUTION

In order to allow the excavation works minimizing the ground loss of confinement effect, soil - cement panels with a maximum depth of about 18m and a cross section of 2,4 x 0,5m², including 0,20m of overlapping, were preliminarily built using the CSM technology. The panels were reinforced with vertical IPE240 hot rolled steel profiles (Euronorm 19-57), spaced in average 1,1m, in order to resist to the earth and ground water pressures, as well as to assure a better control of the retaining structure deformations (Figure 5).

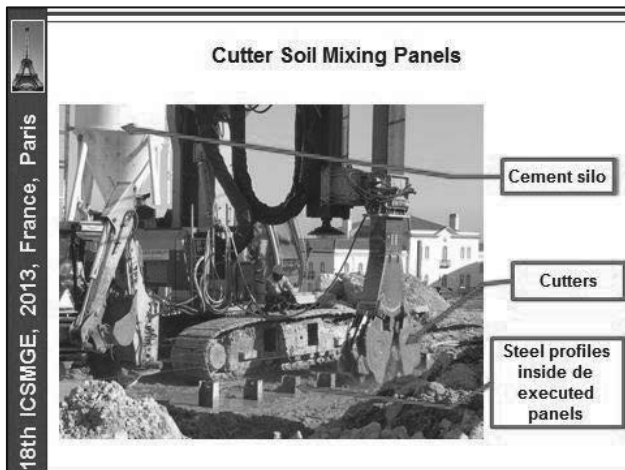


Figure 5. Execution of the soil - cement panels using CSM technology.

The steel profiles were placed inside the soil - cement panels, before the cement started the curing process, and were braced by four or three levels of permanent ground anchors, applied at the reinforced concrete capping beam, as well as at the distribution beams (Figures 6, 7 and 8).

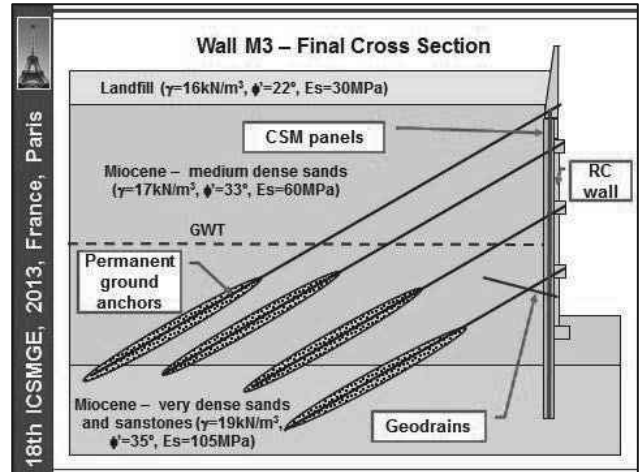


Figure 6. Final cross section of the wall M3.

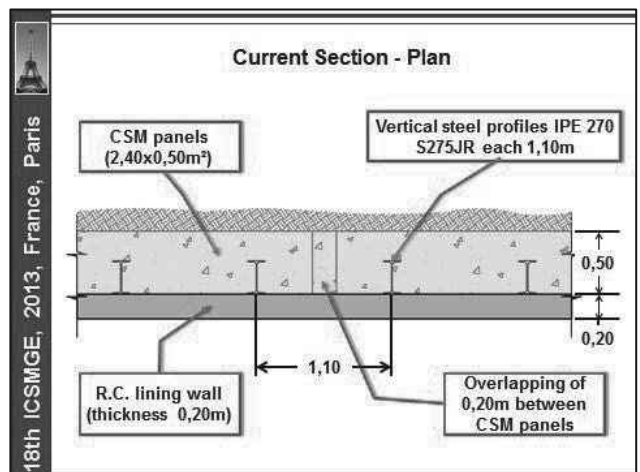


Figure 7. Plan of the wall M3 current section.

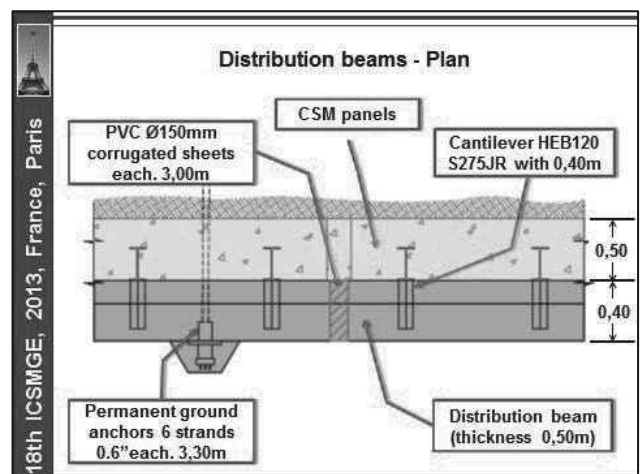


Figure 8. Plan of the wall M3 at the distribution beams section.

As already stated, according to the innovative solution combining the Berlin wall with the CSM technology, the soil - cement panels were designed in order to be integrated on the final earth retaining solution, including the 0,2m thickness lining reinforced concrete (RC) wall and beams (capping and distribution), and also to minimize the water inflow to the

excavation platform (Figure 7, 8 and 9). The preliminary ground improvement effect due to the soil - cement panels allowed the execution of the excavation works without any restrictions, with big advantages on the excavation works schedule, as well as on the RC wall finishing face (Figure 9).

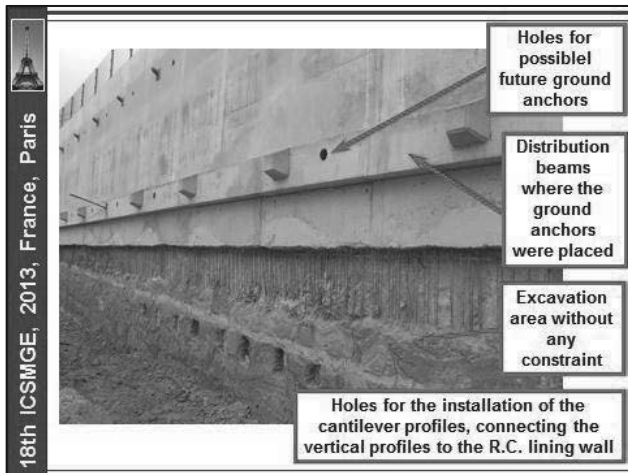


Figure 9. Plan of the wall M3 at the distribution beams section.

The combination of the soil - cement panels with the lining RC wall allowed the construction of a safe and economical solution, overcoming the main disadvantages of the Berlin wall solution (initial solution proposed for the same Project) and spreading the solution application field to almost every kind of geological and geotechnical scenarios, as well as to complex and sensitive neighbourhood conditions.

4 MAIN CONSTRUCTION PHASES

One of the main advantages of the adopted solution was the possibility to reduce the excavation works overall schedule and also to decrease the loss of confinement of the excavated soil and, consequently, to decrease the wall and the neighborhood structures and infrastructures deformations.

The main construction phases are presented on the Figures 10 to 15. As already stated, it should be pointed out the big advantage of the full width excavation, in each level, only possible due to the soil - cement panels ground improvement effect, leading to a big optimization of the construction overall schedule. Due to the versatility of the CSM technology, it should also be pointed out the possibility to apply this solution to almost every kind of geological and geotechnical scenarios, ranging from heterogeneous landfills and soft soils to medium weathered rocks, like the sandstones intersected on present site.

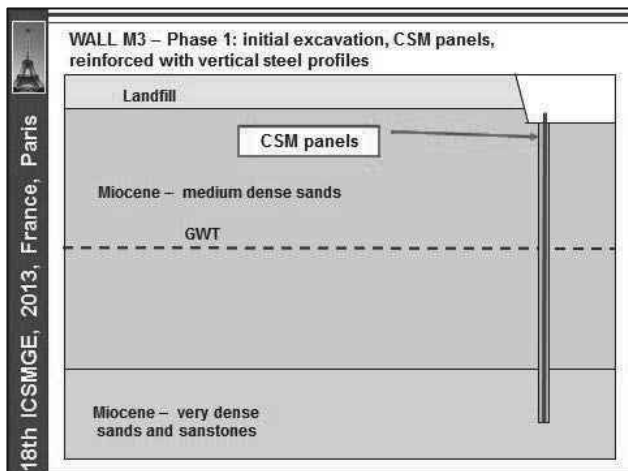


Figure 10. Phase 1.

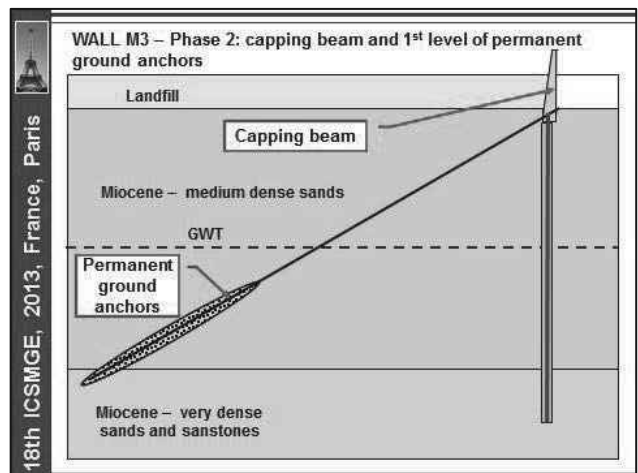


Figure 11. Phase 2.

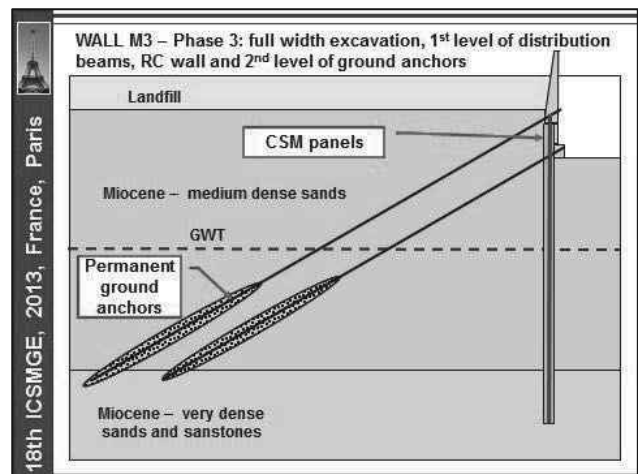


Figure 12. Phase 3.

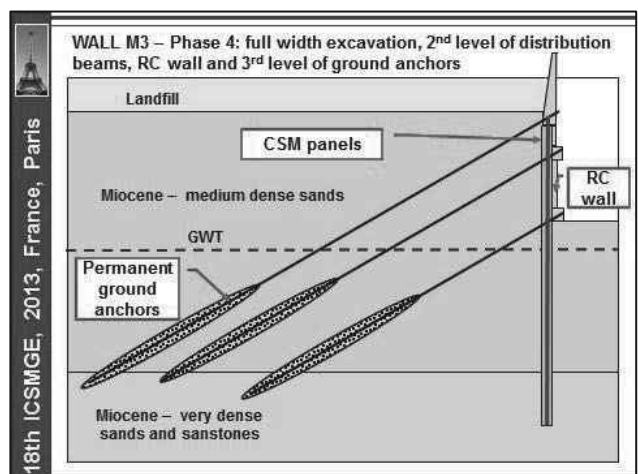


Figure 13. Phase 4.

A tight quality control and quality assurance of the main geotechnical works: soil - cement panels using CSM technology and permanent ground anchors, was implemented, including UCS tests on soil - cement cores and suitability and reception tests on permanent ground anchors (Gomes Correia et al., 2013).

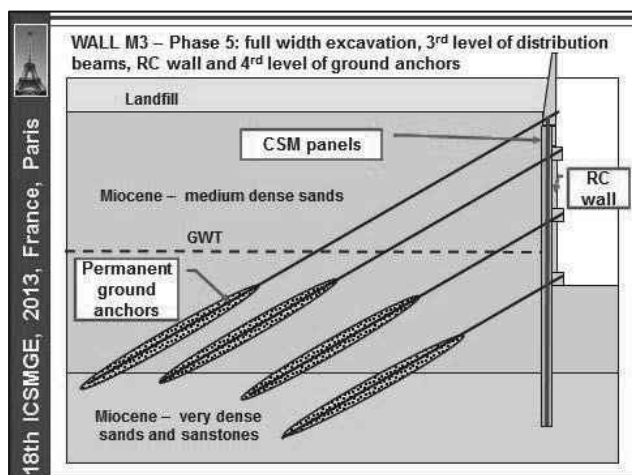


Figure 14. Phase 5.

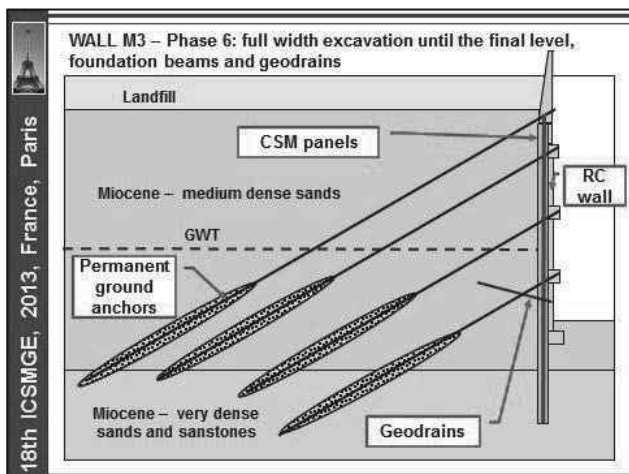


Figure 15. Phase 6.

5 DESIGN

All the soil - cement panels were design in order to achieve an unconfined compression resistance of at least 4,0MPa and a Young Modulus of 1GPa. Due to the soil and water chemical properties, pozolanic cement was adopted. For the design of the adopted solution FEM analysis was carried out, using Plaxis 2D software. The maximum estimated horizontal displacement was about 64mm due to the most critical seismic action (Figure 16).

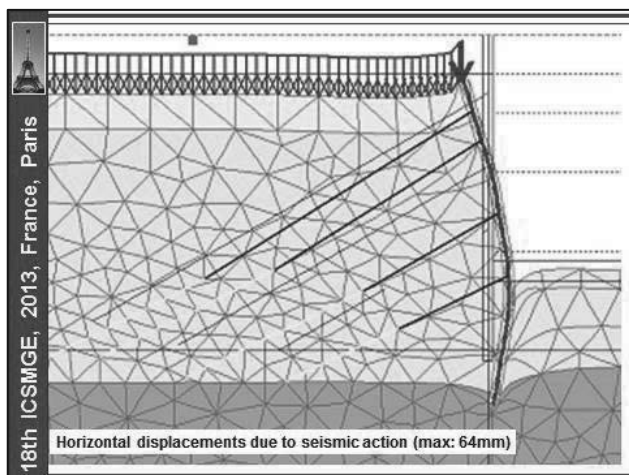


Figure 16. Horizontal displacements according to the FEM model.

6 MONITORING AND SURVEY PLAN

Considering the innovative aspects of the described solutions, a tight monitoring and survey plan was applied, taking into account the need to perform the construction in safe and economic conditions, for both the site and the neighbourhood conditions. In order to accomplish this goal the following equipment's /devices were installed: inclinometers (11un.), topographic targets (65un.) and ground anchors load cells (22un.). Measurements confirmed the excellent overall behavior of the adopted solution, confirming the importance of the previous confinement on the supported soil due to the soil - cement panels, leading, in general, to lower deformations than the ones predicted at the design stage, in spite of some anomalous movements, as presented on Figure 17.

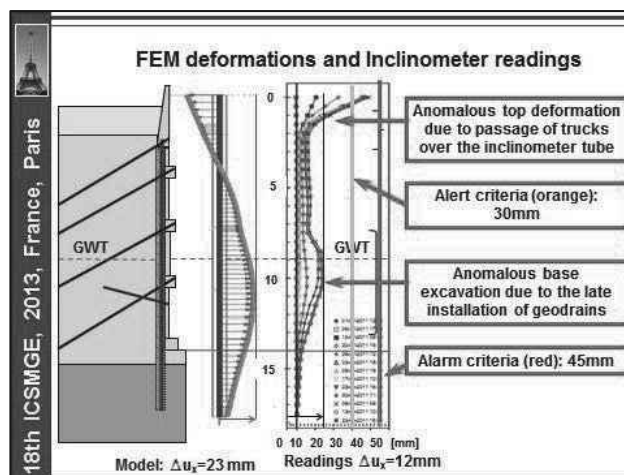


Figure 17. Comparison between predicted FEM deformations and inclinometer readings for static actions.

7 MAIN CONCLUSIONS

As main conclusions it is possible to point out the following advantages of the adopted solution:

- Good confinement of the excavated soils, due to the preliminary ground improvement effect of the soil - cement panels, allowing a very high and safe construction rate;
- Low deformations as confirmed by the monitoring.
- Good wall finishing face and water tightness.
- Environmental advantages associated to the CSM technology, minimizing the excavated ground volume.
- Application field to almost every kind of geological and geotechnical scenarios, as well as to complex and sensitive neighbourhood conditions.

8 ACKNOWLEDGEMENTS

The authors are grateful to the owner of the walls, REFER, for his permission to the presentation of this paper. The construction works were performed by OBRECOL (general contractor) and GEORUMO (geotechnical contractor).

9 REFERENCES

- Gomes Correia A., Tinoco J., Pinto A. and Tomásio R., 2013. An Anchored Retaining Wall in CSM. *Proc. 18th European Conference on Soil Mechanics and Geotechnical Engineering*, Paris, France.
- Pinto A., Tomásio R., Pita X., Pereira A. and Peixoto A. 2011. Cutter Soil Mixing Solutions in Portugal on Hard Soils and Weak Rocks. *Proc. 15th European Conference on Soil Mechanics and Geotechnical Engineering*, September 2011, Athens, Greece, Part 2 - 3.3 - Ground Reinforcement, pp. 1037-1042.

Unusual Geotechnical Solutions at the Leixões Cruise Terminal

Solutions géotechniques inhabituelles au terminal de croisières de Leixões

Pinto A., Pita X., Neves M.

JetSJ Geotecnia Lda

Vaz J.

Dimstrut – Engenharia de Estruturas Lda

ABSTRACT: The aim of this paper is to present the main design and execution criteria related with both cofferdam and foundations solutions, using soil-cement panels, micropiles and bored piles in several applications, at the new Leixões Cruise Terminal, located at the Leixões Port, in Portugal. The Terminal building is being built with one basement on a marine environment, over very difficult geological and geotechnical conditions, which demanded the use of some unusual and integrated geotechnical solutions.

RÉSUMÉ : Dans cet article sont présentés les principaux critères de conception et d'exécution associés aux solutions des parois de soutènement et des fondations, utilisant panneaux de sol - ciment, micropieux et pieux forés, pour le nouveau Terminal de Croisières du Port de Leixões, au Portugal. Le bâtiment, avec un plancher au-dessous du niveau de l'eau est placé dans une ambiance maritime. Ce scénario complexe a demandé l'utilisation de quelques solutions géotechniques peu communes et intégrées.

KEYWORDS: cutter soil mixing, piles, micropiles.

1 INTRODUCTION

The construction of the new Cruise Terminal at Leixões, at the North of Portugal, as a consequence of the constant increase of the cruise traffic, was a challenge from both the geotechnical and structural point of views, mainly due to very difficult and unusual conditions, ranging from the geological and geotechnical scenario to the existent and under operation Leixões Port infrastructures, mainly the South break water, as well as the existent boarding deck (Figures 1 and 2).

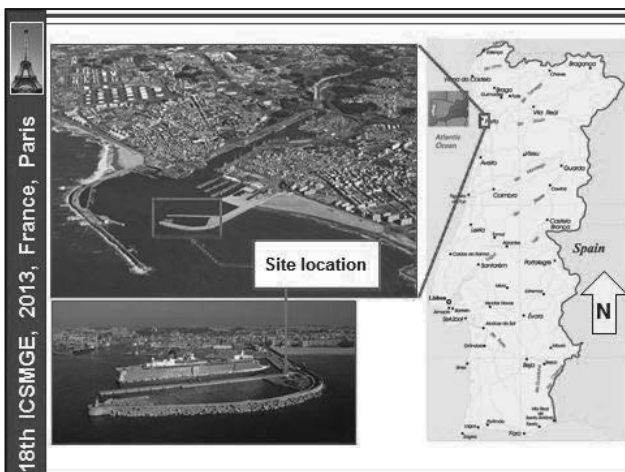


Figure 1. Site location.

According to the Terminal Project it was necessary to build one basement bellow the water table, including several earth retaining structures in order to allow the excavation works on dry conditions leading to a global cofferdam effect. For this purpose soil - cement panels, using CSM technology, reinforced with steel profiles, micropiles (both for foundation and cut off effect) and the existent sheet piles were used. Also pointed out are the adopted special foundations of a very complex structure, including bored piles and micropiles (Figure 3).

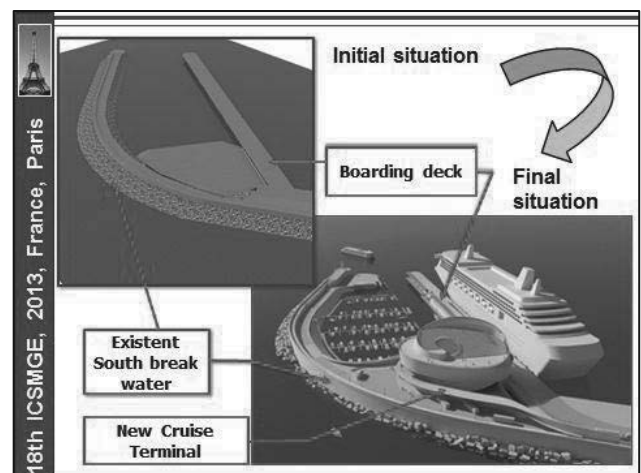


Figure 2. Existent and final situations.

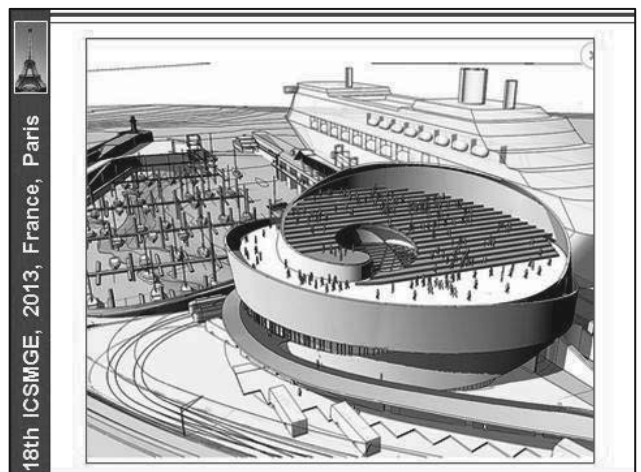


Figure 3. Perspective of the Cruise Terminal building.

2 MAIN CONDITIONS

2.1 Geological and geotechnical conditions

The local geological conditions were homogeneous, but very complex. The excavation works intersected, from the surface, level +5,0m, sandy and silty materials, correspondent to the hydraulic embankment created for working platform purpose. The embankment fill is resting over the bed rock, weathered schist, as previously to the construction of the embankment the existent alluvial material was dredged (Figures 4 and 5).

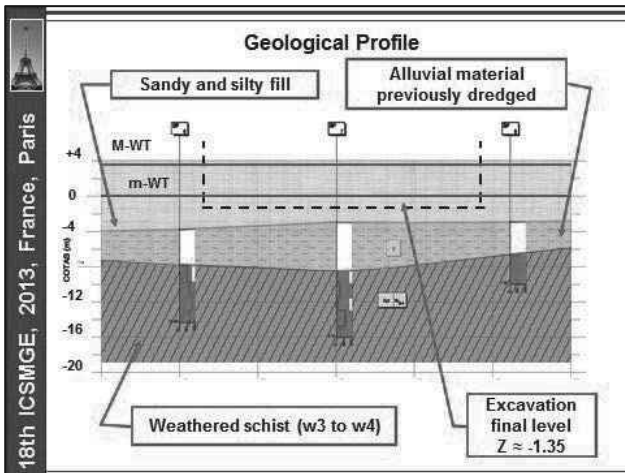


Figure 4. Geological profile.

The water table level ranged from +4,0m to -0,25m according to the Atlantic Ocean tide (Figure 5).

Main Geotechnical Parameters					
Geotechnical Zone	Ground	γ [kN/m ³]	E [kPa]	ϕ [°]	c' [kPa]
ZG1	Sandy and silty fill	16	15.000	20	5
ZG2	Break water stones (rip rap)	22	60.000	25	10
ZG3	Schist	20	120.000	50	100

Water level ranged from +4,0m (high tide) to -0,25m (low tide)

Figure 5. Adopted geotechnical parameters.

2.2. Other conditions

The main neighbourhood conditions included the existent infrastructures, under operation, mainly: the South side break water, accommodating several infrastructures, and the East side cruises boarding deck, a reinforced concrete slab supported by reinforced concrete bored piles. When the embankment was constructed, a sheet pile wall was installed at the boarding border face, in order to improve the hydraulic embankment confinement (Figure 6).

The South side cofferdam walls, as well as of the South side special foundations had to intersect the break water rip rap (8kN to 130kN). This situation was confirmed as an important issue mainly for the execution of the cofferdam walls, as well as for the construction of the bored piles.

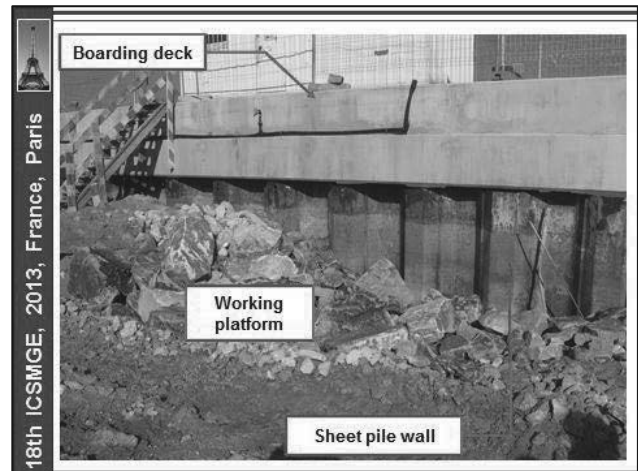


Figure 6. Main neighbourhood conditions: boarding deck.

3 ADOPTED SOLUTIONS

3.1 Global cofferdam

In order to allow the excavation works on dry conditions, three main retaining structures solutions were adopted (Figure 7).

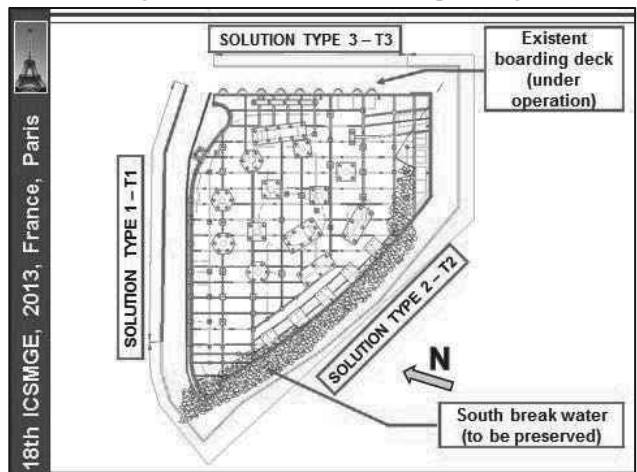


Figure 7. Adopted solutions for the global cofferdam.

Solution type 1 (T1): soil - cement panels with a cross section of 2,4 x 0,5m², including 0,20m of overlapping and 1m of embedment at the bed rock, performed using the CSM technology (Figures 8 to 11), taking into account the experience obtained on previous works (Pinto et al., 2011).

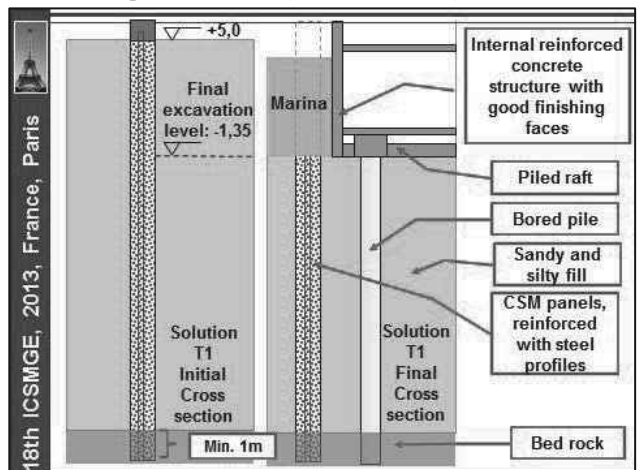


Figure 8. Solution T1 – initial and final cross section.

The soil - cement panels, with UCS resistance not lesser than 4MPa, were reinforced with vertical IPE330 steel profiles (Euronorm 19-57), spaced 0,55m in average, in order to resist to the earth and water pressures, as well as to ensure a better control of the deformations. The steel profiles were placed inside the panels, before the cement started the curing process and capped by a reinforced concrete beam (Figure 8 to 11).

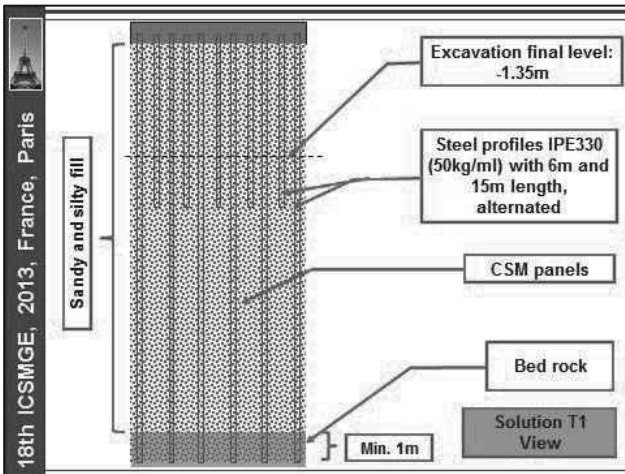


Figure 9. Solution T1 – view.

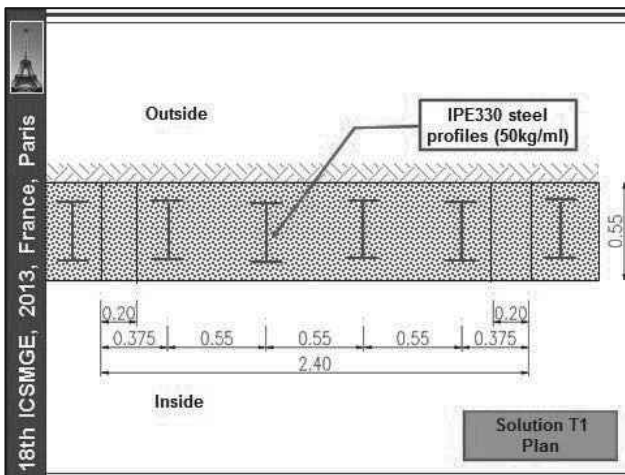


Figure 10. Solution T1 – plan.

The soil - cement panels will be demolished from the internal structure foundation level to the top, in order to allow the reinforced concrete (r.c.) wall with a very good finishing face, being visible from the adjacent marina, (Figure 12).

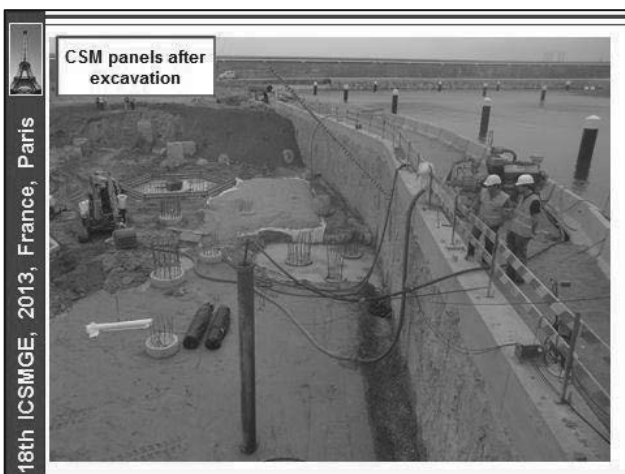


Figure 11. Solution T1 – view of soil-cement panels after excavation.

Solution type 2 (T2): soil - cement panels with a cross section of 2,4 x 0,5m², including 0,20m of overlapping on a height of approximately 6.5m, correspondent to the previous excavation depth, performed in order to replace the break water rip rap by a sandy fill. The panels were built using the CSM technology. Below the soil - cement panels the cofferdam cut off effect was assured through a curtain, performed using alternated slurry cement injections through steel tubes and micropiles N80 ϕ 114,3x12mm, those also with foundation purposes and sealed 4m on the bed rock (Figures 12 to 15).

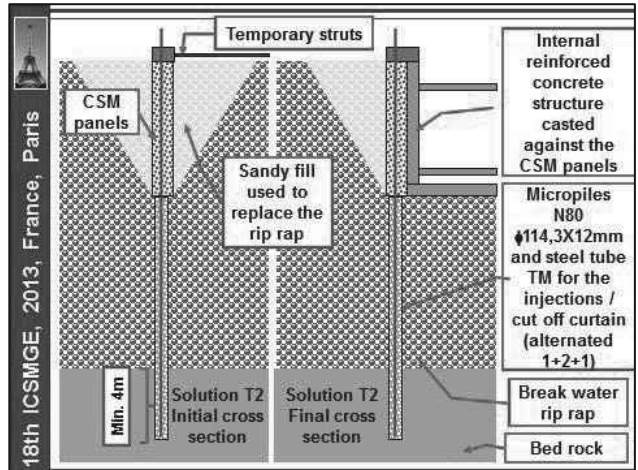


Figure 12. Solution T2 – initial and final cross section.

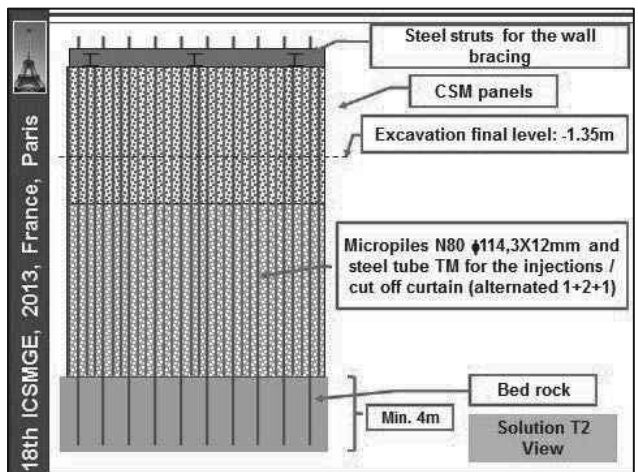


Figure 13. Solution T2 – view.

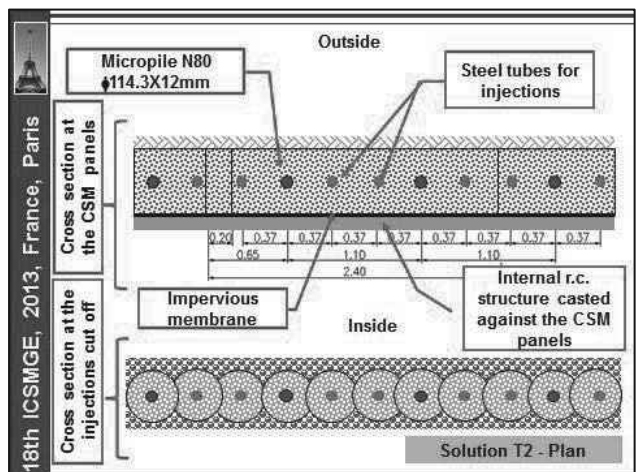


Figure 14. Solution T2 – plan.

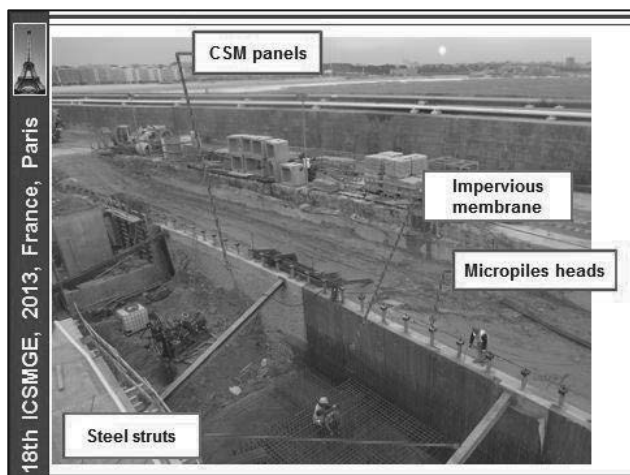


Figure 15. Solution T2 – soil - cement panels after excavation.

Solution type 3 (T3): the existent sheet pile wall was integrated on the global cofferdam, using a bracing system, steel ties, connected to the head of the boarding deck foundation piles (Figure 16).

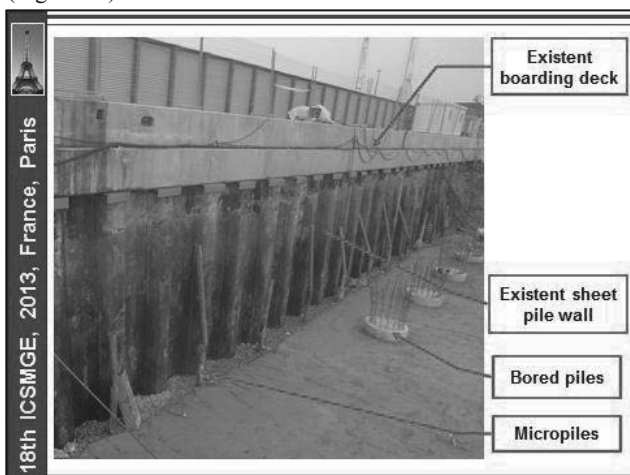


Figure 16. Solution T3 – view of the sheet pile wall after excavation.

3.2 Foundations

For the foundations of the Terminal building reinforced concrete bored piles ($\phi 800\text{mm}$ and $\phi 1200\text{mm}$) and steel micropiles N80 $\phi 139,7 \times 12\text{mm}$ were adopted. Micropiles were used also to resist to both light compression and tension loads, when the structure self-weight was not enough to equilibrate the hydrostatic pressures. Micropiles were designed against corrosion taking into account a sacrificial thickness. All the piles and micropiles were capped by a reinforced concrete raft, cast against an impervious membrane.

4 DESIGN

For the design of the adopted solutions, earth retaining structures and foundations, 2D, including axisymmetric, FEM analysis was carried out, using Plaxis software (Figure 17).

5 MONITORING AND SURVEY PLAN

A monitoring and survey plan was applied taking into account the need to perform the construction in safe and economic conditions, including inclinometers and topographic marks. Measurements confirmed the excellent overall behavior of the adopted solution, with the exception of a local area at solution T1, demanding the implementation of strengthening measures:

inclined steel struts connecting the capping beams to the foundations piles (Figure 18).

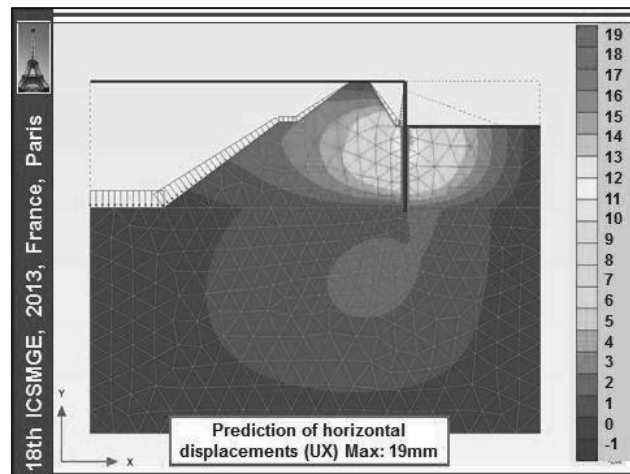


Figure 17. 2D FEM analysis for section T1.

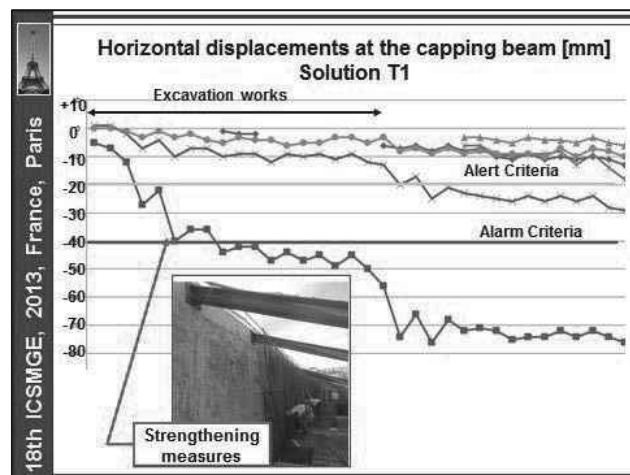


Figure 18. Horizontal displacements at topographic marks - solution T1.

6 MAIN CONCLUSIONS

Taking into account the complex scenario of the presented work, it is possible to point out the following points:

- Good water tightness, mainly due to the cofferdam effect assured by the embedment of the soil - cement panels at the bed rock, as well as due to the injections cut off curtain.
- Low deformations, confirmed by the monitoring results.
- Peripheral r.c. walls with very good finishing faces.

Also very important was the control of both costs and construction schedule.

7 ACKNOWLEDGEMENTS

The authors are grateful to the owner of the Terminal building, APDL (Administração do Porto de Leixões), for his permission to the presentation of this paper. The construction works were performed by OPWAY and FERREIRAS (general contractors) and GEORUMO and HAGEN (geotechnical contractors).

8 REFERENCES

Pinto A., Tomásio R., Pita X., Pereira A. and Peixoto A. 2011. Cutter Soil Mixing Solutions in Portugal on Hard Soils and Weak Rocks. *Proc. 15th European Conference on Soil Mechanics and Geotechnical Engineering*, September 2011, Athens, Greece, Part 2 – 3.3 – Ground Reinforcement, pp. 1037–1042.

Aspects on designing and monitoring a deep excavation for a highly important structure

Aspects de conception et de suivi d'une excavation profonde d'une très importante structure

Popa H., Manea S., Batali L., Olteanu A.

Technical University of Civil Engineering of Bucharest, Geotechnical and Foundations Department, Romania

ABSTRACT: Building large and deep excavations in urban areas is always a complex problem. The geotechnical investigation should be very detailed and the design rigorous. As well, the monitoring of such a work is mandatory. The paper presents a retaining structure from Bucharest, Romania for a deep excavation of 66 x 127 m size in plan and a maximum depth of over 16 m. This open pit was required for building the infrastructure of the largest Cathedral in Romania, the National Redemption Cathedral. The paper presents aspects regarding the geotechnical investigations and interpretation, soil parameters, calculation of the diaphragm wall, anchors and dewatering system, as well as displacement monitoring.

RÉSUMÉ : Les excavations profondes et de grandes dimensions réalisées en milieu urbain représentent toujours un problème complexe. L'investigation géotechnique doit être très détaillée et la conception rigoureuse. De même, le suivi d'un tel ouvrage est obligatoire. L'article présente une structure de soutènement de Bucarest, Roumanie pour une fouille de plus de 16 m de profondeur et ayant 66 x 127 m dimension en plan. Cette excavation a été nécessaire pour construire l'infrastructure de la plus grande Cathédrale de Roumanie, la Cathédrale de la Rédemption du Peuple. L'article présente des aspects concernant l'investigation géotechnique et son interprétation, les paramètres du sol, le calcul de la paroi de soutènement, des ancrages et du système de rabattement de nappe, ainsi que le suivi des déplacements.

KEYWORDS: retaining structure, diaphragm wall, deep excavation.

1 INTRODUCTION

At the present, in Bucharest is under construction the larger orthodox cathedral in Romania, the National Redemption Cathedral. The location of the Cathedral is in the city centre, next to another very large building, the People's House, on a high area called the Arsenal Hill.

The size of the future Cathedral is: length and height of more than 120 m and a width of over 60 m. The Cathedral basement has 2 stories and the total surface of the future cathedral plus the adjacent buildings is of about 11 000 sqm. Figure 1 presents the photo of the concept design of the future cathedral.



Figure 1. Concept design of the future National Redemption Cathedral.

Based on previous analyses of various foundation solutions it was chosen as final solution a cellular raft (basement walls as part of mat) of 4 – 6 m thickness. The raft thickness plus the basement height led to the necessity of excavating a pit of up to

16 m depth. Taking into account the pit depth, as well as its large size (~ 127 m x 66 m) it was chosen as retaining structure a diaphragm wall supported by anchors.

The Cathedral project, including also the deep excavation retaining structure has been submitted to a national contest for choosing the best option.

Paper presents aspects regarding the geotechnical investigation of the site, the design of the diaphragm walls, construction and monitoring the deep excavation.

2 SITE INVESTIGATION

Geotechnical investigation was performed in two stages:

- a preliminary geotechnical study (2008) based on which several preliminary projects were drawn in order to participate to the national contest;
- after selecting the best project, a new detailed geotechnical study was performed by the Technical University of Civil Engineering of Bucharest for the final design of the Cathedral foundations and open pit diaphragm walls.

This geotechnical study comprised the following site investigations: 8 boreholes 25 – 70 m deep, SPT tests, hydro-geological measurements (permeability, analysis of the groundwater flow regime).

Laboratory tests comprised static and cyclic triaxial tests, for determining both shear strength and dynamic parameters of soils. As well, were carried out tests with various stress paths, with unloading – reloading cycles for determining the calculation parameters for the retaining wall. Table 1 presents the main soil parameters obtained from the site and laboratory investigations.

Table 1. Geotechnical parameters

layer	thickness, m	E_{oed} , MPa	$\frac{E_d}{G_d}$, MPa	k_o	ϕ' , °	c' , kPa	N_{SPT}
1 man-made fill	0.6-2.8	-	-	-	-	-	-
2 silty clay	11.4-16.2	7-16	$\frac{56.5}{19.5}$	0.6-0.7	16-23	51-92	10-34
3 sand, gravel	0.9-6.9	30*	-	0.4	35*	-	16-33
4 clay	10.5-16	8.3-11.7	$\frac{54.5}{18.9}$	0.7	9-20	61-113	11-39
5 sand	6.7-7	40*	$\frac{57.8}{20.2}$	0.5	30*	-	23-59
6 clay	21.7-27.8	-	$\frac{71.2}{-}$	-	14	141	-

* - values estimated from SPT tests.

where:

- E_{oed} – oedometric modulus, corresponding to 0.2-0.3 MPa stress interval;
- E_d, G_d – linear deformation modulus and shear modulus for 300 kPa stress;
- k_o – at rest earth coefficient;
- ϕ', c' - drained shear strength parameters;
- N_{SPT} – number of blows from SPT test.

Hydro-geological study emphasized two aquifers: a free level aquifer (layer 3) and a second confined aquifer (layer 5). The excavation will be 2 – 3 m below the groundwater level.

3 RETAINING STRUCTURE

3.1 Geometrical and technological characteristics

The deep excavation was retained using diaphragm walls 80 cm thick, with variable length, from 20 m to 24 m. The lower level of the wall remained constant (+60.50 m), while the upper level varied according to the architectural details of the basement and adjacent buildings (+84.50 m along the long sides and +80.50 m along the short sides of the pit).

Figure 2 presents a layout of the diaphragm wall enclosure and the final excavation levels.

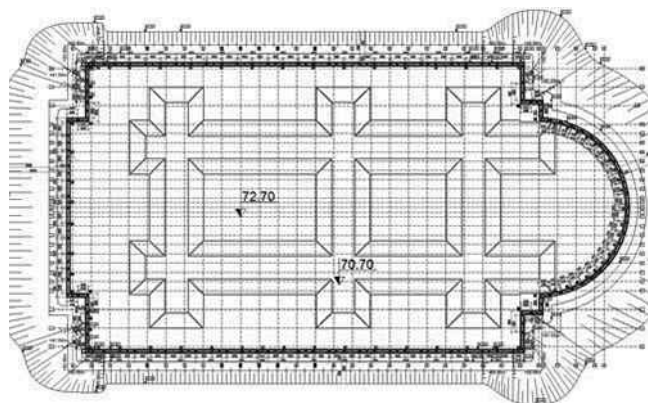


Figure 2. General layout of the diaphragm wall enclosure

The natural ground level varies on the site around +87.0 m, so for the working platforms required for the diaphragm walls execution, a sloped excavation was realized. The final

excavation levels are +72.7 m and +70.7 m (for the 6 m thick raft area), respectively, which led to a maximum excavation level of approx. 16.3 m below the ground level.

It can be seen that the foundation level of the raft is in the sand and gravel layer (layer 2).

The temporary support of the diaphragm wall was ensured using 2 or 3 levels of anchors. The total length of the anchors was comprised between 20 m and 25 m. In the corners were used metallic struts and wale beams.

Figure 3 presents a cross section through the diaphragm wall for the sides with 3 anchor levels.

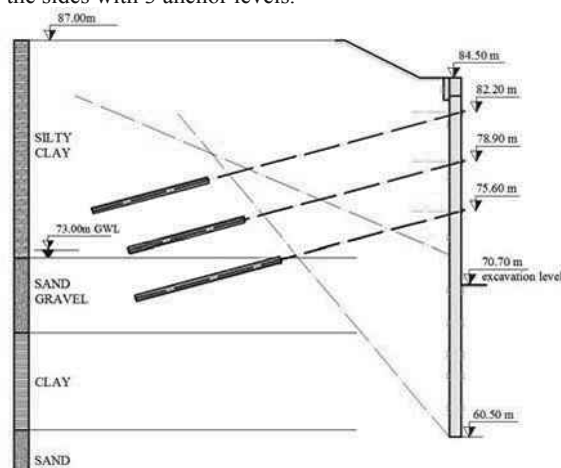


Figure 3. Cross section through the diaphragm wall

For the anchors on 3 levels the characteristics are the following:

- Anchors level 1: +82.20 m
 - inter-axis distance: ~ 1.75 m
 - number of strands in each anchor: 4
 - maximum pull-put force / anchor estimated by calculation (ULS) = 200 kN
- Anchors level 2: +78.90 m
 - inter-axis distance: ~ 1.75 m
 - number of strands in each anchor: 4
 - maximum pull-put force / anchor estimated by calculation (ULS) = 250 kN
- Anchors level 3: +75.60 m
 - inter-axis distance: ~ 1.20 m
 - number of strands in each anchor: 6
 - maximum pull-put force / anchor estimated by calculation (ULS) = 320 kN.

As it can be seen on figure 3, the lowest level of the pit base is 3.0 m below the groundwater level. The soil permeability and the ground level differences led to a water flux in the enclosure of about 90 l/s, unevenly distributed, being higher on the Southern side. Considering these conditions, a dewatering system was designed, comprising 12 wells disposed along the enclosure sides.

3.2 Diaphragm wall calculation

Diaphragm wall calculation was done based on Eurocode 7 (SR EN 1997-1:2004 and the Romanian National Annex SR EN 1997-1/NB). According to the National Annex in Romania, the calculations were performed for design approaches 1 and 3, approach 2 not being recommended by this document.

As well, according to the Romanian technical norm for retaining structures (NP 124-2010), the seismic action was considered on the wall. The seismic coefficient was decreased considering the temporary character of the retaining structure, according to the same technical norm.

Figure 4 shows some of the results obtained for the stresses in the diaphragm wall, corresponding to the side with 3 levels of anchors, for ULS calculation. Calculations were performed

according to technological stages (excavation and installation, anchors pretension) up to the final excavation level.

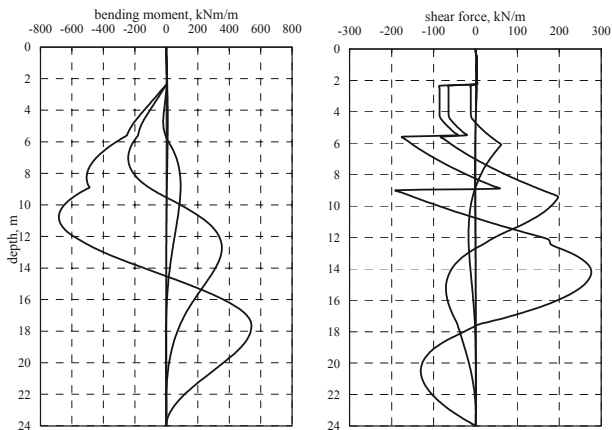


Figure 4. Bending moment and shear force in the diaphragm wall

Figure 5 shows the horizontal displacements of the wall corresponding to the same calculation stages (SLS calculation). It can be seen that the maximum displacements are less than 10 mm, which was confirmed by the inclinometer measurements, presented figure 11.

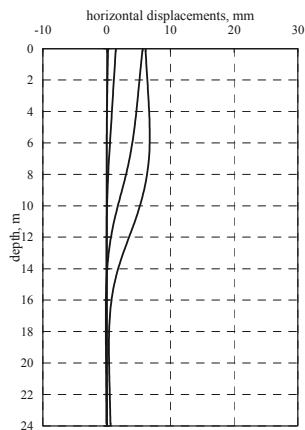


Figure 5. Horizontal displacements of the diaphragm wall

3.3 Aspects during the diaphragm wall execution

Figures 6...9 present some photos taken during the execution of the deep excavation.



Figure 6. Installing the reinforcement cage of the diaphragm wall



Figure 7. Installation of the first level of anchors



Figure 8. Final stage of excavation



Figure 9. Lead waterproofing

As it can be seen in photo figure 9, prior to build the raft a waterproofing layer has been laid on the excavation base. Considering the life time of the cathedral of minimum 500 years, the waterproofing was done with lead, being the only solution guaranteed on such long time. From this point of view, this solution is new for Romanian civil engineering.

3.4 Monitoring the diaphragm wall

The enclosure monitoring was performed by measuring:

- vertical displacements of the wall - measured at the linking beam level using geodetic methods;
- horizontal displacements of the wall - measured at the linking beam level and along the wall depth using inclinometer measurements;
- outflow from the dewatering wells;
- groundwater level inside and outside the enclosure.

Regarding the inclinometer measurements, these were carried out using 6 tubes located in various areas and along different sides of the diaphragm wall (4 on the sides with 3 anchors level and 2 along the sides with 2 anchor levels). A cross section showing the position of the inclinometer tube inside the diaphragm wall is presented in figure 10.

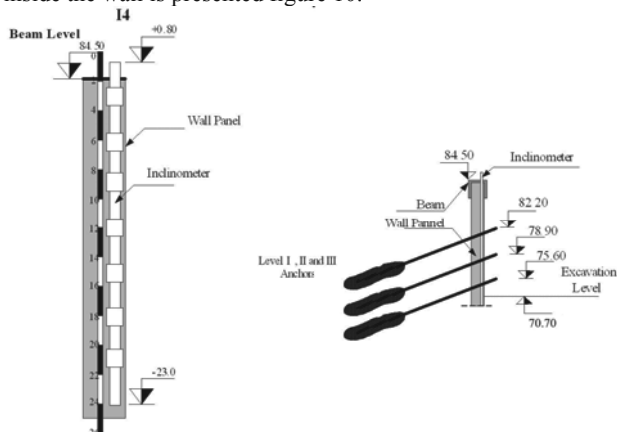


Figure 10. Inclinometer location inside the diaphragm wall

The monitoring of the anchored structure was carried out from April 15 2011 until January 12 2012. The activity during the 9 months of monitoring was according to the technological stages of the excavation works and retaining structure.

The frequency of monitoring activity was established according to preliminary stages of infrastructure works. Due to the construction progress, changes in construction technology flow on site (adjacent traffic infrastructure, frequency and tensioning of anchors system, etc.), weather changes (temperatures on 2012 winter) the frequency of the measurements was increased.

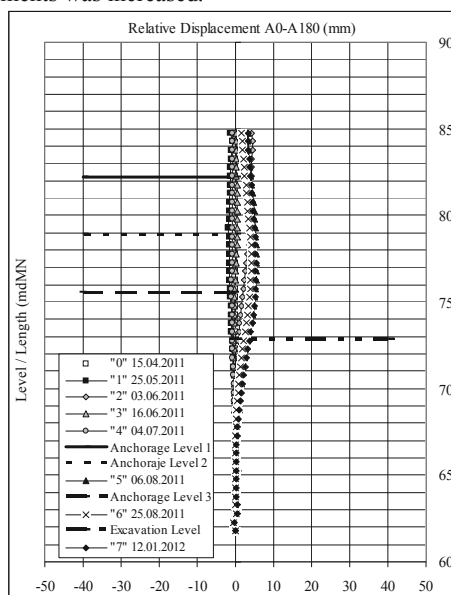


Figure 11. Inclinometer measurements for the diaphragm wall

The main purpose of monitoring activity was to verify design assumptions regarding the deformations of the structure, but also to provide detailed information on the effect induced by the anchors on the retaining wall.

Figure 11 presents a graph of the measured lateral displacement of the wall for the side with 3 anchor levels.

According to measurements, the maximum horizontal displacement of the diaphragm wall didn't exceed, on all sides, 10 mm, confirming the estimation by calculation.

4 CONCLUSIONS

Designing and building a retaining structure for a deep excavation in urban area is always a challenge, taking into account the associated risks. The characteristic parameters of interaction are numerous and their control difficult. For this reason the approach of such works should be done carefully during all stages: geotechnical investigation, design, execution and service.

Paper presents a case study for a deep excavation in centre Bucharest required for the construction of the Redemption Cathedral, which was approached according to Eurocode 7. Considering its size and the supporting system using anchors, this excavation is among the largest in Romania. The anchor supporting system allowed a space-free enclosure and the infrastructure works took place very rapidly.

The work was classified as in geotechnical category no. 3, which imposed a complex approach also from geotechnical investigation, as from design point of view. The execution was permanently monitored and the measurements were compared with the calculations, allowing a rapid intervention if the real behavior would be different from the estimated one.

5 ACKNOWLEDGEMENTS

Authors acknowledge The Romanian Patriarchy and to SC Alfel Construct SRL (general designer) for allowing this paper to be published and for providing some of the data used in this paper.

6 REFERENCES

- SR EN 1997-1:2004 Eurocod 7: Proiectarea geotehnică. Partea 1: Reguli generale.
- SR EN 1997-2:2007 Eurocod 7: Proiectarea geotehnică. Partea 2: Investigarea și încercarea terenului.
- SR EN 1997-1:2004/NB:2007 Eurocod 7: Proiectarea geotehnică. Partea 1: Reguli generale. Anexa națională.
- NP 124-2010 Normativ privind proiectarea geotehnică a lucrărilor de susținere.

FEM-aided design of a novel device for soil anchoring

Conception assistée par éléments finis d'un nouveau système pour l'ancrage des sols

Prisco di C., Pisanò F.
Politecnico di Milano

ABSTRACT: In this paper the pull-out performance of an innovative system for soil anchoring is mechanically interpreted on the basis of a preliminary finite element investigation. The system consists of a tie rod equipped with thick steel sockets, extruding into the soil to increase the overall pull-out bearing capacity. The effectiveness of the anchorage comes from two correlated strength mechanisms: a direct one, associated with the shear/flexural strength of the sockets themselves; and an indirect one, in the form of a remarkable increase in the normal confinement on the tie rod and hence in the available shear strength. Finally, the numerical results are exploited to conceive a design-oriented analytical model for the prediction of the pull-out bearing capacity.

RÉSUMÉ: Dans cet article, le comportement en tension de un nouveau système pour l'ancrage dans les sols est interprété sur la base de une analyse préliminaire avec les éléments finis. Dans le système il y a une bar en métal avec des punçons qui s'extrudent dans le sol pour augmenter la capacité totale de l'instrument. L'efficacité de l'ancrage dérive de deux mécanismes résistants: un qui peut être définis direct, associe a la résistance des punçons, et un indirect, associe à l'incrément du confinement sur la bar. Les résultats numériques ont été utilisés pour définir un model interprétatif du fonctionnement du system d' ancrage.

KEYWORDS: soil anchoring, pull-out, soil–structure interaction, finite element analyses, plasticity

1 INTRODUCTION

The analysis and the design of soil anchors are of major interest to geotechnical engineers in many practical applications, including retaining structures, transmission towers, marine pipelines, etc. For these purposes, the employment of the Finite Element Method (FEM) is progressively increasing, as it overcomes the limitations of most empirical/analytical approaches (Das 1990) in dealing with complex geometries and material non-linearities. On the research side, only a few papers present numerical results about soil anchoring systems, compared to the available experimental data and analytical predictions (see for instance Rowe and Davis (1982a,b), Merifield and Sloan (2006)).

This paper summarizes a recent research activity (di Prisco and Pisanò 2012) concerning the study of a novel device for soil anchoring. This latter is formed by a tie rod equipped with thick steel sockets, which are extruded into the soil to ensure a remarkable pull-out capacity.

To investigate the soil–structure interaction (SSI) mechanisms determining the effectiveness of the system, FEM simulations of pull-out tests have been performed. Then, based on the critical analysis of the numerical outcomes, an analytical model for the estimation of the pull-out capacity has been set up. Despite the approximations introduced, the good agreement between analytical and FEM results is believed to represent the starting point for the conception of a reliable design procedure.

2 FEM SIMULATION OF PULL-OUT TESTS

The novel setup of the anchoring device under consideration is characterized by the presence of internal steel sockets along the tie rod shaft, to be extruded - after the rod installation - into the soil by means of a hydraulic system. Recent in situ pull-out tests have highlighted how socket extrusion ensures a very large bearing capacity (Santoro 2009), much larger than in the usual case of grouted anchorages.

Figure 1 sketches the installation of the anchoring system, composed of the tie rod and the extruded steel sockets, while Figure 2 illustrates the telescopic structure of the sockets. The system is rather flexible in terms of geometrical configuration as the number, the location, and the orientation of the sockets can be freely designed; its installation is extremely fast and inexpensive.

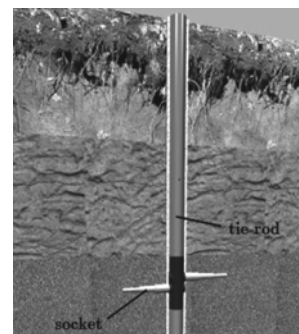


Figure 1. The anchoring system.



Figure 2. The steel sockets.

2.1 FEM model

The geometrical configuration for numerical analyses has been kept as simple as possible, but sufficiently accurate to reproduce the most relevant structural details. If the four sockets

were located at the same vertical level (they are not to allow room for the extruding hydraulic circuits), the anchor would be characterized by four (vertical) symmetry planes. Although this is not exactly true, it has been here assumed for computational convenience that the different socket elevations only slightly violate such symmetries: accordingly, only a quarter of the whole geometry has been considered and discretized.

The FEM mesh employed is shown in Figure 3. The discretization – performed by adopting quadratic tetrahedral elements - is finer around the sockets and the tie rod, i.e. where the solution is expected to exhibit the largest gradients. The external soil boundaries have been placed sufficiently far from the anchor, so as to not affect the global pull-out response.

Since the main purpose of this preliminary study was the highlighting of SSI mechanisms, for the sake of simplicity no sophisticated material models have been considered. In particular, the soil mechanical behaviour has been modelled by means of a simple Mohr-Coulomb perfectly-plastic constitutive relationship with non-associated flow rule (i.e. with different friction and dilatancy angles), while a von Mises perfectly-plastic associated model has been adopted for the anchor structural members. A linear variation along the depth has been introduced for the soil Young modulus, to account for the stiffening induced by the increase in normal confinement. Moreover, as is commonly done in SSI analyses, a widthless perfectly-plastic interface layer has been interposed between the anchor and the surrounding soil to allow both shear and tension detachments.

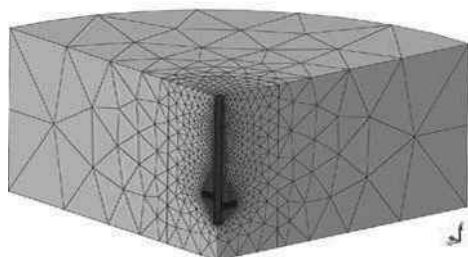


Figure 3. FEM model.

Apparently, the length of the tie rod, i.e., the socket extrusion depth, greatly influences the pull-out capacity of the anchor: as deeper anchors are considered, larger discrete models should be defined, implying an increase in computational costs. Conversely, in order to investigate how the strength contribution coming from the steel sockets is affected by the initial stress state, an approximate approach has been here adopted for the first preliminary analyses. In particular, to simulate a real higher embedment, the same model in Figure 3 has been used for different physical depths, by using an equivalent “embedment surcharge” q_{emb} on the top of the reduced model (obviously, this assumption neglects the frictional pull-out resistance provided by the missing upper soil).

2.2 Main inferences from FEM analyses

In what follows, the main observations derived from the analysis of the preliminary FEM results (with embedment surcharge) are qualitatively summarized.

All the pull-out tests have been performed by imposing a prescribed upward displacement δ at the top of the tie rod, recording the corresponding reaction forces to quantify the global resistance provided by the neighboring soil. While the total pull-out force readily results from the top reaction forces, two distinct contributions can be recognized and estimated on the basis of the FEM outputs. In particular, the global capacity has been split into a first frictional component mobilized along the tie rod, and a second contribution directly carried by the steel sockets.

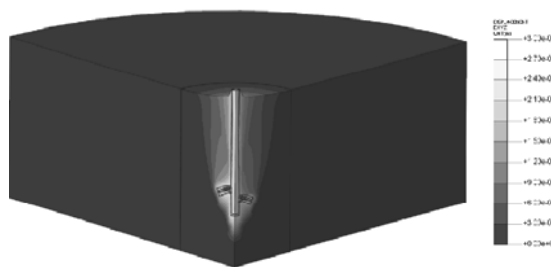


Figure 4.

4. Total displacement contour plot at the onset of failure.

As an example, Figure 4 illustrates the contour plot of the total displacement (absolute value) at the onset of the collapse. The global failure mechanism takes place in the form of a soil wedge surrounding the anchor and moving upward as the anchor itself is pulled-out. Such a failure mechanism is further illustrated in terms of the plastic shear strain in Figure 5: the shear strain concentrations take place along the tie rod and close to the sockets, so that the formation of a failure wedge is apparent.



Figure 5.

5. Plastic shear strain contour plot at the onset of failure.

Figure 6 shows, for four different q_{emb} values, the pull-out curves (force vs. displacement) estimated for the whole anchorage, i.e. four times the force computed for the quarter anchor (this would rigorously hold if the steel sockets were at the same elevation). In all the cases considered, the mechanical response of the anchorage is overall ductile and the limit pull-out load (horizontal plateau) is achieved after quite large displacements. Besides the expected increase in the bearing capacity at larger q_{emb} , it is also worth noting that, owing to the aforementioned spatial variation of the soil Young modulus, the limit load is achieved at about the same displacement level δ .

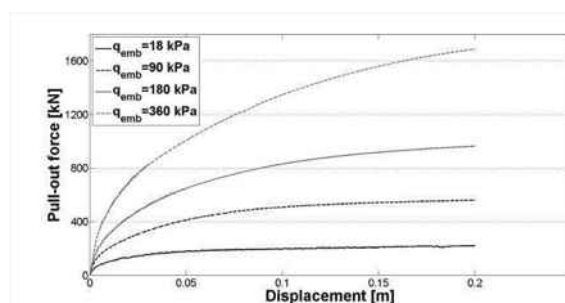


Figure 6. Pull-out responses at increasing embedment surcharge.

Both the above frictional and socket strength contributions have been separately evaluated for all the FEM analyses performed. The obtained values – not reported here for the sake of brevity – show that the lateral frictional forces and the contribution provided by the steel sockets are quantitatively comparable. Such large lateral forces could not be explained by assuming a standard k_0 distribution for the confining stress (k_0 stands for the at rest earth pressure coefficient) all around the tie rod. In contrast, the numerical simulation shows a significant increase in confining stresses as the anchor is pulled-out, up to values much larger than the at rest ones. Figure 7 illustrates the final contour plot of the radial stress, in which the severe perturbation of the initial (linear) at rest distribution is evident.

In the light of these considerations, the influence of the steel sockets on the global pull-out capacity can be said to be twofold. First, the sockets directly sustain a portion F_{socket} of the external load owing to their shear/flexural strength: henceforth, this will be referred to as the “direct effect”. Besides this, an “indirect effect” stems from the formation of a global failure mechanism with a remarkable increase in the radial stress around the tie rod and, therefore, in the mobilizable shear force $F_{lateral}$. For any future design purpose, the necessity of a reliable estimation of both F_{socket} and $F_{lateral}$ is self-evident.



7. Radial stress contour plot at the onset of failure.

3 A DESIGN-ORIENTED ANALYTICAL MODEL

In this section a design-oriented analytical model is defined to estimate each resisting component contributing to the total pull-out capacity of the anchor. The accuracy of the model has been also assessed by comparing the analytical results with the outcomes from full-size FEM analyses, i.e. with no embedment surcharge.

Apparently, the near presence of the tie rod prevents the sockets from being interpreted as isolated deeply buried pipes, so that the force exerted by the soil on each socket (and viceversa) cannot be evaluated via the well-known concept of “uplift coefficient” (or even “break-out coefficient” - see for instance, Rowe and Davis (1982a,b), Merifield and Sloan (2006), White *et al.* (2008)). In contrast, it has been numerically observed that the soil between a single socket and the tie rod behaves as if it was rigidly connected to the anchor, giving rise to a sort of “corkscrew mechanism”.

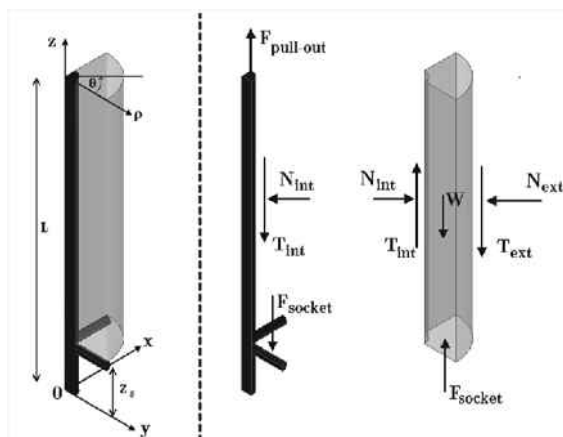


Figure 8. Simplified static scheme for the anchoring system.

To evaluate at the same time both F_{socket} and $F_{lateral}$, the simplified vertical wedge mechanism in Figure 7 (left picture) is considered (the shear force T_{int} coincides with $F_{lateral}$). For the sake of simplicity, the two half-sockets are assumed to be positioned at the same elevation, so that a cylindrical reference frame (ρ, θ, z) can be setup to describe an axisymmetric stress/strain state within the soil wedge (axisymmetric conditions are indeed expected beyond a given distance over the sockets). The right picture in Figure 8 illustrates the reference static scheme, i.e. the forces acting both on the tie rod and the

soil wedge (the rod weight is neglected and boundary reaction forces are not visualized).

From the analysis of all numerical results the following conclusions have been drawn:

1. except for local disturbances next to the sockets, all the stress components are almost linearly distributed along the vertical z -axis;
2. the vertical direct strain component ε_z is much less than the other two (ε_ρ and ε_θ), so that $\varepsilon_z = 0$ can be assumed;
3. the normal force N_{ext} in Figure 8 can be approximately evaluated by assuming a k_p linear distribution for the radial stress σ_r along the outer side of the soil wedge (k_p stands for the passive earth pressure coefficient);
4. the inner and the outer σ_r distributions can be linearly related through a dimensionless constant λ ;
5. the failure distributions of the mobilized friction angle $\phi_{mob} = \arctan(\tau_{z\rho} / \sigma_\rho)$ along the inner and outer sides of the soil wedge exhibit a mean value less than the soil friction angle ϕ and approximately equal to:

$$\tan \phi_{mob}^{lim} = \frac{\cos \phi \cos \psi}{1 - \sin \phi \sin \psi} \quad (1)$$

where ψ is the soil dilatancy angle.

Relationship (1) stems from the fact that, during the pull-out process, the aforementioned soil wedge undergoes a sort of “axisymmetric simple shear loading”. In other words, the loading conditions of the soil elements around the tie rod are highly constrained and similar to those a soil specimen experiences within a so-called simple shear apparatus: as was recently discussed by di Prisco and Pisanò (2011), this implies the material dilatancy to significantly affect the limit shear stress.

The above considerations lead to the formulation of the following system of equations:

$$\begin{cases} T_{int} + F_{socket} = T_{ext} \\ T_{int} = N_{int} \tan \phi_{mob} \\ T_{ext} = N_{ext} \tan \phi_{mob} \\ N_{int} = \lambda N_{ext} \end{cases} \quad (2)$$

with the unknowns N_{int} , T_{int} ($= F_{lateral}$), T_{ext} and F_{socket} (N_{ext} is simply obtained by integrating the k_p - σ_r distribution along the outer surface of the soil wedge). While the equations in system (2) hold at any stage of the loading process, $\phi_{mob} = \phi_{mob}^{lim}$ is to be set at failure - i.e. when the limit frictional capacity is attained along the sides of the soil wedge.

For system (2) to be solved, the determination of the coefficient λ introduced in the previous assumption 4 is required. For this purpose, an original procedure has then been conceived: this is based on the solution of a classical rock engineering problem, concerning the determination of the elastic stress state around a circular cavity (Jaeger *et al.* 2007). For this purpose, an axisymmetric boundary value problem has been posed by assuming that: (i) the soil wedge in Figure 8 is internally elastic; (ii) the direct strain ε_z is nil; and (iii) the vertical stress gradients are much lower than those along the radial direction. While the problem formulation and the solution strategy can be found in di Prisco and Pisanò (2012), the obtained λ expression is reported here:

$$\lambda = \frac{\pi}{4} R(L - z_s) \left(\frac{c_1}{2} - \frac{c_2}{2R^2} \right) \quad (3)$$

where:

$$\left\{ \begin{aligned} c_1 &= \frac{8(R+l)}{\pi(L-z_s)[l^2+2lR+2(1-\nu)R^2]} \\ c_2 &= \frac{8R^2(R+l)(2\nu-1)}{\pi(L-z_s)[l^2+2lR+2(1-\nu)R^2]} \end{aligned} \right. \quad (4)$$

In expressions (3) and (4), R and L are the radius and the length of the tie rod, while l and z_s stand for the length and the elevation (with respect to the bottom of the tie rod) of the steel sockets.

The straightforward solution of system (2) allows of estimating both F_{socket} and T_{int} ($=F_{lateral}$). The soundness of the above assumptions has been verified for all the performed simulations and, in particular, for the full-size analyses (3 m and 7 m embedment) a satisfactory agreement in terms not only of total pull-out force (errors less than 10%) but also of the single contributions has been found. Further confirmation is given in Figures 9 and 10, where the analytical predictions for the radial (a, circular marked line) and shear (b, square marked line) stresses along the inner side of the soil wedge are compared with the FEM results (black solid line).

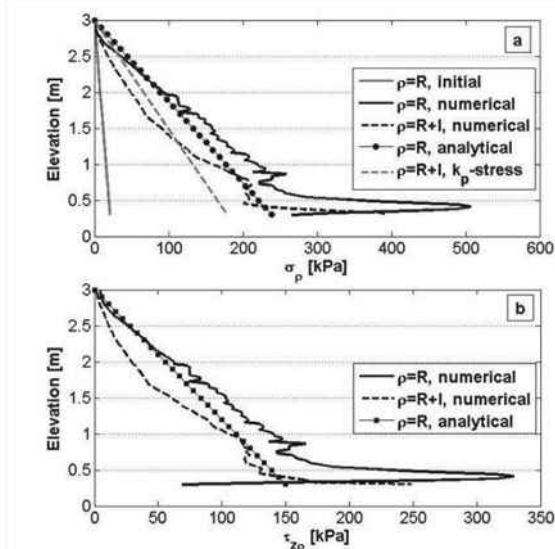


Figure 9. FEM and analytical stress distributions for the full-size model with 3m-embedded sockets.

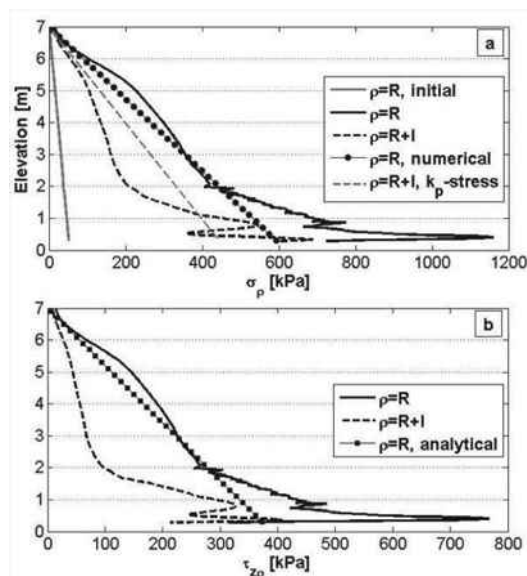


Figure 10. FEM and analytical stress distributions for the full-size model with 7m-embedded sockets.

4 CONCLUSIONS

The pull-out performance of an innovative soil anchoring system has been numerically investigated through FEM analyses. The anchoring device is composed of a tie rod and a set of steel sockets, the latter to be extruded into the soil; former in situ tests have shown the steel sockets largely improve the pull-out performance of the anchorage. The device installation is fast, flexible and inexpensive, while in most cases additional soil grouting becomes optional.

In this work, vertical pull-out tests have been first simulated to explore the SSI mechanisms determining the pull-out capacity of the device, whence the following conclusions have been drawn:

- the steel sockets contribute to the global pull-out capacity in a twofold manner. In a direct way, they sustain a significant part of the total load owing to their shear/flexural strength; they also provide an indirect contribution, by increasing the lateral confinement and the mobilizable friction along the tie rod;
- in all the cases considered, failure develops up to the free surface through a global mechanism involving a cylindrical vertical soil wedge;
- the pull-out strength increases for deeper anchors. Its dependence on socket depth has been found to be, within the investigated range, almost linear;

A simplified analytical model was then proposed to simultaneously estimate the strength contributions – both direct and indirect – given by the sockets. This relies on a set of simplifying hypotheses suggested from the results of FEM simulations, and provides results in good agreement with the numerical outcomes. Although only vertical pull-out tests were considered, the above inferences are believed to apply for inclined anchors as well, since only a slight influence of the initial in situ stresses was found.

The proposed model clarifies the mechanical working conditions of the anchoring system and provides practitioners with a preliminary design framework. In the near future, further efforts will be devoted to analyse the device in the case of more complex geological conditions and, as more experimental results become available, to validate numerical/analytical predictions with respect to in situ measurements.

5 ACKNOWLEDGEMENTS

JOBSSOIL s.r.l and MIDAS/GTS are gratefully acknowledged for the financial support.

6 REFERENCES

- Das B.M. 1990. *Earth anchors*. Elsevier.
- di Prisco C.G. and Pisanò F. 2011. An exercise on slope stability and perfect elasto-plasticity. *Geotechnique* 61 (11), 923-934.
- di Prisco G.C. and Pisanò F. 2012. Numerical modelling and mechanical analysis of an innovative soil anchoring system. Submitted to *Acta Geotechnica*.
- Jaeger J., Cook N.G. and Zimmermann R. 2007. *Fundamentals of rock mechanics*. Wiley-Blackwell
- Merifield R.S. and Sloan S.W. 2006. The ultimate pull-out capacity in frictional soils. *Canadian Geotechnical Journal* 43 (8), 852-868.
- Rowe R.K. and Davis E.H. 1982a. The behaviour of anchor plates in clay. *Geotechnique* 32 (1), 9-23.
- Rowe R.K. and Davis E.H. 1982b. The behaviour of anchor plates in sand. *Geotechnique* 32 (1), 25-41.
- Santoro V.M. 2009. TFEG tensioned elements: from design to implementation. <http://www.jobsoil.it/itfeg.html> 4 (Feb 24 2009).
- White D.J. Cheuk C.Y. and Bolton D. 2008. The uplift resistance of pipes and plate anchors buried in sand. *Geotechnique* 58 (10), 771-779.

Structural Optimization in Geotechnical Engineering

Optimisation de la structure dans la géotechnique

Pucker T., Grabe J.

Hamburg University of Technology, Institute of Geotechnical Engineering and Construction Management

ABSTRACT: Structural optimization methods are used for a wide range of engineering problems. In geotechnical engineering however, only limited experience exists with these methods. The possibilities and difficulties in applying such techniques to geotechnical problems are discussed in this paper and the adaption of the commonly known SIMP-method (Solid Isotropic Material with Penalization) to geotechnical problems is introduced. An application example is used to demonstrate the potential of structural optimization in geotechnical engineering.

RÉSUMÉ : Des méthodes de l'optimisation de la structure sont employés dans beaucoup de disciplines d'ingénieurs. Mais il y a quand-même peu d'expériences dans le domaine de la géotechnique. Les possibilités et les difficultés de l'application de ces procédures d'optimisation dans la géotechnique sont discutées dans cet article. L'application de la méthode SIMP est présenté. Un exemple est présenté pour montrer le potentiel de l'application de cette méthode.

KEYWORDS: topology, optimization, optimisation

1 INTRODUCTION

Structural optimization methods are used for a wide range of engineering problems, for instance in aviation and automotive engineering. In geotechnical engineering however, only limited experience exists with such methods. The possibilities and difficulties in applying these techniques to geotechnical problems are discussed in this paper and the adaption of the commonly known SIMP-method to geotechnical problems is introduced.

1.1 Structural Optimization

Structural Optimization can be classified in three categories. The first category is called topology optimization and describes the main geometry of a design. Topology is a mathematical field used to describe geometrical structures. A geotechnical example of different topologies to stabilize a slope is shown in Figure 1.

Figure 1a) shows the design problem. Different constructions can be used to solve this task, for example a gravity wall (Figure 1b), a single anchored wall (Figure 1c) or a grouted anchored wall (Figure 1d). These three constructions differ in their topology. Some topology optimization algorithms can be found in Bendsøe (1995) or Allaire (2005).

Once a topology is chosen, the shape of the topology can be optimized with regard to the design problem. Concerning the design problem in Figure 1, the topology in Figure 1d is chosen. Figure 2 shows different possibilities to optimize the shape of the topology in Figure 1d during the category shape optimization, for example the variation of the anchor positions (b), of the anchor inclination (c) or the anchor length (d). The variations in Figure 2 b)-d) can be varied regarding an optimization task, for instance the minimization of the bending of the wall or minimization of the installation costs. The application of shape optimization algorithms in geotechnical application has been shown in Kinzler (2007) and Grabe et al. (2010, 2011).

The third category is the dimension optimization of each construction part. Within this category every cross section and dimension is determined. Neither the topology nor the shape can be changed by the dimension optimization. The dimension optimization is the most widely applied category of structural optimization in geotechnical engineering. The shape optimization of Figure 2 results in the shape shown in Figure 3. For this example, possible parameters for the dimension optimization are given in Figure 3.

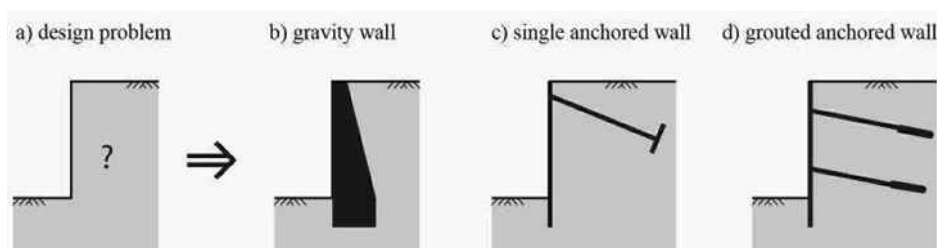


Figure 1. Different topologies for a design problem a): b) gravity wall, c) single anchored wall, d) grouted anchored wall

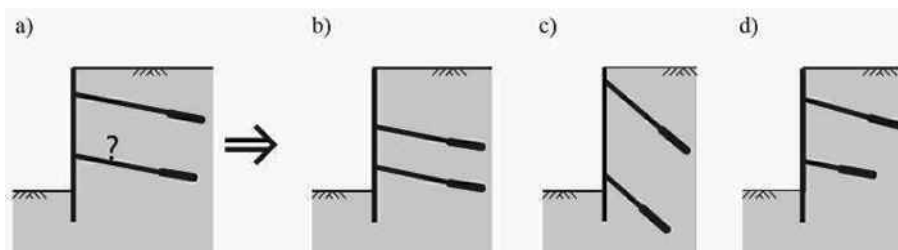


Figure 2. Shape optimization: a) main topology, b) variation 1: anchor position, c) variation 2: anchor inclination, d) variation 3: anchor length

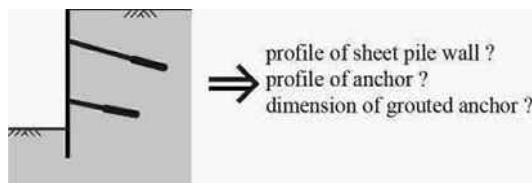


Figure 3. Dimension optimization

2 NUMERICAL OPTIMIZATION ALGORITHM

An iterative algorithm is used to solve the optimization problem numerically. First a topology is created and second its load-displacement behavior is determined using a finite-element analysis. In the next step, the results of the finite-element analysis are interpreted and transmitted to a topology optimization algorithm, which creates a new improved topology. Afterwards step two is performed again.

The SIMP-Method (Solid Isotropic Material with Penalization) after Sigmund (2001) is used as topology optimization algorithm. The algorithm is based on the idea, that the material of the optimized structure already exists in the design domain Ω , but is not optimally distributed. Therefore, the material is equally distributed in the design domain Ω at the beginning of the optimization process. The material distribution changes during the optimization process and the material compacts in areas where it is needed to achieve the optimization task.

The design domain Ω is discretized with finite elements. The material parameters are specified individually for each element depending on the material distribution. The virtual density ρ at a point a has to be between 0 and 1, see Equation 1.

$$\rho(a) = \begin{cases} 0 \rightarrow \text{no material} \\ 1 \rightarrow \text{material} \end{cases} \quad (1)$$

Regarding a geotechnical application, for example a foundation made of concrete, a finite-element with $\rho(a) = 0$ is a soil element and with $\rho(a) = 1$ is a concrete element.

Using the SIMP-Method, the objective function is the minimization of the compliance of the structure in the design domain Ω . Thus, the stiffness of the structure is maximized. The compliance of the structure can be expressed using the internal energy of the system. The internal energy c of an elastic material is defined by Equation 2.

$$c(\mathbf{x}) = U^T K U \quad (2)$$

In Equation 2 U is the global deformation tensor, K the global stiffness matrix and \mathbf{x} the tensor of design parameters. The virtual density $\rho(a)$ matches the design parameters of x_i of the tensor \mathbf{x} at point a .

The minimization of the compliance is restricted by two constraints. The first constraint ensures that the observed system is in equilibrium an every step of the optimization process. Using the finite-element method, this constraint is ensured by Equation 3. F is the global tensor of the external forces.

$$K U = F \quad (3)$$

The second constraint ensures that the volume of the material distributed in the design domain remains constant during the optimization process, see Equation 4. V_δ is the volume of the structure.

$$\int_{\Omega^{mat}} 1 d\Omega = V_\delta \quad (4)$$

Additionally, the design parameters x_i are limited by an upper and an lower bound, such that the optimized material parameters lie within to the physically possible range.

The optimization task for minimal compliance design can be written using Equation 5. U_e is the element deformation tensor, K_e the element stiffness matrix, ρ_e the element virtual density, δ the volume fraction, V_δ the structure volume and V_0 is the volume of the design domain. The values of the material distribution are limited by x_{min} to avoid singularities during the finite-element analysis. Using the algorithm for geotechnical application, this limit is not necessary because the stiffness of an element belongs to the soils stiffness at $x_i = 0$ and cannot tend to zero.

$$\left. \begin{array}{l} \min : \quad c(x) = U^T K U = \sum_e^N (\rho_e)^p U_e^T K_e U_e \\ \text{subject to:} \quad \left. \begin{array}{l} K U = F \\ V_\delta = V_0 \cdot \delta \\ 0 < x_{min} \leq x \leq 1 \end{array} \right\} \end{array} \right\} \quad (5)$$

The penalty p controls the material change-over to ensure complete material change for example from soil to concrete, see Figure 4.

The improved topology in every iteration step is determined using the method of optimal criteria, see Equation 6 (Bendsøe 1995). A positive move-limit m and a numerical damping coefficient $\eta = 0.50$ are introduced, see Bendsøe (1995). The move-limit m limits the change of the topology in each iteration step. The sensitivity of the objective function is expressed in Equation 7. Using the Lagrangian multiplier λ , B_e is defined in Equation 8.

$$\rho_e^{new} \begin{cases} \max(\rho_{min}, \rho_e - m), & \text{if } \rho_e B_e^\eta \leq \max(\rho_{min}, \rho_e - m) \\ \rho_e B_e^\eta, & \text{if } \max(\rho_{min}, \rho_e - m) < \rho_e B_e^\eta < \max(1, \rho_e + m) \\ \min(1, \rho_e + m), & \text{if } \min(1, \rho_e + m) \leq \rho_e B_e^\eta \end{cases} \quad (6)$$

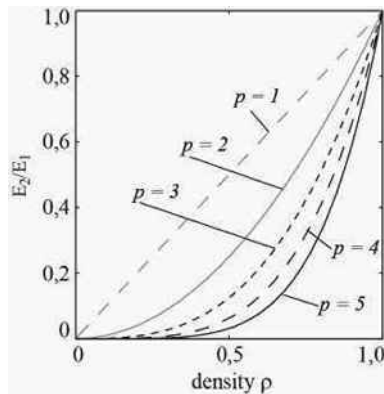


Figure 4: Change-over of the Young's modulus E of two different materials depending on different values of the penalty term p

3 APPLICATION

1.2 Numerical model

The presented topology optimization algorithm is applied to a vertically loaded strip footing foundation. The topology underneath the foundation is to be optimized. The initial width of the foundation is 2 m and the height is 1 m. The load-settlement behavior is simulated in a 2D finite-element analysis. The discretization of the model is shown in Figure 5.

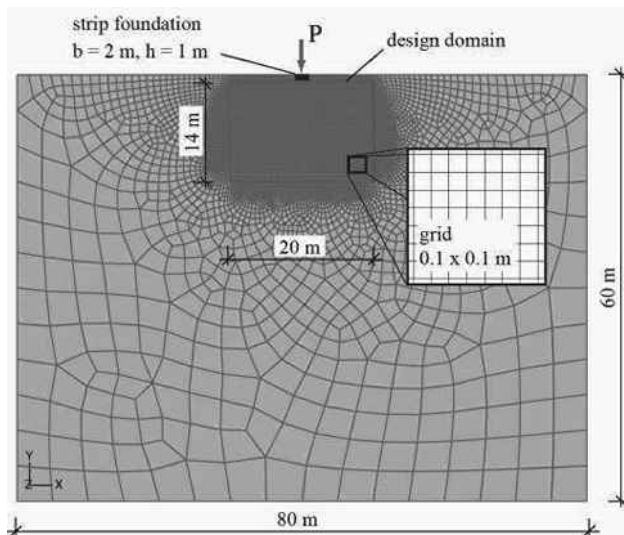


Figure 5. Discretization of the FE-model of a strip foundation with a width of 2 m and a height of 1 m, vertically loaded with 500 kN at the loading point P

The foundation is vertically loaded with 500 kN. The soil and the improved material underneath the strip foundation is modeled using the hypoplastic constitutive model after von Wolffersdorff (1996) with the extension of intergranular strain after Niemunis and Herle (1997). Detailed information can be found in Pucker and Grabe (2011).

$$\frac{\partial c}{\partial \rho_e} = -\frac{\partial c}{\partial \rho_e} p(\rho_e)^{p-1} U_e^T K_e U_e \quad (7)$$

$$\frac{\partial \rho_e}{\partial \rho_e} = \frac{\partial V}{\lambda \partial \rho_e} \quad (8)$$

1.3 Optimization

Three optimizations are performed at different material volumes. The material volume is 2%, 5% and 10% of the design domain. The design domain is 20 m of width and 14 m of height, see Figure 5.

1.4 Results

In Figure 7 the optimized topologies with 2%, 5% and 10% material volume are illustrated. Regarding the 2% material volume, mainly the area at the foundation edges are compacted. Since the foundation can be considered to be rigid, the optimization results can be explained with the theory of a rigid foundation on an elastic half-space, according to which high stresses will occur at the edges of the foundation. The optimization algorithm compacts the material mainly in these areas.

Figure 6 shows the displacement of the soil underneath the foundation with the unoptimized (Figure 6 a) and the optimized (Figure 6 b) structure with a volume of 5%. The settlements can be reduced up to 50%.

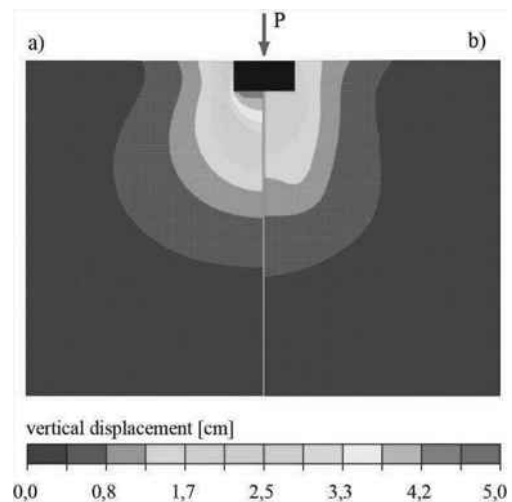


Figure 6. Vertical displacement before (left) and after (right) the topology optimization with 5% material volume

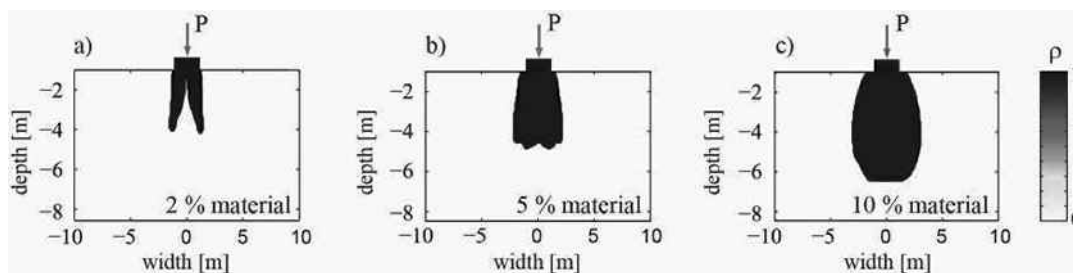


Figure 7. Optimized foundations with a) 2% material volume, b) 5% material volume, c) 10% material volume

The influence of the material volume on the improvement is shown in Figure 8. Figure 8 top shows the material volume over the vertical load P at different settlements. The applicable load at a settlement restriction about 1 cm cannot be significantly improved using more than 2% material volume. Regarding higher settlement restrictions, the increase of the material volume also increases the applicable load P .

The same results can be obtained from the load settlement curves of the improved foundations in Figure 8 bottom. The main improvement is reached with a material volume about 2%.

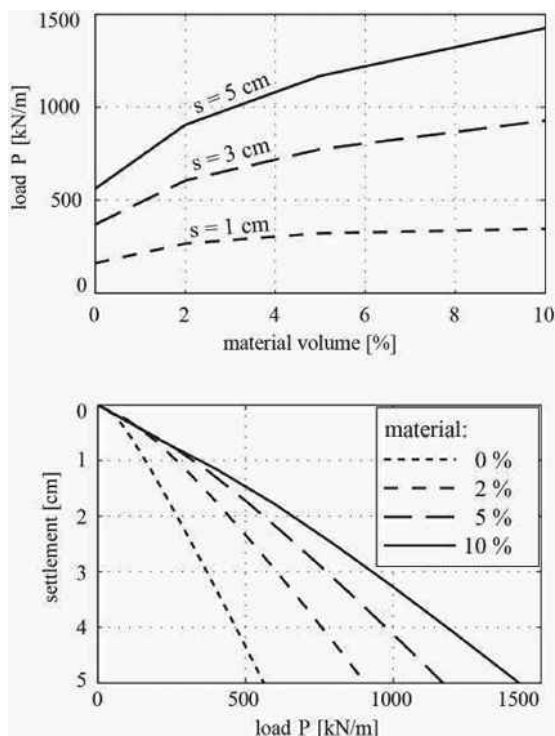


Figure 8. top: load P over material volume at different settlement restrictions; bottom: load-settlement curves of the optimized foundation topologies

1.5 Practical realization

The practical realization of the optimized topologies can be quite difficult. The optimized topologies of the presented example can be realized using the jet grouting method. This method allows the realization of every possible topology restricted by the minimum diameter of a jet grouting body.

Another possibility to realize such topologies is the interpretation of the topologies and the conversion of the topology into standard geotechnical construction parts. The realization of the topology with 2% material can be done using a classical strip foundation topology in combination with micro piles, see Figure 9.

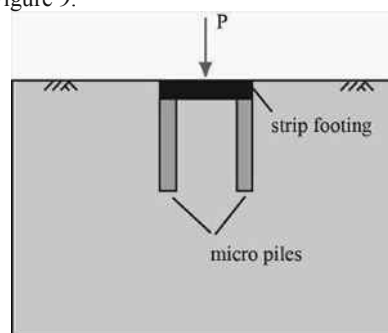


Figure 9. Possible practical realization of the topology with 2% material volume

2 CONCLUSION

The application of topology optimization in geotechnical engineering was presented. The applied SIMP-Method is suitable for geotechnical problems. In the presented example, the settlements of a strip foundation could be reduced up 66%.

Topology optimization in geotechnical engineering has a great potential and can lead to innovative and efficient designs.

3 REFERENCES (TNR 8)

- Allaire G., De Gournay F., Jouve F. And Toader A.-M. 2005. A level-set method for shape optimization. *Control and Cybernetics* 34.
- Bendsøe M.P. 1995. Optimization of structural topology, shape and material. Berlin, Heidelberg, New York
- Grabe J., Kinzler S., Pucker T. And Mardfeldt B. 2010. Untersuchung des Tragverhaltens und der Anwendbarkeit numerischer Optimierungsverfahren für Kaikonstruktionen. *Tagungsband der 31. Baugrundtagung 2010 in München*, 123-129
- Grabe J., Pucker T., Busch P. 2012. Non-linear numerical model for the design process of deep foundations with regard to effects of pile installation. *Proceedings of 9th International Conference on Testing and Design Methods for Deep Foundations 2012 in Kanazawa/Japan*, edited by T. Matsumoto, 55-64
- Kinzler S. 2007. Entwurf einer Pfahlgründung unter Anwendung der Mehrkriterien-Optimierung. *Der Bauingenieur* 82, 367-379.
- Sigmund O. 2001. A 99 line topology optimization code written in Matlab. *Structural and Multidisciplinary Optimization*, 21, 120-127
- Niemunis A. and Herle I. 1997. Hypoplastic model for cohesionless soils with elastic strain range. *Mechanics of Frictional and Cohesive Material*, 2, 279-299
- Pucker T. and Grabe J. 2011. Structural optimization in geotechnical engineering - basics and application. *Acta Geotechnica*, 6, 41-49, DOI: 10.1007/s11440-011-0134-7
- Von Wolfersdorff P.-A.. 1996. A hypoplastic relation for granular materials with predefined limit state surface. *Mechanics of Frictional and Cohesive Material*, 1, 251-271

Role of the facing on the behaviour of soil-nailed slopes under surcharge loading

Rôle du parement sur le comportement des pentes de sol cloué sous surcharge

Sanvitale N., Simonini P., Bisson A., Cola S.

Department of Civil, Environmental and Architectural Engineering - University of Padova - Italy

ABSTRACT: Soil nailing is an economic and efficient method to reinforce soils, involving the insertion of threaded bars into natural unstable slope for increasing the overall stability or into cut slopes during the top-down process of excavation. The retained soil, the resisting reinforcements and the external facing are the main components of a soil-nailed structure. Their composite interactions determine the performance of soil-nail construction in terms of deformations and stability. Even if the international codes deal about the possibility of use rigid or flexible external facing, the role of facing stiffness is not sufficiently studied and evaluated. To this aim, some tests with various facing types, differing in stiffness and continuity, were carried out so far in 1g small scale physical model. The experimental results show the importance of both flexional and axial stiffness of facing in controlling the deformation of the wall during excavation and the maximum surcharge applicable at the rear of wall.

RÉSUMÉ: Le clouage du sol est une méthode économique et efficace pour renforcer le sol en place: il consiste en l'insertion de barres d'acier filetées ou d'autres barres dans les pentes naturelles instables ou dans des talus au cours du processus de l'excavation pour augmenter la stabilité globale. Le sol soutenu, les barres résistantes et le parement extérieur sont les principales composantes d'une structure du sol cloué. Leurs interactions mutuelles déterminent la performance du *soil nailing* en termes de déformations et de stabilité. Même si les codes internationaux considèrent la possibilité d'utiliser des parements extérieurs rigides ou flexibles, le rôle de la raideur du parement n'a pas été suffisamment étudié et évalué. Avec ce but ont été réalisées des épreuves dans un modèle physique avec des parements différents en rigidité et continuité. Les résultats expérimentaux soulignent l'importance de la raideur en flexion et en traction-compression du parement extérieur dans le contrôle de la déformation de la paroi pendant l'excavation, et la valeur maximale de la charge applicable à l'arrière du mur.

KEYWORDS: soil nailing, facing, retaining wall, soil reinforcement, physical model.

1 INTRODUCTION

Soil nailing is an economical and efficient reinforcement technique used as a remedial measure in unstable natural slopes or as retaining structure for excavated slopes. In comparison with other retaining structures, soil nailing permits to reduce the excavated soil volume, saving construction materials and realization time. Its first applications were proposed in France for the Couterre project (Plumelle et al. 1990) and in Germany (Stocker 1976). Even if many studies and researches have been already performed and several national codes or guide lines exist, the role of facing in controlling the deformation of excavated front or the slope overall stability is not completely understood yet.

On this matter, the new code EN 14490:2010 indicates the possible use of three types of facing which are:

- *hard facing* which has to fulfil the function of stabilizing the slope between the nails and shell therefore be dimensioned to sustain the maximum expected destabilizing forces;
- *flexible facing* designed to provide the necessary restrains to the areas of slope face between the bearing plates as well as the erosion control;
- *soft facing* with the primary function of controlling slope erosion in conjunction of vegetation.

Even if the EN 14490:2010 reports some examples for the three types of facing, it does not give precise indications on how to evaluate the forces applied by soil on facing or the stiffness of facing.

In order to improve the understanding of the role of facing on the resistant mechanisms of soil nailing, this paper presents

the results of an experimental program carried out on a 1g small scale physical model of sandy slope reinforced with soil nailing and brought to collapse by surcharge loading: in the tests six facings, differing for continuity and stiffness, were utilized to restrain the soil between nails.

2 PHYSICAL MODEL

The model face is 39.5 cm wide and 40 cm high, with a wall dip angle of 80° (Figure 1). The soil is medium-fine sand from Adige river with the following characteristics (Gottardi and Simonini 2003): mean particle diameter $D_{50} = 0.42$ mm, non-uniformity coefficient $C_u = D_{60}/D_{10} = 2.0$, specific bulk weight $G_s = 2.71$, minimum and maximum dry specific weight $\gamma_{d,min} = 13.6$ kN/m³ and $\gamma_{d,max} = 16.5$ kN/m³, peak friction angle $\phi_{peak} = 42-43^\circ$ and critical friction angle $\phi_{crit} = 35^\circ$.

The sand is prepared in homogeneous layers into a caisson with pluvial deposition method reaching a relative density of about 85%. During deposition the caisson is maintained inclined at 20° to deposit homogeneously the sand also at rear of facing and to simplify the nail installation. In the meanwhile, the cover is fixedly bonded in vertical position, using four wooden blocks behind which will be subsequently removed to simulate the excavation.

The deposition is temporarily stopped to install the nails in 4 horizontal lines and 3 vertical lines, with spacing $s_v = 10.2$ cm and $s_h = 13.2$ cm respectively.

The nails are 32.5 cm long aluminium tubes, with an external diameter of 6 mm and covered with 1 mm thick layer of glued Adige sand. They are perpendicularly connected to the

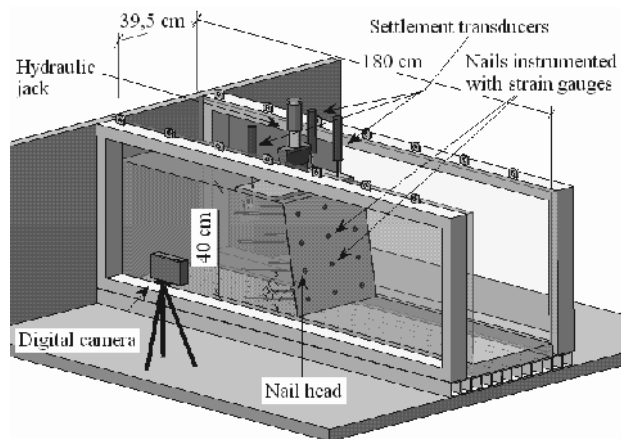


Figure 1 Perspective view of 1g physical model.

facing with a 1.2 cm annular rod and a small steel pin.

The monitoring system includes:

- A load cell between the vertical jack and the plate to measure the load;
- Three vertical displacement transducers recording the plate settlements;
- A digital camera taking lateral images of the model during the entire test. By applying the Particle Image Velocimetry (PIV) technique (White et al. 2003) to the image sequences it is possible to reconstruct the evolution of displacement during the test;
- A laser scanner for monitoring the frontal displacement of the face at some significant load steps. Since the scanner takes about 1 min to complete the scansion, the loading sequence must be temporarily stopped. A small load reduction, due to the occurrence of the soil viscous strains, was observed in this short time interval;
- Eight strain gauges, glued pair by pair, at 2.3, 10.4, 18.5 and 26.7 cm from the face, on the nails located along the central vertical section at 15.3 and 25.4 cm from the top (the central ones). They permit to reconstruct the distribution of axial strain and, consequently, of axial stress along nails.

In order to evaluate which stiffness – i.e. the axial or the flexional ones - mostly influences the soil nailing behaviour during excavation and subsequent plate loading, six tests were performed with different facing types (Table 1 summarises the geometrical and mechanical properties of the various coverings). Four facings, covering the entire excavated front, were: *a*) 4 mm-thick plate of Polymethyl methacrylate (PMMA); *b*) a 0.25 mm-thick sheet of brass (BRASS); *c*) a steel mesh formed by 1-mm wires, perpendicularly welded at 6 mm spacing (MESH); *d*) a steel net formed by 0.24 mm-diameter wires, perpendicularly woven (NET). Three of these continuous coverings have an axial stiffness with the same order of

magnitude but a flexional stiffness decreasing about one order from one to another facing, while the fourth is very deformable both in axial and flexional sense.

The other ones are two discontinuous facing constituted by rectangular tiles in PMMA (obtained by cutting a PMMA cover like that used in test *a*): in these cases the covering ratio, defined as the ratio between the total covered area and the total extension of facing, are respectively equal to 95% (PMMA95) and 25% (PMMA25). Due to this discontinuity the axial stiffness vanishes, so these covers are flexional stiff (like the test *a*) but without any axial stiffness.

Since the soil forming the model is dry sand without cohesion, to avoid the collapse of sand among the tiles or across the mesh holes, a very light and low-resistant geo-synthetic behind them was set up. The same geo-synthetic was also inserted at the rear of the other facings to reach homogeneous test conditions.

After the models being completely set up, they were driven to failure in three steps: 1) application of a uniform load q of 24 kPa on the plate; 2) removing one by one of four wooden blocks, simulating the front excavation; 3) application of an increasing uniform load on the plate up to failure.

3 MODEL RESPONSE DURING EXCAVATION

Figure 2 depicts the vertical displacements of the plate, Δy_p , during the 4 steps of excavations in the all the tests. Even if the plate horizontal displacements, Δx_p , (obtained from the PIV analysis of digital images) are not reported here for brevity, they show a similar trend with the same magnitude order of vertical settlements – i.e. $\Delta y_p/\Delta x_p \approx 1$. Moreover, since the plate is located just at the rear of facing, the horizontal plate displacement may be considered equal to the horizontal displacement of the front tip.

Note that the vertical displacement does not exceed 0.5 mm (equivalent to 0.13% of the slope height) in tests *a* and *b* with very rigid facings (PMMA and MESH), while the maximum displacement, equal to about 2 mm and equivalent to 0.5% of the height, is observed in the tests *d* and *e* with very deformable facing (NET and PMMA25).

It is also interesting to observe that in the test with PMMA95, with discontinuous covering, the displacement does not exceed the 0.27% of the height: this means that the high flexional stiffness of PMMA tiles prevents the soil near to the face to move laterally.

Figure 3 reports the tensile force distribution along the monitored nails at the end of the excavation. Even if the tensile force is determined in few points, it is possible to recognize the typical bell-shaped distribution observed in many applications and described in the international practical guides (i.e. FWHA 2003, Geoguide7 2008). As known, the slope of the lateral segments depends on the shear stresses mobilized at the interface soil-nail in the active and passive zone respectively.

Table 1. Mechanical characteristics of facings adopted in the physical model.

Model	Facing	Covering ratio (%)	Thickness/Wire Diam. (mm)	Wire spacing (mm)	Young modulus E (GPa)	Axial stiffness EA/m (N/mm)	Flexional stiffness EJ/m (Nmm ² /mm)
a	PMMA	100	4	-	3.2	12800	17066.67
b	MESH	100	1	6	210	26180	3318.06
c	BRASS	100	0.25	-	126	31500	236.25
d	NET	100	0.24	1.02	70	3105*	22.66
e	PMMA95	95	4	-	3.2	-	-
f	PMMA25	25	4	-	3.2	-	-

* The axial stiffness of canvas is the mean values obtained from to traction tests performed on two 178mm x 25mm samples.

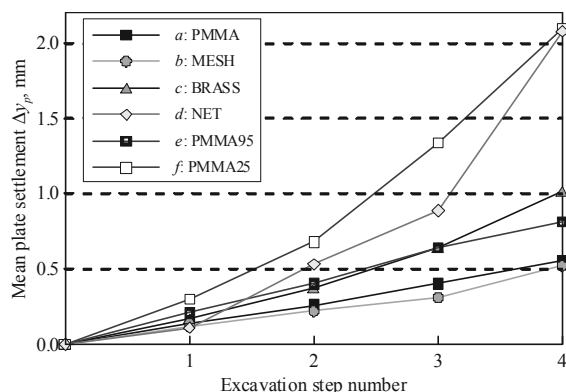


Figure 2. Average plate vertical displacement during four excavation steps in all the tests.

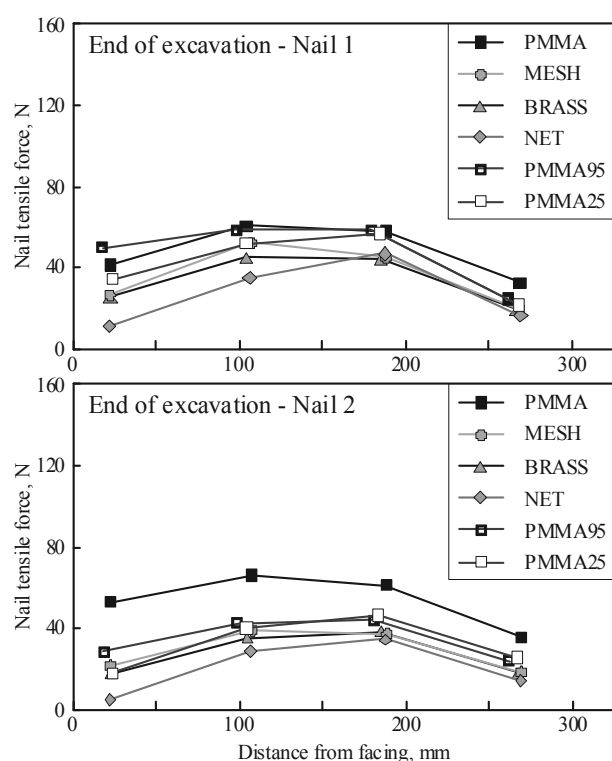


Figure 3. Distribution of tensile force along the monitored nails at the end of excavation: (a) upper nail; (b) lower nail.

The stiffness of facing strongly influences the characteristics of tensile force distribution, such as the slope of two lateral segments, the tensile force at the connection with facing, N_{head} , and the location X_{max} of maximum traction, N_{max} .

The highest N_{head} is reached in tests *a* and *e* (PMMA and PMMA95), with N_{head} gradually decreasing according to the facing deformability: the lowest values are due to tests with NET and PMMA25. On other hand, the difference $N_{max} - N_{head}$ and consequently the slope of segment in the active zone, is less for tests with PMMA and PMMA95, gradually increasing with facing deformability. Finally, X_{max} is located closer to the face in tests with PMMA and PMMA95, while it moves itself from face using deformable covering (NET and PMMA25).

This means that if a rigid facing prevents the soil behind the face to dilate, limiting, as previously explained, the face horizontal displacements. In addition it also reduces the relative soil-nail displacement in the active zone and the increase of shear stress mobilized at this interface. On the contrary, to reduce the face deformation, the nails have to be more stressed by higher soil pressure acting at the rear of facing, because the

soil could not reach the active state condition with the mobilization of the minimum horizontal stress.

4 MODEL RESPONSE DURING PLATE LOADING

Figure 4 plots the load applied to the plate during the phase *c* vs. the mean vertical displacements of the plate. Temporary reductions of the load are evident in the graph and they are due to the temporary stops of loading piston for performing the laser scanner of the front.

Figure 5 compares the spatial distribution of the cumulated shear strains at collapse in tests with PMMA, NET and PMMA25 (for brevity we choose only the most meaningful images): the shear strain distribution is determined by applying the PIV analysis to the lateral images of models.

In all the model tests, failure appears to be combined with localization of shear strain along one or more narrow bands. The mostly well-defined band moves from the plate edge (the one opposite to the face) towards the face base intercepting all the nails and delimiting the wedge pushing on facing: the wedge is characterized by a size related with the maximum load reached in the test: the greater is the maximum load, the larger is the wedge. Other bands, less clear, individuate a wedge like those that typically form below shallow foundations.

Figure 6 plots the distribution of tensile force along the monitored nails when a load of 5,45 kN is applied on the plate: note that at this load level the model *d* is approaching the collapse, and some problems affect the strain-gauge readings (localization of plastic strain in nail n.1 and detachment of one strain-gauge in nail n.2) and the correct evaluation of tension value. Moreover, data from test PMMA95 are not reported in Figure 6, because some problems occurred in the electrical connections induce to consider them not reliable.

These results permit to point out the important role played by the facing. The maximum load supported by the retaining system with rigid facing PMMA, $P_{max,a}$, is about five times greater than the load supported in test with NET, $P_{max,d}$, that represents the minimum load measured in all the tests. Other models support loads in the range 0.83-0.97 $P_{max,a}$ with higher values in tests with MESH and PMMA95, the most rigid covers.

From the comparison suggested in Figure 6 it is evident that the collapse of model *d* is due to the overcoming of the pull-out resistance in the passive zone of soils. The relative soil-nail displacements, cumulated in the active zone as consequence of facing buckling, induced the increase of tensile gradient in the section of nails close to the face. Consequently, also the maximum traction increases significantly: N_{max} in test *d* is 3-4 times greater than that determined in all other tests. This high tensile force has to be compensated by the frictional resistance along the nails in the passive zone. This is evident from Figure 6, because the slopes of the tensile profile in the most internal part of the nails are greater than those characterizing the results

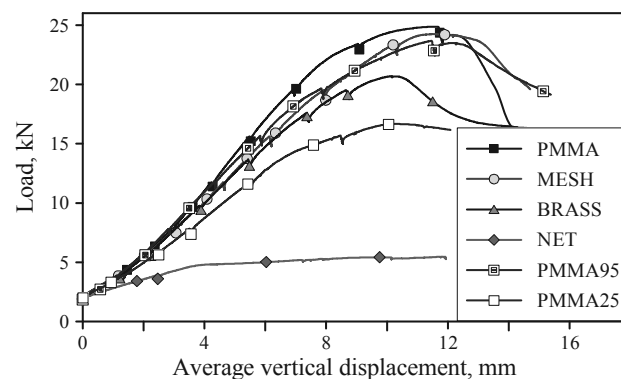


Figure 4. Load on the plate vs. mean settlements during loading phase up to collapse.

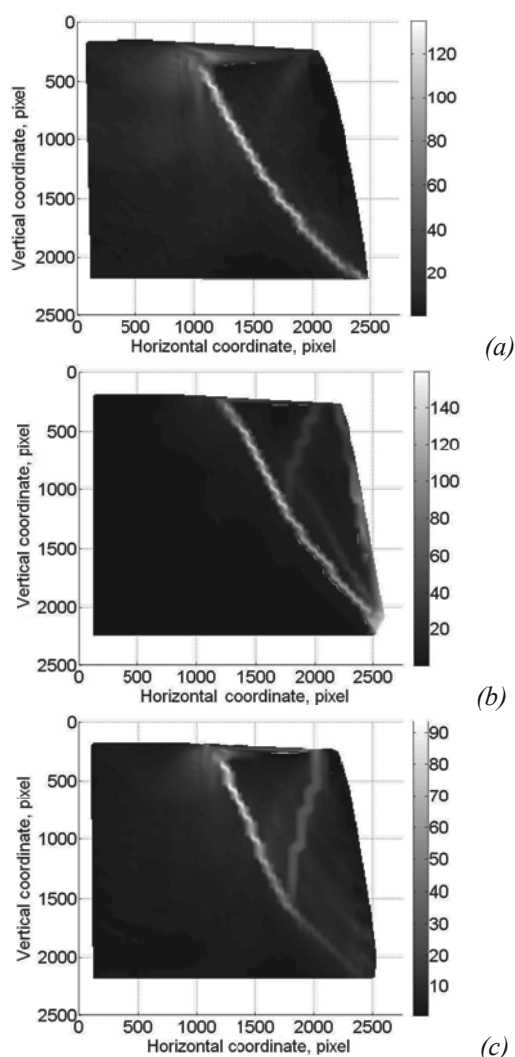


Figure 5. Total shear strain distribution at the face collapse, determined by mean of PIV in tests with PMMA (a), NET (b) and PMMA25 (c).

of other tests. It is important to note that the points marked by an asterisk in Figure 6 are largely overestimated, because approaching the failure the nails underwent to large and concentrated flexional plastic strains, also for the presence of rupture wedge of shallow foundation, and, in this strain state the relationship strain-stress is not linear yet.

Of course the tensile force distributions along nails for all the tests at failure are similar to those recorded for model *d*, even if they are not here reported for sake of brevity.

5 FINAL REMARKS

From the experimental results discussed above it is possible to observe that both flexional and axial stiffness influence the performance of a soil nailing system in excavation and at collapse. If the facing has no continuity, its flexional stiffness can hinder the front deformation during excavation, thus limiting the mobilization of shear stress along nails. In addition, if the facing is flexionally deformable but characterized by low axial deformability, horizontal displacements of the front too can be controlled. In both of the cases, at the end of excavation, the system has still a high level of safety in relation to the global stability problem. On the contrary, the largest deformations accumulated with excavation can reduce the safety margin.

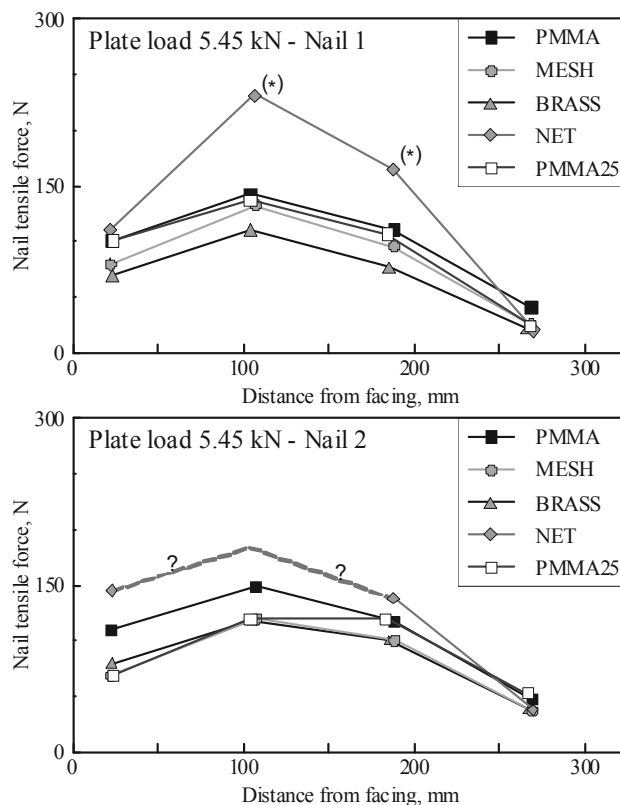


Figure 6. Distribution of tensile force along the monitored nails when the load on plate is equal to 5.45 kN (collapse load of test with NET): (a) upper nail; (b) lower nail. Notes: 1) the tensile data indicated with asterisk (*) are determined from strain-gauge readings at a load of 5.30 kN because at greater loads the nails experimented plastic strains in these positions; 2) The trends indicated with (?) are only presumed, not measured, due to the detachment of the 2nd strain-gauge.

6 ACKNOWLEDGEMENTS

We want to thank the Dalla Gassa s.r.l. (Cornedo Vicentino, Italy), which sponsor this research, and Dr. D.Pilotto and M.Miuzzi for the valuable help given in the experimental tests.

7 REFERENCES

- Geoguide7, 2008. *Guide to Soil Nail design and construction*. Geotechnical Engineering Office, Hong Kong.
- Gottardi G., Simonini P., 2003. The viscoplastic behaviour of a geogrid-reinforced model wall. *Geosynthetics International*, 10: 34-46. ISSN: 1072-6349, doi: 10.1680/gein.2003.10.1.34.
- EN 14490:2010: *Execution of special geotechnical works — Soil nailing*.
- FHWA-IF-03-017, 2003. *Geotechnical Engineering circular No. 7 – Soil Nail Walls*.
- Plumelle C., Schlosser F., Oclage P. and Knochenmus G., 1990. French national research project on Soil Nailing: CLOUTERRE, *Geotechnical Special Publication ASCE*, 25, 660-675.
- Stocker M., 1976. Bodenvernagelung, Vorträge der Baugrundtagung, Nürnberg, *Deutsche Gesellschaft für Erd- und Grundbau e.v.*, Essen.
- White, D.J., Take, W.A. & Bolton, M.D. 2003. Soil deformation measurement using particle image velocimetry (PIV) and photogrammetry, *Géotechnique* 53(7): 619-631.

Geotechnical aspects in sustainable protection of cultural and historical monuments

Les aspects géotechniques dans le développement durable des monuments historiques et culturels

Sesov V., Cvetanovska J., Edip K.
University "Ss Cyril and Methodius" - Skopje
Institute of Earthquake Engineering and Engineering Seismology

ABSTRACT: This paper describes the geotechnical aspects of comprehensive methodology that has been developed at Institute for Earthquake Engineering and Engineering Seismology for protection of cultural and historical heritage. The methodology has been applied on numerous domestic and international projects. Primarily focus is given on geotechnical conditions related to seismic actions because the history showed that many of the historical monuments have been heavily damaged due to earthquakes. Multidisciplinary approach was used to have clear insight of key parameters that driven the seismic potential of the sites. Seismic hazard and risk analysis defined the level of the seismic potential of the sites. Practical implementation of the methodology is described through three case studies for protection of cultural and historical monuments in Macedonia: the St. Mary Peribleptos Church, from the 13th century, located in old town of Ohrid; the mosque Mustafa Pasha in Skopje, from the 15th century and the 19th century Clock Tower located in the city of Prilep. The obtained results point out the significance of involving local site conditions into the seismic assessment and retrofit of historical structures in general.

RÉSUMÉ : Dans cet exposé sont présentés les aspects géotechniques d'une méthodologie qui a été développée à l'Institut de génie sismique et l'ingénierie parasismique pour la protection des monuments historiques et culturels. La méthodologie est appliquée sur plusieurs projets domestiques et internationaux. L'attention est particulièrement donnée sur les conditions géotechniques liées à l'action sismique, puisque l'histoire a démontré que beaucoup de monuments historiques étaient très endommagés lors d'un séisme. Pour obtenir une idée claire sur les paramètres clé gouvernant le potentiel sismique des sites, on a utilisé l'approche multidisciplinaire. Avec l'analyse du risque et l'aléa sismique, on a défini le niveau du séisme potentiel des sites. L'application pratique de la méthodologie est décrit par trois exemples d'études pour la protection des monuments historiques et culturels en Macédoine: l'église Sainte Vierge Marie Peribleptos du 13 siècle, dans la vieille ville d'Ohride, la mosquée Mustafa Pasha de Skopje du 15 siècle et la tour de horloge en Prilep du 19 siècle. Les résultats obtenus montrent l'importance de la prise en compte des conditions locales dans l'estimation sismique et en général, et l'intérêt du retour d'expérience des constructions historiques en général.

KEYWORDS: geotechnical aspects, sustainable protection, historical monuments

1 INTRODUCTION

The problem of deep excavation in highly urbanized area such as the city centre of Skopje has proved to be quite formidable engineering task. In particular the greater depth and the built-up surrounding make it especially difficult. The ever growing prize of a square meter has led to extensive utilization of the underground. Such an idea has been very attractive for the investors which always look for the most economic solution of the underground works, generally constrained by the excavation depth and retaining system.

The tendency to optimize the structures has been an inspiration for the authors to investigate the comparative advantages of different deep excavation retaining systems and their supporting elements. The objective has been to offer a qualitative study which considers all relevant aspects of the underground construction in urban areas.

The paper presents case studies of three different retaining systems used to secure the excavation pits which do not exceed 800m² in base. All of them are located in the area of around 2km, thus share similar ground conditions. There are different limitations and/or specifics on every site, as to the surrounding e.g. existing structures or very frequent streets. The depth of the excavation pit varies from 6.5 to 18m. All retaining systems had been calculated numerically and controlled according to the Eurocode provisions.

1.1 System of soldier H piles with lagging

In the first case example a 7m deep pit should be excavated for the construction of the new National theatre. Larger part of the structure has been already finished, only the part adjacent to the street is left to be erected. The excavation pit is rather narrow only 3.05m in width (enlarging to 6.1m) and 36.65m long, see Figure 1.

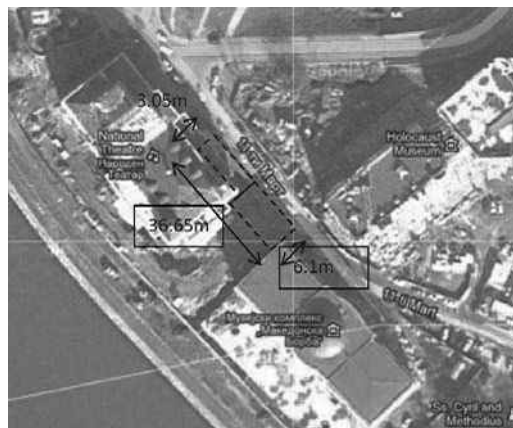


Figure 1. Site location No.1 in front of the new National theatre.

The task has been to secure the pit from only one side (namely from the frequent street which connects the main city square) allowing undisturbed traffic and pedestrian communication. As solution a temporary structure of soldier H piles with lagging has been proposed. The supporting system uses rickers and struts (positioned on -2.0m and -4.65m from the top) acting upon the foundation of the existing structure. There were several arguments in favour of this solution, foremost it is light and suitable for a temporary structure, does not take a lot of space and last but not least it is relatively cheap.

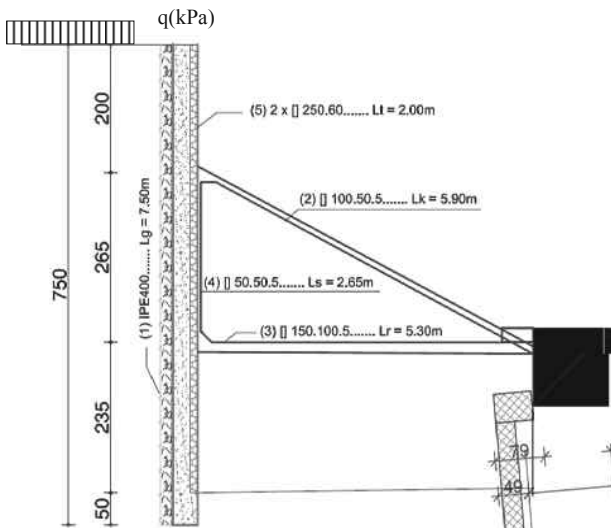


Figure 2. Site location No.1 with RW as soldier H piles with lagging.

The structure is modular consisted of eighteen soldier H piles placed on every 2m with total length of 7.5m. The piles are embedded with depth 0.5m. A steel IPE 40 profile has been chosen according to DIN 1025 B1.5 and DIN 17100 specifications.

The ground profile from 0 to 3m is defined by a layer of fill with pieces of construction material such as bricks and mortar. From 3 to 7.5m there is clayly silt with smaller pieces of construction debris with the following material properties: unit density as $\gamma=19\text{kN/m}^3$, cohesion as $c=5\text{kPa}$, angle of internal friction as $\phi=28^\circ$ and Compressibility modulus as $M_v=8000\text{kPa}$. A standard traffic load with $q=16.67\text{kPa}$ acting on the far away and $p=5\text{kPa}$ on the nearby strip has been assumed.

The problem is calculated using the finite element method using plane and beam element. The structural elements of the wall are assumed to be linear with smeared stiffness as in equivalent plane-strain model. The soil is discretized by Mohr-Coulomb material behaviour. A plot of the total displacements is shown in the Figure 3.

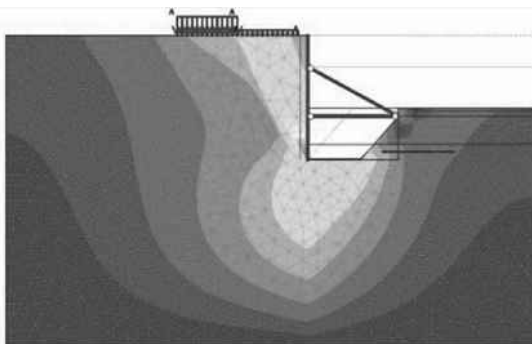


Figure 3. Shading plot of the total displacements.

The maximal total displacement is 64mm registered in the toe of the wall while on the top(-surface) it is around 10 times smaller.

The results of the analysis of soldier H pile wall are presented in the Figure 4.

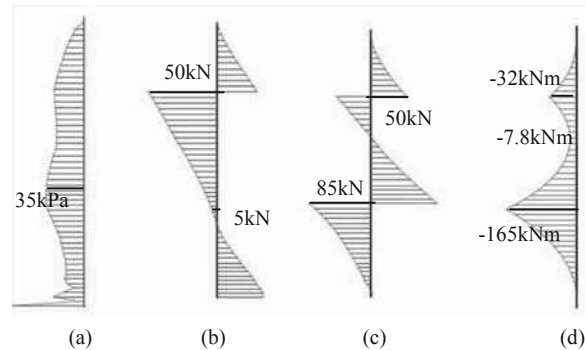


Figure 4. Diagram of (a) Active earth pressure, (b) Axial force, (c) Shear force and (d) Bending moment.

The steel cross sections are calculated according to the provisions in EC3 with $\gamma_s=1.15$. A steel type „Fe235“ with allowable stress of 204MPa has been used.

The rickers prop the wall at -2.0m and are positioned at angle of 23.5 degrees with length of $L_k=6.65\text{m}$. They are designed as a rectangular hollow section [100.50.5]. The struts prop the wall at -4.65m with length of $L_r=6.1\text{m}$. They are designed to accept compression force using rectangular hollow section [150.100.5]. Last but not least, the wooden lagging ($b=25\text{cm}$, $l=182\text{cm}$ and $t=12\text{cm}$) are positioned over the height of 7m between the soldier piles.

Finally, the global stability is controlled using the so-called ϕ -c reduction procedure. A global factor of safety $F_s=1.37$ has been obtained which is larger than 1.1 as recommended value for temporary structure.

1.2 Top to down construction of system with diaphragm wall

Following the site conditions (see Figure 5) a building with five underground floors with depth of -15.86m should be constructed. From two sides there are existing buildings, one of which is adjacent on six floors and one basement while the other one is 3m away with only two floors and shallow basement. From the third side there is very frequent boulevard which leads to the centre and main city square.



Figure 5. Site location No.2 on M.T. Gologanov boulevard.

The base dimension of the excavated pit are 27.65x11.55mn not very large around 320m², but due to the difficult surrounding conditions and the great depth it has been decided to use the top to down approach of construction. The diaphragm wall is considered to be a permanent structural element, which in the first phase carries the horizontal (earth) pressure loads while in exploitation it will be responsible also for the loads from the superstructure. Following the top-down procedure the diaphragm will be supported by the previously constructed RC

slabs, thus enabling the further excavation of the pit. The excavation process and slab support construction is described in Table 1 with respect to the depth h .

Table 1. Excavation phases

Phase	1	2	3	4	5	6	7
h (m)	0.0	-3.5	-6.11	-8.5	-10.9	-13.9	-15.8

The diaphragm RC segments are 2.5m long and 0.4m width organized as primary and secondary. The base plan with depth and sequence of construction is presented in Figure 6.

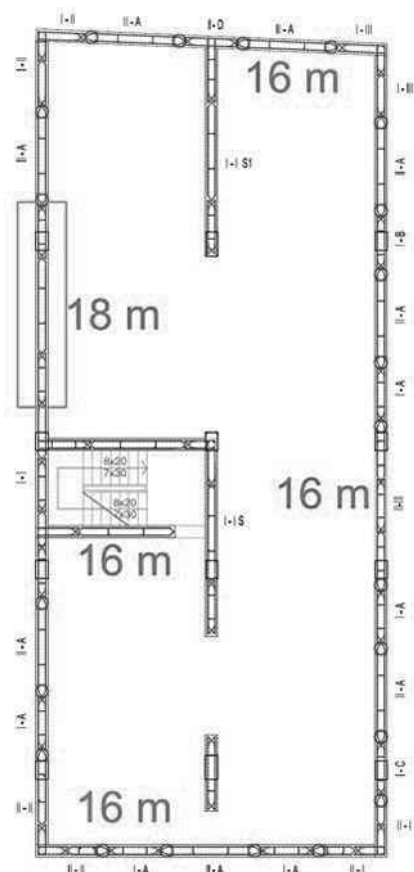


Figure 6. Base plan of primary and secondary diaphragm segments.

The depth is 16m only in one section its 18m due to the requirement necessary for elevator equipment. The soil profile is established through set of field and laboratory investigations which were used to define the material properties given Table 2.

Table 2. Soil properties

Type	h (m)	γ (kN/m ³)	ν (/)	M_c (MPa)	c (kPa)	ϕ (^o)
N	-1.0	17.0	0.30	3	5	18
GW	-3.5	19.0	0.32	30	0	32
M	-4.0	22.0	0.27	35	100	30
M	-10.0	24.0	0.26	45	150	32
M	-20.0	24.0	0.26	55	200	34

where γ is a unit weight, ν is a Poisson's ratio, M_c is Compression modulus, c is cohesion and ϕ is angle of internal friction. They are given for every lithological unit: top layer (N) is a man-made embankment brownish silty clay containing pieces of bricks and roots with a thickness of 1m, followed by layer (GW) is sandy gravel with thickness of 2.5m to 3.7m; continuing as a layers (M) which are Neogene's deposits composed by claylike Marls to highly weathered alveoli. The

underground water is detected at -3.2m below ground surface in layers (GW) while the bottom layers are with low permeability and relatively dry.

In order to obtain more realistic behaviour of the deep excavation process secured by diaphragm wall, the problem has been analyzed using the finite element method. The ground stress-strain state during excavation is determined through a plane-strain finite element model. The soil is discretized as elasto-plastic material using a Mohr-Coulomb definition vis-a-vis the reinforced concrete wall as a linear material. The spatial discretization had been varied depending on the situation and detailing level but in general triangular plane elements with 15 nodes had been used. Two cross sections both in X-X and Y-Y direction had been discretized and calculated. The structural elements were modelled using three node beam elements, see Figure 7.

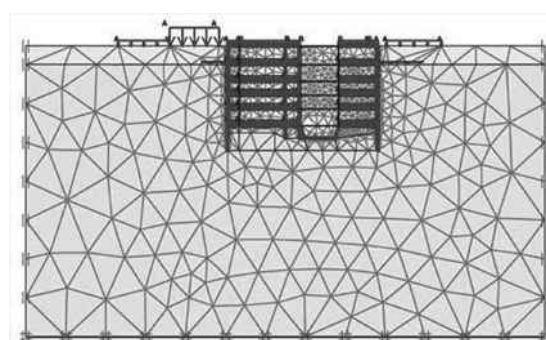


Figure 7. Finite element model of X1-X1 section.

The underground structure has been calculated for two loading combinations, namely the construction loading situation with pit excavation (in 6 phases = 1-diaphragm wall + 5-floor slabs) and exploitation situation (with permanent + temporary + seismic loads). In Figure 8 the total displacements of underground structure is presented for the second loading combination.

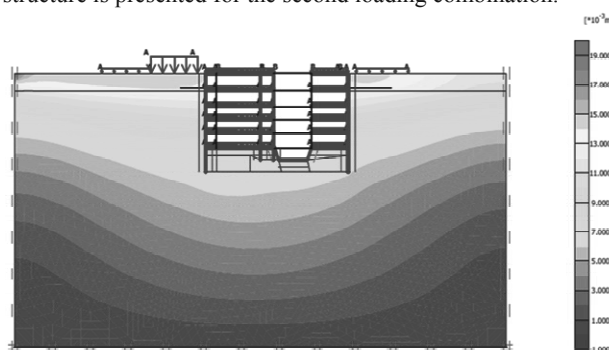


Figure 8. Total displacement of the soil-structure system in X1-X1 section.

The maximal registered displacement is 14mm with predominantly horizontal component (stiff rocking response) due to the seismic loading. According to the stress-strain distribution the internal quantities of the structural elements had been determined. They were used for structural design of elements such as, diaphragm wall, floor slabs and foundation plate. The reinforcement is determined according the EC2 for C35/45 and S500 (with $\gamma_c=1.5$ and $\gamma_s=1.15$). The reinforcement of the diaphragm wall is around $0.8\%A_c$ (area of concrete section). The 47% of the total reinforcement will be used for the diaphragm wall, 18% for the foundation plate and 35% for the floor slabs.

1.3 System of secant pile wall

For the same site (see Figure 5) an alternative solution has been analysed with secant pile retaining wall to secure the excavation pit (27.65x11.55m) but this time with depth of 6.5m. In this scenario only two floors are planned to be constructed using a temporary retaining structure. In the first phase the primary, (reinforced concrete) piles with diameter of 0.6m and length of 7.5m spaced exactly 1.2m should be executed. In the next phase the secondary (concrete) piles with the same diameter but shorter depth of 5.5m are constructed. On the top they are connected by a beam with dimensions 0.6x0.4m as shown in Figure 9.

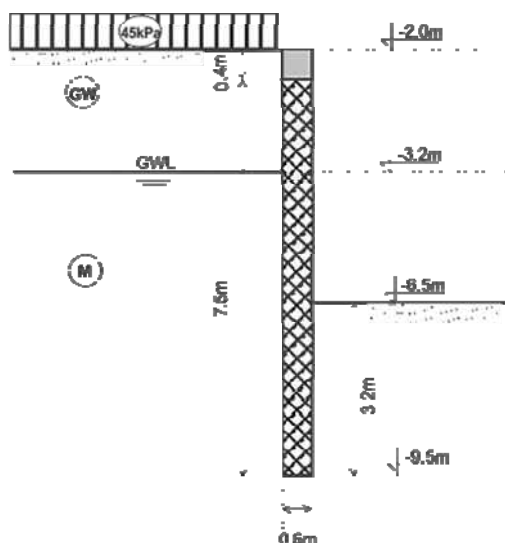


Figure 9. A plan of the secant pile wall in X1-X1 section.

The problem is discretized using three-dimensional finite element model where the soil profile is identical to the one described in Table 2. For the spatial discretization volume elements are used in combination with nonlinear-plastic material definition for the soil and linear-elastic for the concrete. The calculation is used to determine the stress-strain behaviour of the soil-structure interaction system, hence presented through the total displacement in Figure 10.

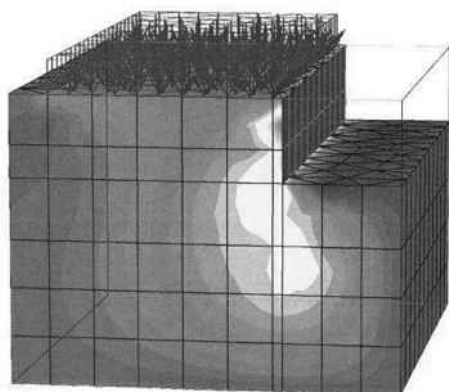


Figure 10. Total displacement of the soil-structure system in X1-X1 section.

A maximal earth pressure of 33.7kN/m² causes horizontal displacement of 9.8mm, which have been considered as acceptable. Furthermore, the diagrams of internal pile quantities are presented in Figure 11.

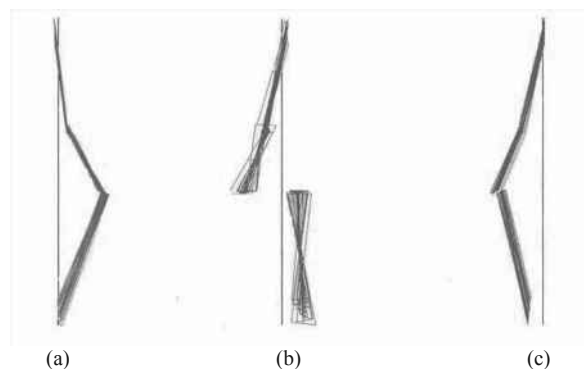


Figure 11. Diagram of (a) Axial force, (b) Shear force and (c) Bending moments in the pile.

The values of the maximal internal quantities: bending moment $M=56.81\text{kNm}$, shear force $Q=43.64\text{kN}$ and axial force is $N=-114.8\text{kN}$. The pile design has been made using interaction (M-N) diagrams for C30/37 providing the following reinforcement: longitudinal $14\phi 16$ (28.2cm^2) and stirrups $\phi 8/20\text{cm}$. Finally, the global stability is controlled where a safety factor $F_s=1.55$ is obtained.

2 CONCLUSIONS

The solder H pile wall with lagging is rarely used in our practice, although it is highly efficient and cost effective for situations where there is no ground water. Also a greater depth can be reached when combined with adequate supporting system e.g. tieback. Nevertheless, in Skopje there are few locations with low GWL. Although very formidable the systems with diaphragm wall are seldom used, partially because there is almost no experience nor there has been clear cost-benefit analysis. For a long period of time it has been thought that the costs are very height, which with the present study had proven not to be the case. Combined with the top-down method of construction where the wall is permanent structure according to our analyses remains very cost effective solution. The secant pile wall technique, in contrast, is very often used in our practice, sometimes in combination with anchors when greater depth is needed. It represents formidable solution but usually takes a lot of the available space and construction time, also brings high expenses since it is often a temporary structure.

Finally, when comparing all retaining structures we had come to conclusion that the diaphragm wall represents a preferred solution for underground construction in highly urbanized (build-up) areas and situations with high ground water level as it is usually the case in Skopje.

3 REFERENCES

- German Society for Geotechnics (Deutsche Gesellschaft für Geotechnik e.V.) 2003. Recommendations on Excavations, Ernst & Sohn Verlag für Architektur und technische Wissenschaften GmbH & Co. KG, Berlin, ISBN 3-433-01712-3.
- Kempfert, H.G. and Gebreselassie, B. 2006. Excavations and Foundations in Soft Soils, Springer-Verlag Berlin Heidelberg, ISBN 540-32894-7.
- Potts, D.M. and Zdravkovic, L. 2001. Finite element analysis in geotechnical engineering: application. Imperial College of Science, Technology and Medicine, Thomas Telford Publishing, Thomas Telford Ltd, ISBN 0-7277 2753-2.
- Moeller G. 2012. Geotechnik. Grunbau, Bauingenieur-Praxis, 2 Ed. Ernst & Sons, A Wiley Company ISBN: 978-3-433-02976-3.
- EN 1997-1:1994 Eurocode 7: Geotechnical design - General rules
- EN 1538:2000 Execution of special geotechnical works – Diaphragm walls

Various use of diaphragm walls for construction of multilevel road junction – Design and monitoring of displacements

Diverses utilisations de parois moulées pour la construction de l'intersection des routes à plusieurs niveaux – Conception et le suivi des déplacements

Siemińska-Lewandowska A., Mitew-Czajewska M.
Warsaw University of Technology, Warsaw, Poland

Tomczak U.
Soletanche Polska Sp. z o.o., Warsaw, Poland

ABSTRACT: The paper presents various use of diaphragm walls for the construction of four-level junction in Warsaw. Diaphragm walls were chosen as a best solution for abutments of 2 viaducts and 1 flyover, foundations (barrettes) under 7 pillars, 60 to 100cm thick retaining walls with total length of over 570 running meters. In the paper detailed technical descriptions, geotechnical conditions, predicted theoretical horizontal and vertical displacements of walls for all mentioned diaphragm wall applications are presented. Finally, the comparison of the results of theoretical analysis and real scale monitoring results (displacements measurements and load tests) in accordance with construction stages is presented and discussed.

RÉSUMÉ : Cet article présente différentes utilisations de parois moulées pour la construction d'une jonction de quatre niveaux à Varsovie. Les parois moulées ont été choisies comme une meilleure solution pour les butées de 2 viaducs et 1 voie surélevée, les fondations (barrettes) sous 7 piliers, des murs de soutènement épais de 60 à 100 cm avec une longueur totale de plus de 570 mètres. Dans le document des descriptions techniques détaillées, des conditions géotechniques, les prévisions de déplacements horizontaux et verticaux théoriques des murs pour toutes les applications de parois moulées mentionnées sont présentés. Enfin, la comparaison des résultats de l'analyse théorique et les résultats en vraie grandeur (mesures de déplacements et de tests de charge) de la surveillance conformément aux étapes de la construction est présentée et discutée.

KEYWORDS: diaphragm wall, deep excavation, foundation, barrettes

1 INTRODUCTION

In Poland nowadays, especially before euro 2012, road network and new motorways connecting Poland and Ukraine with Western Europe are being built. Construction of Warsaw bypass is the place where huge multilevel road junctions are built.

The case discussed in the paper is 3 level road junction consisting of 2 flyovers (indicated as E1, E2 at fig. 1) and 2 viaducts (indicated as W1, W2 at fig. 1). The original building permit design assumed that the abutments and columns were to be founded on large-diameter piles with the diameter 120 and 150 cm. The accompanying RC retaining walls and viaduct abutments were to be erected in traditional formwork. The original design assumed that the embedded part of the junction was to be built with a temporary casing in the form of sheet piling with an RC capping beam at the top. The walls were to be anchored with 1 level of soil nails. Permanent structure was

designed as retaining walls connected with water tight foundation plate. During the execution design stage, due to economical and technological reasons, the solution was much simplified - only diaphragm walls were used for all parts of the structure, i.e. for:

- excavation walls – retaining structures,
- foundations – barrettes of viaduct columns as well as barrettes of columns and abutments of flyovers,
- viaduct abutments – T-shaped diaphragm walls.

The new solution allowed the significant shortening of construction works through the use of diaphragm walls as temporary and permanent structure. Figure 1 presents the general arrangement of the discussed road junction and indicates parts of the structure described in the paper.

In the design stage theoretical displacements and bearing capacities of these structures were calculated. During construction, at each of discussed structure parts, the real

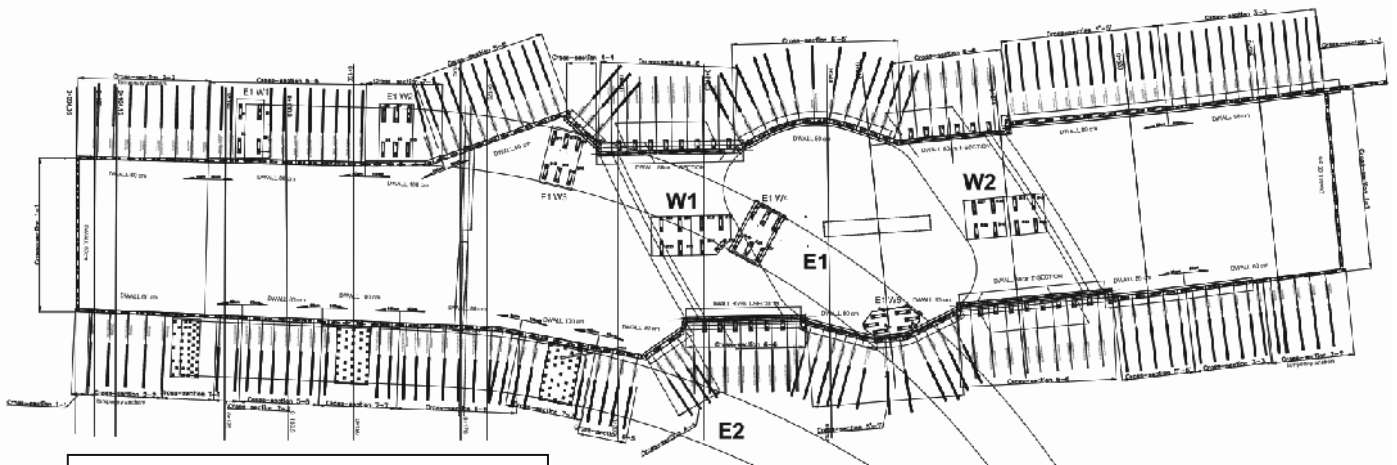


Fig. 1 General arrangement

horizontal displacements and settlements were measured and compared to theoretical values calculated in the design stage. It has allowed an assessment of the correctness of the solution.

2 GEOTECHNICAL AND HYDROLOGICAL CONDITIONS

The ground in the land plot consists mainly of Quaternary formations: river sediments and glaciofluvial deposits as well as glacial deposits. In the entire area involved in the investment, the near-surface layers below man-made fills consist of medium-dense and dense sands and gravels reaching down to the max. depth of 18.8 m. Below (the layer roof from 10.6 to -18.8 m), there are glacial clays, deposited in the form of stiff sandy clays, clayey sands and, locally, silty clays. The layer of anthropogenic soils is not very thick: maximum thickness: 2.2m, average thickness: about 0.5-1.00 m.

Within the entire area, a continuous ground water table was found in the layer of glaciofluvial sands. The ground water table was located at about -4.5 m below the ground level. Occasionally, the water table was confined by lenses of cohesive soils.

3 DIAPHRAGM WALLS AS A RETAINING WALL

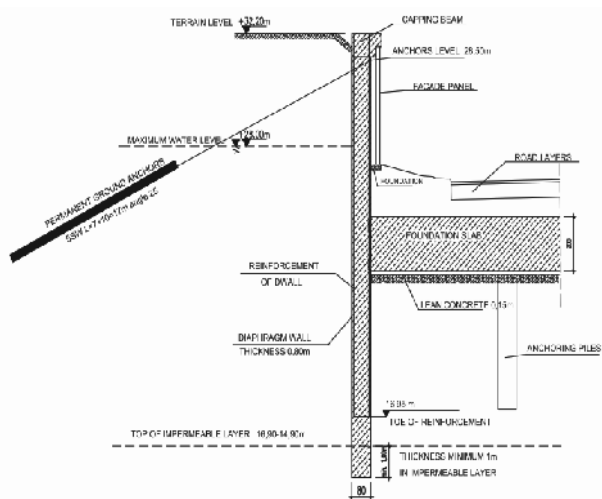


Fig. 2 Typical cross-section of the excavation wall; 80cm thick diaphragm walls, anchored using permanent anchors.

Due to variable embedding of the excavation below the ground level, down to the maximum depth of 10 m below the ground level, diaphragm walls with 3 different thickness values were implemented, namely 60 cm, 80 cm and 100 cm. Moreover, different types of protective measures were implemented to ensure stability of casing walls, i.e:

- temporary ground anchors, 600 kN capacity (cross – section 2-2),
- permanent ground anchors, 600 - 700 kN capacity (cross-sections 3-3, 4-4, 5-5),
- permanent ground anchors in the area of T-shaped D-walls, 700 kN capacity (cross section 6-6).

Some parts of walls remained not supported (cantilever walls) due to the small height of excavation (cross-section 1-1) or possible colisions with pile foundations outside the wall (cross-section 7-7).

In total 148 ground anchors were executed (18 temporary and 130 permanent) and 31 permanent ground anchors for abutments.

Diaphragm walls along the entire perimeter of the facility (including the transversal walls) were embedded at least 1 m down into the impermeable layer, in order to minimise the inflow of water into the excavation (fig 2). Due to unbalanced hydrostatic pressure, the ground slab was anchored with

displacement piles in its central part in the deepest excavation (fig 2).

Diaphragm walls were designed to resist loads resulting from soil pressures and from service loads at the ground surface generated by vehicles and stored materials, amounting to $q=12,0$ kPa in the zone removed by at least 1.5 m from the wall face, and loads generated by heavy traffic, amounting to $q=30$ kPa. Additionally, the design considered a load generated with vehicle K located on the roadway located in close vicinity of the diaphragm wall, in compliance with standard PN-85/S-10030 Bridges. Loads.

Static analysis of diaphragm walls were made using dependent pressures method (PAROI). 7 typical calculation cross-sections were verified. Typical results of calculations – bending moments and displacements – are shown at fig. 3. Maximum theoretical values of horizontal wall displacements are as follows:

- cantilever D-wall - 6 mm;
- D-wall and temporary ground anchors - 15 mm;
- D-wall and permanent ground anchors - 12mm;
- T-shaped D-walls - 8mm.

Corresponding bending moments amount to 180 kNm/m up to 700 kNm/m.

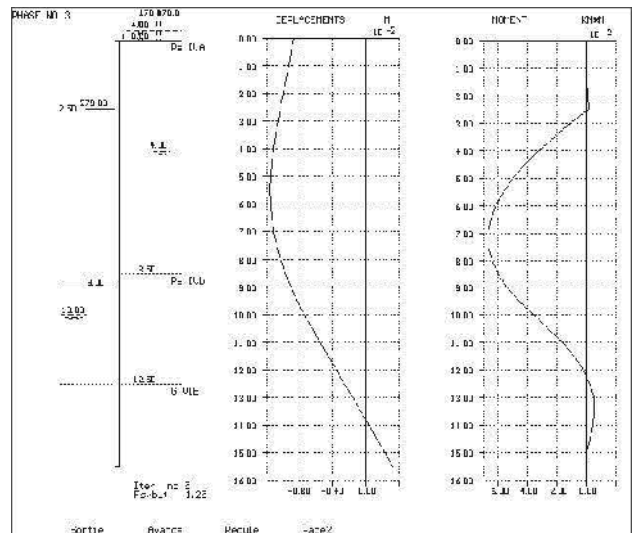


Fig. 3 Theoretical values of bending moments and horizontal displacements for 80cm thick D-wall with permanent ground anchors (cross-section 5-5) in the final construction stage.

Benchmarks for geodesic measurements were located on the capping beam of diaphragm walls, spaced every 50 m at the maximum. Measurements were carried out for particular stages of execution of works on site, at least once every month or more frequently.

Construction stages were as follows:

- site preparation, sub-base preparation, construction of guide walls and D-walls with RC capping beam – reference measurement,
- excavation 0,5m below the anchoring level – measurement 1,
- execution and stressing of ground anchors – measurement 2,
- final excavation – measurement 3,
- verification of displacements during the execution of driven piles – subsequent measurements.

Particular attention was paid to measurements of wall displacements in the vicinity of works consisting in driving displacement piles in, in order to anchor the ground slab. In the view of the presence of a layer of silty sands, designers were concerned about the impact of dynamic pile driving on the load-carrying capacity of ground anchors, whose bearing plates are

embedded in these sands. The monitoring of displacements of the capping beams of diaphragm walls showed that their maximum value reached 10 mm for an 80 cm thick wall, anchored with permanent anchors. In the case of other cross-sections, displacements were smaller and reached up to 8 mm. No increased displacements of the diaphragm wall were observed during the process of pile driving.

Design works had to face additional difficulties resulting from the very complex shape of the facility, involving 4 abutments (T-shaped D-walls, cross-section 6-6) and curved walls that encased the roundabout (cross-section 5'-5'). Both the excavation bottom and the top of the walls and the capping beam were located in slopes. Due to this fact combined with variable thickness and varied strut methods, almost every single reinforcing cage of a diaphragm wall was of different type. Therefore, the contractor who constructed diaphragm walls was forced to stick strictly to the schedule of execution of particular sections, without any possibility of introducing changes during the works.

4 DIAPHRAGM WALLS AS FOUNDATIONS FOR PILLARS AND COLUMNS

A foundation on barrettes (parts of diaphragm walls) – instead of large-diameter piles (\varnothing 120/150) implemented in the construction design – was designed for 5 supports of the flyover E1 (4 pillars and 1 abutment) and viaducts pillars – viaducts: W1 and W2 (fig.1). The barrettes – as fragments of diaphragm walls – have a very large base. Therefore, they can transmit very high loads. For this reason, they are very useful for structures subjected to very high loads, as in this particular case of bridge structures.

The replacement, for instance, of the support consisting of 11 piles that were 150 cm in diameter with 6 barrettes resulted in a considerable acceleration of works, which brought about a measurable financial result in this particular case. Typical arrangement of the pillar foundation is shown at fig. 4.

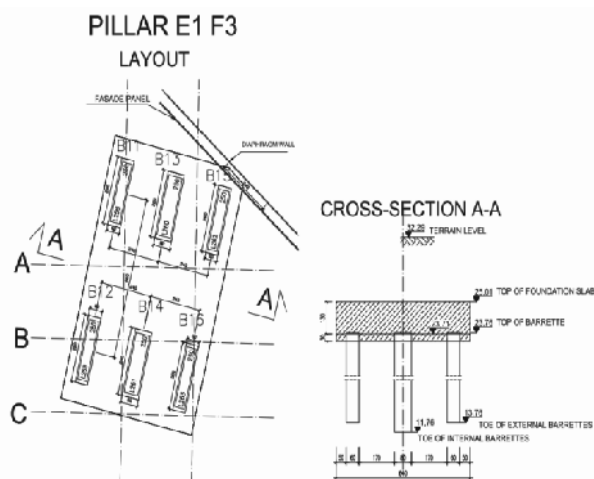


Fig.4 Typical pillar foundation arrangement

Barrettes implemented as foundations for pillars had the following dimensions: 0.6x2.80 m and 0.8x2.8m. They were from 10.0 to 15.0 m long. They transmitted vertical forces reaching the max. value of 7600 kN and the bending moment reaching the max. value of 4996 kNm. In total 44 barrettes were erected.

Internal forces and moments for each barrette were calculated using ROBOT software, modelling supports loaded by a possible most unfavourable load combination. Due to unsymmetrical loading of supports each barrette had different loading (both - compression as well as tension) and different bending moments in both directions.

For each of barrettes additional boreholes were made in order to verify geotechnical conditions. Only then the design of lengths and calculation of bearing capacities of barrettes were made. It was considered that barrettes were founded in the stiff sandy clay layer and the shaft friction was calculated considering 2 geotechnical layers along barrettes, i.e. stiff sandy clays and medium dense to dense fine and silty sands.

Base bearing capacities and shaft frictions were calculated basing on the regulations of PN-83-B-02482 Foundations. Bearing capacity of piles and piles foundations.

A base injection system was designed for all barrettes, in order to ensure as high load-carrying capacity of a barrette as possible, while ensuring minimum settlements. In each support, one barrette was selected to be subjected test vertical loads, supposed to confirm the adapted geotechnical parameters were correct. The results of test loading showed that the load-carrying capacity of barrettes was higher than necessary, while the settlements were smaller than admissible.

Vertical loading tests of barrettes was carried out for 6 barrettes that were gradually loaded up to the maximum of 150% of the calculation force. After reaching 100% of design load the barrettes were unloaded in order to measure the resulting permanent settlement. Analogical procedure was used after reaching 150% calculation force. Permanent settlements at the 150% force (i.e. 5286 - 10397 kN) did not exceed 4 mm, while they reached 2 mm for 100% of the calculation force (i.e. 3524 - 6931 kN). The barrette (dimensions: 0.6x2.8m, length: 13.1m) subjected to the greatest load experienced maximum settlement of 4.35 mm at the load of 10397 kN, where permanent settlement reached 2.91 mm. The results of settlement measurements during test loading of barrettes are compiled in table 1.

Table 1. The results of vertical loading tests of barrettes – settlements.

No.	Dimensions	Settlements for 100%Q		Settlements for 150%Q	
		temporary	permanent	temporary	permanent
B8	2,8x0,8 x10,0m	6001 kN		9002 kN	
		3,96mm	1,61mm	7,54 mm	3,53 mm
B12	2,8x0,6 x10,0m	3524 kN		5286 kN	
		1,33mm	0,75mm	2,82mm	1,71mm
B18	2,8x0,6 x10,0m	5889 kN		8834 kN	
		2,36mm	1,32mm	4,56mm	2,69mm
B31	2,8x0,6 x12,0m	5989 kN		8984 kN	
		2,53mm	1,32mm	5,29mm	3,09mm
B24	2,8x0,6 x13,1m	6931 kN		10397 kN	
		1,99mm	1,08mm	4,35mm	2,91mm
B41	2,8x0,6 x14,0m	4594 kN		6891 kN	
		1,80mm	1,14mm	4,17mm	2,84mm

As a part of interpretation of the test loading results auxiliary graphs were plotted as shown at fig. 5, in order to help calculate the bearing capacity of barrettes.

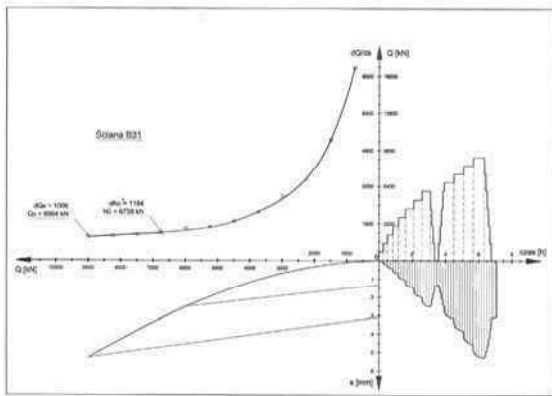


Fig. 5 Static load test result

5 DIAPHRAGM WALLS AS VIADUCT ABUTMENTS

The contour of the casing of the lowest level of the junction contained 4 viaduct abutments (viaduct W1 and W2). They were designed as 80 cm thick T-shaped diaphragm walls. Additional limitations were imposed for these fragments of diaphragm walls with respect to both horizontal and vertical displacements, caused by the selection of appropriate bearings. Additional permanent anchors were implemented – fig. 6, in order to minimize horizontal displacements of walls. In total, in the area of viaduct abutments, 31 permanent ground anchors of the 700kN capacity, were erected.

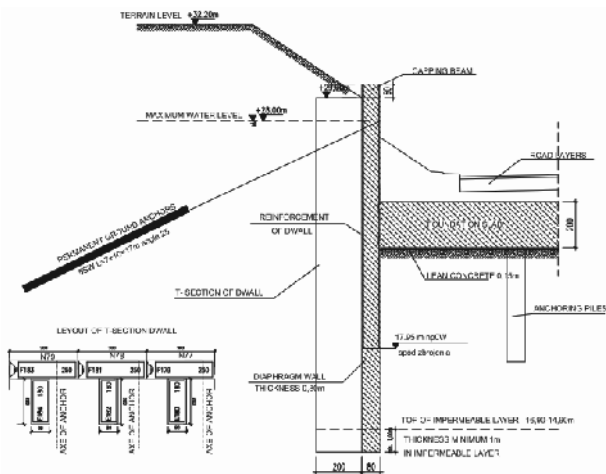


Fig. 6 Typical T-shaped D-wall cross-section for the W2 viaduct abutment.

Due to the fact that abutments were founded in the same stiff sandy clay layer as remaining barrettes made for the foundations of pillars, additional, special loading tests were not carried out for the T-shaped diaphragm walls. Bearing capacities of T-shaped barrettes were calculated by interpolation of the results of tests loadings of individual barrettes executed in the near vicinity of abutments. Additional limitations were imposed for T-shaped diaphragm walls with respect to horizontal displacements. In order to comply with limitations and minimize horizontal displacements of walls additional permanent anchors were implemented. The design load of permanent anchors was verified during acceptance tests. Each anchor was stressed up to 125% of its design load and after stabilization of creeping it was blocked at 80% of its design load. There were no excess permanent or elastic strains of anchor tendons measured, in accordance with regulations of

the code: PN-EN 1537 Execution of special geotechnical works. Ground anchors.

6 SUMMARY AND CONCLUSIONS

The results of diaphragm walls (as retaining walls) horizontal displacements measurements confirmed the correctness of static analysis of walls and prediction of their displacements, both made during design stage. Maximum value of horizontal displacement reached 10 mm for an 80 cm thick wall, anchored with permanent anchors and it didn't exceed neither theoretical nor permissible values. In the case of all other cross-sections, displacements were smaller and reached up only to 8 mm.

The results of vertical loading tests made for the barrettes confirmed the value of calculated theoretical bearing capacity being 7600 kN to be correct.

There were no significant horizontal displacements of T-shaped diaphragm walls noted (measured).

The new solution applied in the execution design (replacing the original one from the building permit design) was correct and resulted in significant savings due to the use of only one technology for the foundation and the retaining system (diaphragm walls) of the entire 3 level road junction construction. Most of the savings were obtained as a result of significant shortening of construction works.

7 REFERENCES (TNR 8)

- Soletanche Polska Sp. z o.o. 2010 Design of diaphragm walls for Łopuszańska-Kleszczowa junction, Warsaw
- Soletanche Polska Sp. z o.o. 2010 Design of anchors for Łopuszańska-Kleszczowa junction, Warsaw
- Soletanche Polska Sp. z o.o. 2008 Design of barrettes for Łopuszańska-Kleszczowa junction, Bydgoszcz
- GEOTECH Sp. z o.o. 2010 Geotechnical documentation for Łopuszańska-Kleszczowa junction, Warsaw
- PN-EN 1538 Execution of special geotechnical works – Diaphragm walls.
- PN-EN 1537 Execution of special geotechnical works – Ground anchors.
- PN-83/B-02482 Foundations. Bearing capacity of piles and piles foundations.

Effects of plane shapes of a cofferdam on 3D seepage failure stability and axisymmetric approximation

Effets des formes planes d'un batardeau sur la stabilité après une rupture par infiltration tridimensionnelle et sur l'approximation axisymétrique

Tanaka T., Kusumi S., Inoue K.

Department of Agricultural and Environmental Engineering, Kobe University, JAPAN

ABSTRACT: In the excavation of soil with a high ground water level, seepage failure is often a problem. For excavations over a large area, seepage failure is a problem in two dimensions. In contrast, the more the region of a cofferdam is restricted, the greater the seepage flow concentrates three-dimensionally. This three-dimensionally concentrated flow lowers the safety factor for seepage failure more than under the two-dimensional condition. In this paper, seepage failure experiments were conducted under three-dimensional flow conditions for various cases of penetration ratios of sheet piles and analyses of FEM seepage flow and stability against the seepage failure of soil were carried out using the Prismatic failure concept 3D. The critical hydraulic head differences obtained by experiments and the theoretical values are examined for several cases. Effects of plane shapes of a cofferdam on the theoretical critical hydraulic head differences and axisymmetric modeling of three-dimensional seepage failure are also discussed.

RÉSUMÉ : Dans le cas de l'excavation d'un sol où le niveau des eaux souterraines est élevé, la rupture par infiltration constitue souvent un problème. Lorsque l'excavation est effectuée sur une grande surface, la rupture par infiltration devient alors un problème en deux dimensions. En revanche, plus la zone du batardeau est limitée, plus le flux d'infiltration se concentre en trois dimensions. Or, comparé à ce qui se passe dans un contexte bidimensionnel, ce flux concentré de manière tridimensionnelle réduit davantage le facteur sécurité lié à une rupture par infiltration. Dans cet article, nous décrivons les expériences sur la rupture par infiltration menées dans les conditions d'un flux tridimensionnel pour divers ratios de pénétration dans des palplanches. Nous y rapportons aussi les analyses du flux d'infiltration et de la stabilité suivant le modèle FEM par rapport à la rupture par infiltration du sol, menées à l'aide d'un concept prismatique de rupture en trois dimensions. Nous avons examiné, pour plusieurs cas, les rapports de niveau hydraulique obtenus dans les expériences et la théorie. Les effets des formes planes d'un batardeau sur les rapports de niveau hydraulique critiques d'ordre théorique et la modélisation axisymétrique de la rupture par infiltration tridimensionnelle y sont également évoqués.

KEYWORDS: three dimensional seepage failure (3DSF), surface shape of a cofferdam, axisymmetric modeling of 3DSF

1 INTRODUCTION

In the excavation of soil with a high ground water level, sheet piles or diaphragm walls are often used to retain soil and water. Under such conditions, seepage flow occurs through the soil, and seepage failure is often a problem. For excavations over a large area, seepage failure is a problem in two dimensions. In contrast, the more the region of a cofferdam is restricted and the deeper the penetration of the sheet piles, the greater the seepage flow concentrates three-dimensionally within it. The three-dimensionally concentrated flow lowers the safety factor for seepage failure more than under the two-dimensional condition (Nikkei construction, 2001). Such a case must be treated in three dimensions.

In this paper, seepage failure experiments were conducted under three-dimensional flow conditions for various cases of total depths of soil, T , and penetrated depths of sheet piles, D , with a plane shape of a cofferdam of 1:2. Analyses of FEM seepage flow and stability against the seepage failure of soil were carried out using the Prismatic failure concept 3D. The hydraulic head differences at deformation in the experiment, H_p , and theoretical critical hydraulic head differences based on the Prismatic failure concept 3D, H_c , are examined for the same cases. The theoretical critical hydraulic head differences for various plane shapes of a cofferdam, e.g., short to long length of 1:1, 1:2, 1:3, and 1:4, were calculated, and the effects of plane shapes of a cofferdam on the theoretical critical hydraulic head differences are discussed. The axisymmetric modeling of three-dimensional seepage failure is also discussed.

2 THREE DIMENSIONAL EXPERIMENTS

2.1 Test apparatus

A test apparatus was designed to study 3D seepage failure of soil within a cofferdam as shown in Figure 1. In the experiment, one quarter of the three dimensional region is examined. The seepage tank is made of stainless steel, 1,000mm wide, 1,300mm high and 1,000mm deep. The front of the tank is made of transparent glass for observation of the behavior of soil particles inside and the right side of the tank is equipped with 283 piezometer holes for the measurement of pore water pressures. A cofferdam is mounted on the right/front side with surface size 200mm×400mm. Seepage water flows through a sand model under the difference in water head H between the downstream water level at the top of the right-hand-side drainage hole and the upstream water level kept constant by the constant-head device.

2.2 Test material and test cases

In seepage failure experiments, uniform fine sand (Lake Biwa Sand 3: under 850 μ m mesh, 50% grain size D_{50} =0.283 mm, specific gravity G_s =2.67 and uniformity coefficient U_c =1.40) was used. Seventeen tests E0301 to E0317 were conducted. The following notation is used: T_1 and D_1 are the total depth of soil and penetration depth of sheet piles on the upstream side, T and D are those on the downstream side, d ($=D_1-D$) is the excavation depth for the excavation model, and D_r is the relative density of soil. For a no-excavation model, $T_1=T$, $D_1=D$ and $d=0$ are applied.

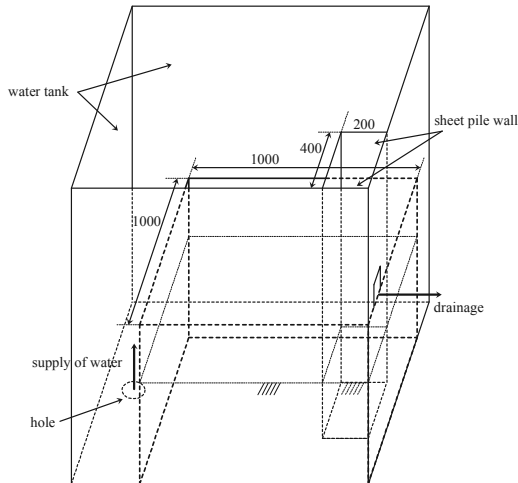


Figure 1. Schematic sketch showing test apparatus

3 EXPERIMENTAL RESULTS

3.1 $H-Q_{15}$ curve and change in shapes of soil surface

Figure 2 shows the $H-Q_{15}$ curve for test E0317, where Q_{15} is the discharge at 15 degrees Centigrade. It is observed from Figure 2 that Q_{15} increases linearly with increasing H until a certain value H_d . H_d value is referred to as the hydraulic head difference at which the $H-Q_{15}$ curve diverts from linearity. As stated below, at almost the same point as H_d , the soil surface begins to settle on the upstream side and rise on the downstream side. This is because, just at this point, the soil loosens on the downstream side, the void space enlarges, permeability of the soil grows larger, and discharge increases non-linearly with H . As H increases beyond H_d , Q_{15} becomes larger with increasing H more steeply than before, and the ground finally collapses at the hydraulic head difference at failure H_f .

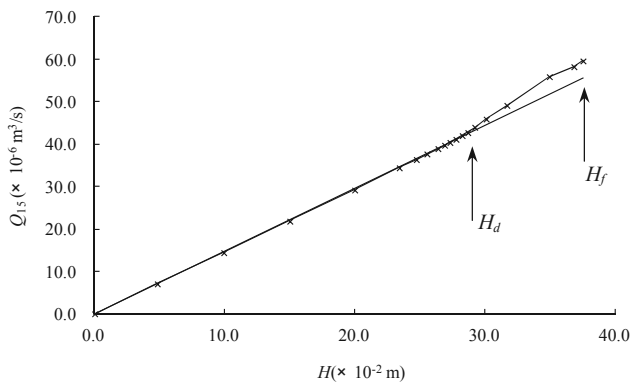


Figure 2. $H-Q_{15}$ curves for test E0317

The heights of the soil surface are measured at several chosen points along the measurement line shown in Figure 3. The measurement line is a bisector of the right angle of the inside corner of the rectangular diaphragm wall. Figures 4 (a)-(c) show the changes in shape of the surface of the sand model along the surface height measurement line with increase in H , from $H=4.81$ cm at the first step to $H=36.78$ cm at one step before failure. The model sand is in a stable state at early steps of H (Figure 4(a)). When H increases beyond a certain value H_y , the model sand changes in shape near the sheet pile wall. The surface of the soil in the vicinity of the sheet pile wall subsides on the upstream side and rises on the downstream side (Figure 4(b)). The value of H_y is referred to as the hydraulic head difference at onset of deformation. It was found from a series of

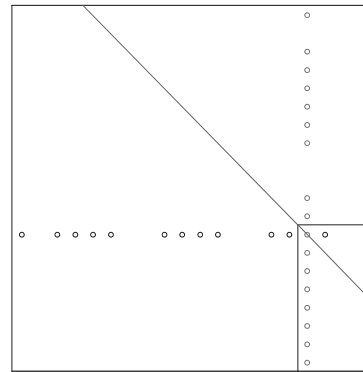
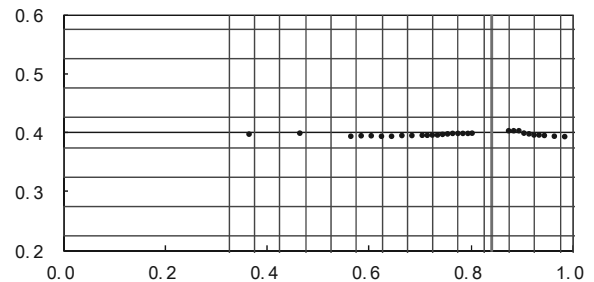
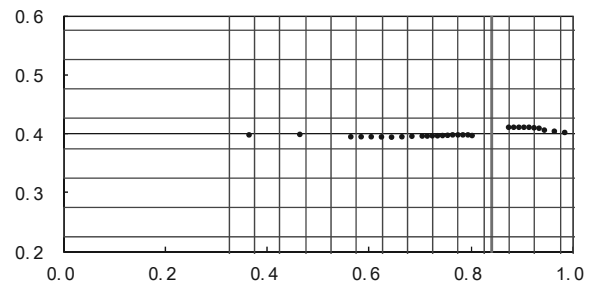


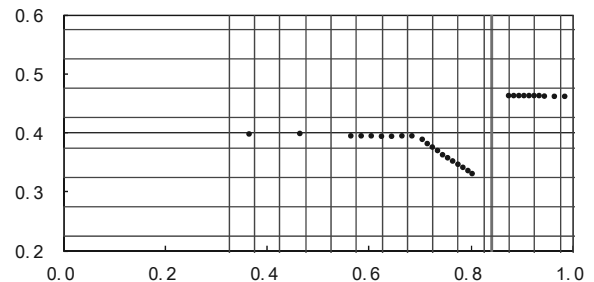
Figure 3. Measurement line of the height of soil surface



(a) At the early step of H ($H=4.81$ cm)



(b) At the H value just beyond H_y ($H=30.06$ cm)



(c) At the one step before failure ($H=36.78$ cm)

Figure 4. Changes in shape of surface of sand model along the surface height measurement line with increase in H

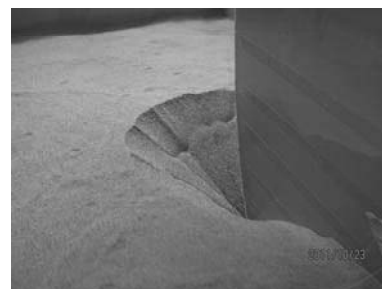


Figure 5. A close-up photo of the upstream inverse conical shape at $H=36.78$ cm (E0317)

tests that the experimental results lead to the interesting conclusion $H_y = H_d$.

Subsidence of the upstream soil surface and rising of the downstream soil surface proceed with steps of increasing H . The upstream soil surface is an inverse conical shape centered at the outer corner of the rectangular diaphragm wall. A close-up photo of the upstream inverse conical shape is shown in Figure 5 at $H=36.78\text{cm}$ (E0317). The rise in the downstream soil surface occurs uniformly within a certain width from the sheet pile wall. As H increases and approaches H_f , the upstream subsidence shows a clear inverse conical shape, and sand particles are observed to roll down the slope of the upstream soil surface (Figure 4 (c)).

4 STABILITY ANALYSES –RESULTS AND DISCUSSIONS–

4.1 Prismatic failure concept 3D

The Prismatic failure concept 3D presented by Tanaka et al. (2012) is used for estimating the stability against seepage failure of soil. In the Prismatic failure concept 3D, we assume that the body of soil lifted by seepage water has the shape of a prism with a certain height and width adjoining the sheet pile wall. The rise of the prism is resisted by the submerged weight, W' , and frictions F_{RL} and F_{RCR} on the left and right sides and F_{RF} and F_{RCB} , on the front and back sides. The safety factor F_s with respect to the rise of the prism, which is subjected to the excess pore water pressure on its base, U_e , is given as:

$$F_s = \frac{W' + F_{RL} + F_{RCR} + F_{RF} + F_{RCB}}{U_e} \quad (1)$$

For the hydraulic head difference H between up- and downstream sides, safety factors, F_s , are calculated for all of the prisms within a cofferdam. The safety factor F_s takes the minimum $F_{s\min}$ for a certain prism among all of the prisms. The calculation is iterated for another hydraulic head difference, H , until the condition whereby $F_{s\min}$ becomes nearly equal to 1.0 is found. $H=H_c$ at which the condition $F_{s\min}=1.0$ is applied is defined as the critical hydraulic head difference. The prism with a value of $F_{s\min}=1.0$ among all of the prisms for $H=H_c$ is defined as the critical prism. We could say that the critical prism is separated from the underlying soil at its base when H exceeds H_c . Safety factors using the Prismatic failure concept 3D when considering frictions are discussed below.

4.2 Relationship between hydraulic head differences H_c (by theory) and H_y (by experiment)

For Lake Biwa sand 3 of $D_r=50\%$, the theoretical hydraulic head difference by the Prismatic failure concept 3D, H_{PF} [Tanaka et al. 2012] is analyzed taking the anisotropy of the test sand to be $k_{xy}/k_{zz}=1.20$ [Tanaka et al. 2011]. Figure 6 shows the relationship between D/T and $H_c\gamma_w/T\gamma'$ for a no-excavation model. The experimental results are also plotted in Figure 6. It is observed from Figure 6 that the calculated critical hydraulic head differences H_{PF} are very close to the measured H_y . The Prismatic failure concept 3D thus proved to be a useful method for calculating critical hydraulic head difference at the onset of deformation of soil within a cofferdam. The same is true of the excavation model.

4.3 Effects of surface shape of a cofferdam on H_c

Let us consider a cofferdam whose surface shape is rectangular with the shorter length at B and longer length at L (see Figure 7). Four cases of $B:L=1:1, 1:2, 1:3$ and $1:4$ are analyzed for constant values of $B=0.2\text{m}$ and $W=0.8\text{m}$. Figure 8 shows the relationship between D/T and $H_c\gamma_w/T\gamma'$. It follows from Figure 8 that:

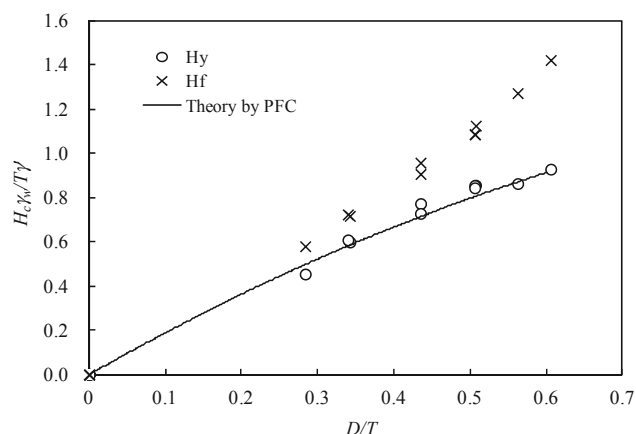


Figure 6. Relationship between D/T and $H_c\gamma_w/T\gamma'$ for no excavation model

- (1) H_c gives the lowest value in the case of 1:1.
- (2) For the same value of penetration ratio of sheet piles, D/T , the critical hydraulic head differences, H_c , are given as follows in order of increasing magnitude: $1:1 < 1:2 < 1:3 < 1:4$.
- (3) For the same value of a short length, the more the longer length increases, the smaller the effect of the longer length on H_c becomes. H_c in the case of 1:3 almost equals the H_c in the case of 1:4 for the same value of D/T .
- (4) For a small value of D/T , all of the H_c values are nearly equal in cases of 1:1, 1:2, 1:3, and 1:4.

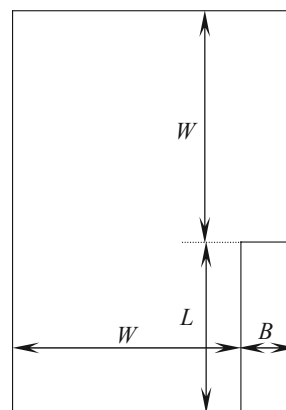


Figure 7. Plane shape of a cofferdam

5 AXISYMMETRIC MODELING OF THREE-DIMENSIONAL SEEPAGE FLOW

In the experiment, one quarter of the three dimensional region is examined as stated earlier. The surface shape of the cofferdam is rectangular with the shorter length at 1 and longer length at 2. Considering an inscribed circle in the shorter side of the rectangle as shown in Figure 9, an axisymmetric seepage flow through the soil is used to model such a three-dimensional flow.

Let us consider the three dimensional and approximate axisymmetric conditions: $T=40\text{cm}$, $D=20\text{cm}$ and $R=20\text{cm}$ for the non-excavation sand models, where R is the radius of the circular wall in the axisymmetric condition. Figure 10 shows the relationship between the penetration ratio of sheet piles D/T and the non-dimensional value of H_c , $H_c\gamma_w/T\gamma'$. It is found from Figure 10 that the three dimensional seepage failure phenomena are well approximated using axisymmetric seepage failure. For further details, the following points may be made:

- (1) $D/T \leq 0.40$ H_c values are larger in the AXS flow than in the 3D flow; in particular the approximate accuracy with respect to H_c , $(H_{c\text{AXS}} - H_{c\text{3D}})/H_{c\text{3D}}$, is about +17% for $D/T=0.27$. This

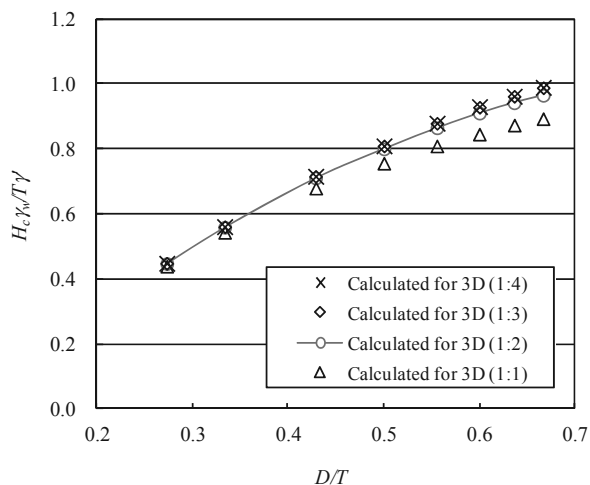


Figure 8. Relationships between D/T and $H_c \gamma_w / T \gamma'$ for various plane shapes

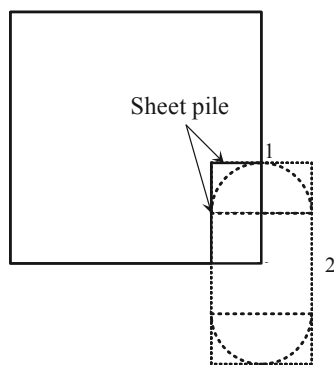


Figure 9. Plane figure of the 3D test apparatus (axisymmetric modeling)

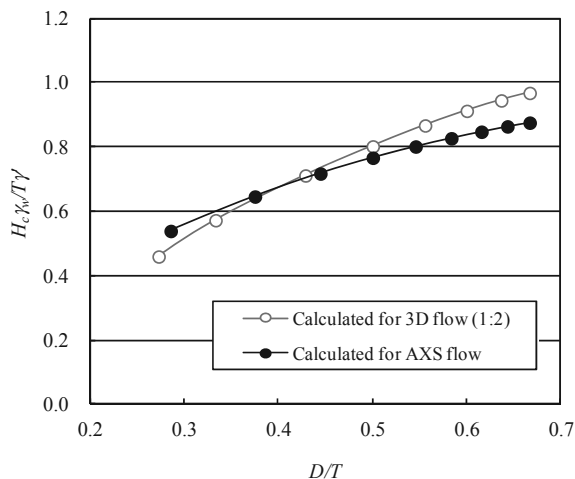


Figure 10. Relationship between D/T and $H_c \gamma_w / T \gamma'$ (Axisymmetric modeling of 3D flow)

means that assuming that the 3D flow is the same as AXS flow leads to an overestimation of H_c , and generates unreasonable results with respect to seepage failure.

(2) $D/T > 0.40$ H_c values are smaller in the axisymmetric case than in the three-dimensional case; the approximate accuracy, $(H_{c, \text{AXS}} - H_{c, \text{3D}})/H_{c, \text{3D}}$, is about -9% for $D/T = 0.67$. This means that assuming that the 3D flow is the same as AXS flow leads to an underestimation of H_c , and generates uneconomical designs with respect to the H_c value.

For the same value of D/T , the H_c values are given as follows in order of increasing magnitude: $B:L = 1:1 < 1:2 < 1:3 < 1:4$ as stated in Section 4.3. The same axisymmetric approximation is

applied in these four cases. So, the difference in H_c between 3D and AXS flows changes, and the approximate accuracies, $(H_{c, \text{AXS}} - H_{c, \text{3D}})/H_{c, \text{3D}}$, are given as -2% (1:1), -9% (1:2), -11% (1:3) and -12% (1:4) for $D/T = 0.67$.

6 CONCLUSIONS

Seepage failure experiments were conducted under three-dimensional flow conditions for various cases of total depths of soil, T , and penetrated depths of sheet piles, D , and analyses of FEM seepage flow and stability against the seepage failure of soil were carried out using the Prismatic failure concept 3D (pfc 3D). From discussions, the following results were obtained:

(1) With an increase in the hydraulic head difference between up- and downstream, H , the discharge at 15°C , Q_{15} , increases linearly for a smaller value of H , but changes abruptly and non-linearly beyond the point $H=H_d$. H_d is referred to as the hydraulic head difference at an abrupt change of the $H-Q_{15}$ curve.

(2) In correlation with the above phenomenon regarding the H and Q_{15} relationship, the height of the soil surface changes at the front (downstream) and rear (upstream) of the sheet piles. When H increases beyond H_y , a downstream rise and upstream drop of the soil surface occur. H_y is referred to as the hydraulic head difference at the onset of soil deformation.

(3) Sand particles move from up- to downstream sides under the bottom edges of the sheet piles. The upstream soil surface is an inverse conical shape centered at the outer corner of the rectangular diaphragm wall.

(4) The experimental results led to the interesting conclusion that $H_y=H_d$.

(5) The hydraulic head differences at deformation in the experiment, $H_y (=H_d)$, are nearly equal to the theoretical critical hydraulic head differences based on the pfc 3D, H_c .

The theoretical critical hydraulic head differences for various plane shapes of a cofferdam, e.g., a short to long length of 1:1, 1:2, 1:3, and 1:4, were calculated, and the following results were obtained:

(6) H_c gives the lowest value in the case of 1:1.

(7) For the same value of the penetration ratio of sheet piles, D/T , the critical hydraulic head differences, H_c , are given as follows in order of increasing magnitude: $1:1 < 1:2 < 1:3 < 1:4$.

(8) For the same value of a short length, the more the longer length increases, the smaller the effect of the longer length on H_c becomes. H_c in the case of 1:3 almost equals the H_c in the case of 1:4 for the same value of D/T .

(9) For a small value of D/T , all of the H_c values are nearly equal in cases of 1:1, 1:2, 1:3, and 1:4.

The axisymmetric modeling of three-dimensional seepage failure was discussed, concluding as follows:

(10) With respect to the seepage failure problem, axisymmetric seepage flow through soil within a cylindrical wall can be used to model such a three-dimensional flow. The magnitudes of the critical hydraulic head differences $H_{c, \text{3D}}$ (in three dimensions) and $H_{c, \text{AXS}}$ (axisymmetric model) are given as follows for the 3D case of 1:2 and its axisymmetric model: $H_{c, \text{3D}} < H_{c, \text{AXS}}$ for $D/T \leq 0.40$, and $H_{c, \text{3D}} > H_{c, \text{AXS}}$ for $D/T > 0.40$.

7 REFERENCES

- Nikkei Construction. 2001. Shortage of penetration depth of sheet piles, Nikkei Business Publications, 37-38, 2001.9.28.
- Tanaka T., Naganuma H., Shinha M., Kusumi S. and Inoue K. 2011. Anisotropic permeability of soil on 3D seepage failure experiments, *Procs. of the 68th annual meeting of the Kyoto Branch of Japanese Society of Irrigation, Drainage and Rural Engineering*, 3-5 - 3-6.
- Tanaka T., Hirose D. and Kusumi S. 2012. Seepage failure of sand within a cofferdam in three dimensions -Prismatic failure concept 3D and analytical consideration-, *Report of Research Center for Urban Safety and Security*, Kobe University, No.12, 285-299.

Stability and dewatering problems of deep excavations in Bratislava

Les problèmes de stabilité et d'assèchement des excavations profondes dans la ville de Bratislava

Turček P., Frankovská J., Súľovská M.

Faculty of Civil Engineering, Slovak University of Technology in Bratislava, Slovakia

ABSTRACT: Geotechnical design and execution of deep excavations of high-rise buildings in urban areas are presented in the paper. Design of retaining structure and subsoil behaviour based on the results of in situ measurement during execution with the aim to minimise the settlement of high-rise building are discussed. Limited space on the surface and ground conditions in Bratislava are important factors for design of foundations. Quaternary sediments, coarse grained soils, mainly sands and gravels reach down to the depths of 12 to 20 m, Neogene sediments, mainly clays and silty sands with confined ground water level occur deeper. Ground water level occurs from 2 to 6 m below the surface level. Several examples of excavations where the risks of local hydraulic failure were present are analysed. The paper summarizes stability and dewatering problems associated with design and execution of deep excavations in the city of Bratislava.

RÉSUMÉ : La conception géotechnique et l'exécution des fouilles profondes de bâtiments de grande hauteur dans les zones urbaines sont présentées dans le document. La conception de structure de soutènement et le comportement du sous-sol sur la base des résultats des mesures in situ lors de l'exécution dans le but de minimiser le tassement des bâtiments de grande hauteur sont discutés. L'espace limité sur la surface et les conditions du sol à Bratislava sont des facteurs importants pour la conception des fondations. Les sols à gros grains du Quaternaire, principalement les sables et graves descendent jusqu'aux profondeurs de 12 à 20 m, les argiles du Néogène et les sables silteux avec une nappe en charge se trouvent plus profonds. Le niveau de la nappe se trouve de 2 à 6 m en dessous du niveau de la surface. Plusieurs exemples de fouilles sont présentés où les risques d'une défaillance hydraulique locale ont été analysés. Le document résume les problèmes de stabilité et d'assèchement associés à la conception et à l'exécution des excavations profondes dans la ville de Bratislava.

KEYWORDS: retaining structure, deep excavations, geotechnical design, subsoil behavior

1 INTRODUCTION

Geological conditions in Bratislava are determined mostly by Quaternary sediments of the Danube river, Neogene sediments and Cenozoic crystalline rocks (biotite granites to granodiorites, diorite and gneisses) of Carpathians. The most important construction activities in last 20 years have been concentrated in the Danube area, with the Quaternary sediments (coarse grained soils, mainly sands and gravels) with thickness of 12 to 15 m, in the city of and in near vicinity of Bratislava. South and southeastward the depth is increasing, up to 400 m under Gabčíkovo (27 km from Bratislava). The Quaternary sediments are underlayed by fine-grained Neogene marine sediments with typical altering of fine grained and coarse grained sediments. Fine grained sediments are classified as clays from firm to very stiff consistency. Coarse grained sediments are classified as dense sands, silty fine sands and clayey sands. Under the Neogene deposits there are the same crystalline rocks as on the northern side of Bratislava (Kopecký, Černý, 2008). Underground water has two main horizons. One is underground water in Quaternary deposits with free water table donated by water from precipitation and from Danube river. The second horizon is groundwater confined in the Neogene deposits. The water is pressurized and recharged by underground water flowing from nearby Male Karpaty Mts.

Limited space on the surface and ground conditions in Bratislava are the important factors for design of foundations. Three examples of deep excavation where the risk of local hydraulic failure was present are analysed.



Legend:
Cenozoic crystalline rocks: ■ biotite granites, granodiorites, diorites,
Quaternary deposits: ■ slope deposits, ■ river deposits

Figure 1. Geological map of Bratislava region and location of case studies.

2 EXCAVATION FOR BUSINESS CENTER ON KARADZICOVA STREET

The first case study is excavation situated on the left side of Danube River in the city centre on Karadzicova street. Foundation pit was constructed for the high-rise building with 30 floors and 3 underground floors. The longer side of the foundation pit with the dimensions of 200x39 m and depth of 11.4 m was adjacent to existing buildings, two sides were

adjacent to streets and only one short site was open to free space. This layout requires minimisation of horizontal deformation of the retaining structure. Furthermore, there was interest to use all space available on the construction lot, i.e. to exclude technologies that would interfere with the ground plan and decrease the usable volume of the underground floors.

In the first section of the foundation pit up to the depth 4.5 m, where dry conditions were expected, the soil nailing was used as support. The jet grouted wall in deeper section was anchored by one level of ground anchors 15 m long, with 25° inclination, the anchor force was 670 kN and spacing of the anchors 1.6 m. The retaining wall was prestressed in vertical direction due to the necessity to carry large bending moments (bending moment of 1332 kNm per meter of wall was expected by full excavation of the pit); this pre-stressing was supposed to limit the horizontal deformation (see fig. 2 and 3).

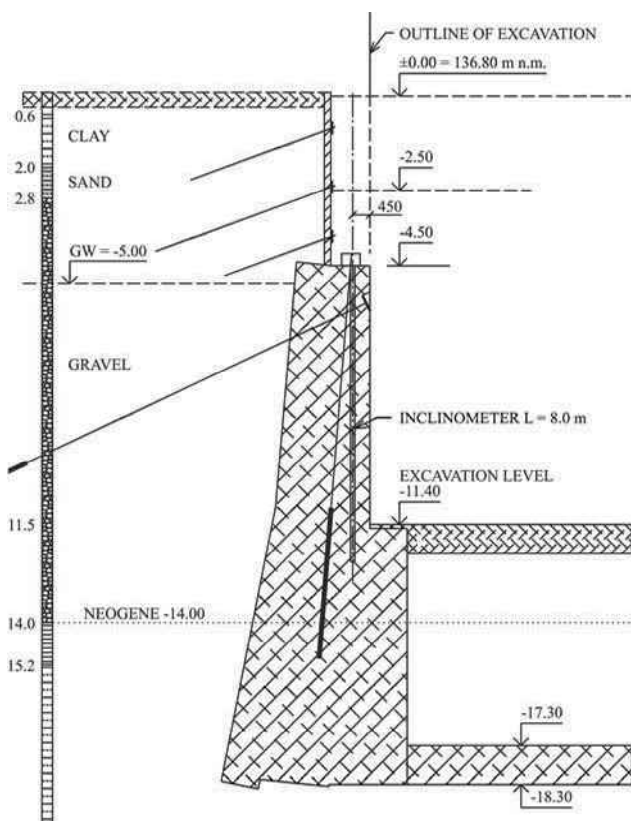


Figure 2. Cross section of retaining structure made by soil nailing and jet grouting.

According to geotechnical investigation the Neogene soils with high permeability are expected at the excavation base. Therefore a sealed bottom of the foundation pit was proposed by overlapping short columns constructed by jet grouting. This solution proved to positively influence the settlement of the building. Horizontal deformation in the level of the retaining wall 3.3 mm and 19.15 mm in the lower embedded part under the bottom of the excavation (in the direction of the excavation) were expected in geotechnical design. By full excavation the toe of retaining wall was expected to move into the foundation pit by 52.56 mm. Nine inclinometers were installed around the foundation pit in the wall constructed by jet grouting. The example of measurements from inclinometer no. 3, where the highest deformations (not higher than 2 mm in the direction into the pit) were indicated, is on figure 4.

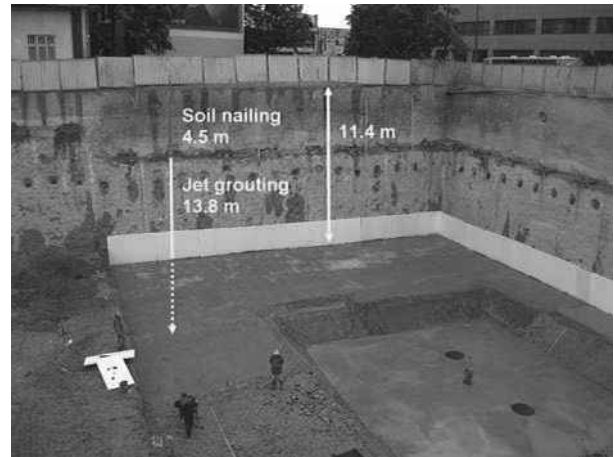


Figure 3. View into the excavation. Retaining structure made by soil nailing and jet grouting.

Similar results with even lower deformations were measured by other inclinometers. This favourable outcome was achieved thanks to high stiffness of the retaining wall prestressed in vertical direction. The stiffness of weak sandy clays under the bottom of excavation has been increased by constructing a horizontal barrier by jet grouting.

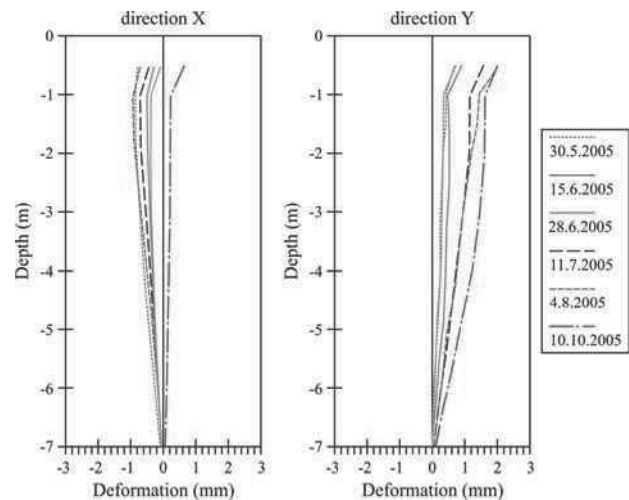


Figure 4. Horizontal deformations of retaining structure during construction.

3 EXCAVATION FOR RIVER PARK

The second case study is the foundation pit with dimensions of 265x53.5 m and depth of 9.0 m (fig. 5) situated directly at Danube riverside (in the distance of 12 m to Danube river). Retaining walls for foundation pit were designed as a secant pile wall embedded 1m into the weathered rock base. Danube coarse grained soils are well-known by their susceptibility to piping. The analysis of the risk of filtration failures is important in geotechnical design. Risk of the internal erosion (structural erosion) is affected by granularity of gravel or sand soils, situated in this region. Therefore the analysis of seepages effect on safety of construction and its subsoil it is necessary to carefully observe mainly development of filtration velocities or hydraulic gradients, which are decisive from the viewpoint of reviewing filtration stability of soils (Bednárová et al., 2010). According to geotechnical investigation the value of permeability coefficient (hydraulic conductivity) of gravel k is in the range from 1.5×10^{-2} to 6.5×10^{-3} m/s. The characteristic value of k equal to 1×10^{-5} m/s was evaluated from the results of water pressure tests. The permeability coefficient $k = 1 \times 10^{-7}$

m/s was used in pile walls design (representing mainly leakages between the piles). Seepage in the foundation pit consists of wall and bottom rate of seepage. The seepage through the pile wall on section 1 was 0.008 l/s and can be obtained from equation

$$q_{wl} = \frac{k_s}{2 t_s} (H^2 - d^2) = 7.7 \times 10^{-6} \text{ m}^3 \text{ s}^{-1} \quad (1)$$

where H is the height of the water column, d embedding of the wall under the bottom of the foundation pit.

The predicted flow rate at the pit through walls was 2.12 l/s in the section farther from Danube and 2.23 l/s in the section closer to Danube.

Flow rate through the bottom was determined by the relation

$$Q_b = k i A_d = 0.0567 \text{ m}^3/\text{s} = 56.7 \text{ l/s} \quad (2)$$

The total rate of seepage can be given as

$$Q = Q_{w1} + Q_{w2} + Q_b = 61.55 \text{ l/s} \approx 62 \text{ l/s} \approx 223 \text{ m}^3/\text{h} \quad (3)$$

In case the groundwater level reaches 138.0 m above sea level (i.e. level of the pile heads), the rate of seepage in the pit increases to 266 m³/h.

At the beginning of water pumping, static reserve of groundwater from closed space was pumped from the foundation pit besides the inflow. The volume of saturated gravels is 92170 m³, of which volume of water by the assumption of 25 % active porosity is 23043 m³. This amount of water is presumed to be pumped in 9 days (during excavation works) when pumping more water than 30 l/s over pumped water flow into the foundation pit.

In order to secure dry foundation pit it was recommended to modify the length of the piles according to the actual conditions even though it might result in longer piles in certain sections compared to the design. Seven pumping wells with diameter 600 mm were proposed with recommendation to verify the actual pumped amounts. Contractor did not trust the assumption of the calculation and constructed 10 wells.

During the excavation of the foundation pit, a measuring of the groundwater movement was performed at all 10 pumping wells (water was permanently pumped only from 2 wells).

Parameters of groundwater movement were determined by the single borehole indicator method, based on the principle of diluting the indicator. NaCl was used as the indicator. Evaluating NaCl concentration was performed by the Radelkis OK 104 tool/instrument on battery source, which recorded the conductivity of the saline solution. Sensors of the Radelkis set with prolonged cable were used as detectors. The value of filter speed (v_f) in each depth level, as well as the average value for the whole measured wall, was calculated according to the relation

$$v_f = \frac{\pi d \beta}{4 \alpha \delta t} \ln \frac{c_0 - c_p}{c - c_p} \quad (4)$$

where d is the inner diameter of the borehole ($d = 0.8$ m);

α - coefficient of drainage impact of the borehole; base on comparable experience the value $\alpha = 2$ was used;

β - ratio used for volume decreasing ($\beta = 1$);

δ - coefficient considering the sealing impact on the ratio of flow concentration ($\delta = 1$);

t - time equal to the difference between c_0 and c ;

c_0 - initial concentration of the indicator;

c - concentration in time t ;

c_p - background of the indication substance before indicating the environment.

Average value of filter speed for the test section can be determined by the relation

$$\bar{v}_f = \frac{\sum v_{fi} \Delta h_i}{\sum \Delta h_i} \quad (5)$$

Evaluated filter speed in all measured objects depend on the location and ground conditions (gravel). No well showed an anomaly of permeability of depth that would indicate increased inflows from certain depth level or from the bottom of the foundation pit. In 2 wells where the water was pumped, filter speed in the range of 1.4 to 4.7 x 10⁻³ m/s was measured, while in other cases it was $v_f = 2.2 \times 10^{-4}$ to 6.7 x 10⁻⁵ m/s. Very low seepage ratio was measured in line where jet grouting by the pile wall was performed, which proves reliability of the sealing system. Depth division of the filter speeds confirmed non-homogeneity of the gravel location (in some depth the sand fraction was missing).



Figure 5. Foundation pit with dimensions of 265 x 53,5 m and depth of 12 m next to Danube river.

Stable pumping at 20 l/s decreased the groundwater head under the level of excavation base. Decreasing the groundwater head in the area of the foundation pit and evaluation of the movement tests by diluting method indicated that lesser amount of water is required to be pumped from the foundation pit than expected amount of water in the project design (62 l/s). In conclusion it was stated that the retaining structure created a foundation pit with required sealing function.

When preparing the base foundation for placing the underlying concrete, the excavation in the north-western corner of the foundation pit deepened for 0.3 m more than was necessary and minor water seepage occurred along the pile wall that held at the same level for several days. It was confirmed by leveling that the groundwater head in the wet area by the pile wall was 0.48 m bellow the upper edge of the base concrete and held at the same level. Performed test of natural conductivity of the water seepage helped in identifying its origin. Two locations of leakage were confirmed in the wet area along the pile wall. It was evaluated as the water seepage into the foundation pit area through the contact of the piles connection in the wall where the discontinuities in the rock massive were collectors of the water. Drainage to the nearest active pumping well had to be installed in order to solve the problem. At the same time it was necessary to replace existing soil by gravel without the sand fraction in the foundation pit area and thoroughly compact the layers of this soil replacement, in order to eliminate the risk of higher deformations of the future base structure.

4 DEEP EXCAVATION IN PETRZALKA

Quaternary gravel sediments on the right side of Danube were characterized as loose to medium dense coarse grained soils with the values of density index I_D varying from 0.25 to 0.63

and deformation modulus $E_{def} = 30$ up to 112 MPa according to geological investigation by dynamic penetration testing up to the depth 40m. Locally in layers with fine-grained gravel with minimal sand filling the value if I_D was 0.15 and deformation modulus $E_{def} = 16$ MPa. Average thickness of the quaternary gravels was 13 m. Neogene sediments were represented mostly by sandy clays (*saCl*) with firm filling of clay, with sand locations with addition of fine-grained soil (less than 15 %), to a small extent also with silts of middle plasticity to clays of high plasticity in depths of 19.8 to 20.6 m and 25.3 to 26.4 m. The value E_{def} determined by dynamic penetration tests was 20 to 28 MPa in Neogene soils.

Contact stress in base foundation of the high building was 500 to 800 kPa. Limit settlement determined the type of foundation (rafts or piles). Based on the information about disproportionately high compressibility of the subsoil, ground treatment by deep vibratory compaction was performed. Base foundation was located in the depth of 4.0 m under the surface. The raft is 1.4 m thick, in deepened parts 2.0 m. Density of compaction points was in raster of 2.2 x 2.4 m for stress of 800 kPa, under pad footings and strip footings in raster 2.5x 2.5 m to 1.75 x 3.5 m for stress of 500 kPa and under pads and strips in raster 1.8 x 1.8 m for stress of 800 kPa. The length of the piles for stress of 800 kPa was in depth of 3.0 m from the working base under the surface 10,0 m (i.e. till the Neogene in the depth of 13.0 m), shortened to 7 m in area with load of 500 kPa.

This arrangement was based on previous comparable experience in Quaternary gravel sediments of Bratislava where the verified deformation modulus of the vibrated gravel columns reached the average value of E_{def} equal to 500 MPa and increasing of the deformation modulus of average environment was proved by the values E_{def} from 250 to 300 MPa. The calculation of the average deformation modulus of improved subsoil in the area A in question is according to the relation

$$E_{def} = \frac{A_g E_g + A_s E_s}{A} \quad (6)$$

where A_g is the area of vibrated stone columns
 E_g – deformation modulus of the vibrated stone columns
 A_s – area of the unimproved soil
 E_s – deformation modulus of the unimproved soil

After constructing the vibrated stone columns, dynamic penetration tests were performed, located in the middle of the vibrated stone columns. Increase in the deformation modulus with depth was also proved, which was taken into account in the calculation of predicted settlement based on the monitored data. Average value of $E_{def} = 284$ MPa was measured under the base foundation up to depth of 2 m. The predicted final settlements are summarized in the table 1.

Table 1. The values of settlement calculated for different foundations.

Foundation	Settlement s (mm)
Spread foundation without soil improvement	104.46
Spread foundation with soil treatment by stone columns (E_{def} based on comparable experience)	67.01
Spread foundation with soil treatment by stone columns (E_{def} based on site testing)	64.55
Pile foundation	73.97

During the construction of the high building the vertical and horizontal deformations were monitored. The measured value of settlement after consolidation process reached 52.2 mm.

5 CONCLUSIONS

The key value in the design of high building foundation in deep excavation pits is the limit usability state. Most questions are raised by the simulation of soil deformation characteristics and expected groundwater inflows. Good prognosis of deformations is based on combination of determining correct soil deformation characteristics verified by laboratory and field tests in the whole deformation zone and selecting the right calculation method. The project must respond to the architect's requirements by suitable design, its monitoring and potential modification of stiffness of the retaining structure, subsoil and additional sealing elements.

Geotechnical design and execution of deep excavations of high-rise buildings in urban areas are presented in the paper. Design of the retaining structure and subsoil behaviour based on the results of in situ measurement during execution with the aim of minimising the settlement of high-rise building are discussed. The paper summarizes stability and dewatering problems associated with design and execution of deep excavations in the city of Bratislava. The results of geotechnical calculations have been compared to the results of in-situ measurements.

6 ACKNOWLEDGEMENTS

The present work has been supported by the project of the Slovak Science Agency VEGA No. 1/0241/13 and by the Ministry of Education, Science, Research and Sport of the Slovak Republic within the bounds of OPVaV project No. 26220220140.

7 REFERENCES

- Bednárová, E. Minárik, M. Grambličková, D. Sabo, J. 2010. Flood Protection of Bratislava and its Specifics from the Viewpoint of Geological Composition of Surrounding Environment. In: *XIVth Danube-European Conference on Geotechnical Engineering: Proceedings*. Slovak University of Technology in Bratislava, Slovakia, 7 p.
- Kopecký M. Černý M. 2008. Landslides remediation of railway cut in Bratislava. *Czech Journal Silnice a železnice*. 3/2008. Part Foundation
- Ťavoda O. and Šabo A. *Foundation below groundwater*. ALFA, Bratislava, 1986, 272 pp.
- Turček P. and Hulla, J. *Foundation engineering*. JAGA, Bratislava, 2004, 360 pp.
- Turček, P. and Súľovská M. Using the observation method for foundation of high-rise buildings. In: *Proceedings of the 14th European Conference on Soil Mechanics and Geotechnical Engineering*. Vol. 2. Madrid, 2007, Millpress Rotterdam. p. 419 – 422.

Managed remediation of a large Victorian gravity quay wall using the observational method

Stabilisation d'un grand mur de quai de l'époque Victorienne gérée en utilisant la méthode observationnelle

Turner M J, Smith N A
Applied Geotechnical Engineering, UK

ABSTRACT: The paper describes on-going work to control the stability of a large gravity quay wall at a port on the western seaboard of the UK, which has had a history of instability dating back over several decades. In 1999 further ground movements of the wall were triggered by leakage from a fractured water main in the quayside behind the wall. This caused severe settlement damage to the quay and associated storage warehouses on the quayside. Monitoring of the affected area of the wall was established in early 2000, with additional ground investigations and instrumentation to supplement existing data. By the end of September 2000 the worst affected parts of the wall were moving outwards at a rate of 10mm/day. The movements were initially arrested by groundwater lowering. Subsequently additional remedial measures consisting of anchors and shear keys were designed and installed to provide physical restraint. The Owner wished to minimise capital expenditure and instead to use an observational approach (Peck 1969) and to respond to the information obtained. The work had therefore attained what was regarded as an acceptable steady state, with continued managed remediation to ensure that the wall's stability is maintained and the Owner can continue to use the berthing facilities.

RÉSUMÉ: Le document décrit les travaux en cours pour contrôler la stabilité d'un grand mur de quai dans un port de la côte ouest du Royaume-Uni, qui avait un historique d'instabilité datant de plusieurs décennies. En 1999, de nouveaux mouvements de terrain et du mur furent déclenchés par une fuite d'eau due à une rupture de tuyaux d'alimentation en eau du quai qui étaient derrière le mur. Ceci causa des dommages graves au quai et aux entrepôts de stockage sur le quai. La surveillance de la zone affectée du mur commença au début de 2000, avec addition d'instruments de mesure supplémentaires et investigations complémentaires du sol pour compléter les données existantes. À la fin de Septembre 2000, les zones les plus touchées du mur se déplaçaient vers l'extérieur à une vitesse de 10mm/jour. Les mouvements furent arrêtés par l'abaissement des eaux souterraines. Par la suite d'autres mesures correctives constituées de tirants d'ancrage et de piles pour éviter les glissements furent conçues et installées pour assurer la contention physique du mur. Le propriétaire souhaitait minimiser l'investissement initial et préférait utiliser une approche observationnelle (Peck 1969) en réponse aux informations obtenues. Le mur était assez stable pour utiliser le quai en continuant l'application opportune des mesures correctives pour assurer la contention du mur, et le propriétaire peut continuer à utiliser les installations d'accostage.

KEYWORDS: gravity walls; long-term monitoring; long-term displacements; ground anchors; water pressures; effects of dewatering.

1 INTRODUCTION

A section of harbour wall at a port on the western seaboard of the UK has a history of instability dating back over more than thirty years. Measurements taken in the 1980s had indicated that the maximum total horizontal movement of the wall up to that date had been more than 400mm. In 1999 further ground movements of the wall were triggered by leakage from a fractured water main in the quayside behind the wall. This caused outward movements along a length of over 80 metres, and severe settlement damage to the quay and associated storage warehouses on the quayside.

The harbour works were constructed at the end of the 19th Century. The wall is a gravity structure of mass concrete and masonry with sandstone "plums". At its top, it is some 17 metres above the harbour bed level; it is about 2 metres wide at its crest, increasing to almost 9 metres at its base. There is a large tidal range at the site.

After the 1999 movements, monitoring of the affected area of the quay wall was established in early 2000, with additional ground investigations to supplement existing data and to confirm the wall dimensions and the ground/groundwater conditions behind the wall. Inclined meters and piezometers were also installed to monitor water levels and the wall behaviour. Survey lines were established perpendicular to the wall and extending back to stable reference markers remote from the wall, with intermediate reference points to measure lateral and vertical movements in the ground behind the wall.

By mid-2000 the monitoring data showed a deteriorating situation, with outward movements of the wall accelerating from an initial value of around 15 to 20mm per month to as much as 100mm/month, and increasing. By the end of

September of that year the worst affected parts of the wall were moving outwards at a rate of 10mm/day, and measures were put in place to stabilise the wall immediately in the short term, together with further works to ensure the stability of the quay wall in the medium term.

This current paper describes these measures and the long term monitoring of the wall over the past decade.

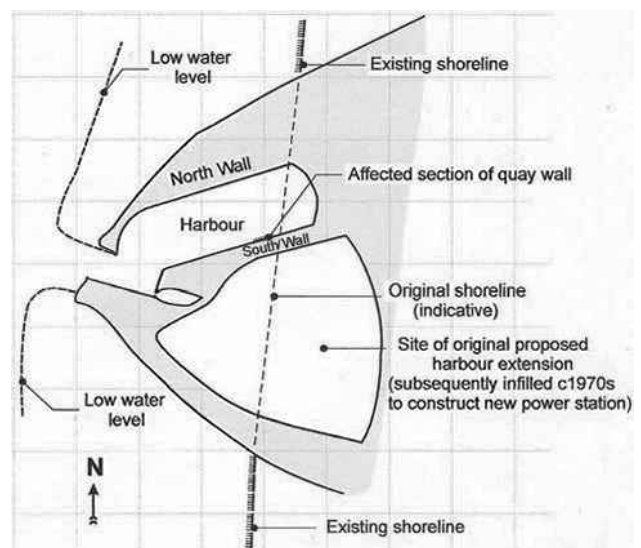


Figure 1. Outline plan of the site.

2 BRIEF HISTORY OF THE SITE

The harbour walls were constructed in the dry within a large embayment formed by advancing two curved embankments from the shore to meet at a central point, which would form the entrance to the harbour, as illustrated on Figure 1. This entrance point was closed by a temporary dam for the construction works and the site was drained by pumping. The harbour was then excavated in the dry.

A typical section through the quay wall is shown on Figure 2. The walls were constructed of mass concrete and, in the larger sections, large sandstone “plums” were incorporated into the concrete. The quay was intended for both passenger and livestock traffic. In view of the large tidal range provision was made for loading and off-loading at any state of the tide. This was achieved by constructing access-ways through the wall at two levels. These were connected to subways and stairways on the landward side of the wall. On the seaward side the quay wall was fronted by a heavy timber staging with continuous landings at the necessary levels to give access from the steamers into the subways.

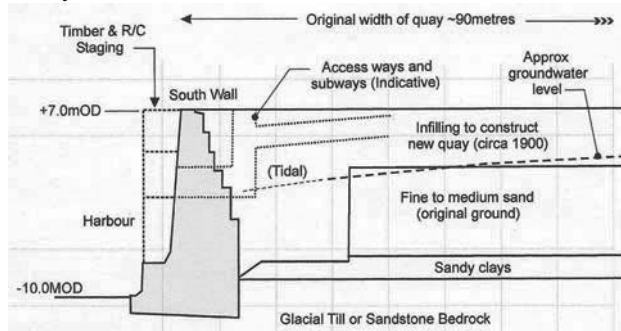


Figure 2. Typical cross-section through quay wall.

As illustrated on Figure 1, the affected quay, known as the ‘South Quay’ was constructed on the harbour side of a central spine embankment within the construction site. To the south of this, the remaining area was planned as a future extension to the harbour, but this extension was never constructed. In the 1970s this area was infilled and a large power station constructed on the site

In the early 1980s surface settlement was noted behind a 40m long section of the quay wall. This was repaired by infilling and releveling to grade. Further repairs were undertaken in 1988, when a maximum settlement of 400mm was reported on the quay surface prior to reconstruction. Following these repair works the quay surface settled a further 30mm of settlement within a year, and the worst-affected area was reported as extending over an 85 metre length of the wall, although the effect was also discernible beyond this. Crane rails which had been relaid along the quayside in 1972 were found to have deviated by up to 100mm towards the harbour over a 100m length of the quay wall.

Detailed surveys taken in 1991 indicated that the South Quay was showing a distinct bulge of as much as 430mm towards the harbour, and the zone of movement extended for some 200m along the wall. Shortly after these measurements were taken, a break occurred in a water main some 13m behind the crest of the wall, due to the continuing outward displacement of the quay wall. At this time a remedial works solution using high capacity ground anchors was proposed, but not proceeded with.

In late 1999 a further major leak occurred from a fractured water main near the centre of the previous movements, causing accelerated wall movements and severe ground settlements beneath the quay itself. The next sections describe subsequent evaluation and remedial works following this particular incident.

3 GROUND INVESTIGATIONS AND OBSERVATIONS (2000-2001)

In early 2000 Applied Geotechnical Engineering was requested by the port owner to undertake investigations as to the cause of the movements and to advise on the measures required to stabilise the South Quay wall.

A targeted ground investigation was commissioned, to supplement information available from previous investigations undertaken in 1990/1992. In addition, inclinometers were installed at five locations along the crest of the affected length of wall and were continued through the base of the wall and any superficial soils into bedrock at depth. A further three inclinometers were installed behind the wall to monitor the behaviour of the retained soils. Water observation boreholes were also installed behind the quay wall to monitor groundwater conditions.

In addition a series of “traverse lines” was established perpendicular to the wall and extending back to stable ground well beyond any zone of influence of the wall movements. These were monitored by conventional surveying techniques to determine horizontal and vertical displacements.

3.1 Geology and Ground Conditions at the Site

The ground was raised behind the masonry quay walls using the material excavated to form the harbour. Beneath these surface construction materials, the South Quay is underlain by fine to medium grained sands of Quaternary age. In some places these are underlain by soft sandy silty clays. These materials rest upon either Glacial Till (typified as reddish brown, stony, clayey silts), or, more commonly, directly onto bedrock. At the western end of the quay, bedrock consists of sandstones with subordinate marls of Permo-Triassic age. Over the eastern end older sandstones and siltstones of Upper Carboniferous Namurian (Millstone Grit) age are present. The boundary between the two rock formations is formed by a large fault, trending in a NNW – SSE direction, which cuts at right angles across the line of the South Quay, slightly west of its central point, and close to the centre point of the historic movement of the wall. The fault zone was also identified during the construction of the power station to the south.

This fault zone is associated with heavy flows of groundwater under artesian or sub-artesian pressures. Before the power station was constructed a freshwater lake formed in the area of the old proposed harbour extension.

The investigations led to the conclusion that groundwater flows from this source to the south of the South Quay were the root cause of the wall instability, as described below.

3.2 Groundwater observations

It was soon apparent from the monitoring data that the movement of the wall was driven by the groundwater held behind it. The rate of drainage of the water below the wall was relatively slow, so that the difference in water levels between the front and the back of the wall was highest at low tide, as shown in Figure 3. At these points the wall would ratchet forward, and not quite recover its original location as the tide level rose. By inference, the effect was greatest at times of high tidal difference (Spring tides).

The water observation standpipes confirmed that close to the quay wall, water levels varied tidally between about +4m OD and +1.4mOD. Some fifty metres south of the face of the quay wall, water levels varied between +2.9 and +2.7m OD with the tide. At a distance of 100 metres groundwater levels were almost static, with very little discernible tidal variation, and were around +3.7m OD.

It was also noted that the salinity of the groundwater changed from south to north. In the south the groundwater was fresh or brackish. Close to the quay wall the salinity altered with the tide. At low tide it was brackish or fresh. At high tide, as

seawater clearly flooded behind the wall, the groundwater became salty.

There was therefore a discernible hydraulic gradient from the power station site in the south, northwards towards the quay wall. It was also clear that the bulk of the groundwater was fresh water, flowing from the power station site towards the South Quay. In addition it was quite possible that concentrated groundwater flow was occurring in the fault zone in the vicinity of the harbour, although in the location of the South Quay the zone was buried beneath a cover of Glacial Till.

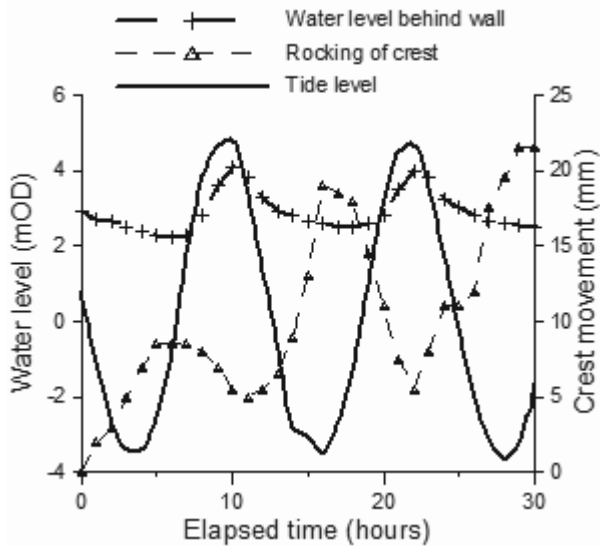


Figure 3 Water levels and crest movements, 13-14 Oct 2000.

The analyses showed that the high groundwater level behind the quay wall was the predominant driver of the instability and the observed wall movements.

3.3 Wall Movements (2000)

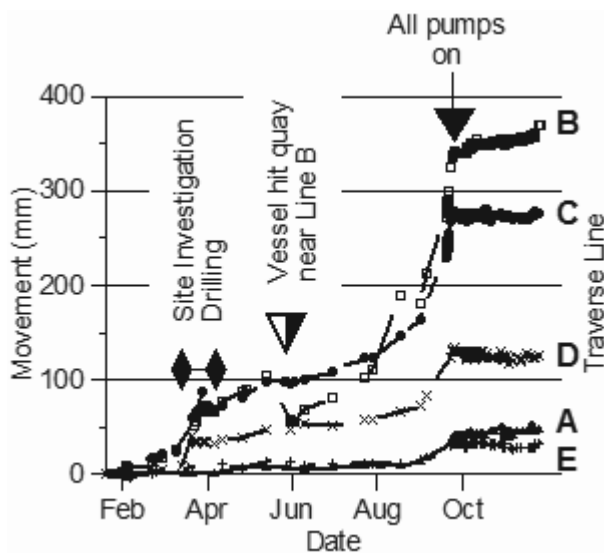


Figure 4. Crest movements during 2000.

The displacements of the quay wall measured at the traverse lines are illustrated on Figure 4. It can be seen that there was a noticeable effect upon outward wall displacements while the site investigation works were being undertaken in April 2000. Figure 4 also shows that the rate of outward movement also began to increase markedly in September of that year, and was accelerating. By September 2000 the worst affected area of the quay wall (Traverse Lines B and C on Figure 4) had recorded between 270 and 350mm of outward movement, relative to their

values in January of that year. At this time the analysis, design and procurement of the remedial works was still being progressed, but, based upon the evidence of the increased wall movements during the investigation work, contingency plans had already been put in place to deal with such a situation. Eleven dewatering wells were installed in a line behind the quay wall at approximately 10m centres, to lower the ground water level behind the wall. At that time the wall was moving forward by more than 10mm per day at the worst affected part, and was rocking measurably with the tide. The pumps were started as soon as the wells were connected, over a three day period, the first three being commissioned on 17 October and the balance by 19 October 2000.

As soon as the first pumps were started, the wall movement virtually ceased, as can be seen from Figure 4. Measurements eight days later showed that the amplitude of the rocking motion was less than half its magnitude prior to pumping. With the wall stabilised, work on installing permanent drainage and ground anchors could begin. The effects of the dewatering upon the groundwater levels behind the wall are illustrated on Figure 5.

A feature of Figure 5 is that a distinct 'plateau' can be seen in the levels recorded for the water immediately behind the quay wall. The level of the retained water is drawn down to 0.0mOD by the pumping wells as the tide falls. It does not fall below this level, however, giving the step-like feature in the graph. The 0.0mOD level coincides with the invert level of the lower access-ways through the quay wall, which were open to the sea. When the tide was above 0.0m, on a falling tide, the retained water was clearly draining through these accessways, as well as being removed by the pumping wells. Once the tide fell below this level, then the pumping wells alone were removing the retained water, and, on the evidence of these readings, could only maintain the retained water at about the 0.0mOD level against the fresh water flowing from the landward side of the quay wall.

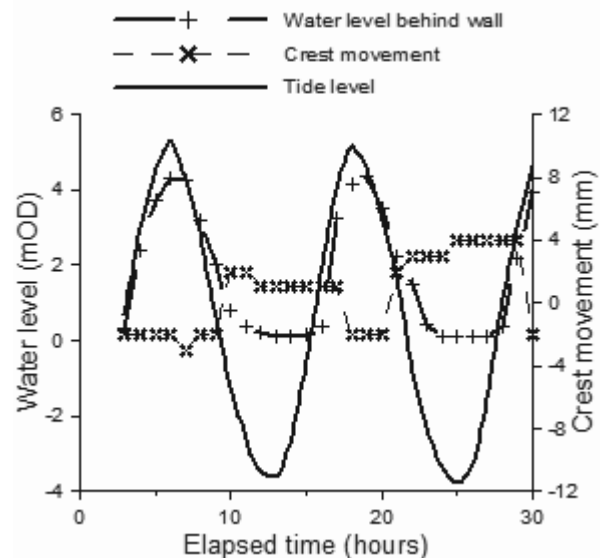


Figure 5. Water levels and crest movements 27-28 Oct 2000.

4 OUTLINE OF INTERIM REMEDIAL MEASURES (2001 – 2002)

It was recognised from the outset that the efficiency of the wells was likely to deteriorate in the medium term due to bio-fouling. Hence, additional measures were designed to provide physical restraint to the worst affected section of the wall. These consisted of seventeen 1050kN permanent rock anchors installed through the face of the wall at an inclination of 43° to the vertical; twenty-four 525 or 626kN permanent anchors through the crest of the wall inclined to landward at 10° to the

vertical and approximately thirty near-vertical 63.5mm diameter shear keys into rock beneath the base of the wall.

In addition, a series of sub-horizontal drainage wells were installed through the quay wall at a level of +0.0m OD, to speed the drainage of the retained soils.

These works were completed in early 2002.

5 WALL BEHAVIOUR 2002 – 2012

The dewatering wells were shut off in April 2002 and the wall behaviour was monitored.

The response of the wall in terms of its outward movement as measured by the inclinometers and the traverse line surveys is illustrated in Figure 6.

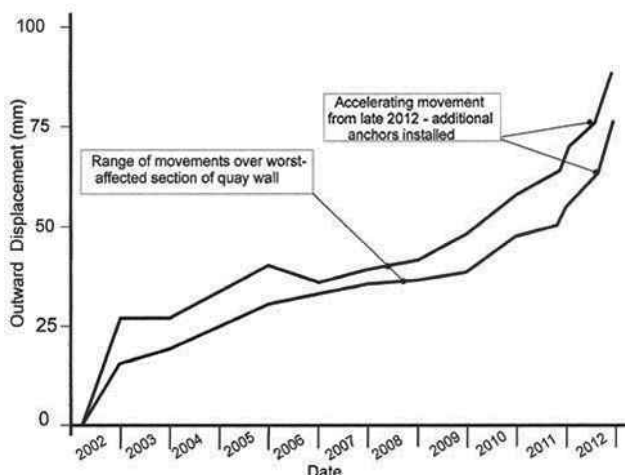


Figure 6. Wall displacements at crest level 2002 to 2012. (Toe displacements similar but generally smaller.)

Initial wall movements over the first 5-6 months were between 5 and 10mm at the crest and toe of the wall as the anchors took up further load. Load increases in the 43° anchors were typically between 50 and 200kN over this period.

By the end of 2002 the movements had stabilised at around 16 to 26mm at the crest, and 15 to 20mm at the toe. These data confirmed that the predominant mode of movement of the quay wall in the most active area was by sliding along a plane coincident with or close to the interface between the base of the wall and the underlying strata.

Over the next 3 years outward crest movements over the anchored section had increased to 30 to 40mm relative to the April 2002 readings and toe movements were between 35 and 40mm. Loads in the 43° anchors had increased by between 200 and 250kN. It had been planned to complete the main remediation works within this 3-year timeframe, but the monitoring works had demonstrated that movements were remaining controllable. The main works were put on hold, therefore and a watching brief was maintained on the wall. Based upon the previous readings, a movement criterion of 10mm/year had been adopted as a signal that further support works needed to be put in place.

By 2009 the loads in some 43° anchors were approaching or exceeding 1200kN – 15% above their design loads. Any anchors found to be in excess of this load level were being relaxed to avoid overstressing.

Outward wall movements over the anchored section generally continued at a rate of around 3 to 5mm per year.

By 2012, however, inclinometer and traverse line readings were indicating that outward wall movements were reaching 10 to 12mm per year, and the loads in the 43° anchors were increasing at an average of around 150 to 300kN per year. Additional interim measures were undertaken at the end of 2012, when a further six 1800kN capacity 43° anchors were installed through the face of the wall over the anchored section.

The aim of these works is to reduce outward movements back to acceptable levels.

These additional limited-scope works are intended to allow the continued limited working of the quay, consistent with the current requirements of the Port. As demand rises or operational needs change at the Port, then full remediation works will be implemented to upgrade the South Quay facilities to meet this demand.

For reference, the data from Figures 4 and 6 have been combined on Figure 7 to illustrate the relative degrees of movement measured at the crest of the quay wall over the worst affected section from 2000 to the present day. The figure clearly shows the rapid, and probably catastrophic, accelerating rates of movement in 2000, before the dewatering was switched on, followed by the relatively slow but continuing movements over the next 9-10 years, but increasing latterly.

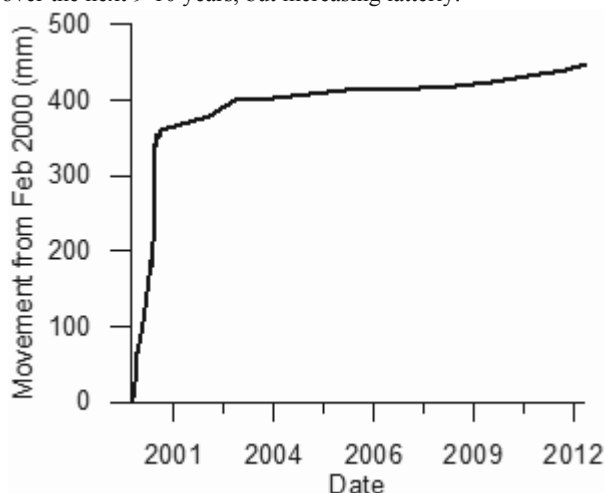


Figure 7 Wall crest movements between February 2000 and June 2012

6 SUMMARY AND CONCLUSIONS

The long-term monitoring of this 19th Century harbour wall over the last twelve years in particular, (but with records extending back over thirty years) has given a unique opportunity to gain an insight into the behaviour and relative ‘flexibility’ of such structures. The data gained from this work highlight the importance of monitoring such structures once they are perceived to be ‘at risk’, and the need to establish ‘trigger values’ related not just to overall movements but to rates of movement, and, in particular where rates of movement are seen to be accelerating over time.

7 ACKNOWLEDGEMENTS

The authors acknowledge with thanks the permission and co-operation of the port owners and their engineers in gathering and collating the data obtained from these monitoring works and allowing their publication in this paper.

8 REFERENCE

Peck R. B. 1969. Avantages and limitations of the observational method in applied soil mechanics. *Géotechnique* 19 (2), 171-187.

Concrete panel walls – Current development on interaction of earthworks, geosynthetic reinforcement and facing

Comportement des parements béton de murs de soutènement en sols renforcés – interaction entre les sols remblayés, le renforcement et le parement

Vollmert L., Niehues C.

BBG Bauberatung Geokunststoffe GmbH & Co. KG, Espelkamp, Germany

Pachomow D.

Technische Universität Cottbus, Cottbus, Germany

Herold A.

IBH – Herold & Partner Ingenieure, Weimar, Germany

Verstraaten W.

KWS Infra b.v., De Meern, The Netherlands

ABSTRACT: Reinforced soil structures have become an appropriate construction method for infrastructural buildings. Several types of facing are commonly used. Full height panels or segmental panels with a certain height are mainly used for flyover constructions and bridge abutments. The design of the constructions depends on the stiffness of the facing element. Large scale test with loads up to 450 kPa at laboratory conditions as well as on site test with one year of continuous measurement under weathering conditions are presented and compared to analytical design and calculations using commercial finite element software. The results indicate that this type of structure can be designed on the safe side using current design standards and benefits given by the interaction of stiff geogrid reinforcement and soil.

RÉSUMÉ : Les ouvrages en remblai renforcé sont devenus une méthode de construction adaptée aux projets d'infrastructures. Plusieurs types de parement sont couramment utilisés. Des panneaux de pleine hauteur, ou panneaux segmentaires avec une certaine hauteur, sont principalement utilisés pour les constructions surélevées et les culées de pont. La conception de ces ouvrages dépend de la rigidité de l'élément de parement. Cet article présente des essais réalisés à grande échelle avec des charges allant jusqu'à 450 kPa, en condition de laboratoire ainsi que sur site, avec une année de mesure en continu en condition de vieillissement. Les résultats sont comparés à la conception analytique et aux calculs réalisés à l'aide d'un logiciel commercial d'éléments finis. Les résultats montrent que ce type d'ouvrage peut être conçu de façon sécuritaire suivant les normes de conceptions actuelles et les avantages apportés par l'interaction d'une géogridde rigide avec le sol.

KEYWORDS: geosynthetic reinforced walls, concrete, design, testing, execution, DIN EN 14475, EBGEO, BS8006

1 INTRODUCTION

Creating robust and sustainable constructions in geotechnical engineering has become an upcoming topic in terms of reduction of carbon footprint as well as on cost reduction on PPP projects. Combining technologies for slim precast concrete panels with stiff geosynthetic reinforced walls allows for the use of local and in some cases even treated soils.

In the last years recent research has led to further understanding of reinforcing interaction, leading to design approaches published in EBGEO and allowing for a reduction of lateral stress on the facing constructions.

Design of precast panels in practice requires attention to the transport phase as well as on the construction steps during execution and serviceability limit state.

2 DESIGN OF REINFORCED STRUCTURES

DIN EN 14475, the British design code BS8006 as well as the German design recommendations EBGEO are state-of-the-art standards in order to safeguard the constructions.

Special attention has to be paid to the design of the facing, as these elements are directly exposed to the environment and deformations of the construction can be seen immediately. The mentioned design codes do not give a unique calculation of lateral stress acting on the facing elements. DIN EN 14475 already differentiates between several types of facing elements, depending on the stiffness:

- Rigid facings, e.g. full height panels

- Semi-flexible facings, e.g. concrete blocks without rigid connections, gabion baskets
- Flexible facings, e.g. wrap-around method

The lateral stress has to be different from the active earth pressure calculated according to Rankine's theory due to the geosynthetic reinforcing elements, "nailing" the fictive failure zone. As this becomes a hyper static system, the earth pressure distribution on the facing is indifferent.

Nevertheless, the design has to be proper and worked out on the safe side, so additional information has to be gained from sites and large scale tests, especially taking influence of water, subsoil settlements and installation conditions (compaction, construction steps, etc.) into consideration.

3 CURRENT DEVELOPMENT

3.1 *Lateral stress on facing*

Pachomow et al. (2007) collected several test-field data of executed walls in heights between 2.0 m and up to 30 m, with information concerning the lateral pressure on the facing given. It is interesting that the lateral stress gained by self-weight of the construction remained within a range of up to 50 kPa, although significant higher values would have been expected especially for high walls.

Normalising the height of all test field data, and recognising that nearly all data are linked to non-cohesive soils as well as to slope inclinations between 70° and 90°, the relationship between the vertical and lateral stress can be compared to the

active earth pressure coefficient, being expected in the range of 0.2 and 0.35, depending on the theory and boundary conditions. Figure 1 indicates that the normalised lateral stress on the facing is significantly less for reinforced structures. Furthermore, the data indicate that the absolute height might not have a decisive influence at all, but the normalised one.

Ruiken et al. (2010) have demonstrated the arching effects close to the facing of a geogrid-reinforced soil sample, using biaxial tests at plane strain conditions. The degree of arching and the absolute value of stress reduction depends on the lateral movement of the facing as well as on the degree of reinforcement, see also Bussert (2006).

Based on full scale tests using several commonly known reinforcing products varying in a small range of nominal strength from 40 kN/m up to 55 kN/m a clear tendency can be obtained concerning the stiffness, described by the secant modulus J of the products:

$$J \text{ [kN/m]} = \text{strength } F \text{ [kN/m]} / \text{strain } \varepsilon \text{ [\%]} \quad (\text{eq. 1})$$

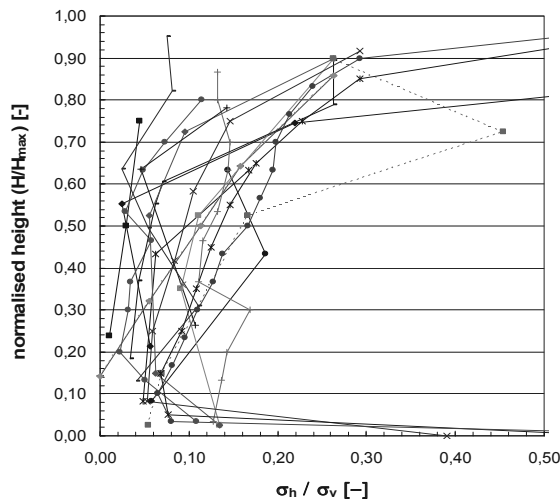


Figure 1. Compiled data of lateral stress to facing, presented at normalized height and relationship between normal load σ_h and lateral pressure σ_v .

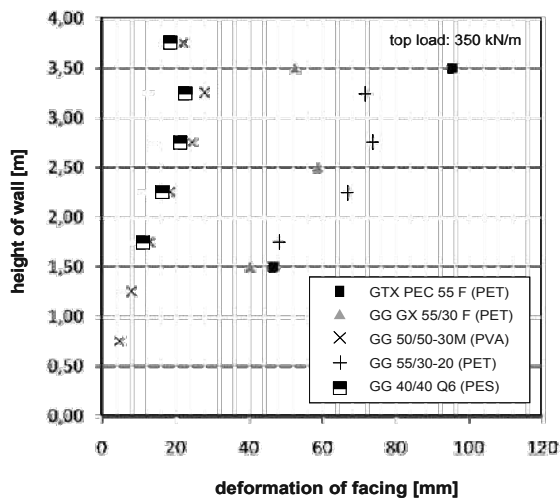


Figure 2. Deformation of full scale walls with semi-flexible facing, depending on the product (Pachomow & Herold, 2009).

Figure 2 shows preliminary results of a 4.0 m high construction using a weak facing system and a load beam 1.0 m behind the wall surface, applying a top load of up to 350 kPa. The deformation varies significantly depending on the type of product. All products performed satisfactory in an acceptable

range, while some products allow for higher loads and show an enhanced performance in terms of serviceability.

4 EUROPEAN DESIGN CODES

Exemplarily the mostly used design codes in Europe, BS 8006 and EBGEO 2010, dealing with reinforced earth will be discussed in the following.

Following the basic principles of designing reinforced soil, based on the results shown in Chapter 3, EBGEO allows further for a reduction of the lateral stress as compared to the Rankine's active earth pressure. The well-known coefficient for the lateral active earth pressure k_{ak} is just used as basic parameter (eq. 2), taking the inclination of the wall as well as the soil parameters (e.g. angle of internal friction ϕ') into consideration. The correction factor η_G as per Figure 3 is then applied, knowing well that using the lateral active earth pressure k_{ak} as basic parameter is just an interim solution up to full understanding and modeling of reinforced earth. In the upper part of the construction respectively on the actual construction level, the earth pressure due to compaction (not shown in Figure 3, typically up to 25 kPa) becomes decisive, but is going to be superimposed by the earth pressure resulting from the self-weight of the construction.

$$E_{\text{Facing}} = (\eta_g * k_{a_{gh,k}} * \gamma_k * H_i * \gamma_G + \eta_q * k_{a_{qh,k}} * q * \gamma_Q) * l_v \quad (\text{eq. 2})$$

- with
- E_{Facing} Earth pressure on facing [kN/m]
- η_g, η_q Matching coefficient [-]
- $k_{a_{gh,k}}, k_{a_{qh,k}}$ Coefficient active earth pressure [-]
- γ_k Weight of the soil [kN/m³]
- H_i Covering [m]
- q Traffic load [kN/m²]
- γ_G, γ_Q Partial safety factor DIN 1054 [-]
- l_v Vertical space between layers [m]

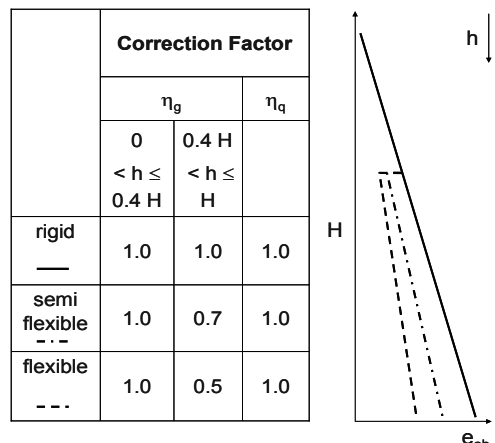


Figure 3. Correction factors applied to k_{ah} according to EBGEO, 2010.

In opposition to EBGEO, the earth pressure following BS 8006 is calculated using the active earth pressure coefficient k_{ah} for the structure, superimposed by k_0 in the upper part. The reduced stress acting on the front of the construction depending on the stiffness of the wall-facings is considered by a reduction of the connection stress, e.g. by 25 % in the upper 60 % of wall height using wrap-around method.

The BS 8006 concept results in having the highest connection stress requirements at the footing of the construction, while research and lessons learned from failures indicate to have the highest stress levels at approx. 1/3 height starting from the bottom of the walls.

Nevertheless, the reduction of the lateral earth pressure of both concepts has a direct influence on the design of reinforced walls and allows for steep walls with a friction connection between e.g. blocks and reinforcement.

5 LARGE-SCALE TEST IN SITU

5.1 Design and set-up

In addition to the large scale tests on full height panel walls performed by Pachomow, a full scale trial has been performed by KWS Utrecht, Netherlands, supported by NAUE, Germany. While under laboratory conditions high loads up to 450 kPa could have been applied to the structure, in situ the influence on installation procedure, weathering (changes of moisture-content and temperature) and long term effects caused by the thermoplastic characteristics of the used high strength Polyester geogrid could be investigated. Figure 4 gives the cross section of the test set-up for the in-situ test with geometry comparable to the laboratory test.

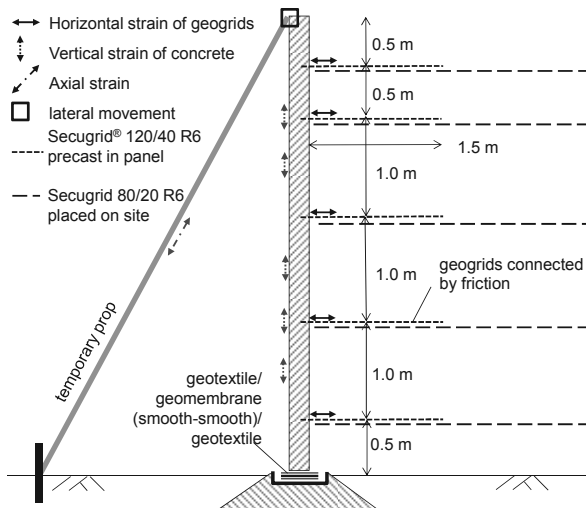


Figure 4. Test setup full height panel wall, KWS Utrecht

To reduce the required amount of structural steel for the construction, the panel has not been designed using conventional design methods, but taking the results from laboratory test explained in Chapter 4 into consideration. Therefore, the design configuration has been optimized, assuming the load distribution given in EBGeo, applying an overall safety to the earth pressure distribution of 1.5 (assumption).

The load distribution has been applied to the panel design, testing several static systems and designs to optimize the amount of required structural steel. At the end, the system could be optimized for transport steel only.

To make the system as easy as possible, only 1.5 m long strips of the reinforcement have been precast to the concrete (Figures 4, 5a). The required length of the reinforcement to fit the overall safety according to EBGeo has been placed on site, just overlapped by friction. For the earth pressure distribution, satisfactory pull-out resistance of the strips from the reinforced backfill has to be ensured.

Several types of instrumentation have been used, taking the static principle of $\Sigma H = 0$ into consideration. The sum of forces acting on the backside of the panel shall be equal to the forces

acting on the geogrids, the temporary prop, added by the friction on the toe of the panel.

Therefore, the toe of the panel has been designed as plain bearing, using geosynthetic components for sliding purposes with tested and well-known friction parameters for back-analysis of the forces acting at the toe. Temporary wooden wedges, applied during placing the panel, have been removed after the installation of the first 1.5 m of backfill material, so lateral movement of the panel toe was possible but has not been observed.

Further on, it had to be ensured that the material used is applicable to the use in concrete, as it is given here by independent testing and applying a partial reduction factor for environmental influences to the polyester material of 1.18 [-].

To predict stress, strain and lateral movement of the stage construction, finite element (FE) analysis have been worked out using PLAXIS 2D, 2011. These calculations are also usable for comparing the measurements and predictions for the reference times $t_0 \dots t_5$ charged as indicator for significant changes in the static system with construction stage and time, Figure 5.

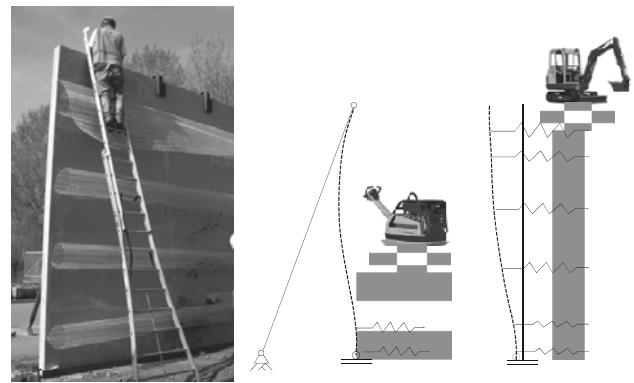


Figure 5a. Installation procedure and expected deformations of wall.

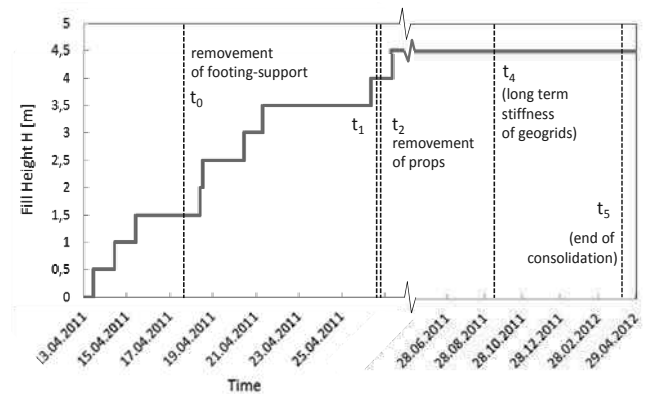


Figure 5b. Time schedule of construction.

5.2 Measuring strain and back-calculation of stress

For the back-analysis of horizontal forces from strain recordings, the corresponding stress has to be known. This can be read from isochronous stress-strain curves, as far as they are available. For the used material here, Secugrid[®] made from polyethylenterephthalat (PET), the curves are given. The back-analysis for representative times t_0 , t_1 and t_2 (see Figure 7) has been worked out using the isochronous curve for 1 hour, representative for the situation immediately after compaction of soil. As this gives conservative values of stress, no further differentiation is required.

For the time t_4 and t_5 , long term stiffness has been calculated using the isochronous curve for 1000 h, also giving

conservative values for stress, as t_4 is approx. at 2880 h and t_5 at 6500 h.

5.3 Main findings

Up to the date of printing, the construction is approximately one year in service. Data recording is available continuously during installation and in sequences during the service period. Within the service period, also 24h-measurements have been done to get an impression of temperature changes within the wall. Figure 6 gives the strain recording for the total time, indicating a very low level of strain of less than 1%, as it has to be expected. Nevertheless, only the three layers on the bottom get a significant loading. Two layers of geogrids on the top are up to now not taking any load. As these layers are mainly designed for a top-load of the construction not performed yet, the results fit with the expectations.

Removing the prop (t_1 to t_2) has been expected to increase the strain in the upper layers of the geogrids. Actually, this could not be found on site. The absolute values of strain (and therefore stress) at each layer remained stable.

For the sum of horizontal loads, compiled for the representative time t_0 to t_5 , measured forces as well as forces from FE-calculation and analytical approach by classical earth pressure theory can be compared. Friction at the toe of the wall, forces on the temporary prop as well as forces at the geogrids, measured right behind the wall, have to be compiled.

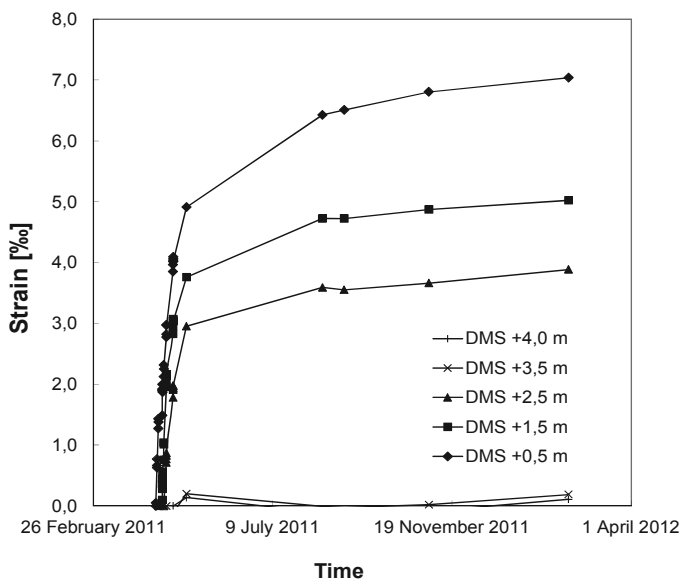


Figure 6. Entire strain recordings of the geogrids (DMS: strain gauge applied to geogrid).

For time t_0 to t_4 , the results gained by PLAXIS come quite close to the results gained from measurements in situ, Figure 7. Taking the rotation backwards due to settlements into consideration (time t_5), PLAXIS gives a significant increase in stress, not be found on site.

In comparison to the measurements, results given by classical earth pressure have not been found to represent the reality for this combination of reinforcement and facing, neither the laboratory one nor the in-situ one. The difference is at least between 30% and 40% and therefore in line with the current status of research on reinforced soils. Compared to the design situation according to EBGEO, a reduction of lateral stress for the load case “unit weight of structure” and therefore a correction factor $\eta_g \geq 0.7$ would be acceptable from the author’s point of view.

6 SUMMARY

Full scale laboratory tests have been performed for a full height panel wall, combined with a geogrid-reinforced soil structure. Tests are performed at loads up to 450 kPa according to bridge abutments as well as at dynamic loadings.

A comparable setup of a full scale panel wall has also been tested in situ. Monitoring of the reinforced wall allows for satisfactory back-analysis of the constructions steps.

The measured stress conditions fit with the expected low stress approach for the combined structure, given by FE-analysis. The findings combine the current results of international research and updated design approaches (EBGEO) also for full height panel walls. They allow for the consideration of a reduced earth pressure distribution in design as well as for simplified construction.

Due to limitations, the setup and results cannot be transferred to all combinations of reinforcement, soil and panel-systems, but allow for further analysis by FE calculations.

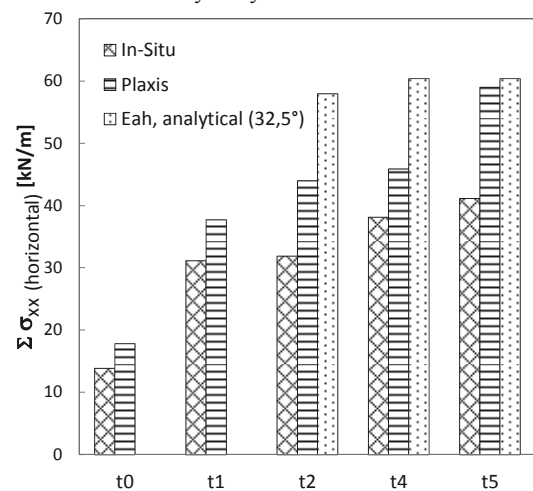


Figure 7. Comparison of measured lateral stress in situ, prediction by FE-analysis and prediction by classical earth pressure theory

7 REFERENCES

- EBGEO - Recommendations for Design and Analysis of Earth Structures using Geosynthetic Reinforcements. 2nd Edition. Published by German Geotechnical Society (DGGT). Ernst & Sohn, Berlin, 2011.
- DIN EN 14475, 2006-04: Execution of special geotechnical works - Reinforced fill.
- BS 8006-1, 2010-10: Code of practice for strengthened/reinforced soils and other fills.
- Pachomow, D., Vollmert, L. & Herold, A. (2007): „Der Ansatz des horizontalen Erddrucks auf die Front von KBE-Systemen“. Tagungsband zur 10. FS-KGEO 2007.
- Ruiken, A., Ziegler, M., Vollmert, L. & Duzic, I. (2010): “Recent findings about the confining effects of geogrids from large scale laboratory testing”. 9th International Conference on Geosynthetics, Brazil, 2010.
- Bussert, F. (2006): „Verformungsverhalten geokunststoffbewehrter Erdstützkörper – Einflussgrößen zur Ermittlung der Gebrauchstauglichkeit“. Dissertation. TU Clausthal, Schriftenreihe des Instituts für Geotechnik und Markscheidewesen, Heft 13/2006.
- Pachomow, D. & Herold, A. (2009): „Zum Last-Verformungsverhalten von KBE-Konstruktionen im Frontbereich“. Vortrag zum VI. Geokunststoff-Kolloquium in Bad Wildungen der NAUE GmbH & Co. KG, Espelkamp.

The influence of bond stress distribution on ground anchor fixed length design. Field trial results and proposal for design methodology

L'influence de la répartition des contraintes sur les tirants d'ancrage de longueur fixe. Résultats de planche d'essais et proposition de méthodologie de conception

Vukotić G.
Kellerterra, S.L.

González Galindo J., Soriano A.
Universidad Politécnica de Madrid

ABSTRACT: This paper presents a brief analysis and comparison of different recommendations for a ground anchor fixed length design and a load transfer capacity at grout-ground interface, comparing it with the full scale test results recently carried out in Spain. Simple methodology for ground anchor routine design is proposed, incorporating efficiency factor as a conceptual control of anchor capacity, and fixed length criteria to determine range of application of conventional anchors, with single fixed length unit, or Single Bore Multiple Anchors (SBMA). Ground anchors discussed in this paper are cement pressure grouted, formed by pre-stressed strand tendons that are installed in soil or rock.

RÉSUMÉ: Cet article présente une brève analyse et la comparaison des différentes recommandations pour la conception de tirant d'ancrage de longueur fixe et la capacité de transfert de charge à l'interface coulis-sol, en le comparant avec les résultats d'essais à échelle réelle obtenus en Espagne au cours des dernières années. Une méthodologie simple pour la conception de tirant d'ancrage est proposée; elle intègre le facteur d'efficacité comme un contrôle conceptuel de la capacité de l'ancrage et les critères de longueur fixe pour déterminer le champ d'application des tirants d'ancrage conventionnels, d'unique longueur fixe, ou d'ancrages multiples en un unique forage (SBMA pour ses sigles en anglais). Les tirants d'ancrage décrits dans ce document sont injectés à pression au moyen d'un coulis de ciment et sont formés par un faisceau de câbles d'acier précontraints qui sont installés dans le sol ou la roche.

KEYWORDS: anchor, fixed length, bond stress, efficiency factor.

1 INTRODUCTION

Nowadays anchors represent a key medium to sustain and strengthen slopes formed by instable soils and fractured rocks, and to ensure the stability of various types of gravity structures.

Regarding bond stress and load transfer capacity at the grout-ground interface, most procedures for anchor design are empirical values or formulas derived by local experiences, very difficult to extrapolate for different locations or execution systems. The design procedure is often simplified, considering direct proportionality between fixed anchor length and its load capacity, as it is prevailing practice in Spain and South America.

However, since late 1960s numerous authors demonstrate bond stress or skin friction distribution to be highly non-uniform at all stages of loading, with high bond stress mobilization along reduced fixed length. In the following chapters, based on presented references and analysis of the field trial results recently performed in Spain, the methodology for anchor fixed length design is proposed.

2 DESIGN OF THE FIXED ANCHOR LENGTH

2.1 Current practice

Design assumption of uniform load distribution along the fixed anchor length is not only limited to usual methodology and standards in Spain and South America but is internationally generally adopted. Considering this hypothesis the ultimate or capacity of the anchor is commonly expressed as follows:

$$T_{ult} = \pi \cdot d \cdot L_{fix} \cdot \tau_{ult} \quad (1)$$

where: d = anchor diameter, L_{fix} = anchor fixed length and τ_{ult} = ultimate bond stress.

This formula differs from experimental and theoretical evidence that corroborate that there is no linear dependency of ultimate capacity on fixed anchor length.

2.2 Non-uniform bond stress distribution

It is fully acknowledged by numerous researchers that the distribution of stress along the fixed anchor length is non-uniform, both at low stress levels and at failure. This phenomenon results from the general incompatibility between elastic modulus and corresponding deformation of the anchor strands, cement grout and ground.

Field tests on instrumented conventional anchors, reported by Muller (1966), Berrardi (1967), Ostermayer (1974), Ostermayer and Scheele (1977), Mastrantuono and Tomillo (1977), Barley (1995) and Briaud et al. (1998), showed that when applying the initial load the bond stress is concentrated over the proximal length of the fixed anchor, leaving a significant part of the fixed length towards distal end unstressed. By the evolution of the load the bond stress concentration zone is transferred along the fixed anchor as the bond stress along either the tendon/grout or grout/ground interface is exceeded.

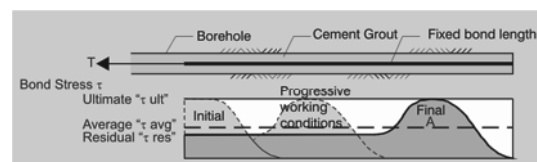


Figure 1. Development of bond stress distribution along a fully bonded fixed anchor length (Barley 1995).

Simultaneously, due to progressive debonding, stress at the proximal end reduces to residual values. The bond stress concentration zone reaches distal end of the anchor just before the failure, as it can be seen in Figure 1.

The same mechanism of a non-linear load and bond distribution was confirmed by laboratory full-scale test accomplished by Weerasinghe (1993). It is also important to mention investigation done by Coates and Yu (1970), which studied stress distribution around a cylindrical anchorage in triaxial stress field using finite element methods. The results emphasize the non-uniform bond stress distribution for the ratio of the elastic modulus of the anchor material (E_A) and the rock (E_R) less than 10 ($E_A/E_R < 10$), which is very common for wide range of rocks and soils in which anchors are usually constructed.

2.3 Efficiency factor

There have been a number of attempts to quantify the non-uniform load distribution and to introduce effects of progressive debonding into Formula 1. Casanovas (1989) recommended design based on definition of apparent fixed length (L_{ve}) over which the ultimate bond stress can be mobilized:

$$L_{ve} = \left(\frac{L_{fix}}{L_0} \right)^{\frac{1}{\log(0.1 \cdot \frac{\tau_{ult}}{\tau_0})}} \cdot L_0 \quad (2)$$

where: L_{ve} = apparent fixed length over which τ_{ult} (kN/m²) operates, L_0 = reference length of 1 m, τ_0 = reference value of 1 kN/m².

To understand better efficiency factor concept it is possible to analyze Figure 1 and to compare area A_s , that corresponds to the final and maximum load stage, with the total area below τ_{ult} .

$$f_{eff} = \frac{Area.A}{Area.below.\tau_{ult}} \quad (3)$$

Then, ultimate anchor capacity can be expressed as follows:

$$T_{ult} = \pi \cdot d \cdot L_{fix} \cdot \tau_{fix} \cdot f_{eff} \quad (4)$$

Research based on over 60 full scale tests performed on different anchor fixed lengths, installed in wide range of soil (clays, silty clays, sandy clays, boulder clay and glacial till), permitted development of the concept of the efficiency factor (Barley 1995 and 1997, Barley and Windsor 2000). Figure 2 presents the distribution of the values of the efficiency factor (f_{eff}) against anchor fixed length, and the best fit curve can be expressed by following expression:

$$f_{eff} = 1,6 \cdot \left(\frac{L_{fix}}{L_0} \right)^{-0,57} \quad (5)$$

It is important to emphasize that Barley's efficiency factor is quite consistent with Ostermayer (1974) diagrammatic presentation of the ultimate medium skin friction against fixed length for similar soil characteristics and anchor construction process, as it can be seen in Figure 2.

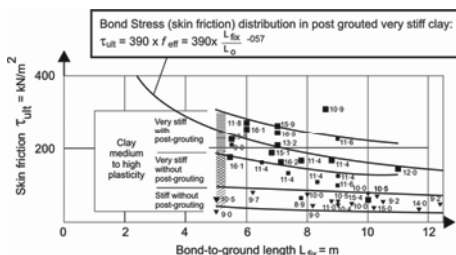


Figure 2. Ostermayer's (1974) boundary lines vs. Barley's (1995) efficiency factor.

Barley (1995) also suggested the efficiency factor for sands, correlating efficiency with the fixed length and the friction angle:

$$f_{eff} = (0,91) \frac{L_{fix} \cdot \tan \varphi}{L_0} \quad (6)$$

One of the most extensive attempts to model construction technique, characteristics and behaviour of anchors have been accomplished by Mecsi (1995), based on analysis of results from numerous installed and monitored anchors.

Analytical solution and simple graphical method based on the theory of expanded cylindrical cavity provide the possibility to define the approximate pull-out capacity. The Analysis of load distribution for the known anchor geometry and rigidity permits determination of the specific pull-out resistance of a 1 m anchor length (t_{ult}) and the length of the fully mobilised bond stress (L_b). Considering that only reduced percentage of maximum bond stress can be mobilised over the remaining fixed anchor length ($L_{fix} - L_b$), the ultimate anchor capacity can be expressed by the following expression:

$$T_{ult} = \tau_{ult} \left[L_0 + \frac{1}{k} \text{th} [k \cdot (L_{fix} - L_0)] \right] \quad (7)$$

$$k = \sqrt{\frac{\tau_{ult}}{E_{steel} \cdot A_{steel} \cdot \Delta_{ult}}} \quad (8)$$

where: k = rigidity index, E_{steel} = steel deformation modulus, A_{steel} = steel tendon area, Δ_{ult} = elongation of the shear strength length ($L_{fix} - L_0$).

Based on data from Ostermayer and Scheele (1997), Woods and Barkhordari (1997) proposed efficiency factor for its incorporation in the expression for ultimate capacity of low-pressured anchors in sand (Formula 10), recommended in BS 8081 (1989), which is a function both of fixed anchor length and friction angle:

$$f_{eff} = \exp(-0,05 \cdot \frac{L_{fix}}{L_0} \cdot \tan \varphi) \quad (9)$$

where: L_0 = reference length of 1 m.

$$T_{ult} = f_{eff} \cdot L_{fix} \cdot n \cdot \tan(\varphi) \quad (10)$$

2.4 Single Bore Multiple Anchors - SBMA

This system involves the installation of a multiple unit anchors into a single borehole, with enough short unit lengths to reduce or even to avoid the progressive debonding. Each unit is formed by individual tendon and is loaded with the corresponding unit stressing jack, mobilizing its own capacity independently of other unit anchors.

Application of this system permits the unlimited theoretical total fixed length, while conventional anchors formed by only one unit do not provide beneficial effects in load capacity for fixed length superior to 10 m as is stated by numerous authors and design guidelines or codes.

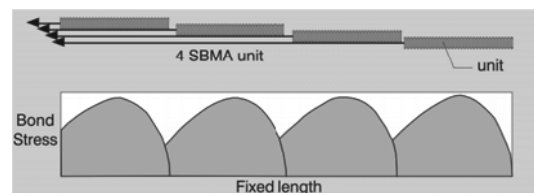


Figure 3. Development of bond stress along a four unit single bore multiple anchor (Barley, 1997).

Total fixed lengths of 10 to 20 m are frequently used in all types of soils, achieving high anchor capacities (2000 to 5000 kN) that are almost three times greater than the normal conventional anchors capacity values (Barley 1997, Barley and Windsor 2000). A comparison of load distribution between conventional and SBMA anchor is presented in Figure 3.

3 GENERAL FIELD TEST DETAILS

The results of full-scale field tests, undertaken to verify the influence of the fixed anchor length on the ultimate capacity (T_{ult}) and the average bond stresses (τ_{ault}) obtained at failure in gravelly sands, silty clays and clayey marl are presented in this chapter.

Investigation test were done according to the Test Method 1 (EN 1537), with incremental load cycles from a datum to ultimate load. The test involved very strict measurement of tendon displacement versus applied load and, at the peak of each cycle, measurement of tendon displacement versus time. Anchors subjected to investigation were high-pressure grouted, designed to fail at grout/ground interface. Field tests were carried out near previously performed boreholes to establish better correlation between obtained data and soil characteristics.

Values of efficiency factor presented in Table 1, 2, 3 and 4 are calculated comparing average bond stresses (τ_{ault}) of SBMA units and conventional anchors, considering that units that formed SBMA anchors with fixed length of 2.5 – 3.0 m were short enough to avoid progressive debonding effects. Due to that hypothesis it can be assumed that efficiency factor for individual units of SBMA anchor have the value of 1.

To avoid possible influences and collaboration of the free anchor length on pull-out capacity and bond stress distribution, fixed units of all test anchors were separated by specially designed compressible joints that prevent load transmission from fixed to free anchor length.

3.1 Test results in gravelly sand

The trial anchors, six SBMA with two units (in total 12 units) and two conventional anchors, were executed in dense to very dense gravelly sand, with silt content that varied from 5 to 15%, at depth of 20 to 30 m.

SBMA anchors were formed by two units of 2.5 m fixed length, while conventional anchors had fixed length of 7.5 m. Diameter of all test anchors was of 178 mm. The following table shows ranges of obtained results:

Table 1. Test results for pressure grouted 178 mm diameter anchors in gravelly sands.

N°/Type of Anc.	L_{fix} m	T_{ult} kN	τ_{ault} kN/m ²	f_{eff}
6 SBMA (12 units)	2.5	780–960	558-687	1
2 Conventional	7.5	1880-1920	445-455	0.65-0.8

It is worthy to mention that values of the obtained ultimate load capacities are very consistent with Ostermayer and Scheele (1978) diagrammatic presentations of the load capacity against fixed length (see Figure 4).

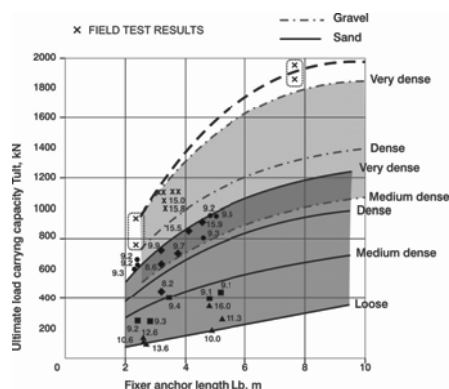


Figure 4. Ultimate load capacity obtained in field test vs. values proposed by Ostermayer and Scheele for sand and gravel (1977).

3.2 Test results in silty clays

Table 2 summarizes results for trial anchors, 2 SBMA with two units (in total 4 units) and two conventional anchors, performed in stiff silty clay (CL) at depth of 15 to 25 m. SBMA anchors were formed by two units of 2.5 m fixed length, and conventional anchors had fixed length of 8.0 m. Diameter of all test anchors was of 160 mm.

Table 2. Test results for pressure grouted 160 mm diameter anchors in silty clays.

N°/Type of Anc.	L_{fix} m	T_{ult} kN	τ_{ault} kN/m ²	f_{eff}
SBMA (4 units)	2.5	400–440	318-350	1
2 Conventional	8.0	915-950	227-236	0.65-0.74

3.3 Test results in clayey marl

The trial anchors were carried out in two different sites with similar soil characteristics, stiff to very stiff clayey marl (CH-CI), with sand proportion less than 10%.

3.3.1 Test site A

The trial anchors were constructed at depth of 20 m, with diameter of 150 mm. SBMA anchors were formed by two units of 3 m fixed length, and conventional anchors had fixed length of 11 m.

Table 3. Test results for pressure grouted 150 mm diameter anchors in clayey marl – Test site A.

N°/Type of Anc.	L_{fix} m	T_{ult} kN	τ_{ault} kN/m ²	f_{eff}
2 SBMA (4 units)	3.0	450	318	1
2 Conventional	11.0	785	110-152	0.35-0.48

Results presented in Table 3 demonstrate high inefficacy of fixed anchor lengths longer than 8 or 10 m.

Efficiency factor for 11 m long fixed length obtained comparing average bond stresses varies from 0.35 to 0.48. It is important to emphasize that results feet well with efficiency factor values proposed by Barley (1995), as it can be seen in Figure 5.

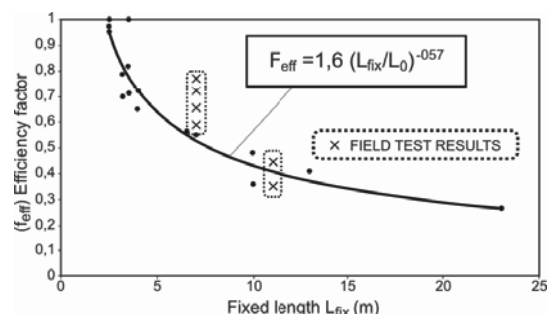


Figure 5. Efficiency factor obtained in field tests in silty clays and clayey marlvs. values proposed by Barley (1995).

3.3.2 Test site B

The trial anchors were executed at depth of 30 to 35 m, with diameter of 178 mm. SBMA anchors were formed by two and three units of 2.5 and 3 m, while conventional anchors had fixed length of 7.5 m.

Table 4. Test results for pressure grouted 178 mm diameter anchors in clayey marl – Test site B.

N ^o /Type of Anc.	L _{fix} m	T _{ult} kN	τ _{ult} kN/m ²	f _{eff}
8 SBMA (18 units)	2.5	450-540	322-386	1
2 Conventional	7.5	960-1080	230-254	0.59-0.79

3.4 Summary

An extensive series of field anchor tests performed in different soils showed that:

- there is no direct proportionality between fixed anchor length and its ultimate load capacity;
- obtained values of the average ultimate bond stresses in cohesive soils fit well with Ostermayer's (1974) diagrammatic presentation of skin friction against fixed length, while results obtained in gravelly sands fit well with Ostermayer and Scheele (1978) presentation of ultimate load capacity vs. anchor length;
- ranges of obtained efficiency factors are consistent with tendency of values proposed by Barley (1995);
- efficiency factor can be considered as a conceptual control of anchor ultimate capacity;
- fixed anchor lengths longer than 10 m do not contribute significant beneficial effects on capacity.
- SBMA anchors permits construction of high anchor capacities that approach more than two times that of the conventional anchors which utilize long inefficient fixed length.

4 PROPOSAL FOR DESIGN METHODOLOGY

Based on the information presented in previous chapters, proposal for design methodology for cement grouted anchors formed by steel tendons is presented below, considering most important parameters that define its capacity, like: soil characteristics, execution process, ultimate and average bond capacity, fixed length, type of anchors (conventional or SBMA), stress distribution and efficiency factor.

Emphasis is placed on the effects of progressive debonding that cause the non-uniform stress distribution along the fixed length, with efficiency factor as a conceptual control of anchor capacity. Due to the number of parameters that enter the analysis, recommended methodology has an iterative character, as it can be seen in Figure 6. Some of the most important steps of the flow chart are commented below.

Phase I: Evaluation of the site subsoil conditions and relevant properties of in situ soil and rock, as a factor that directly influence steps in the Phase II (construction system and skin friction estimation).

Phase II: For the skin friction estimation it is recommended to use at least two sources, taking into account the concept or formula that will be applied for the anchor design. If pre-design load tests are performed to evaluate ultimate anchor load capacity, construction process has to be exactly the same as planned for production anchors, and fixed lengths should be similar with test anchors. For the first iteration anchor length is calculated considering uniform bond stress distribution (Equation 1). If calculated fixed length is larger than 5 m, construction process can be reconsidered (Alternative A), varying anchor diameter or type of grouting, with objective to reduce fixed length up to 5 m. Other option (Alternative B) is to introduce directly the efficiency factor.

Phase III: If the fixed length obtained considering non-uniformity is in the range between 5 and 10 m, two alternatives are proposed. First alternative considers conventional type of anchor, with unique fixed length unit calculated taking into account efficiency factor (f_{eff}) – Equation 2. Another alternative

is the application of SBMA. In this case fixed length of each unit that forms SBMA is calculated considering corresponding efficiency factor (f_{eff}) – Equation 3.

If the fixed length, obtained considering non-uniformity is greater than 10 m it is recommended to apply SBMA anchors.

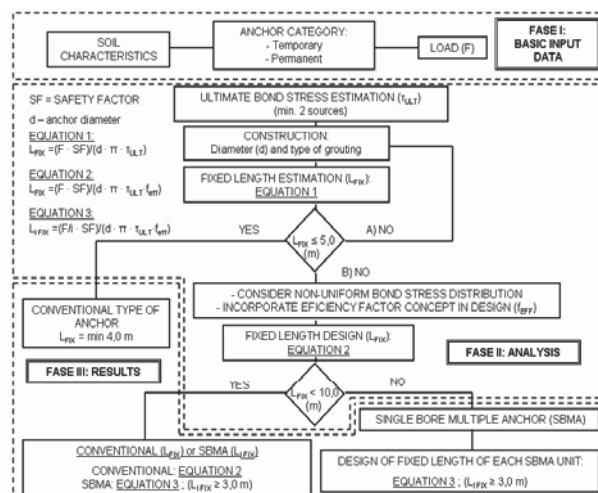


Figure 6. Flow chart for design of fixed anchor length.

5 REFERENCES

- Barley A.D. (1995). Theory and Practice of the Single Bore Multiple Anchor System. *Proc. Int. Symposium Salzburg*. Balkema Rotterdam, pp 293-301.
- Barley A.D. (1997). The Single Bore Multiple Anchor System. *Proc. Int. Conf.: Ground anchorages and anchored structures*. London, pp. 65-75.
- Barley A.D. and Windsor, C.R. (2000). Recent advances in ground anchor and grout reinforcement technology with reference to the development of the art. *GeoEng 2000, Int. Conf. on Geotechnical and Geological Engineering*. Melbourne, pp. 1083-1094.
- Berardi G. (1967). Sul Comportamento Deglie Ancoraggi Immersi in Terreni Diversi. *Universidat Genoa, Inst. Contr. Sc. Serie III* (60), pp 18-19.
- Briaud J.L., Powers W.F. and Weatherby D.E. (1998). Should Grouted Anchors Have Short Tendon Bond Length?. *Journal of Geotechnical and Geoenvironmental Engineering ASCE*, pp. 110-119.
- BrS 8081 (1989). British Standard Code of Practice for Ground Anchorages. BSI, London.
- Casanovas (1989). Anchoring in rock. Elsevier Scientific Publishing Company, pp 0-33.
- Coates D.F. and Yu Y.S. (1970). Three dimensional stress distribution around a cylindrical hole and anchor. *Proc. of 2 Int. Conf. on Rock Mechanics*. Belgrade, pp. 175-182.
- EN 1537 European Standard (2010). Execution of special geotechnical work – Ground Anchors.
- Mesci J. (1997). Some Practical and Theoretical Aspects of Grouted Soil Anchors. *Proc. of Int. Conf. Ground Anchorages and Anchorages Structures*. London, pp. 119-130.
- Muller H. (1966). Erfnungenmit Verakurungen System BBRV in Fels- und Lock-ergensteinen. *Schweizerische Bauzeitung*, 84 (4), pp. 77-82.
- Ostermayer H. (1974). Construction carrying behavior and creep characteristics of ground anchors. *Int. Conf. On Diaphragm Walls and Anchorages. I.C.E. London*, Septiembre 18-20, pp. 141-151.
- Ostermayer H. and Scheele F. (1977). Research and Ground Anchors in Non-Cohesive Soils. *Géotechnique* 3, pp. 92-97.
- Weerasinghe R.B. (1993). The Behaviour of Anchorages in Weak Mudstone. PhD Tesis, University of Bradford.
- Woods R.I. and Barkhordari K. (1997). The Influence of Bond Stress Distribution on Ground Anchor Design. *Proc. of Int. Conf. Ground Anchorages and Anchorages Structures*. London, pp. 55-64.

The sustainability and assessment of drystone retaining walls

Le développement durable et l'évaluation des murs de soutènement en pierres sèches

Warren L., McCombie P.
University of Bath

Donohue S.
Queens University Belfast

ABSTRACT: The art of drystone walling is a highly sustainable traditional practise which uses local materials and craftsmen. As no mortar is used they have low embodied carbon, and much repair work or rebuilding can be carried out using very little if any new materials. However local practices developed to suit local materials, leading to a range of construction styles, making them difficult to assess. This paper examines a range of construction styles of drystone retaining walls in use across the United Kingdom. Understanding of the substantial variations of construction style is essential to enable proper assessment of these structures. Different frictional and weathering characteristics, and the naturally occurring shapes of stone found in an area, all affect the ways in which the stones have traditionally been assembled into walls. Ease of construction also plays a part, as the craftsman will naturally wish to achieve a robust construction in a way that is economical of time and effort. Aesthetics may be very important, for both client and craftsman. It is also shown that construction style is influenced by the location and function of the structures, with harbour walls particularly likely to have unique characteristics, and the reasons for this are explored.

RÉSUMÉ : L'art de la pierre sèche est une pratique hautement durable traditionnelle qui utilise des matériaux et des artisans locaux. En l'absence de mortier, elles ont une faible carbone incorporé, et les travaux de réparation ou de reconstruction bien peut exiger très peu ou pas de nouveaux matériaux. Cependant les pratiques locales développées pour répondre à des matériaux locaux, conduisant à une gamme de styles de construction, ce qui les rend difficiles à évaluer. Cet article examine une gamme de styles de construction de murs de soutènement en pierres sèches utilisées dans l'ensemble du Royaume-Uni. Compréhension des variations importantes du style de construction est essentielle pour permettre une évaluation adéquate de ces structures. Différentes caractéristiques de frottement et aux intempéries, et les formes naturelles de pierre trouvés, affectent la façon dont les pierres ont traditionnellement été assemblés. Facilité de construction joue également un rôle. L'esthétique peut être très important, à la fois pour le client et l'artisan. Il est également démontré que le style de construction est influencée par l'emplacement et la fonction des structures, avec des murs du port particulièrement susceptibles d'avoir des caractéristiques uniques, et les raisons de cette situation sont explorées..

KEYWORDS: Drystone, Construction styles, Assessment

1 INTRODUCTION.

Throughout the UK there are many different styles and types of walling to be found. Most styles can be categorised as horizontal construction, vertical construction or random construction (Figure 1). Each has its own unique features and is often associated with certain areas of the country and corresponding rock types. Horizontal construction is often found with more blocky types of stone such as limestones, which can be stacked in a more conventional fashion; the stones are also sometimes worked to give a better fit. Horizontal construction is probably the most common type of construction within the UK. Vertical construction is mainly associated with slate type stones that can be tightly packed and may be less successful in a horizontal configuration. Random construction is mainly associated with more granitic type rocks which are hard to work and are often irregular in shape. These styles are sometimes found in combination in a single wall with a single type of stone, and there are variations such as the herringbone construction, found in parts of Cornwall.

It could be argued that every drystone retaining wall works in essentially the same way, as every wall is essentially a gravity retaining wall that relies on the frictional forces between the stone for stability. However, each style is likely to use the mechanical properties of the stones in different ways to achieve the required coherence. The failure and movement of horizontally constructed walls is comparatively well documented and understood (Mundell, 2009) when compared to

the other construction styles. The mechanical differences between the styles are explored below.

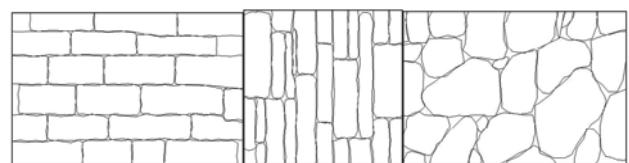


Figure 1. Different wall styles found in the United Kingdom: horizontal construction, vertical construction, random construction.

1.1 Horizontal Construction

Experimental testing and numerical modelling (McCombie et al. 2012, Mundell et al. 2009, Colas et al. 2010, Villemus et al. 2007) have shown that the overturning moment due to the horizontal component of earth pressure is resisted in part by the vertical component acting in downwards shear on the back of the wall, with very small deformations for well-constructed walls in a normal condition. As walls become overloaded the deformations can become considerable, often showing the classic bulged profile as the walls adapt their shape to the higher applied load (Figure 2). Ultimately, the walls will typically overturn, though if a smooth stone is used the wall or a part of it may slide forwards first. If the wall is constructed in a well-bonded manner, with stones overlapping, then a tensile strength can develop along the length of the wall which greatly assists in

the redistribution of load, and helps give the wall substantial ductility. This behaviour is dependent upon a horizontal construction. A less beneficial consequence of horizontal construction is the reliance on through stones to connect coursed layers of stone at the front and back of the wall across an infill of rubble. These stones are necessarily larger than those used for the rest of the construction, and there may not be sufficient to ensure that the wall behaves monolithically, giving a greater chance of movement and hence failure.



Figure 2. 2.4m high test wall at the University of Bath showing a classic bulged profile in a limestone wall of horizontal construction.

1.2 Vertical Construction

There has been no notable published research into vertical or random forms of construction, but some indications of how they perform may be inferred from observations, in relation to the behaviour of horizontal constructions.



Figure 3. Model test showing concrete blocks partially rotated and wedged in against the sides of the test box.

Discussions with wallers who use the vertical form of construction, and detailed observations carried out in Somerset and Cornwall, suggest that vertical construction is reliant on compressional pre-stressing forces. In the majority of vertically constructed walls all stones either penetrate the full width of the wall, or are tightly packed throughout the wall depth creating an effectively continuous cross section. During construction pre-stressing is induced through the wedging of stones at regular

intervals which when combined with the overall confinement from the rest of the wall produces a compressional force. As the walls are backfilled, material will fill any remaining gaps at the back of the wall further strengthening the wedging. Evidence of this is shown in work carried out by Bailey (2008) in conjunction with Mundell (2009) (Figure 3). In Bailey's work during initial experiments using smaller individual blocks it was found that the backfill became wedged between the blocks making them virtually impossible to remove from the testing box. This was a nuisance for these tests, but gives useful information about the mechanical wedging of other wall types.

1.3 Random Construction

Random construction is likely to have features common to both the horizontal and vertical construction methods, however the variable morphology of the stones in random construction make it difficult to make generalised assumptions regarding any further mechanisms involved. However, it can be seen that an absence of bonding prevents the development of tensile strength along the wall face, whilst the lack of alignment of vertical stones prevents useful pre-stressing. Randomly constructed walls must rely much more on the size and weight of individual stones.

Table 1. Locations, principal stone types, and principal construction styles in this study.

Location	Geology	Wall Construction
Boscastle, Cornwall, UK	Slate	Vertical Herringbone
Mousehole, Cornwall, UK	Granite	Random
Dartmoor, Devon, UK	Igneous Intrusion	Random
Brompton Regis, Somerset, UK	Morte Slate	Vertical
Northleach, Gloucestershire, UK	Limestone Formations	Horizontal
Bath, Somerset, UK	Interbedded Limestone	Horizontal

The use of these different styles is often found to relate to the types of stone available in a given area. Horizontal construction is often found where stones are more block like in their nature, either naturally or by easy working to desired shapes. The stones used in horizontal construction are often stone types with more frictional surfaces, such as limestones, which help the stones to transfer loading more than any other mechanisms which might occur within the wall. Vertical construction seems more likely to be used with more slaty type materials. Due to its laminated nature slate is often found with a comparatively thin cross section that lends itself more to this style. This form of construction is likely to be beneficial for stones such as slate which have comparatively low surface friction because shear load from earth pressure is transmitted through contact between the rough edges of the stones rather than the smooth surfaces. Random construction is often found where stone is difficult to work e.g. granitic areas or where there is a variety of local stone types, which may all be used in conjunction within a wall. The geology of an area therefore has considerable influence on the locally dominant forms of construction, but it is still possible to see different styles within the same wall (Table 1).

2 SPECIFIC CONSTRUCTION STYLES – HARBOUR WALLS

Although wall construction style is often a reflection of locally available stone, sometimes the construction style reflects the purpose of the wall. Probably the best examples of this are the harbour walls found around the United Kingdom. Many of these walls are of significant age - parts of the quay in Mousehole are reported to date back to 1390 (Cornwall-online.co.uk) suggesting that they are well suited to their usage. Mousehole is also unusual when looking at harbour walls as much of it is uncut random rubble.



Figure 4. Wall at Mousehole, Cornwall, containing of large blocks.

It is typical when looking at harbour walls to find vertical construction as you would find with slate type materials, but they can be on a far larger scale to that found in a typical wall. Stones may also be shaped to suit vertical construction even if they are not usually built in the fashion, or are constructed from slate sheets far larger than you may expect to find in a typical vertically constructed wall. This is likely to be linked to the convenience of transport material by water, allowing larger stones to be transported. The vertical construction and larger stone sizes are both advantages in harbour construction. The verticality of the stone helps to prevent uplift by presenting a small bottom face for waves to act on, and provides better drainage for sea water, both during the changing tides and under wave penetration. Being drystone and hence free draining is better suited to harbour construction than most other wall types, in which any water which penetrated the wall under wave pressure may not flow out quickly under gravity alone, inducing extra pressures on the rear of the wall. Having a more massive construction provides better protection from wave action as a greater force is needed to move individual stones within the wall. The voided nature of drystone is also likely to help with wave energy dissipation as waves will break up into the wall on impact, as opposed to being reflected or running up and over an impermeable concrete wall.

Research has been carried out into the construction and tradition of drystone harbours by Richard Tufnell (2012) which he presented at the 13th International Dry Stone Walling Congress in September 2012

3 UNDERSTANDING CONSTRUCTION AND ASSESSMENT

Many of the current drystone retaining structures were constructed around 100 years ago with no records of how or exactly when they were constructed. Even many of the modern walls are constructed based on rules of thumb, with little or no input from engineers. Many of these walls have remained stable for a number of years and still continue to do so, retaining a significant proportion of various transport infrastructures throughout the United Kingdom, as well as being used in other applications such as harbour walls and domestic use.

Since the majority of these structures have been built, the loadings that they are subjected to have increased, particularly on the road networks. This combined with the increasing age of the walls and the need to be able to replace or repair walls before collapse means that improved assessment drystone retaining wall stability is increased. The assessment of these structures by engineers is often tricky due to the lack of formal engineering input during their design, as well as a lack of knowledge of failure mechanisms, unlike with more modern retaining structures. Assessing these structures in the same way as modern structures is inappropriate due to their un-mortared nature and inherent flexibility, which means that obvious deformation within the wall does not automatically mean that the wall is unsafe. Guidance on assessment can be found in work by O'Reilly and Perry (2009) and through the various publications by the dry stone walling association. However much of the guidance given is qualitative and relies on the judgement of the engineer assessing the wall as to whether it is safe or not. Where an engineer is familiar with drystone walls in general and the walls he is looking at in particular, then a reasonable assessment is likely to be made. However if an engineer has little to no experience of drystone walls they may take the walls' natural deformations and oddities to be signs of failure, and hence make an inaccurate or insecure judgement. This in turn may lead to walls unnecessarily being taken down and replaced with less sustainable modern alternatives which are out of keeping with their surroundings. It could also lead to a failure which should have been prevented

In order to improve assessment of these structures further engineering knowledge of them is required, both in terms of overall structural behaviour and the effects of properties of individual elements. This should include consideration of how these factors might change with time, such as the weathering of the stone. By understanding generic wall behaviour and how different factors affect this new assessment techniques can be developed that can enable the engineering judgement to be better informed.

It is also important to note the modifications that are often made to drystone retaining walls, often in good faith, which can be detrimental to the wall's health. For example, it is common practise for dry stone walls to be grouted or pointed either in an effort to prevent further movement, or to protect the base of a wall from salt spray, particularly in limestone areas. However in doing so the drainage paths through the wall are often blocked, thus taking away one of the main advantages of drystone retaining walls, which is that due to their un-mortared nature they are free draining. This can cause a build-up of water pressures behind the wall which did not exist before, and ultimately lead to collapse. The grouting of a wall will probably reduce its flexibility, which can be detrimental in two ways. If the wall is less ductile then it is unable to redistribute load concentrations, or distribute load away from weak areas, which could result in a local failure leading to a general collapse. On the other hand, a local crack which might allow a safe redistribution of load might give serious concern.

Unfortunately as with most retaining type walls a number of harbour walls are also being grouted. This is potentially understandable in harbour walls as over time wave action is likely to have caused some visible damage to the wall, and it

may be deemed necessary to protect the wall. However due to their voided nature these walls often need more grout than initially estimated and there is no guarantee that the grouting has been done sufficiently to fill all the voids in a wall. It is also difficult to know where the injected grout ends up. Grouting not only stops the draining of water that enters the wall through wave and sea action, but also most harbour walls retain land behind them so that the grouting will also prevent the drainage of groundwater, which as before exerts extra pressures on the wall and potentially causes failure.

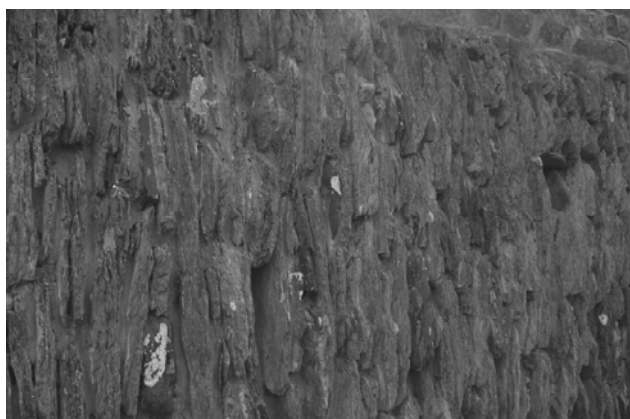


Figure 5. Grouted wall of vertical construction at Port Gavern, Cornwall

A general difficulty of assessing walls which have failed is that due to their un-mortared nature, all that is usually left of a failed section of wall is a pile of rubble that is almost impossible to analyse, and it cannot be assumed that adjacent standing sections give a true indication of the form of a failed section. Some judgement may be able to be made about the foundations or conditions of the backfill but little can be said about the wall. Increasing the understanding of how these walls work as well as improving assessment it may make it easier for engineers to use drystone walling in new build projects or to replace existing damaged walls, rather than their more modern and less sustainable counterparts.

3.1 Appearance Vs. Wall Quality

When assessing a drystone wall much weight might be given to the appearance of the wall at its face. This can be deceiving, especially as the way in which walls are finished is likely to have changed over the years. It is likely that the majority of walls built a hundred years or more ago had greater emphasis on function, whereas aesthetics are likely to be an important factor in choice of drystone walling today. This means that quality of the aesthetics is easily taken as a proxy for quality of construction, but just because the wall face looks even and is cleanly finished does not mean that the wall behind will be to the same standard - and vice versa. For example, wallers cite cases where freestanding walls have appeared to be well constructed and have a good finish but have failed within months of being built, because instead of being constructed with properly packed filling they have been filled with pea shingle with no through stones, preventing the wall from performing as a monolith. In another case a waller was asked by a client to build a small retaining wall which was to have a hedge planted in front of it, so ultimately was not worried about the finished appearance of the wall. He also did not want any wastage of the stone, whereas normally a certain amount of stone is left at the end where stones have been shaped or just not used in the wall. However this wall was built to no less a standard than other walls he had built for the same client which had a very high quality of finish to them.

4 THE SUSTAINABILITY OF DRYSTONE WALLS

As with most constructions the sustainability of drystone walls must also be considered. When considering drystone structures this will also include the ecology impacts of the walls providing habitat and shelter for both animals and plants.

Drystone walls are naturally very sustainable structures and with the current imperative of low carbon structures are an almost ideal solution. Their main advantage is a lack of mortar, this not only means that the walls lack the embodied carbon associated with the mortar, but that when repair or rebuild is required very little if any new material is required. This does however depend on the stone type; for example a limestone wall is more likely to need some new material as limestone is prone to decay from water and frost. Traditionally walls have been built with materials local to where the wall was built, as with most vernacular structures, and this has continued through the generations of wall builders so that even today new materials are usually obtained from local quarries or sources well known to the waller. This means that there is minimal transport of materials, thus reducing the embodied carbon within a drystone wall. Drystone walls also provide an excellent habitat for a variety of animals and plants and various research has been carried out where drystone walls have been highlighted. (Hynes and Fairley 1978, Cody and Cody 1972,)

5 CONCLUSIONS

Drystone retaining walls of horizontal construction have dominated scientific work to date, but regional construction styles which have developed in response to the type of stone available or particular requirements may behave in significantly different ways. It is important that these differences are understood if the stability of walls is to be assessed correctly.

6 REFERENCES

- Bailey, C. 2008. Model Tests of Dry Stone Retaining Walls. *MEng Dissertation: University of Bath: Dept. Architecture and Civil Engineering*.
- Cody, M.L., Cody, C.B.J. 1972. Territory Size, Clutch Size and Food in Populations of Wrens. *The Condor*. Vol.74. pp. 473-477.
- Colas, A.S., Morel, J.C., Garnier, D. 2010. Full-scale Field Trials to Assess Dry-Stone Retaining Wall Stability, *Engineering Structures*, Vol. 32, pp. 1215-1222.
- Cornwall-Online, Mousehole-West Cornwall, Available from: <http://www.cornwall-online.co.uk/westcornwall/mousehole.htm> [Accessed 5th November 2012]
- Hynes, J.A., Fairley J.S. 1978. A Population Study of Fieldmice in Dry-Stone Walls. *The Irish Naturalists Journal*, Vol. 19. pp. 180-184.
- McCombie, P., Mundell, C., Heath, A., and Walker, P. 2012. Drystone Retaining Walls: Ductile Engineering Structures with Tensile Strength. *Engineering Structures*, 45.
- Mundell, C. 2009. Large Scale Testing of Drystone Retaining Structures. *PhD Thesis: University of Bath: Dept. Architecture and Civil Engineering*
- Mundell, C., McCombie, P., Bailey, C., Heath, A., and Walker, P. 2009. Limit-equilibrium assessment of Drystone Retaining Structure. *Proceedings of the Institution of Civil Engineers-Geotechnical Engineering*, 162 (4), pp. 203-212
- O'Reilly, M.P., Perry, J., 2009. Drystone Retaining Walls and their Modifications – Condition Appraisal and Remedial Treatment. *CIRIA, London*.
- Tufnell, R., 2012. Dry Stone and the Sea: Techniques and Traditions of Dry Stone Harbours and Jetties in the British Isles. *13th International Dry Stone Walling Congress* (Unpublished at time of writing)
- Villemus, B., Morel, J.C., Boutin, C. 2007. Experimental Assessment of Dry Stone Retaining Wall Stability on a Rigid Foundation. *Engineering Structures*. Vol.29, pp. 2124-2132.

Numerical modelling of groundwater flow around contiguous pile retaining walls

Modélisation numérique des écoulements des eaux souterraines autour d'écrans de soutènement de pieux contigus

Wiggan C. A., Richards D.J., Powrie W.

University of Southampton, Southampton SO17 1BJ, United Kingdom

ABSTRACT: Pore water pressure constitutes a significant proportion of the lateral load acting on a retaining wall. Consequently, guidelines often mandate that the worst case hydraulic conditions are applied in the design of retaining walls. This invariably dictates that retaining walls are treated as impermeable unless special consideration is given to the maintenance of drainage systems or to the prevention of infiltration. Contiguous pile retaining walls are, however, by their nature permeable unless considerable effort is expended to prevent seepage through gaps. If allowed, this seepage can result in reduced active side pore water pressures. Numerical simulations were conducted to determine the impact on pore water pressures of varying the pile gap (x) to diameter (d) ratio, x/d , in a contiguous pile retaining wall. A relationship between x/d and the effective bulk wall permeability, k_p was derived, and applied to two-dimensional simulations representing a contiguous pile wall. The results show that pore pressures behind the retaining wall reduced significantly with increased x/d .

RÉSUMÉ: La pression de l'eau interstitielle constitue une part importante des charges latérales agissant sur les parois d'un mur de soutènement. Par conséquent, les règles de l'art imposent que les pires conditions hydrauliques soient considérées dans la conception d'un mur de soutènement. Cela impose invariablement que les murs de soutènement soient considérés comme imperméables à moins que des considérations particulières soient données à l'entretien des systèmes de drainage ou à la prévention des infiltrations. Les murs de soutènement constitués de pieux contigus, sont cependant perméables (de par leur structure), à moins que des efforts considérables soient déployés pour empêcher les infiltrations à travers les intervalles. Ces infiltrations peuvent entraîner une réduction des pressions interstitielles effectives. Des simulations numériques ont été réalisées afin de déterminer l'impact des variations de l'espace entre palplanches (x), de diamètre (d), de ratio, x/d , sur les pressions interstitielles d'un mur de soutènement constitué de pieux contigus. Une relation entre le ratio x/d et la réelle perméabilité du mur, k_p a été déduite et appliquée à un modèle à deux dimensions représentant un mur en pieux contigus. Les résultats montrent que les pressions interstitielles derrière le mur de soutènement diminuent significativement lorsque le ratio x/d augmente.

KEYWORDS: Pore water pressure, numerical modelling, retaining wall, seepage forces, surface settlement

1 INTRODUCTION

Guidelines generally require that the most onerous tenable pore water pressure distribution is adopted for the design of subsurface retaining structures. For example, Eurocode 7 recommends that, unless reliable drainage can be provided or infiltration prevented, retaining walls should be designed with the water table at the ground surface (BSI, 2004). This can however cause over-conservative and unnecessarily expensive engineering solutions which go against the ethos of sustainable development. It would be advantageous if, based on the bulk permeability of the structure, the hydraulic loads on retaining walls could be treated as reduced.

There is however limited research into how the geometry influences hydraulic loads on retaining walls although, according to CIRIA 580, 'economic advantages' might be derived if through-wall seepage is allowed (Gaba et al. 2003). This is due mainly to the reduction in pore pressures because of through-wall seepage. Research into ways of facilitating through-wall seepage and quantifying its effect is necessary.

1.1 Research in hydraulic loads around retaining structures

Previous research has not generally sought to distinguish between the long-term pore water pressure distributions around different types of retaining walls. For example, Potts and Burland (1983) and Hubbard et al. (1984) showed that the long-term pore pressures behind a secant pile retaining wall recovered to near their pre-construction values as might be

expected of an impermeable wall in fine soils. Powrie et al. (1999) and Carder et al. (1999) observed a reduction in pore pressures following construction of a contiguous pile retaining wall at Woodford. The pore pressures at Woodford however, did not return to their pre-construction values in the long-term. This reduction was attributed at the time to under-drainage to the more permeable chalk layer and therefore no consideration was given to the possible contribution of through-wall seepage. However Clark (2006) and Richards et al. (2007) have shown that there was a reduction in long-term pore pressures measured at a contiguous pile retaining wall in over-consolidated clay at Ashford. The pore pressures have not returned to their pre-construction values. Although there is underdrainage to the more permeable Weald Clay at Ashford, there is evidence that the long-term reduction in pore pressure can be attributed to through-wall seepage.

In contrast to retaining walls, there has been significant research into methods of reducing pore water pressures acting on shallow tunnels and on tunnels acting as drains. Despite an earlier assumption by Atkinson and Mair (1983) that groundwater loadings do not change significantly in the presence of varying hydraulic conditions, it has been shown by numerical analyses that segmented tunnel linings do in fact allow seepage of groundwater which contributes to reduced pore water pressures around tunnels in fine grained soils. Pore pressures at segmented lined tunnels approach atmospheric values and increase with distance away from the tunnel (Shin et

al. (2002), Lee and Nam (2006), Bobet and Nam (2007) and Arjnoi et al. (2009)).

The corresponding reductions in axial forces and stresses on segmented tunnel linings in comparison with fully waterproofed linings are significant, although inconsistent. For example Arjnoi et al (2009) observed a 20% reduction, Lee and Nam (2001) 25%, Potts et al. (2002) up to 30% and Lee and Nam (2006) up to a 70% reduction.

1.1.1 Surface settlement

Notwithstanding the potential advantages of allowing through-structure seepage, some detrimental effects have been noted in the analyses of shallow tunnels which might be relevant to through-wall seepage. Significant settlements have been observed associated with segmented lined tunnels acting as drains in fine grained soils. For example, Yoo (2005) noted that settlement was proportional to the amount of drawdown in the groundwater levels around the tunnel. Consolidation settlement, ρ due to the drawdown of groundwater level may be estimated in a similar manner by considering the one dimensional stiffness modulus, E'_0 of the soil as shown in equations 1 and 2 (Roberts et al. 2007).

$$E'_0 = 400\sigma'_v \tag{1}$$

$$\rho = \frac{D_w S_{av}}{E_{0av}} \tag{2}$$

where σ'_v , D_w , S_{av} and E_{0av} are the vertical effective stress, thickness of the soil layer, unit weight of water and average drawdown respectively.

In this paper, pore water pressure variations around contiguous pile retaining walls are investigated numerically. An expression for the resulting effective bulk wall permeability k_p , is derived. This is then applied to two dimensional analyses of contiguous and secant pile retaining walls to highlight the advantages of a semi-permeable structure.

2 NUMERICAL ANALYSES

Numerical simulations were conducted using the finite difference geotechnical application FLAC2D (ITASCA, 2012). The investigations were undertaken in two phases. Horizontal flow was simulated in phase 1 to determine how pore pressures and steady state flow vary with x/d in order to derive an expression for k_p/k_s . This relationship was then applied to a vertical plane flow in phase 2 and the pore pressures calculated.

Preliminary analysis, not included in this report, were carried out to establish i) suitable boundary locations, ii) the size of the numerical grid and iii) the limiting value of x/d . Grid boundaries were selected such that x/d did not influence the far-field conditions. It was determined that increasing x/d above 2 did not significantly impact the results.

2.1 Model soil and wall properties

An elastic constitutive soil model was used in all analyses. Elastic properties of bulk and shear moduli were used instead of Young's modulus and Poisson's ratios. The soil and model pile section and the model wall in phases 1 and 2 respectively were represented by grid elements attached directly to the soil grid without the use of interface elements so as to allow cross-boundary flow. Uncoupled groundwater flow analyses which ignored the impact of mechanically induced pore pressures were performed.

2.2 Derivation of bulk wall permeability, k_p

The simulations started with a 'wished into place' model pile section and the water level at the surface. Pore pressures at the

discharge surface shown in figure 1 were lowered incrementally corresponding to pressure drops U_i for each step. Steady state discharge and pore pressures were measured and fluid flow-paths tracked for different pile gap to diameter ratios x/d .

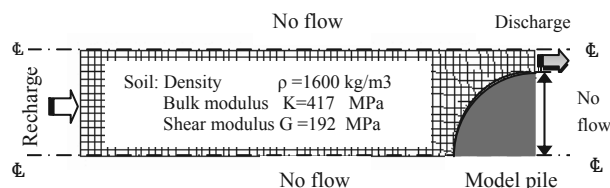


Figure 1. Plan of typical numerical grid showing boundary conditions for phase 1 analyses.

2.2.1 Results and discussion

Darcy's equation for steady state flow (Eq. 3) was applied using the parameters Δl , h_1 , and h_2 indicated in figure 2 and the values compared with the numerically derived flow rates (Q_i) in figure 3 at pressure differences, U_i .

$$Q = A_p k_p \frac{h_1 - h_2}{\Delta l} \tag{3}$$

where $(h_1 - h_2)/\Delta l$ is the hydraulic gradient between the distance of influence and the discharge surface (see Figure 2). (The distance of influence was selected as the point beyond which the hydraulic gradient was uniform).

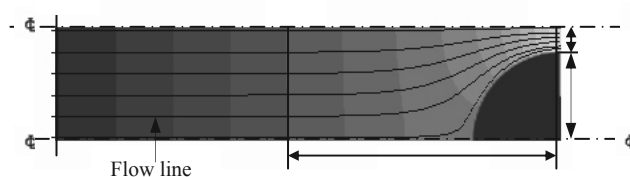


Figure 2. Calculating bulk wall permeability, k_p and flow-paths.

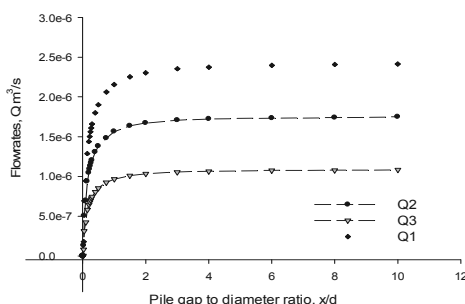


Figure 3. Steady state flow-rates, Q_i at various pressure drops U_i .

The resulting bulk wall permeability was calculated for a soil permeability $k_s = 2 \times 10^{-5}$ m/s and plotted for three values of U_i (see Figure 4). The empirical hyperbolic relationship between the pile gap to diameter ratios x/d and permeability ratios k_p/k_s derived in the phase 1 simulation is given in equation 4.

$$\frac{k_p}{k_s} = \frac{4 \frac{x}{d}}{1 + 4 \frac{x}{d}} \tag{4}$$

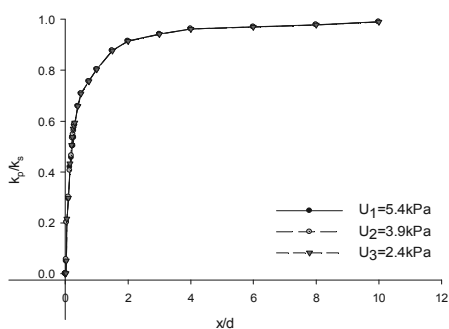


Figure 4. Calculated permeability from FLAC2D simulations.

2.3 Application of derived expression to 2D analyses

The aim of phase 2 simulations was to test the application of the permeability expression derived in phase 1.

2.3.1 Procedure

A continuous wall was used to represent the contiguous pile retaining wall. The model wall thickness (t) was calculated by equating the second moments of area (I) of the different cross-sections (A) as outlined by Powrie et al (1999) (Eq. 5). This gave a result similar to the stiffness approach adopted by Day and Potts (1993) (see Eq. 6 and 7).

$$I_p = I_m \tag{5}$$

$$tE_{eq} = EA \tag{6}$$

$$E_{eq} = EI \tag{7}$$

where E_{eq} and E are the equivalent model wall stiffness and material Young's modulus respectively.

The simulations commenced as before with a 'wished into place' model wall. Pore pressures were varied corresponding to U_i as before for different pile gap to diameter ratios, x/d .

2.3.2 Results and discussion

It was observed that flow patterns for the 'permeable' walls deviated from the classically accepted flow around an impermeable retaining wall especially at higher values of x/d . This seems to suggest that through-wall flow is taking place for $x/d > 0.0$ as shown in figure 5.

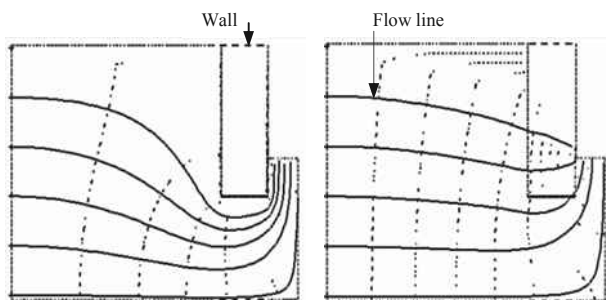


Figure 5. Tracked flow-paths for $x/d=0$ and $x/d=0.1$. Note these are not intended to be flownets, hence the flow elements are not "square".

2.3.3 Pore pressure distribution

Pore pressures ratios P_i/P_0 are plotted against normalized distance (L/d) from the model wall in figure 6 for various values of x/d .

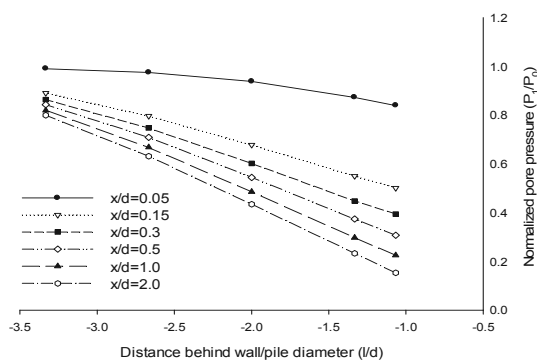


Figure 6. Normalised pore pressures for different x/d against distance (L/d) from the wall.

It was observed that pore pressures at each position behind the wall decreased with x/d as the equivalent permeability increased. Further analyses have shown that the pore pressures and hence hydraulic head reduce towards the wall (Figure 7).

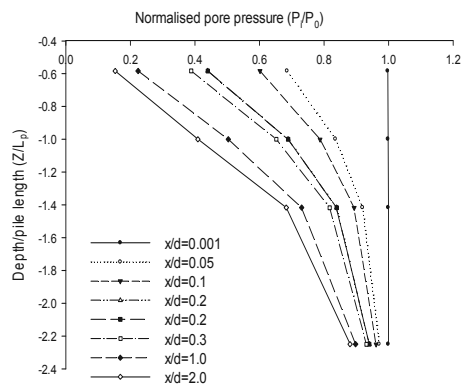


Figure 7. Normalised pore pressure versus normalized depth below soil surface for different values of x/d .

2.3.4 The effect of seepage on surface settlement

Surface settlements increased as the bulk permeability of the wall increased (see Figure 8). The calculated settlement values were compared with an estimated solution which uses the one dimensional stiffness modulus (Roberts et al 2007). It was noted that the 1D stiffness modulus method over-predicted surface settlement at higher x/d as shown in Figure 9. This is unsurprising as in this approach all volume change is assumed to manifest as vertical settlement.

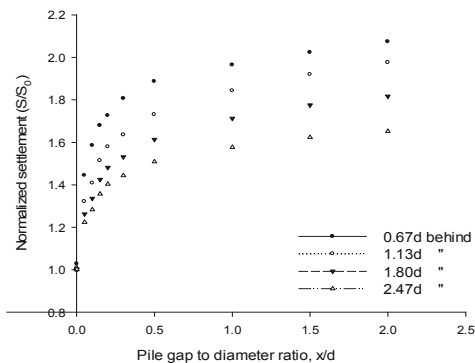


Figure 8. Normalised settlement increases with soil/structure permeability.

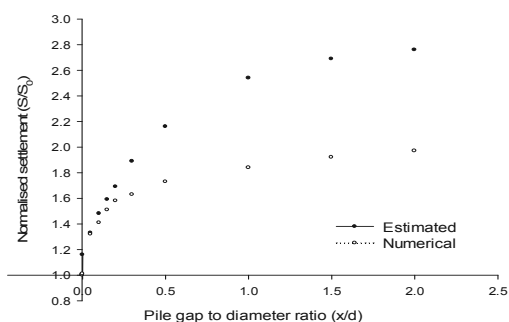


Figure 9. Comparison of analytical and numerical solutions for surface settlement variation with x/d .

2.5 Secant versus Contiguous Pile Retaining Walls

Comparisons were made between retaining walls formed of contiguous and secant piles 20m long with 10m excavation depth in homogeneous soil. Figure 10 shows that the pore pressure profiles are slightly less than hydrostatic for the secant and significantly less than hydrostatic for the contiguous pile wall.

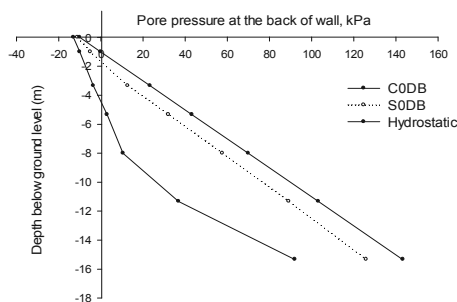


Figure 10. Comparison of pore pressure profiles for secant and contiguous pile walls against hydrostatic pressure.

3 CONCLUSIONS

Limited research has previously been carried out on the influence of retaining wall geometry on the development of hydraulic loads on the active side. Numerical simulations presented in this paper have shown that the pore pressure magnitude behind bored pile retaining walls reduces with increasing pile gap to diameter ratio, x/d . This reduction in lateral loads however is accompanied by an increase surface settlement. However, the potential benefits of allowing through-wall seepage are likely to be greater than the drawbacks.

4 ACKNOWLEDGEMENTS

Funding for this research was provided by the Engineering and Physical Sciences Research Council, (EPSRC) grant number EP/F063482.

5 REFERENCES

Arjinoi, P., Jeong, J.H., Kim, C.Y., & Park, K.H. 2009. Effect of drainage conditions on porewater pressure distributions and lining stresses in drained tunnels. *Tunnelling and Underground Space Technology*, 24, (4) 376-389.

Atkinson, J.H. & Mair, R.J. 1983. Loads on Leaking and Watertight Tunnel Linings, Sewers and Buried Pipes due to Groundwater. *Geotechnique*, 33, (3) 341-344

Bobet, A. & Nam, S.W. 2007. Stresses around pressure tunnels with semi-permeable liners. *Rock Mechanics and Rock Engineering*, 40, (3) 287-315.

BSI 2004, Eurocode 7: Geotechnical design Part 1, General Rules. EN1997-1:2004, British Standard Institution.

Carder, D.R., Watson, G.V.R., Chandler, R.J., & Powrie, W. 1999. Long-term performance of an embedded retaining wall with a stabilizing base slab. *Proceedings of the Institution of Civil Engineers-Geotechnical Engineering*, 137, (2) 63-74.

Clark, J. 2006. Performance of a propped retaining wall at the Channel Tunnel Rail Link, Ashford. PhD University of Southampton.

Day, R.A. & Potts, D.M. 1993. Modeling Sheet Pile Retaining Walls. *Computers and Geotechnics*, 15, (3) 125-143

Gaba, A.R., Simpson, B., Beadman, D.R., & Powrie, W. 2003. Embedded retaining walls: guidance for economic design. *Proceedings of the Institution of Civil Engineers-Geotechnical Engineering*, 156, (1) 13-15.

Hubbard, H.W., Potts, D.M., & Miller, D. 1984. Design of the retaining walls for the M25 cut and cover tunnel at Bell Common. *Geotechnique*, 34, (4) 495-512

ITASCA. Fast Lagrangian Analysis of Continua in 2 Dimensions. User Manual. Itasca Consulting Group[7.0]. 2012. Minneapolis, USA. Ref Type: Computer Program

Kolymbas, D. & Wagner, P. 2007. Groundwater ingress to tunnels - The exact analytical solution. *Tunnelling and Underground Space Technology*, 22, (1) 23-27.

Lee, I. M. & Nam, S. W. 2001, The study of seepage forces acting on tunnel lining and tunnel face in shallow tunnels. *Tunnelling and Underground Space Technology*, 16, (1) 31-40.

Lee, I. M. & Nam, S. W. 2006, Seepage Force Considerations in Tunnelling, In *International Symposium on Underground Excavation and Tunnelling*.

Potts, D. M., Axelsson, K., Grande, L., Schweiger, H., & Long, M. Guidelines for the use of advanced numerical analysis. 2002. Thomas Telford Publishing. Ref Type: Edited Book

Potts, D. M. & Burland, J. B. 1983, Numerical investigation of retaining wall at Bell Common Tunnel.

Powrie, W., Chandler, R.J., Carder, D.R., & Watson, G.V.R. 1999. Back-analysis of an embedded retaining wall with a stabilizing base slab. *Proceedings of the Institution of Civil Engineers-Geotechnical Engineering*, 137, (2) 75-86.

Richards, D.J., Powrie, W., Roscoe, H., & Clark, J. 2007. Pore water pressure and horizontal stress changes measured during construction of a contiguous bored pile multi-propped retaining wall in Lower Cretaceous clays. *Geotechnique*, 57, (2) 197-205.

Roberts, T.O.L., Roscoe, H., Powrie, W., & Butcher, D.J.E. 2007. Controlling clay pore pressures for cut-and-cover tunnelling. *Proceedings of the Institution of Civil Engineers-Geotechnical Engineering*, 160, (4) 227-236.

Shin, J.H. 2010. Analytical and combined numerical methods evaluating pore water pressure on tunnels. *Geotechnique*, 60, (2) 141-145.

Shin, J.H., Addenbrooke, T.I., & Potts, D.M. 2002. A numerical study of the effect of groundwater movement on long-term tunnel behaviour. *Geotechnique*, 52, (6) 391-403.

Yoo, C.S. 2005. Interaction between tunnelling and groundwater, Numerical investigation using three dimensional stress pore pressure coupled analysis. *Journal of Geotechnical and Geoenvironmental Engineering*, 131,)2= 497β513.

Geosynthetic Reinforced Soil Wall Performance under Heavy Rainfall

La performance du mur en sol renforcé par géosynthétiques sous de fortes pluies

Yoo C., Jang D.W.

Dept. of Civil and Environmental Engineering, Sungkyunkwan University, Suwon, Korea

ABSTRACT: Global warming is now considered to be one of the greatest threats to earth. The direct consequence of the temperature increase due to the global warming include a rise in sea levels and a change in the amount and pattern of precipitation. Since the amount pattern of precipitation have of paramount implications to short and long-term performance of geo-structures, geo-engineers should pay attention to the issue of global warming. In this paper, the results of laboratory investigation into the effect of rainfall on the performance of geosynthetic reinforced soil wall (GRSW) are presented. A series of model tests were performed using reduced scale model walls, which were reduced from a full-scale GRS wall according to the similitude law. The model GRSWs were subjected to cycles of wetting and drying process with different rainfall intensities but with a same amount. The results show that the cycles of wetting and drying associated with a heavy rainfall may induce additional wall displacement and reinforcement strains in GRSWs, and that such trends have significant implications to GRSW stability, especially for walls designed with marginal factor of safety in terms of long-term performance.

RÉSUMÉ : Le réchauffement climatique est aujourd'hui considéré comme l'une des plus grandes menaces pour la terre. Les conséquences directes de l'augmentation de température due au réchauffement climatique incluent notamment l'élévation du niveau des mers et un changement dans la quantité et le régime des précipitations. Ces paramètres ayant des implications primordiales sur les performances à court et à long terme de géo-structures, les géo-ingénieurs devraient prêter attention à la question du réchauffement climatique. Dans cet article, les résultats des études en laboratoire sur les effets de fortes précipitations pour la performance des murs en sol renforcé par géosynthétiques (GRSW) sont présentés. Une série d'essais sur modèles réduits a été réalisée avec des modèles réduits d'un mur à pleine échelle GRS suivant la loi de similitude. Les modèles GRSW ont été soumis à des cycles de mouillage et de séchage avec des intensités pluviométriques différentes. Les résultats montrent que les cycles de mouillage et de séchage associés à une forte pluie peuvent provoquer un déplacement supplémentaire du mur et les tensions dans le renforcement, et que ces tendances ont des implications importantes pour les GRSW conçus avec un faible facteur de sécurité en termes de performance à long terme

KEYWORDS: Climate change, Rainfall, Reduced-scale model test, Matric suction, Pore water pressure

1 INTRODUCTION

Since the early 20th century, Earth's mean surface temperature has increased by about 0.8°C with about two-thirds of the increase occurring since 1980. A climate model projects that the global surface temperature will probably rise further 1.1 to 6.4°C during the twenty-first century (IPCC 2007). An increase in global temperature will cause sea levels to rise and will change amount and pattern of precipitation as well. Korea is no exception from the issue of global warming. The Korean Meteorological Administration (KMA) has made a report on climate change characteristics during the period of 1996–2005 that the mean temperature has increased by 0.6°C from the last 30 year mean temperature during the period between 1971 to 2000 (KMA 2008). The annual precipitation has also increased by 11%. It is projected that the temperature increase will be as great as 4°C with an annual precipitation increase of 17% by the end of 21st century. Since the increase in precipitation has of paramount implications to short and long-term performance of geo-structures, geo-engineers should pay attention to the issue of global warming.

In response to the need for addressing the effect of rainfall on geo-structures for design and construction, a number of studies have been undertaken. Most of the available studies are, however, focused more or less on the effect of rainfall on natural slopes (Gasmo et al. 2000, Tsaparas et al. 2002, Zhan and Ng 2004, Cai and Ugai 2004, Cheuk et al. 2005, Garcia et al. 2006, Rahardio et al. 2007, Rahimi et al. 2011) except Blake et al. (2003) and Yoo et al. (2008a, 2008b) in which the effect

of rainfall on retaining structures was investigated. More specifically, Yoo et al. (2008a, 2008b) investigated the effect of rainfall on GRSWs using a series of limit equilibrium analyses within the framework of unsaturated shear strength, coupled with transient infiltration analyses. Much still need to be studied on the subject of the effect of rainfall on geo-structures.

In this paper, the results of a laboratory investigation into the effect of rainfall on the performance of geosynthetic reinforced soil wall (GRSW) are presented. A series of model tests were performed using reduced scale model walls, which were reduced from a full-scale GRS wall according to the similitude law. The model GRSWs were subjected to cycles of wetting and drying process with different rainfall intensities but with the same total rainfall.

2 REDUCED SCALE MODEL TEST

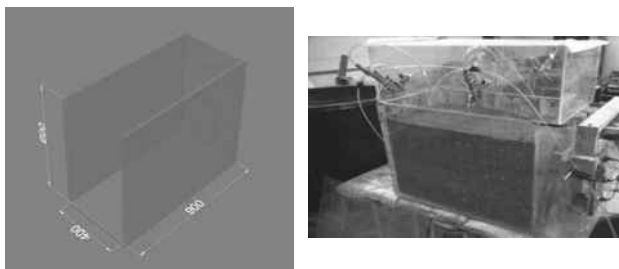
A series of reduced scale model tests were performed with due consideration of the wetting and drying process. Details of the model tests and the results are given in the subsequent sections.

2.1 Model wall and backfill soil

The reduced scale model tests were performed using 0.5 m high reduced scale model GRSWs constructed in a test box, having dimensions of 0.9 m x 0.4 m in plan and 0.6 m in height, made of 2 cm thick Plexiglas as shown in Figure 1. The test box was made sufficiently rigid to maintain the plane-strain condition during test. The wall facing, made of 0.5 cm thick Plexiglas,

was hinged at the bottom of the test box so as to allow lateral displacement to occur during the wetting and drying process.

The backfill soil was a non-plastic poorly-graded sand, commonly known as decomposed granite soils (DCG) in Korea, classified as SP as per ASTM 2487 (ASTM 1992) with the effective size (D_{10}), uniformity coefficient (C_u), and coefficient of curvature (C_c) of 0.36 mm, 5.3 and 1.1, respectively. The soil was compacted to 70% of its maximum unit weight ($19kN/m^3$) to create reinforced as well as retained zones. The estimated effective internal friction angle (ϕ') using a series of consolidated-undrained (CU) triaxial compression tests with pore pressure measurements at a density corresponding to the as-compacted state was determined as approximately 35° with a shear stress intercept of 8 kPa.

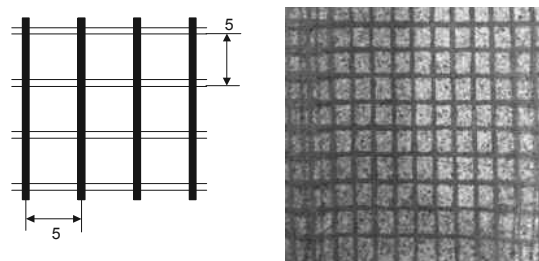


(a) Test box (unit mm)

(b) photo of model GRSW

Figure 1. Test box and model GRSW

A non-woven geotextile was used as reinforcement. Note however that the tensile strength of the non-woven geotextile was intentionally reduced by creating 5 mm x 5 mm square holes (Figure 2) to have an ultimate tensile strength of $3.8 \times 10^{-2} kN/m$. Six layers of reinforcement, 35 cm in length each, were placed at a vertical spacing of 6 cm (Figure 3). The reinforcement layers were firmly connected to the wall facing by bolting.



Unit [mm]

(a) square hole size

(b) photo of model reinforcement

Figure 2. Model geotextile reinforcement

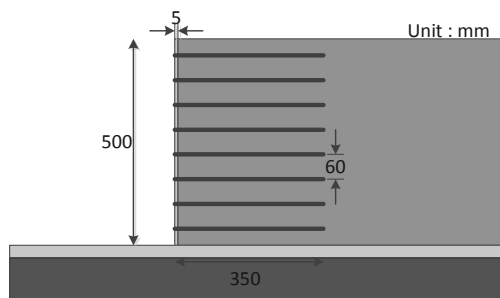


Figure 3. Schematic sectional view of model GRSW

2.2 Rainfall simulation

Three cycles of wetting and drying were applied to the model walls to simulate the natural weather condition. Two rainfall intensities (I_r) were considered, i.e., 18.7 mm/h and 56.2 mm/h

for a given total precipitation of 450 mm. The duration of the rainfall for the case with $I_r = 18.7 mm/h$ was therefore 24 hours while 8 hour duration was used for the case with $I_r = 56.2 mm/h$. Note that these rainfall conditions were based on the actual rainfall occurred in 2011 in Kyoung-Gi province, Korea. Followed after each wetting process was a 24 hour drying period prior to the ensuing wetting to observe the wall behavior during the repeated wetting and drying.

The rainfall was simulated by spraying water at the top of the backfill using spray guns with 15HP compressor and a 20W water motor (Figure 4).

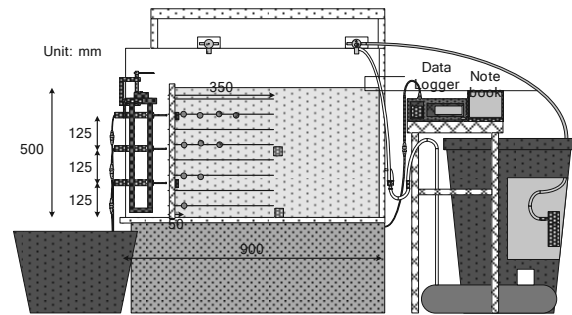


Figure 4. Schematic diagram of rainfall simulator

2.3 Instrumentation

The performance of the model GRSW under a series of wetting and drying cycles was evaluated in terms of wall facing displacements, pore water pressures, and reinforcement strains. The layout of instrumentation program is shown in Figure 5.

As shown, the horizontal displacements of the wall facing were measured by using three LVDTs having gauge length of 100 mm, placed at locations along a vertical row. In addition, the wetting and drying cycle induced reinforcement strains were measured using high-elongation strain gauges, manufactured by Tokyo Sokki Kenyujo Company (Model YFLA-5-5L) which were mounted directly onto the selected reinforcement layers in one array. Also installed at the back of the reinforced zone were two pore pressure cells (Model BPR-A-200 kPa) at the bottom (0 mm) and 250 mm above the wall base. The volumetric water content of the backfill soil during the wetting and the drying process was also measured using a tensiometer (Model EC-5).

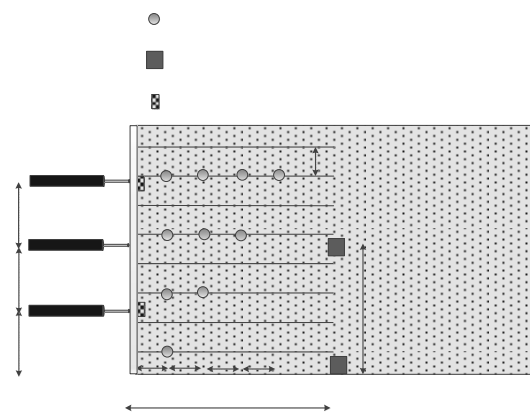


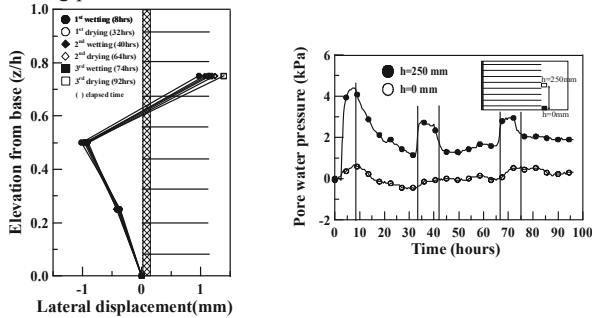
Figure 5. Instrumentation layout

3 RESULTS AND DISCUSSION

3.1 General behavior

Figure 6 show the measured data for the rainfall intensity of $I_r = 56.2 mm/h$. As mentioned, the 56.2 mm/h intensity rainfall

lasted for 8 hours for wetting. As shown in Figure 6(a), the wall displacement increased about 1 mm during the 1st cycle of wetting after which no significant increase was recorded. The pore water pressures measured at the bottom and the mid-height at the back of reinforced zone tended to increase during the first wetting period as great as 4 kPa, followed by gradual decreases during the ensuing 24 hour drying period as shown in Figure 6(b). As observed in the wall displacement, the largest increase in the pore water pressure was measured during in the first wetting period.



(a) wall displacement (b) pore pressure
Figure 6. Wall displacement and pore pressure ($I_r = 56.2 \text{ mm/h}$)

Shown in Figure 7 are the measured reinforcement strains in the selected reinforcement layers. Of salient features are twofold. First, the reinforcement strains tended to steadily increase over the repeated wetting and drying cycles unlike the wall displacements and the pore water pressures which showed cycles of fluctuation during the wetting and drying process. Second, larger strains, as great as 0.015%, are measured in the upper reinforcement layers than in the lower layers due possibly to the downward movement of wetting front caused by the rainfall infiltration.

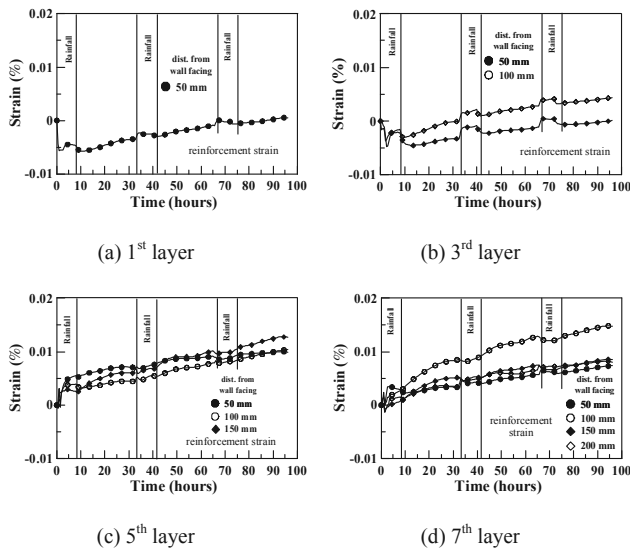


Figure 7. Reinforcement strains ($I_r = 56.2 \text{ mm/h}$)

Figure 8 shows the time variation of volumetric water content (θ) measured at 160 mm above the wall base at the back of the reinforced zone. As shown, the initial volumetric water content of 0.05 at the measuring point sharply increased to 0.35 after which it remained constant over the remaining wetting period. During the drying period, θ then sharply decreased to 0.2 and remained constant during the entire drying period. A similar trend can be observed in the following cycles suggesting that the cycles of the wetting and drying with the rainfall intensity and duration considered in this study may increase the water content of the backfill soil.

The results shown here indicate that the repeated cycles of wetting and drying associated with a heavy rainfall may induce additional wall displacement and reinforcement strains in GRSWs. Such results suggest that the weather induced wetting drying has significant implications to GRSWs designed with marginal factor of safety in terms of long-term stability.

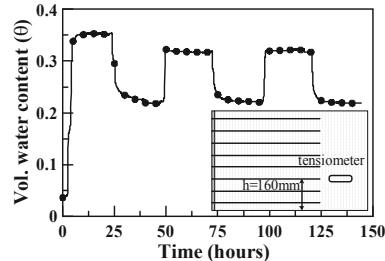
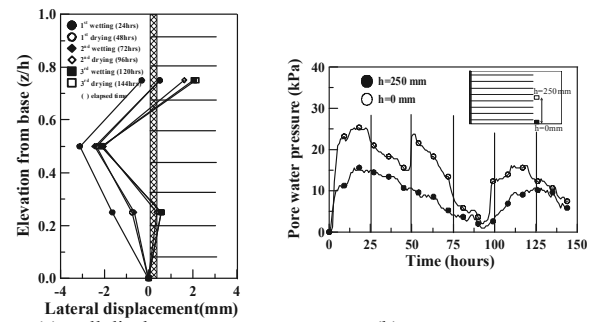


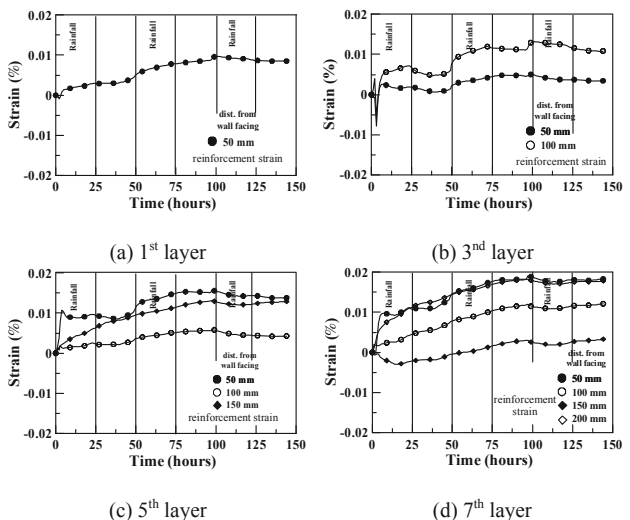
Figure 8. Time variation of volumetric water content (θ)

3.2 Effect of rainfall intensity

Figures 9 and 10 show the measured wall displacements and the reinforcement strains for the case with a rainfall intensity of 18.7 mm/h. Note that the total rainfall was kept same at 450 mm as in the case of $I_r = 56.2 \text{ mm/h}$ but with a longer wetting period of 24 hours. The discrepancies in the wall performance between the two cases can therefore be thought to stem from the rainfall intensity.



(a) wall displacement (b) pore pressure
Figure 9. Wall displacement and pore pressure ($I_r = 18.7 \text{ mm/h}$)



(c) 5th layer (d) 7th layer
Figure 10. Reinforcement strains ($I_r = 18.7 \text{ mm/h}$)

The direct comparison between the two cases reveals that the case with the smaller rainfall intensity but with the longer duration generally induces larger wall displacements and reinforcement strains except for the pore water pressure measured at the back of reinforced zone. Considering the backfill soil being a high permeability soil, these results

contradict those reported by Cai and Ugai (2005) as well as Rahardjo et al. (2007) which were based on a numerical study. A further study is therefore warranted to confirm the effect of rainfall intensity. It can however be stated that the rainfall intensity is a controlling factor for the performance of a GRSW during rainfall infiltration as reported by Rahardjo et al. (2007) in their study concerning natural slopes.

4 CONCLUSIONS

In this study, the results of laboratory investigation into the effect of rainfall on the performance of a geosynthetic reinforced soil wall (GRSW) using reduced scale model tests are presented. The model GRSWs were subjected to cycles of wetting and drying process with different rainfall intensities but with the same total rainfall. The results show that the cycles of wetting and drying associated with a heavy rainfall may induce additional wall displacement and reinforcement strains in GRSWs, and that such trends have significant implications to GRSWs with marginal factor of safety in terms of long-term performance. The effect of rainfall intensity for a given total rainfall is such that the case with a smaller rainfall intensity but with a longer duration generally induces larger wall displacements and reinforcement strains except for the pore water pressure measured at the back of reinforced zone. Although a further study is required to confirm the effect of rainfall intensity, it can be concluded that the rainfall intensity is a governing factor for the performance of a GRSW during rainfall infiltration.

5 ACKNOWLEDGEMENT

This research is supported by Grant No. 20100008227 from the Basic Research Program of the Korea Science & Engineering Foundation. The financial support is gratefully acknowledged.

6 REFERENCES

- ASTM 1992. Standard test method for classification of soils for engineering purposes. ASTM D2487-90, Annual Books of ASTM Standards, West Conshohocken, PA., 4.08, 326-336.
- Cai, F. and Ugai, K. 2005. Numerical Analysis of Rainfall Effects on Slope Stability. *International Journal of Geomechanics*, 4(2), 69-78.
- Cheuk, C.Y., Ng, C.W.W., and Sun, H.W. 2005. Numerical experiments of soil nails in loose fill slopes subjected to rainfall infiltration effects. *Computers and Geotechnics*, 32(4), 290-303.
- Garcia, E.F., Gallage, C.P.K., and Uchimura, T. 2006. Unsaturated infiltration on artificial embankments reinforced with geosynthetics. *Prof. of 8th International Symposium on Geosynthetics*, Kuwano and Koseki (eds). 1417-1420.
- Gasmo, J.M., Rahardjo, H., and Leong, E.C. 2000. Infiltration effects on stability of a residual soil slope. *Computers and Geotechnics*, 26, 145-165.
- IPCC 2007. Summary for Policymakers" (PDF). *Climate Change 2007: The Physical Science Basis. Contribution of Working Group I to the Fourth Assessment Report of the Intergovernmental Panel on Climate Change*. http://ipcc-wg1.ucar.edu/wg1/Report/AR4WG1_Print_SPM.pdf.
- Korean Meteorological Administration 2008. Report on Climate Change and Mitigation: Dept. of Climate Change Response: Climate Change Information Center, (in Korean).
- Rahardjo, H., Ong, T.H., Rezaur, R.B., and Leong, E.C. 2007. Factors controlling Instability of Hogeneous Soil Slopes under Rainfall. *Journal of Geotechnical and Geoenvironmental Engineering*, ASCE, 133(12), 1532-1543.
- Rahimi, A., Rahardjo, H., Leong, E. C. 2011. Effect of Antecedent Rainfall Patterns on Rainfall-Induced Slope Failure, *Journal of Geotechnical and Geoenvironmental Engineering*, ASCE, 137(5), 483-491
- Tsaras, I., Rahardjo, H., Toll, D.G., and Leong, E.C. 2002. Controlling parameters for rainfall-induced landslides. *Computers and Geotechnics*, 29(1), 1-27.
- Yoo, C., Kim, S.B., and Jung, H.S. 2008a. A numerical investigation on effect of vertical drainage system on geosynthetic reinforced soil wall during rainfall. *Journal of Korean Geotechnical Engineering*, 24(5), 99-106.
- Yoo, C., Kim, S.B., and Han, J.Y. 2008b. A numerical investigation on stability of geosynthetic reinforced soil wall during rainfall. *Journal of Korean Geotechnical Engineering*, 24(12), 1-12.
- Zhan, L.T. and Ng, C.W.W. 2004. Analytical Analysis of Rainfall Infiltration Mechanism in Unsaturated Soils. *International Journal of Geomechanics*, 4(4), 273-284.

Proceedings of the 18th International Conference on Soil Mechanics and Geotechnical Engineering **CHALLENGES AND INNOVATIONS IN GEOTECHNICS**

*Actes du 18^e Congrès International de Mécanique
des sols et de Géotechnique*

DÉFIS ET INNOVATIONS EN GÉOTECHNIQUE

The 18th International Conference on Soil Mechanics and Geotechnical Engineering (Paris 2013) was devoted to "Challenges and Innovations in Geotechnics". The call for abstracts was based on a large series of themes covering most aspects of Geotechnical Engineering and around 800 abstracts were received from the Member Societies. According to the ISSMGE new vision for strengthening the role of the Technical Committees, the papers were distributed to the corresponding Technical Committees, which then selected the General Reporters, the Invited Speakers and the Poster presentations. The involvement of TCs (which could also propose Workshop Sessions on an independent basis) was enthusiastic and successful, which probably explains the success of the Conference with more than 1500 delegates.

The four volumes of the Proceedings contain the Terzaghi Oration, the Honour lectures, the Special lectures followed by the papers presented according to the relevant TC and introduced by the TC General Report. All volumes, together with late papers, will also be made available online free of charge. These volumes will provide a state of the art and serve as an essential reference for practitioners, academics and researchers involved in Soil Mechanics and Geotechnical Engineering.

Le 18^e Congrès International de Mécanique des sols et de Géotechnique (Paris 2013) a été dédié aux « Défis et Innovations en Géotechnique ». L'appel à résumé était ouvert sur un large éventail de thèmes couvrant la plupart des aspects de la Géotechnique ; les Sociétés Membres ont sélectionné environ 800 résumés. En cohérence avec le souhait de la Société Internationale (SIMSG) de renforcer le rôle des Comités Techniques (CTs), les contributions ont été transmises aux CTs correspondants, en charge de choisir les Rapporteurs Généraux, les Orateurs Invités et les Présentations sur Posters. L'implication des CTs, qui pouvaient en outre proposer des sessions d'Atelier à leur convenance, a été enthousiaste et fructueuse ; ceci explique probablement le succès du Congrès avec plus de 1500 délégués.

Les quatre volumes des Actes contiennent l'Allocution Terzaghi, les Conférences Honorifiques, les Conférences Spéciales, suivies des contributions, réunies par CT, et précédées du Rapport Général du CT correspondant. L'ensemble, accompagné des contributions complémentaires, sera mis en ligne sur le Web, en accès libre. Ces volumes constituent un état de l'art et serviront de référence essentielle pour les praticiens, les enseignants et les chercheurs en Mécanique des Sols et en Géotechnique.

Paris 2013

